N/0002653--073

Hydrologic Data for the Groundwater Flow and Contaminant Transport Model of Corrective Action Units 101 and 102: Central and Western Pahute Mesa, Nye County, Nevada

Revision No.: 1

January 2021

Prepared for U.S. Department of Energy under Contract No.DE-NA0002653.

Available for sale to the public from:

U.S. Department of Commerce
National Technical Information Service
5301 Shawnee Road
Alexandria, VA 22312
Telephone: 800.553.6847
Fax: 703.605.6900
E-mail: *orders@ntis.gov*
Online Ordering: *http://www.ntis.gov/help/ordermethods.aspx*

Available electronically at *http://www.osti.gov/bridge*

Available for a processing fee to U.S. Department of Energy and its contractors, in paper, from:

U.S. Department of Energy
Office of Scientific and Technical Information
P.O. Box 62
Oak Ridge, TN 37831-0062
Phone: 865.576.8401
Fax: 865.576.5728
Email: *reports@adonis.osti.gov*

N/0002653--073

HYDROLOGIC DATA FOR THE GROUNDWATER FLOW AND CONTAMINANT TRANSPORT MODEL OF CORRECTIVE ACTION UNITS 101 AND 102: CENTRAL AND WESTERN PAHUTE MESA, NYE COUNTY, NEVADA

Revision No.: 1
January 2021
Navarro
c/o U.S. DOE
100 N. City Parkway, Suite 1750
Las Vegas, NV 89106

Prepared for U.S. Department of Energy under Contract No.DE-NA0002653..

TABLE OF CONTENTS

TABLE OF CONTENTS (CONTINUED)

TABLE OF CONTENTS (CONTINUED)

TABLE OF CONTENTS (CONTINUED)

TABLE OF CONTENTS (CONTINUED)

LIST OF FIGURES

LIST OF FIGURES (CONTINUED)

LIST OF FIGURES (CONTINUED)

LIST OF FIGURES (CONTINUED)

LIST OF TABLES

LIST OF TABLES (CONTINUED)

LIST OF PLATES

NUMBER **TITLE**

LIST OF ACRONYMS AND ABBREVIATIONS

General Acronyms and Abbreviations

3-D	Three dimensional
acre-ft	Acre-feet
acre-ft/yr	Acre-feet per year
AFFCR	Alkali Flat/Furnace Creek Ranch
amsl	Above mean sea level
bgs	Below ground surface
BLM	Bureau of Land Management
BWSD	Beatty Water and Sanitation District
CADD	Corrective action decision document
CAI	Corrective action investigation
CAIP	Corrective action investigation plan
CAP	Corrective action plan
CAS	Corrective action site
CAU	Corrective action unit
CDF	Cumulative density function
CR	Closure report
CV	Coefficient of variability
DEM	Digital elevation model
DGV	Moderately dense to dense grassland vegetation
DMV	Dense meadow and woodland vegetation
DoD	U.S. Department of Defense
DOE	U.S. Department Energy
DRI	Desert Research Institute
DWV	Dense wetland vegetation
ECDF	Empirical cumulative distribution function
EM	Environmental Management
EOI	Effective open interval
ET	Evapotranspiration
FFACO	*Federal Facility Agreement and Consent Order*
FGE	Forced-gradient experiment
ft	Foot

LIST OF ACRONYMS AND ABBREVIATIONS (CONTINUED)

ft/day	Feet per day
ft/yr	Feet per year
gal/min	Gallons per minute
GMWL	Global meteoric water line
HDD	Hydrologic data document
HFM	Hydrostratigraphic framework model
HGU	Hydrogeologic unit
HSU	Hydrostratigraphic unit
ID	Identification number
in./yr	Inches per year
ISPID	Integrated Sampling Plan Identifier
K	Hydraulic conductivity
kg/m^3	Kilograms per cubic meter
km	Kilometer
KPa	Kilopascal
K-S	Kolmogrov-Smirnov
kt	Kiloton
LANL	Los Alamos National Laboratory
LLNL	Lawrence Livermore National Laboratory
L/mg	Liters per milligram
LMWL	Local meteoric water line
m	Meter
m/day	Meters per day
m^2	Square meter
m^3	Cubic meter
m^3/day	Cubic meters per day
m^3/yr	Cubic meters per year
MBS	Moist bare soil
MCL	Maximum contaminant level
Mgal	Million gallon
mg/L	Milligrams per liter
mHSU	Modified hydrostratigraphic unit
mi	Mile

LIST OF ACRONYMS AND ABBREVIATIONS (CONTINUED)

M&O	Management and operating
mmol/L	Millimoles per liter
mm/yr	Millimeters per year
Mt	Megaton
MWAT	Multiple-well aquifer test
NA	Not applicable
NAD	North American Datum
NDEP	Nevada Division of Environmental Protection
NGRT	Noble gas recharge temperature
NNSS	Nevada National Security Site
NSMC	Null space Monte Carlo
NTS	Nevada Test Site
NTTR	Nevada Test and Training Range
NWIS	National Water Information System
OWB	Open water
pCi/L	Picocuries per liter
PER	Preemptive review
PEST	Parameter estimation
PM-OV	Pahute Mesa-OasisValley
PRISM	Parameter-Elevation Regressions on Independent Slopes Model
QA	Quality assurance
QAP	Quality assurance plan
QC	Quality control
R^2	Coefficient of determination
RMS	Root mean square
SAV	Submerged and sparse emergent aquatic vegetation
SDWA	*Safe Drinking Water Act*
SGV	Sparse to moderately dense grassland vegetation
SI	International System of Units
SNJV	Stoller-Navarro Joint Venture
Ss	Specific storage
Ss_f	Fracture specific storage
Ss_m	Matrix specific storage

LIST OF ACRONYMS AND ABBREVIATIONS (CONTINUED)

SSV	Sparse to moderately dense shrubland vegetation
SWNVF	Southwestern Nevada Volcanic Field
TM	Thermatic Mapper
UCL	Unclassified
UGTA	Underground Test Area
USAF	U.S. Air Force
USGS	U.S. Geological Survey
UTM	Universal Transverse Mercator
VPDB	Vienna Pee Dee Belemnite
VSMOW	Vienna Standard Mean Ocean Water
WIPP	Waste Isolation Project Plant
YF/CM	Yucca Flat/Climax Mine
YMP	Yucca Mountain Project
°C	Degrees Celsius
°F	Degree Fahrenheit
% meq/L	Percent milliequivalents per liter

Stratigraphic, Geologic, Hydrostratigraphic, and Hydrogeologic Unit Abbreviations and Symbols

Note: Stratigraphic and hydrostratigraphic unit assignments and respective symbols are complex. Refer to Plate 1 for additional stratigraphic and hydrostratigraphic unit descriptions and acronyms.

AA	Alluvial aquifer
ATCCU	Ammonia Tanks caldera confining unit
ATCU	Argillic tuff confining unit
ATICU	Ammonia Tanks intrusive confining unit
ATMLFA	Ammonia Tanks mafic lava-flow aquifer
ATWTA	Ammonia Tanks welded-tuff aquifer
BA	Benham aquifer
BMICU	Black Mountain intrusive confining unit
BFCU	Bullfrog confining unit
BRA	Belted Range aquifer
BWCU	Buttonhook Wash confining unit

LIST OF ACRONYMS AND ABBREVIATIONS (CONTINUED)

BWWTA	Buttonhook Wash welded-tuff aquifer
CA	Carbonate aquifer
CCICU	Claim Canyon intrusive confining unit
CCU	Clastic confining unit
CFCM	Crater Flat composite unit
CFCU	Crater Flat confining unit
CHICU	Calico Hills intrusive confining unit
CHLFA	Calico Hills lava-flow aquifer
CHLFA1	Calico Hills lava-flow aquifer 1
CHLFA2	Calico Hills lava-flow aquifer 2
CHLFA3	Calico Hills lava-flow aquifer 3
CHLFA4	Calico Hills lava-flow aquifer 4
CHLFA5	Calico Hills lava-flow aquifer 5
CHVTA	Calico Hills vitric-tuff aquifer
CHZCM	Calico Hills zeolitized composite unit
CPA	Comb Peak aquifer
DVA	Detached volcanic aquifer
DVCM	Detached volcanic composite unit
FCCM	Fortymile Canyon composite unit
FCCU	Fluorspar Canyon confining unit
FCLLFA	Fortymile Canyon lower lava-flow aquifer
FCULFA	Fortymile Canyon upper lava-flow aquifer
FCWTA	Fortymile Canyon welded-tuff aquifer
FCWTA1	Fortymile Canyon welded-tuff aquifer 1
GCU	Granite confining unit
IA	Inlet aquifer
ICU	Intrusive confining unit
IICU	Intracaldera intrusive confining unit
KA	Kearsarge aquifer
LCA	Lower carbonate aquifer
LCA3	Lower carbonate aquifer-thrust plate
LCCU	Lower clastic confining unit
LCCU1	Lower clastic confining unit - thrust plate

LIST OF ACRONYMS AND ABBREVIATIONS (CONTINUED)

LFA	Lava-flow aquifer
LPCU	Lower Paintbrush confining unit
LVTA2	Lower vitric-tuff aquifer 2
mCCU	Modified clastic confining unit
mCFCM	Modified Crater Flat composite unit
mCHLFA5	Modified Calico Hills lava-flow aquifer 5
mCHZCM	Modified Calico Hills zeolotic composite unit
mCPA	Modified Comb Peak aquifer
mFCCM1	Modified Fortymile Canyon composite unit 1
mFCCM2	Modified Fortymile Canyon composite unit 2
mFCCM3	Modified Fortymile Canyon composite unit 3
mFCCU	Modified Fluorspar Canyon confining unit
FCLMLFA	Fortymile Canyon lower mafic lava-flow aquifer
FCULFA1	Fortymile Canyon upper lava-flow aquifer 1
FCULFA2	Fortymile Canyon upper lava-flow aquifer 2
FCULFA3	Fortymile Canyon upper lava-flow aquifer 3
FCULFA4	Fortymile Canyon upper lava-flow aquifer 4
FCULFA5	Fortymile Canyon upper lava-flow aquifer 5
FCULFA6	Fortymile Canyon upper lava-flow aquifer 6
FCULFA7	Fortymile Canyon upper lava-flow aquifer 7
FCUMLFA	Fortymile Canyon upper mafic lava-flow aquifer
FCWTA	Fortymile Canyon welded-tuff aquifer
MGCU	Mesozoic granite confining unit
mLPCU	Modified Lower Paintbrush confining unit
MPCU	Middle Paintbrush confining unit
mRMWTA1	Modified Rainier Mesa welded-tuff aquifer 1
mRMWTA2	Modified Rainier Mesa welded-tuff aquifer 2
mTCA	Modified Tiva Canyon aquifer
mTSA	Modified Topopah Spring aquifer
mUPCU	Modified Upper Paintbrush confining unit
PBPCU	Post-Benham Paintbrush confining unit
PBRCM	Pre-Belted Range composite unit
PCM	Paintbrush composite unit

LIST OF ACRONYMS AND ABBREVIATIONS (CONTINUED)

PLFA	Paintbrush lava-flow aquifer
PMNICU	Pahute Mesa Northern Extension intrusive confining unit
PVFA	Paintbrush vitric-flow aquifer
RMICU	Rainier Mesa intrusive confining unit
RMWTA	Rainier Mesa welded-tuff aquifer
RVICU	Redrock Valley intrusive confining unit
SCCC	Silent Canyon Caldera Complex
SCICU	Silent Canyon intrusive confining unit
SPA	Scrugham Peak aquifer
SWA	Stockade Wash aquifer
TCA	Tiva Canyon aquifer
TCFZ	Thirsty Canyon Fault Zone
TCL	Thirsty Canyon Lineament
TCU	Tuff confining unit
TCVA	Thirsty Canyon volcanic aquifer
THCM	Tannenbaum Hill composite unit
THCU	Tannenbaum Hill confining unit
THLFA	Tannenbaum Hill lava-flow aquifer
TMA	Timber Mountain aquifer
TMCC	Timber Mountain caldera complex
TMCM	Timber Mountain composite unit
TMLVTA	Timber Mountain lower vitric-tuff aquifer
TMUWTA	Timber Mountain upper welded-tuff aquifer
TMWTA	Timber Mountain welded-tuff aquifer
TSA	Topopah Spring aquifer
UCCU	Upper clastic confining unit
UPCU	Upper Paintbrush confining unit
VTA	Vitric-tuff aquifer
WTA	Welded-tuff aquifer
WWA	Windy Wash aquifer
YMCFCM	Yucca Mountain Crater Flat composite unit
YVCM	Younger volcanic composite unit

LIST OF ACRONYMS AND ABBREVIATIONS (CONTINUED)

Symbols for Elements and Compounds

Ar	Argon
Br	Bromide
C	Carbon
Ca	Calcium
Cl	Chloride
CO_2	Carbon dioxide
Cs	Cesium
DIC	Dissolved inorganic carbon
F	Fluoride
^{3}H	Tritium
$^{3}He/^{4}He$	Helium-3/helium-4
HCO_3	Bicarbonate
He	Helium
I	Iodide
K	Potassium
Kr	Krypton
Mg	Magnesium
Na	Sodium
Ne	Neon
pmc	Percent modern carbon
Pu	Plutonium
SO_4	Sulfate
Sr	Strontium
Tc	Technetium
Xe	Xenon
$\delta^{2}H$	Delta deuterium
$\delta^{13}C$	Delta carbon-13
$\delta^{18}O$	Delta oxygen-18
$\delta^{34}S$	Delta sulfur-34

1.0 INTRODUCTION

This hydrologic data document (HDD) has been prepared for Corrective Action Units (CAUs) 101 and 102, Central and Western Pahute Mesa, in order to support the development of a groundwater flow and contaminant transport model. Central and Western Pahute Mesa are two of the five CAUs on the Nevada National Security Site (NNSS) (formerly the Nevada Test Site [NTS]) used for underground nuclear testing (Figure 1-1). The nuclear tests resulted in groundwater contamination in the vicinity of the underground test areas. As a result, the U.S. Department of Energy (DOE), Environmental Management (EM) Nevada Program is currently conducting a corrective action investigation (CAI) of the Pahute Mesa underground test areas. This work is a part of the Underground Test Area (UGTA) Activity in accordance with the *Federal Facility Agreement and Consent Order* (FFACO) (1996, as amended).

The CAU groundwater flow and transport model is composed of two pieces, a flow model and a transport model, that together provide the contaminant boundary forecasts required by the FFACO. The hydrologic data necessary for the flow model portion of the CAU model are presented in this report. The transport data necessary for the transport model portion of the CAU model will be provided in a separate report.

This report is a revision to the HDD first published in 2004 (SNJV, 2004a). A considerable amount of characterization activities including well drilling, development, testing, multiple-well aquifer testing, sampling, and analysis has taken place since 2004, resulting in a large body of published work that became available since 2004. This revision to the HDD incorporates the results of these additional characterization activities.

This section provides a brief summary of the UGTA Activity background, the history of the CAUs, a presentation of the purpose and scope of the work described in this document, and quality assurance (QA) activities, followed by an outline of this document's contents.

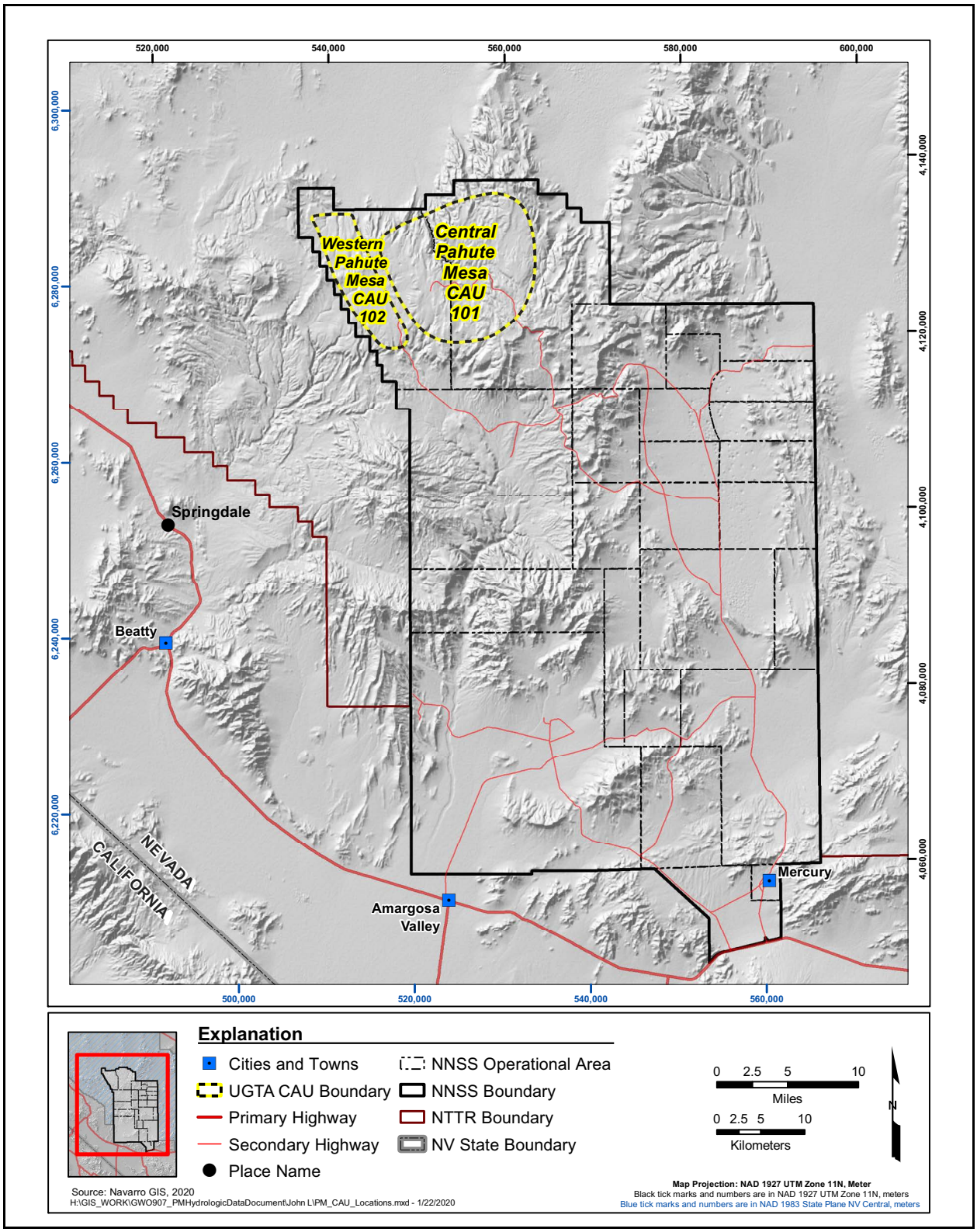

Figure 1-1
Location of the Pahute Mesa CAUs

1.1 Background

A brief overview of the UGTA Activity and site history are presented in the following subsections.

1.1.1 UGTA Activity Background

Between 1951 and 1992, DOE and the U.S. Department of Defense (DoD) conducted underground nuclear testing at the NTS (now the NNSS). To ensure protection of the public and the environment from the radiological contamination resulting from these tests, the FFACO (1996, as amended) established a regulatory process to identify sites of potential historical contamination and to implement proposed corrective actions. "UGTA" was the name given to the CAUs representing the underground nuclear testing locations. The FFACO identified a strategy (FFACO, Appendix VI, Section 3.0) to address the UGTA contaminated sites. The UGTA Activity is managed by EM Nevada Program.

Since 1996, the Nevada Division of Environmental Protection (NDEP) has regulated DOE's corrective actions through the FFACO (1996, as amended). The individual locations covered by the agreement are known as corrective action sites (CASs), and they are grouped into CAUs. The UGTA CAUs are Frenchman Flat, Central Pahute Mesa, Western Pahute Mesa, Yucca Flat/Climax Mine (YF/CM), and Rainier Mesa/Shoshone Mountain. Central Pahute Mesa (CAU 101) and Western Pahute Mesa (CAU 102), shown in (Figure 1-1), and together referred to as "Pahute Mesa," are addressed together due to their adjacent locations and common groundwater regimen as well as similarities in testing practices, geology, and hydrology. Given the adjacent locations of CAUs 101 and 102 and commonality between them, a single groundwater flow and transport model will be developed that encompasses both CAUs. In this report, all references to this model will be to the CAU model without inclusion of the distinction that the model represents both CAUs 101 and 102.

The FFACO UGTA strategy is implemented through a four-stage approach that comprises the following: (1) Corrective Action Investigation Plan (CAIP), (2) Corrective Action Investigation (CAI), (3) Corrective Action Decision Document (CADD)/Corrective Action Plan (CAP), and (4) Closure Report (CR) and long-term monitoring. There are multiple decision points within this strategy that require NDEP concurrence before the project can proceed to the next step. Currently, the Pahute Mesa CAUs are in the second stage, the CAI stage.

In accordance with this strategy, a CAIP was developed for the Pahute Mesa CAUs. Upon getting NDEP approval in 1999 (DOE/NV, 1999), the project proceeded to the CAI stage with data evaluation, collection, and analysis, documented in reports, that would be required to support a CAU flow and transport model. The development of a CAU groundwater flow and transport model is a major step in the CAI stage of the FFACO UGTA strategy. A flow and transport model was developed and presented to DOE and NDEP for review and approval as required by the UGTA strategy (SNJV, 2006, 2007, and 2009b). Based on the internal reviews, NDEP decided that the model was not yet acceptable for CADD/CAP studies; however, the primary FFACO UGTA strategy was achievable for the Pahute Mesa CAUs. Hence, a Phase II of the CAI activities was begun in 2009 with the development of a Phase II CAIP (NNSA/NFO, 2014), first published in 2009. A considerable amount of characterization activities have been conducted since 2004 including well drilling, development, testing, multiple-well aquifer testing, sampling, and analysis; resulting in a large body of published work that became available since 2004 (these documents are referenced in later sections where information from them is used).

The FFACO describes a four-component approach for achieving the primary objective of the UGTA strategy, which is to define perimeter boundaries for each CAU over the next 1,000 years (FFACO, 1996 as modified). These four components are (1) data collection, (2) modeling, (3) iterative model evaluation and monitoring, and (4) land use policies. As formally defined in the FFACO, a contaminant boundary is a probabilistic model-forecast perimeter and a lower hydrostratigraphic unit (HSU) boundary that delineates the extent of radionuclide-contaminated groundwater from underground testing over 1,000 years. Simulation modeling of contaminant transport is to be used to forecast the location of contaminant boundaries within 1,000 years and must show the 95th percentile of the model results (boundary outside of which only 5 percent of the simulations exceed the *Safe Drinking Water Act* [SDWA] standards). Thus flow and transport modeling to forecast areas of current and future contamination for 1,000 years forms an essential part of the UGTA strategy.

1.1.2 Pahute Mesa Background

Brief overviews of the operational history and work conducted to date are presented in this subsection.

Pahute Mesa was used as an underground nuclear testing area of the NTS (now the NNSS) for 27 years, from 1965 to 1992 (NNSA/NFO, 2015b). A total of 85 nuclear tests were conducted at Pahute Mesa. Three of these tests (SCHOONER, PALANQUIN, and CABRIOLET) were shallow and are not considered as a part of the UGTA Activity. (Although these three corrective action sites are not assigned to UGTA as defined in the FFACO [1996, as amended], they will be included in the Pahute Mesa CAU model for completeness because of known contamination at Well PM-2 that likely came from SCHOONER.) Nuclear tests conducted at Pahute Mesa that are of interest to the UGTA Activity are those detonated in deep (from 225 meters [m] to 1,425 m depth below ground surface [bgs]) vertical shafts. A total of 82 such underground nuclear tests were conducted in Pahute Mesa; 37 of these were at or below the water table, and 45 were above the water table. The announced yield ranges for these tests are between 20 kilotons (kt) to more than 1 megaton (Mt). The 82 tests on Pahute Mesa produced 60.2 percent of the radiologic inventory for the entire NNSS site, based on curies (Finnegan et al., 2016). Media contaminated by the underground nuclear tests on Pahute Mesa are geologic formations within the unsaturated and saturated zones. Transport in groundwater is the primary mechanism of migration for the subsurface contamination away from the Pahute Mesa underground nuclear tests.

Major data collection activities completed since the initiation of Phase II work at Pahute Mesa are noted below. New data analysis activities are presented throughout the report.

- The Pahute Mesa Phase II CAIP for CAUs 101 and 102 (NNSA/NFO, 2014) was developed.
- New data have been collected and added to the datasets. Eleven wells have been installed and tested.
- Sixteen multiple-well aquifer tests (MWATs) were conducted on Pahute Mesa between 2009 and 2014 (Garcia et al., 2017).

1.2 Task Purpose and Scope

The purpose and scope of the analysis of hydrologic data for the Pahute Mesa CAUs are presented in the following subsections.

1.2.1 Purpose

The purpose of the tasks documented in this report was to analyze relevant information available for the hydrologic components of the groundwater flow system of Pahute Mesa and vicinity. The information will be used to develop the Pahute Mesa CAU flow model. Some of the information will be directly incorporated into the modeling. Other data may only be used indirectly, and some may be judged inappropriate for the modeling effort. For example, precipitation distributions that significantly exceed the groundwater basin discharges cannot be used without adjustment to balance the water budget (see Sections 6.0 and 7.0). Other information, such as hydraulic conductivity (see Section 5.0), will be calibrated during the modeling effort and will only be used to designate permissible ranges during the model calibration to observed water levels and measured transmissivities.

Specific task objectives were as follows:

- Compile available hydrologic data and supporting information that may be relevant to the Pahute Mesa CAI.
- Assess the level of quality of the data and associated documentation.
- Analyze the data to derive expected values or spatial distributions, and estimates of the associated uncertainty and variability.

1.2.2 Scope of Work

The scope of this task includes the assessment of data and information relevant to groundwater flow in the Pahute Mesa subsurface. The data and interpretations are derived from a variety of sources including historical documents, new data collected in wells drilled specifically for the purpose of characterization of the Pahute Mesa-Oasis Valley (PM-OV) flow system, and recent published reports, including the hydrostratigraphic framework model (HFM) document (DOE/EMNV, 2020).

Data types of interest include hydraulic properties (conductivity, specific storage), precipitation recharge, natural groundwater discharge, well discharge, hydraulic heads, and groundwater chemistry. Descriptions of these data types are provided in Section 4.0.

The previous version of this document (SNJV, 2004a) relied heavily on data analysis that included (1) literature searches, (2) data/information compilation, (3) data documentation, (4) data documentation qualification, (5) data quality evaluation, (6), and data assessment and interpretation activities. Since that time, many technical reports have been published and, where possible, these interpretations, many from peer-reviewed reports, are used directly in this report.

The area of investigation is defined by the PM-OV groundwater basin. As described in the update to the CAIP (DOE/EMNV, 2020b) (Figure 1-2), it encompasses the Pahute Mesa CAUs and areas located downgradient that may be impacted by these CAUs. The PM-OV groundwater basin is generally considered to be closed in that total discharge in Oasis Valley is balanced by recharge within the PM-OV groundwater basin. As such, the boundary of the PM-OV groundwater basin is considered a no-flow boundary. The southeast boundary of the basin is the boundary between the Pahute Mesa and Rainier Mesa flow systems. From this conceptual model, all the radionuclides in the groundwater of Pahute Mesa will move toward the discharge area in Oasis Valley. The Pahute Mesa CAU flow and transport model area will encompass the entire PM-OV groundwater basin (Figure 1-2) to ensure that intra-groundwater basin influences on the groundwater flow system are included. This area more than includes the northwestern portion of the NNSS and adjacent lands to the west, south, and north managed by the U.S. Air Force (USAF) and the Bureau of Land Management (BLM). The groundwater flow model area is the same as the PM-OV area (Figure 1-2), which is contained within the PM-OV HFM domain.

Even though the area of interest is limited to the PM-OV area, information considered to be relevant to this task may be obtained from other nearby sites. Nearby sites include other underground test areas, the Yucca Mountain site, and other sites located within the NNSS region. The justification for the transfer of data from other sites is documented in Appendix B.

1.3 Quality Assurance

QA measures consistent with the UGTA Activity Quality Assurance Plan (QAP) (NNSA/NFO, 2015a; DOE/EMNV, 2018b) have been taken to control quality during the performance of all UGTA data analysis tasks. These measures include data documentation qualification, data quality assessment, checking procedures, software QA, use of standard methodologies, technical and peer reviews, and corroboration through models.

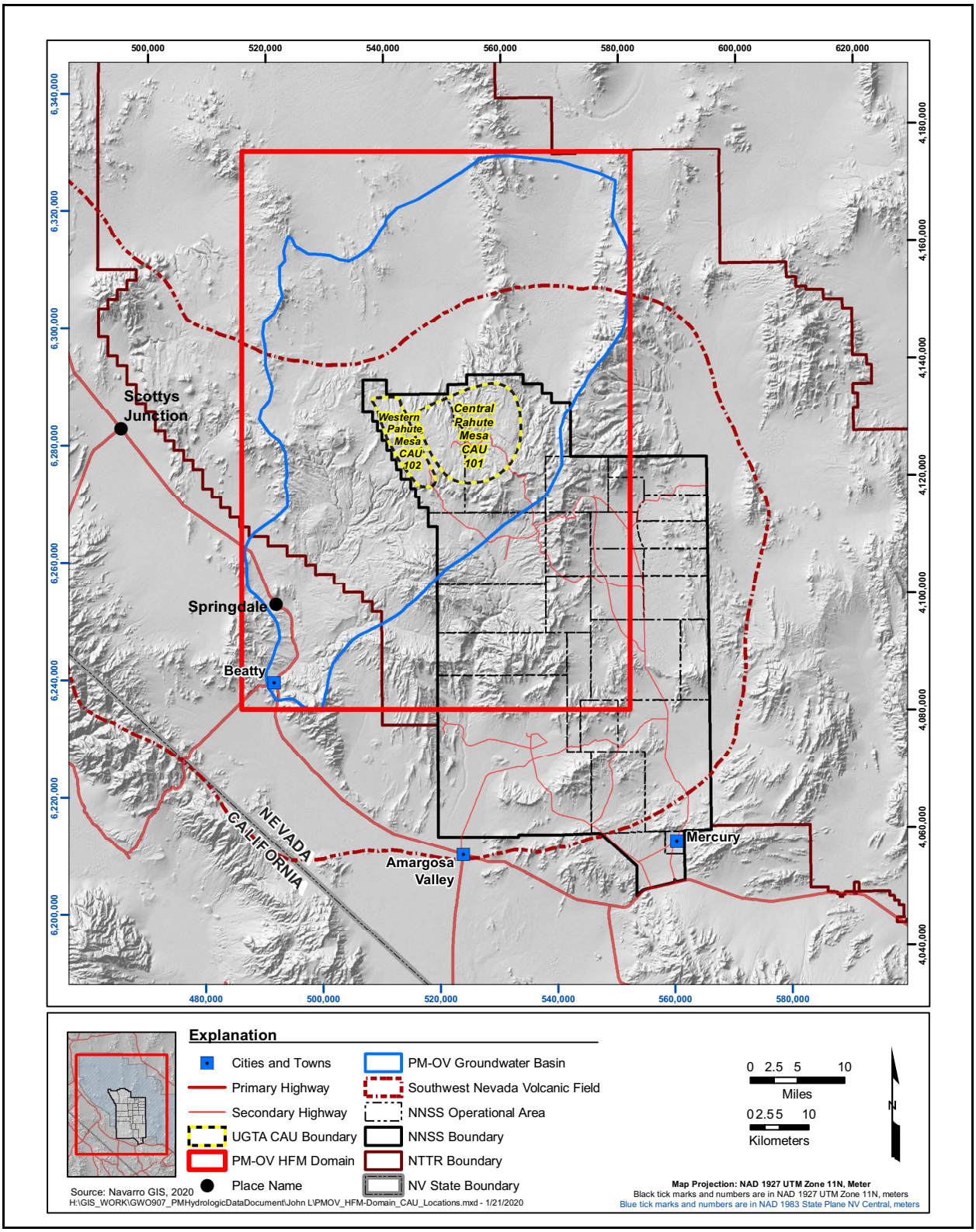

Figure 1-2
Investigation Areas and the PM-OV HFM for the Pahute Mesa CAUs
Sources: DOE/NV, 1999; Navarro, 2019a

Data Quality Assessment

In accordance with the UGTA QAP (NNSA/NFO, 2015a; DOE/EMNV, 2018b), the processes for the management, control, and transfer of data must include verification of transcription and data transfer; and assurance that data used in reports, analyses, models, and interpretive works are traceable to their source, and data manipulations are checked.

Checking Procedures

Various checking procedures were designed for quality control (QC) purposes. Checking procedures applicable to the UGTA data analysis include those developed for transcription of data, generation of figures, tables and logs, and performance of calculations. Data compiled by project personnel are subjected to the checking procedures before inclusion in the appropriate dataset. Much of the available data are composed of data gathered and compiled by agencies external to the UGTA Activity. Data from other organizations are obtained following their organization policies and procedures that are UGTA QAP compliant.

Standard Methodologies

To the extent possible, standard and widely accepted methodologies should be used in the development of the interpretive products. The various methodologies used are too numerous to list here; however, they are described and referenced in the sections of this document that discuss their use in the data analysis process.

Technical and Peer Reviews

The review process constitutes an important measure of product quality and is used throughout the performance of the data analysis activities. The review process may include internal and external technical reviews. Internal reviews are performed by individuals who are subject matter experts within the UGTA Activity. External reviews may be conducted as directed by DOE.

1.4 Document Organization

This document consists of 12 sections and 3 appendices:

- Section 1.0 provides a description of the project background, the purpose and scope of this data analysis task, QA and QC considerations, and a description of the documentation of the CAU model.
- Section 2.0 describes the regional setting and local hydrostratigraphic framework of the PM-OV area. These descriptions are presented to support the analysis of the hydrologic data presented in this document.
- Section 3.0 provides a brief overview of the modeling approach proposed for the Pahute Mesa CAUs and a more detailed description of the approach used to simulate groundwater flow.
- Section 4.0 presents the approach used to assess the available hydrologic data.
- Section 5.0 describes the compilation and analysis of hydraulic conductivity and specific storage data.
- Section 6.0 describes the compilation and analysis of the available precipitation recharge data.
- Section 7.0 describes the compilation and analysis of the available surface discharge data.
- Section 8.0 describes the compilation and analysis of water-level data to derive hydraulic heads.
- Section 9.0 describes the evaluation of existing stress response data from MWATs for use in the Pahute Mesa CAU flow model.
- Section 10.0 describes the lateral boundary fluxes for the Pahute Mesa CAU flow model.
- Section 11.0 describes the compilation and analysis of groundwater chemistry data.
- Section 12.0 provides a list of references used in the document.
- Appendix A contains information in support of the hydrostratigraphic model layers and stratigraphy described in Section 2.0.
- Appendix B contains a justification of the use of non-direct datasets for developing parameter distributions for the Pahute Mesa modeling effort.
- Appendix C contains a description of the hydraulic head dataset used in the Pahute Mesa modeling effort.
- Appendix D contains responses to NDEP comments on the draft version of this document.

2.0 REGIONAL SETTING AND LOCAL HYDROSTRATIGRAPHIC FRAMEWORK

Selected components of the PM-OV HFM are summarized in this section to support the hydrologic data assessment presented in this report. Components described include the regional setting and local hydrostratigraphic framework.

2.1 Regional Setting

The PM-OV groundwater basin, which coincides with the boundaries of the Pahute Mesa CAU model and is contained within the PM-OV HFM, as defined in Fenelon et al. (2016) (Figure 2-1), is part of the Death Valley regional groundwater flow system. A conceptual model of the PM-OV groundwater flow system of the NNSS was developed during the regional evaluation (DOE/NV, 1997), and the area was modified and enlarged in subsequent investigations (BN, 2002; Fenelon et al., 2016; Halford et al., 2000; DOE/EMNV, 2020b). Summary descriptions of the NNSS regional hydrogeologic framework and groundwater occurrence and movement are presented in the following subsections.

2.1.1 Regional Hydrogeologic Framework

The hydrogeologic framework used in the PM-OV HFM is based on the conceptual hydrologic system established for the NNSS area by Winograd and Thordarson (1975) and Blankennagel and Weir (1973). This early work was summarized and updated by Laczniak et al. (1996), the UGTA Phase I hydrostratigraphic regional modeling team (IT, 1996d), and the UGTA Phase II hydrostratigraphic framework modeling team (NSTec, 2014). The PM-OV HFM report (DOE/EMNV, 2020a) supersedes previous draft (NSTec, 2014) and published Pahute Mesa HFM reports. The PM-OV HFM contains the relevant details, summary discussion, and supporting information regarding the history and development of the HFM.

The rocks of the NNSS have been classified using a two-level classification scheme, in which hydrogeologic units (HGUs) are grouped to form HSUs (Prothro, 2009a; DOE/EMNV, 2020a). The HGUs are used to categorize rocks according to their ability to transmit groundwater, which is mainly a function of the rocks' primary lithologic properties, degree of fracturing, and secondary mineral

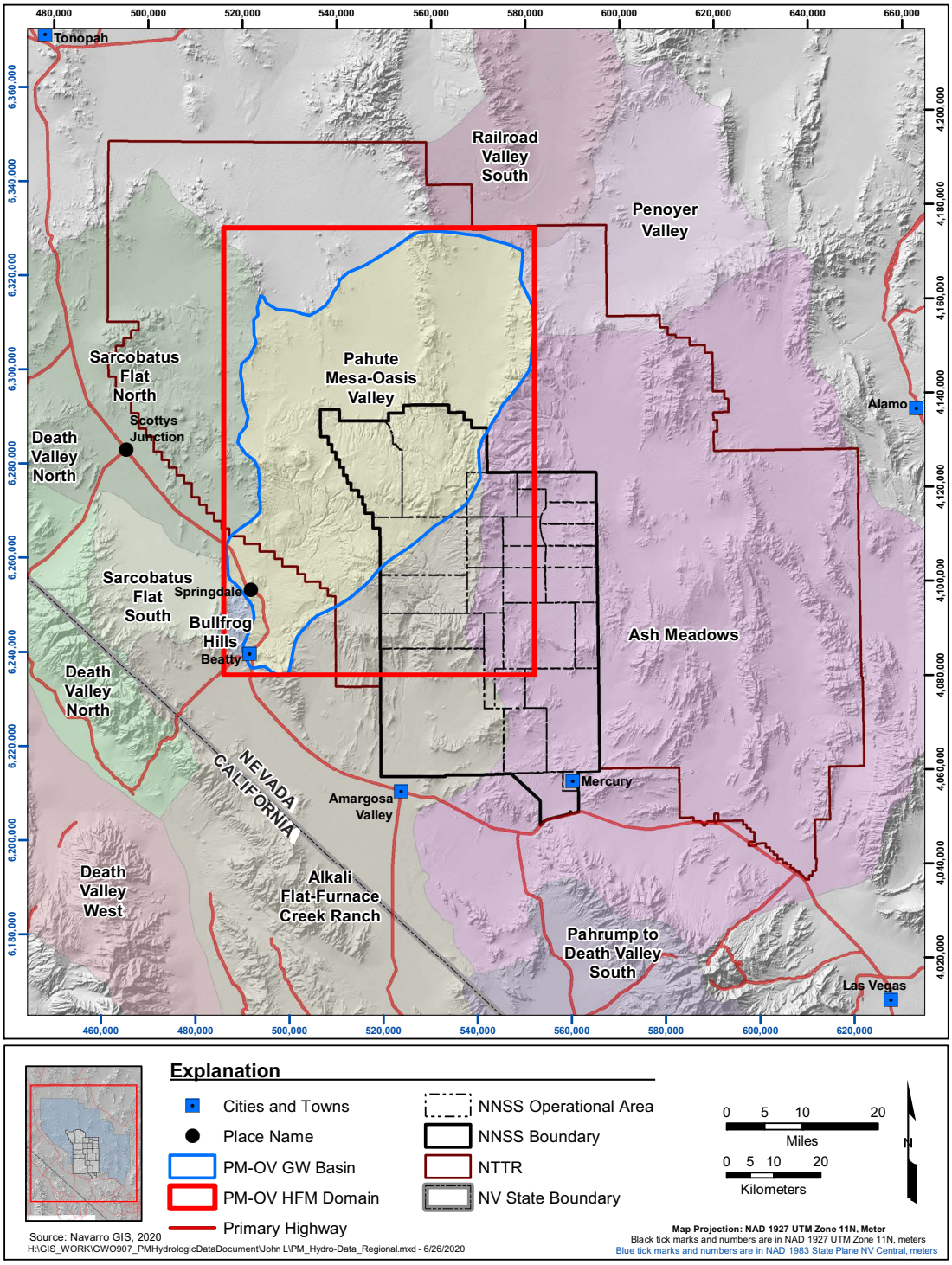

Figure 2-1
Features of the PM-OV HFM Groundwater Flow System Region

alteration. The complex hydrologic properties of the volcanic rocks of the NNSS and vicinity are best addressed in terms of HGUs (Blankennagel and Weir, 1973; Winograd and Thordarson, 1975). The concept of HSUs that are made up of groups of similar HGUs is also very useful in volcanic terrains because stratigraphic units can differ greatly in hydrologic character, both laterally and vertically. The HSUs serve as "layers" in the PM-OV area and NNSS CAU-scale HFMs. Further discussion and explanation of HGUs and HSUs are found in Sections 2.1.1.1 and 2.1.1.3.

The Pahute Mesa Phase II HFM was expanded to include the entire PM-OV groundwater basin area, as defined in Fenelon et al. (2016). The additional area to the north, south, east, and west significantly increasing the size of the model domain. This new model domain is the basis for the PM-OV HFM and fully incorporates the Pahute Mesa Phase II HFM. This additional area resulted in an increase in the number of structural elements (i.e., faults and caldera margins) and HSUs in the PM-OV HFM. Surface mapping, geophysics, and limited borehole information provide the majority of data in the new areas. The lower data density (e.g., fewer boreholes and lower resolution geophysics) of the northern extension results in a lower resolution of the modeled HSU distribution in this area. However, given the minimal amount of recharge and the presence of confining and composite units under the depositional basins in the northern extension (i.e., Gold Flat and Kawich Valley), there is only a minimal impact regarding geologic uncertainty.

The following subsections summarize the components that make up the PM-OV HFM, addressing HGUs, stratigraphy, HSUs, and structural features, respectively.

2.1.1.1 Hydrogeologic Units

The rocks of the NNSS and UGTA CAUs have been classified in terms of one of nine HGUs, which are the alluvial aquifer (AA), four volcanic HGUs, two intrusive HGUs, and two HGUs that represent the pre-Tertiary rocks (Table 2-1). Additionally, Table 2-2 provides a definition and brief description of significant hydrologic properties of each HGU. Section 5.0 provides a description of hydraulic parameter data reviewed and included in this document. Section 4.0 of the PM-OV HFM report (DOE/EMNV, 2020a) provides additional detailed discussion of the HGUs present in the model.

Alluvial HGU

The deposits of alluvium (AA) fill the main depositional basins of the NNSS, and generally consist of an unconsolidated to partially consolidated mixture of boulders, gravel, sand, silt, and clay derived

Table 2-1
Summary of Hydrologic Properties for HGUs at the NNSS Used in the PM-OV HFM

HGU [a]			Fracture Density [b,c]	Relative Hydraulic Conductivity [c]
Alluvial aquifer (AA)			Very Low	Moderate to Very High
Vitric-tuff aquifer (VTA)			Low	Low to Moderate
Welded-tuff aquifer (WTA)			Moderate to High	Moderate to Very High
Lava-flow aquifer (LFA) [d]	Pumiceous lava	Vitric	Low	Low to Moderate
		Zeolitic	Low	Very Low
	Stoney lava and vitrophyre		Moderate to High	Moderate to Very High
	Flow breccia		Low to Moderate	Low to Moderate
Tuff confining unit (TCU)			Low	Very Low to High
Intracaldera intrusive confining unit (IICU)			Low to Moderate	Very Low
Granite confining unit (GCU)			Low to Moderate	Very Low
Carbonate aquifer (CA)			Low to High (Variable)	Low to Very High
Clastic confining unit (CCU)			Moderate	Very Low to Low [e]

[a] See Table 2-2 for hydrogeologic nomenclature.
[b] Including primary (cooling joints in tuffs) and secondary (tectonic) fractures.
[c] The values presented are qualitative estimates based on data from published (IT, 1996b; Blankennagel and Weir, 1973; and Winograd and Thordarson, 1975) and unpublished sources (i.e., numerous UGTA, LANL, and LLNL drill-hole characterization reports).
[d] Abstracted from Prothro and Drellack (1997).
[e] Fractures tend to be sealed by the presence of secondary minerals.

LANL = Los Alamos National Laboratory
LLNL = Lawrence Livermore National Laboratory

from volcanic and Paleozoic sedimentary rocks (Slate et al., 1999). Overall, the alluvium is typically thin and unsaturated over much of the PM-OV HFM. Only in the deeper depositional basins (e.g., Gold Flat, Kawich Valley, and Oasis Valley) is the alluvium thicker and saturated below the water table.

Volcanic HGUs

The volcanic rocks within the study area can be categorized into four HGUs based on primary lithologic properties, degree of fracturing, and secondary mineral alteration. The HGUs are VTAs (e.g., nonwelded, bedded, and reworked); TCUs (zeolitic and/or argillic altered volcanic rocks); WTAs (welded vitric to devitrified ash-flows); and LFAs. These HGUs host some, if not most, of the important flow paths for the PM-OV HFM.

Table 2-2
HGUs of the PM-OV HFM

HGU	Typical Lithologies	Hydrologic Significance
Alluvial aquifer (AA)[a]	Unconsolidated to partially consolidated gravelly sand, eolian sand, and colluvium; thin, basalt flows of limited extent	Has characteristics of a highly conductive aquifer, but less so where lenses of clay-rich paleocolluvium or playa deposits are present.
Vitric-tuff aquifer (VTA)	Bedded tuff; ash-fall and reworked tuff; vitric	Constitutes a volumetrically minor HGU. Generally does not extend far below the static water level due to tendency to become zeolitized under saturated conditions. Significant interstitial porosity (20 to 40 percent) and matrix permeability. Typically insignificant fracture permeability.
Welded-tuff aquifer (WTA)	Welded ash-flow tuff; vitric to devitrified	Degree of welding greatly affects interstitial porosity (less porosity as degree of welding increases) and permeability (greater fracture permeability as degree of welding increases).
Lava-flow aquifer (LFA)	Rhyolite lava flows; includes flow breccias (commonly at base) and pumiceous zones (commonly at top)	Generally, a caldera-filling unit (with exceptions; i.e., ER-20-12). Hydrologically complex; wide range of transmissivities; fracture density and interstitial porosity differ with lithologic variations.
Tuff confining unit (TCU)	Zeolitized bedded tuff with interbedded, but less significant, zeolitized, nonwelded to partially welded ash-flow tuff	May be saturated but measured transmissivities are very low. May cause accumulation of perched and/or semi-perched water in overlying units. Where fractured TCU may have higher hydraulic conductivity.
Intracaldera intrusive confining unit (IICU)	Highly altered, highly injected/intruded country rock and granitic material	Assumed to be impermeable. Conceptually underlies each of the Southwestern Nevada Volcanic Field (SWNVF) calderas and Calico Hills. Developed for this study to designate basement beneath calderas as different from basement outside calderas.
Granite confining unit (GCU)	Granodiorite, quartz monzonite	Relatively impermeable; forms local bulbous stocks, north of Rainier Mesa and Yucca Flat; may contain perched water.
Carbonate aquifer (CA)	Dolomite, limestone	Transmissivity values differ greatly and are directly dependent on fracture frequency.
Clastic confining unit (CCU)	Argillite, siltstone, quartzite	Clay-rich rocks are relatively impermeable; more siliceous rocks are fractured, but with fracture porosity generally sealed due to secondary mineralization.

[a] AA is also an HSU in the PM-OV HFM.

VTA, nonwelded and bedded, rocks are primarily found above the water table and have only limited extent in the PM-OV HFM below the water table. VTA HGUs are typically dominated by matrix permeability and porosity and do not usually support extensive fracture systems. Vitric tuffs (i.e., nonwelded and bedded) are frequently altered to zeolites and clays, in part based on extended exposure to saturated conditions, relatively high, matrix porosity, permeability, and the reactive

nature of the vitric (volcanic glass) material itself. The formation of zeolites and clays significantly reduces the permeability of the rock.

TCUs are altered volcanic rocks (i.e., zeolitic or argillically altered) that act as confining units. Zeolitic and argillic alteration affects the volcanic glass material. Common zeolitic minerals include clinoptilolite and mordenite. As alteration progresses, matrix porosity typically remains similar to the unaltered rock while the matrix permeability is significantly reduced. The reduction of permeability occurs due to the growth of zeolite and clay minerals in the pore space of the vitric rocks. However, because both zeolites and clays can store water within their respective structures, there is only a minor change in porosity. Zeolitic and argillic rocks do not typically support well-developed fracture systems. Where the TCUs occur at higher elevations (e.g., Pahute Mesa and Rainier Mesa) perched water zones may form on the top of the unit (Winograd et al., 1975; Fenelon et al., 2016; Jackson et al., 2018).

WTAs, such as welded ash-flow tuffs, are widely distributed within the HFM. These HGUs are typically devitrified (i.e., crystallized), but may be vitric and have minimal matrix porosity and permeability. However, they fracture more readily and are dominated by fracture permeability and porosity. These fractures consist of both thermal-related (i.e., cooling joints) and tectonic-related fractures. Overall, they have relatively high permeability (Blankennagel and Weir, 1973; Winograd and Thordarson, 1975; Laczniak et al., 1996; IT, 1996d; Prothro and Drellack, 1997). Welded ash-flow tuffs are typically widely distributed within and outside the source caldera.

LFAs, also may be devitrified (i.e., crystallized) or vitric. However, lava flows tend to have more erratic and localized distributions, and are typically found within the source caldera. LFAs are also dominated by fracture porosity and permeability. An LFA (Calico Hills lava-flow aquifer 5 [CHLFA5]) identified during drilling of Well ER-20-12 is a significant exception, to the norm of an LFA being located inside the caldera margins, and is located outside the known caldera boundaries.

Pre-Tertiary HGUs (Paleozoic and Precambrian)

The pre-Tertiary rocks beneath the study area are categorized as one of two HGUs based on primary lithologic properties, degree of fracturing, and secondary mineral alteration. The two HGUs are CCUs or CAs.

CCUs are composed of siliciclastic rocks (e.g., quartzites, siltstones, and shales) and typically are aquitards or confining units. Siliciclastic rocks may be fractured. However, these fractures are typically filled by secondary mineralization (e.g., calcite, silica). The siliciclastic confining units form the base of the PM-OV HFM (DOE/EMNV, 2020a).

CAs, limestone and dolomite rocks, tend to be aquifers (Winograd and Thordarson, 1975; Laczniak et al., 1996). The carbonate rocks that comprise the CA have a wide variation in their hydrologic properties. Matrix permeability and porosity is typically low unless enhanced by fracturing or solution activities (e.g., fault or solution breccia) (Winograd et al., 1975).

Intrusive HGUs

The intrusive confining unit (ICU) category includes IICUs and the GCU. These rocks are relatively impermeable and are considered to behave as a confining unit. The IICUs conceptually underlie the calderas of the SWNVF, as well as other calderas in the PM-OV HFM. The GCU, which consists of Mesozoic age granitic stocks (i.e., granodiorite and quartz monzonite), is exposed to the north of Rainier Mesa and Yucca Flat areas of the model.

The distribution of these units in the subsurface is unknown. The Climax stock in extreme northern Yucca Flat (Houser et al., 1961; Walker, 1962; Maldonado, 1977) and the Gold Meadows stock in the extreme eastern part of the PM-OV model area (Snyder, 1977) may serve as analogs for the GCU.

2.1.1.2 Stratigraphic Units

An idealized stratigraphic section is shown in Figure 2-2 and has been grouped and subdivided, in part according to work and mapping completed at the NNSS and surrounding area over the past 50 years (e.g., Ekren et al., 1971; Slate et al., 1999; Warren, 2000a; Fridrich et al., 2007). Extensive mapping and multiple drill holes allow the detailed subdivision of these units over a significant portion of the area of interest.

Note that while many of the stratigraphic units are widely distributed, their various properties and characteristics (e.g., welding, thickness, porosity, permeability, alteration) may vary significantly with distance from their source. Section 4.0 of the PM-OV HFM report (DOE/EMNV, 2020a), in addition to the previously referenced reports, provides additional detail regarding stratigraphic units, their extent, and properties.

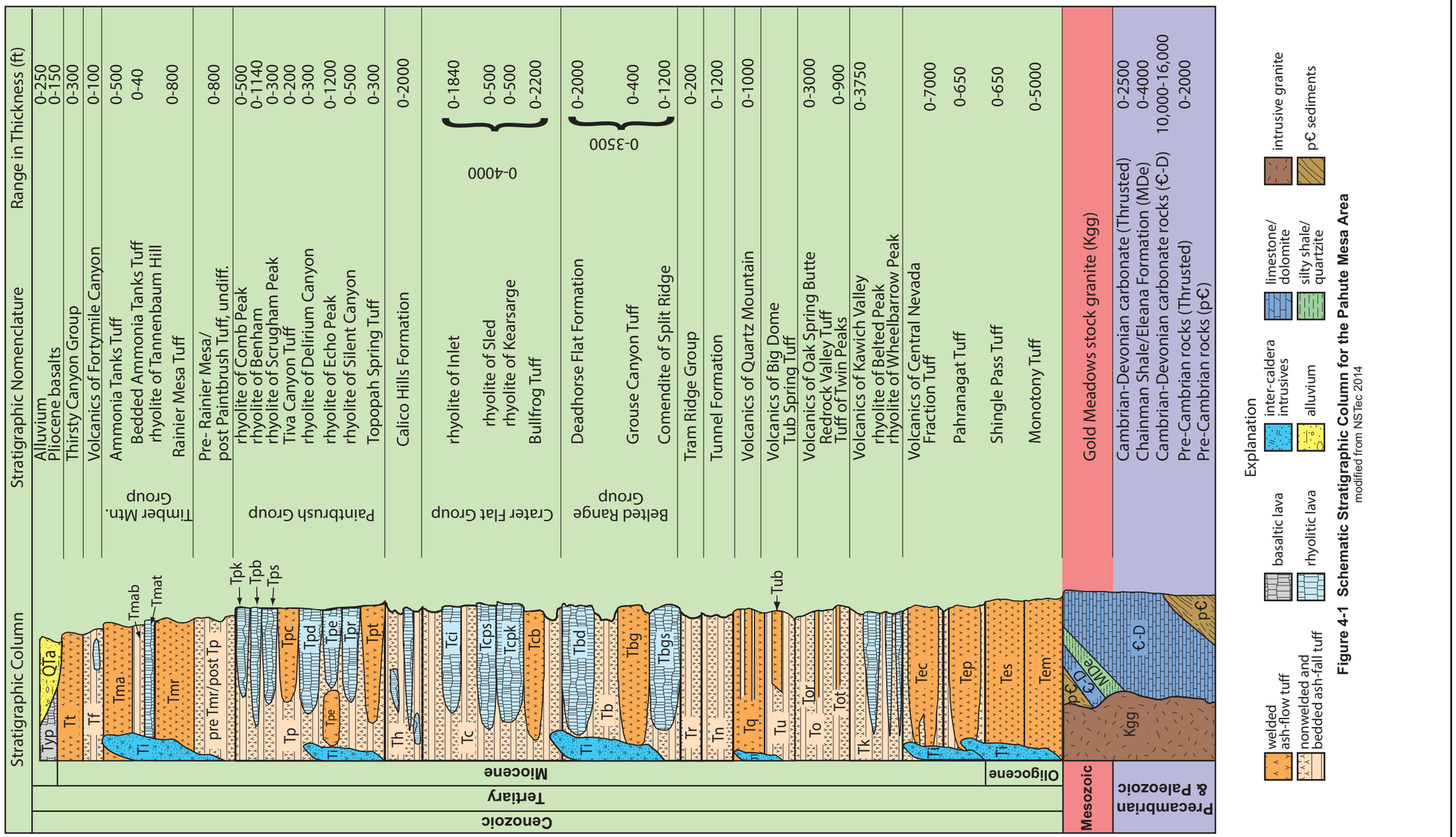

Figure 4-1 Schematic Stratigraphic Column for the Pahute Mesa Area
modified from NSTec 2014

Figure 2-2
Schematic Stratigraphic Column for the PM-OV HFM
Source: Modified from NSTec, 2014

2.1.1.2.1 Quaternary (Q)

The Quaternary units in the PM-OV HFM are principally alluvium, colluvium, and younger basalt flows. The alluvium consists of fine (clay/silt/sand) to coarse (gravel/cobble) material that is unconsolidated to partially consolidated and frequently exhibits some level of sorting, grading, and bedding.

Alluvial material has undergone some transport and sorting from its source area to the point of deposition. In some of the depositional basins (e.g., Gold Flat and Kawich Valley), fine-grained playa sediments, mostly silts and clays, have been deposited. These sediments inhibit downward infiltration of surface water, limiting recharge to the underlying groundwater system. Colluvium typically consists of relatively coarser and more angular material than alluvial sediments and has not been transported far from the parent source. Alluvium and colluvium are typically unsaturated except where they occur in deeper depositional basins (e.g., Gold Flat, Kawich Valley, and Oasis Valley) (DOE/EMNV, 2020a). Ekren et al. (1971) and Slate et al. (1999) have noted that the base of the Tertiary section is marked by the presence of coarse gravels, composed of Paleozoic material, which may or may not contain altered volcanics. This unit appears to be similar to the Paleocolluvium identified in Yucca Flat.

The basalt lava flows, vents, and cones in the model area are primarily Pliocene to Holocene in age and exhibit some level of permeability based on fracturing and other permeable zones (e.g., flow breccias and scorrias). However, most of these flows are above the water table and typically are unsaturated in the PM-OV HFM area (Slate et al., 1999).

2.1.1.2.2 Tertiary (T)

Tertiary units in the PM-OV HFM consist principally of igneous units with minor sediments. The volcanic rocks include pyroclastic rocks (i.e., ash-flows, ash-falls), lava flows, and small intrusive bodies.

Pyroclastic rocks are made up of a spectrum of welded to nonwelded ash-flows, nonwelded ash-falls, and bedded (including reworked) material. Porosity and permeability are controlled, in part, by degree of welding, alteration, and fracturing (initial thermo-mechanical and subsequent tectonic). As a general rule, the greater the degree of welding, the greater the fracturing and hence permeability and porosity. Conversely, the lesser the degree of welding and crystallization, the greater

the potential alteration (zeolitic or argillic) and the lower the fracture frequency and subsequent permeability and porosity.

Alteration, both zeolitic and argillic, principally occurs in vitric nonwelded, bedded, and reworked tuffs. These rocks have been saturated (i.e., below a paleo or current water table) for some duration. Alternatively, the rocks may have been affected by a hydrothermal system (e.g., Cactus Range, Gabbard Hills).

Zeolitic rocks (e.g., portions of the Paintbrush, Calico Hills, and Crater Flat Formations) typically have moderate to high porosity similar to when they were vitric. However, they have lower permeability. The reduction of permeability occurs due to the growth of zeolite and clay minerals in the pore space of the vitric rocks. However, because both zeolites and clays can store water within their respective structures, there is only a minor change in porosity.

A number of the pyroclastic (stratigraphic) units are of large volume and are widely distributed throughout the area of interest (e.g., Topopah Spring, Tiva Canyon, Rainier Mesa, and Ammonia Tanks) (DOE/EMNV, 2020a; Appendix C, Table C-1). These stratigraphic formations have been further subdivided based on rock properties (e.g., welding and crystallization) and comprise multiple HSUs. Many of the younger volcanics (e.g., Thirsty Canyon Group) have surface expression, and are above or down to just below the water table and are unsaturated to partially saturated. These younger units may have substantial vitric portions. Surface expressions of the nonwelded to reworked portions of these younger units may have been heavily dissected by geologic processes (e.g., erosion and faulting).

Lava flows, which were initially deposited on the surface and have been buried by subsequent lava or pyroclastic flows, have a more erratic and limited distribution compared to pyroclastic flows. They also show a marked zoning to their rock properties such as permeability and porosity. Much of the variability exhibited by lava flows is controlled by the thickness of the different zones within the flow and the subsequent alteration.

In a typical rhyolitic LFA (e.g., CHLFA 5), the outer zone is composed of pumiceous material that may be zeolitized and relatively impermeable. This is followed by one to three zones of densely welded vitric to crystallized lava that may be heavily fractured. Finally, a lower zone can be present that may also be zeolitized and impermeable (Prothro and Drellack, 1997). See Figure 2-3 for a

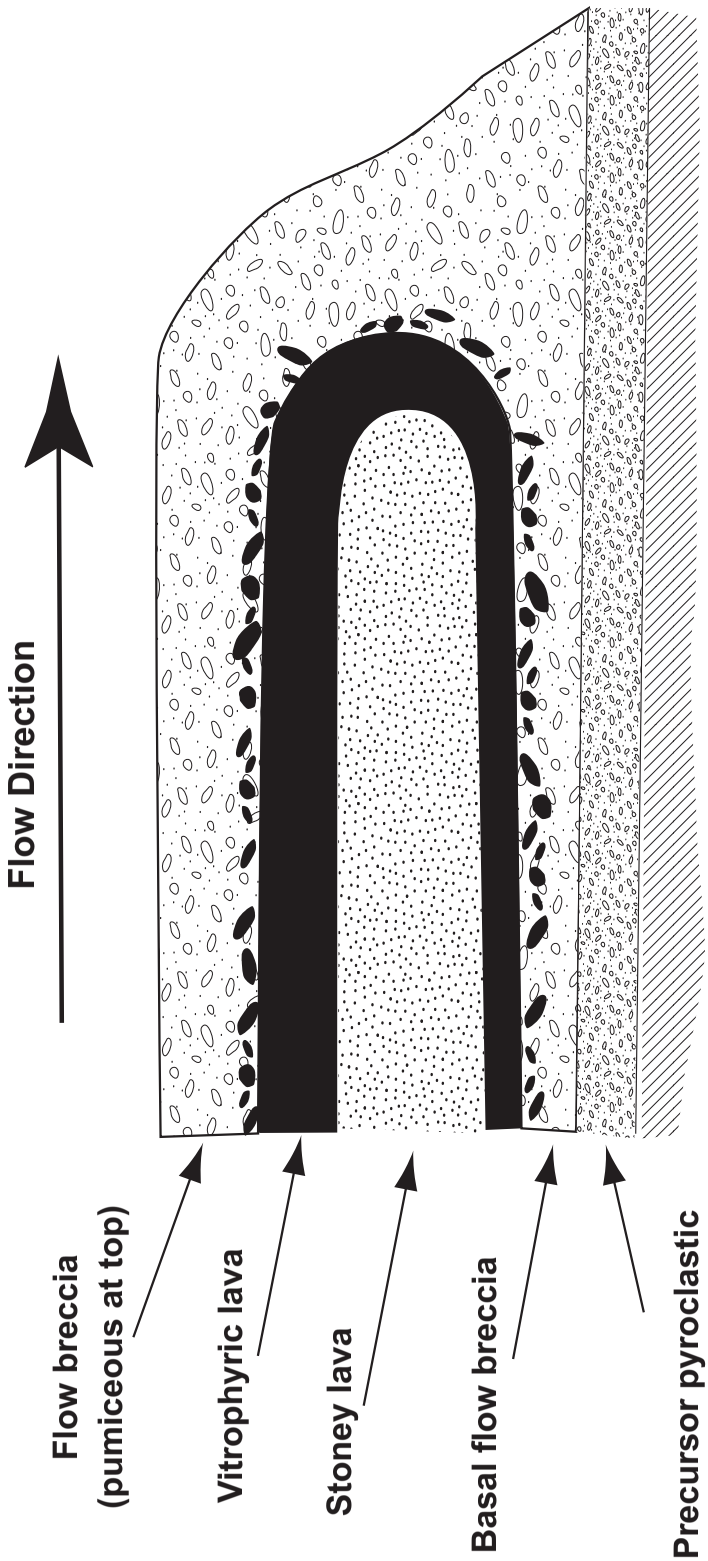

Figure 2-3
Schematic Section through a Rhyolitic Lava Flow
Source: Modified from Cas and Wright, 1987

schematic view of a rhyolitic lava flow. The PM-OV HFM report (DOE/EMNV, 2020a) provides a more detailed discussion of LFAs and their properties.

2.1.1.2.3 Mesozoic (Mz)

Cretaceous granitic (i.e., granodiorite and quartz monzonite) intrusive units (e.g., Gold Meadows Stock) are GCUs and make up the Mesozoic units present in the PM-OV HFM. These units are relatively impermeable and are treated as confining units. They are poorly exposed in the Rainier Mesa area. There are a number of other small intrusives exposed in the northern portion of the PM-OV HFM (DOE/EMNV, 2020a).

2.1.1.2.4 Precambrian and Paleozoic (Pz)

Paleozoic units are composed of a mixture of siliciclastic (e.g., quartzite, siltstone, and shales) units and carbonate sediments (e.g., limestone and dolomite). Siliciclastic units, CCUs, are typically confining units; and the carbonates, CAs, tend to behave as aquifers. Many of the carbonates exhibit low permeability and porosity unless subsequently enhanced by solution or tectonic activity. The Precambrian units in the area are composed predominantly of silicilastic sediments and meta-sediments with one known outcrop of crystalline basement material in the Trappman Hills on the western side of the PM-OV HFM.

2.1.1.3 Hydrostratigraphic Units

HSUs are groupings of contiguous stratigraphic units that have a particular hydrogeologic character, such as being either an aquifer (unit through which water moves readily) or a confining unit (a unit that generally is of relatively low permeability). An HSU may contain several HGUs. Definitions, from the PM-OV HFM report (DOE/EMNV, 2020a), for the 77 HSUs are provided in Table A-1 (see Appendix A), and a correlation chart with all CAUs on the NNSS is provided on Plate 1. HSUs are listed in approximate order from surface to basement.

The HSUs stratigraphic position is based on volcanic stratigraphy, lithologic properties related to depositional environment, post-depositional alteration, and degree of welding. Outside the caldera complexes, structural relationships depicted on hand-drawn cross sections, surface map data, and borehole lithostratigraphic logs were used to assist in determining the distribution of volcanic HSUs. The Warren et al. (2000b) block model was also used for additional guidance in this area. Volcanic

units within the caldera complex were mapped as horizontal layers because they typically have very low dips. The PM-OV HFM report (DOE/EMNV, 2020a) provides the rationale and detailed information regarding model parameters and stratigraphy.

Additionally, the dominant lithology of some units may change or pinch out laterally (e.g., LFA close to the source vents, WTA further away, and finally nonwelded TCU or VTA at distal edges). Another simplification addresses the caldera roots. In the PM-OV HFM area, the plutonic or hypabyssal igneous rocks that likely occur at depth below the calderas are modeled as ICUs, which are similar in their hydrologic properties to the GCU.

2.1.1.4 Structural Features of the PM-OV HFM

Geologic structural features are an important part of the hydrologic framework of the groundwater flow system of the PM-OV area. They define the geometric configuration of the flow domain, including the distribution, thickness, and orientation of rock units. The depositional patterns of many of the geologic units occurring in the area may have been strongly influenced by syn-volcanic structures, including caldera faults and some normal faults. Figure 2-4 provides an overview of some of the significant structures incorporated into the PM-OV HFM and their spatial relationship to discharge areas. Geologic structures on the NNSS, Nevada Test and Training Range (NTTR), and surrounding areas were identified on the basis of surface mapping (Ekren et al., 1971; Slate et al., 1999; Fridrich et al., 2007; Sweetkind and Drake, 2007; Prothro et al., 2009b), drilling activities, and geophysical data collection (Mankinen et al., 2003; Hildenbrand et al., 1999; Grauch et al., 1999; Ferguson et al., 1994; Warren et al., 2000b). Section 3.0 of the PM-OV HFM report (DOE/EMNV, 2020a) provides more detailed discussion and information.

The PM-OV HFM includes a total of 105 structural elements that are either faults or calderas. Faulting (e.g., caldera related, and Basin and Range), for example, may result in juxtaposition of units with different hydrologic properties or influence depositional thickness. Structures themselves may influence flow patterns by acting as conduits for flow or barriers to flow (Prothro et al., 2009b; DOE/EMNV, 2020a). For example, data collected during the drilling of Well ER-20-12 in 2015 indicate that the Ribbon Cliff Structural Zone has greater offset than previously suspected and may have enhanced the hydraulic connectivity to HSUs south of the zone (NNSA/NFO, 2016). Faults included in the PM-OV HFM were those with the greatest offset, through-going structures, or that seem to form significant structural/hydraulic boundaries.

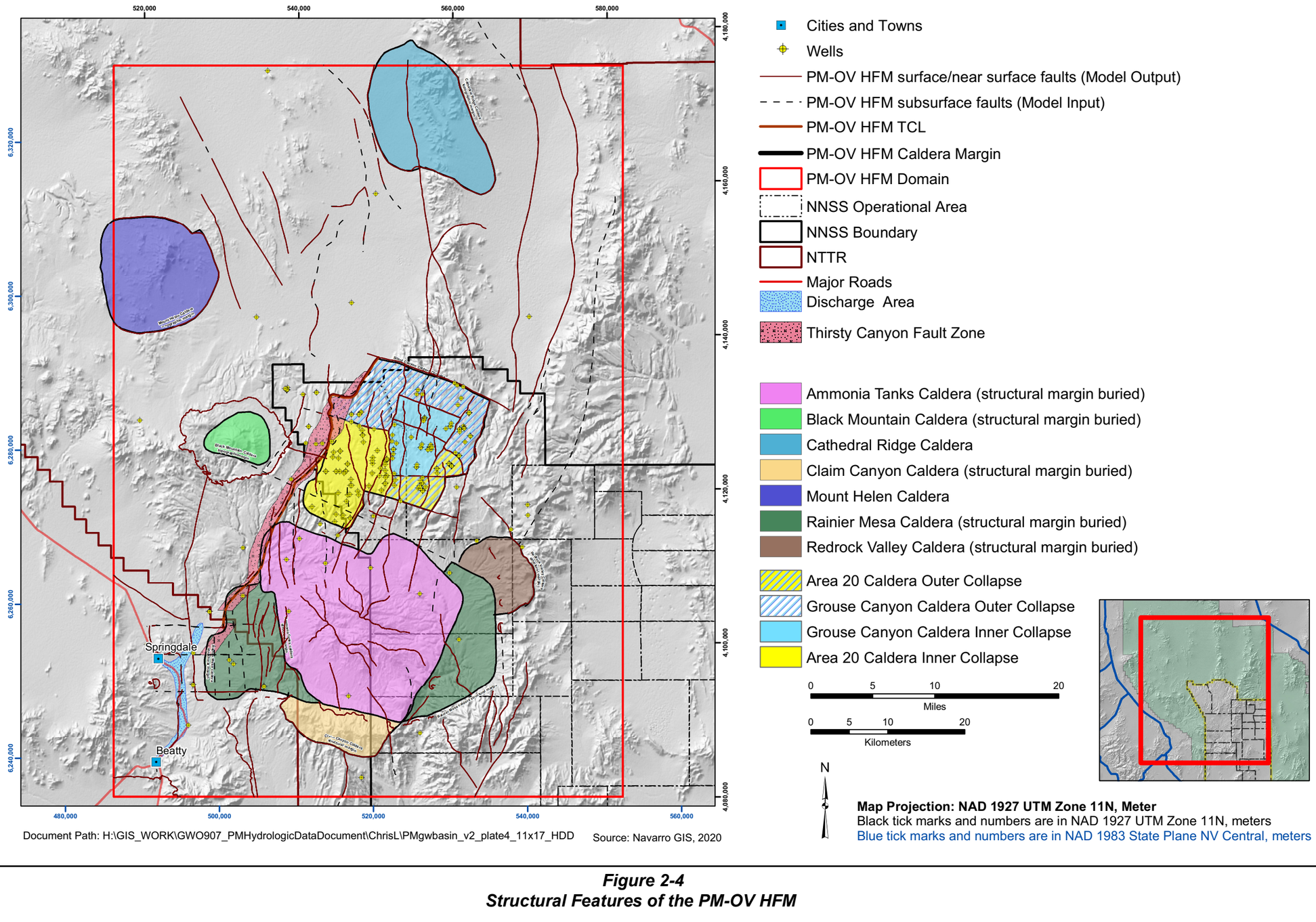

Figure 2-4
Structural Features of the PM-OV HFM

The Thirsty Canyon Lineament (TCL) (Mankinen et al., 1999; Grauch et al., 1999) and related Thirsty Canyon Fault Zone (TCFZ) (Hildenbrand et al., 1999; Mankinen et al., 2003) are important features of the PM-OV HFM (Navarro, 2019; DOE/EMNV, 2020a). Development of the TCL and the TCFZ concepts and subsequent incorporation into the PM-OV HFM are discussed in detail in Wurtz et al. (2018). The TCL is a north–northeast-trending, geophysically inferred feature that has been identified on regional gravity and aeromagnetic maps (Mankinen et al., 1999 and 2003).

The lineament extends from just west of Well ER-EC-8, north–eastward beneath western Pahute Mesa east of the Black Mountain caldera to the southern edge of Gold Flat. Hildenbrand et al. (1999) suggested that the TCL represents a fault zone, rather than a single structure, and that the fault zone is an older structure that may have influenced subsequent caldera activity. Geophysical and geologic profiles across the lineament by Mankinen et al. (1999 and 2003) indicate that the lineament is characterized by a zone of en echelon faults 2 to 3 kilometers (km) (1.2 to 1.9 miles [mi]) wide. Figure 2-5 provides views of the gravity data, interpreted cross sections (profiles), locations of cross sections (profiles), and stratigraphic information regarding units in the TCFZ.

Nine calderas have been included in the PM-OV HFM. These calderas reflect a variety of geometries and collapse processes. Caldera-collapse processes include the "piston," down-sag, trap-door, and piecemeal collapse. Some of the calderas seem to have collapsed along pre-existing linear faults, resulting in polygonal boundaries (Kane et al., 1981; Ferguson et al., 1994).

2.1.2 Groundwater Occurrence and Movement

Figure 2-1 is a map depicting the PM-OV groundwater basin, including the flow system boundary and adjacent groundwater flow basins. Groundwater in the PM-OV groundwater basin generally flows to the south–southwest. Hydraulic property data for rocks relevant to the PM-OV HFM have been reassessed and are presented in Section 5.0 of this document. A comprehensive hydrologic conceptual model of groundwater flow in the PM-OV groundwater basin is given in Halford and Jackson (2020).

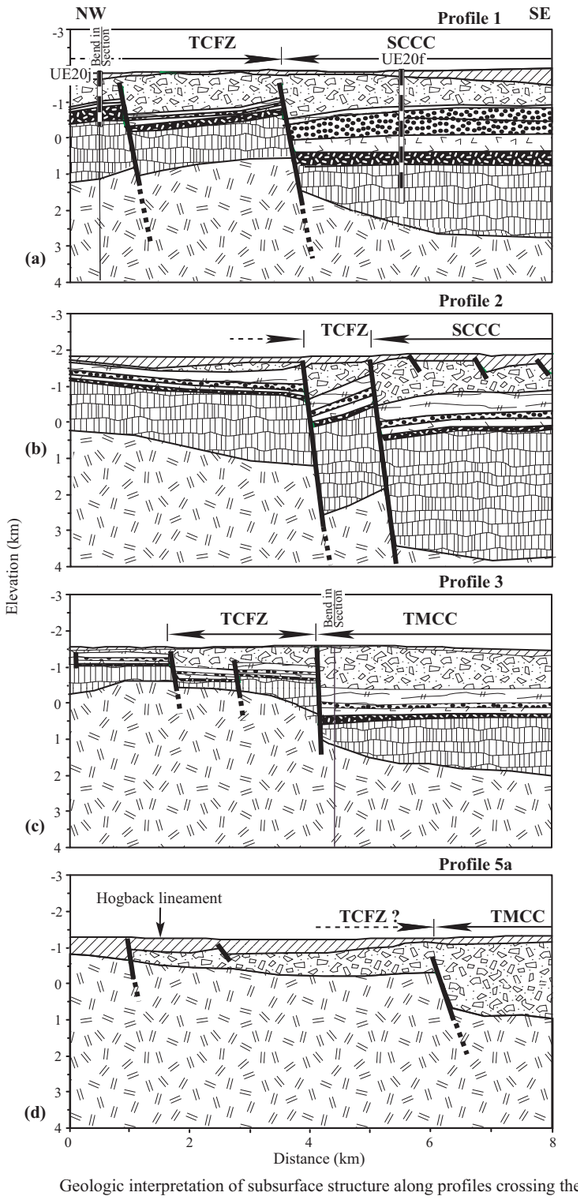

Geologic interpretation of subsurface structure along profiles crossing the Thirsty Canyon lineament. Vertical exaggeration is 0.6.
(**Modified from Mankinen et al., 2003**)

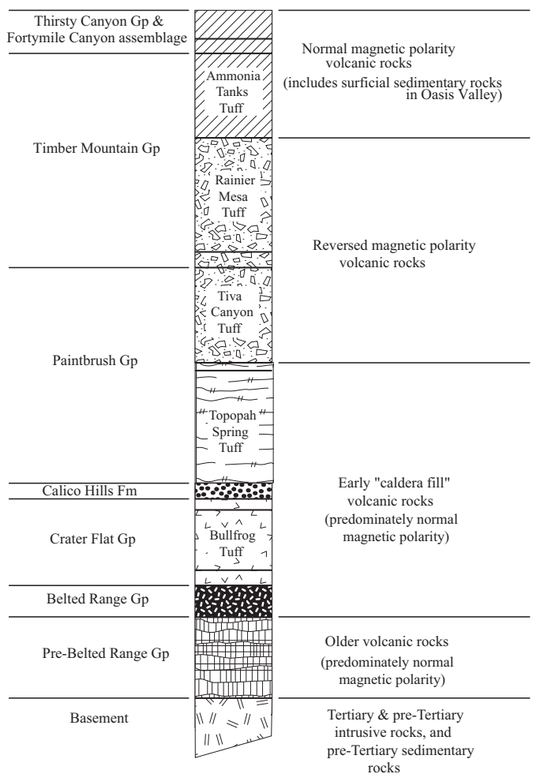

Generalized volcanic stratigraphy of the study area. Unit patterns are the same as shown in our geologic interpretations of the geophysical models. Horizontal lines in the column denote unit boundaries within the larger volcanic groups. Only the names of the major stratigraphic subdivisions are shown on the column. Unit thicknesses schematically depict the erupted magma volumes as estimated by Sawyer and others (1994). (**Modified from Mankinen et al., 2003**)

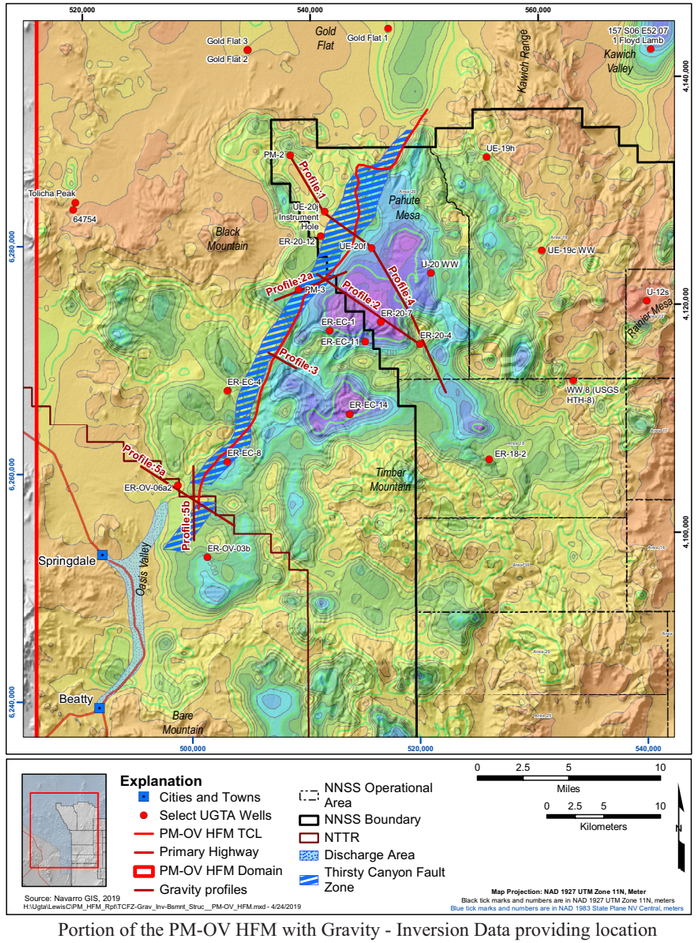

Portion of the PM-OV HFM with Gravity - Inversion Data providing location of the Thirsty Canyon Lineament as used in the PM-OV HFM
Figure also shows PM-OV Discharge Area and inferred Thirsty Canyon Fault Zone

(Gravity - Inversion Data **Modified from USGS MF-2381-E**)
(Thirsty Canyon Fault Zone **Modified from Mankinen et al., 2003**)

Mankinen, E.A., T.G. Hildenbrand, C.J. Fridrich, E.H. McKee, and C.J. Schenkel. 2003. Geophysical Setting of the Pahute Mesa - Oasis Valley Region Southern Nevada, Report 50. Reno, NV: Nevada Bureau of Mines and Geology, University of Nevada Mackay School of Mines.

Blakely, R.J., and D.A. Ponce. 2001. Map Showing Depth to Pre-Cenozoic Basement in the Death Valley Ground-water Model Area, Nevada and California. Miscellaneous Field Studies Map MF-2381-E. Scale 1:250,000. Denver, CO: U.S. Geological Survey.

Figure 2-5
Geophysical and Geologic Information Related to the Thirsty Canyon Lineament and Fault Zone of the PM-OV HFM

2.1.2.1 Groundwater Occurrence

Within the NNSS and surrounding area, groundwater occurs in alluvial, volcanic, and carbonate materials. Saturated alluvial materials are present in Oasis Valley, Kawich Valley, and Gold Flat. Saturated Tertiary volcanics are present throughout the PM-OV basin. The distribution and thickness of AAs and VAs are highly variable throughout the PM-OV HFM, and many HSUs are interpreted to be discontinuous. In most instances, AAs are confined to a valleys bounded by mountain ranges and are localized discontinuous aquifers in the PM-OV basin.

Within the PM-OV flow system, the shallowest depth to groundwater is zero in the Oasis Valley discharge area where springs discharge to the land surface compared to more than 610 m (2,000 feet [ft]) beneath Pahute Mesa on the northern portions of the NNSS (IT, 1996c; DOE/NV, 1997). Table C-3 in Appendix C provides water-level information, as available, from wells used in this report. Perched groundwater is found locally throughout the NNSS and occurs within and on top of the TCUs and, to some extent, overlying units. In the highlands, springs emerge from perched groundwater lenses. Spring discharge rates are low, and this water mostly is used by wildlife.

2.1.2.2 Groundwater Movement

Within the PM-OV groundwater flow system, groundwater movement is partially controlled by hydrologic properties of the rocks, which are influenced by geologic conditions.The general direction of groundwater flow in the PM-OV groundwater basin is from north to south and east to southwest. The direction of groundwater flow is locally influenced in areas where structural and geologic conditions have controlled the distribution and thickness of aquifer and confining units. In some areas of the PM-OV flow system, groundwater encounters structural and geologic conditions, such as structural highs composed of confining units such as the lower clastic confining unit (LCCU), that promote an upward flow component. The upward flow component brings water to discharge at the surface at springs (e.g., springs in the Beatty-Oasis Valley area).

Groundwater recharge results from precipitation in the higher elevations, primarily Pahute Mesa, Rainier Mesa, and Timber Mountain. Additional groundwater recharge may take place in the Kawich Range and the Belted Range (Hevesi et al., 2003; Middleton et al., 2019). Most of recharge occurs from spring snow melt following winters of above-normal precipitation (Jackson and Fenelon, 2018). Infiltration occurs along stream channels, and minor infiltration potentially occurs in playas.

Recharge rates and distributions have been estimated for the model area and are described in Section 6.0.

Within the PM-OV groundwater basin, groundwater discharges to the surface in the form of springs, seeps, and evapotranspiration (ET) in Oasis Valley. Artificial discharge occurs as groundwater pumpage from water-supply wells (public and domestic), agricultural, and stock wells, and industrial wells. Public, domestic, and industrial water-supply wells for the NNSS produce water from the carbonate, volcanic, and AAs. South of the NNSS, private and public water-supply wells are completed in the AA. Discharge from the PM-OV area is discussed in Section 7.0.

2.2 HSU Model Development

The approach followed to develop the PM-OV HFM is summarized in this subsection. The model area is shown in Section 1.0 (Figure 1-2).

The PM-OV HFM was constructed using EarthVision, Version 10 (Dynamic Graphics, 2019), a three-dimensional (3-D) geologic model building and visualization software package. Input data included the Pahute Mesa Phase II HFM (BN, 2002; NSTec, 2014); new drill-hole data from Well ER-20-12 (NNSA/NFO, 2016); digital elevation model (DEM) data; outcrop, geologic, and fault data from surface geologic mapping for the northern extension of the model; and relevant geophysical and interpretive data for the TCL and TCFZ (Wurtz et al., 2018; Navarro, 2019a; DOE/EMNV, 2020a).

Where necessary, the data were supplemented with control points generated from geophysical data, cross sections, and structure-contour maps. A control point is a manually generated data point used to facilitate the automated contouring of data. During development, the model underwent an iterative process of model builds, internal geologic reviews, and QA/QC checks.

Historically, an initial HSU model was constructed based on the conceptual model of the NNSS hydrologic system described by Winograd and Thordarson (1975). Additional modifications and refinements were made by personnel from the U.S. Geological Survey (USGS) and various DOE contractors, resulting in the PM-OV HFM. For details regarding model development and refinement, see the Pahute Mesa Extended HFM Data Document (Navarro, 2019a) and the PM-OV HFM report (DOE/EMNV, 2020a).

2.3 PM-OV HFM Summary

An HFM has been built for the PM-OV groundwater flow system. Figure 2-6 provides a 3-D view of the PM-OV HFM. Details regarding the HFM and model development may be found in the PM-OV HFM report (DOE/EMNV, 2020a) and the Pahute Mesa Extended HFM Data Document (Navarro, 2019a), respectively. Figure 2-7 provides a north–northeast to south–southwest HSU cross section along the general flow direction and a west–east HSU cross section perpendicular to the general groundwater flow direction. Both of these cross sections are from the PM-OV HFM (DOE/EMNV, 2020a), where additional cross sections and detailed information regarding this CAU-scale model can be found.

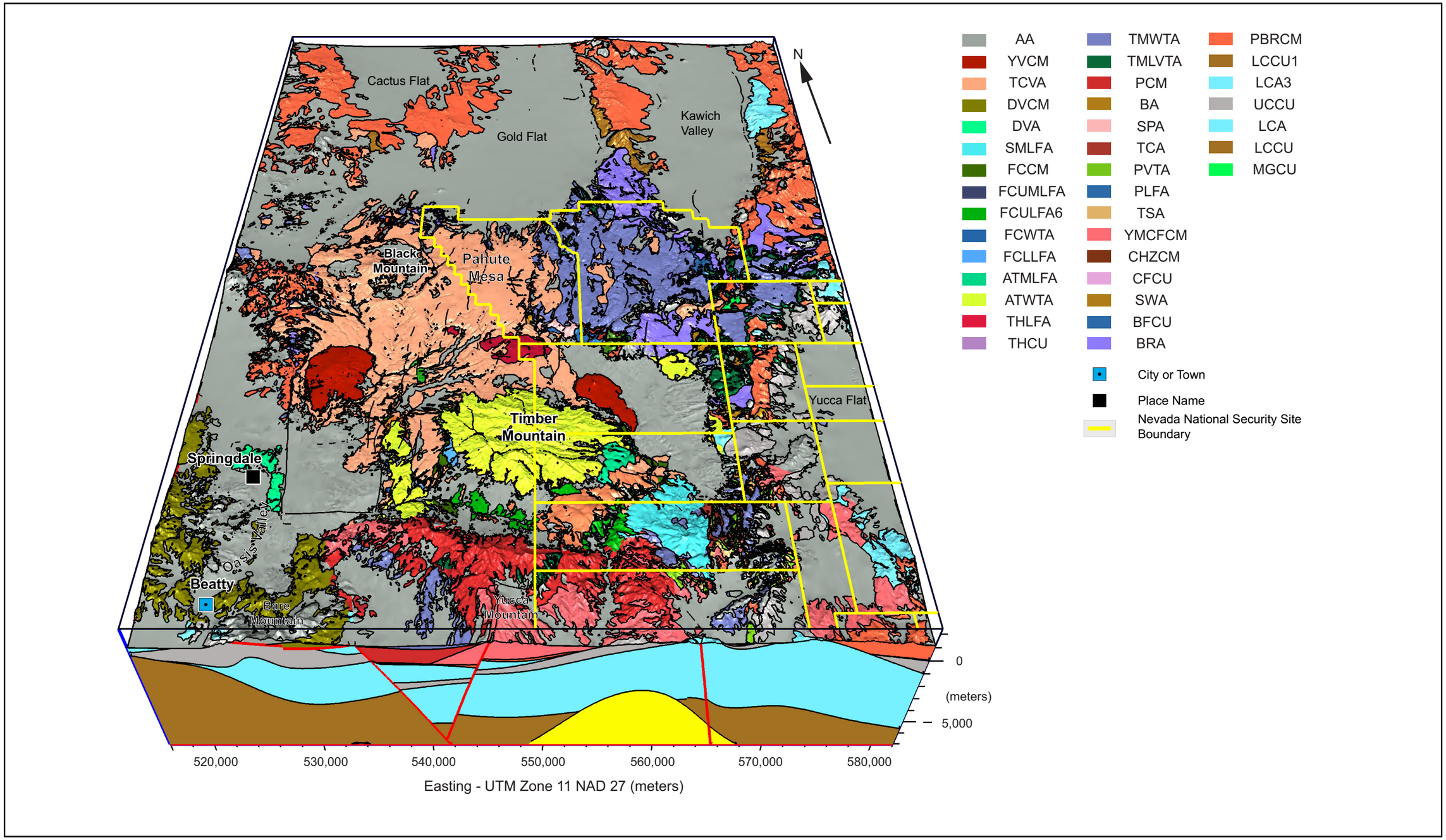

Figure 2-6
3-D View of the Hydrostratigraphic Model of the PM-OV Area

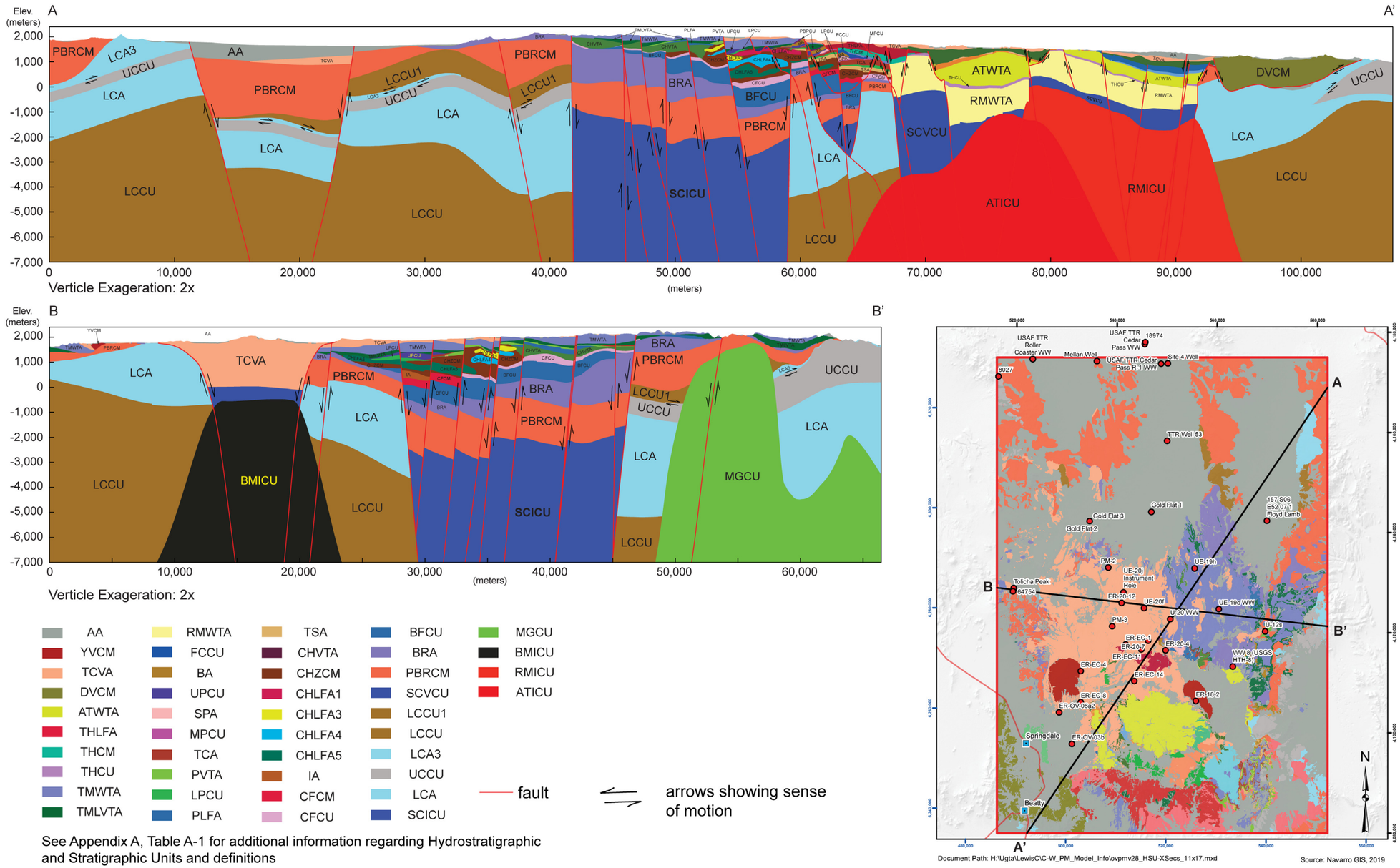

Figure 2-7
North–Northeast to South–Southwest and West–East Cross Sections through the PM-OV HFM

3.0 CAU MODELING APPROACH

This section presents an overview of the CAU modeling approach and data requirements.

3.1 Overview of CAU Modeling Approach

Underground nuclear testing on Pahute Mesa included a total of 82 nuclear tests in deep vertical shafts with the majority of the detonations taking place near or below the water table (DOE/NV, 1997; SNJV, 2004c). Groundwater flow from these sources flows through diverse and structurally complex rocks (Laczniak et al., 1996). The FFACO (1996, as amended) strategy stipulates that modeling (numerical, conceptual, and/or analytical) of the hydrogeologic setting, the radiologic source term, and flow and contaminant transport be used to forecast areas of current and future contamination for 1,000 years. Given the complexity of the system, sources, and processes controlling transport, computer models will be required to meet the objectives of the FFACO strategy. The modeling approach for groundwater flow and transport begins with characterization of the system, development of conceptual models based on assumptions of system processes, and representation of these processes mathematically. Mathematical models are then implemented on a computer to represent the system.

A four-component approach is used to achieve the primary objective of the UGTA strategy, which is to define perimeter boundaries for each CAU over the next 1,000 years (FFACO, 1996 as modified). These four components are (1) data collection, (2) modeling, (3) iterative model evaluation and monitoring, and (4) land use policies. Modeling (numerical, conceptual, and analytical) of the hydrogeological setting, the radiologic source term, and flow and contaminant transport to forecast areas of current and future contamination for 1,000 years forms an essential part of the UGTA strategy.

The modeling forecasts of contamination transport provide the fundamental basis for identifying contaminant boundaries. A ***contaminant boundary*** is formally defined as a probabilistic model-forecast perimeter and a lower HSU boundary that delineates the extent of

radionuclide-contaminated groundwater exceeding the radiological standards of the SDWA from underground testing over 1,000 years.

The important components of the Pahute Mesa CAU flow and transport model include (1) a conceptual model of groundwater flow and potential contaminant transport; (2) the HFM, which incorporates understanding of the geology underlying the Pahute Mesa CAUs; (3) the HST model, which represents the nature, extent, and relevant composition of the potential contamination sources that result from the underground detonations within the CAU; and (4) groundwater flow and contaminant transport models of the saturated zones underlying the CAU.

The complex geological setting and groundwater pathways within and downgradient of the NNSS combined with limitations in obtaining sufficient characterization data for these systems results in uncertainty in the model forecasts of ***contaminant boundaries***. The uncertainty includes both statistical (variability and parametric or knowledge uncertainty) and structural uncertainty (numerical model and conceptual model uncertainty). Pahute Mesa is unique compared to other testing areas because of a greater amount of hydrologic, transport, and radionuclide concentration data with which to calibrate the model. This relative wealth of data will provide a substantial reduction in parameter and model uncertainty. The uncertainty will be evaluated through integrated Monte Carlo simulations and alternative models of contaminant transport that investigate the range of parameters values that provide calibration to observed hydrogeologic data. Alternative approaches are not planned unless necessary to achieve acceptable calibrations.

To ensure fidelity of the CAU model to the physical system, the CAU model will undergo internal technical reviews, acceptance by both EM Nevada Program and NDEP, and a second technical review by an external review panel before the model is deemed acceptable for further model evaluation studies. During model evaluation, the model is evaluated against new information to enhance confidence in the model forecasts. Following the model evaluation, the CAU model is presented to DOE and NDEP for acceptance as a tool for making regulatory closure decisions.

3.2 Integrated 3-D Model Development

The CAU flow and transport models will consist of an integrated set of models. Some of these models will focus on a small-scale (relative to the CAU) process such as radionuclide release from source regions, and flow and transport in the Bench area subregion (the area between the Silent Canyon

caldera complex [SCCC] and Timber Mountain caldera complex [TMCC]); and others will be directed toward models to understand CAU-scale processes such as matrix diffusion in fractures. The models (referred to as "components" or "process models") support the CAU predictive model. Essential aspects of the processes described by the detailed process models must be represented in the CAU model to be able to make defensible contaminant boundary forecasts. This representation will include the uncertainty associated with the process or parameters.

The integrating numerical model will be a 3-D flow and transport simulator that captures the complex geologic structure including HSUs of variable thickness, faults, and offsets, as well as complex transport processes associated with reactive solutes and fractured rock. The CAU groundwater flow model will be corroborated by the regional groundwater flow model (Halford and Jackson, 2020), the PM-OV groundwater basin delineation model (Fenelon et al., 2016), and recharge models (Fenelon et al., 2016; Middleton et al., 2019) to determine appropriate model boundaries and estimate groundwater flows through the system. The CAU contaminant transport model requires the CAU groundwater flow model and will utilize input from the hydrologic source term model to provide initial radionuclide concentrations.

3.3 Conceptual Flow Model Components

The hydrologic conceptual model for the PM-OV groundwater flow system is presented in Halford and Jackson (2020). The conceptual model defines the important elements of the flow system, including the components of the water balance (recharge, discharge, and changes in storage) and hydrogeologic controls on groundwater flow. Several key findings of the conceptual model are as follows.

Recharge occurs primarily in upland areas as a result of spring snow melt during years of above-normal winter precipitation. At present, most well discharge occurs in Oasis Valley. Historically, most groundwater withdrawals in the PM-OV basin since predevelopment (pre-1950) have occurred from about 10 NNSS wells in Pahute and Buckboard Mesas. Groundwater withdrawals from three water-supply wells by Beatty Water and Sanitation District (BWSD) provide drinking water to the city of Beatty, Nevada, and Beatty pumping has dominated the pumping in the PM-OV basin only since 2000.

The groundwater flow system is considered to be in steady-state based on observations of temporal trends in water levels in wells. It is noted that there are a few small regions where non-steady water levels are observed, but these are of limited spatial extent and do not warrant separate treatment (Jackson and Fenelon, 2018). The PM-OV system is believed to have balanced recharge and discharge. That leads to the expectation that the boundaries of the PM-OV basin can be treated as no-flow for the purposes of modeling.

Blankennagel and Weir (1973) and Frus and Halford (2018) have shown that the largest transmissivity occurs in the first 1,500 ft below the water table. This indicates that the majority of the groundwater flow will also occur in the shallower portions of the aquifers. Permeability is spatially variable within units; therefore, the ability to accommodate intra-HSU heterogeneity should be considered.

Faults are important structural features. They can displace permeable units against low-permeable confining units, effectively creating barriers to flow. Faults may also create zones of enhanced permeability in the near vicinity of faults due to increased fracturing. The model will be designed to include specific structural features, with emphasis on the features located downgradient of underground nuclear tests. As demonstrated by the work of Garcia et al. (2017) and Lu et al. (2020), flow models can be calibrated to Pahute Mesa hydraulic data with heterogeneous conductivity fields, without explicitly invoking grid-block scale anisotropy. The CAU flow model will incorporate inhomogeneity with the use of HSUs and explicitly included faults, as well as pilot points to capture variations within conductivity zones.

3.4 CAU Model Development Process

The process of model development, as it is applied to the CAU model, involves following a modeling protocol: a series of steps that build support in demonstrating that a given site-specific model is capable of producing meaningful results. This increases confidence in the model predictions. To ensure fidelity of the CAU model to the physical system, UGTA follows a multi-step process that includes (1) establishment of model purpose, (2) development of conceptual model, (3) selection of a computer code, (4) model design, (5) model calibration, (6) sensitivity and uncertainty analyses, (7) predictive simulations, (8) presentation of model results, and (9) review of model predictions.

3.5 Data Requirements

Data requirements for the Pahute Mesa CAU flow model fall into the three categories listed below.

Groundwater Flow

Data types required for the Pahute Mesa CAU flow model include transmissivity (or hydraulic conductivity), storage parameters (for simulating transient aquifer responses), precipitation recharge, lateral boundary fluxes, and hydraulic heads. These data types are the subject of this document and are discussed in detail in the following sections. Groundwater chemistry data are used to corroborate the groundwater flow paths determined by the model.

Contamination Sources and Extent

Potential contaminants are currently located in the 82 test locations and downgradient areas in Central and Western Pahute Mesa. Additionally, three near-surface tests (SCHOONER, PALANQUIN, and CABRIOLET) were conducted within this area as a part of the Plowshare program. Although these three corrective action sites are not assigned to the UGTA Activity as defined in the FFACO (1996, as amended), they will be included in the Pahute Mesa CAU model for completeness. The HSTs from SCHOONER, PALANQUIN, and CABRIOLET will be placed at the water table; thus, unsaturated zone modeling will not be needed.

Groundwater sampling has identified several locations where contaminant plumes have migrated downgradient of tests. These locations include observations of radionuclides downgradient of the tests HANDLEY, BENHAM, and CHESHIRE. The observed migration of radionuclides provides key information on groundwater flow direction that is not available from hydraulic data alone. Using the SDWA concentration of tritium (^{3}H) (20,000 picocuries per liter [pCi/L]) as a concentration of interest (CFR, 2019), the extent of downgradient migration observed on Pahute Mesa is about 4.25 km from the working point of the BENHAM underground test. Only ^{3}H has been observed in groundwater downgradient of underground nuclear tests in concentrations exceeding the SDWA standards. Other radionuclides are observed below their respective SDWA standards, but significant concentrations (defined as between 0.1 and 0.5 of the maximum contaminant level [MCL]) are observed only in locations where ^{3}H concentrations are more than 500 times greater than the MCL. At ^{3}H concentrations of 20,000 pCi/L, other radionuclide concentrations are well below 1 percent of their respective MCLs. This suggests that modeling of ^{3}H will dominate the contaminant

boundary calculation and that although the time frame of interest based on the FFACO is 1,000 years, ^{3}H radioactive decay reduces the time frame when radionuclides are expected to exceed their MCLs to the next 150 years or so. If one assumes pure radionuclide decay of ^{3}H starting with a concentration of 1.0×10^{9} pCi/L, it takes almost 200 years for the ^{3}H to decay below the SDWA standard of 20,000 pCi/L. Many of the tests were conducted about 50 years ago, so that leaves about 150 years left. Considering the 1,000-year time frame of interest (which is closer to 150 years for ^{3}H) and ^{3}H travel distances since nuclear testing on Pahute Mesa ended, the potential downgradient location of the contaminant boundary is likely to extend another 2 or 3 km from its current location. Based on current groundwater monitoring downgradient of tests, concentrations of radionuclides other than ^{3}H are not expected to influence the location of the contaminant boundary. One of the goals of the Pahute Mesa CAU flow model is to evaluate potential flow paths from underground nuclear tests to Oasis Valley to be used to design a monitoring network to provide assurance that ^{3}H and other radionuclides, in aggregate, do not exceed the SDWA standards in groundwater accessible to the public. The information on the unclassified hydrologic source term and radionuclide data for Central and Western Pahute Mesa will be documented in a separate report.

Transport Parameters

Major data types of interest include effective porosity, dispersivity, matrix porosity, matrix diffusion, sorption coefficients, and colloid-facilitated transport parameters. Note that for the purpose of modeling, effective porosity and matrix porosity are considered to be transport parameters rather than hydrologic parameters as they are required input variables in the contaminant transport model. Details for these parameters will be documented in a separate report.

3.6 Groundwater Flow Modeling Approach and Data Requirements

The following subsections describe the approach used for the CAU flow model and the associated data requirements. The CAU transport modeling approach will be documented in a separate report.

Steps for developing the CAU flow model include the following:

- Identify Simulation Objectives.
- Define CAU Geologic Model Domain.
- Define CAU Flow Model Parameters.
- Define CAU Flow Model Boundaries and Boundary Conditions.
- Develop Numerical Model.

- Generate CAU Model Grid.
- Calibrate CAU Flow Model.
- Perform Parameter Sensitivity and Uncertainty Analyses.
- Identify Data Requirements.

3.6.1 Simulation Objectives

Simulation objectives for the groundwater flow and transport model are defined in Appendix VI of the FFACO (1996, as amended). Briefly, the objective is to develop a tool for predicting contaminant migration from source locations through the subsurface of Pahute Mesa. The predictions forecast locations of specified contaminant concentrations for assessment of the contaminant boundary and to provide a basis for risk assessment as well as for the design and siting of monitoring wells. The transport portion of the modeling is dependent on the prior development of a robust groundwater flow model.

3.6.2 CAU Geologic Model Domain

The next step in the strategy, defining the geologic model domain, has already been completed. The boundaries of the geologic model were chosen to encompass the lateral extent of the PM-OV groundwater basin, which includes the contaminant source areas, recharge areas, and discharge areas. The Pahute Mesa CAU flow and transport models will be developed within the boundaries of the PM-OV groundwater basin.

3.6.3 CAU Flow Model Parameters

Specific data types needed to support groundwater flow modeling include storage properties, transmissivity or hydraulic conductivity, groundwater recharge, discharges, lateral boundary fluxes, steady-state hydraulic heads and drawdowns. Parameter distributions were developed based on review and analysis of available data and information. This information is the subject of this report.

3.6.4 CAU Flow Model Boundaries and Boundary Conditions

The next stage of the process is identification of the CAU flow model boundaries and boundary conditions. When selecting boundaries for a flow and transport model, natural physical boundaries of the aquifer system (such as recharge and discharge zones, impermeable rock, and groundwater divides) are preferred because they provide easily described hydraulic boundary information. The

boundaries of the CAU flow and transport model should incorporate all relevant radionuclide sources and important hydrogeologic features, and encompass the area of expected radionuclide transport over the time period of interest.

The CAU flow model domain extent will extend to the PM-OV groundwater-basin boundaries. The PM-OV groundwater basin is largely isolated from surrounding groundwater basins by low-permeability rocks and groundwater divides. Overall, inter-basin flow between the PM-OV groundwater basin and adjacent basins is thought to be insignificant (Fenelon et al., 2016). These boundaries will be within the geologic model boundaries. Lateral boundary conditions will be no flow at the groundwater basin boundaries. These lateral boundaries are consistent with groundwater basins delineated in the Death Valley regional groundwater flow model (Halford and Jackson, 2020). The recharge model will provide fluxes for the model surface that, in total, account for the discharge at Oasis Valley. The bottom of the model will encompass the source area of the deepest tests and will allow in excess of 500 m of saturated zone at the PM-OV basin's lowest point, located within Oasis Valley. The majority of the transmissivity occurs within the upper 1,200 m of the subsurface, or as stated by Frus and Halford (2018), within the first 500 m beneath the water table. Hydraulic conductivity below 1,800 m bgs is typically less than 0.1 feet per day (ft/day) (0.03 meters per day [m/day] (see Section 5.2.2.5).

3.6.5 Develop Numerical Model

The MODFLOW 6 code (Langevin et al., 2017), developed by USGS, was chosen for the Pahute Mesa CAU-scale flow and transport model (SNJV, 2009b). MODFLOW 6 is based on a generalized control-volume finite-difference approach in which a cell can be hydraulically connected to any number of surrounding cells. MODFLOW 6 can use fully structured or unstructured spatial discretization that allow cell connections through inactive grids or discontinuous layers. Specific capabilities include the following:

- 3-D
- Finite volume formulation
- Complex geometries with unstructured grids
- Coupled to the MODPATH particle-tracking module for some grid configurations

- Coupled to the FloPy Python based pre- and post-processor for grid generation
- Multiple models can be coupled together that allow parameter and boundary condition exchanges between models
- Available source code that can be compiled on any computing platform

Documentation includes a description of the mathematical models and numerical methods used by MOFLOW 6 (Langevin et al., 2017). MODFLOW 6 uses "packages" that deal with a single aspect of the groundwater simulation. There are three general types of hydrologic packages: (1) internal flow packages that simulate flow between adjacent cells or handle storage changes for model cells; (2) simplified stress packages for simulating features such as rivers, wells, and recharge; and (3) advanced stress packages that involve solving some form of a water budget equation for the stress features, such as a stream, lake, MWATs, or unsaturated zone.

PEST, a software package developed by Watermark Computing (2000), provides a nonlinear parameter estimation routine that can be used to automatically calibrate a model. PEST can be used with any existing modeling computer code for model calibration without making any changes to that code.

FlowPy (USGS, 2019) is a Python package developed by USGS for creating, running, and post-processing MODFLOW based models. Users can define the model grid using one of the three discretization packages within MODFLOW 6: (1) a structured discretization package for defining regular MODFLOW grids consisting of layers, rows, and columns, (2) a discretization by vertices package for defining layered unstructured grids consisting of layers and cells, and (3) a general unstructured discretization package for defining flexible grids composed of cells and their connection properties.

Grid Generation

Simulations of flow and transport, including particle tracking, in 3-D domains representing the complex hydrostratigraphy described in the hydrogeologic models will be conducted on spatially variable grids that conform to the HSU contacts and have cell size refinement near faults. The spatially varying grids will capture source areas and complex structures such as faults with higher resolution than other areas where coarser discretization is sufficient.

The method developed for the flow of information from hydrogeologic interpretation through grid generation has the following steps. The process begins with incorporation of a given hydrogeologic digital model using EarthVision (Dynamic Graphics, 2015). EarthVision is a suite of software applications used for geospatial analyses. Elevations describing the surface of each HSU and traces of each fault are extracted from the EarthVision model and become inputs to the grid generation software. Possible candidates for high resolution include fault zones and thin HSUs. Calibration efficiency can be increased by keeping the flow model grids coarse, then adding higher resolution to source regions and plume pathways for the transport simulations. A process for transferring hydrogeologic framework model information from an EarthVision model to inputs required by the grid generation software will be developed and tested. An important aspect of the grid generation process will be efficiency so that grids can be adjusted during the model calibration. FloPy based scripts will be used to transfer the HFM information into the grid generation and groundwater model software that can easily be modified and rerun.

Flow Model Calibration

Calibration consists of determining model parameter values such that simulated steady-state heads, drawdowns, and fluxes are consistent with observed or target values. The parameters for a CAU flow model will include the recharge distribution along with permeabilities and storativities of the HSUs and faults in the model. Specified observations for a CAU flow model will include steady-state heads, aquifer stress responses to groundwater withdrawal, transmissivity measurements, discharge at springs and the total amount of groundwater flow moving through the PM-OV basin. These data provide “targets” for the calibration process. Data required for calibration include well locations, locations of open intervals, HSUs represented by open intervals, transient and steady-state head measurements in wells, well pumping rates, spring discharge volumes, ET areas and volumes, basin water budget, and transmissivity estimates.

Model parameterization will use a combined zonation-pilot point approach. The pilot point method estimates parameters at discrete locations throughout the model domain and interpolates the pilot point values onto the model mesh (RamaRao et al., 1995). Pilot points allow for spatial heterogeneity in rock properties and calibration to transmissivity estimates, where transmissivity is spatially variable within a single HSU. Initial model calibrations will assume HSU and fault zones are homogeneous. Heterogeneity will be added to the HSU and fault zones as needed to calibrate the model. Pilot points within specific HSU zones will be added as needed to adequately calibrate the

model. Similar to the hydraulic conductivity parameterization, the recharge distribution may require pilot points to improve the model calibration. Initially, the model will be calibrated to data by adjusting the conductivities and storativities using a fixed recharge distribution obtained from the cited literature. If this calibration is found to be unsatisfactory, the recharge distribution may then be treated as a calibration variable to obtain a better match to the observed data.

PEST runs the model initially and calculates the sum of weighted squared differences between model-generated and target data. This sum is referred to as the "objective function." PEST then repeatedly runs the flow model to guide the adjustment of parameters until the objective function is minimized. In principle, PEST can be set up to adjust the model parameters until simulated values match measured values within the CAU flow model domain and simulated flows through the CAU flow model match those estimated at basin outflow locations. Due to random and systematic errors, there will always be some discrepancy between modeled and measured values. PEST attempts to minimize this discrepancy and provides estimates of uncertainty in the results. Because the flow model must be run many times during calibration, this part of the process requires heavy usage of computing resources. A model calibration will be specific to the hydrogeologic model and calibration targets. A priori alternative models will not be identified in advance of model calibration. Rather, alternatives will be identified, if needed, to enhance the calibration to observations. Alternative geologic models or changes in calibration targets, if needed, will require new calibrations.

Tikhonov regularization supplements the information content of a calibration dataset with expert knowledge that compensates for a deficit of information in the calibration dataset (Doherty, 2018). Regularization augments the measurement objective function with a regularization objective function that penalizes for departures from a preferred condition. Tikhonov regularization observations will be specified with equations derived from the geostatistical structures used to interpolate pilot point values onto the model mesh. This information defines preferred differences between pilot points and penalizes large differences between pilot point values. Initial pilot point values for hydraulic conductivity will be the average hydraulic conductivity from pump-scale aquifer test data within the HSU, which provide a fall-back position if the pilot points parameters are insensitive to the observation data.

As PEST proceeds through the inversion process, PEST relaxes the regularization constraints in order to achieve fits with heterogeneous parameters. The relaxation takes place through reduction of the

regularization weight factor (Doherty, 2018). If there is strong evidence for the existence of parameter heterogeneity in the observation data, PEST will estimate the heterogeneous parameters. The initial regularization objective function is always zero when starting with homogeneous pilot point values, which facilitates making homogeneity the preferred condition.

The model hydraulic properties will be estimated by simultaneously calibrating multiple 3-D flow models using identical parameterization. The models will include a steady-state model of pre-development flow conditions and transient stress response models of the Pahute Mesa MWATs. The steady-state model provides initial conditions for the transient stress response models. All models will share the same outflow and recharge boundary conditions, hydraulic conductivity, and specific storage values. The temporal separation of the various Pahute Mesa MWATs and well responses will be evaluated to determine the number of transient models needed.

The steady-state CAU flow model will be calibrated to steady-state water levels, spring discharges, total basin flow, and transmissivity measurements. The transient flow models will include additional calibration data from the drawdowns seen in wells responding to the MWATs.

In contrast to the Phase I modeling (SNJV, 2009b), datasets of radionuclide concentration data are now available in and around the Bench area and west of the NNSS at Wells PM-3 and ER-20-12, which can be used to assess transport simulations. Three main plumes have been identified, which appear to be associated with the HANDLEY, BENHAM, and CHESHIRE nuclear tests. In addition to the radionuclide data, more detailed estimates of flow directions and recharge have been recently performed using naturally occurring groundwater geochemical and isotopic tracer data (Navarro, 2020).

After the flow calibration process is completed, a verification of the calibration for transport simulations will be assessed by inspecting simulated and measured radionuclide concentrations at well locations. If simulated and measured values are significantly different, an evaluation will be conducted to determine whether the mismatch is caused by a flow issue such as incorrect pathline direction, or a transport parameter problem. Additionally, geochemical data may inform the calibration by providing independent estimates of groundwater flow paths.

Sensitivity Analysis

Sensitivity analysis is a systematic process of varying the magnitude of model inputs and determining the effect on model outputs such as hydraulic head and flux. Sensitivity analyses are conducted before and after calibration of the flow model. Sensitivity analyses conducted before model calibration help identify parameters that can be estimated. Sensitivity analyses conducted after model calibration help identify parameters that affect the model results. The sensitivity analysis process can be automated using the PEST utility SENSAN.

Global Uncertainty Analysis

The Pahute Mesa CAU flow model will be a highly parameterized groundwater model and may have more parameters than can be estimated uniquely on the basis of the calibration dataset. The model calibration can present an ill-posed inverse problem and may not have unique parameter-estimation solutions. There can be many alternative calibration sets with alternative flow fields that have similar fits to the calibration data. Therefore, it may be necessary to perform a global uncertainty analysis that examines many optimized parameter sets which are determined from many different initial parameter sets. PEST's null space Monte Carlo (NSMC) method uses a special technique to sample all parameters by using information regarding the parameter and null spaces of the Jacobian matrix to efficiently create many alternative models that have similar fits to the calibration data. The need for NSMC will be determined after calibration has successfully been achieved. One reason is that NSMC is computationally burdensome, requiring potentially hundreds of full calibrations (each requiring up to 1,000 simulations). During the Yucca Flat model evaluation (Navarro, 2018), two or three alternative cases chosen by expert opinion were shown to adequately span the range of uncertainty determined by the NSMC.

Data Requirements

Specific data types needed to simulate groundwater flow are shown in Figure 3-1. The data include geologic data, hydraulic head data, groundwater recharge estimates, discharge estimates, and hydraulic conductivity or transmissvity. Geologic data are described in Section 2.0. Hydraulic head data serve as a target to which the flow model is calibrated. Hydraulic gradients, as discussed in Section 8.6, are also used as calibration targets. Note that in Figure 3-1, well construction information is included in several places. The well defines the open interval, but well construction information is considered known. Recharge refers to either lateral flow across the CAU-model boundary into the

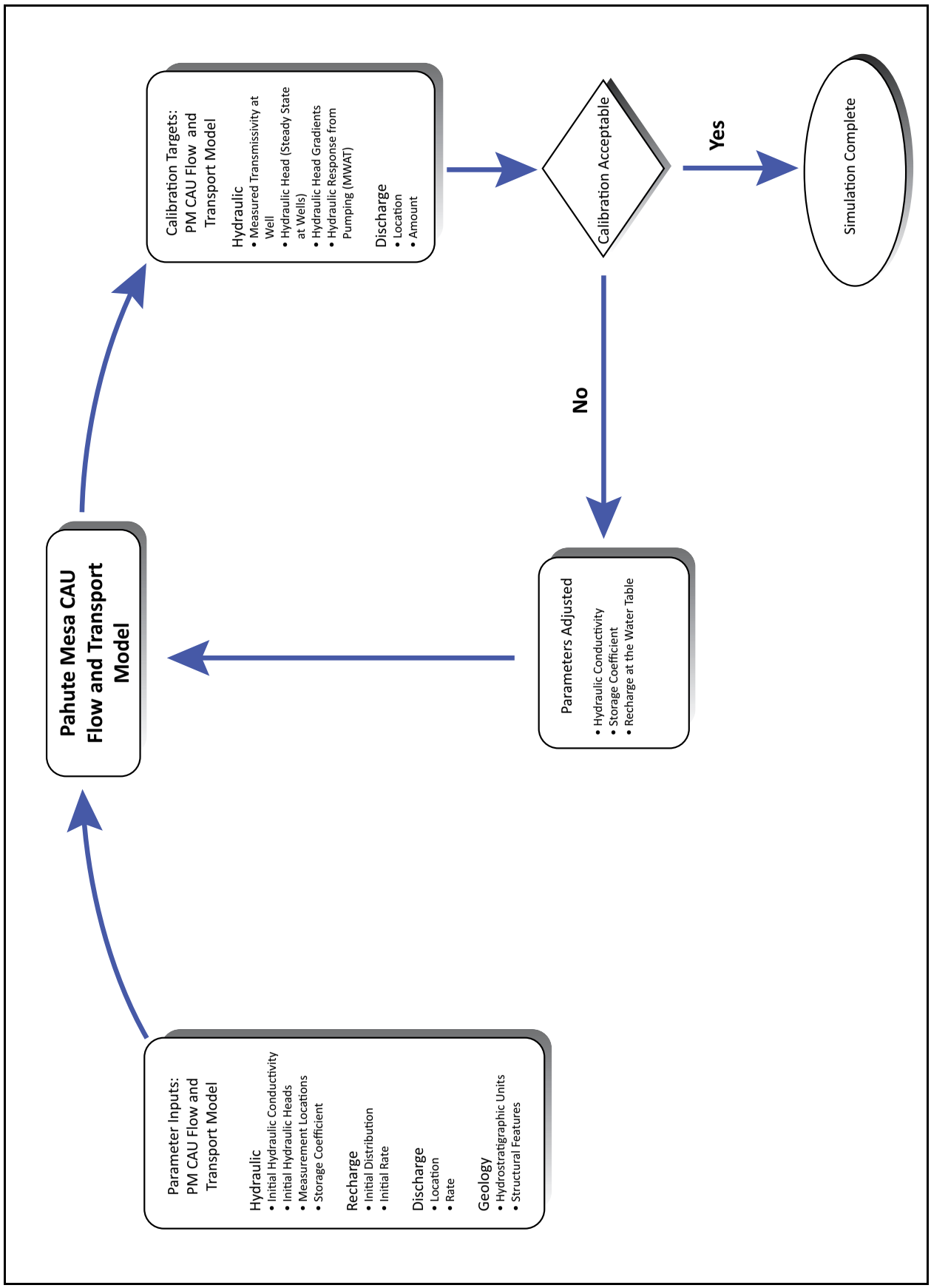

Figure 3-1
Data Types and Utilization in the Groundwater Flow Model

model or recharge that enters from the land surface. Discharge is the lateral flow across the CAU-model boundary out of the model or natural discharge to the surface (e.g., ET, springs, seeps) or groundwater pumped from wells. The hydraulic conductivity is a measure of the water-transmitting ability of the aquifer system. Hydraulic conductivity may be heterogeneous, and may vary from location to location within an aquifer unit and vary across geologic units. Nonetheless, measured transmissivity will also be a calibration constraint. An understanding of the natural geochemical system may provide constraints on the flow model for the Pahute Mesa CAUs. The various data types are described in Section 4.0.

4.0 DATA ANALYSIS

Data analysis is the process of compiling, assessing, and interpreting available data in preparation for flow and transport modeling. Data come in a wide variety of types, from a wide variety of sources, and represent a wide variety of scales. The process of analyzing the data can be summarized in the following steps, which are explained in detail in this section: (1) compilation of existing data in the study area; (2) transfer of applicable data from outside the PM-OV area; and (3) analysis of the data, including calculation of the expected values, range of uncertainty, statistical distribution, and discussion of data limitations.

4.1 Data Compilation

The compilation of existing data is a multiple step process of identifying existing data, acquiring the data, and compiling the data into structured databases. As will be discussed later, certain data inputs required for CAU-scale flow models necessitate data processing through numerical models representing semi-analytical solutions to the flow equations. For example, specific storage and hydraulic conductivity obtained from single-well pump-scale aquifer tests must be estimated from the resulting drawdown data using models. Data types of interest and data sources are discussed in the following subsections.

4.1.1 Data Types

Major data types of interest to this report are hydrologic parameters and supporting information. These data include hydraulic properties, precipitation recharge, discharge to the surface, lateral boundary fluxes, hydraulic heads, aquifer stress responses, and groundwater chemistry. Descriptions of these parameters are provided in Section 4.1.2.

The following types of supporting information are recorded, as required and when available:

- Site or core information
- Chemical constituent
- Method of data collection or type of test
- Scale of measurement

- Date of data collection
- Stratigraphic unit
- Lithology
- Alteration
- HSU
- Method of data analysis
- Observed parameter value
- Parameter spatial distribution
- Uncertainties
- Any references relating to the data records
- Any noted deficiencies

References to the specific sources of information are provided along with the data. A general description of the data sources is provided in Section 4.1.3.

4.1.2 Description of Hydrologic Data Types

Information needed in support of the groundwater flow model include hydraulic properties, precipitation recharge, discharge to the surface, lateral boundary fluxes, hydraulic heads, and groundwater chemistry.

Hydraulic Properties

Important hydraulic properties include hydraulic conductivity (transmissivity), hydraulic conductivity anistropy, and specific storage coefficients.

The hydraulic conductivity of the geologic units determines the volumetric flow rate of groundwater movement in response to the hydraulic gradient. Data types relating to hydraulic conductivity required by the model are horizontal hydraulic conductivity, horizontal anisotropy ratio (north–south to east–west) and vertical hydraulic conductivity, which is specified in the model as a horizontal to vertical anisotropy ratio. Values of measured hydraulic conductivity will be used in two ways. First, the range of measured values provides an uncertainty range within which the values may be varied during model calibration. Second, the values will be used during the uncertainty analyses to prevent unrealistic realizations.

Inputs required by the numerical codes used for the CAU scale models typically consist of permeabilities or hydraulic conductivities at computational nodes/volumes/cells. However, the water flow and hydraulic head information obtained from hydraulic testing of wells corresponds to the

entire production interval. Well test analysis methods typically yield a transmissivity value that represents the hydraulic conductivity integrated over the production interval, but in some cases represents the entire thickness of the aquifer. The thickness used to calculate the average hydraulic conductivity from the transmissivity is often uncertain. Thus, well tests determine transmissivity with greater confidence than the hydraulic conductivity. The transmissivity provides a constraint on the depth integrated hydraulic conductivity.

Specific storage is another property of the geologic units that affects the pattern of groundwater flow, during transient conditions. Transient, or non steady-state, flow conditions are caused when time-varying natural or artificial stress is placed on an aquifer.

Precipitation Recharge

Under natural conditions, recharge occurs from precipitation when infiltration moves below the root zone and reaches the water table. Recharge is an important component of the hydrologic system. The areal distribution of the recharge affects the rate and direction of groundwater flow. The velocity of groundwater is indirectly a function of the amount of recharge entering the flow system. Surface infiltration leads to recharge, but it can be diverted laterally before reaching the water table by occurrence of layers with conductivity contrasts. Recharge rates are usually estimated because direct measurements are difficult to obtain. Recharge rates may be adjusted during the groundwater flow model calibration.

Surface Discharge

Under natural conditions, discharge from the groundwater system to the surface occurs by spring flow and by ET. Discharge may also be induced by anthropological activities such as well pumping. Discharge ranges and spring elevations may be used during the steady-state flow model calibration process. Well pumping rates may be used to simulate transient conditions and calibrate the model to drawdown observations during MWATs.

Lateral Boundary Fluxes

Under natural conditions, subsurface flow can occur across the lateral boundaries of the delineated groundwater flow system. The subsurface inflow and outflow rates are referred to as lateral boundary fluxes. Overall, inter-basin flow between the PM-OV basin and adjacent basins is thought to be

insignificant (Fenelon et al., 2016). Because the Pahute Mesa CAU flow model domain will coincide with the PM-OV groundwater basin boundaries defined by Fenelon et al. (2016), the lateral boundaries will be no-flow.

Hydraulic Heads

Hydraulic heads define the pressure condition in the aquifer system. They are mostly derived from measured water levels. Land surface elevations at the locations of known regional springs may also be used to approximate spring-pool elevations at these locations. Existing spring data and water-level data measured in wells and boreholes located within the PM-OV area and vicinity were analyzed to derive a hydraulic head dataset. Hydraulic heads for locations inside of the model area are used as targets during the calibration process of the groundwater flow model.

Groundwater Chemistry

Groundwater chemistry and isotopic data provide important information to corroborate groundwater recharge, discharge, and flow paths. Groundwater chemistry data are not incorporated as input in the flow model; rather, interpretations of groundwater chemistry data are used to support calibration of the model. These interpretations also provide an independent check on groundwater flow paths and travel times.

4.1.3 Data Sources

A great many sources for the data have been identified. In many cases, existing databases developed as part of the NNSS regional groundwater flow and transport modeling (DOE/NV, 1997) were used as starting points. These data were supplemented with new data collected as part of ongoing UGTA field investigations and existing data not previously identified.

Most of the new data evaluated in this report for the Pahute Mesa Area come from numerous organizations including the NNSS management and operating (M&O) contractor, LLNL, LANL, Desert Research Institute (DRI), USGS, and the DOE Environmental Program Services contractor. Historical data are available in many publications. Typically, much of the data have been compiled during the preparation of the CAIP (DOE/NV, 1999), but these data need to be supplemented with new data and newly identified existing data.

Site-Specific Data

Site-specific data refers to data collected within, or near, the boundaries of the CAU study area, which is defined as the PM-OV groundwater basin area (Figure 1-2). These are directly applicable to the HSUs within the study area.

Yucca Mountain Data

Yucca Mountain is the proposed geologic storage location for commercial high-level waste in the United States. A great deal of high-quality data has been collected and analyzed during investigations of the Yucca Mountain site. The northern portion of the Yucca Mountain Project (YMP) site is located within the southern portion of the PM-OV HFM domain. The geology in the YMP region has many similarities with the geology of the Pahute Mesa CAUs as well as a number of differences. A process was developed to assess the transferability of YMP data for use in the Pahute Mesa CAU flow model. The justification for using Yucca Mountain data was presented as Appendix B in the previous version of this document (2004a).

Other Data

In some cases, the data from much more distant sites may be used to estimate parameter values. Data from distant sites will only be used in cases where the data from the study area or the YMP site are non-existent or are very limited. As with the YMP data, the transferability of all data will be assessed prior to use in the Pahute Mesa CAU flow model.

4.2 Data Transfer Methodology

It has been proposed that using data from other sites to reduce flow and transport parameter uncertainty is an appropriate approach when developing models in a sparse data environment (Freeze et al., 1990), such as that of the Kawich Valley, Gold Flat, and Black Mountain areas of PM-OV groundwater model. This type of approach incorporates flow and transport parameter data from investigations of similar environments for parameters to be used in modeling of the study area. Utilization of data from other sites can be both a cost-effective and necessary step for a modeling effort in a sparse data environment. Nearby sites considered as potential sources of additional data for the Pahute Mesa CAUs are other UGTA CAUs and Yucca Mountain. Rock genesis and evolution

factors that influence flow and transport parameters, the general transfer methodology, and the case of YMP data transfer are described in this section.

4.2.1 Rock Genesis and Evolution Factors Influencing Flow and Transport Parameters

Numerous factors may influence the flow and transport of groundwater in the subsurface environment in a variety of ways. The following subsections focus on rock genesis and evolution factors that influence rock characteristics and, therefore, flow and transport parameters. These factors include the overall geologic history of the area, lithology, alteration, stress history, and groundwater chemical composition. The general process of data transfer is provided in Appendix B. This process differs from work reported in previous Stoller-Navarro Joint Venture (SNJV) documents (2004a and b). A significant change is that much of data results are now available through published reports that have followed internal review processes. Secondly—and, perhaps, more importantly—much more direct data are available for Pahute Mesa, which has reduced the need for non-direct data. In some cases, the extension of the model area into Gold Flat has brought data from outside the project. However, those data are no longer a direct input to the forecasts of radionuclide migration, but rather serve to extend the model boundaries away from the area of interest.

4.2.2 General Transfer Methodology

The use of flow and transport data from other study areas to develop parameter distributions for flow and transport modeling of UGTA CAUs can be justified by examining specific similarities that may exist between various investigation areas. It must be shown that there is a sufficient similarity that exists between the two areas, taking into account the various factors mentioned in the previous subsection. A general approach for the transfer of data from one area to another may be accomplished using the following strategy:

- For each parameter of interest, sites need to be identified that may contain data of the same type.
- Degrees of similarity—in terms of geological setting, geographical distance, and rock types—need to be identified between the identified sites and Pahute Mesa.
- Once the sources of the flow and transport parameter data are identified, the factors affecting the specific parameter need to be clarified. For example, if it can be shown that a parameter is

influenced by lithology, then transfer of data from another HSU or another site with similar lithology would increase confidence in the use of transfered data.

- Finally, if sufficient data for the purpose of statistical comparison are present in the original study area, a comparison can be made of the datasets (data references are located within the specific data discussions, as appropriate). If it can be shown that the two datasets have comparable distributions, data from the original study can be augmented with those from other areas. While this approach is unlikely to substantially alter measures of central tendency, adding additional comparable data may provide increased confidence in the estimation of the range of uncertainty in the data.

4.2.3 YMP Data Transfer

The Yucca Mountain Site Characterization Project implemented one of the largest hydrologic and geologic characterization studies of volcanic rocks ever conducted. The proximity and similar hydrogeologic environment of the Yucca Mountain area and Pahute Mesa make it particularly attractive as a source of potential data for the UGTA modeling effort. A detailed rationale for the transfer of data from the YMP was provided in SNJV (2004a, Appendix B); however, a brief summary is presented here:

- Both areas are located in the SWNVF.
- Volcanic rocks in both areas are the result of similar depositional processes.
- Both areas contain similar lithologic units and even lithologic units from the same source area.
- Both areas have experienced similar types of alteration, including devitrification and zeolitization of volcanic material.
- Both areas have undergone similar types of regional tectonic stresses, resulting in a similarity in the two areas regional fracture orientations.
- Both have similar groundwater chemistry.

As a result of the two areas' similarities, the use of flow and transport parameter data from the Yucca Mountain area can be justified in helping to develop parameter distributions for the Pahute Mesa CAU flow modeling effort. Note that the data are actually transferred on an HSU-by-HSU basis. In others words, data for a given parameter are transferred only between HSUs that have relevant similar characteristics.

4.3 Data Analysis Methods and Limitations

For each dataset presented in this report, the data and method of analysis are described. Data limitations may be related to the level of data documentation, the data collection method, the data analysis method, or other factors (such as the scale of the data) that may limit confidence in the values. Within the discussion of each dataset, data limitations will be noted.

5.0 HYDRAULIC PARAMETER DATA

Hydraulic parameters play a vital role in simulating groundwater movement. Specifically, hydraulic conductivity and related parameters such as transmissivity and anisotropy are the most often used parameters in groundwater modeling. The storage coefficient is another hydraulic parameter of interest because it is needed for transient simulations of groundwater flow. This assessment provides a range of hydraulic conductivities and specific storage coefficients for the major HSUs in the Central and Western Pahute Mesa CAUs.

5.1 Objectives

The specific objectives for the hydraulic parameter assessment include the following:

- Compile and evaluate available hydraulic conductivity and specific storage data for use in the Pahute Mesa CAU flow modeling.
- Determine appropriate ranges and distributions of hydraulic conductivity and specific storage for the HSUs and HGUs of the PM-OV HFM with sufficient data.
- Identify whether outliers in the hydraulic conductivity distributions are associated with poor-quality data.
- Identify whether known faults are altering the rock properties by investigating correlations of hydraulic conductivity with distance to faults.
- Assess the relationship of hydraulic conductivity with depth.

5.2 Hydraulic Conductivity

Hydraulic conductivity is a parameter for groundwater flow modeling that determines the volumetric flow rate in response to the hydraulic gradient. Representative hydraulic conductivities for the formations to be modeled, at the scale over which the model is discretized, are integral to producing defensible model predictions. The values used for the hydraulic conductivities of HSUs in the simulation of groundwater flow and transport should be consistent with available information to provide confidence in the reasonableness of the simulations. The following subsections present the

analysis of hydraulic conductivity data that will be used to guide parameterization and calibration of the groundwater flow model.

It is acknowledged that reducing transmissivity estimates from well-testing data to hydraulic conductivity is problematic because the subsurface intervals contributing flow can be considerably smaller than the tested interval. However, large-scale groundwater models such as the Pahute Mesa CAU flow model simulate groundwater flow with transmissivity parameterized as hydraulic conductivity. The calibration approach for the Pahute Mesa CAU flow model will not directly use the hydraulic conductivity estimates obtained in this analysis. The model calibration will use transmissivity estimates as the calibration targets and the hydraulic conductivities derived from this analysis as a guide to the permissible range of values for hydraulic conductivity that will be optimized during model calibration.

5.2.1 Scales of Hydraulic Conductivity Measurements

Testing used to determine hydraulic conductivity is conducted at three generalized scales: laboratory scale, slug-scale aquifer test, and pump-scale aquifer test.

The laboratory scale comprises measurements made on small samples (typically of about 1,000- to 2,000-cubic centimeter volume) removed from the natural environment by various means and placed into a test apparatus in the laboratory. Rock/core samples tested are necessarily intact, and exclude features (such as fractures) that occur on larger scales or are not preserved in handling. The measurements generally represent the hydraulic conductivity of the intact rock matrix. Unconsolidated materials may be reasonably preserved in their natural state or repacked for testing. The laboratory-scale data are discussed as “core-scale data” throughout this section.

The slug- and packer-scale aquifer tests are conducted in situ on fairly short test intervals (typically in the range of about 50 to 500 ft in Pahute Mesa wells) using small volumes of water (less than 100- to several hundred gallons) to induce pressure pulses that equilibrate in a relatively short period (ranging from several seconds to several days). These methods test a relatively small volume of rock in the immediate area of the borehole, and the results may be substantially influenced by near-borehole conditions that reflect drilling damage to the formation and effects from the well completion. The small volumetric stress on the rock unit associated with these methods is insufficient to measure the hydraulic conductivity of large-scale fracture networks. The majority of hydraulic

conductivity data for Pahute Mesa is derived from slug-scale aquifer tests. A large number of slug-scale aquifer tests using packers were conducted to characterize emplacement boreholes for nuclear tests during the 1960s. Multiple tests were run over a series of short adjacent intervals along deep open boreholes to evaluate the variation of hydraulic conductivity in the rocks.

The pump-scale aquifer tests are conducted in situ on short to long well completion intervals (typically in the range of 100 to 1,000 ft or more) (30 to 300 m or more), moving relatively large volumes of water to induce pressure change and possibly dewatering responses in the test formation over relatively long periods of time (typically several hours to several days). These methods test much larger volumes of rock extending large distances from the borehole and may extend to observation wells. The response in the pumping well may be substantially affected by near borehole conditions reflecting drilling damage and non-linear losses in the well screen and pump string. However, responses measured in remote observation wells provide data unaffected by local formation damage and nonlinear flow. In addition, tests with observation wells can also provide directional property data. Depending on the length of the test, the test may reveal different aspects of the formation response that are related to time or distance from the well.

5.2.2 Hydraulic Conductivity Data Analysis

The hydraulic conductivity dataset is derived from several sources consisting of (1) single-well aquifer tests, including pump- and slug-scale aquifer tests performed on Pahute Mesa wells (Frus and Halford, 2018), (2) borehole flow logs including hydraulic conductivity with depth (Oberlander et al., 2007) and (3) numerical models of MWATs including hydraulic conductivity distributions within HSUs (Garcia et al., 2017). The single-well tests comprise the vast majority of the data and were primarily used in hydraulic conductivity analysis. The datasets from Oberlander et al. (2007) and Garcia et al. (2017) are presented apart from the single-well test datasets.

The single-well test dataset consists of 360 individual well completions and 1,468 analyses of transmissivity/hydraulic conductivity. The majority of the single-well data are slug-scale aquifer tests, which include 310 of the 360 aquifer tests. The remainder of the tests are constant or variable rate pump-scale aquifer tests. The number of aquifer tests analyzed was much greater than the number of actual tests because some responses to a water-level displacement were interpreted multiple times using different analytical models by different investigators. Frus and Halford (2018) standardized the aquifer test results and identified the best transmissivity estimate for each well. Generally,

International System of Units (SI) of measurement are used in this document. However, British Engineering units are used as well to be consistent with the units used in the source document (e.g., Frus and Halford [2018], and Fenelon et al. [2016]), which allow simple comparison of the analysis presented in both documents. The convention used is that the units found in the source document are stated first with a conversion of the units following in parentheses.

A large body of field data shows that formation hydraulic conductivity obtained from slug-scale aquifer tests is systematically lower than that obtained from pump-scale aquifer tests (Bradbury and Muldoon, 1990; Rovey and Cherkauer, 1995). Rovey and Cherkauer (1995), among others, have interpreted these results as a scale-dependency of hydraulic conductivity which is theoretically postulated (Dagan, 1986; Neuman, 1990). In contrast, Butler and Healey (1998) suggest that the difference in values is due to altered near-well conditions from incomplete development and vertical anisotropy.

Analysis of the hydraulic conductivity data included separate evaluations of pump- and slug-scale aquifer test data to determine statistics for the hydraulic conductivity within the HGUs and HSUs of the PM-OV HFM at each scale. Analysis of core-scale data is excluded because it is not appropriate data for use in large-scale modeling. Analysis was conducted using all data within the area defined by the Pahute Mesa PM-OV HFM. This provides the best site-specific data available for the Pahute Mesa HSUs and HGUs.

The analysis provides statistics for each HSU and HGU at each test scale, including the mean, standard deviation, and number of data points. Each dataset having a sufficient number of data points was evaluated for conformance to a log-normal distribution. The 95-percent confidence interval was calculated for datasets for which a distribution was determined. Summary tables are presented of the analysis results.

The incremental slug-scale aquifer test data with depth provide a dataset to evaluate the depth decay and the vertical variability of hydraulic conductivity within HSUs. These data may also be used to validate the general conceptual model of the hydraulic character of WTA and LFA HSUs. The variability of lithology with depth must be considered when analyzing the hydraulic conductivity data for depth decay because the variability of hydraulic character in different HGUs may mask the variability of hydraulic conductivity with depth dependence. For example, the change of hydraulic

conductivity across a TCU to WTA transition can be much greater than the change in hydraulic conductivity with depth within a continuous TCU or WTA section.

5.2.2.1 Methodology

This subsection summarizes the approach and methods used during the assessment of the hydraulic parameter dataset for the Pahute Mesa CAUs. The following approach was used to define ranges for hydraulic conductivity for the HSUs and HGUs in the Pahute Mesa PM-OV HFM:

- Transmissivity data were compiled from Frus and Halford (2018). Information associated with each entry included the location, tested interval effective open interval (EOI) top and bottom, type of test, method of analysis, HSU and HGUs within the tested interval, data quality, and the source of the information.

- Hydraulic conductivity is the unit value for formation transmissivity. The pump- and slug-scale aquifer test data are reported as transmissivity and the transmissivity values are applied to the HSUs and HGUs as hydraulic conductivity by dividing the value of transmissivity by the tested interval thickness. The mid-point depth of the test interval is used to assign the test depth.

- In fractured rock materials such as those present within the Pahute Mesa CAUs, three types of hydraulic conductivities can be defined: bulk hydraulic conductivity, fracture hydraulic conductivity, and matrix hydraulic conductivity. For the pump- and slug-scale aquifer test data, a generalized measurement over a vertical interval is termed the bulk transmissivity. In cases where the formations are fractured, the bulk transmissivity will be similar to the fracture-associated transmissivity because the matrix transmissivity is significantly lower.

- Within each scale-dependent dataset, the data were further grouped by HSU, HGU, and HGU within each HSU. A nominal hydraulic conductivity was identified for each data grouping. Often the tested interval will contain multiple HSUs and HGUs. Data for each HSU or HGU were analyzed using various threshold fractions of HSU or HGU within the EOI (e.g., 0.5, 0.75, and 1.0) to identify the HSU or HGU that is represented by the test. Increasing the threshold fraction significantly reduces the available data for each HSU or HGU, and a fraction of 0.75 was selected as the best compromise of retaining sufficient quantity of data and retaining data that adequately represent the HSU or HGU. Where flow logging data are available, the logging under stressed conditions is also used to determine the hydraulic conductivity within individual HSUs (Oberlander et al., 2007).

- In some cases, more than one aquifer test or interpretation of an aquifer test is available for a well completion. The single best aquifer test results for each well, as identified by Frus and Halford (2018), was used to evaluate the hydraulic conductivity. The hydraulic conductivity data were then transformed to log base 10 values for analysis based on the expectation of a log-normal distribution for this property. The scale-specific datasets were then used for

various other analyses, including the spatial variability of hydraulic conductivity and the depth dependence of hydraulic conductivity, as appropriate.

- The resulting sets of unique location and depth-specific hydraulic conductivity values were then statistically analyzed to determine the range, mean, standard deviation, correspondence to a log-normal probability distribution, and the 95-percent confidence interval where there were sufficient data. The results are presented in tables and displayed graphically.

Typically, hydraulic conductivity variability has been found to be distributed according to a log-normal distribution (Neuman, 1987). Where there were sufficient data (10 data points), the datasets for each HSU at each scale were tested for conformance with a log-normal distribution. The Kolmogorov-Smirnov (K-S) statistic was calculated for each grouping. The K-S statistic is a measure of the maximum difference, in probability space, between the empirical cumulative density function (CDF) and the assumed theoretical CDF (Benjamin and Cornell, 1970). An estimate of the range of uncertainty in the log-normal parameters can be determined from the K-S test statistic for an assumed level of significance. The K-S statistic upper and lower bounds were calculated at the 5-percent level of significance and were plotted along with the empirical data and fit distribution.

The spatial distribution of the hydraulic conductivity data is discussed first to show the extent to which the available data represent the Pahute Mesa CAUs. Figure 5-1 is a map showing the locations of wells and boreholes for which hydraulic conductivity (or permeability) data are available. This constitutes all the data identified for Pahute Mesa CAUs that are within the PM-OV HFM. The locations are identified with two different symbols corresponding to the scale of test information (pump- or slug-scale aquifer test). In some cases, both pump- and slug-scale aquifer test data are available at a single location. The data are not uniformly distributed throughout the area of the PM-OV HFM. Rather, the slug-scale aquifer test data are clustered in areas where nuclear tests were conducted. The pump-scale aquifer test data cover a larger area and extend into the area southwest of the nuclear testing along the flow path to the discharge areas in Oasis Valley, and largely represent the UGTA Phase I and II wells.

5.2.2.2 Analysis Results

The single-well testing interrogated approximately 237,000 linear feet of open borehole. Testing data are only available for 37 of 77 HSUs and 7 of the 9 HGUs within the PM-OV HFM.

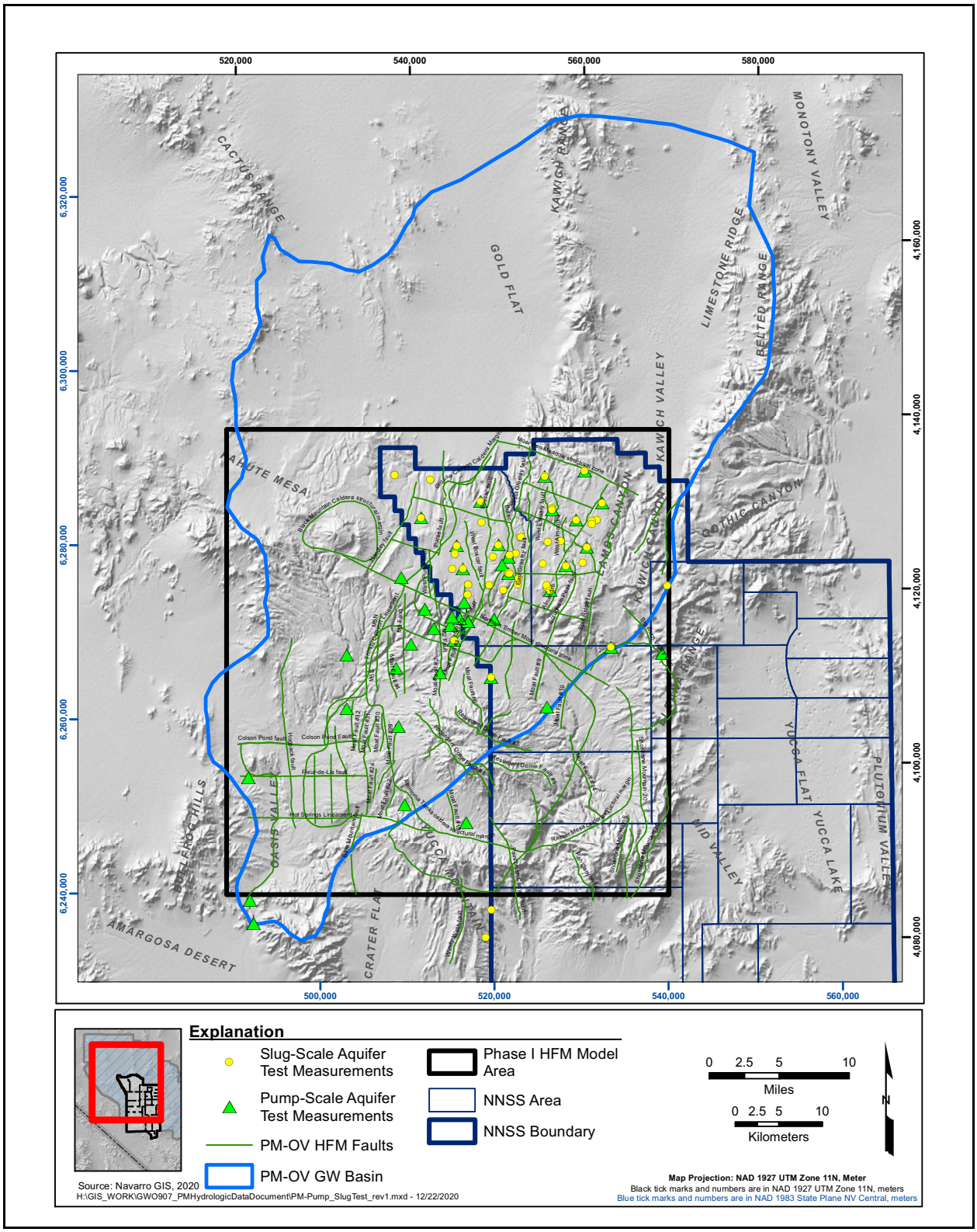

Figure 5-1
Locations of Wells and Boreholes with Hydraulic Conductivity Data

Data from wells located within the PM-OV HFM area were sorted into individual datasets for each scale of test, and then sorted into groups for each HSU, HGU, and HGU within HSU. Probability distributions were evaluated for log normality at the K-S 5-percent level of significance for each group with sufficient data.

HSU Groupings

Table 5-1 summarizes the fraction each HSU occupies within the total length of the tested open borehole from all tested wells. The BRA HSU occupies the largest tested fraction (0.35) of the total tested interval length; and the PBRCM, BFCU, CHZCM, and CHLFA HSUs additionally occupy large fractions compared to the other HSUs (0.15, 0.10, 0.082, and 0.065; respectively).

Table 5-1
Aquifer Test Interval Total Thickness Fraction of Each HSU
(Page 1 of 2)

HSU	HSU Fraction of All Test Intervals	HSU	HSU Fraction of All Test Intervals	HSU	HSU Fraction of All Test Intervals
BRA	3.41E-01	LPCU	1.48E-02	SPA	2.27E-03
PBRCM	1.48E-01	FCCM	1.41E-02	TMWTA	1.80E-03
BFCU	1.00E-01	THCU	6.87E-03	THCM	1.39E-03
CHZCM	8.23E-02	FCWTA	6.58E-03	BWWTA	1.17E-03
CHLFA	6.45E-02	BWCU	5.83E-03	FCCU	1.12E-03
IA	2.94E-02	TMUWTA	5.64E-03	MPCU	8.76E-04
ATWTA	2.73E-02	FCULFA	5.49E-03	PBPCU	6.13E-04
CFCM	2.71E-02	BA	4.86E-03	PLFA	3.63E-04
TCA	1.91E-02	ATCU	4.80E-03	KA	1.69E-04
RMWTA	1.76E-02	CPA	4.30E-03	CHVTA	1.60E-04
CFCU	1.72E-02	TCVA	3.94E-03	TMLVTA	1.80E-06

Table 5-1
Aquifer Test Interval Total Thickness Fraction of Each HSU
(Page 2 of 2)

HSU	HSU Fraction of All Test Intervals	HSU	HSU Fraction of All Test Intervals	HSU	HSU Fraction of All Test Intervals
TSA	1.66E-02	THLFA	3.76E-03		
UPCU	1.56E-02	LCA3	2.72E-03		

ATCU = Argillic tuff confining unit
ATWTA = Ammonia Tanks welded-tuff aquifer
BA = Benham aquifer
BFCU = Bullfrog confining unit
BRA = Belted Range aquifer
BWCU = Buttonhook Wash confining unit
BWWTA = Buttonhook Wash welded-tuff aquifer
CFCM = Crater Flat composite unit
CFCU = Crater Flat confining unit
CHLFA = Calico Hills lava-flow aquifer
CHVTA = Calico Hills vitric-tuff aquifer
CHZCM = Calico Hills zeolitic composite unit
CPA = Comb Peak aquifer
FCCM = Fortymile Canyon composite unit
FCCU = Fluorspar Canyon confining unit
FCULFA = Fortymile Canyon upper lava-flow aquifer
FCWTA = Fortymile Canyon welded-tuff aquifer
IA = Inlet aquifer
KA = Kearsarge aquifer
LCA3 = Lower carbonate aquifer-thrust plate
LPCU = Lower Paintbrush confining unit
MPCU = Middle Paintbrush confining unit
PBPCU = Post-Benham Paintbrush confining unit
PBRCM = Pre-Belted Range composite unit
PLFA = Paintbrush lava-flow aquifer
RMWTA = Rainier Mesa welded-tuff aquifer
SPA = Scrugham Peak aquifer
TCA = Tiva Canyon aquifer
TCVA = Thirsty Canyon volcanic aquifer
THCM = Tannenbaum Hill composite unit
THCU = Tannenbaum Hill confining unit
THLFA = Tannenbaum Hill lava-flow aquifer
TMLVTA = Timber Mountain lower vitric-tuff aquifer
TMUWTA = Timber Mountain upper welded-tuff aquifer
TMWTA = Timber Mountain welded-tuff aquifer
TSA = Topopah Spring aquifer
UPCU = Upper Paintbrush confining unit

Table 5-2 summarizes the hydraulic conductivity data grouped by HSU from the pump-scale aquifer tests. Pump-scale aquifer test data are only available for 11 HSUs, and are only available for aquifer or composite unit type HSUs. The largest hydraulic conductivity was seen in the TSA HSU, and the lowest hydraulic conductivity was seen in the PBRCM HSU. The BRA HSU has 7 pump-scale aquifer tests and is the HSU with the largest number of tests meeting the criteria of each interval being composed of at least 75 percent of the HSU. Figure 5-2 illustrates the experimental data CDF for the BRA with the K-S bounds for the HSU grouped pump-scale aquifer test. The number of hydraulic conductivity values from the other HSUs is insufficient for evaluating log normality.

Table 5-3 summarizes the hydraulic conductivity data grouped by HSU from the slug-scale aquifer tests. An adequate amount of data to characterize the HSU is only available for the BRA, PBRCM, BFCU, CHLFA, CHZCM, and IA HSUs. Data are limited to a few data points each for the other HSUs. The mean and standard deviations of the slug-scale aquifer test hydraulic conductivities are very similar for the HSUs with sufficient data for fitting distributions, regardless of whether the HSU is an aquifer, composite unit, or confining unit. The hydraulic conductivity values are generally

Table 5-2
Pump-Scale Aquifer Test Hydraulic Conductivity Data Analyzed by HSUs

HSU	Mean Log10 K (ft/day)	Standard Deviation Log10 Ks (ft/day)	Number of Data Points
TSA	1.71E+00	NA	1
ATWTA	1.32E+00	NA	1
FCULFA	1.04E+00	NA	1
BA	1.04E+00	NA	1
CPA	7.29E-01	NA	1
CHLFA	4.69E-01	6.41E-01	2
BRA	2.08E-01	9.35E-01	7
LCA3	5.93E-02	NA	1
TCA	-3.81E-01	1.42E+00	3
RMWTA	-4.88E-01	1.87E+00	3
PBRCM	-1.23E+00	8.98E-01	2

K = Hydraulic conductivity
NA = Not applicable

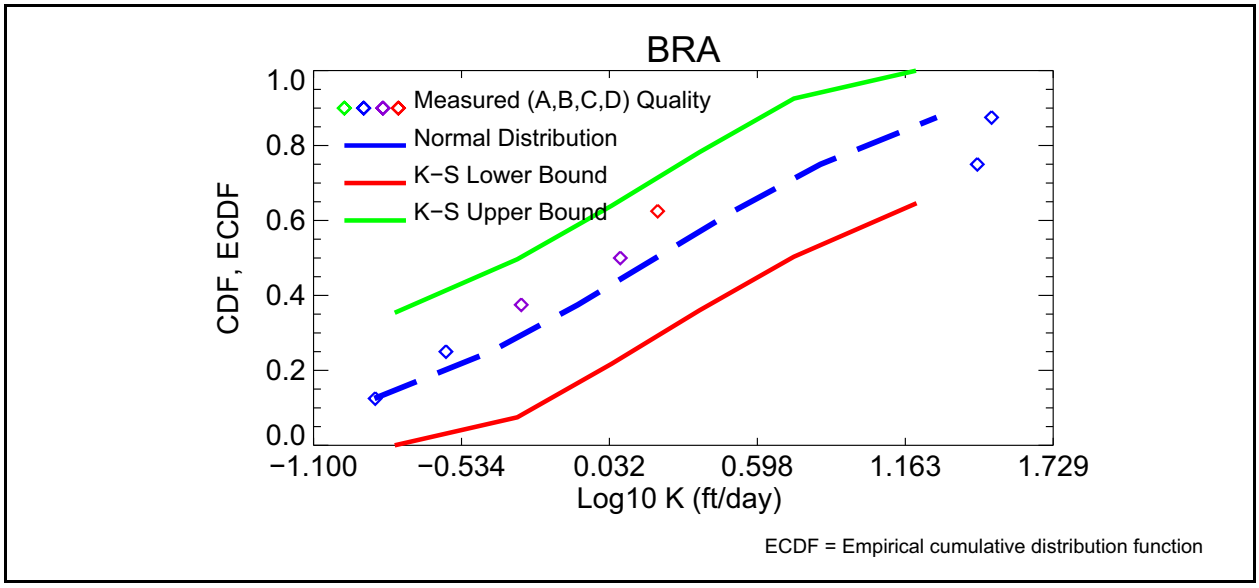

Figure 5-2
Hydraulic Conductivity CDF from Pump-Scale Aquifer Tests within HSU Groupings

within an order of magnitude of each other. Figure 5-3 illustrates the experimental data CDFs with the K-S bounds for the HSU grouped slug-scale aquifer test data for HSUs. The measured data are plotted

Table 5-3
Slug-Scale Aquifer Test Hydraulic Conductivity Data Analyzed by HSUs

HSU	Mean Log10 K (ft/day)	Standard Deviation Log10 Ks (ft/day)	Number of Data Points	Log Normal [a]
ATWTA	-8.60E-01	1.15E+00	7	NA
TCA	-1.18E+00	NA	1	NA
CHVTA	-1.27E+00	NA	1	NA
THCU	-1.30E+00	6.20E-01	3	NA
CHLFA	-1.36E+00	5.56E-01	24	Yes
IA	-1.65E+00	7.76E-01	13	Yes
RMWTA	-1.84E+00	7.53E-01	3	NA
CHZCM	-1.87E+00	7.29E-01	24	Yes
CFCM	-1.87E+00	6.60E-01	9	NA
PLFA	-1.88E+00	5.34E-01	3	NA
UPCU	-1.96E+00	2.19E-01	4	NA
ATCU	-1.98E+00	3.96E-01	2	NA
BRA	-2.00E+00	9.20E-01	107	Yes
PBPCU	-2.00E+00	NA	1	NA
CFCU	-2.05E+00	1.02E+00	3	NA
LPCU	-2.18E+00	NA	1	NA
PBRCM	-2.19E+00	1.21E+00	27	Yes
BFCU	-2.30E+00	9.10E-01	25	Yes
KA	-2.34E+00	5.70E-01	2	NA
THLFA	-2.82E+00	NA	1	NA
TSA	-3.86E+00	NA	1	NA

[a] Log normality is evaluated for distributions with 10 points or greater.

in Figure 5-3 with a color code denoting the quality of the data. The data of low quality are distributed throughout the hydraulic conductivity distributions and do not explain outliers in the distributions.

HGU Groupings

Table 5-4 summarizes the fraction of total tested interval thickness that each HGU occupies. The LFA HGU occupies the largest fraction (0.40) of the total test interval thickness. The TCU and WTA occupy the majority of the remaining length and have fractions of 0.37 and 0.21, respectively.

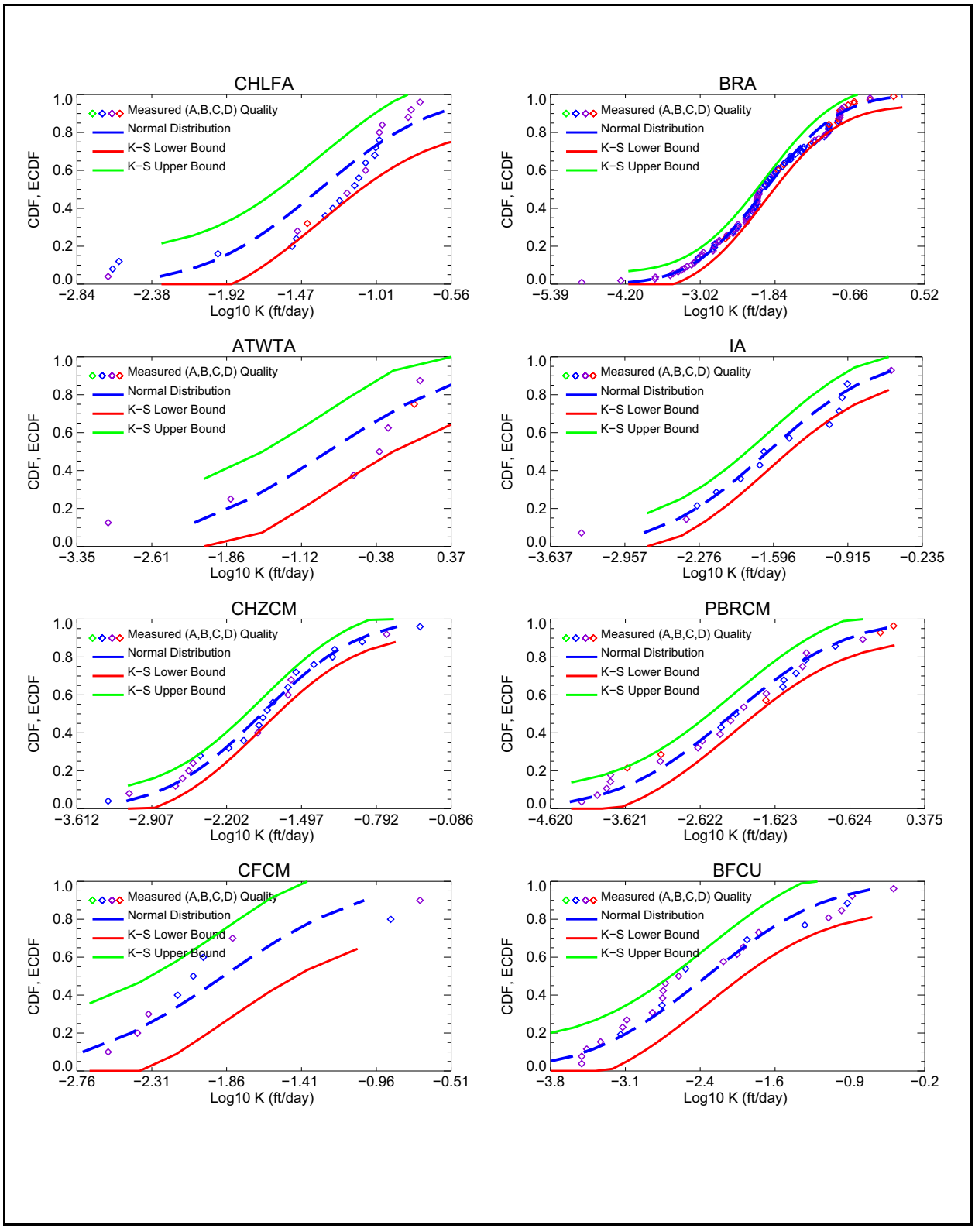

Figure 5-3
Hydraulic Conductivity CDF from Slug-Scale Aquifer Tests within HSU Groupings

Table 5-4
Aquifer Test Interval Total Thickness Fraction of Each HGU

HGU	Fraction of Total EOI Thickness in Each HGU	HGU	Fraction of Total EOI Thickness in Each HGU
LFA	4.05E-01	ICU	4.91E-03
TCU	3.68E-01	CA	2.72E-03
WTA	2.14E-01	AA	2.91E-04
VTA	5.53E-03		

Tables 5-5 and 5-6 summarize the pump- and slug-scale aquifer test hydraulic conductivity data grouped by HGU, respectively. Figures 5-4 and 5-5 illustrate the experimental CDFs of the pump- and slug-scale aquifer test hydraulic conductivity data, respectively. The LFA mean hydraulic conductivity is slightly higher than the WTA, but the two HSUs are hydraulically similar based on the variability seen in the data. Three pump-scale aquifer tests were performed in a well with the EOI composed of greater than 75 percent confining unit (TCU). The average hydraulic conductivity of the TCU is moderately lower than the LFA and WTA HGUs.

Table 5-5
Pump-Scale Aquifer Test Hydraulic Conductivity Data Analyzed by HGUs

HGU	Mean Log10 K (ft/day)	Standard Deviation Log10 Ks (ft/day)	Number of Data Points	Log Normal [a]
LFA	6.54E-01	7.73E-01	10	Yes
WTA	9.78E-02	1.57E+00	8	NA
CA	0.087	NA	1	NA
TCU	-1.38E-02	1.06E+00	3	NA

[a] Log normality is evaluated for distributions with 10 points or greater.

The mean hydraulic conductivity of the slug-scale aquifer test data grouped by HGU are very similar among the HGUs and are generally within an order of magnitude of each other. This finding is consistent with Garcia et al. (2017), in that most HSUs in the Bench area are heterogeneous and the aquifer and confining unit HSUs can have similar average hydraulic behaviors.

Table 5-6
Slug-Scale Aquifer Test Hydraulic Conductivity Data Analyzed by HGUs

HGU	Mean Log10 K (ft/day)	Standard Deviation Log10 Ks (ft/day)	Number of Data Points	Log Normal [a]
VTA	-1.48E+00	3.74E-01	2	NA
LFA	-1.68E+00	8.88E-01	102	Yes
ICU	-1.86	NA	1	NA
WTA	-1.96E+00	1.03E+00	47	Yes
TCU	-2.23E+00	8.40E-01	86	Yes

[a] Log normality is evaluated for distributions with 10 points or greater.

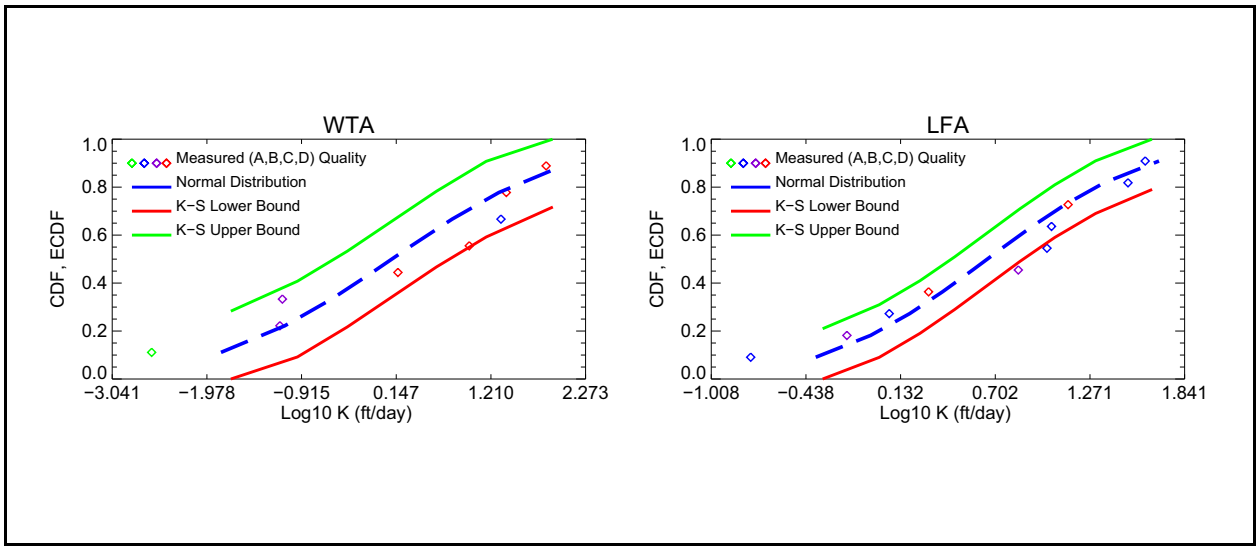

Figure 5-4
Hydraulic Conductivity CDF from Pump-Scale Aquifer Tests within HGU Groupings

HGU Groupings within HSUs

Table 5-7 summarizes the hydraulic conductivity data, and Figure 5-6 illustrates the experimental CDFs of the hydraulic conductivity data grouped by HGU within HSUs for the slug-scale aquifer tests. An adequate amount of data for discerning HGU hydraulic conductivity trends within HSUs is only available from the slug-scale aquifer testing data. The mean hydraulic conductivity among groupings from slug-scale aquifer test data are generally similar. The pump-scale aquifer test data are too sparse for ascertaining trends among HGUs within HSUs.

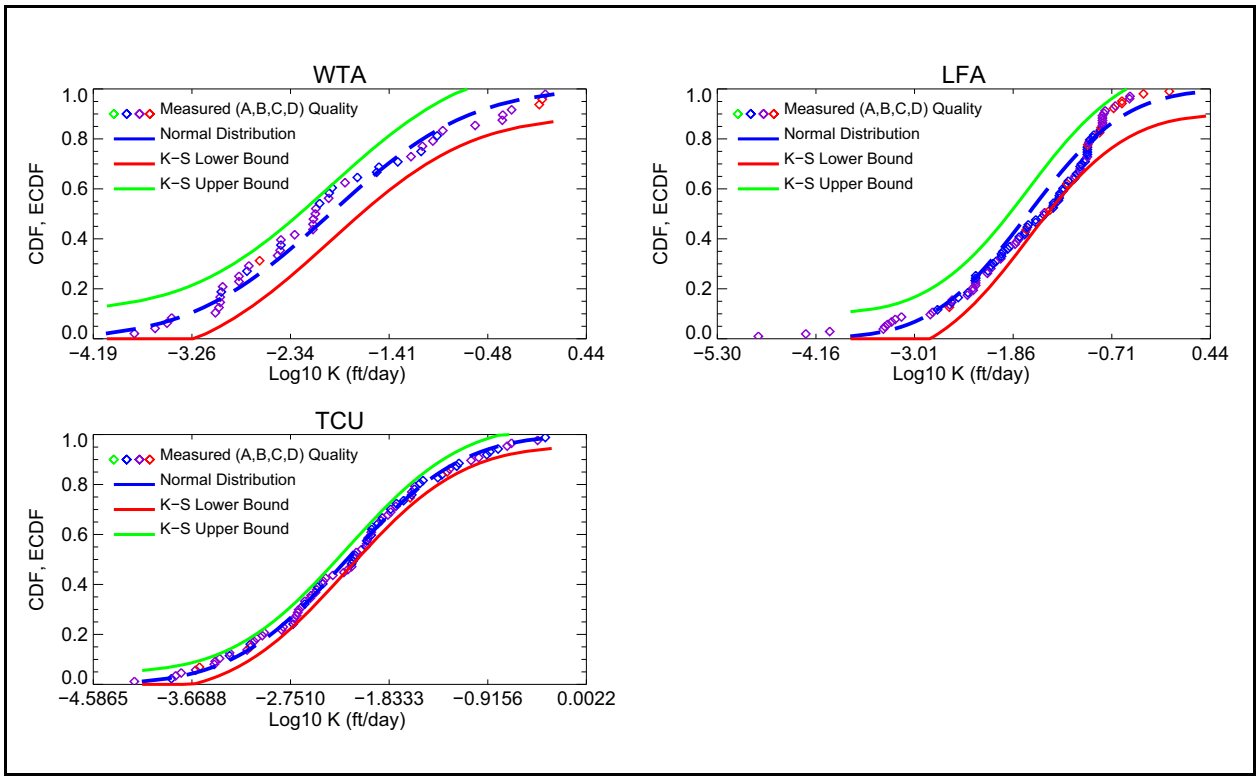

Figure 5-5
Hydraulic Conductivity CDF from Slug-Scale Aquifer Tests within HGU Groupings

5.2.2.3 Flow Logging Estimates of Hydraulic Conductivity

Many of the Pahute Mesa wells have flow log information obtained from aquifer testing. During well development and testing, borehole flow logging was performed while the wells were being pumped. The resulting logs can be used to infer flowing intervals with depth. Flow logging of the Phase I ER-EC wells was performed in the pumped completion. However, flow logging of the Phase II wells was performed within the piezometers that are open to the annular space between the main screen and the formation. Russell et al. (2011) performed an analysis of the flow logs collected under stressed conditions at ER-20-8-2 to determine the extent to which measurements of flow within the piezometer can be representative of the entire borehole and concluded that calculating horizontal hydraulic conductivities from the available data is unwarranted because any such calculation would be subject to large uncertainties. Halford (2011) simulated flow from the formation to the main well through the annular fill and piezometers for ER-20-8-2 and ER-EC-11, and reached similar conclusions. Because the flow logging performed in the piezometers is unreliable, flow logging data from the Phase II wells cannot be used to estimate the hydraulic conductivity distribution within the well completion.

Table 5-7
Slug-Scale Aquifer Test Hydraulic Conductivity Data Analyzed by HGUs within HSUs

HSU	Mean Log10 K (ft/day)	Standard Deviation Log10 Ks (ft/day)	Number of Data Points	Mean Log10 K (ft/day)	Standard Deviation Log10 Ks (ft/day)	Number of Data Points	Mean Log10 K (ft/day)	Standard Deviation Log10 Ks (ft/day)	Number of Data Points
	WTA			LFA			TCU		
ATCU	-1.93E+00	3.32E-01	2	NA	NA	NA	NA	NA	NA
ATWTA	-8.60E-01	1.15E+00	7	NA	NA	NA	NA	NA	NA
BFCU	-1.31E+00	6.18E-01	5	-2.79E+00	6.09E-01	16	NA	NA	NA
BRA	-2.26E+00	8.83E-01	31	-1.77E+00	9.67E-01	54	-2.31E+00	2.96E-01	4
CFCM	NA	NA	NA	-2.23E+00	2.95E-01	5	-2.07E+00	1.10E-01	2
CFCU	NA	NA	NA	NA	NA	NA	-1.67E+00	1.10E+00	2
CHLFA	NA	NA	NA	-1.25E+00	4.34E-01	20	-2.63E+00	1.95E-02	2
CHVTA	NA	NA	NA	NA	NA	NA	-1.271	NA	1
CHZCM	NA	NA	NA	NA	NA	NA	-1.87E+00	7.43E-01	23
IA	-1.328	NA	1	-1.66E+00	8.05E-01	12	NA	NA	NA
KA	NA	NA	NA	-2.741	NA	1	-1.937	NA	1
LPCU	NA	NA	NA	NA	NA	NA	-2.117	NA	1
PBPCU	NA	NA	NA	NA	NA	NA	-2	NA	1
PBRCM	-1.35E+00	2.13E-01	2	-2.02E+00	2.80E+00	2	-2.42E+00	1.12E+00	16
PLFA	-1.944	NA	1	-1.85E+00	7.53E-01	2	NA	NA	NA
RMWTA	-1.81E+00	8.06E-01	3	NA	NA	NA	NA	NA	NA
TCA	-1.109	NA	1	NA	NA	NA	NA	NA	NA
THCU	NA	NA	NA	NA	NA	NA	-1.27E+00	6.55E-01	3
THLFA	NA	NA	NA	-2.824	NA	1	NA	NA	NA
TSA	-3.802	NA	1	NA	NA	NA	NA	NA	NA
UPCU	NA	NA	NA	NA	NA	NA	-1.96E+00	2.19E-01	4

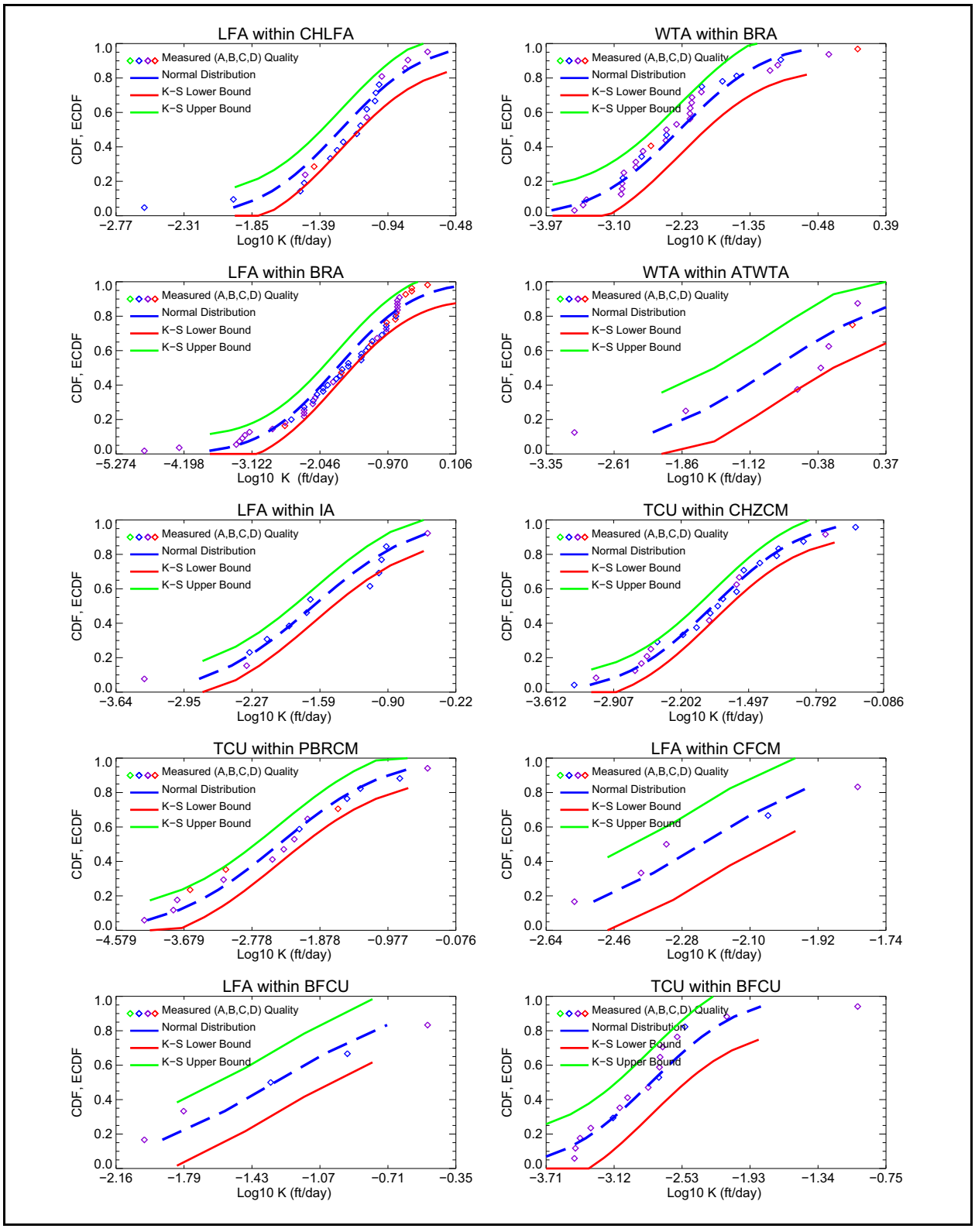

Figure 5-6
Hydraulic Conductivity CDF from Slug--Scale Aquifer Tests for HGU within HSU Groupings

Oberlander et al. (2007) calculated hydraulic conductivity with depth for the Phase I ER-EC wells using the borehole flow logging data and associated the hydraulic conductivity values with specific hydrogeologic characteristics such as stratigraphic unit, HSU, HGU, lithology, and secondary mineral alteration. Table 5-8 presents average hydraulic conductivity by well and Phase I HFM HSUs, and Table 5-9 presents average hydraulic conductivity by well and Phase I HFM HGUs.

Table 5-8
Hydraulic Conductivity Data by Phase I HFM HSUs Estimated by Oberlander et al. (2007, Modified from Table 31)

Well	HSU Log10 Average K (ft/day)								
	FCCM	TMCM	TCVA	TMA	BA	UPCU	TCA	TSA	CFCM
ER-EC-1	NA	NA	NA	NA	2.0	1.1	0.9	1.4	1.6
ER-EC-2a	-0.2	-0.2	NA	NA	NA	NA	NA	NA	NA
ER-EC-4	NA	NA	2.0	1.7	NA	NA	NA	NA	NA
ER-EC-5	NA	1.8	NA	NA	NA	NA	NA	NA	NA
ER-EC-6	NA	NA	NA	NA	1.2	NA	NA	NA	NA
ER-EC-7	1.8	NA	NA	NA	NA	NA	NA	NA	NA
ER-EC-8	1.7	1.3	NA	NA	NA	NA	NA	NA	NA

TMA = Timber Mountain aquifer
TMCM = Timber Mountain composite unit

Table 5-9
Hydraulic Conductivity Data by Phase I HFM HGUs Estimated by Oberlander et al. (2007, Modified from Table 30)

Well	HGU Average Log10 K (ft/day)			
	WTA	TCU	LFA	AA
ER-EC-1	1.2	1.1	2.0	NA
ER-EC-2a	-0.9	-0.2	NA	-0,5
ER-EC-4	1,7	NA	2.0	1.4
ER-EC-5	1.8	NA	NA	NA
ER-EC-6	NA	NA	1.2	NA
ER-EC-7	NA	NA	1.8	NA
ER-EC-8	NA	1.7	NA	NA

Oberlander et al. (2007) summarized that most of the HSUs do not have an association with hydraulic conductivity, and the average values for WTA, LFA, and TCU HGUs are similar. The similarity of

HGUs is possibly indicating that the hydraulic conductivity of fractures is similar among the volcanic HGUs and that the frequency of fractures determines hydraulic conductivity. Furthermore, the Oberlander et al. (2007) analysis by lithologic unit found the average hydraulic conductivity seems to be unaffected by the degree of welding in tuff. The nonwelded tuff, partly welded tuff, moderately welded tuff, and densely welded tuff have hydraulic conductivity values over similar ranges. However, the average hydraulic conductivity values for lava are generally greater than for other lithologic units (Oberlander et al., 2007).

5.2.2.4 Numerical Modeling Estimates of Hydraulic Conductivity

Phase II data collection program included drilling and testing of 11 new wells that are downgradient of the testing locations in Area 20. Water levels in these wells, along with other Pahute Mesa wells, have been measured continuously with pressure transducers by Navarro and USGS. Water-level observations during well development and aquifer testing in these wells can be interpreted as MWATs (see Section 9.0). Garcia et al. (2017) performed simultaneous interpretation of the 16 MWATs to estimate hydraulic properties on Pahute Mesa. Hydraulic properties of aquifers and confining units were estimated by interpreting drawdowns from the MWATs using a 3-D hydrogeologic framework and multiple numerical groundwater-flow models. Individual models for each MWAT were simultaneously calibrated using identical hydrogeologic properties.

The numerical modeling of Garcia et al. (2017) used a modified version of the PM-OV HFM. The existing 55 HSUs in the PM-OV HFM were subdivided and grouped into 22 modified HSUs (mHSUs) so that groundwater-flow models could reproduce the observed hydraulic responses between pumping and observation wells. Hydraulic properties within each mHSU were spatially variable and distributed with pilot points during model calibration (RamaRao et al., 1995).

Most mHSUs evaluated were hydraulically similar in the area investigated by the 16 MWATs, where simulated drawdown exceeded 0.05 ft (Garcia et al., 2017). Hydraulic conductivity distributions in the mHSUs typically spanned between more than 2 and more than 4 orders of magnitude for the 75th and 95th percentiles, respectively (Table 5-10 and Figure 5-7). Ranges of hydraulic conductivity in mHSUs overlapped greatly among many mHSUs, and the differences between HSUs were considered small relative to the variability within individual mHSUs (Garcia et al., 2017).

Table 5-10
Simulated Hydraulic-Conductivity Estimates for mHSUs from Garcia et al. (2017, Table 10)

mHSU	Geometric Mean K (ft/day)	Standard Deviation (ft/day)	mHSU	Geometric Mean K (ft/day)	Standard Deviation (ft/day)
mFCCM1	0.2	8	mUPCU	0.1	7
mFCCU1	<0.002	98	mMPCU	0.2	9
mFCCM2	0.5	14	mTCA	0.3	8
mFCCU2	<0.001	87	mLPCU	0.07	5
mFCCM3	0.3	5	mTSA	0.2	6
mFCCU3	<0.001	15	mCHLFA1	3	4
mRMWTA1	0.07	8	mCHLFA5	0.9	12
mRMWTA2	2	9	mCHZCM	1	6
mRMCM	<0.001	11	mCFCM	0.4	5
mFCCU	0.2	5	mCCU	0.002	12
mCPA	3	9			

5.2.2.5 Depth Decay of Hydraulic Conductivity

The hydraulic conductivity is expected to decrease with depth in many situations because the pore spaces, or fractures, through which water flows are expected to close under the increasing overburden pressure at greater depths. Additionally, deeper units are generally older and may have greater mineral precipitation or alteration that seals pore space. Depth versus hydraulic conductivity trends may be specific to individual HSUs or HGUs according to variations in physical properties affecting the hydraulic conductivity and the response to increasing effective stress with depth. Because much of the slug-scale aquifer testing consisted of multiple tests in each borehole using packers over short adjacent intervals, it possible to evaluate depth decay at specific well locations.

Figures 5-8a through 5-8c illustrate the hydraulic conductivity data versus depth for each well analyzed. A decreasing linear trend is frequently observed in the hydraulic conductivity with increasing depth, although the data show great scatter. The depth versus hydraulic conductivity is plotted for data in the dominant HGU for each well with multiple hydraulic conductivity measurements. The depth-dependent hydraulic conductivity relationship is more obscure when data from many wells within each HGU are viewed in aggregate. A trend of decreasing hydraulic

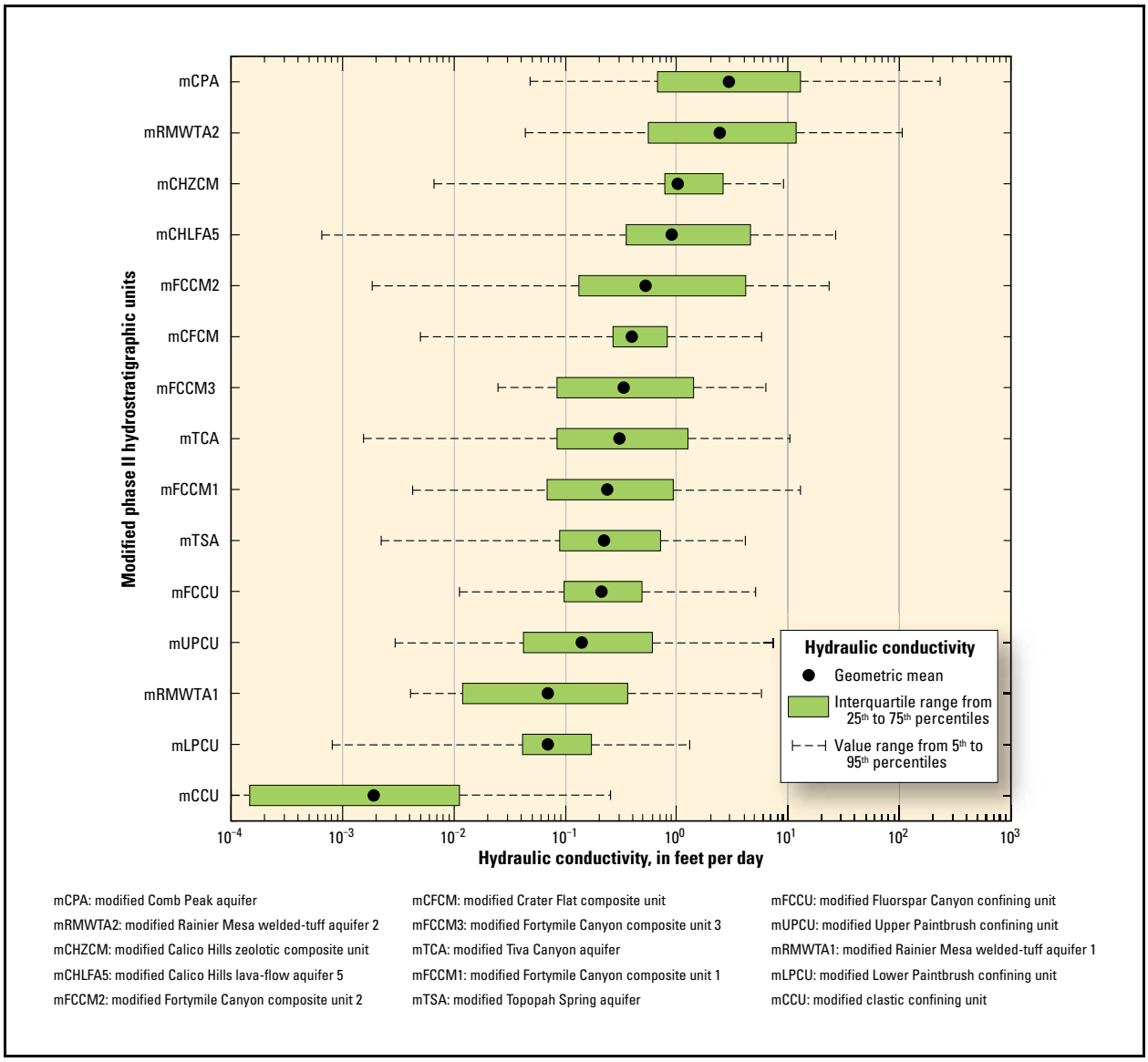

Figure 5-7
Estimated Hydraulic Conductivity Distributions for Modified HSUs in the Area Investigated by 16 MWATs as Estimated by Garcia et al. (2017, Figure 24)

conductivity with depth was seen in 31 of the 40 of the wells analyzed when the slug-scale aquifer test data were plotted for the each HGU.

Figure 5-9 presents the hydraulic conductivity versus depth from pump- and slug-scale aquifer testing. Very low hydraulic conductivity occurs at all tested depths, but the highest hydraulic conductivity values (in excess of 1 ft/day [0.3048 m/day]) occur within 4,000 ft (1,220 m) of the surface. Hydraulic conductivity below 6,000 ft bgs (1,800 m) is less than 0.1 ft/day (0.03 m/day). The following approach to depth dependence of hydraulic conductivity is being proposed for use in the

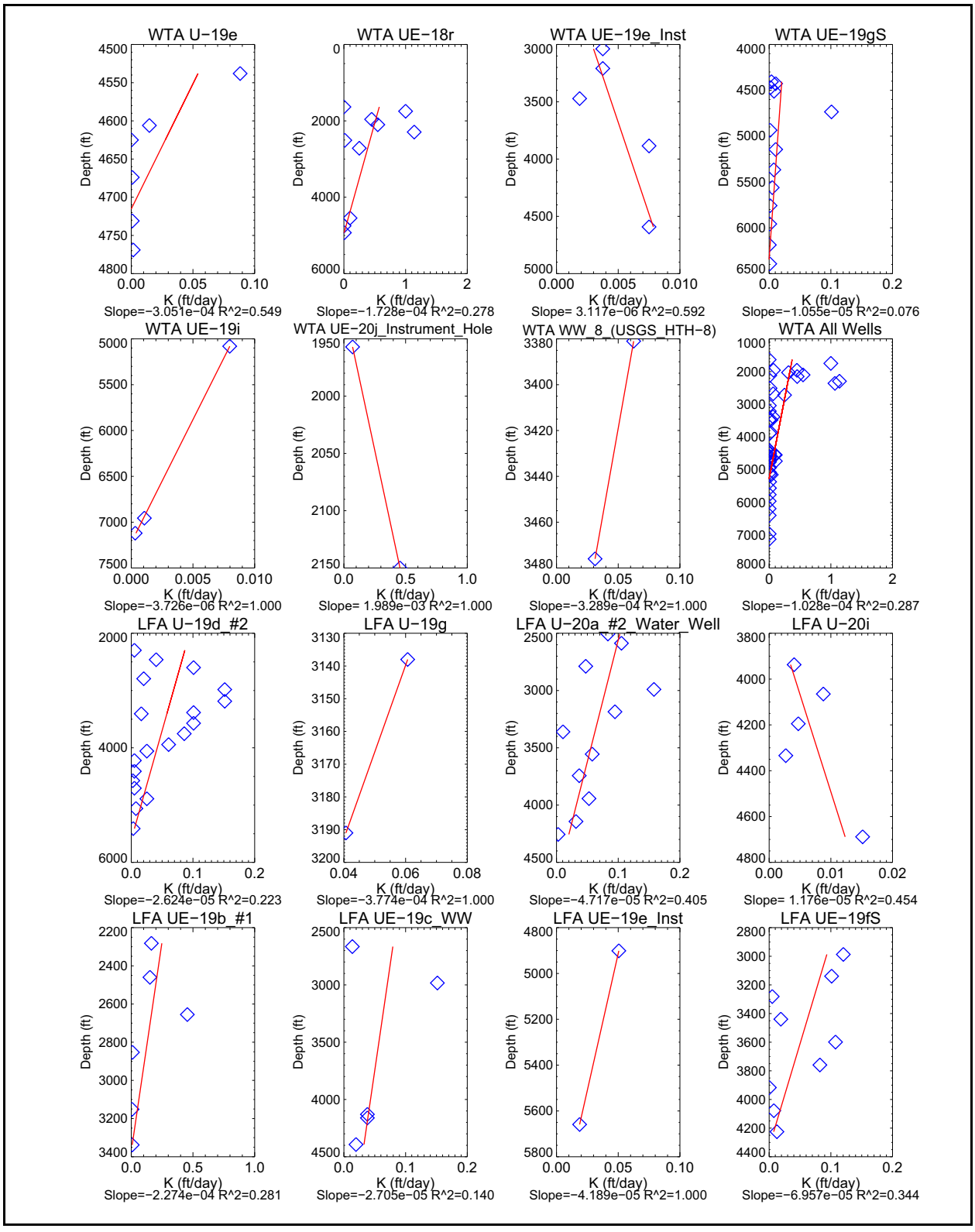

Figure 5-8a
Hydraulic Conductivity versus Depth for Dominant HGUs within Each Well

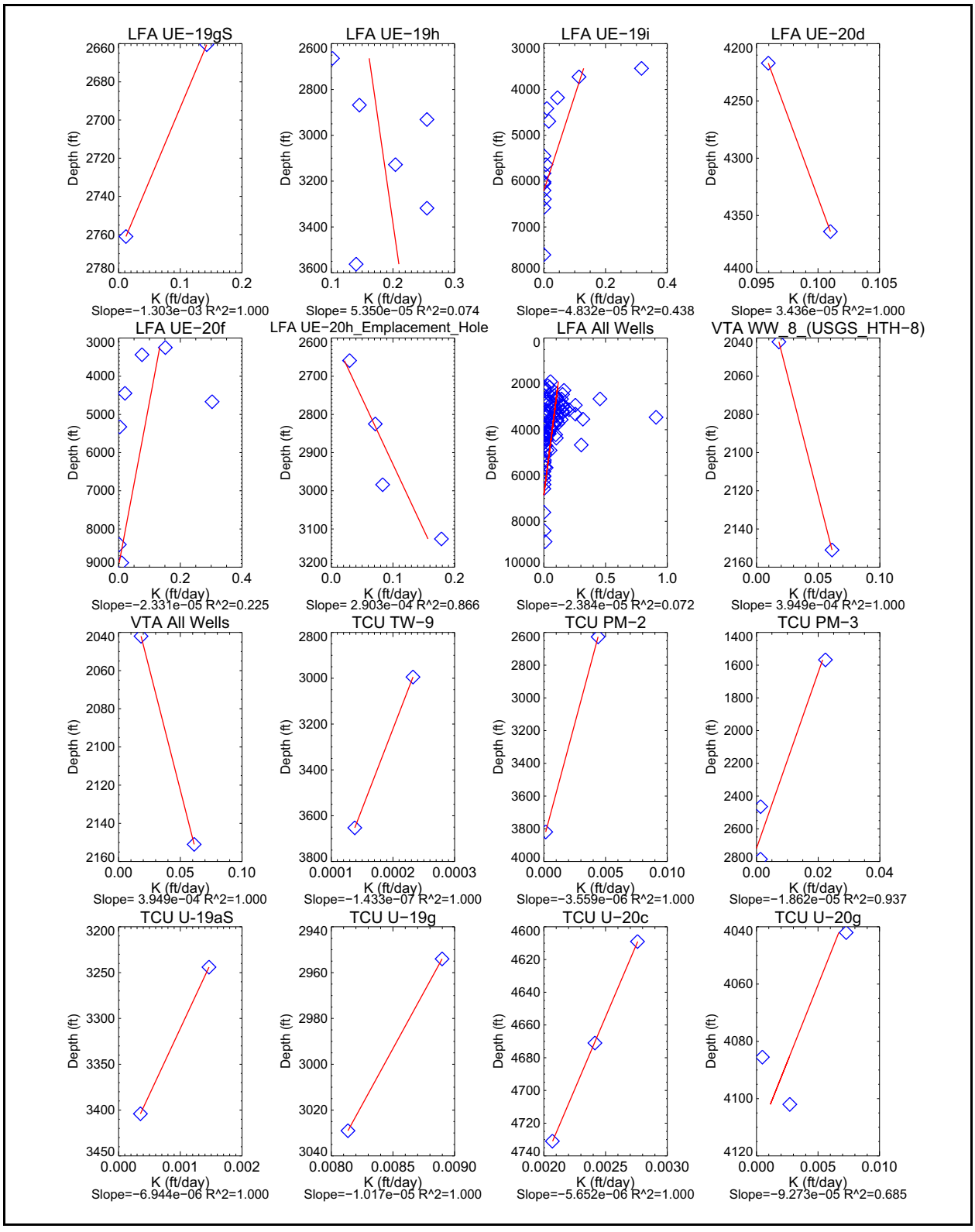

Figure 5-8b
Hydraulic Conductivity versus Depth for Dominant HGUs within Each Well (cont.)

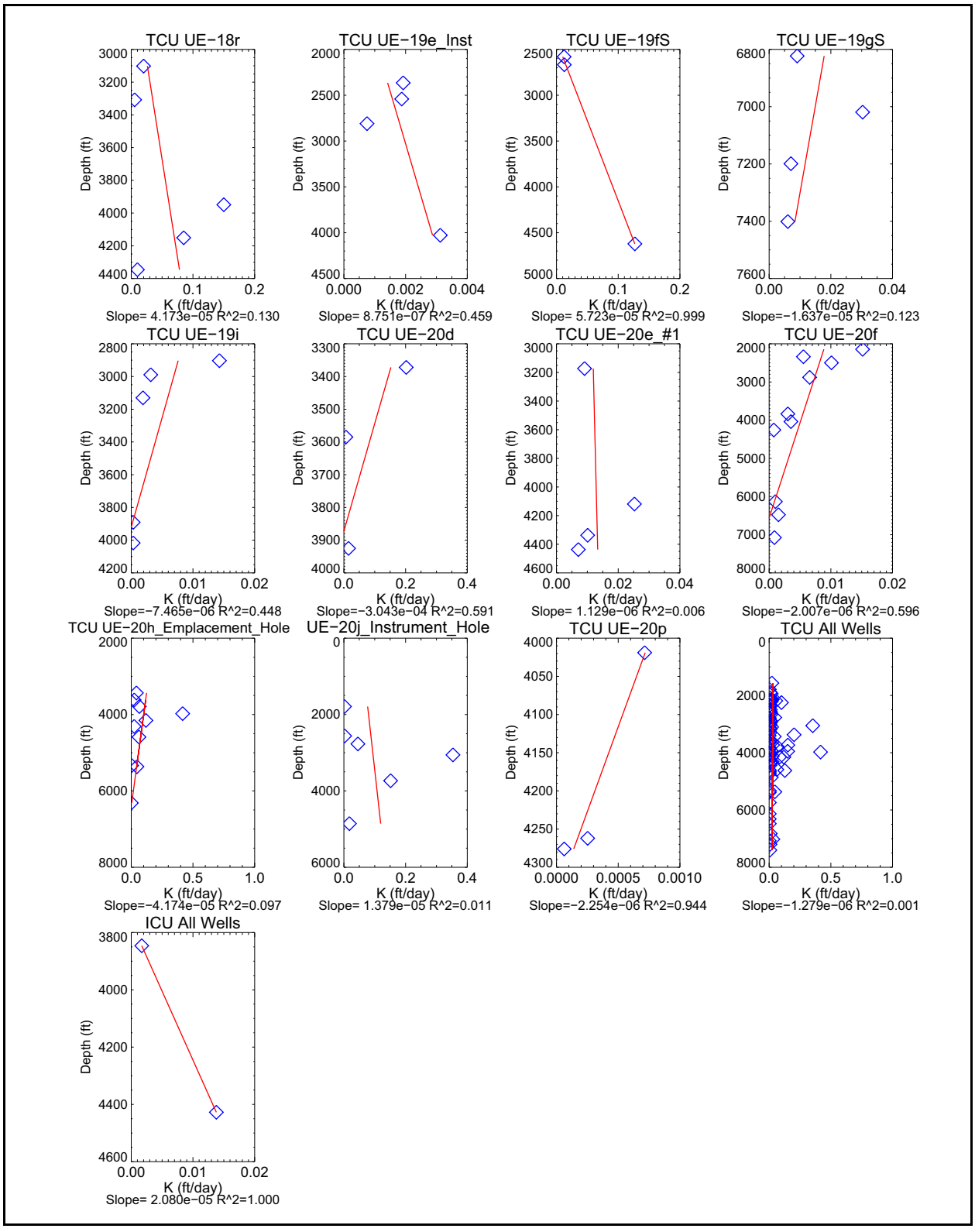

Figure 5-8c
Hydraulic Conductivity versus Depth for Dominant HGUs within Each Well (cont.)

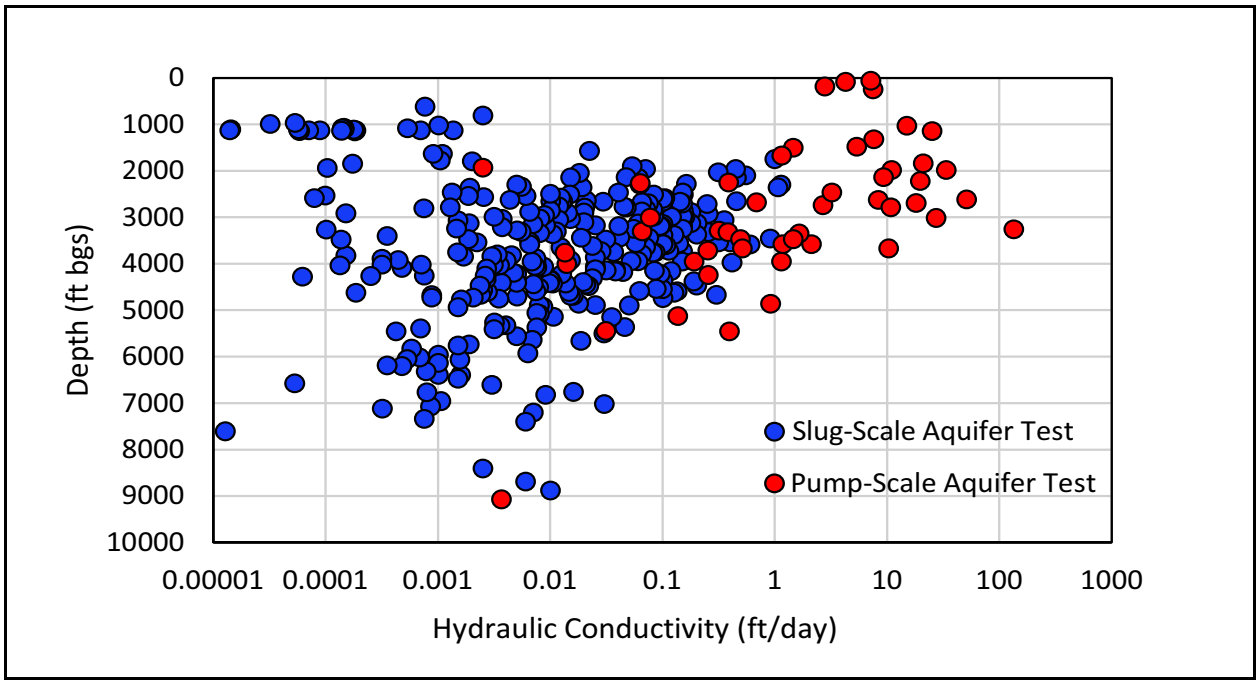

Figure 5-9
Pump- and Slug-Scale Aquifer Test Hydraulic Conductivity versus Depth

calibration of the Pahute Mesa CAU flow model. For the depth intervals up to 1,500 m bgs (4,500 ft), no depth dependence will be assumed. It is in this depth range that well-specific data indicate no clear trend with depth. At greater depths, a depth dependence will be used to transition to a insignificant hydraulic conductivity at depths greater than 6,000 ft bgs (1,800 m) or at the model's bottom depth. The model's depth should exceed the maximum expected radionuclide source depth within the source area and the maximum depth is approximately 6,000 ft bgs (1,800 m) for the largest detonations at 5 cavity radii below the working point based on the maximum unclassified yield (e.g., HANDLEY, BOXCAR, and MUENSTER detonations) (NNSA/NFO, 2015b).

5.2.2.6 Fault Influences on Hydraulic Conductivity

Faults at the NNSS tend to form relatively narrow-width (less than 100-m [300-ft]) fault zones that have flow properties that vary from fault to fault as well as along individual faults. Fault zones resulting from the most recently active zone probably form the most permeable fault zones, but only where they cut the stronger and more consolidated HGUs such as WTA, LFA, and CA. Where these faults intersect TCU, they likely form zones of enhanced fracture permeability, but the permeability may be less than the fault zones in the stronger HGUs (Prothro et al., 2009b).

The relationship between hydraulic conductivity and distance to the nearest fault was analyzed by evaluating trends on scatter plots of hydraulic conductivity versus distance to the nearest fault. Trends were evaluated to test the hypothesis that regional fault structures may either enhance or inhibit hydraulic conductivity with decreasing distance from the structures. The populations of pump- and slug-scale aquifer test hydraulic conductivity are largely separated because of scale-dependency of hydraulic conductivity (Section 5.2.2), and the relationship between hydraulic conductivity and distance to faults was investigated independently for the two populations of hydraulic conductivity.

No correlation between the slug-scale aquifer test hydraulic conductivity and distance to faults was found. The absence of a relationship between distance to faults to slug-scale aquifer test hydraulic conductivity is likely due to two causes. The first is the limited scale of the slug-scale aquifer test data, which only test a relatively small volume of rock in the immediate area of the borehole. The second cause is the slug-scale aquifer testing locations. Slug-scale aquifer tests beneath Pahute Mesa were primarily intended to locate low-permeability rocks suitable for the testing of nuclear devices (Blankennagel, 1967; Blankennagel and Weir, 1973), and test locations were selected to avoid faults because of the possibility of detonation venting to the surface through fault-damaged zones.

Figure 5-10 presents a linear regression of pump-scale aquifer test data of the logarithm of the hydraulic conductivity versus distances to faults. Most data are within 2 mi of a fault, and no trend of increasing hydraulic conductivity with decreasing distance to faults is seen when all data are evaluated together. The coefficient of determination increases significantly when the data are grouped by decreasing distance to faults. A correlation between proximity to faults and hydraulic conductivity is seen at a distance of 1,000 ft, although the amount of data becomes limited as the distance is decreased. The coefficient of determination is 0.05 at 5,000 ft, 0.37 at 2,000 ft, and 0.73 at 1,000 ft. An enhanced permeability zone of 1,000-ft width is consistent with the observations of fault zones at the NNSS by Prothro et al. (2009).

5.2.2.7 Anisotropy

Anisotropy is a concept that provides for a directional dependency of hydraulic conductivity. In fractured aquifer systems where there is a dominant fracture orientation caused, for example, by regional large-scale stresses in the earth's crust, the hydraulic conductivity may be preferably aligned with fracturing (Reeves et al., 2017). The anisotropy concept was applied in the analysis of the BULLION forced-gradient experiment (FGE) (IT, 1998) to explain the direction differences in

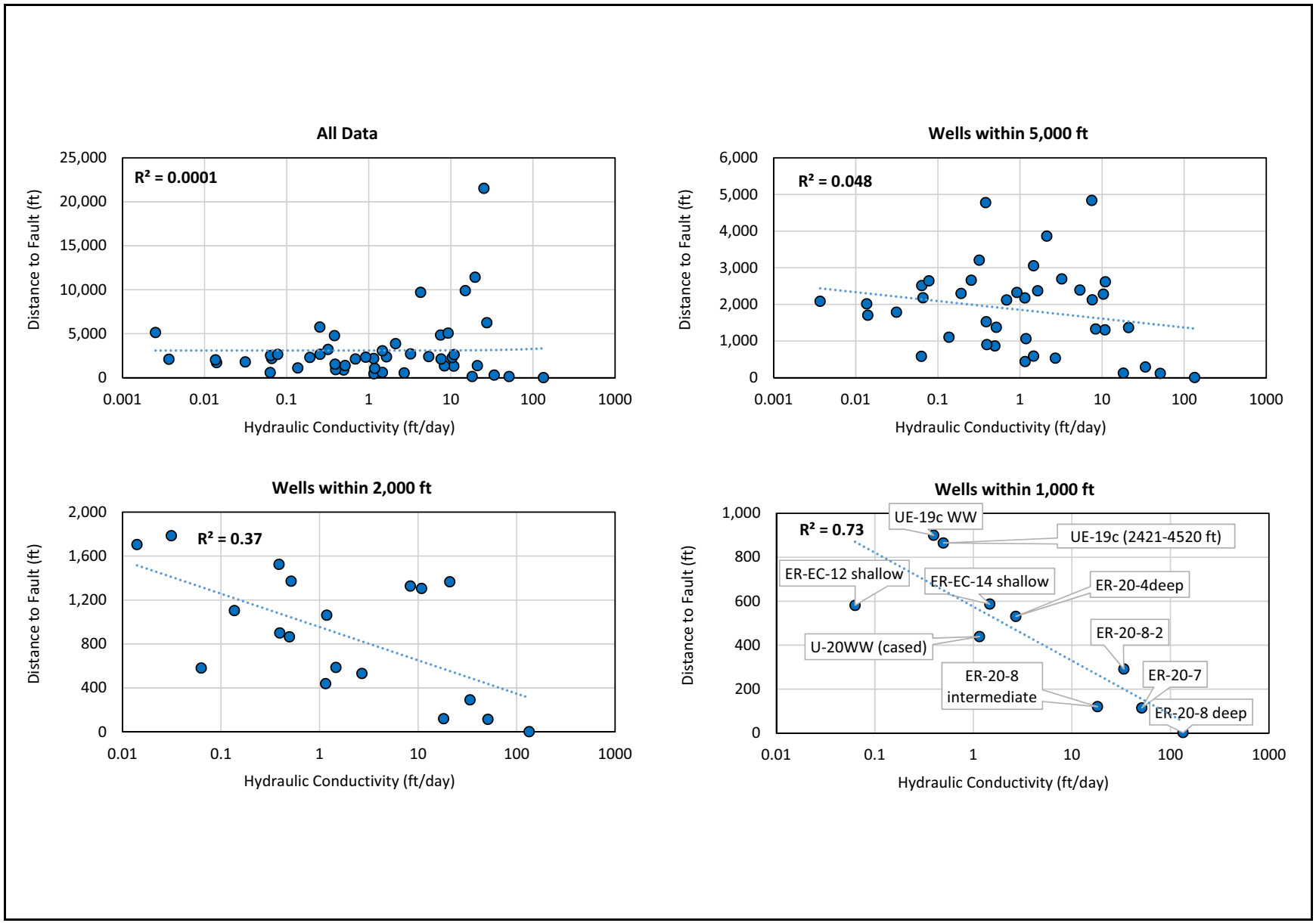

Figure 5-10
Hydraulic Conductivity from Pump-Scale Aquifer Tests versus Distance to Faults

hydraulic responses caused by pumping. For the BULLION modeling, a horizontal anisotropy value near 7 was applied to selected model layers to better match hydraulic responses to pumping. In a later analysis of hydraulic responses to pumping of wells in the Bench area (Garcia et al., 2017), spatial heterogeneity rather than anisotropy was used to explain differences in hydraulic responses.

5.2.3 Summary and Conclusions of Hydraulic Conductivity Analyses

The hydraulic conductivity data derived from single-well testing of Pahute Mesa wells have been compiled and analyzed. The data were sorted into individual datasets for each scale of test, and then sorted into bins for each HSU, HGU, and HGU within HSU.

Pump-scale aquifer test hydraulic conductivity data are only available for 11 HSUs, and are only available for aquifer or composite unit type HSUs. The largest hydraulic conductivity was seen in the TSA and AWTA HSUs. The hydraulic conductivity of pump-scale aquifer test aquifer HGUs (WTA and LFA) is several times higher than confining unit HGU (TCU), but there is a large amount of overlap in the range of hydraulic conductivity values.

The majority of the Pahute Mesa wells are screened across multiple HSUs or HGUs, making the amount of data primarily representative of a single type of rock from pump-scale aquifer testing very limited. The moderate difference seen between aquifer and confining unit HGU pump-scale aquifer test data may be partially explained by the confounding effect of multiple HSUs or HGUs being present within well screens.

The amount of slug-scale aquifer test hydraulic conductivity data is considerably larger than pump-scale aquifer test data. The mean hydraulic conductivity of the slug-scale aquifer test data grouped by HSU and HGU are very similar regardless of hydraulic character (e.g., aquifer or confining unit) and are generally within an order of magnitude of each other. The character of the slug-scale aquifer test data is very similar regardless of HGU or HSU. This similarity of the slug-scale aquifer test data among the different HGUs and HSUs may have several explanations including the following:

- The volume of aquifer interrogated by the slug-scale aquifer tests is insufficient to find a larger-scale fracture network, which could lead to a possibly incorrect conclusion of aquifer HSUs being undifferentiated from confining HSUs.

- Fractured rock is ubiquitous across Pahute Mesa, and the fractures present in the material control hydraulic conductivity to a greater extent than the lithology.

- The slug-scale aquifer testing was significantly affected by altered near-well conditions (i.e., borehole damage from drilling).

- Pump-scale aquifer test data are only available for a small number of aquifer or composite unit HSUs. The CDFs derived from this data likely do not capture the full range of hydraulic conductivity inherent in the HSUs.

- Packers did not effectively isolate the tested intervals, and measurement limitations prevented accurate characterization very low- and high-transmissivity areas. Within very permeable intervals, water levels could not be measured with sufficient frequency. Within very low-permeability intervals, time constraints inhibited measuring recovery (Frus and Halford, 2018).

Generally, the variability of hydraulic conductivity within a group is larger than the variability across groups. This suggests that the HSU or HGU groups do not identify unique hydraulic conductivity values in most cases. This further suggests that other factors such as degree of fracturing dominate the hydraulic conductivity of most tested intervals. These findings are consistent with Garcia et al. (2017) and Oberlander et al. (2007) in that most HSUs in the Bench area are heterogeneous, and the aquifer and confining unit HSUs can have similar hydraulic behaviors.

The data of low quality and high quality are distributed throughout the hydraulic conductivity distributions for the groupings by HSU or HGU, and low quality cannot be used as an explanation for the outliers seen in the datasets.

A general trend of decreasing hydraulic conductivity with depth is seen in Pahute Mesa hydraulic conductivity data regardless of the tested rock types (aquifer and confining unit). Very low hydraulic conductivity occurs at all tested depths, but the highest hydraulic conductivity values (in excess of 1 ft/day) generally occur within 4,000 ft of the surface. Hydraulic conductivity below 6,000 ft bgs is less than 0.1 ft/day.

The relationship between hydraulic conductivity and distance to the nearest fault was analyzed by evaluating trends on scatter plots of hydraulic conductivity versus distance to the nearest fault for the pump- and slug-scale aquifer test data. A strong correlation between proximity to faults is seen in the pump-scale aquifer test data at a distance of less than 1,000 ft, but the amount of data becomes limited as the distance is decreased. No correlation between the slug-scale aquifer test hydraulic conductivity

and distance to faults was found, likely due to the limited scale of the slug-scale aquifer test data or the location of slug-scale aquifer tested wells being selected to avoid faults.

5.3 Specific Storage

The specific storage (Ss) of a saturated aquifer is defined as the volume of water that a unit volume of aquifer releases from storage under a unit decline in hydraulic head (Freeze and Cherry, 1979). Specific storage is used to assess storage property variability because it removes the effects of unequal test intervals from the data.

Most of the transmissivity estimates at Pahute Mesa have been derived from analysis of the drawdown in the pumped wells. Storage parameter values in single-well analyses are uncertain due to many effects (e.g., unknown effective well radius, well bore storage, well skin). Given the accuracy of estimates of specific storage derived from single-well test data, upper and lower bounds for specific storage (Ss), both fracture specific storage (Ss_f), and matrix specific storage (Ss_m) were calculated using upper and lower bound values for compressibility and porosity. The values used for compressibility (jointed and sound rock as well as water) are from Freeze and Cherry (1979, page 55). The values used for porosity were taken from the YF/CM Phase I flow and transport model document (N-I, 2013). Although this report was prepared for YF/CM, the estimates for the volcanics given in the report are not exclusive to YF/CM; they are based on sitewide data. In addition, the report provides estimates of porosity for the LCA that are not available at this time from Pahute Mesa data. These parameter values are listed in Table 5-11.

The ranges for the storage parameters were calculated based on the theory of confined storage using general values from the literature bounding the possible values of the parameters. Specific storage was calculated using the following formula (Freeze and Cherry, 1979):

$$Ss = \rho g\,(\alpha + n\beta) \qquad (5\text{-}1)$$

where:

ρ = Density
g = Gravity
α = Bulk matrix compressibility
n = Matrix porosity
β = Water compressibility

Table 5-11
Storage Parameter Constraints

Parameter	LCA		TSA		TMWTA	
	Upper Bound	Lower Bound	Upper Bound	Lower Bound	Upper Bound	Lower Bound
Fracture Specific Storage (Ss_f) [1/m]	9.79E-05	9.79E-07	9.78E-05	9.78E-07	9.78E-05	9.78E-07
Matrix Specific Storage (Ss_m) [1/m]	9.96E-06	9.78E-08	1.20E-05	1.19E-06	1.12E-05	9.78E-08
Bulk Compressibility [m^2/N]	1.00E-08	1.00E-10	1.00E-08	1.00E-10	1.00E-08	1.00E-10
Matrix Compressibility [m^2/N]	1.00E-09	1.00E-11	1.00E-09	1.00E-11	1.00E-09	1.00E-11
Fracture Porosity	2.00E-02	2.00E-04	6.00E-03	1.00E-04	6.00E-03	1.00E-04
Matrix Porosity	4.20E-02	0.00	5.05E-01	2.53E-01	4.42E-01	0.00

The Ss_f values derived in this manner for volcanic rocks range between 9.8E-07 and 9.8E-05 1/m. The Ss_m values derived in this manner for volcanic rocks range between 9.8E-08 and 1.2E-05 1/m. In similar fashion, the Ss_f values derived in this manner for the lower carbonate aquifer (LCA) range between 9.8E-07 and 9.8E-05 1/m. The Ss_m values derived in this manner for the LCA range between 9.8E-08 and 1.0E-05 1/m.

In addition to the estimates for specific storage described above, estimates were developed by spectral analysis using earth-tide response data for water levels measured in a single depth interval for Wells ER-EC-1, ER-EC-2A, ER-20-1, ER-20-5-1, ER-20-1, ER-20-5-3, and ER-20-7; in two depth intervals for Wells ER-20-4 and ER-20-8; and in three depth intervals for Wells ER-EC-6, ER-EC-11, ER-EC-12, and ER-EC-13. The methodology is based on the relationship derived by Bredehoeft (1967) to estimate specific storage of an aquifer. Implementation of the methodology is described in the Wells ER-20-8 and ER-20-4 Well Development and Testing Analyses report (N-I, 2012), where the specific storage estimates for both Wells ER-20-8 and ER-EC-11 are given. The remaining estimates are given in the Wells ER-EC-12 and ER-EC-13 Well Development and Testing Analyses report (Navarro, 2018). The water-level data for these analyses were obtained from the Pahute Mesa 2010 Long-Term Monitoring Program (N-I, 2011).

The estimates of specific storage developed for Wells ER-20-8 and ER-EC-11 are given in Table 5-12. The remaining estimates are given in Table 5-13.

Table 5-12
Specific Storage Estimated for Wells ER-20-8 and ER-EC-11
(Page 1 of 2)

Well	Screen Interval	Type of Fit	Specific Storage Using M2 (1/m)	Specific Storage Using O1 (1/m)
ER-20-8	Deep	Using Theoretical/Fit Amplitudes	2.03E-06	2.55E-06
		Using Spectral Amplitudes	2.02E-06	3.10E-06
ER-20-8	Intermediate	Using Theoretical/Fit Amplitudes	3.96E-06	4.55E-06
		Using Spectral Amplitudes	3.87E-06	6.05E-06

Table 5-12
Specific Storage Estimated for Wells ER-20-8 and ER-EC-11
(Page 2 of 2)

Well	Screen Interval	Type of Fit	Specific Storage Using M2 (1/m)	Specific Storage Using O1 (1/m)
ER-EC-11	Deep	Using Theoretical/Fit Amplitudes	1.09E-06	9.66E-06
		Using Spectral Amplitudes	9.90E-07	1.06E-06
ER-EC-11	Intermediate	Using Theoretical/Fit Amplitudes	1.09E-06	9.75E-07
		Using Spectral Amplitudes	9.90E-07	1.05E-06
ER-EC-11	Shallow	Using Theoretical/Fit Amplitudes	1.09E-06	2.33E-06
		Using Spectral Amplitudes	1.79E-06	2.40E-06

Note: M2 and O1 are earth-tide constituents (Cutillo and Bredehoeft, 2011).

Table 5-13
Specific Storage Estimated from Earth Tides for Select Pahute Mesa Wells
(Page 1 of 3)

Well	Screen Interval	Type of Fit	Specific Storage Using M2 (1/m)	Specific Storage Using O1 (1/m)
ER-EC-1	Multiple	Using Theoretical/Fit Amplitudes	2.75E-06	2.42E-06
(Unvented)	Multiple	Using Spectral Amplitudes	2.59E-06	2.66E-06
ER-EC-1	Multiple	Using Theoretical/Fit Amplitudes	2.64E-06	2.17E-06
(Vented)	Multiple	Using Spectral Amplitudes	2.58E-06	2.05E-06
ER-EC-2A	Shallow	Using Theoretical/Fit Amplitudes	1.94E-06	1.79E-06
(Unvented)	Shallow	Using Spectral Amplitudes	1.96E-06	1.59E-06
ER-EC-6	Shallow	Using Theoretical/Fit Amplitudes	3.87E-06	4.04E-06
(Unvented)	Shallow	Using Spectral Amplitudes	4.04E-06	4.35E-06
ER-EC-6	Intermediate	Using Theoretical/Fit Amplitudes	1.71E-06	1.60E-06

Table 5-13
Specific Storage Estimated from Earth Tides for Select Pahute Mesa Wells
(Page 2 of 3)

Well	Screen Interval	Type of Fit	Specific Storage Using M2 (1/m)	Specific Storage Using O1 (1/m)
(Unvented)	Intermediate	Using Spectral Amplitudes	1.64E-06	1.63E-06
ER-EC-6	Deep	Using Theoretical/Fit Amplitudes	1.61E-06	1.36E-06
(Unvented)	Deep	Using Spectral Amplitudes	1.52E-06	1.39E-06
ER-EC-12	Shallow	Using Theoretical/Fit Amplitudes	1.45E-06	1.00E-06
(Unvented)	Shallow	Using Spectral Amplitudes	1.09E-06	9.37E-07
ER-EC-12	Intermediate	Using Theoretical/Fit Amplitudes	3.35E-06	1.91E-06
(Unvented)	Intermediate	Using Spectral Amplitudes	3.44E-06	2.27E-06
ER-EC-12	Deep	Using Theoretical/Fit Amplitudes	9.10E-06	3.60E-06
(Unvented)	Deep	Using Spectral Amplitudes	7.66E-06	4.30E-06
ER-EC-13	Shallow	Using Theoretical/Fit Amplitudes	4.68E-06	3.59E-06
(Unvented)	Shallow	Not enough data for spectral analysis	NA	NA
ER-EC-13	Intermediate	Using Theoretical/Fit Amplitudes	3.61E-06	2.74E-06
(Unvented)	Intermediate	Not enough data for spectral analysis	NA	NA
ER-EC-13	Deep	Using Theoretical/Fit Amplitudes	3.24E-06	2.41E-06
(Unvented)	Deep	Not enough data for spectral analysis	NA	NA
ER-20-1	Main	Using Theoretical/Fit Amplitudes	6.24E-05	1.40E-05
(Vented)	Main	Using Spectral Amplitudes	6.62E-05	1.64E-05
ER-20-4	Shallow	Using Theoretical/Fit Amplitudes	6.04E-06	6.45E-06
(Unvented)	Shallow	Using Spectral Amplitudes	6.37E-06	5.99E-06

Table 5-13
Specific Storage Estimated from Earth Tides for Select Pahute Mesa Wells
(Page 3 of 3)

Well	Screen Interval	Type of Fit	Specific Storage Using M2 (1/m)	Specific Storage Using O1 (1/m)
ER-20-4	Deep	Using Theoretical/Fit Amplitudes	3.36E-06	4.04E-06
(Unvented)	Deep	Using Spectral Amplitudes	3.45E-06	3.75E-06
ER-20-5-1	Main	Using Theoretical/Fit Amplitudes	1.07E-05	7.71E-06
(Vented)	Main	Using Spectral Amplitudes	9.87E-06	9.32E-06
ER-20-5-3	Main	Using Theoretical/Fit Amplitudes	1.53E-06	1.47E-06
(Vented)	Main	Using Spectral Amplitudes	1.45E-06	2.15E-06
ER-20-7	Main	Using Theoretical/Fit Amplitudes	6.96E-06	3.45E-06
(Vented)	Main	Using Spectral Amplitudes	7.95E-06	3.00E-06

Table C-1 in Appendix C of this report provides the location, elevation, and EOIs of select wells and boreholes in the Pahute Mesa area. In addition, the table includes the primary and secondary (if any) HSUs present in the open interval(s). Aligning the estimates of Ss given in Tables 5-12 and 5-13 with the primary HSUs listed in Table C-1 yields a breakdown of the Ss estimates by HSU.

Table 5-14 shows the breakdown of the estimated Ss values by primary HSU. Figure 5-11 shows the theoretical limits of Ss as well as the estimates of Ss by HSU developed using earth tides. Reference to Figure 5-11 shows the estimates developed using earth tides, which with one exception, fall within the bounds of the theoretical limits. The exception is the upper limit estimated for the TCA at Well ER-20-1. The value estimated at Well ER-20-1 appears to be an outlier, as the estimates for the TCA at Wells ER-EC-11, ER-EC-12, and ER-20-8 all have estimated maximum values that are approximately an order of magnitude lower.

Additional estimates of specific storage were developed through numerical modeling. The first of these are documented in the report detailing modeling of the BULLION FGE (IT, 1998). The second are derived from modeling done by USGS personnel for the hydraulic characterization of volcanic

Table 5-14
Estimates of Specific Storage from Earth-Tide Analyses by Primary HSU

HSU	Minimum Specific Storage (1/m)	Maximum Specific Storage (1/m)	Number of Estimated Values
BA	1.79E-06	4.04E-06	2
CFCU	3.36E-06	9.10E-06	2
CHLFA	1.45E-06	6.37E-06	2
CHZCM	1.52E-06	2.03E-06	2
FCCM	1.94E-06	4.68E-06	2
FCULFA4	3.24E-06	3.61E-06	2
TCA	9.90E-07	6.62E-05	4
TSA	9.90E-07	1.07E-05	4
UPCU	1.64E-06	1.71E-06	1

Sources: Values estimated using the M2 signal as reported in N-I (2012) and Navarro (2018).

rocks in Pahute Mesa (Garcia et al., 2017). The BULLION FGE analyses produced a range of specific storage values between 1.13E-06 and 1.79E-05 1/m.

Garcia et al. (2017) reports on the use of numerical models to estimate hydraulic parameters by fitting simulated drawdowns to observed drawdowns from MWATs conducted in the Pahute Mesa area (Sections 5.2.2.4 and 9.0). Specific storage values were among the hydraulic parameters estimated. HSUs, as described in the PM-OV HFM (Navarro, 2020), were combined to form modified HSUs, and the values reported pertain to those modified HSUs.

Table 5-15 lists the modified HSUs, geometric means, and associated standard deviations of the estimated specific storage values determined in Garcia et al. (2017). Table 7 of Garcia et al. (2017) shows how the modified HSUs are defined. Table 5-15 shows that the numerical modeling yielded more Ss estimates than have been developed using earth tides. The values estimated in Garcia et al. (2017) are lower than those estimated using earth tides, generally by an order of magnitude or more. The estimates based on earth tide analyses vary between a low of 9.9E-07 to a high of 6.62E-05 1/m. The analyses performed for Garcia et al. (2017) have a geometric mean of 1.0E-07 1/m and range from approximately 6.1E-09 to 3.1E-07 1/m.

Figures 5-12 and 5-13 are plots showing the geometric means for the Ss values estimated by Garcia et al., 2017).

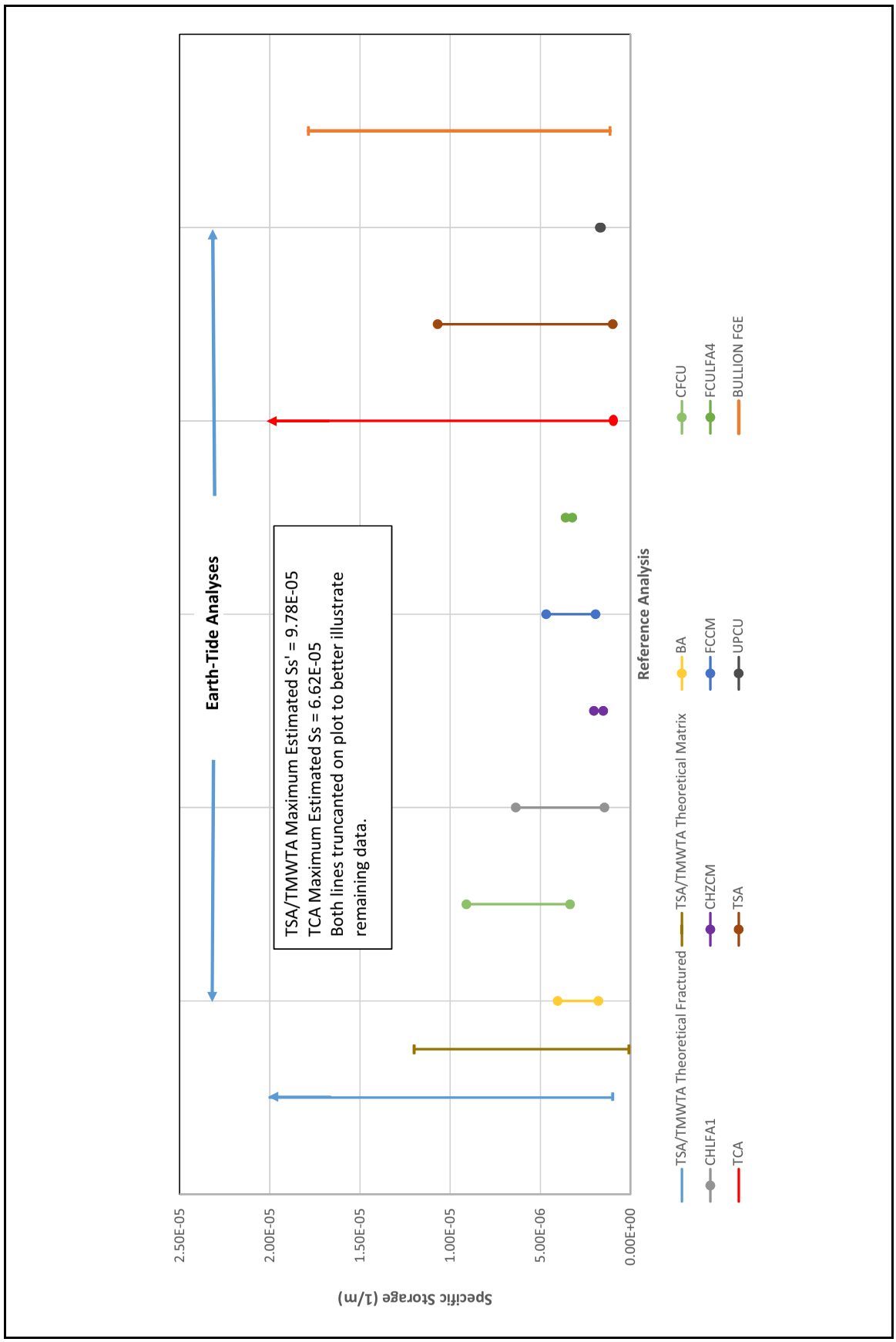

Figure 5-11
Theoretical and Estimates of Specific Storage Developed Using Synthetic Earth Tides

Table 5-15
Estimated Specific Storage Values Determined by Garcia et al. (2017)

Modified HSU	Geometric Mean (1/m)	Standard Deviation
mFCCM1	1.22E-08	1.22E-07
mCCU	3.05E-07	6.10E-08
mCFCM	2.44E-08	3.05E-08
mCHLFA1	3.05E-07	1.22E-07
mCHLFA5	3.05E-08	1.52E-07
mCHZCM	3.05E-07	3.05E-07
mCPA	3.05E-07	6.10E-07
mFCCM2	2.13E-07	1.83E-07
mFCCM3	1.83E-08	6.10E-08
mFCCU	3.05E-07	3.05E-08
mFCCU1	3.05E-07	9.14E-08
mFCCU2	3.05E-07	9.14E-08
mFCCU3	3.05E-07	6.10E-08
mLPCU	1.22E-08	3.05E-08
mMPCU	1.52E-07	1.22E-07
mRMCM	3.05E-07	6.10E-08
mRMWTA1	6.10E-09	3.05E-08
mRMWTA2	1.83E-07	1.22E-07
mTCA	2.74E-07	3.05E-07
mTSA	3.05E-07	6.10E-07
mUPCU	9.14E-09	3.05E-08

Source: Modified from Garcia et al., 2017, Table 11

5.3.1 Uncertainty in the Values of Specific Storage Estimated

The “theoretical” estimates of specific storage developed are based on widely accepted parameter values (e.g., density, gravity, bulk compressibility) and an established relationship defining specific storage (Freeze and Cherry, 1979).

To develop the estimates of specific storage using earth-tide analyses, time-frequency analysis was conducted on water-level data gathered through the Pahute Mesa long-term head monitoring program (N-I, 2011). Because no direct measurements of earth tides were available, theoretical models were used to generate synthetic earth-tide time series. Comparison of the time-frequency spectrum of the water-level data and the earth-tide time series allows the calculation of amplitude ratios for specific

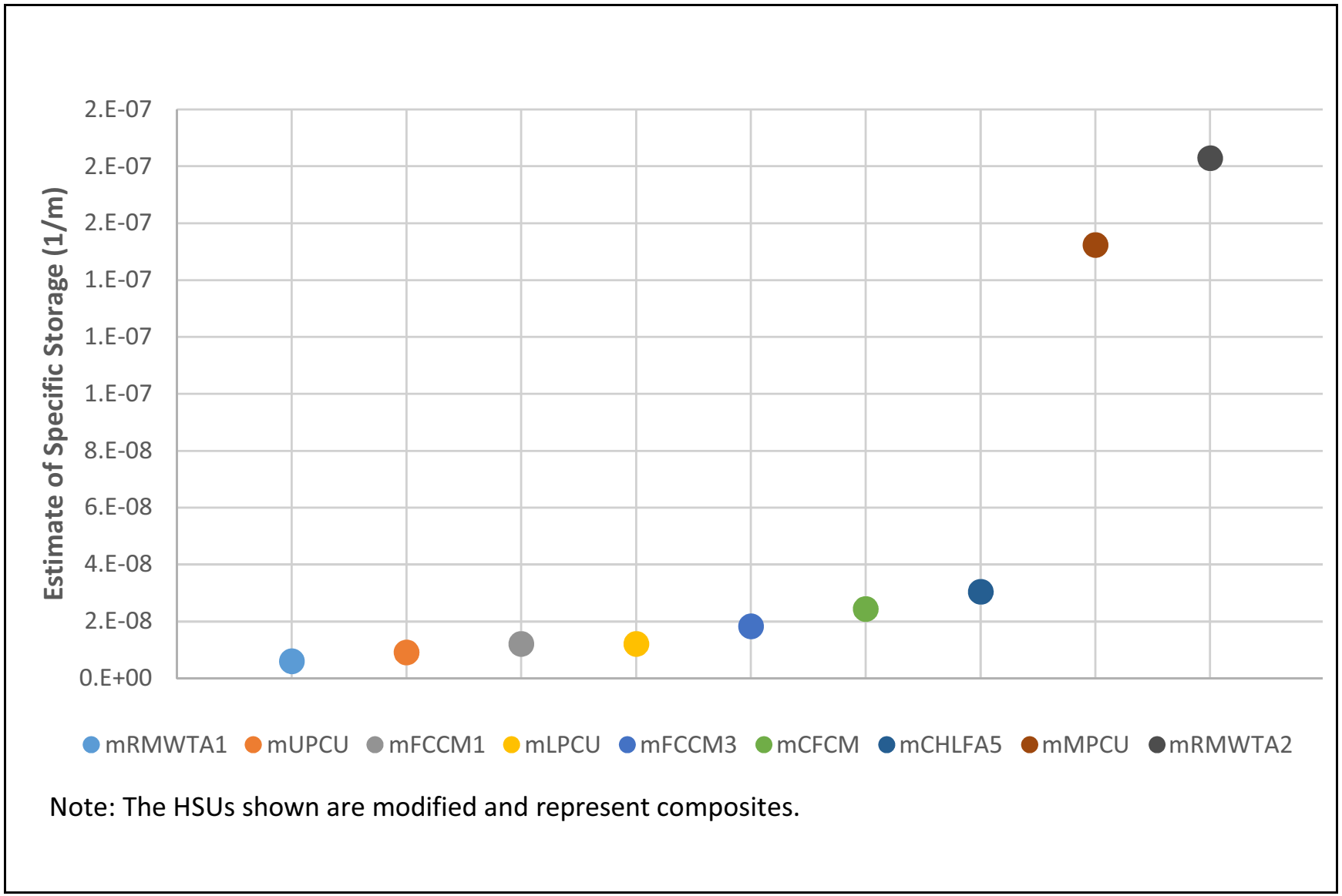

Figure 5-12
Specific Storage Estimates Developed by Garcia et al. (2017)

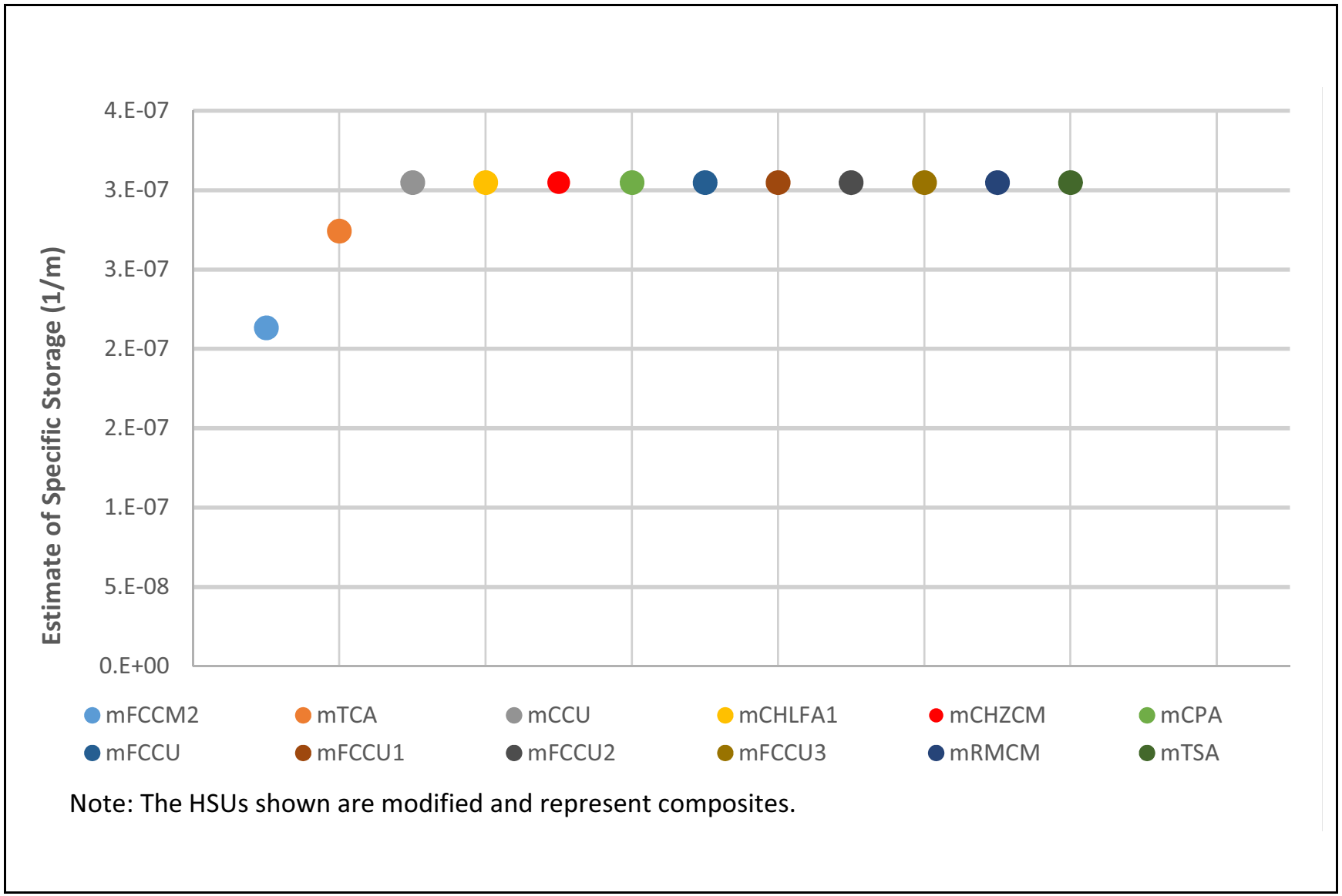

Figure 5-13
Additional Specific Storage Estimates Developed by Garcia et al. (2017)

frequencies in the earth-tide spectrum, which are then used to estimate specific storage for the different monitoring locations. As noted above, the range of "theoretical" specific storage values span the range of values developed using this method; however, no estimate of the uncertainty of the values was assigned.

The estimates of specific storage given by USGS (Garcia et al., 2017) were developed through numerical modeling fitting observed drawdowns during pump-scale aquifer tests to those simulated. The approach taken to this work was rigorous; however, estimates of the uncertainty in the values given are not provided.

The range of estimated specific storage values given by analysis of the BULLION FGE (IT, 1998) is large but generally consistent with those estimated using the definition of Ss. These estimates were derived through numerical modeling of the experiment and no specific estimates of the uncertainty of the values is given.

5.3.2 Summary of Specific Storage Estimates

The two main sources for estimated values of Ss are the analyses based on the use of earth tides (N-I, 2012; Navarro, 2018) and those estimated through the use of numerical modeling to estimate hydraulic parameters by matching simulated drawdowns to those observed due to hydraulic testing in the Pahute Mesa area (Garcia et al., 2017). The values of Ss estimated using earth tides range from a low of 9.9E-07 to a high of 6.62E-05 1/m. The analyses performed for Garcia et al. (2017) range from approximately 6.1E-09 to 3.1E-07 1/m.

The values of Ss estimated using earth tides generally agree with the theoretical range for fractured rock of 9.78-07 to 9.78E-05 1/m. If the high value of Ss for the TCA at Well ER-20-1 is not used, the high value of Ss estimated using earth tides drops to 1.1E-05 1/m. The values of Ss estimated by Garcia et al. (2017) are generally one to two orders of magnitude lower than the theoretical range and that developed using earth-tide analyses (N-I, 2012; Navarro, 2018). Underestimation of model-estimated specific storage values may be attributed to overestimation of the aquifer thicknesses contributing to flow.

6.0 PRECIPITATION-DERIVED RECHARGE

The PM-OV groundwater basin (Figure 2-1) is part of the Death Valley regional groundwater flow system. The basin extends from Gold Flat and Kawich Valley in the north to the terminus in Oasis Valley in the southwest. Altitudes in the study area range from about 3,300 ft (1,000 m) near Beatty to about 8,300 ft (2,500 m) in the Kawich and Belted Ranges in the northernmost areas. The groundwater flow system of the PM-OV area is replenished by areal recharge from precipitation on the volcanic highlands such as Pahute Mesa. An estimated 5,900 acre-feet per year (acre-ft/yr) (7,268,800 cubic meters per year [m^3/yr]) of groundwater discharges in Oasis Valley (Reiner et al., 2002). Subsurface discharge from Oasis Valley to the Amargosa Desert through alluvium in southern Oasis Valley is estimated at about another 100 acre-ft/yr (123,200 m^3/yr) (Reiner et al., 2002), and an additional estimated 300 acre-ft/yr (369,600 m^3/yr) of surface water in the Amargosa River flows southward out of Oasis Valley. The total estimated recharge generated within the PM-OV groundwater basin from precipitation derived recharge infiltration is 6,300 acre-ft/yr (7,761,600 m^3/yr), assuming the groundwater system is in steady-state and recharge equals discharge. Overall, inter-basin flow between the PM-OV groundwater basin and adjacent basins is thought to be insignificant, except south of Beatty, where there is 400 acre-ft/yr of surface and subsurface interbasin flow (Fenelon et al., 2016).

Estimating the quantity and spatial distribution of precipitation derived recharge is an important aspect of the PM-OV groundwater flow system and is difficult within the arid environment of the NNSS region. This section reviews three different studies that estimate recharge within the PM-OV groundwater basin.

6.1 Objectives

The objective of this data analysis activity is to estimate precipitation recharge rates and their spatial distribution over the PM-OV groundwater basin, including the associated uncertainties. The resulting recharge distributions will be used during the development of the CAU-scale groundwater flow model.

6.2 Approach

Several modeling studies have been recently performed to estimate the net infiltration (recharge) since the Phase I CAU modeling effort. These studies can be used to define the upper boundary conditions and constrain the water balance for the CAU flow model. The approach was to review the pertinent modeling studies on recharge for the PM-OV area. The resultant recharge volumes and areal distributions were then evaluated and compared to identify those most applicable to the development of a groundwater flow model for the PM-OV groundwater basin. Limitations to the models were also evaluated. This approach yielded a range of recharge volumes and areal distributions that can be used to limit the reasonable amount of recharge that could be occurring in the PM-OV area.

6.2.1 Recharge Model Descriptions

The following sections describe the recharge models considered in support of the Pahute Mesa CAU flow model. Each of the models used different approaches and input datasets, as discussed in the individual model descriptions below.

Fenelon et al. (2016) defined the PM-OV groundwater basin area based on regional water-level contours, geologic controls, and balancing of groundwater discharges in the PM-OV groundwater basin and adjacent basins against available water from precipitation. The recharge used in the study was estimated using three methods: (1) the modified Maxey-Eakin method (Maxey and Eakin, 1951); (2) a soil-water balance method coded in the INFIL code (Hevesi et al., 2003); and (3) a local-scale analysis of the PM-OV groundwater basin delineation using a numerical groundwater-flow model that matched measured water levels, groundwater discharges, and transmissivities. The recharge estimated using the INFIL model was from a published recharge distribution and was subsequently scaled to balance observed discharges. The recharge estimated with the Maxey-Eakin and INFIL code includes the entire area of the Death Valley regional groundwater flow system on a 1,000-m-resolution grid. The recharge estimated with the numerical model only includes the PM-OV groundwater basin on a 300-m-resolution grid.

LANL (Middleton et al., 2019) estimated net infiltration rates for the PM-OV area using an updated version of INFIL code (USGS, 2008b) to constrain the water balance for groundwater flow models being developed for the PM-OV flow system. The area for the estimated recharge corresponds to the Phase I transport model area (SNJV, 2009b) and does not cover the entire PM-OV groundwater basin

as defined by Fenelon et al. (2016). The spatial distribution of recharge is estimated on a 50-m-resolution grid.

6.2.1.1 Modified Maxey-Eakin as Applied by USGS

The application of the modified Maxey-Eakin method is documented in *Delineation of the Pahute Mesa-Oasis Valley Groundwater Basin, Nevada* (Fenelon et al., 2016). The following is taken from the document:

> "*Recharge was estimated from the Parameter-elevation Regressions on Independent Slopes Model (PRISM) (PRISM Climate Group, 2012) precipitation distribution that was scaled to match measured discharge. The approach used an empirical basin-balance method analogous to the Maxey-Eakin method (Maxey and Eakin, 1951; Avon and Durbin, 1994). The method simultaneously balances estimates of recharge with discharge in all basins. Recharge rates are estimated by multiplying annual precipitation amounts within specified precipitation ranges by coefficients that represent the fraction of precipitation that is converted to recharge. Precipitation for the area within each range is summed by groundwater basin and multiplied by a fitted coefficient to estimate precipitation-derived recharge. Recharge is balanced against discharge simultaneously within each basin by varying the coefficients for each precipitation range to get a best fit. A rule was applied that requires a precipitation range with a higher precipitation rate to have a coefficient that is equal to or greater than a range with a lower rate. This was done because it is assumed that as precipitation increases, a larger percentage is available for recharge. The best fit is measured by minimizing the root mean square (RMS) error of the differences between discharge and recharge in each groundwater basin using the Microsoft Excel® Solver. A best fit is obtained by manually changing the precipitation ranges, iteratively balancing recharge and discharge, and comparing RMS errors between models with different ranges until the error is minimized. A groundwater basin balance with an RMS error of about 2,000 acre-ft/yr is considered reasonable, given the uncertainties in recharge, discharge, and basin boundaries.*

When applying the Maxey-Eakin approach, Fenelon et al. (2016) balanced recharge against discharge simultaneously within the PM-OV and surrounding basins that comprise the Death Valley regional groundwater flow system (Figure 6-1). The Maxey-Eakin model agreement with the target recharge and discharge for each groundwater basin had an RMS error of 1,300 acre-ft/yr (1,601,600 m^3/yr) and required scaling of only two precipitation ranges: 120–490 and 490–790 millimeters per year (mm/yr) (4.8–19 and 19–32 inches per year [in./yr]). The fitting error is considered acceptable relative to the uncertainties in the PRISM precipitation distribution, discharge estimates, and delineation of

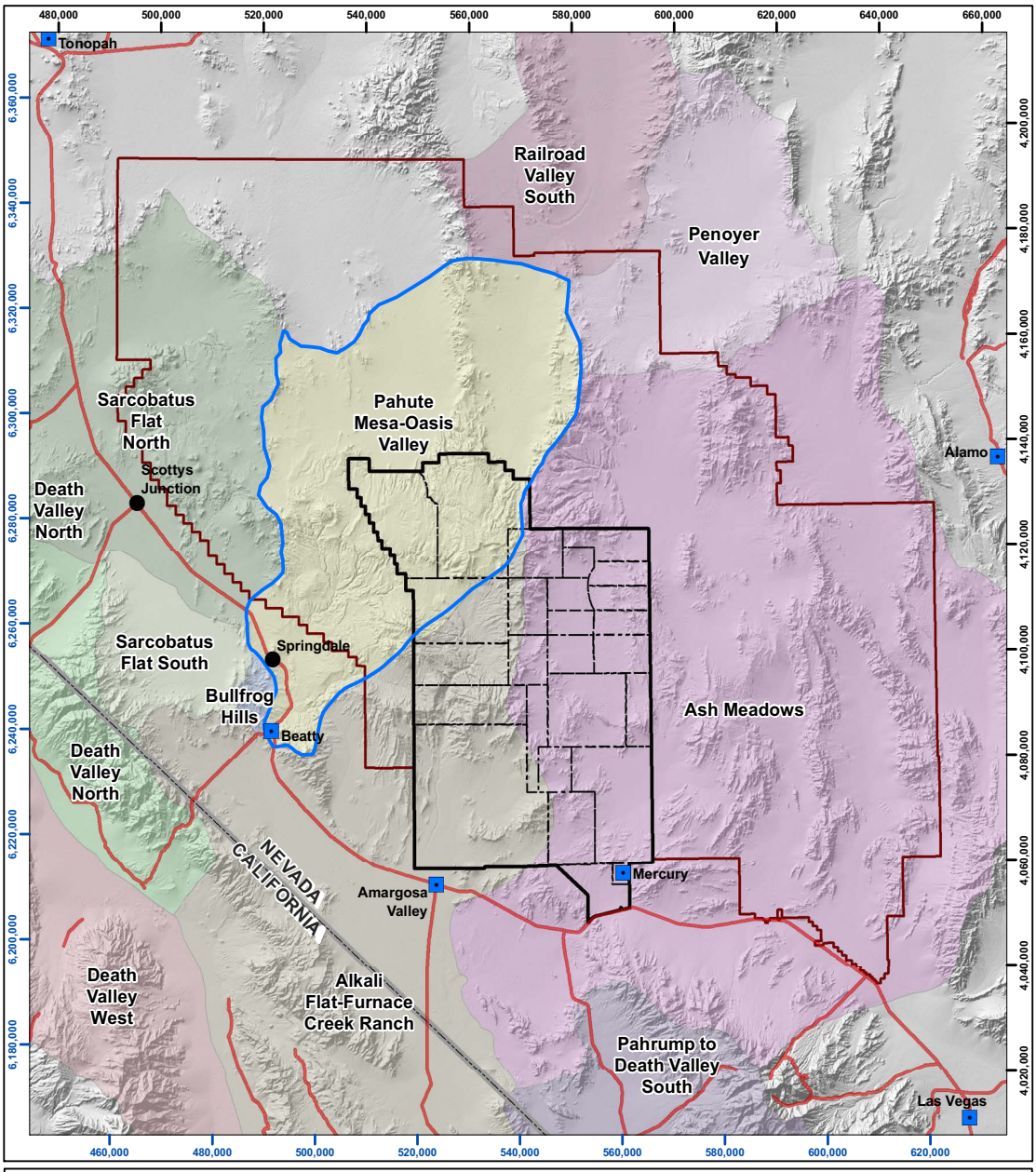

Figure 6-1
PM-OV and Surrounding Basins within the Death Valley Regional Groundwater Flow System
Source: Modified from Plate 1 of Fenelon et al., 2016

groundwater basins. The total recharge amount for the PM-OV groundwater basin was estimated as 6,159 acre-ft/yr (7,587,888 m^3/yr) (Fenelon et al., 2016).

Figure 6-2 presents the distribution of recharge from application of the Modified Maxey-Eakin method that is within the PM-OV HFM model domain. The recharge rates are 1 to 5 mm/yr (3.9E-02 to 0.20 in./yr) throughout the PM-OV groundwater basin and are spatially uniform compared to the recharge rates estimated with the INFIL code (see Sections 6.2.1.2 and 6.2.1.4).

6.2.1.2 INFILv3 Model as Applied by USGS

The INFIL method of estimating net recharge, as applied by USGS, is documented in *Simulation of Net Infiltration and Potential Recharge Using a Distributed-Parameter Watershed Model of the Death Valley Region, Nevada and California* (Hevesi et al., 2003). This model estimated the recharge distribution for the Death Valley region, which includes 42 hydrographic areas and subareas, of which the PM-OV is one. The recharge distribution was subsequently updated (Belcher and Sweetkind, 2011). The following description of the INFILv3 method is taken from Hevesi et al. (2003):

> "*To estimate the magnitude and distribution of potential recharge in response to variable climate and spatially varying drainage basin characteristics, the INFILv3 model uses a daily water-balance model of the root zone with a primarily deterministic representation of the processes controlling net infiltration and potential recharge. The daily water balance includes precipitation (as either rain or snow), snow accumulation, sublimation, snow-melt, infiltration into the root zone, evapotranspiration, drainage, water content change throughout the root-zone profile (represented as a 6-layered system), runoff (defined as excess rainfall and snow melt) and surface water run-on (defined as runoff that is routed downstream), and net infiltration (simulated as drainage from the bottom root-zone layer). Potential evapotranspiration is simulated using an hourly solar radiation model to simulate daily net radiation, and daily evapotranspiration is simulated as an empirical function of root zone water content and potential evapotranspiration. The model uses daily climate records of precipitation and air temperature from a regionally distributed network of 132 climate stations and a spatially distributed representation of drainage basin characteristics defined by topography, geology, soils, and vegetation to simulate daily net infiltration at all locations, including stream channels with intermittent stream-flow in response to runoff from rain and snow-melt. The temporal distribution of daily, monthly, and annual net infiltration can be used to evaluate the potential effect of future climatic conditions on potential recharge.*"

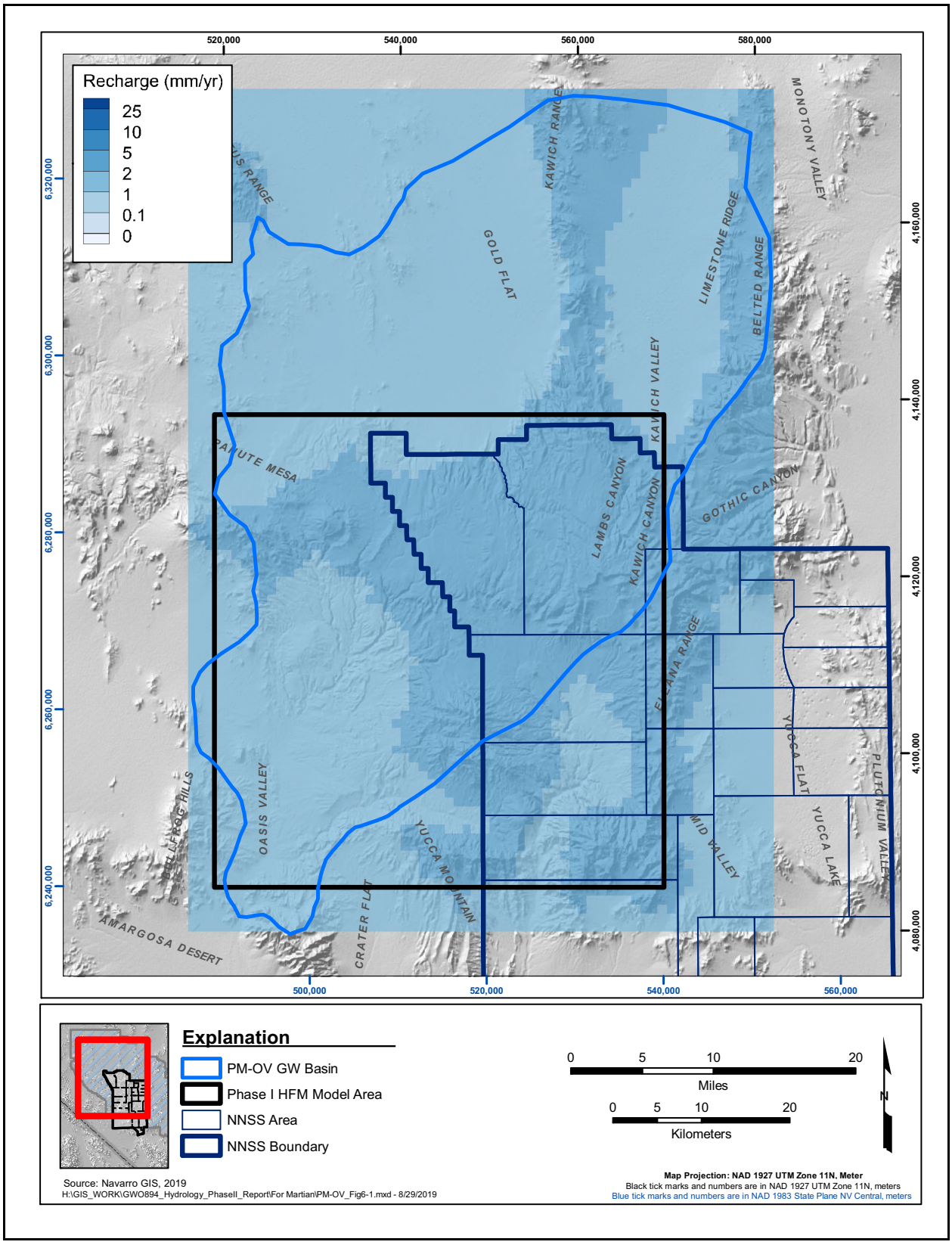

Figure 6-2
Modified Maxey-Eakin Recharge Distribution within the PM-OV HFM Area, as Estimated by Fenelon et al. (2016, Appendix B) Using the PRISM Model

The relative distribution of recharge estimated by the INFIL code was assumed correct, as published, but the absolute amount was allowed to be scaled up or down during the balancing analysis. The best fit used a multiplier of 0.9. The overall balance using the INFIL recharge dataset was significantly worse than the balance from the modified Maxey-Eakin method. The RMS error for INFIL was 4,200 acre-ft/yr (5,174,400 m^3/yr), as compared to 1,300 acre-ft/yr (1,601,600 m^3/yr) for the Maxey-Eakin method. An acceptable target error is about 2,000 acre-ft/yr (2,464,000 m^3/yr). The total recharge amount for the PM-OV groundwater basin was estimated as 9,016 acre-ft/yr (11,107,712 m^3/yr) (Fenelon et al., 2016).

Figure 6-3 presents the distribution of recharge rates resulting from the application of the INFIL code that is within the PM-OV HFM model domain. Recharge is highest in the highlands of the Kawich and Belted Ranges, Rainier Mesa and eastern Pahute Mesa. Recharge is also high in some of the washes including Fortymile Wash and the Amargosa River channel. Recharge becomes lower toward western Pahute Mesa. Little or no recharge occurs in Gold Flat and the Kawich Valley. The pattern of recharge exhibits a large amount of spatial variability compared to the recharge rates estimated with the Maxey-Eakin method.

6.2.1.3 Local-Scale Analysis Using a Numerical Model Applied by USGS

The numerical groundwater model used in the local-scale analysis of basin delineation is documented in *Delineation of the Pahute Mesa-Oasis Valley Groundwater Basin, Nevada* (Fenelon et al., 2016). A single-layer, groundwater-flow model was constructed to simulate steady-state water levels within the delineated PM-OV groundwater basin boundary. The recharge rates used by the numerical model were calibrated using a total of 355 pilot points, and recharge rates were interpolated from pilot points to model cells with kriging. Initial conditions for the recharge distribution were based on a conceptual model of recharge created from PRISM (PRISM Climate Group, 2012), geology at the water table, slope of land surface, and runoff accumulation distributions. The following is taken from Fenelon et al. (2016):

> *"Internal consistency* [of the Basin Delineation] *was tested by calibrating a numerical model of groundwater flow to water-level, land-surface, transmissivity, and discharge observations in the PMOV groundwater basin. Estimated recharge rates and transmissivities in the numerical model also were constrained to expected values from the conceptual model."*

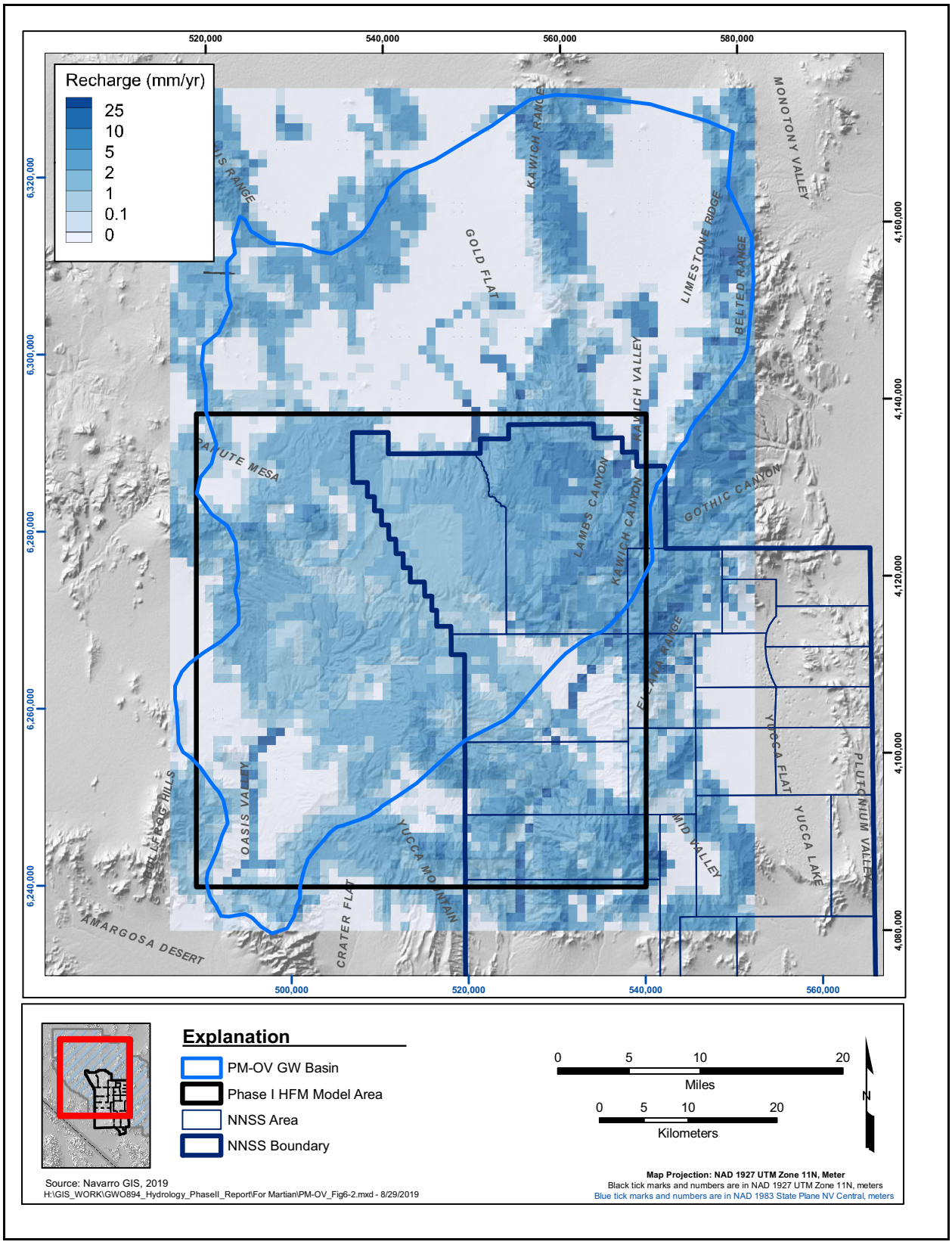

Figure 6-3
Recharge Distribution within the PM-OV HFM Area, as Estimated by Fenelon et al. (2016, Appendix B) Using the INFIL.v3 Model (Hevesi, 2006)

> *"A recharge distribution was estimated for the PMOV model based on a conceptual model that areas with higher precipitation rates have higher recharge rates and precipitation falling on low-permeability rocks moves laterally until it can infiltrate more permeable materials."*
>
> *"Distributed recharge is conceptualized as a piece-wise linear function of total annual precipitation, as defined by the 1981–2010 distribution of precipitation in PRISM (PRISM Climate Group, 2012). A two-stage relation between precipitation and total potential recharge (infiltration and runoff recharge) is assumed. The water available for recharge was estimated from precipitation in excess of 0.4 ft/yr, consistent with the modified Maxey-Eakin method. From 0.4 to 1 ft/yr, the proportion of recharge increases from 0 to 1 percent of the annual precipitation (fig. 7A). For more than 1 ft of annual precipitation, the slope of the function increases more than tenfold, so that about 7 percent of precipitation is converted to recharge at a precipitation rate of 1.5 ft/yr."*
>
> *"In areas of low-permeability bedrock, a small (less than 0.01 ft/yr) volume of water is conceptualized to infiltrate directly into the low-permeability bedrock, but most available water is assumed to run off and infiltrate down-gradient on alluvial fans (fig. 8). Recharge from runoff was estimated in Gold Flat and Kawich Valley, where water levels indicated that some local recharge from runoff was occurring. The volume of water available for recharge on fans was halved because runoff is subject to greater evaporative losses in alluvial channels. Recharge is assumed not to occur on valley floors, which were defined as areas with land-surface slopes of less than 1.5 percent. The valley floors have clay-rich soils, low precipitation rates, and warm air temperatures, which promote retention of soil water and evapotranspiration.The relation between total conceptual recharge and precipitation in excess of 1 ft/yr was adjusted so that the cumulative volume of annual recharge totaled 5,900 acre-ft, equal to the groundwater discharge from Oasis Valley."*

The total recharge amount for the PM-OV groundwater basin was simulated as 6,001 acre-ft/yr (7,393,232 m^3/yr), which includes 100 acre-ft/yr of subsurface discharge that occurs through a narrow section of saturated alluvium at the terminus of Oasis Valley (Fenelon et al., 2016). Figure 6-4 presents the distribution of recharge simulated by the numerical model. Recharge exceeds 25 mm/yr (1 in./yr) in the highest elevation of eastern Pahute Mesa and lower (typically 2 to 5 mm/yr) (0.08 to 0.3 in./yr) in the lower elevations, western end of Pahute Mesa.

6.2.1.4 INFILv3 Model as Applied by LANL

The application of the INFIL code to a portion of the PM-OV groundwater basin is documented in *Net Infiltration Models for the Pahute Mesa Area* (Middleton et al., 2017). This work is a refinement of previous studies and uses daily data from 26 meteorological stations in the NNSS area. Daily water

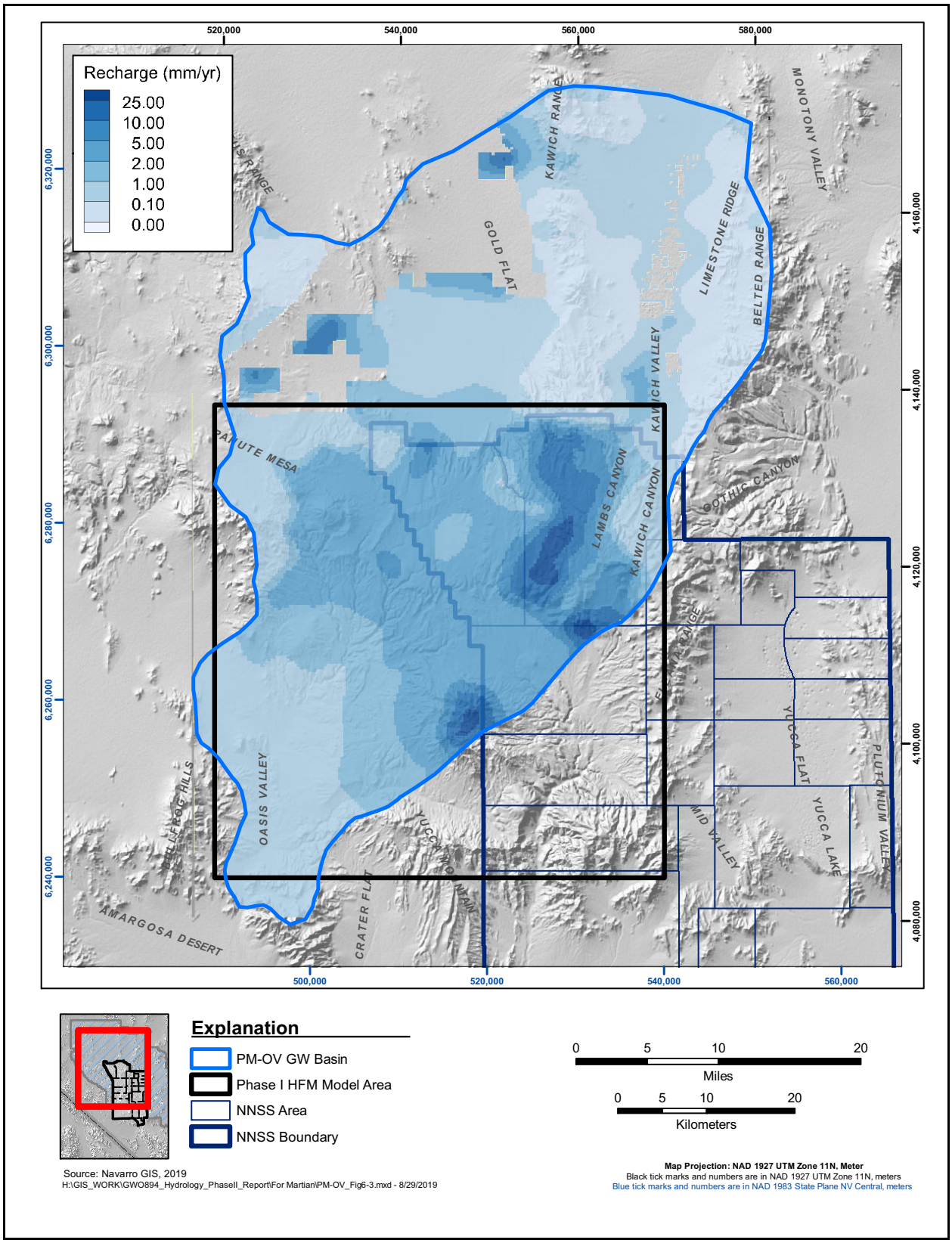

Figure 6-4
Simulated Recharge Distribution from Steady-State Groundwater Flow Model of the PM-OV Groundwater Basin by Fenelon et al. (2016)

balances were calculated for each multilayer cell using a 50-by-50-m-resolution DEM, which allowed surface topographic features, geology, and soil and vegetation characteristics to be defined with greater precision than could be represented in previous infiltration studies using the INFIL code, which were performed on a regional scale. The following description is taken from Middleton et al. (2017):

> "*This study estimates net infiltration rates for the Pahute Mesa-Oasis Valley (PM-OV) area that can help constrain the water balance for groundwater flow models being developed for the PMOV flow system. The study uses a spatially-distributed, local water balance model—INFIL3.0 (USGS, 2008a, b)—to calculate the amount of water entering and leaving a soil/bedrock column and estimate long-term net infiltration rates below the root zone. Five maps of spatially distributed net infiltration were produced with the INFIL3.0 infiltration model for the Pahute Mesa Flow and Transport Model domain. Daily water balances were calculated for each multilayer cell in a roughly 50-by-50-km digital elevation model (DEM) for the study area. The DEM had a 50-by-50-m resolution, which allowed surface topographic features, geology, and soil and vegetation characteristics to be defined with greater precision than could be represented in past regional infiltration studies using INFIL2.0 (Hevesi et al., 2003). The INFIL3.0 model uses measurements of daily precipitation (rain and snow), minimum and maximum daily temperature, potential evapotranspiration (PET), soil properties and thickness, and vegetation type and density as inputs to calculate daily water balance components in each cell. These daily water balance components include surface infiltration, runoff and run-on, actual evapotranspiration (ET), sublimation, changes in soil moisture storage and deep drainage (net infiltration).*"

> *"Five different infiltration models are presented in this report, which are differentiated primarily by slope-dependent soil hydraulic conductivities that reflect shorter residence time of surface water on sloping terrain and using alluvium-like soil and bedrock parameters in river channels and streambeds to enhance infiltration beneath these features. The basic spatial pattern of net infiltration is similar among the maps, which differ primarily in the magnitude of the infiltration and how it is apportioned between channel and non-channel areas.*"

Figure 6-5 illustrates the boundary of the PM-OV groundwater basin identified by Fenelon et al. (2016) along with the INFILv3 recharge rate (Phase I transport model area boundary). The PM-OV groundwater basin extends to the north of the INFILv3 model study area into Gold Flat, the Kawich Range, and Kawich Valley. The southeast quadrant of the INFILv3 infiltration study area is part of the Alkali Flat/Furnace Creek Ranch (AFFCR) flow system and does not discharge to Oasis Valley. An estimated 2,000 acre-ft/yr of recharge occurs north of the INFILv3 model area within the PM-OV

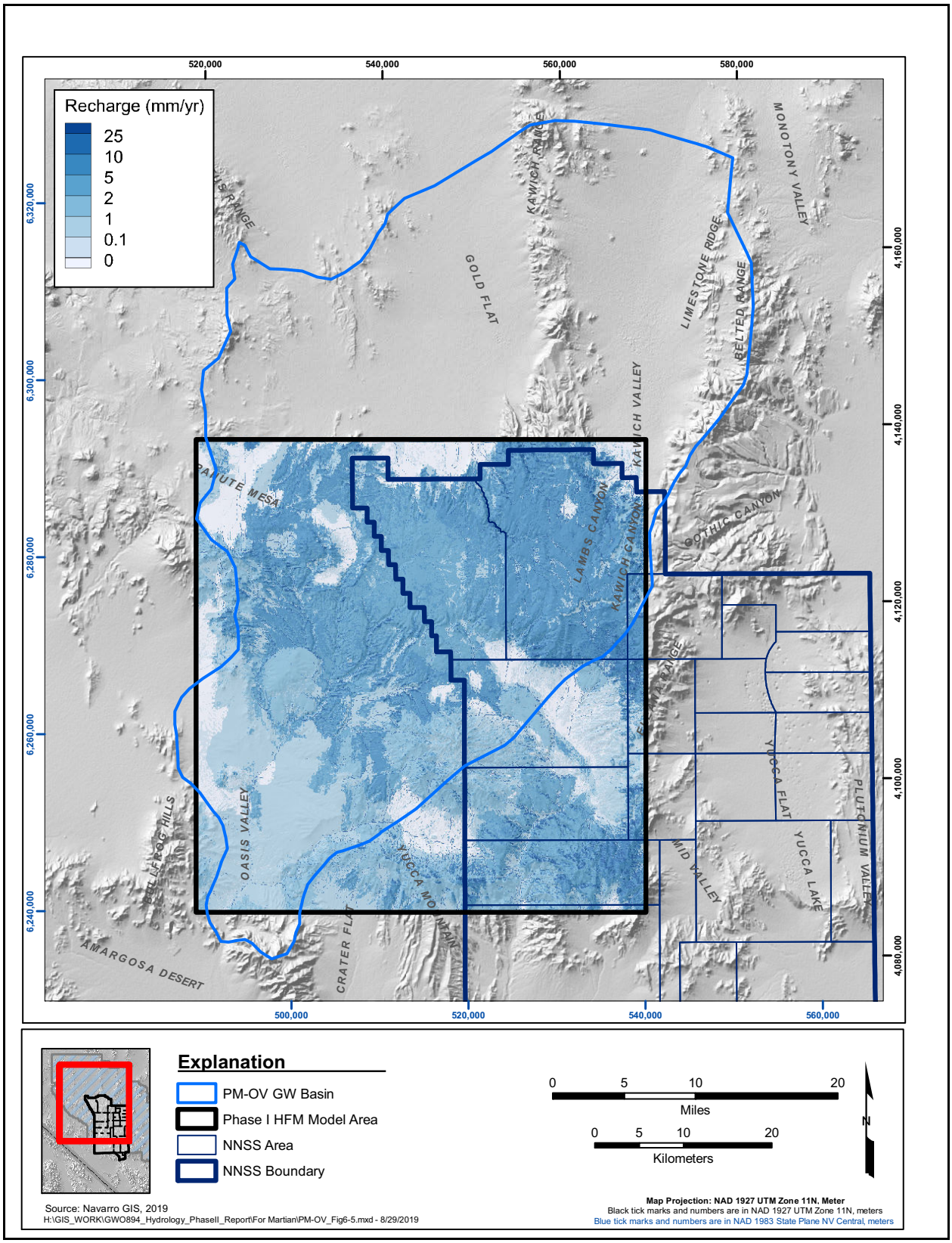

Figure 6-5
LANL INFIL Code Recharge Distribution from Model 4

groundwater basin, and another 2,000 acre-ft/yr of recharge occurs in the southeast quadrant of the INFILv3 model area that is within the AFFCR groundwater basin (Middleton et al., 2019).

The basic spatial pattern of recharge reflects the topographic influences on precipitation and the estimated spatial distribution of soil and rock properties. Each of the models predict that recharge beneath alluvium on the valley floors is negligibly small compared with most upland areas except beneath ephemeral washes. Recharge is strongly correlated with the soil's storage capacity. Larger values of soil storage capacity delay drainage and allow more transpiration (Middleton et al., 2019).

Table 6-1 presents the annual net infiltration rates, based on 54 years of meteorological data over the model domain and the annual recharge volume over the model area that is located within the PM-OV groundwater basin. The average recharge rate is approximately 3 to 6 mm/yr (0.12 to 0.24 in./yr), and the annual recharge volume is approximately 4,000 to 9,000 acre-ft/yr (4,928,000 to 11,088,000 m^3/yr) within the PM-OV groundwater basin. The results of five different infiltration models are presented in Table 6-1. The annual recharge volumes presented in Table 6-1 should include an additional 2,000 acre-ft/yr to represent the area north of the INFILv3 model domain that is within the total PM-OV groundwater basin but was not included in the model. Figure 6-5 presents the distribution of recharge within the INFILv3 model domain for model 4. Recharge is higher (5 to 10 mm/yr) toward the higher elevations (eastern end of Pahute Mesa) and lower (typically 2 to 5 mm/yr) toward the lower elevations (western end of Pahute Mesa) where precipitation rates are lower.

Table 6-1
Annual Net Infiltration Rates by LANL Models

Model Number	Average Recharge (mm/yr)	Annual Recharge Volume in Model Domain (acre-ft/yr)	Annual Recharge Volume in Model Domain within PM-OV Groundwater Basin (acre-ft/yr)*
1	3.1	6,778	4,199
2	6.2	13,766	8,991
3	4.8	10,620	7,296
4	5.4	11,893	8,164
5	3.5	7,637	4,597

*Annual volume does not include an estimated 2,000 acre-ft/yr occurring north of the INFILv3 model domain.

6.3 Precipitation Recharge Uncertainty

Fenelon et al. (2016) concluded that with reasonable groundwater basin delineations, there is sufficient derived recharge to supply the discharge occurring within the PM-OV groundwater basin. The water balance within the PM-OV groundwater basin is also constrained by balances in adjacent groundwater basins, as each of the basins requires sufficient recharge water to supply discharge areas. Groundwater discharges to Oasis Valley have been well-characterized (Reiner et al., 2002), and inter-basin flow between the PM-OV groundwater basin and adjacent basins is thought to be insignificant (Fenelon et al., 2016).

Middleton et al. (2019) compared estimates of recharge rates and annual recharge volumes within the PM-OV groundwater basin from the LANL application of the INFILv3 code and three other studies using the Maxey-Eakin approach (Rush, 1970; SNJV, 2004a) and the groundwater chloride mass-balance approach (Cooper et al., 2013). Without consideration of mass-balance constraints from discharge volumes within the PM-OV groundwater basin and the surrounding basins, the total volume of annual recharge within the PM-OV groundwater basin varied within a factor of 5 among the various studies.

Sensitivity and uncertainty analyses of annual ET were conducted by Laczniak et al. (2001) as part of their ET study of the Death Valley regional groundwater flow system. The objective of the sensitivity analysis was to identify the input parameters that have the greatest effect on the annual ET values, and the objective of the uncertainty analysis was to quantify the uncertainty associated with estimates of annual groundwater discharge by ET from the nine discharge areas of the Death Valley flow system, which includes the PM-OV discharge areas. The ET estimates ranged between approximately 4,200 to 8,900 acre-ft/yr (7.7E+06 to 1.1E+07 m^3/yr). With consideration of mass-balance constraints from discharge volumes, uncertainty in the total recharge occurring within the PM-OV groundwater basin is likely a factor of 2. However, on a local scale within the basin, the uncertainty associated with spatial variability of recharge is higher.

6.4 Precipitation Recharge Summary

To define upper boundary conditions for the flow model, the quantity and spatial distribution of recharge are needed. Four recharge analyses have recently been performed to estimate the quantity and spatial distribution of recharge within the PM-OV groundwater basin. The analyses included a

modified Maxey-Eakin (1951) approach, a local-scale numerical model, and two different applications of the INFIL code. These models used different approaches and input datasets of basin hydrological parameters. However, the basic spatial pattern of recharge reflects the topographic influences on precipitation. Recharge is higher toward the higher elevations at the eastern end of Pahute Mesa and lower toward the lower elevation on the western end of the mesa. Recharge is near zero at the PM-OV groundwater basin terminus in Oasis Valley.

The Maxey-Eakin approach is an empirically derived method relating recharge to precipitation zones from a base precipitation map. Recharge rates are estimated by multiplying annual precipitation amounts within specified precipitation ranges by coefficients that represent the fraction of precipitation that is converted to recharge (Maxey-Eakin, 1950). Fenelon et al. (2016) balanced recharge against discharge simultaneously within the PM-OV and surrounding basins, when applying the Maxey-Eakin approach.

The INFIL code model calculates a daily water-balance model of the root zone. The daily water balance includes precipitation, snow accumulation, sublimation, snow-melt, infiltration into the root zone, ET, and drainage. Surface water runoff is defined as excess rainfall or snow-melt and surface water run-on is defined as runoff that is routed downgradient. The USGS application of the INFIL code (Fenelon et al., 2016) was taken from the INFILv3 model for the Death Valley regional groundwater flow system (Hevesi, 2006) and balanced simultaneously against discharge rates using a multiplier. The overall balance using the INFIL recharge dataset was significantly worse than the balance from the modified Maxey-Eakin method. The RMS error for INFIL was approximately twice as large as the acceptable target error of about 2,000 acre-ft/yr.

The USGS local-scale analysis used ensured that groundwater data from the PM-OV groundwater basin are internally consistent with the defined basin boundary delineation. A numerical, single-layer, steady-state, groundwater-flow model was created that matched measured water levels, groundwater discharges, and transmissivities. Initial conditions for the recharge distribution were based on a conceptual model that areas with higher precipitation rates have higher recharge rates and precipitation falling on low-permeability rocks moves laterally until it can infiltrate more permeable material. Recharge was then calibrated and distributed in the numerical model with a total of 355 pilot points, and recharge rates were interpolated from pilot points to model cells with kriging.

The LANL INFILv3 model is a refinement of previous INFIL code studies that used daily data from 26 meteorological stations in the NNSS area. Daily water balances were calculated for each multilayer cell using a 50-by-50-m-resolution DEM, which allowed surface topographic features, geology, and soil and vegetation characteristics to be defined with greater precision than could be represented in previous infiltration studies using the INFIL code. Five different infiltration models were created, which used different slope-dependent soil hydraulic conductivities that reflect shorter residence times of surface water on sloping terrain and used alluvium-like soil and bedrock parameters in river channels and streambeds to enhance infiltration beneath these features (Middleton et al., 2019).

The recharge distribution, as defined by the modified Maxey-Eakin method, may not be appropriate for use in the Pahute Mesa CAU flow model because it was primarily intended to provide gross water balances between basins. A more precise approach may be needed to define the local distribution near the nuclear testing areas. The recommended approach for simulating recharge within the CAU-scale model is to use the local scale analysis from Fenelon et al. (2016) or the recharge from the INFIL code (Middleton et al., 2019) with a scaling factor to bring the total recharge into balance with the estimated discharges As was done in the USGS local-scale analysis modeling, the recharge distribution may require adjustment during the model calibration, and the pilot point method can be used. The recharge distributions from Fenelon et al. (2016) or Middleton et al. (2019) can be used as initial conditions. The discharge estimates at specific locations from Reiner et al. (2002) will be specified, and the total basin discharge along with spring elevations will be used as observations in the model calibration. The uncertainty analysis should consider that the total recharge occurring within the PM-OV groundwater basin is likely certain within a factor of 2, but on a local scale within the basin, the uncertainty associated with the spatial variability of recharge can be much greater.

7.0 GROUNDWATER DISCHARGE

Within the PM-OV basin, most groundwater discharge to the surface occurs naturally in the form of ET and springs at the Oasis Valley discharge area. Some groundwater is also withdrawn from the flow system at wells. The area of interest to this activity includes the PM-OV basin as defined by Fenelon et al. (2016) (Figure 2-1). The purpose, approach, and results of the analysis of the data available on groundwater discharge to the surface are presented in this section.

7.1 Objectives

The general purpose of this data analysis activity is to define locations and rates of groundwater discharge to the surface occurring within the PM-OV basin.

The specific objectives are as follows:

- Identify locations of natural discharge.
- Provide estimates of mean rates of discharge.
- Provide information on well discharge rates.
- Assess and quantify associated uncertainties.

7.2 Approach

The approach used to complete the data analysis of groundwater discharge to the surface depended on the major data types (i.e., natural discharge and well discharge).

Natural Discharge

Natural discharge to the surface from the PM-OV basin occurs in the form of springs and ET in the Oasis Valley discharge area. However, because of the processes involved, these two forms of discharge are not independent. In Oasis Valley, most groundwater discharged from springs does not leave the valley by surface flow. Surface water flow out of the valley occurs mostly through the Amargosa River on an intermittent basis. Spring water either re-infiltrates into the flow system or evaporates. Thus, the majority of the groundwater discharged by springs is effectively lost from the groundwater system through ET within the discharge area. In addition, ET estimates include water

that moves up from the underlying regional flow system into the shallow flow system (Reiner et al., 2002). Total spring discharge could provide a lower bound for ET estimates; however, spring flow rates are difficult to measure at the numerous seeps and at spring locations that are inaccessible. The net natural groundwater discharge to the surface is, therefore, best approximated by an estimate of ET. Thus, the approach used to analyze the natural discharge information is as follows:

- Review and summarize the available ET studies for the PM-OV area and vicinity.
- Evaluate their level of documentation.
- Evaluate the level of quality.
- Describe the ET areas, and estimate their extent
- Provide estimates of mean annual ET rates and the associated range of uncertainty.

Well Discharge

Wells of interest to this activity are only those that pumped or have been pumping for longer than a year. Discharge data collected during short-term pumping such as that conducted during well testing are not included. The approach to analysis of the well discharge data was as follows:

- Compile available historical well pumping data.
- Assess pumping record completeness.
- Estimate groundwater withdrawal from domestic wells.
- Calculate or estimate annual discharge rates.

7.3 Data Types Required

Data types required for ET and well discharge are as follows:

ET Data

- Location and extent of ET areas within the Oasis Valley discharge area
- Estimates of mean annual ET rates for each area
- Estimates of uncertainty associated with annual ET rates for each area

Well Discharge Data

- Site identification (ID) name/number
- Site coordinates
- Dates discharge rate measured
- Discharge measurement

These data were acquired from published reports prepared by USGS. USGS is a project participant and has QA procedures in place that are the equivalent to those of UGTA's. These data are acceptable for inclusion in the model.

7.4 Available Data Description

Available data for natural groundwater discharge and well discharge are summarized in the following subsections. An assessment of the quality of the documentation and the data is also provided.

7.4.1 Natural Surface Discharge

Prior to the 1990s, only two reports provided estimates of ET for the Oasis Valley discharge area: Malmberg and Eakin (1962), and Blankennagel and Weir (1973). Starting in 1993, USGS, in cooperation with DOE, initiated a series of studies to refine and improve previous estimates of groundwater discharge for the NNSS region, including the Oasis Valley discharge area. The first study was focused on the Ash Meadows discharge area (Laczniak et al., 1999). The second study was initiated in 1996 and was focused on Oasis Valley. Estimates based on early measurements of ET at Oasis Valley during this study were made by Laczniak (1996) and were reported in the regional model report (DOE/NV, 1997; IT, 1996a). The results of the completed Oasis Valley study were later published by Reiner et al. (2002). During the same period of time, Laczniak et al. (2001) estimated annual ET for discharge areas located within the Death Valley regional groundwater flow system, including the Oasis Valley discharge area.

Malmberg and Eakin (1962) estimated the annual ET for Oasis Valley as part of a reconnaissance study. An estimate of the annual ET was calculated as the product of the acreage and the average ET rate. The ET area was delineated using vegetation and soil maps available at the time. The average ET rate was estimated from ET rates reported for other areas of the southwestern United States having similar phreatophytes as Oasis Valley (Lee, 1912; Robinson, 1958; White, 1932; Young and Blaney, 1942). Their estimate of ET was about 7,000 cubic meters per day (m^3/day) (2,000 acre-ft/yr) (Malmberg and Eakin, 1962). Malmberg and Eakin (1962) also estimated spring discharge rates for selected springs of Oasis Valley.

Blankennagel and Weir (1973) later reported that annual groundwater discharge from Oasis Valley might exceed the Malmberg and Eakin (1962) estimate by a factor of 2 or more (greater than

14,000 m^3/day [4,800 acre-ft/yr]). Their estimate was based on unpublished USGS studies conducted at the time by Beetem and Young of USGS.

Early measurements of ET during the Oasis Valley study later reported by Reiner et al. (2002) confirmed the findings reported by Blankennagel and Weir (1973). Using the early measurements of ET, Laczniak (1996) estimated the range of ET from the Oasis Valley discharge area to be between 5,000 to 8,000 acre-ft/yr (17,000 to 27,000 m^3/day). This range was used in the regional model (DOE/NV, 1997).

Reiner et al. (2002) conducted a comprehensive study on groundwater discharge in the Oasis Valley. This study was initiated to address the concern raised by Blankennagel and Weir (1973) and later by the findings of studies by Johnson (1993), Nichols et al. (1997), and Laczniak et al. (1999) suggesting that ET rates for local phreatophytes may be higher than those used by Malmberg and Eakin (1962) for Oasis Valley. The purpose of this study was to estimate groundwater discharge by quantifying ET, estimating subsurface outflow, and compiling groundwater withdrawal data. In addition to discharge by ET, Reiner et al. (2002) also measured spring discharge and groundwater levels to help evaluate ET and characterize hydrologic conditions. The main objective was to refine and improve the current estimates of ET from the Oasis Valley discharge area.

The study included an extensive field data collection program and detailed analyses. The method used by Reiner et al. (2002) to quantify ET is similar to that used by Laczniak et al. (1999) for the Ash Meadows discharge area. This method is a refinement of the Malmberg and Eakin (1962) method. Refinements include the incorporation of satellite imagery and remote-sensing techniques to better define the ET units, and the use of long-term micrometeorological data to calculate ET rates for each ET unit. In addition, nearly continuous measurements of water level collected during the study were used to build confidence in the locations and quantities of ET.

Laczniak et al. (2001) published the results of studies on groundwater discharge in the Death Valley regional groundwater flow system. The purpose of their study was to estimate mean annual ET from discharge areas located within the Death Valley flow system, including Oasis Valley. The approach used by Laczniak et al. (2001) was basically the same as the one used by Reiner et al. (2002) and Laczniak et al. (1999). For the Oasis Valley discharge area, Laczniak et al. (2001) used most of the data that had been collected by Reiner et al. (2002) at the time. However, their estimates of mean annual ET for the Oasis Valley discharge area are slightly different from those reported by Reiner

et al. (2002) due to differences in data interpretation. In addition to mean annual ET, Laczniak et al. (2001) presented estimates of uncertainty associated with annual ET using Monte Carlo simulations.

7.4.2 Well Discharge

The pumping data, their sources, and prioritization for further evaluation are discussed in this subsection.

Groundwater is withdrawn from the flow system from several wells located within or near the PM-OV area. These wells have been classified into the following groups:

- NNSS water-supply wells
- Beatty municipal wells
- Domestic water wells
- Livestock water wells

Pumping data for the NNSS water-supply wells are compiled on a monthly and yearly basis by USGS from records provided by the NNSS M&O contractor. Pumping data for the Beatty municipal wells are recorded by the Beatty Water and Sanitary District (BWSD) and were obtained from USGS.

7.5 Natural Surface Discharge

The studies conducted by Reiner et al. (2002) and Laczniak et al. (2001) were selected to provide estimates of natural discharge for this activity because of their high level of quality. The following description of natural discharge from the Oasis Valley discharge area was summarized from the reports prepared by Reiner et al. (2002) and Laczniak et al. (2001).

7.5.1 Description of Oasis Valley Discharge Area

Natural groundwater discharge to the surface within the PM-OV area and vicinity occurs by springflow or ET within the Oasis Valley discharge area.

Reiner et al. (2002) report that approximately 75 springs and seeps are mapped throughout Oasis Valley. Spring flow rates range from less than 1 gallon per minute (gal/min) to more than 200 gal/min. Water temperatures had previously been reported to be between about 16 degrees Celsius (°C) (60 degrees Fahrenheit [°F]) to more than 38 °C (100 °F) (White, 1979; McKinley et al., 1991). Reiner et al. (2002) grouped the springs of Oasis Valley according to their hydrogeologic setting into

seven groups as presented in Table 7-1 and Figure 7-1. Except for Group 7 (Bullfrog Hills) which consists of perched springs, all other groups are believed to be regional springs. The source of water is believed to be a portion of the groundwater flowing in the volcanic rocks of Western Pahute Mesa (Reiner et al., 2002). In general, these source areas are consistent with the end-member water types identified by Rose et al. (2002) in the PM-OV flow system. It is also likely that as one moves to the south, the springs discharge some mixture of groundwater from recharge areas, as well as contributions from overland flow and reinfiltration of spring discharge, that occurred further to the north.

Table 7-1
Description of Springs Occurring in Oasis Valley [a]

Group Number	Group Name	Probable Cause	Source
1	Colson Pond	Transmissivity change across the Colson Pond fault	Likely fed by water flowing from the north and northeast
2	Oasis Mountain Hogback	Abrupt westward thinning of the WTA across the Hogback fault	Likely fed by water flowing from Pahute Mesa
3	Amargosa River	Transmissivity change and disruption in aquifer continuity across the Beatty fault	Likely fed by a mixture of the water flowing into Oasis Valley from the east, west, and north
4	Hot Springs	Upward flow along the Hot Springs fault (elevated water temperatures [about 105 °F])	Likely fed by flow from the east and north, possibly Timber Mountain and/or Pahute Mesa
5	Lower Amargosa River	--	Probably fed primarily by water flowing from the north through Oasis Valley
6	Upper Amargosa River	Transmissivity change and disruption in aquifer continuity across the Beatty fault	Likely fed by inflow from the north and northwest (White, 1979)
7	Bullfrog Hills	Permeability changes within the WTA caused by hydrothermal alteration	Likely fed by local recharge to nearby highlands and therefore perched

Source: Adapted from Reiner et al., 2002

-- = Not available

[a] See Figure 7-1 for locations.

Once at the surface, groundwater emerging from springs and seeps is captured in local marshes and small pools, or is channeled into free-flowing drainages. It then evaporates into the atmosphere or infiltrates valley fill deposits. The valley fill aquifer also receives water from the regional WTA both by diffuse or preferential, fault-associated upward flow. Water in the valley fill aquifer maintains a

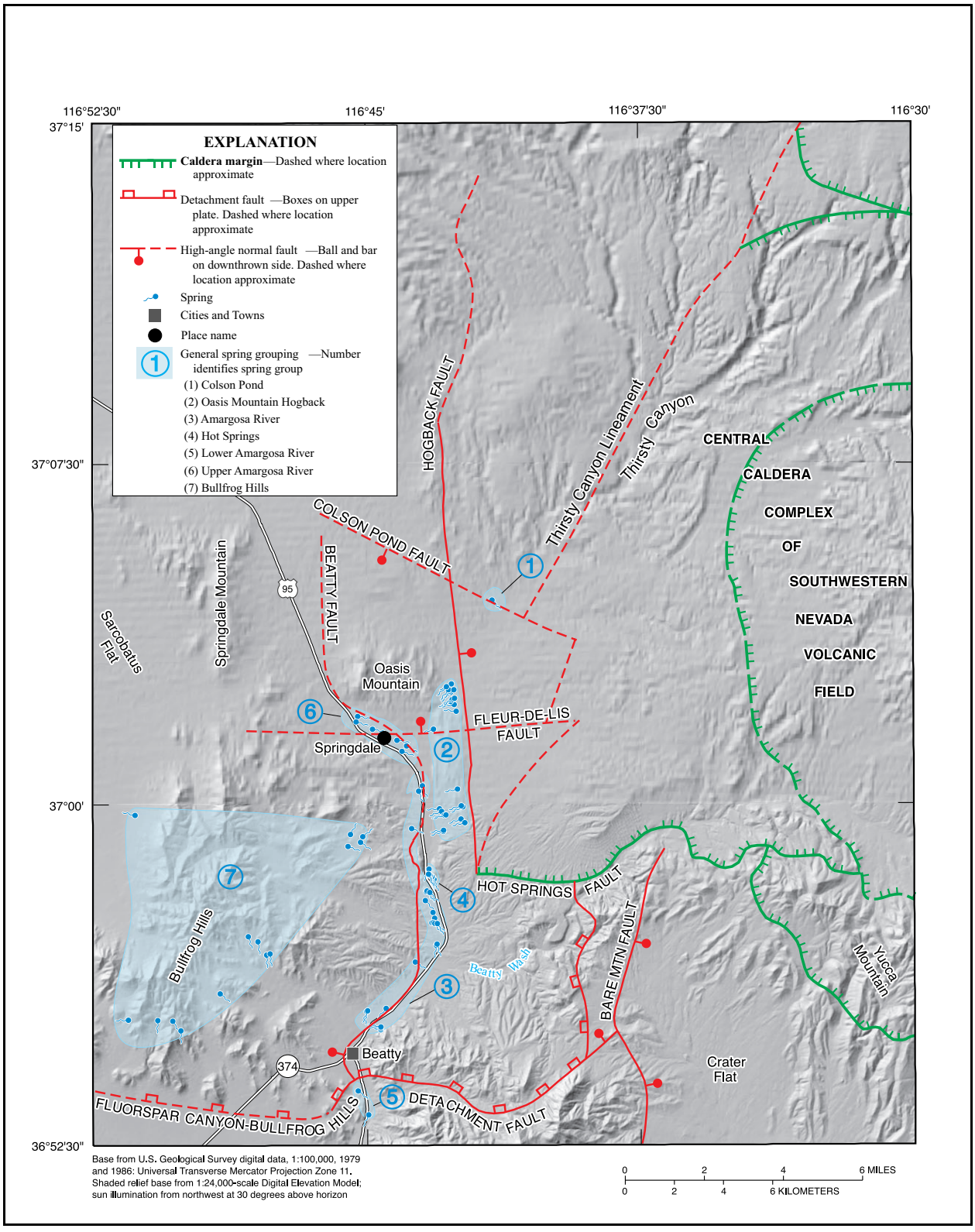

Figure 7-1
General Spring Locations and Major Structural Features Controlling Spring Discharge in Oasis Valley
Source: Reiner et al., 2002

variety of plants within the discharge area and vicinity, including grasses, reeds, shrubs, and trees. This vegetation serves as a major vehicle for natural discharge from the area through transpiration.

Little surface water flows out of Oasis Valley except during short periods that follow occasional, intense rainstorms (Reiner et al., 2002). The main drainage is the Amargosa River, which is an intermittent stream. Only reaches located directly downgradient from major springs or spring-fed streams flow on a continuous basis. A small amount of water leaves Oasis Valley via the Amargosa River and through the subsurface across the Amargosa River Narrows (Reiner et al., 2002). An estimated 300 acre-ft/yr flows southward out of the Oasis Valley via the Amargosa River. An additional subsurface discharge to the Amargosa Desert through alluvium is estimated at 100 acre-ft/yr (Fenelon et al., 2016).

7.5.2 Methodology

Reiner et al. (2002) approximated the natural loss of groundwater to the surface from the Oasis Valley discharge area with an estimate of the ET from areas of groundwater discharge. Such an estimate not only includes water losses by springs and seeps, but also water flowing upward from the regional WTA into the AA.

The method used by Reiner et al. (2002) and Laczniak et al. (2001) to quantify ET from the Oasis Valley discharge area is similar to that used by Laczniak et al. (1999) for the Ash Meadows discharge area.

As stated by Laczniak et al. (2001), the method is based on the following assumptions:

- ET rates vary with the health, density, and type of vegetation; and with the wetness of the soil.
- Within a given discharge area, ET rates can be generalized on the basis of similarities in vegetation and soil conditions.

The method consists of the following four basic steps:

1. ET units, which are defined as areas of similar plant cover and soil cover, are identified and mapped using Landsat Thermatic Mapper (TM) imagery. Spatial changes in vegetation and soil covers are interpreted from remotely sensed spectral reflectance data and used to delineate ET units on the basis of spectral similarities identified from the TM imagery.

2. ET rates are calculated from field measurements of micrometeorological data (localized) using the Bowen-ratio method. An annual ET rate is then estimated for each of the ET units by averaging all ET rates available for sites located within that unit. The ET rates are then adjusted by removing water contributed by local precipitation from the estimates.

3. Annual ET from each ET unit is computed as the product of the unit's acreage and ET rate.

4. Total ET is calculated by adding estimates of annual ET computed for ET units.

In addition, water-level and spring discharge fluctuations may be used to verify the locations and relative magnitude of ET.

7.5.3 ET Units

In both studies (i.e., Reiner et al., 2002; Laczniak et al., 2001), the TM data used to classify ET units within the Oasis Valley area were imaged June 13, 1992 (scene identification number LT5040035009216510, Figure 7 in Reiner et al.'s report [2002]). Reiner et al. (2002) and Laczniak et al. (2001) decided to use the June 1992 TM imagery for the following reasons:

- June is a period of high vegetation vigor.
- 1992 had slightly above-normal precipitation.
- The authors wanted to be consistent with the Ash Meadows ET study (Laczniak et al., 1999).

ET unit definitions were very similar in the two studies (Table 7-2). However, in addition to the nine ET units defined by Reiner et al. (2002), Laczniak et al. (2001) defined two new ET units (9 and 10) to segregate areas dominated by sparse woodland vegetation, and areas dominated by open playa, respectively.

As shown in Table 7-2, the two studies yielded very similar results in terms of ET unit differentiation for the Oasis Valley discharge area. The areas were, however, not identical for some of the ET areas. The difference was due to difficulty in discriminating between the two grassland ET units, labeled sparse to moderately dense grassland (SGV) and moderately dense to dense grassland (DGV) by Reiner et al. (2002) and sparse grassland and dense to moderately dense grassland by Laczniak et al. (2001) (Table 7-2). This difficulty led to two different interpretations. Laczniak et al. (2001) interpreted some of the grassland classified as moderately dense grassland cover by Reiner et al. (2002) as dense grassland (DGV). This resulted in different ET unit areas for the two units (Table 7-2).

Table 7-2
ET Units Determined from Spectral Analysis of Satellite Imagery Data, Oasis Valley Discharge Area, Nevada, June 13, 1992
(Page 1 of 2)

Laczniak et al. (2001)			Reiner et al. (2002)		
ET Unit ID	**ET Unit Area (m^2)**	**General Description of ET Unit**	**ET Unit ID**	**ET Unit Area (m^2)**	**General Description of ET Unit**
0	0	Area of no significant ET from groundwater source (unclassified); water table typically greater than 50 ft bgs.	UCL	0	Area of no substantial ET from groundwater source (unclassified); water table typically greater than 20 ft bgs; soil very dry.
1	4,047	Area of open water, primarily reservoir or large spring pool.	OWB	4,047	Area of open water, primarily spring pool or pond.
2	20,234	Area of submerged aquatic vegetation; includes sparse emergent vegetation and shallow part of open water areas; perennially flooded; water at surface.	SAV	16,187	Area of submerged and sparse emergent aquatic vegetation; includes primarily shallow part of open water areas; perennially flooded; water at surface.
3	161,874	Area dominated by dense wetland vegetation, primarily tall reedy and rushy marsh plants, typically tule, cattail, or giant reed; perennially flooded; water at surface.	DWV	161,874	Area dominated by dense wetland vegetation, primarily tall reedy and rushy marsh plants, typically tule, cattail, or giant reed; perennially flooded; water at surface.
4	3,767,627	Area dominated by dense meadow and forested vegetation, primarily trees, meadow grasses, or mixed trees, shrubs, and grasses; trees include saltcedar, mesquite, or desert willow; water table typically ranges from a few ft to about 20 ft bgs; soil moist to dry.	DMV	3,366,988	Area dominated by dense meadow and woodland vegetation, primarily trees, meadow and marsh grasses, or mixed trees, shrubs, and grasses; trees include desert ash and cottonwood, with some desert willow and mesquite; water table typically ranges from above land surface to about 20 ft bgs; soil wet to dry.
5	2,610,225	Area dominated by dense to moderately dense grassland vegetation, primarily saltgrass, and/or short rushes with an occasional tree or shrub; intermittently flooded; water table typically less than 5 ft bgs; soil wet to moist.	DGV	1,375,932	Area dominated by moderately dense to dense grassland vegetation, primarily saltgrass, and/or short rushes with an occasional tree or shrub; intermittently flooded; water table typically less than 10 ft bgs; soil wet to moist.
6	3,893,079	Area dominated by sparse grassland vegetation, primarily salt and bunch grasses but also includes areas of very low density shrubs (mesquite); water table typically ranges from a few ft to about 12 ft bgs; soil dry.	SGV	4,916,935	Area dominated by sparse to moderately dense grassland vegetation, primarily salt and bunch grasses with occasional tree or shrub; water table typically ranges from a few ft bgs to about 10 ft bgs; soil damp to dry.

Table 7-2
ET Units Determined from Spectral Analysis of Satellite Imagery Data, Oasis Valley Discharge Area, Nevada, June 13, 1992
(Page 2 of 2)

Laczniak et al. (2001)			Reiner et al. (2002)		
ET Unit ID	**ET Unit Area (m^2)**	**General Description of ET Unit**	**ET Unit ID**	**ET Unit Area (m^2)**	**General Description of ET Unit**
7	327,796	Area dominated by moist bare soil; vegetation very sparse, primarily grasses; intermittently flooded, water table typically near land surface throughout most of the year but in some areas declines to a maximum depth of about 5 ft bgs during late summer and early fall; soil typically moist.	MBS	412,780	Area dominated by moist bare soil; vegetation very sparse, primarily grasses; intermittently flooded, water table typically near land surface throughout most of the year but in some areas declines to a maximum depth of about 5 ft bgs during late summer and early fall; soil wet to moist.
8	3,265,816	Area dominated by sparse to moderately dense shrubland vegetation, primarily greasewood, rabbitbrush, wolfberry, and seepweed; water table typically ranges from about 5 ft to about 20 ft bgs; soil dry	SSV	3,609,799	Area dominated by sparse to moderately dense shrubland vegetation, primarily greasewood, rabbitbrush, and wolfberry; water table typically ranges from about 5 ft bgs to about 20 ft bgs; soil damp to dry.
9	--	Area dominated by sparse woodland vegetation, primarily mesquite; water table typically ranges from about 10 to 40 ft bgs; soil dry.	--	--	--
10	4,047	Area dominated by open playa, primarily bare soil, often encrusted with salts; water table ranges from about 5 to 40 ft bgs; soil typically dry but can be moist for short periods after intermittent flooding.	--	--	--

Source: Laczniak et al., 2001; and Reiner et al., 2002

m^2 = Square meter

-- = No data or not applicable

Notes: UCL = Unclassified; OWB = Open water; SAV = Submerged and sparse emergent aquatic vegetation; DWV = Dense wetland vegetation; DMV = Dense meadow and woodland vegetation; DGV = Moderately dense to dense grassland vegetation; SGV = Sparse to moderately dense grassland vegetation; MBS = Moist bare soil; SSV = Sparse to moderately dense shrubland vegetation.

The values of total ET area were very similar: Reiner et al. (2002) estimated the total ET unit area to be 13,864,542 m^2 (3,426 acres), whereas Laczniak et al. (2001) estimated the total to be 14,054,745 m^2 (3,473 acres). The difference in total ET area and other differences in ET unit areas derived from these two studies are minor. The values of total ET area reported by Reiner et al. (2002) and Laczniak et al. (2001) are also comparable to the 15,378,068 m^2 (3,800 acres) of phreatophytes

estimated by Malmberg and Eakin (1962). The ET unit distribution generated by Laczniak et al. (2001) is presented in Figure 7-2.

The accuracy of the classification method as applied to the Oasis Valley discharge area was assessed by Reiner et al. (2002) using the same method as Laczniak et al. (1999) for the Ash Meadows discharge area. In this method, a select number of sites are assigned to ET units on the basis of field observation. The assigned ET unit areas are then compared with those assigned using the classification procedure. The overall accuracy is calculated as the ratio of the number of sites correctly classified to the total number of sites compared.

The overall accuracy calculated by Reiner et al. (2002) for Oasis Valley was 88 percent. This accuracy is comparable to that reported by Laczniak et al. (1999), 86.6 percent, for the Ash Meadows discharge area. Reiner et al. (2002) also calculated an average accuracy of individual classes to be 91 percent. Both Reiner et al. (2002) and Laczniak et al. (1999) concluded that these accuracy values are above the acceptability criterion established by Anderson et al. (1976).

7.5.4 ET Rates and Volumes

ET rates and volumes, as derived by Reiner et al. (2002) and Laczniak et al. (2001), are described in this subsection.

Reiner et al. (2002) and Laczniak et al. (2001) derived ET rates for the ET units they defined differently. Reiner et al. (2002) derived ET rates from data they collected during their study of Oasis Valley and from data collected at Ash Meadows by Laczniak et al. (1999). ET rates were calculated from field measurements of micrometeorological data (localized) collected from five sites located within the Oasis Valley discharge area between 1996 and 2000, using the energy budget method (Bowen-ratio solution [Bowen, 1926]) (Table 7-3). Data obtained from nine similar ET sites in nearby Ash Meadows (Laczniak et al., 1999) were used to supplement their data (Table 7-3). An annual ET rate was then estimated for each of the ET units by averaging all ET rates available for sites located within that unit (Table 7-3). Laczniak et al. (2001) used ET rates estimated in other studies of areas located in the NNSS region. Their primary sources of data were the same as Reiner et al. (2002), which are, ET rates derived from field measurements of micrometeorological data at Oasis Valley (Reiner et al., 2002) and Ash Meadows (Laczniak et al., 1999). However, Laczniak et al. (2001) supplemented these data with rates estimated in other selected studies of ET

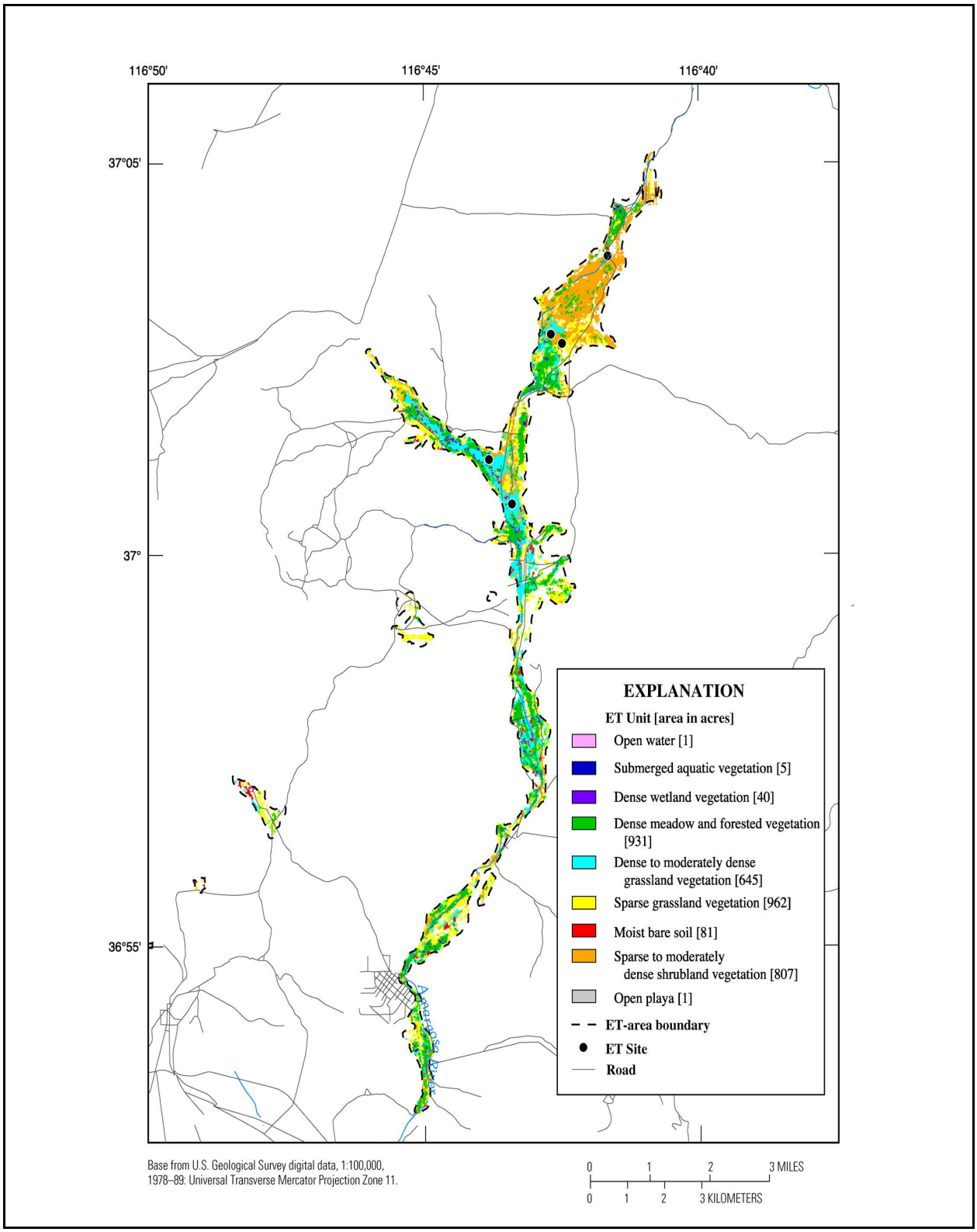

Figure 7-2
Locations of ET Units as Defined by Laczniak et al. (2001) for Oasis Valley

Table 7-3
ET Rates Used To Compute Annual ET from Oasis Valley Discharge Area

ET Unit ID[a]	Average ET Rate[b] (m/day)	Site Name	Location	Site Identifier	Estimated ET Rate (m/day)	Source
OWB	7.182E-03	Peterson Reservoir	AM	PRESVR	7.182E-03	Laczniak et al. (1999)
SAV	7.182E-03	Peterson Reservoir	AM	PRESVR	7.182E-03	Laczniak et al. (1999)
DWV	3.257E-03	Fairbanks Swamp	AM	FSWAMP	3.265E-03	Laczniak et al. (1999)
DMV	2.756E-03	Carson Meadow	AM	CMEADW	2.873E-03	Laczniak et al. (1999)
		Springdale	OV	SDALE	2.622E-03	Reiner et al. (2002)
DGV	2.672E-03	Fairbanks Meadow	AM	FMEADW	2.564E-03	Laczniak et al. (1999)
		Rogers Spring 2	AM	RGSPR2	2.697E-03	Laczniak et al. (1999)
SGV	1.670E-03	Middle Oasis Valley	OV	MOVAL	2.079E-03	Reiner et al. (2002)
		Bole Spring South	AM	BSSOUT	1.570E-03	Laczniak et al. (1999)
		Rogers Spring 1	AM	RGSPR1	1.603E-03	Laczniak et al. (1999)
		Upper Oasis Valley Middle	OV	UOVMD	1.361E-03	Reiner et al. (2002)
MBS	2.171E-03	Lower Crystal Flat	AM	LCFLAT	2.154E-03	Laczniak et al. (1999)
		Bole Spring North	AM	BSNORT	2.171E-03	Laczniak et al. (1999)
SSV	1.002E-03	Upper Oasis Valley Lower	OV	UOVLO	1.152E-03	Reiner et al. (2002)
		Upper Oasis Valley Upper	OV	UOVUP	5.177E-04	Reiner et al. (2002)

Source: Reiner et al., 2002

[a] ET unit descriptions are given in Table 7-2.
[b] Average rate is computed as arithmetic mean of measured rates for each ET unit except for SSV. The average rate for SSV is an area-weighted average.

Notes: AM = Ash Meadows; OV = Oasis Valley.

throughout the region. ET rates for each ET unit are presented as ranges in Table 7-4. For each ET unit, the range is inclusive of all ET rates calculated for Ash Meadows (Laczniak et al., 1999) and Oasis Valley (Reiner et al., 2002), and the estimated rates obtained from the literature.

Both Laczniak et al. (2001) and Reiner et al. (2002) adjusted the ET rate values by subtracting local precipitation contributions. The local precipitation component was assumed to be equal to the mean, annual, long-term precipitation of 4.175 10^{-04} m/day (1.37 10^{-03} ft/day). Uncertainty in the precipitation adjustment is due to errors in the estimate of the average annual precipitation and to the fact that the actual quantity of local precipitation contained in the unadjusted ET rates is unknown.

Table 7-4
Ranges of ET Rates for ET Units Classified In Major Discharge Areas of Death Valley Regional Groundwater Flow System, Nevada and California

ET Unit ID	Estimated ET Rate (m/day)		Source (by order of significance)
	Minimum	Maximum	
0	0	0	NA
1	7.015E-03	7.349E-03	Laczniak et al. (1999)
2	6.764E-03	7.099E-03	Laczniak et al. (1999)
3	3.090E-03	3.591E-03	Laczniak et al. (1999)
4	2.505E-03	3.340E-03	Laczniak et al. (1999); Reiner et al. (2002); Johnson (1993); Weeks et al. (1987); Gay and Fritschen (1979); Walker and Eakin (1963)
5	2.088E-03	3.090E-03	Laczniak et al. (1999); Reiner et al. (2002); Walker and Eakin (1963)
6	5.010E-04	1.921E-03	Laczniak et al. (1999); Reiner et al. (2002); Czarnecki (1997); Nichols (2001)
7	1.837E-03	2.505E-03	Laczniak et al. (1999)
8	5.845E-04	2.088E-03	Reiner et al. (2002); Nichols (1993); Nichols (2001); Walker and Eakin (1963)
9	5.845E-04	1.503E-03	Reiner et al. (2002); Walker and Eakin (1963); Young and Blaney (1942)
10	8.351E-05	5.845E-04	DeMeo et al. (1999); Nichols (2001); Czarnecki (1997)

Source: Laczniak et al., 2001

Surface-water inflow contributions were not accounted for in the estimate of the ET rate due to a lack of data, even though it could be a substantial part of the ET rate in Oasis Valley. The adjusted ET rates are presented in Table 7-5.

Mean annual groundwater ET values calculated by Reiner et al. (2002) and Laczniak et al. (2001) are presented in Table 7-5. Mean annual groundwater ET from each ET unit was calculated by multiplying the unit's area by the adjusted mean groundwater ET rate. Mean annual groundwater ET from the Oasis Valley discharge area was estimated by summing the mean annual groundwater ET from all ET units. The estimates of the mean annual groundwater ET derived by Laczniak et al. (2001) and Reiner et al. (2002) for the Oasis Valley discharge area are very similar.

The estimates of mean annual groundwater ET made by Laczniak et al. (2001) and Reiner et al. (2002) differ from that of Malmberg and Eakin (1962, p. 25) by a factor of 3. The extent of ET area

Table 7-5
Estimated Mean Annual ET and Groundwater ET by ET Unit from Oasis Valley Discharge Area

Laczniak et al., 2001						Reiner et al., 2002					
ET Unit ID	Area (m^2)	ET Rate (m/day)	Annual ET (m^3)	Mean ET Rate (m/day)[a]	Mean Annual ET (m^3)	ET Unit ID	Area (m^2)	ET Rate (m/day)	Annual ET (m^3)	Mean ET Rate (m/day)[a]	Mean Annual ET (m^3)
1	4,047	7.182E-03	11,101	6.764E-03	9,868	OWB	4,047	7.182E-03	10,608	6.764E-03	9,991
2	20,234	7.098E-03	51,806	6.681E-03	49,339	SAV	16,187	7.182E-03	41,938	6.764E-03	39,471
3	161,874	3.507E-03	209,692	3.090E-03	185,022	DWV	161,874	3.257E-03	197,357	2.839E-03	172,687
4	3,767,627	2.589E-03	3,577,092	2.171E-03	2,960,352	DMV	3,366,988	2.756E-03	3,330,396	2.338E-03	2,837,004
5	2,610,225	2.589E-03	2,466,960	2.171E-03	2,096,916	DGV	1,375,932	2.672E-03	1,356,828	2.255E-03	1,134,802
6	3,893,079	1.002E-03	1,480,176	5.845E-04	826,432	SGV	4,916,935	1.670E-03	2,960,352	1.253E-03	2,220,264
7	327,796	2.255E-03	271,366	1.837E-03	222,026	MBS	412,780	2.171E-03	333,040	1.754E-03	259,031
8	3,265,816	1.587E-03	1,850,220	1.169E-03	1,356,828	SSV	3,609,799	1.002E-03	1,356,828	5.845E-04	764,758
9	--	--	--	--	--	--	--	--	--	--	--
10	4,047	4.175E-04	1,233	8.351E-06	--	--	--	--	--	--	--
Total	14,054,745	1.921E-03	9,867,840	1.503E-03	7,647,576	--	13,864,542	1.921E-03	9,621,144	1.420E-03	7,400,880

[a]Subtract precipitation rate from ET rate (Precipitation rate = 4.175E-04 m/day).

m^3 = Cubic meter

-- = No data or not applicable

estimated by Malmberg and Eakin (1962) is similar to the estimates made by Laczniak et al. (2001) and Reiner et al. (2002) (within about 10 percent). The ET rate, however, was much smaller at about one-third of the average rates estimated by Laczniak et al. (2001) and Reiner et al. (2002).

7.5.5 Water-Level and Spring Discharge Measurements

Reiner et al. (2002) measured groundwater levels and spring discharge rates in the Oasis Valley discharge area during their investigation to gain additional insight into the ET process. They also estimated annual discharge from springs in Oasis Valley for comparison with their ET estimate.

Reiner et al. (2002) measured depth-to-water levels in several shallow wells located throughout the discharge area. The data exhibited a wide range in annual and daily fluctuations between and within the ET units. Reiner et al. (2002) generally observed a declining water table in the summer and fall, and a rising water table in the winter and spring. They also observed a decrease in the magnitude of daily fluctuations during periods of higher ET rates when the water table was near the surface. Reiner et al. (2002) concluded that even though seasonal and daily changes in water levels may indicate the occurrence of ET; their magnitude is not always indicative of ET rates. This is because factors other than ET affect water levels. The observations of Reiner et al. (2002) are consistent with those of Laczniak et al. (1999) in their study of the Ash Meadows discharge area.

Reiner et al. (2002) also measured spring discharge at several springs and channels. Channel measurement sites were located downgradient of groups of springs and seeps where direct measurements could not be made. The annual maximum discharge at channel sites was observed in the winter and early spring when ET was at a minimum. The annual minimum discharge was observed from late spring to early fall when ET was increasing or at a maximum. Reiner et al. (2002) found that flow rates made at spring sites were not seasonally dependent and exhibited smaller fluctuations than those measured at channel sites. Not only did the channel site measurements exhibit larger fluctuations, but they also were more variable. Reiner et al. (2002) attributed the larger fluctuations to seasonal changes in ET primarily. They found no relationship between the rates of spring flow and ET.

The estimate of spring discharge made by Reiner et al. (2002) is about 3,700,440 m^3/yr (3,000 acre-ft/yr). This estimate excludes flow from numerous seeps or springs for which measurements are not available. Their estimated groundwater discharge by ET (7,268,800 m^3/yr)

(5,900 acre-ft/yr) is about 2 times greater than the estimated spring discharge. This value does not include the spring discharge in Bullfrog Hills. Differences are due to the exclusion of unavailable data for some springs and seeps and to diffuse and fault-associated upward leakage into the AA from the underlying aquifer.

7.5.6 Sensitivity and Uncertainty Analyses of Annual ET

Sensitivity and an uncertainty analyses were conducted by Laczniak et al. (2001) as part of their ET study of the Death Valley regional groundwater flow system. The objective of the sensitivity analysis was to identify the input parameters that have the greatest effect on the annual ET values. The objective of the uncertainty analysis was to quantify the uncertainty associated with estimates of annual groundwater discharge by ET from the nine discharge areas of the Death Valley flow system, including the Oasis Valley discharge area. The method and results for the Oasis Valley discharge area analyses are summarized in the appendix of the report by Laczniak et al. (2001).

7.5.6.1 Method

The analyses were conducted using Crystal Ball Version 4.0 (Decision Engineering, 1996), a Microsoft Excel add-in designed to implement the Monte Carlo method. The following input parameters were required for each of the discharge areas considered by (Laczniak et al., 2001):

- The ET unit area
- The ET rate for each ET unit
- The annual precipitation rate

Each input parameter was assumed to be normally distributed. Each normal distribution was described by a mean and a coefficient of variability (CV), defined as the standard deviation divided by the mean. The mean of each input parameter is the value of the parameter as estimated by Laczniak et al. (2001, Tables 5 and 7).

The ET unit area CV was assumed to be 10 percent. This value is based on the results of the ET unit classification accuracy assessment conducted by Laczniak et al. (1999) and Reiner et al. (2002) for the Ash Meadows and Oasis Valley discharge areas, respectively. As stated previously, this accuracy is about 90 percent.

The CV for each ET rate was calculated from ranges listed in Table 7-4. The CV for each precipitation rate was calculated from measurements given in Tables 8 and 9 in Laczniak et al.'s report (2001). CV values for these input parameters were calculated assuming that the ranges represent ±2 standard deviations of a normal population (95 percent of the measurements are contained in the range).

Each Monte Carlo realization consisted of four steps:

1. Random selection of a value from the normal distribution of each input parameter
2. Subtraction of the selected precipitation rate from the selected ET rate of each ET unit
3. Calculation of the mean annual ET from each ET unit by multiplying the adjusted ET rate by the corresponding area
4. Calculation of total areas and total ET for each discharge area by addition of corresponding values for all ET units

Sample size testing showed that a sample size of 1,000 realizations would be sufficient to produce stable estimates of annual ET probability distributions.

The sensitivity of each parameter was measured by rank correlation (correlation based on ranks rather than on values).

7.5.6.2 Results

Results of the Monte Carlo simulations conducted by Laczniak et al. (2001) for the Oasis Valley discharge area are presented in this subsection.

Table 7-6 contains the simulated mean annual ET from the Oasis Valley discharge area by ET unit. Values shown in Table 7-6 are simulated means of 1,000 Monte Carlo realizations.

The sensitivity of each parameter was measured by rank correlation. The five most sensitive input parameters for the Oasis Valley discharge area are shown in Table 7-7. The sensitivity of the precipitation rate is negative because it is subtracted from the ET rate to calculate the adjusted ET rate.

Table 7-6
Simulated Mean Annual ET from Oasis Valley

ET Unit ID	Oasis Valley ET Unit ID	Area (m^2)	ET Rate (m/day)	Annual ET (m^3)	Adjusted ET Rate (m/day)[a]	Mean Annual ET (m^3)
1	OWB	4,047	7.182E-03	10,608	6.764E-03	9,991
2	SAV	20,234	7.098E-03	52,423	6.681E-03	49,339
3	DWV	160,660	3.507E-03	205,621	3.098E-03	181,692
4	DMV	3,757,914	2.589E-03	3,550,819	2.171E-03	2,978,114
5	DGV	2,619,128	2.580E-03	2,466,713	2.163E-03	2,067,559
6	SGV	3,892,270	9.937E-04	1,411,718	5.762E-04	818,537
7	MBS	326,177	2.246E-03	267,418	1.837E-03	218,696
8	SSV	3,271,482	1.603E-03	1,914,484	1.186E-03	1,415,912
9	—	—	—	—	—	—
10	—	4,047	4.175E-04	617	—	—
Total	—	14,054,745	—	9,880,175	—	7,740,087

Source: Laczniak et al., 2001

[a] Mean annual precipitation used in Monte Carlo simulations is 2.923E-04 m.

-- = No data or not applicable

Note: Data are simulated means of 1,000 realizations.

Table 7-7
Parameters Having the Greatest Effect
on Simulated Annual ET Measured by Rank Correlation

ET Unit	Parameter	Rank Correlation
ET Unit 8	Annual ET Rate	0.56
ET Unit 6	Annual ET Rate	0.43
All	Annual Precipitation	-0.35
ET Unit 4	Area	0.35
ET Unit 5	Annual ET Rate	0.29

Source: Laczniak et al., 2001

Laczniak et al. (2001) found that, generally, the precipitation rate is always one of the more sensitive input parameters. They also found that the two most sensitive parameters are typically the precipitation rate and the ET rate associated with the largest ET unit. This, however, was not the case for Oasis Valley. The ET rate associated with ET unit 8 is the most sensitive parameter, even though ET units 4 and 6 have the largest areas. According to Laczniak et al. (2001), this anomaly can be

explained in part by (1) the low CV of the ET rate for ET unit 4 (0.07) relative to that of ET units 6 and 8 (0.29 and 0.28, respectively; Table 11), and (2) the high ET rate of ET unit 8 relative to ET unit 6.

Oasis Valley, which has nine ET units and only a small area of open playa, has a CV of 0.12. Assuming that CV is a reasonable estimator of the relative uncertainty, Laczniak et al. (2001) found that the discharge estimates for Oasis Valley and those of the Tecopa/California Valley area are most certain (0.12 and 0.11, respectively).

Additional analyses were performed to examine the uncertainty associated with the classification procedure and to evaluate uncertainty related to the assumption of a 10 percent CV for ET unit areas. The effects of correlation between the classified ET units were found to be minimal. The results of testing the 10 percent CV for ET unit areas indicate that the predicted uncertainty in the estimate is nearly proportional to the CV of the area.

Table 7-8 shows the summary statistics of simulated annual ET from 1,000 Monte Carlo realizations for the Oasis Valley discharge area.

Table 7-8
Summary Statistics of Simulated Annual ET from 1,000 Monte Carlo Realizations for the Oasis Valley Discharge Area

Statistic	Value	Unit
Mean	7,754,945	m^3
Median	7,758,646	m^3
Minimum	5,142,416	m^3
Maximum	11,005,189	m^3
Standard Deviation	953,487	m^3
Lower 95th Percentile Bound	5,886,111	m^3
Upper 95th Percentile Bound	9,623,780	m^3
Coefficient of Variability	0.12	unitless

Source: Modified from Laczniak et al., 2001

Note: Upper and lower 95th percentile bound calculated by subtracting and adding 1.96 standard deviations from the mean.

7.6 Well Discharge

The locations of pumping wells located within the PM-OV area and close vicinity are shown in Figure 7-3.

7.6.1 Well and Pumping Record Description

In the PM-OV groundwater basin, groundwater was pumped from several water-supply wells located on and off the NNSS. (Figure 7-3).

The pumping wells were grouped into two categories: NNSS wells and non-NNSS wells. All of the wells considered are located within the PM-OV boundary.

7.6.1.1 NNSS Water-Supply Wells

NNSS water-supply wells of interest are located in Areas 19, 20, and 18.

Area 19

Four water-supply wells were installed in Area 19 on the NNSS: UE-19b 1 WW, UE-19c WW, UE-19e WW, and UE-19gS WW. Groundwater withdrawal data for these and other NNSS water-supply wells were recompiled by USGS from totalizing flowmeter readings.

UE-19b 1 WW was located in Central Pahute Mesa (Figure 7-3). It was installed as a water-supply well in 1964. The well had a total depth of 1,371.6 m bgs. The open interval was from a depth of 667.5 to 1,371.6 m bgs within the BRA HSU. The pumping record for this well is available for a few months in 1964 and 1965. The data are insufficient to calculate yearly totals. The well was plugged and abandoned in May 1966.

UE-19c WW is located near the center of Area 19 on Pahute Mesa. It was originally drilled in 1964 as an exploratory hole to determine the adequacy of the site for underground nuclear testing. During drilling, the drill pipe became stuck at a depth of approximately 2,587.4 m bgs. As a result, the hole was abandoned. UE-19c WW was then completed as a water-supply well in 1975 and was again recompleted in 1992. The current well depth is 2,587 m bgs. The well is open to the BRA HSU from a depth of 737.9 to 2,401.8 m bgs, and to the PBRCM HSU from a depth of 2,401.8 to 2,587.4 m bgs.

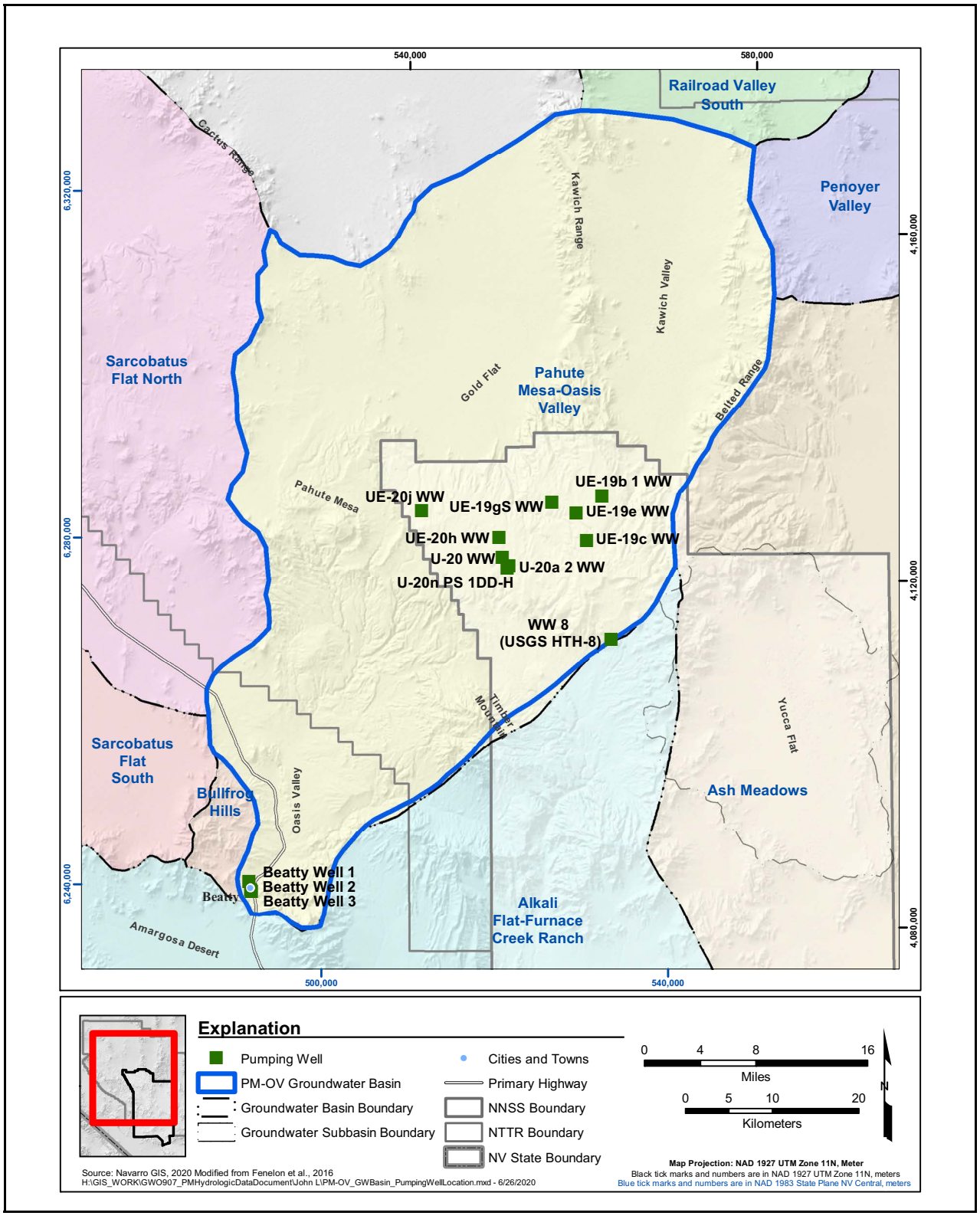

Figure 7-3
Locations of Pumping Wells in the PM-OV Area and Vicinity

UE-19e WW was located in Central Pahute Mesa (Figure 7-3). It was installed as a water-supply well in 1964 with a total depth at 1,981.2 m. The well was open to the BFCU HSU from a depth of 754.38 to 894 m bgs, and to the BRA HSU from a depth of 894 to 1,830.47 m bgs. The pumping record for this well is available for years 1965 through 1969. This well was plugged and abandoned in September 1975.

UE-19gS WW was located in Central Pahute Mesa (Figure 7-3). It was installed as a water-supply well in 1965 with a total depth at 2,286 m bgs. The well was open to the BRA HSU from a depth of 807.72 to 2,002.5 m bgs, and to the PBRCM HSU from a depth of 2,002.5 to 2,286 m bgs. The well pumping record for this well is available for the years 1965 through 1975. After 1969, it was only pumped for one month in 1971. This well was plugged and abandoned in January 1976.

Area 20

Four water-supply wells were installed in Area 20 of the NNSS: U-20 WW, U-20a 2 WW, UE-20h WW, and UE-20j WW. In addition, significant quantities of groundwater were discharged from Well U-20n PS 1DD-H.

U-20 WW is located in western Pahute Mesa (Figure 7-3). It was installed as a water-supply well in 1982 with a total depth at 996.1 m (3,268.0 ft). The open interval is from 692.2 to 996.1 m bgs within the CHZCM, CHLFA1, and CHLFA4 HSUs.

UE-20j WW was installed in 1964 to a total depth of 5,690 ft bgs. The well was cased to a depth of 1,740 ft bgs. Between 1964 and 1969, a total of some 179 acre-feet of groundwater was withdrawn from the BRA and PBRCM. The well was instrumented and grouted in 1969.

U-20a 2 WW was located in western Pahute Mesa (Figure 7-3). It was installed as a water-supply well in 1963 with a total depth at 1,371.6 m. The well was open to the CHZCM, CHLFA1, and CHLFA4 HSUs from a depth of 629 to 1,371.6 m bgs. The pumping record for this well is available for years 1964 through 1969. This well was plugged and abandoned in January 1976.

UE-20h WW is located in western Pahute Mesa, north of U-20 WW (Figure 7-3). It was installed as a water-supply well in 1964 with a total depth at 2,196.69 m. The well is open to the CHZCM, CHLFA3, and CHLFA4 HSUs from a depth of 763.82 to 1,653.8 m bgs, to the BFCU HSU from a depth of 1,653.8 to 2,196.4, and to the CFCM from a depth of 2,196.4 to 2,196.69 m bgs. The

pumping record for this well is available for a few months in 1965. It is unknown whether this well was pumped in 1966. This well was recompleted as an emplacement hole for the REX underground test, which took place on February 24, 1966.

In addition, approximately 18 acre-ft of groundwater were pumped from Well U-20n PS 1DD-H (3,025 ft bgs). However, significant quantities of groundwater were not pumped from any completion of this well post-1985. The groundwater pumped in 1985 was pumped from the CHZCM from a depth of 2,417 to 3,080 ft bgs.

Area 18

Only one water-supply well is located in Area 18: Water Well 8. This well is located on the far eastern edge of PM-OV basin (Figure 7-3). It was installed in 1962. The total depth is 1,676.10 m (5,499 ft). The well is open to the BRA HSU from a depth of 381 to 542.5 m bgs. Since 2010, this is the only NNSS well in the PM-OV basin that has produced significant quantities of water.

7.6.1.2 Oasis Valley Wells

Groundwater withdrawal data were compiled from USGS records (USGS and DOE, 2019; Elliot and Moreo, 2018). The groundwater withdrawal records for wells located on the NNSS are complete through 2018; however, the latest compilation of local public water-supply records and estimates of non-municipal use was complete through 2010 only. The largest water user for more than the past 20 years has been the BWSD, the main water supplier of municipal water to the town of Beatty, Nevada. Homes and ranches located outside of Beatty but within PM-OV basin obtain their water from springs and non-municipal wells.

Currently, BWSD pumps groundwater from three wells located in PM-OV groundwater basin (Figure 7-3). Beatty Well No. 1 is located near Beatty (Figure 7-3). The well is open to the AA HSU from a depth of 28.96 to 48.77 m bgs. Beatty Well No. 2, and Beatty Well No. 3 are open to the AA HSU from a depth of 27.43 to 59.44 m bgs, and 21.336 to 39.62 m, respectively. Pumping records for these wells are available through 2010.

7.6.1.3 Mine Wells

As of 2019, there are no active mining operations in the PM-OV groundwater basin. However, there is some active exploration that requires limited intermittent use of groundwater. The amount of groundwater that may be required for future mineral exploration and production is unknown and is a source of uncertainty.

7.6.2 Historical Pumping Volumes

For wells located within the boundaries of the PM-OV basin, the total yearly groundwater withdrawals at 5-year intervals for the period 1985 to 2010 are shown in Figure 7-4. The pumping rates for wells both on and off the NNSS through 2010 were taken from Elliot and Moreo (2018). The pumping rates for wells on the NNSS for the years of 2015 and 2018 were taken from a database maintained by USGS (USGS and DOE, 2019).

Figure 7-4 shows the respective components of the groundwater pumping (i.e., both on and off the NNSS). Figure 7-4 shows that overall pumping through 1995 was much higher than post-1995. The drop in groundwater pumping on the NNSS reflects the end of nuclear testing in 1992. The drop in groundwater pumping off the NNSS between 1995 and 2000 reflects the closure of a mine outside of Beatty, Nevada, in 1998. Although the pumping rates off the NNSS since 2010 are not readily available, there have been no significant changes in population, land use, or in mining activities since then, and it is reasonable to assume that the volumes of groundwater pumped have not changed significantly. Pumping rates on the NNSS in the PM-OV groundwater basin were totaled for the years of 2015 and 2018. Total pumpage was 27,470 m^3/yr (22.3 acre-ft/yr) and 32,400 m^3/yr (26.3 acre-ft/yr), respectively. Both yearly totals are lower than the 2010 value of 43,000 m^3/yr (34.9 acre-ft/yr). Well WW-8 was the only actively pumped well on the NNSS in the PM-OV groundwater basin during the years of 2015 and 2018.

7.7 Limitations

Limitations associated with the ET estimates and well discharge data are discussed in this subsection.

Limitations associated with the ET estimates are as follows:

- The assumption that ET is negligible in areas other than the Oasis Valley area discharge area is supported by a lack of vegetation, soil dryness, and greater depths to water. It could, however,

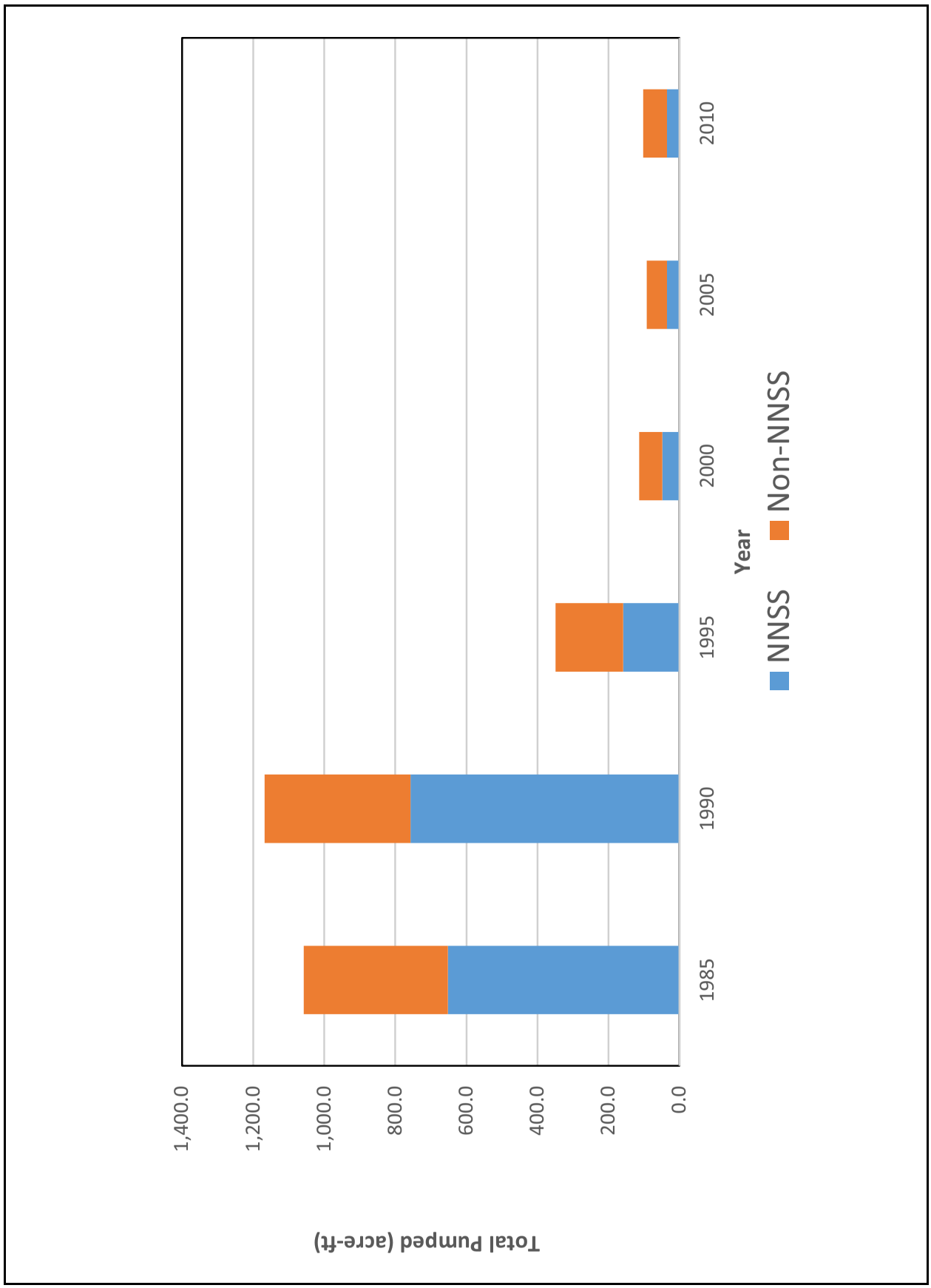

Figure 7-4
Total Estimated Groundwater Withdrawals within the PM-OV Area for Select Years

still result in some error. The volumetric loss would be minimal because the rate of ET from these areas is likely to be less than 0.01 feet per year (ft/yr) as shown by Andraski (1997) in his study of soil-water movement in the Mojave Desert of Nevada. Andaski (1997) estimated water fluxes from water potential and temperature data. From these data, he concluded that isothermal liquid, isothermal vapor, and nonisothermal vapor fluxes need to be included in the conceptual model of unsaturated flow at the study sites. Estimated vapor fluxes ranged between approximately 4.0E-09 and 5.0E-04 ft/yr.

- The use of the 1992 TM imagery to delineate the ET unit area, a year of slightly above-normal rainfall, may have led to an overestimate of ET. The use of TM imagery from multiple years would likely result in area estimates that would be more representative of the desired long-term ET average.

- The mean annual ET estimates of each ET unit were computed from Oasis Valley and Ash Meadows data acquired over a relatively short period of a few years. These data may not be representative of long-term averages.

- It is assumed that most of the water flowing at the surface is either lost to ET or infiltrated into the AA. Thus, overland flow is not factored out of the total ET estimate.

- Other limitations include (1) the assumption that all springflow is ultimately evaporated or transpired from within the bounds of one of the ET units, (2) the short-term nature of the data used to compute mean values, (3) the limited number of sites used to estimate ET from each ET unit, (4) the uncertainty in the adjustment applied to remove precipitation from ET estimates, and (5) the non-inclusion of local groundwater recharge from areas outside ET unit boundaries (Reiner et al., 2002).

7.8 Summary

Groundwater discharge to the surface within the PM-OV area and vicinity occurs by natural means and by withdrawal from wells.

Natural discharge to the surface in the area of interest is best approximated by an estimate of ET. Laczniak et al. (2001) and Reiner et al. (2002) used TM imagery to delineate the ET subareas (ET units), and field data to estimate the ET rates. The mean annual ET was calculated by Reiner et al. (2002) to be 5,900 acre-ft/yr (7,268,800 m^3/yr) and by Laczniak et al. (2001) to be about 6,275 acre-ft/yr (7,730,800 m^3/yr). Reiner et al. (2002) estimated groundwater discharge from Oasis Valley by all means, including subsurface flow and wells, and found that ET represents about 90 percent of the discharge from that area. Discharge by ET constitutes the majority of natural discharge to the surface from the PM-OV groundwater flow system. A range of uncertainty for the ET was derived by Laczniak et al. (2001) using Monte Carlo simulations of annual ET. The range of

annual ET is between 4,170 and 8,930 acre-ft/yr (5,142,378 and 11,005,109 m^3/yr or between 14,089 and 30,151 m^3/day).

Up to eight wells per year have been used to withdraw groundwater at rates of over 4 acre-ft/yr since 1985 within the PM-OV groundwater basin. However, that number of wells has diminished with time. By way of example, in 1985 five wells on the NNSS and three municipal supply wells for the town of Beatty, Nevada, pumped at high rates. By 2010, only one well on the NNSS and three municipal wells for Beatty were pumped at high rates. However, the amount of groundwater discharged through wells is small compared to that of natural discharge. Even the 1990 discharge of approximately 1,200 acre-ft/yr (1,478,000 m^3/yr) represents only 20 percent of the ET estimate. The 2010 discharge of approximately 100 acre-ft/yr (125,850 m^3/yr) represent less than 2 percent of the ET estimate.

8.0 HYDRAULIC HEADS

Potentiometric data for the Pahute Mesa area and vicinity were collected and analyzed to support development of a steady-state CAU groundwater flow model for Pahute Mesa. Observed hydraulic heads are derived from depth-to-water measurements, well information, and spring locations. This section provides a description of the potentiometric data including the data types, compilation, and analysis.

8.1 Objectives

The objective was to identify representative steady-state hydraulic heads for the Pahute Mesa area and vicinity from the available potentiometric data for use in flow model calibration in a steady-state condition, including interpretation of flow directions and gradients. During steady-state conditions, all aspects of groundwater flow remain constant, including recharge, discharge, water-level elevations, and geochemical properties. For the purposes of this analysis, every attempt was made to identify heads representative of stable flow conditions in the basin for use in the steady-state model calibration. Stable flow conditions are considered to be those under which the water level remains reasonably constant. Water-level measurements that do not represent static heads in the regional aquifer system are identified and excluded from the potentiometric data, or the data are reduced to a mean value. The transient measurements can include the effects of infiltration from precipitation, barometric-pressure changes, earth tides, groundwater pumpage, and seismic events caused by tectonic activity or underground nuclear testing. The transient aspects of the water-level measurements are included in the uncertainty estimated for each steady-state hydraulic head value.

8.2 Approach

The following approach was used to evaluate the available potentiometric data:

- Collect, compile, and qualify existing potentiometric data for the Pahute Mesa area and vicinity.
- Review temporal trends in the potentiometric data using hydrographs and statistical analysis of the water elevations.

- Identify a subset of the hydraulic head data that is representative of steady-state conditions for the PM-OV area and vicinity; this dataset includes the location of the measurement point, the water-level elevation, water-level uncertainty, and the HSU(s) represented.

- Identify the potentiometric data uncertainty.

- Calculate horizontal and vertical gradients, and create a gradient dataset that can be used for model calibration.

8.3 Data Types

The data needed to assess hydraulic heads include general site information, depth-to-water data, well construction information, and hydrostratigraphic information. A site is defined as a spring, well, test hole, or a separate completion zone within a well. The specific data types needed are as follows:

General Site Information

- Unique site identifier
- Site location
- Land-surface elevation
- Uncertainty in land-surface measurement

Depth-to-Water Data

- Depth-to-water measurement
- Date of measurement
- Site status at the time of the depth-to-water measurement
- Status of nearby sites at the time of the depth-to-water measurement
- Water temperature
- Accuracy of the depth-to-water measurement

Well Construction Information

- Total depth of well
- Slotted casing interval(s) (top and bottom)
- Gravel/sand pack interval(s) (top and bottom)
- Well deviation
- Open hole interval(s) (top and bottom)

Stratigraphic/Hydrostratigraphic Data

- Well hydrostratigraphy
- Well stratigraphy
- Well lithology

Measurements of land surface-elevation and depth-to-water are the primary data required to calculate hydraulic heads. The additional data are used for site description, data qualification, uncertainty evaluation, identification of the EOI, and HSU assignment.

8.4 Data Compilation

Well water-level data for the PM-OV area and vicinity were obtained from the USGS National Water Information System (NWIS) database (USGS, 2015). In addition, land surface elevations from springs were included to supplement the available water-level data.

8.4.1 Depth-to-Water and Spring Data

Fenelon (2015a, b, and c) developed contour maps to represent the predevelopment hydraulic-head distribution within the PM-OV aquifer systems. Developing the contour maps included performing a the transient-effects analysis to identify which water-level measurements collected during periods of onsite groundwater activity (pumping and underground nuclear testing) actually represent predevelopment conditions. Fenelon (2015a, b, and c) compiled and analyzed more than 19,000 depth-to-water records representing 617 well completions from the USGS NWIS database. The period of record spans from 1941 to 2015. In addition, Fenelon (2015a, b, and c) included 75 springs to supplement the available water-level data.

8.4.2 General Site Information

The general site information of interest includes location, land-surface elevation, EOI, and hydrostratigraphy. For springs, site information of interest includes location, land surface elevation and hydrostratigraphy to a depth of 100 m bgs.

8.4.2.1 EOI Definition

Well construction data are used to identify the EOI for a given site. The EOI and stratigraphy information are then used to identify the HSU or units associated with each site. The process of defining an EOI is described in the following text.

Well construction data of primary interest are the depths to the top and bottom of each open interval within a given completion zone, or the total depth for open boreholes. The term “open interval” refers

to any type of opening through which water may flow from the rock formation into the borehole. Examples of open intervals include open borehole (uncased), or the intervals in which well screens and perforated casing are gravel packed.

An EOI was defined for each site for which well construction data are available. Determination of the top of the EOI was based upon whether the water level was above or below the top of the open interval. The bottom of the EOI was defined as the bottom of the open interval.

If the average water level was below the top of the open interval, then the EOI was defined as follows:

- Depth of EOI top = steady-state water-level depth
- Depth of EOI bottom = the bottom of the screen or sand/gravel pack

If the estimated steady-state water level was above the top of open interval, then the EOI was defined as follows:

- Depth of EOI top = depth to top of screen or sand/gravel pack
- Depth of EOI bottom = depths to either the bottom of the screen or sand/gravel pack

For cases where the well screen depth is unknown or the borehole was open, the EOI was defined as the length of the saturated thickness.

- Depth of EOI top = average depth-to-water measurement
- Depth of EOI bottom = total depth (or depth to top of backfill)

8.4.2.2 HSU Assignment

Water levels were assigned to HSUs based on the identified effective well screen of each well and the HSU structures extracted from the PM-OV HFM. The wells with hydrostratigraphic information were used to develop the PM-OV HFM, so the extracted HSUs are accurate at these well locations. For springs, assignment of HSUs was made based on the HSU occurring from land surface to 100 m bgs.

8.5 Steady-State Hydraulic Heads

The identification of steady-state hydraulic heads and a measure of their uncertainty are discussed in the following subsections. For the purposes of constructing a groundwater flow model, a set of hydraulic heads consistent with natural and undisturbed groundwater flow system conditions needs to be identified. Ideally, this dataset is derived from water levels measured prior to the start of pumping

and underground nuclear testing in the PM-OV area, and represent predevelopment hydrologic conditions.

As part of the water-level analysis by Fenelon (2015a, b, and c), each water level was evaluated to be representative one of the following three hydrologic conditions: (1) natural predevelopment conditions, (2) transient conditions resulting from nearby nuclear testing, and (3) transient conditions resulting from pumping. Assignment of a water level as predevelopment-condition assumed that human activity has not affected or has minimally affected the water level. Of the 617 well completions analyzed for this study, 412 of the wells had at least one water level identified as representative of predevelopment conditions, and 374 of the wells are located within the PM-OV HFM. The predevelopment water levels identified by Fenelon (2015a, b, and c) are selected as the target heads for the steady-state CAU flow model. In addition to the steady-state water levels, the land surface elevation at spring locations provide additional target heads. Figure 8-1 illustrates the steady-state and spring water-level sites.

8.5.1 Steady-State Water-Level Uncertainty

Although the steady-state water levels are identified as not having impacts from human activity, the water levels change over time due to the effects of infiltration from variable precipitation, barometric pressure, and earth tides. The uncertainty due to variability in steady-state heads were estimated through evaluation of the hydrographs. The hydrographs were prepared with the objective of presenting information relevant to understanding the amount of variability in hydraulic head and prioritizing hydraulic head data for use as model calibration points. A total uncertainty was estimated for each steady-state hydraulic head value. The total uncertainty includes uncertainties associated with the following:

- Depth-to-water measurement
- Land-surface elevation
- Borehole deviation
- Barometric effects
- Variability in steady-state water levels
- Variability in groundwater temperatures

The predevelopment water levels reported by Fenelon (2015a, b, and c) included an estimate of water-level measurement accuracy and land surface accuracy for each well. Most of the water-level altitudes computed from depth-to-water measurements are considered accurate to within 5 ft (1.5 m)

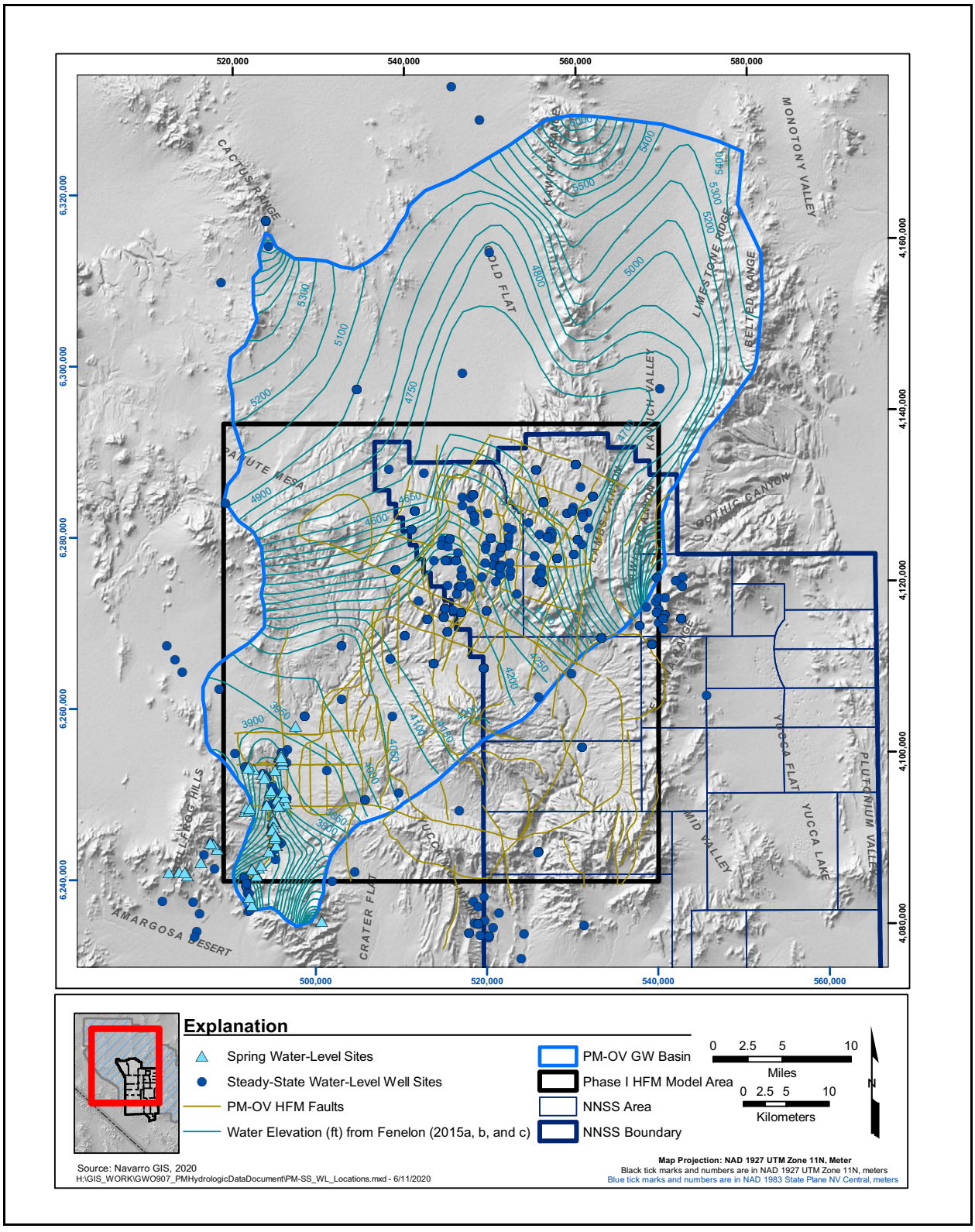

Figure 8-1
Pahute Mesa Steady-State Water-Level Sites from Well and Spring Locations

or less, depending on the method of measurement. Most of the land surface altitudes are considered accurate to within 1 ft (0.3 m). However, the land surface altitudes for many wells are only accurate to within 20 ft (6 m). The water-level measurement and land surface accuracies reported by Fenelon (2015a, b, and c) are used for the depth-to-water and land-surface elevation uncertainty.

Within the water levels reported by Fenelon (2015a, b, and c), the errors caused by borehole deviation in the conversion from depth-to-water to water-level altitude generally are less than 0.5 ft (0.15 m). Where the errors are known to be larger, the measured water levels are corrected for borehole deviation (Elliott and Fenelon, 2010). The uncertainty associated with borehole deviation is assumed to be 0.5 ft (0.15 m) for all wells.

Changes in barometric pressure can cause fluctuations in water levels of confined and semi-confined aquifers. Barometric pressure and water level are inversely related and an increase in barometric pressure causes a decrease in water level. The water levels reported by Fenelon (2015a, b, and c) are not corrected for barometric pressure. Therefore, an uncertainty in the water levels due to the effects of barometric pressure was estimated. In the vicinity of Pahute Mesa, the barometric-pressure changes are most pronounced when regional storms occur during the fall, winter, and spring seasons. Water-level modeling of distal well response to constant-rate test pumping by Navarro (2015 and 2016) determined that the fluctuations in water levels due to barometric effects are generally less than 1 ft (0.3 m) during the fall, winter, and spring seasons. A 1-ft (0.3-m) uncertainty is used to represent barometric effects on water-level elevations for all wells.

Another source of uncertainty derives from the departures from long-term average water levels caused by temporal variability in recharge and ET. In instances where many measurements are available over a long time period, there is a high likelihood that those values accurately represent the variability. However, if fewer measurements are available, there is a significant potential that measurements do not accurately represent variability in water levels due changes in recharge over time.

Inspection of the hydrographs from wells with a 10-year or longer monitoring period was used to estimate steady-state water-level uncertainty. The steady-state water-level timescale in the PM-OV basin is more than 25 years and may be about a century (Jackson and Fenelon, 2018). Ideally, only water-level records exceeding 25 years would be used to estimate water-level uncertainty, but these criteria would eliminate most wells, and the observed information would be neglected. Clearly, some

wells have less water-level variability than others, and this information should be acknowledged. For example, water levels in Well UE-19h have only varied less than 0.5 m over a 22-year period. In contrast to Well UE-19h, ER-12-1 has a strong response to recharge (Jackson and Fenelon, 2018) and has varied more than 14 m over the same time period.

Of the 374 steady-state water-level wells within the PM-OV HFM, 57 wells meet the 10-year criteria, and these points are illustrated with symbols scaled by the logarithm of the water-level range in Figure 8-2. Among the wells with a monitoring period of more than 10 years, those wells near the PM-OV basin boundaries or outside of the PM-OV basin have the greatest variability. These wells include the Rainier Mesa wells (ER-12-1, U-12s, and UE-12t6); wells within Fortymile Wash (UE-29a1 HTH, UE-29a2 HTH, and USW UZN91); and wells near the Cactus Range (TTR Antelope Mine Wells 1, 2, and 3; and TTR Sulfide Mine). One notable exception is Well U-19bh, which has a rising trend in response to episodic recharge from multiple wet winters between 1995 and 2016. The water level in this well has risen approximately 4 m after recovering from drilling. Excluding the Rainier Mesa, Fortymile Wash, and Cactus Range wells, the water-level variability is generally less than 2 m. The observed variability is used to estimate water-level uncertainty in wells with more than 10 years of monitoring and an uncertainty of 2 m is assumed to represent wells with a shorter monitoring period. The water-level variability seen in the wells with extensive hydrograph data and the assumed 2-m uncertainty for wells without extensive records include barometric effects.

8.5.2 Temperature Effects on Water Levels

The hydraulic head at each well opening is equated to the water-level altitude in the well. However, hydraulic heads at well screens below the water table may be different due to differences in water temperature, and the measured hydraulic head in the well may not represent the true hydraulic head in the formation open to the well. Water column temperatures affect the water levels by altering the density of the column of water in the well and, thus, the length of the water column above the well screen. The water level in the well with the higher temperature will be greater than the water level in the well with the lower temperature at the same bottom hole pressure. The different temperatures in wells can be caused by variability of rock thermal conductivity, geothermal hot spots, and groundwater flow. The well water levels compiled by Fenelon (2015a, b, and c) are not corrected for temperature effects.

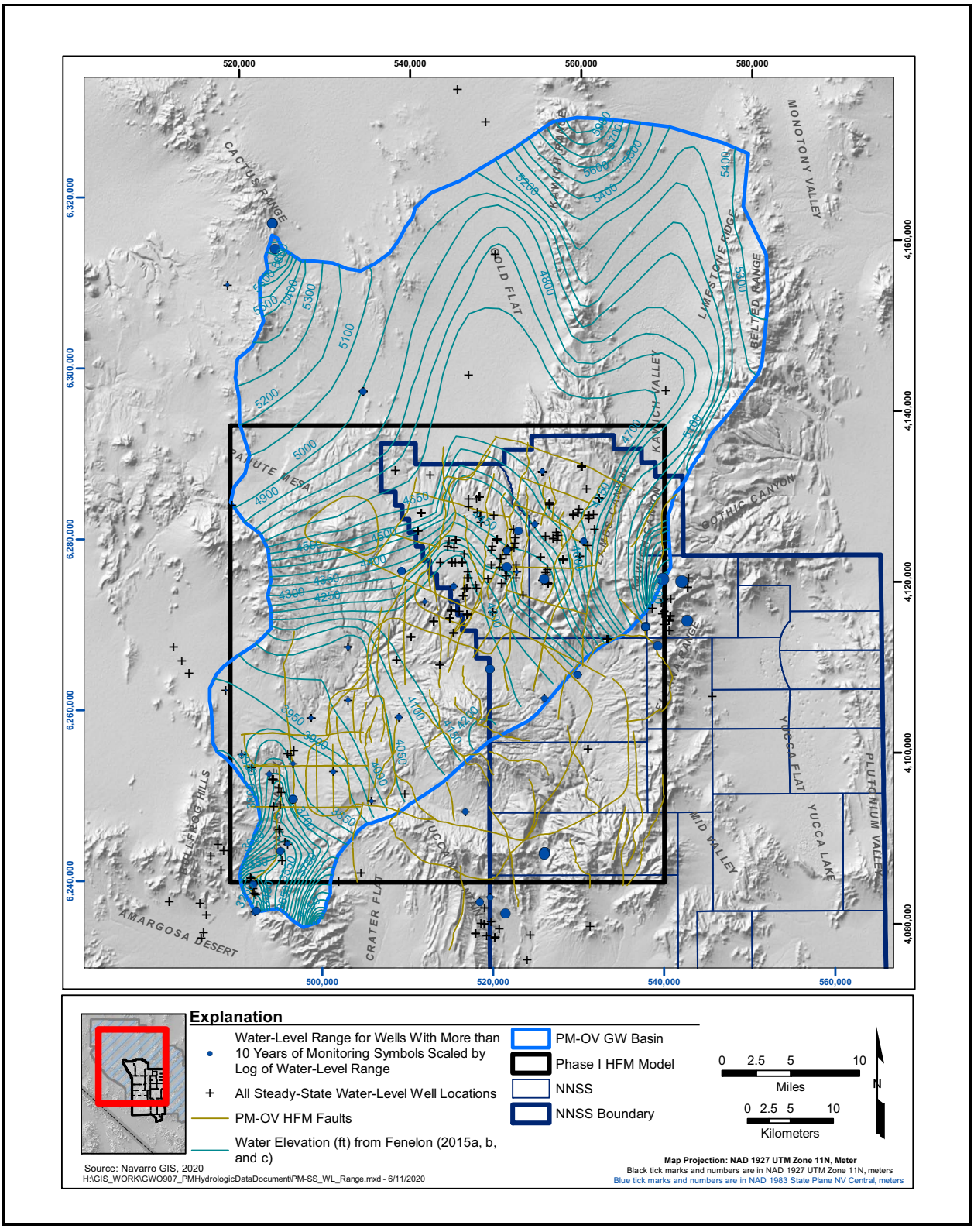

Figure 8-2
Locations of Pahute Mesa Steady-State Water-Level Sites Illustrating Water-Level Variability

Several Pahute Mesa wells have anomalously high or low temperatures. In order to compare the pressure head from different wells at the well screen depths, the density of the water column in each of the wells needs to be similar. Therefore, the density of the water column must be considered in the pressure head calculation or treated as uncertainty in the pressure head. The effects of water column temperature on bottom hole pressure are the greatest for wells with large water column heights, and many Pahute Mesa wells have water columns in excess of 1,000 m.

For deep wells, the water in the well will not be a single temperature but will have a gradient from the depth of the completion interval to the water surface. Reiner (2007) compiled groundwater temperature data for wells at and in the vicinity of the Nevada Test Site during the years 2000–2006, and groundwater temperature profiles were collected in 73 wells. Pottorff et al. (1987) evaluated the hydrologic utility of borehole temperatures in Areas 19 and 20 of Pahute Mesa. Carle (2016) used the Reiner (2007) data, Pottorff et al. (1987) data, and temperature data collected by UGTA activities to calculate the water column pressure at various depths considering the variation of water temperature and gravity within Pahute Mesa boreholes.

A total of 44 wells located within the vicinity of Pahute Mesa with usable temperature data were used to calculate the bottom hole pressure head. The bottom hole pressures and departures from water levels were calculated at the well screen center. The bottom hole pressure should be calculated at the well screen depth that is most productive and representative of the larger aquifer system connected to the well screen. However, the most productive interval is rarely known and highly uncertain.

The correction of water levels for variable density due to variable temperatures in the water columns is simply the expression of bottom hole pressure using common units of pressure for the different wells. The pressure can be expressed in pressure units (e.g., kilopascal [KPa], or pressure head in units of length using a common water density). Using the average water density or average temperature of all wells to calculate the average density will minimize the average pressure head departure for all wells undergoing temperature effect correction. The average borehole density from the analysis of Carle (2016) is 994.3 kilograms per cubic meter (kg/m^3), which corresponds to a temperature of 34.2 °C at standard pressure. The pressure head departures from the water column height range between -16 m to + 1.8 m. The pressure head departures normalized by the water column length (uncertainty per meter of water column) range from -0.0081 to +0.0034 m/m.

The pressure head departures were not used to correct water levels, but are treated as an uncertainty in the water levels. The uncertainty from temperature effects for wells without temperature profiles is estimated from the wells with temperature data. The uncertainty is proportional to the water column height and is estimated as 0.3 percent of the column height.

Ideally, the water column temperature profile will be nearly linear, reflecting the geothermal gradient due to heat conduction, and a linear model fit to the available temperature data could be used to estimate temperature profiles in wells without temperature data. However, the Pahute Mesa temperature profile data have a large amount of variability due to the variability of rock thermal conductivity, groundwater flow, and geothermal hot spots. Figure 8-3 illustrates all temperature data analyzed and a linear regression model fit. The linear fit is poor, and estimating the well screen pressure uncertainty due to temperature effects would not be an improvement over simply estimating the uncertainty as 0.3 percent of the water column length.

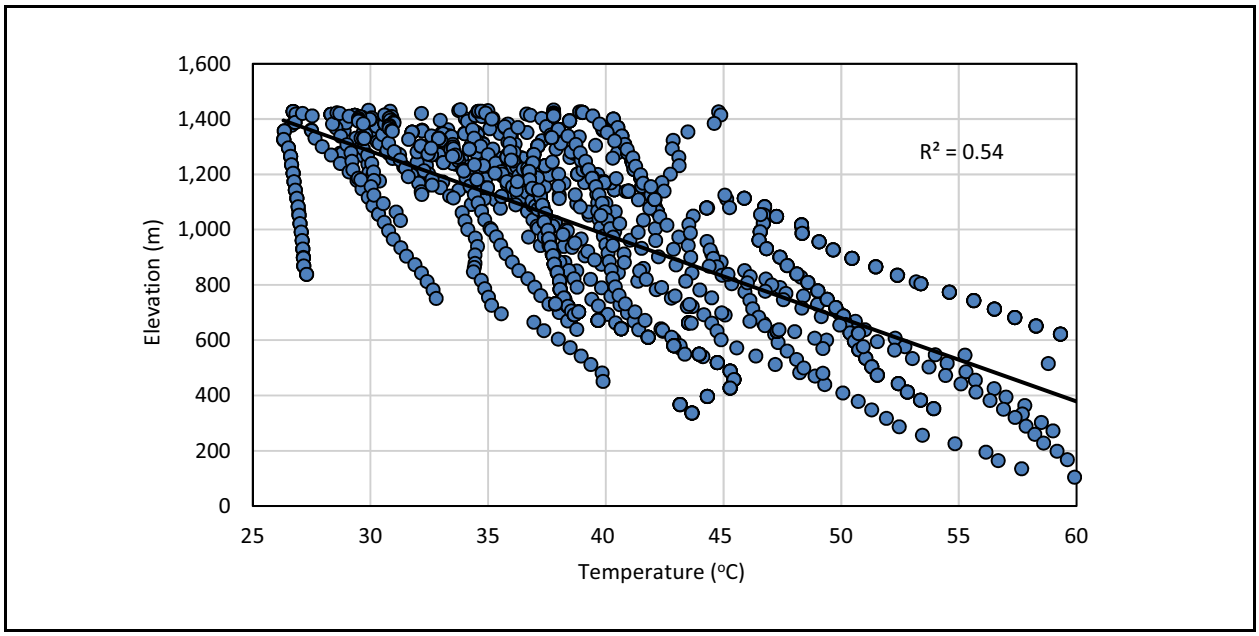

Figure 8-3
Linear Regression Model Fit to Temperature Profile Data

8.5.3 Impacts of Water-Level Uncertainty on Flow Direction

Uncertainty in water levels imparts uncertainty in the water-level gradients and the inferred direction of water flow. If the magnitude of water-level uncertainty is large compared to the water-level difference between wells, the direction of flow cannot be reliably ascertained. Because the

water-level difference between wells generally increases with distance between wells, the relative uncertainty in the estimates of flow direction is expected to decrease with increasing well spacing. For example, the distance between Wells ER-20-11 and ER-EC-15 is approximately 3 km, and the steady-state water-level difference between these wells is approximately 2 m, which is approximately the same as the water-level uncertainty at these wells. In contrast, the distance between Wells ER-20-11 and ER-EC-8 is approximately 17 km, and the steady-state water-level difference between these wells is approximately 50 m, suggesting the flow direction and gradient can be more reliably estimated at a scale of 17 km compared to 3 km.

The relationship between distance and flow direction uncertainty was investigated by calculating the horizontal gradient direction over various length scales (2, 5, and 10 km) from the water-level data that Fenelon (2015a) used to construct the potentiometric surface map of Pahute Mesa. For wells with multiple completions, preference was given to heads from wells open to transmissive intervals; or wells with long open intervals, heads with low uncertainty, and heads consistent with surrounding wells (Fenelon 2015a). All water-level data within various distances of each well were identified, and a plane was fit through the data using linear regression. The azimuth and the dip of the resulting plane were used to approximate the flow direction and gradient. An example of these calculations, including the effect of water-level uncertainty on gradient calculation, is presented in Appendix C. The uncertainty analysis described here was used to select appropriate distances between the well pairs used in the model calibration. Hydraulic head gradients between various well pairs are reported in Table C-4.

Uncertainty in the gradient calculations was introduced by sampling 1,000 realizations assuming the total water-level uncertainty is a uniform random variable with the distribution bounds of -1/2 the total water-level uncertainty to +1/2 the total uncertainty. Each realization results in a unique flow direction and gradient estimate. The 2.5 percentile and 97.5 percentile values of the calculated gradient and dip azimuth capture the 95th percentile interval and are used to estimate the uncertainty range of the horizontal gradient.

The uncertainty discussed here is the parametric uncertainty in the gradient direction resulting from uncertainty in the water-level data assuming the potentiometric surface is a plane at the scale of the calculation. This is not a complete assessment of flow direction uncertainty and should not be interpreted as such. This approach does not address conceptual uncertainties such as those arising due

to recharge variability or the amount of available data in various regions of Pahute Mesa. These sources of uncertainty can be addressed during the flow model development and calibration using alternate calibrated models, sensitivity studies, or NSMC analysis (Doherty et al., 2010).

Figure 8-4 illustrates the 2.5 and 97.5 percentile gradient directions for a 2-, 5-, and 10-km length scale. Clearly, calculating the gradient using a distance scale of 2-km imparts excessive uncertainty to the gradient and gradient direction because the head difference between wells within close proximity of one another is similar in magnitude to the water-level uncertainty. The uncertainty in gradient and gradient direction are significantly reduced using regression to all wells within 5-km distance and further reduced using a 10-km distance because the water-level difference between wells, due to the natural gradient, becomes larger compared to the water-level uncertainty; and, additionally, more wells are used to calculate the plane representing the water table. The flow directions depicted in Figure 8-4 at the 10-km-length scale are generally consistent with the qualitative potentiometric surface contours interpreted by Fenelon (2015a). Convergent flow occurs toward a potentiometric trough in southwest Area 20 and flow directions continue down through Thirsty Canyon to the discharge area in Oasis Valley.

8.6 Steady-State Flow System Behavior

The direction and rate of radionuclide transport away from the former underground testing areas within Pahute Mesa is controlled, in part, by the groundwater flow potential (gradient). The difference in hydraulic head across a given area defines the groundwater flow potential. The following subsections present an analysis of the pattern of hydraulic heads gradients. The results will be used to guide the use of steady-state heads and gradients for calibration of the flow model.

8.6.1 Horizontal Water-Level Gradients and Structural Controls

The Pahute Mesa subsurface is primarily composed of volcanic rock originating from multiple Miocene-age calderas. Groundwater flow occurs along faults and the interconnected fracture systems that developed during cooling and shrinking of the lava flows and welded tuffs (Blankennagel and Weir, 1973). Rhyolite lavas and partly to densely welded ash-flow tuffs are the principal volcanic-rock aquifers. Rhyolite lavas generally have the highest permeabilities, but may be restricted areally and in thickness. Welded ash-flow tuffs are slightly less permeable than the lavas but are widespread and thick; therefore, they may provide lateral continuity for water to move through the

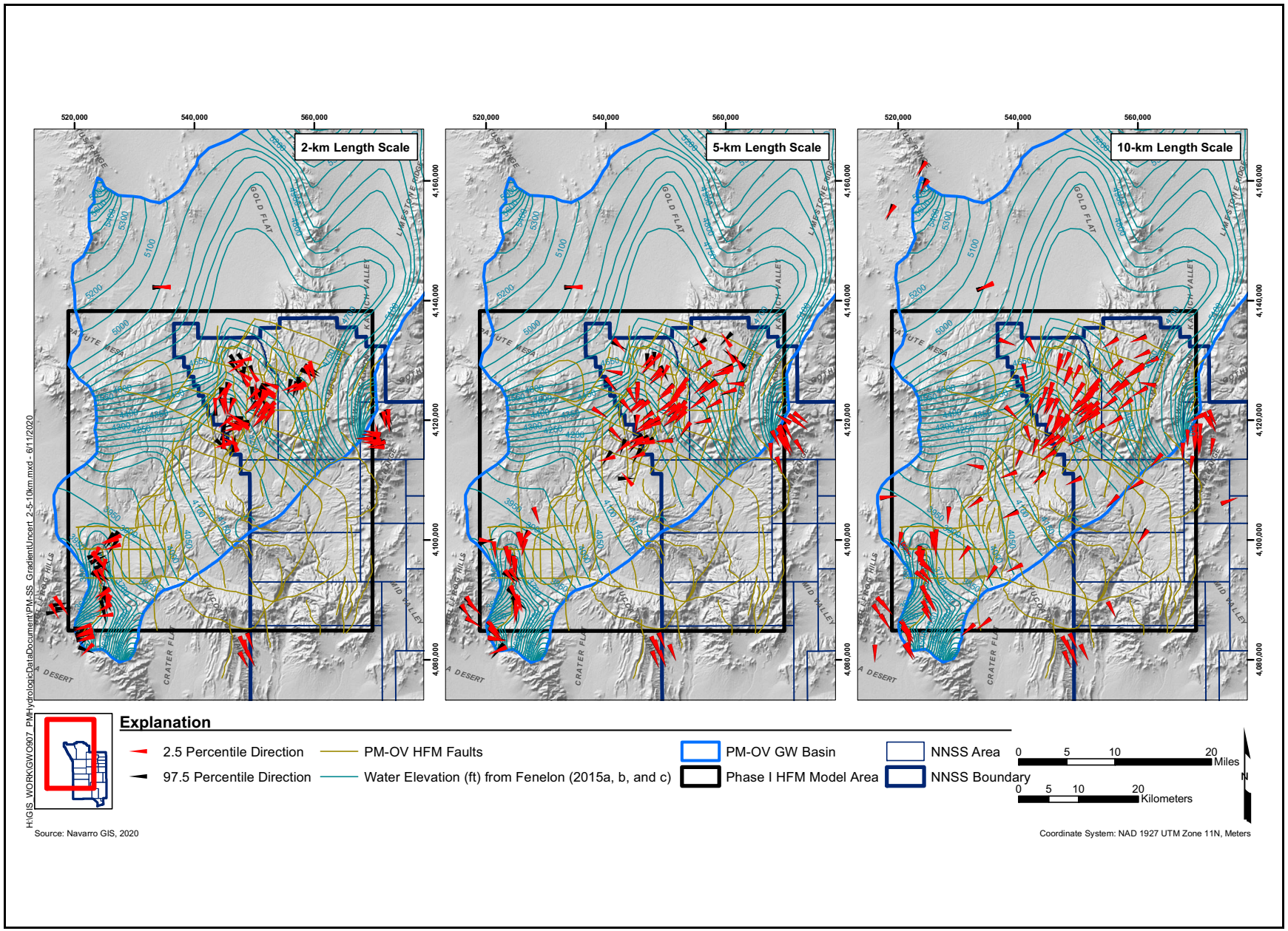

Figure 8-4
Pahute Mesa Gradient Direction Uncertainty at Specific Wells Estimated Using Neighboring Wells within 2, 5, and 10 km

Note: Locations with a single red arrow have nearly identical 2.5 and 97.5 percentile gradient directions.

regional flow system (Fenelon et al., 2016). Partially welded and nonwelded ash-flow and ash-fall tuffs have limited fracture networks and, as a result, typically are the confining units, especially where they are zeolitized (Fenelon et al., 2016).

One of the striking characteristics of Pahute Mesa (and the NNSS in general) is the degree of faulting. The faulting is due to Basin-and-Range extension tectonic activity and multiple stages of caldera collapse associated with the nested SCCC and TMCC. The generally accepted zonation of fault-related rocks include (1) a low-permeability fault core of narrow width that is adjacent to the slip plane and composed of granulated wall rock; (2) a high-permeability damage zone of brecciated and fractured rock surrounding the fault core; and (3) a protolith of relatively undamaged rock at some distance from the fault (Rawling et al., 2001; Caine et al., 1996). Faults may act as either conduits of groundwater flow, if characterized by open fractures, or barriers to flow, if associated with fine-grained gouge or increased alteration of nearby rocks. Faults also may be neutral to groundwater flow or a barrier-conduit (core limiting flow across the fault, damage enhancing flow along it) (Protho et al., 2009b).

The hydraulic gradient is related to the geologic structures, hydraulic properties of the rock, and location of recharge areas. The relationship between structure and hydraulic gradient was investigated by calculating the horizontal gradient over various length scales (2, 5, and 10 km) using linear regression from the water-level data from Fenelon (2015a) and comparing the stratigraphy extracted from the Phase II HFM to the gradient. The hydraulic heads are the steady-state head estimates from Fenelon (2015a) that were used to construct the potentiometric surface map of Pahute Mesa.

Figures 8-5 through 8-7 illustrate the hydraulic gradient for the 2-, 5-, and 10-km length scales. At each well location, the mean value for the appropriate scale was used from the uncertainty realizations described above. Locations with low, medium, and high gradient are illustrated with yellow, orange, and red circles, respectively, that are located at the well location used to calculate the gradient. Fewer gradient locations are illustrated in Figure 8-5 compared to Figures 8-6 and 8-7 because at some locations, there are no wells within 2 km of one another. The average horizontal gradient between Area 19 of the NNSS and Oasis Valley is approximately 0.005. Figure 8-7 indicates that using a length scale of 10 km to calculate gradients may average local areas of high or low gradient across hydrogeologic features such as faults and juxtapositioned stratigraphy. The gradients in Areas 19 and 20 become very similar, and the “low” category is nearly eliminated using a

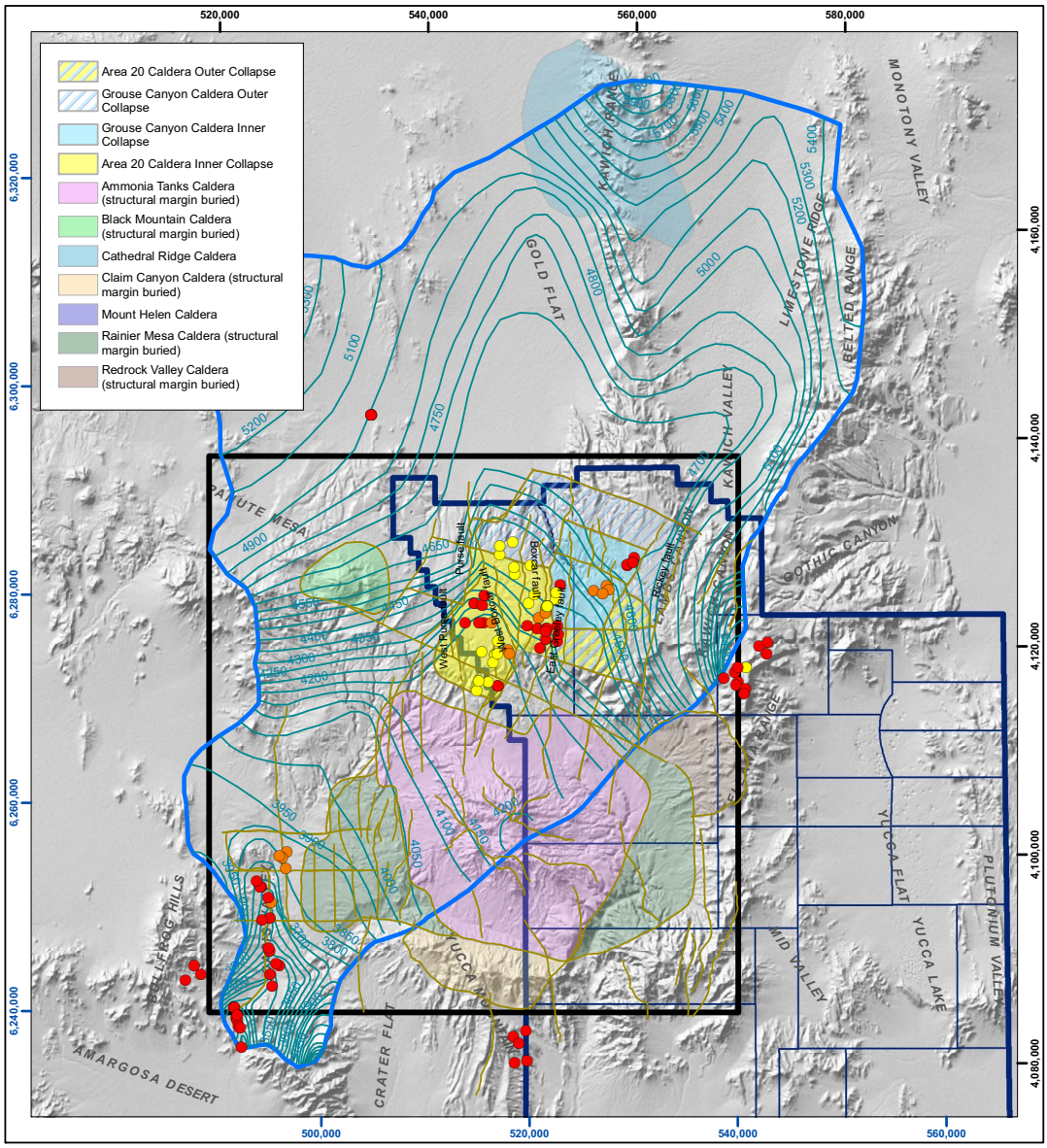

Figure 8-5
Pahute Mesa Steady-State Water-Level Gradient at a 2-km Length Scale

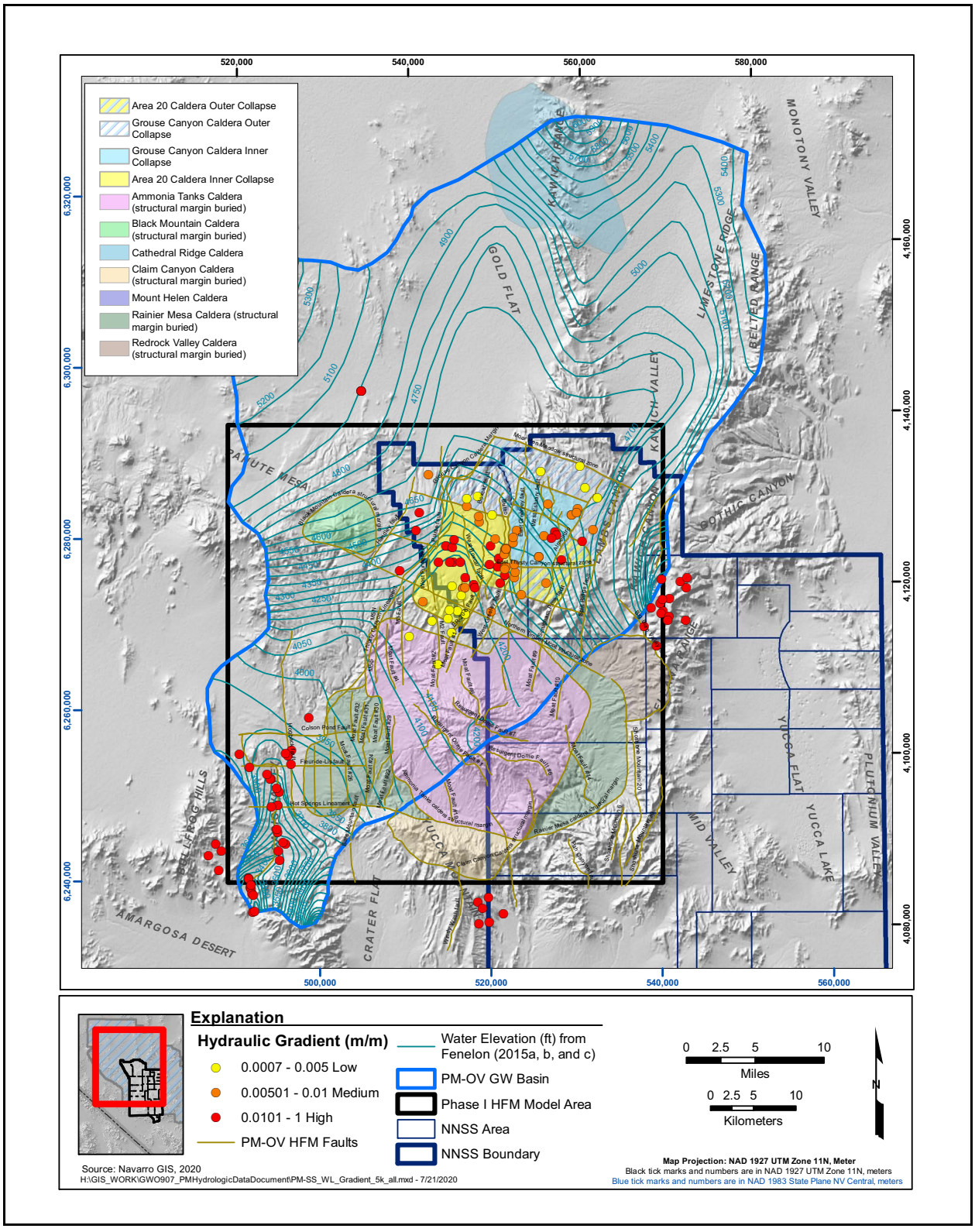

Figure 8-6
Pahute Mesa Steady-State Water-Level Gradient at a 5-km Length Scale

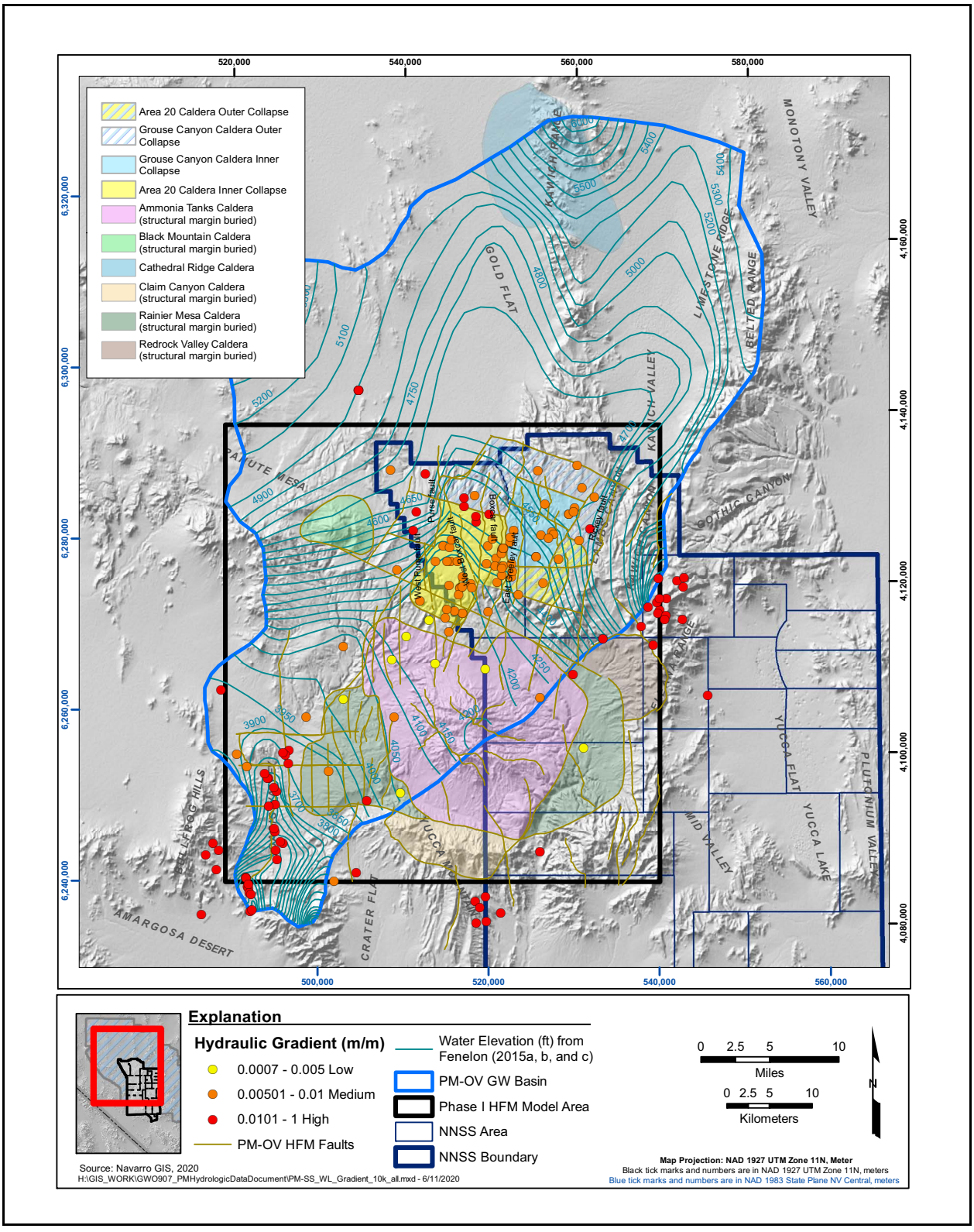

Figure 8-7
Pahute Mesa Steady-State Water-Level Gradient at a 10-km Length Scale

10-km-regression distance. Figure 8-6 and the gradient direction and uncertainties illustrated in Figure 8-4 suggest a length scale of approximately 5 km adequately preserves local gradients and has acceptable gradient uncertainty. The following areas of distinct geologic structure that influence the hydraulic gradient are identified.

Eastern Silent Canyon Caldera

This area is between the East Greeley and Rickey faults within the SCCC (Figure 8-6). The hydraulic gradient is generally low in the northern half of this area due to the presence of the extensive and productive BRA near the water table. The hydraulic gradient in the south is generally medium to high due to the presence of the thick BFCU near the water table.

Western Silent Canyon Caldera

This area includes the northern area between the East Greeley and West Boxcar faults where the dominant HSU in which testing was conducted is the CHZCM (Figure 8-6). Within the northern area, the hydraulic gradient is generally low due to several high-permeability rhyolitic lava flows. The migration of radionuclides in this area is likely controlled by the distribution of rhyolite lavas in the CHZCM. The steepening of the hydraulic gradient near West Boxcar fault corresponds to an increase in the percentage of poorly permeable zeolitized tuff in the saturated zone (Blankennagel and Weir, 1973). It is also possible that groundwater is redirected southward by the Boxcar and West Boxcar faults. The Boxcar and West Boxcar faults are located between most of the wells in this area. The faults could have a low-permeability core, or the juxtaposition of aquifers to confining units could restrict flow across the faults. The migration of radionuclides in the area between the Boxcar and Purse faults is likely controlled by the distribution and continuity of the Paintbrush welded tuffs (TCA and TSA) and rhyolitic LFAs (BA, CPA, and SPA).

West of the Purse Fault

The Purse fault may behave as a structural barrier to groundwater flow and provides a discontinuity between flow paths in the aquifers to the east and to the west of the fault (Figure 8-6). The discontinuity results in heads that are several hundred feet higher west of the caldera and groundwater flow that is predominantly parallel to the discontinuity (SNJV, 2006). The Purse fault coincides with the northwestern boundary of the SCCC and separates two groundwater systems with distinct

compositions. The groundwater chemistry in the upper Thirsty Canyon, west of the Purse fault, is distinct from Pahute Mesa groundwater immediately to the east (SNJV, 2006).

Southwest Area 20 and the Bench Area

The Bench area is a transitional area between the SCCC and TMCC (Figure 8-6). A southwest trending trough in the potentiometric surface begins in Area 20 and extends through the Bench area to the southwest and down through Thirsty Canyon. The trough may be attributed to several causes, including the following:

1. The potentiometric surface trough coincides with a zone of higher transmissivity. The high transmissivity may be due to fracturing associated with the caldera margin, or a thick accumulation of intra-caldera tuffs in the Area 20 caldera. Faults within southwest Area 20 and the Bench area do not behave as hydraulic barriers to cross-flow and may hydraulically connect the ash-flow aquifers and LFAs in this area (see Section 9.4.1). Transmissivities are especially high just southwest of the NNSS in the Bench area, as a result of thick rhyolite lava flows near the water table (Fenelon et al., 2016).

2. The TCL may behave as a conduit along the axis due to the lineament being a high-permeability fault zone. The potentiometric trough is nearly coincident with the lineament. The water levels west of lineament and the Purse fault are 200 ft higher, suggesting the lineament may also behave as a barrier to cross flow. It is uncertain whether the juxtaposition of rocks with different permeabilities across faults or low-permeability fault cores are responsible for the apparent flow barrier seen across the TCL. During aquifer testing in Southwest Area 20 and the Bench area, drawdowns were seen across structural blocks and faults (Garcia et al., 2017), but the Purse fault may be beyond the area influenced by aquifer testing.

3. The Purse and West Purse faults on the western margin of the trough and the Boxcar and West Boxcar faults on the eastern part of the structural trough may restrict flow into the structural block. Restricted inflow and low recharge combined with the high transmissivity result in a small flow of groundwater moving through this area under a relatively small hydraulic gradient.

Single-well testing at ER-EC-12 revealed that the TCA and TSA have low transmissivity interpreted to be from the extensive hydrothermal alteration filling the fracture system, which may be a large-scale heterogeneity in the southeast corner of the Bench area (N-I, 2014). Single-well testing of ER-EC-15 indicates that this low-transmissivity area may also include TCA and TSA at ER-EC-15 (Navarro, 2015). However, the analysis of distal well drawdown in response to the ER-20-11 constant-rate test detected a drawdown in the deep (CHZCM/CFCU) completion of ER-EC-12.

Western Timber Mountain Moat

The northwestern portion of the Timber Mountain caldera between the Bench area and the Timber Mountain resurgent dome is associated with the Ammonia Tanks caldera. Flow will transition in a complicated way through the caldera moat into two units: the FCCM and TMCM around the northwest flank of the Timber Mountain resurgent dome. The gradient begins to increase in the central area of the western Timber Mountain moat, possibly due to constriction of the flow paths due to the Timber Mountain resurgent dome or transition to lower permeability rock in this area. The gradient is increased compared to the gradient in the Bench area. Distances between wells in this area are greater than 5 km, and the interpretation of the gradient must rely on the potentiometric contours.

West Side of the Ammonia Tanks Caldera

This is the area west of the Timber Mountain dome extending along the western ring fracture zone of the Ammonia Tanks portion of the TMCC (Figure 8-6). Groundwater flow in this area parallels the strike of the western ring-fracture zone coinciding with an area of sub-parallel basin-and-range faults. The gradient increases near the entrance to Oasis Valley in part due to narrowing of the groundwater basin, the presence of low-permeability rock, and reduction in volcanic rock thickness.

Oasis Valley Discharge Area

Outflow from Oasis Valley is controlled by a deep confining unit of siliciclastic rocks, which underlies the southern part of the PM-OV flow system and crops out near Oasis Valley. The confining unit may force water upward through faults in the area. The potentiometric contours surrounding this valley exhibit a prominent “V” shape along the valley near the terminus of the PM-OV groundwater basin (Figure 8-6). Most of the water that flows through the Pahute Mesa area of the NNSS is assumed to be discharged by springs and seeps in Oasis Valley (Fenelon et al., 2016). The gradient in the Oasis Valley discharge area is much higher than the average PM-OV gradient due to further narrowing of the groundwater basin and reduction in volcanic rock thickness.

8.6.2 Vertical Water-Level Gradients and Structural Controls

Recharge in the PM-OV groundwater basin occurs on volcanic highlands such as Pahute Mesa and Timber Mountain, and as infiltration of runoff from highlands onto alluvial fans (Fenelon et al., 2016). Typically, areas of highest altitude receive the most precipitation, and the largest amount of

recharge and semi-perched and perched groundwater (water separated from the regional groundwater flow system by low-permeability rock) is common throughout the Pahute Mesa region. Distinguishing whether a hydraulic head is anomalous relative to heads in the regional alluvial-volcanic aquifer is needed to accurately determine the vertical gradients in the regional aquifer. The subset of water levels located within the PM-OV HFM area not identified as being anomalous was extracted from the Fenelon (2015a, b, and c) data and was analyzed to determine the vertical gradients. Furthermore, the Fenelon (2015a, b, and c) water-level data flagged as "less than" or "greater than" were discarded. The vertical gradients at 34 unique locations were calculated from the head in the highest and lowest water-level intervals in each well using the distance between the EOI centers.

Figure 8-8 illustrates the well locations with vertical gradient data. Vertical groundwater gradients are generally neutral to downward in most of Area 19, and transition toward neutral to upward in Area 20 and upward in Oasis Valley. The following areas of distinct geologic structure that influence the vertical hydraulic gradient are identified.

Western Rainier Mesa

A strong downward vertical gradient occurs in the eastern part of the Pahute Mesa Phase II HFM, near Rainier Mesa. This is an area of low-permeability siliciclastic rock and high recharge.

North of the Purse Fault

The vertical gradients on the northwest side of the Purse fault are downward, but the wells with multiple vertical completions are limited to Wells UE-20j, ER-20-12, and PM-3. At ER-20-12, the TMWTA is separated from the lower HSUs by the low-permeability UPCU. Vertical gradients are downward from the TMWTA to the HSU below the UPCU, but upward from the deeper HSUs to the UPCU. Water levels in the lower HSUs at ER-20-12 are similar to those east of the Purse fault.

Eastern Silent Canyon Caldera within Area 19

Vertical groundwater gradients are generally neutral to downward in most of Area 19. Many of the wells in the eastern part of the caldera are completed in the extensive and productive BRA, and the heads in these wells are relatively stable or decrease with depth. One exception to the vertical gradient

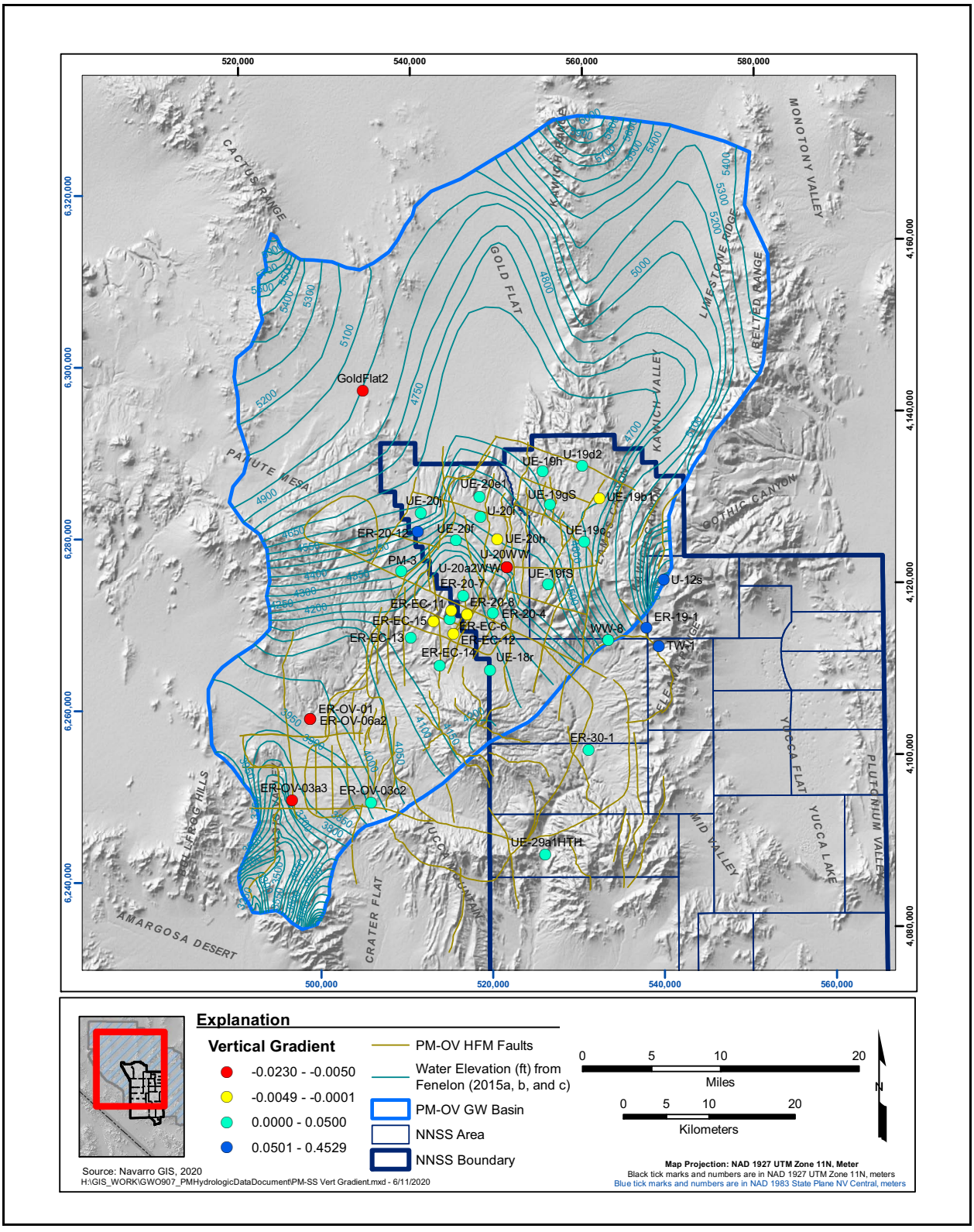

Figure 8-8
Pahute Mesa Vertical Water-Level Gradients at Multi-Level Wells

trend is Well UE-19i. Thick sequences of the CFCU and BFCU overlie the BRA at this location, thereby creating confining conditions.

Western Silent Canyon Caldera within Area 19 and to the Bench Area

The vertical gradients become more variable in the western part of Area 19 and into Area 20. The vertical gradients generally transition from downward to upward between eastern Area 19 to southwestern Area 20. Blankennagel and Weir (1973) observed that in most of the drill holes in the western and central parts of the caldera, fractured rhyolites and welded tuffs constitute the significant aquifers. These aquifers are separated by thick sections of ash-fall and ash-flow tuffs that have low permeabilities that may be low enough to create confined aquifers.

Oasis Valley

Vertical hydraulic gradients in Oasis Valley are generally upward, indicating a groundwater discharge zone.

8.7 Summary

The primary objective of the potentiometric data analysis was to derive a set of steady-state hydraulic head and gradient data that can be used to support the development of the Pahute Mesa CAU flow model. This dataset was prepared through the collection and compilation of existing depth-to-water and spring data, and estimation of water-level uncertainty using hydrograph and statistical analyses. The resulting hydraulic head dataset is provided in Appendix C. General site information for wells, boreholes, or completions located within the PM-OV HFM is presented in Table C-1 and site information for springs is provided in Table C-2. The hydraulic head dataset is provided in Table C-3. Also included in Table C-3 is the number, minimum, maximum, and standard deviation of the measurements used to determine the steady-state values along with the uncertainties assigned to each steady-state head. The resulting gradient dataset is provided in Table C-4.

A vertical gradient analysis showed a strong downward vertical gradient at the water table in the area of Rainier Mesa. This gradient is consistent with recharge occurring on Rainier Mesa. Vertical groundwater gradients are generally neutral to downward in most of Area 19, and transition toward neutral to upward in Area 20 and upward in Oasis Valley.

A secondary objective of this data analysis was to investigate possible structural controls on horizontal and vertical gradients, and flow directions. The hydraulic gradient is related to the geologic structures and location of recharge areas. The relationship between structure and hydraulic gradient was investigated by calculating the horizontal gradient over various length scales and comparing the stratigraphy extracted from the Phase II HFM to the gradient. The hydraulic gradient is generally low in areas of productive aquifers. These areas include the BRA and rhyolitic lava flows in the SCCC, and the highly fractured transitional area between the SCCC and TMCC located in southwest Area 20. The TCL and Purse fault may behave as structural barriers due to the juxtaposition of aquifers to confining units or the presence of low-permeability fault cores. The latter explanation is less likely because pumping signals were seen across structural blocks during aquifer test analyses (Garcia et al., 2017).

9.0 MULTIPLE-WELL AQUIFER TESTS

Phase II data collection program included drilling and testing of 11 new wells that are downgradient of the testing locations in Area 20. Water levels in these wells, along with other Pahute Mesa wells, have been measured continuously with pressure transducers by Navarro and USGS. Water-level observations during well development and aquifer testing in these wells can be interpreted as MWATs. A total of 38 completions within 26 well locations have aquifer stress responses to groundwater withdrawals that can be used in calibration of the CAU groundwater flow model.

9.1 Objectives

The purpose of this data analysis activity was to evaluate the existing stress response data from the MWATs for use in the Pahute Mesa CAU groundwater flow model. The data will be used to estimate transmissivity and storage properties during model calibration.

9.2 Approach

The approach used to evaluate the MWAT data includes the following:

- Collect, compile, and qualify existing groundwater stress response data for the Pahute Mesa area and vicinity.
- Identify the drawdown uncertainty.

9.3 Data Types

The data needed to assess hydraulic heads include general site information, pumping rates in tested wells and drawdowns in responding wells. A site is defined as a well or a separate completion zone within a well. The specific data types needed are as follows:

General Site Information

- Unique site identifier
- Site location

Aquifer Test Information

- Pumping schedules
- Water-level time series
- Water-temperature time series
- Barometric-pressure time series
- Drawdown observation time series
- Uncertainty of the drawdown observations

9.4 Data Compilation

Phase II data collection activities between November 2009 and September 2016 included well development and testing of 10 wells located within the Bench area (SNJV, 2009a), and 1 additional well located northwest of the Bench (Well ER-20-12). The wells contain single or multiple completions and, for the wells with multiple completions, the individual completions were hydraulically isolated during pump-scale aquifer testing using packers. The pumping along with the drawdowns seen in the observation well network associated with each tested interval can be considered individual aquifer tests, thereby providing a total of 16 MWATs (Figures 9-1 and 9-2). The distal location of ER-20-12 from observation wells prohibits the well development and testing data from this well being interpreted as an MWAT.

Garcia et al. (2017) performed simultaneous interpretation of the 16 MWATs to estimate hydraulic properties on Pahute Mesa. Hydraulic properties of aquifers and confining units were estimated by interpreting drawdowns from multiple aquifer tests using a 3-D hydrogeologic framework and multiple groundwater-flow models. Individual models for each MWAT were simultaneously calibrated using identical hydrogeologic properties. The data compiled by Garcia et al. (2017) represent the available stress-responses that will be used to calibrate the CAU groundwater flow model. Data collected during the 16 MWATs included pumping schedules and continuous water-level, temperature, and barometric-pressure measurements. Water levels and temperatures were measured continuously or intermittently in the observation wells, background wells, and pumping wells from November 2009 to October 2014.

9.4.1 Aquifer Tests

Wells pumped during the 16 MWATs contained a main casing with one, two, or three completions. Packers or bridge plugs in the main casing were used to isolate completions, allowing the individual completions to be pumped during testing. The individual completions within wells with

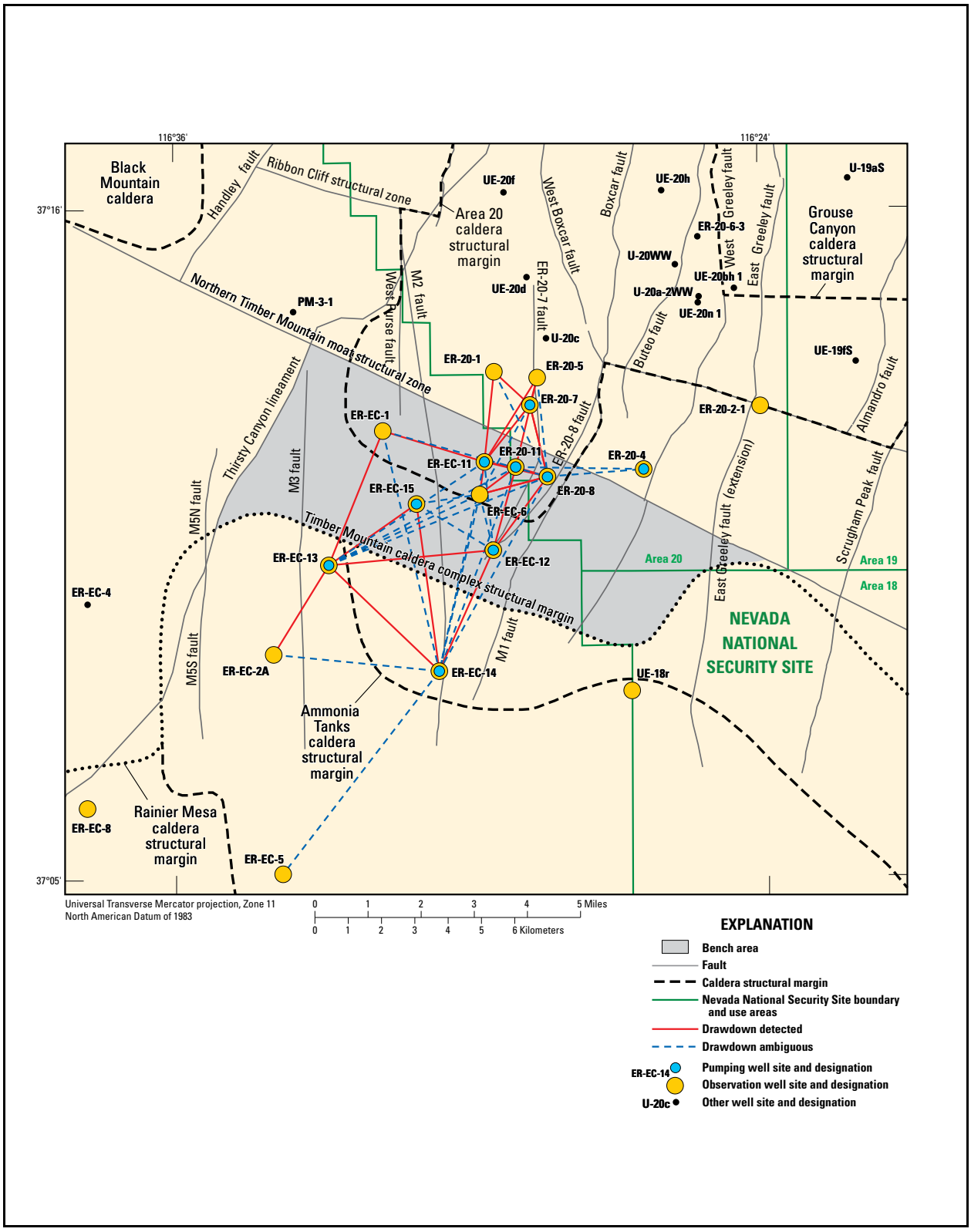

Figure 9-1
Location of Well Sites and Hydraulic Connections between Pumping and Observation Wells Associated with MWATs at Pahute Mesa
Source: Garcia et al., 2017, Figure 10

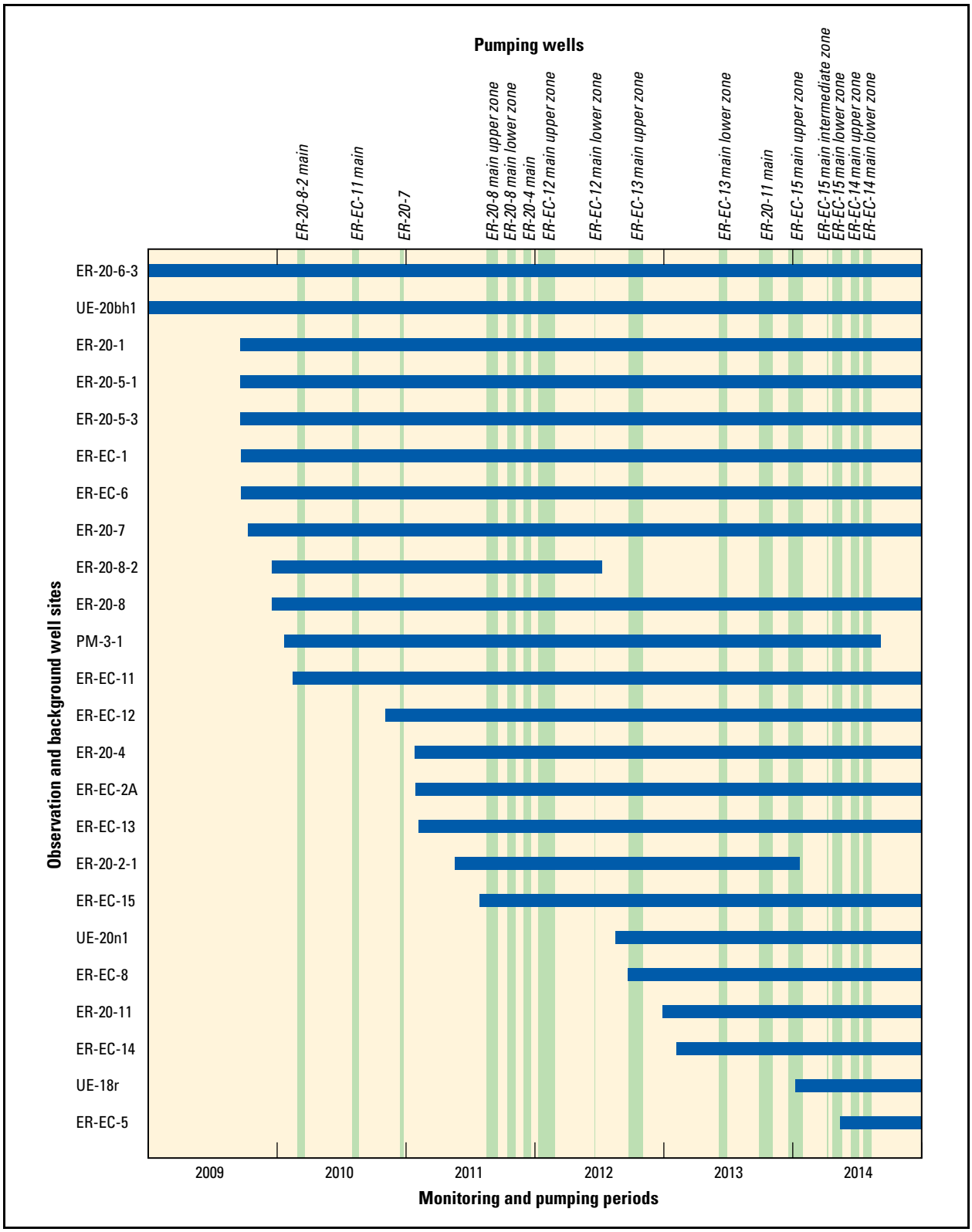

Figure 9-2
Monitoring and Pumping Periods for the Pahute Mesa MWATs
Source: Garcia et al., 2017, Figure 6

multiple-completions are designated main upper zone, main intermediate zone, or main lower zone. Several of the pumping wells also contained piezometers completed in the annulus alongside the main completion zone or in shallower or deeper zones in the borehole. Piezometers in multiple-completion wells were used as observation wells.

Each aquifer test typically consisted of three phases during a 30-day pumping schedule. Well development and step-drawdown tests were done during the first 10-day period. No pumping was performed during the second 10-day recovery, and aquifer testing was performed during the third 10-day period. Pumping periods were briefer in low-productivity wells, where pumping could not be sustained (e.g., ER-EC-12 main lower zone, and ER-EC-15 main intermediate and lower zones) (Garcia et al., 2017); and were longer in duration at ER-20-11 because of the high yield and the potential to observe hydraulic influence due to the pumping at surrounding wells.

Table 9-1 presents the pumping wells, pumping periods, and volume discharged during each MWAT. Pumping rates during well development and testing were typically 100 to 300 gal/min, and total discharge volumes were 2 to 8 million gallons (Mgal) over the well development and testing period with a few exceptions. The exceptions are the TCA and TSA completions in Wells ER-EC-12 and ER-EC-15, which could only support much lower pumping rates. Single-well hydraulic testing in the ER-EC-12 main lower zone and ER-EC-15 main intermediate and lower zones revealed that the TCA and TSA at these locations have low transmissivities more akin to aquitards than aquifers, even though the two units tested often behave as aquifers at other Pahute Mesa wells. The low transmissivity is interpreted to be from extensive hydrothermal alteration filling the fracture system, which may represent a large-scale herogeneity along the flow path to Oasis Valley (Navarro, 2015 and 2018).

9.4.2 Drawdowns

The drawdowns analyzed by Garcia et al. (2017) were estimated using water-level models. Water-level models were calibrated using the observed water levels because distal drawdowns during aquifer tests can be obscured by environmental fluctuations such as barometric pressure changes, earth tides, and recharge events in the water-level record. The water-level models provide a mechanism for distinguishing environmental fluctuations from pumping-induced drawdown in complex hydrogeologic systems. The water-level models transform the pumping stresses using Theis (1935) analytical models. Environmental water-level fluctuations are approximated with

Table 9-1
Pumping Wells, Pumping Periods, and Volume Discharged during Each MWAT

Pumping Well Name	Period of Well Development and Aquifer Testing (mm/dd/yyyy)		Approximate Discharge Rate (gal/min)	Approximate Volume Discharged (Mgal)
	Start	End		
ER-20-4 main	08/30/2011	09/21/2011	250–280	5.2
ER-20-7	09/14/2010	09/24/2010	280	2.4
ER-20-8 main upper zone	05/18/2011	06/27/2011	110–140	3.1
ER-20-8 main lower zone	07/15/2011	08/08/2011	105–130	3.1
ER-20-8-2 main	11/28/2009	12/18/2009	130	1.9
ER-20-11 main	06/11/2013	08/05/2013	245–285	10.8
ER-EC-11 main	04/30/2010	05/19/2010	270–300	5.5
ER-EC-12 main upper zone	10/11/2011	11/28/2011	83–100	2.3
ER-EC-12 main lower zone	02/29/2012	03/19/2012	10–40	<0.1
ER-EC-13 main upper zone	06/22/2012	07/13/2012	240–300	5.1
ER-EC-13 main lower zone	07/21/2012	03/29/2013	200–300	8.5
ER-EC-14 main upper zone	03/14/2014	04/07/2014	150	4.0
ER-EC-14 main lower zone	04/18/2014	05/12/2014	220–270	7.0
ER-EC-15 main upper zone	09/17/2013	10/29/2013	119–124	3.0
ER-EC-15 main intermediate zone	12/18/2013	01/10/2014	9–13	<0.1
ER-EC-15 main lower zone	01/22/2014	02/18/2014	20–21	0.5

modeled time series of barometric pressure, earth-tide signals, and background water levels to account for recharge or any other natural stress on the groundwater system (Halford et al., 2016; Garcia et al., 2013).

Drawdown detection was classified as undetected, detected, or ambiguous using water-level modeling for more than 200 pumping-observation well pairs. Drawdown was classified as undetected where the signal-to-noise ratio was less than 2, indicating drawdown could not be reliably differentiated from the noise. Drawdown was classified as detected where the signal-to-noise ratio was greater than 10; drawdown was above a detection threshold of 0.05 ft; and correlation with environmental water-level fluctuations was unlikely (Garcia et al., 2017). Of the 206 drawdown detections evaluated, 93 well drawdowns were classified as detected; 59 drawdowns were ambiguous; and 54 well pairs had no drawdown (Table 9-2).

Table 9-2
Summary of MWAT Observed Drawdowns (ft) for Pumping- and Observation-Well Pairs [a]
(Page 1 of 2)

Observation Well Name	Pumping Well Name										
	ER-20-4 main	ER-20-7	ER-20-8 main upper and lower zones	ER-20-8-2 main	ER-20-11 main	ER-EC-11 main	ER-EC-12 main upper and lower	ER-EC-13 main upper zone	ER-EC-13 main lower zone	ER-EC-14 main upper and lower zones	ER-EC-15 main upper, intermediate, and lower zones
ER-20-1	--	0.16	--	(0.06)	--	0.07	--	--	--	--	--
ER-20-2-1	U	--	U	--	--	--	--	--	--	--	--
ER-20-4 deep (main)	206	--	(<0.05)	--	(0.03)	--	--	--	--	--	U
ER-20-4 shallow	2.42	--	U	--	U	--	--	--	--	--	U
ER-20-5-1	--	0.16	(0.03)	(0.05)	0.07	0.1	--	--	--	--	U
ER-20-5-3	--	0.17	(0.02)	(0.06)	0.14	0.12	--	--	--	--	U
ER-20-7	--	9.5	0.1	(0.04)	0.24	0.23	--	U	U	--	U
ER-20-8 deep (main lower zone)	(0.07)	0.12	1.2-4.0	0.25	0.65	0.17	--	--	--	(0.02)	U
ER-20-8 intermediate (main upper zone)	U	(0.04)	0.22-16	0.34	0.61	(0.05)	--	U	--	(0.03)	U
ER-20-8 shallow	--	0.07	0.26-0.8	0.46	0.6	(0.15)	--	(0.02)	U	U	U
ER-20-8-2	U	--	0.38	6	--	--	(0.03)	--	--	--	--
ER-20-11	--	--	--	--	112	--	--	--	(0.02)	(0.03)	--
ER-EC-1	--	--	(0.04)	(0.05)	--	0.12	--	0.07	0.08	(0.07)	--
ER-EC-2A	--	--	U	--	U	--	--	(0.04)	0.05	(0.04)	U
ER-EC-5	--	--	--	--	--	--	--	--	--	(0.04)	--
ER-EC-6 deep	--	(0.08)	0.13	(0.04)	0.45	0.55	(0.04)	U	--	(0.03)	(0.05)
ER-EC-6 intermediate	--	(0.07)	0.16	0.1	0.76	0.41	(0.05)	U	(0.03)	(0.03)	(0.04)
ER-EC-6 shallow	--	(0.09)	0.2	0.13	0.85	0.45	(0.04)	--	(0.02)	U	(0.04)
ER-EC-8	--	--	--	--	U	--	--	--	U	(0.02)	U
ER-EC-11 deep (main lower zone)	--	0.09	0.18	--	0.71	126	(0.03)	U	(0.02)	(0.04)	U
ER-EC-11 intermediate (main upper zone)	--	0.1	0.16	0.13	0.71	--	(0.04)	U	(0.02)	(0.04)	U
ER-EC-11 shallow	--	0.13	0.22	0.12	0.87	1	(0.04)	U	(0.02)	--	U

Table 9-2
Summary of MWAT Observed Drawdowns (ft) for Pumping- and Observation-Well Pairs [a]
(Page 2 of 2)

Observation Well Name	Pumping Well Name										
	ER-20-4 main	ER-20-7	ER-20-8 main upper and lower zones	ER-20-8-2 main	ER-20-11 main	ER-EC-11 main	ER-EC-12 main upper and lower	ER-EC-13 main upper zone	ER-EC-13 main lower zone	ER-EC-14 main upper and lower zones	ER-EC-15 main upper, intermediate, and lower zones
ER-EC-12 deep	--	--	0.1	--	0.21	--	U	(0.03)	U	(0.04)	U
ER-EC-12 intermediate (main lower zone)	--	--	0.08	--	0.06	--	457	--	--	(0.08)	U
ER-EC-12 shallow (main upper zone)	--	--	0.03	--	0.09	--	371	0.06	0.05	0.19	0.06
ER-EC-13 deep (main lower zone)	--	--	U	--	U	--	--	1.7	293	0.09	U
ER-EC-13 intermediate (main zone)	--	--	U	--	U	--	--	59	2	0.09	U
ER-EC-13 (shallow)	--	--	U	--	U	--	--	0.1	0.02	0.08	U
ER-EC-14 deep (main lower zone)	--	--	--	--	(0.04)	--	--	--	0.08	1.1-12	(0.03)
ER-EC-14 shallow (main upper zone)	--	--	--	--	(0.01)	--	--	--	0.07	2.2-137	(0.03)
ER-EC-15 deep (main lower zone)	--	--	U	--	--	--	(0.09)	(0.03)	(0.02)	0.25	90
ER-EC-15 intermediate (main intermediate zone)	--	--	U	--	U	--	(0.05)	0.07	U	0.39	146
ER-EC-15 shallow (main upper zone)	--	--	U	--	U	--	(0.05)	0.08	0.08	0.22	94
UE-18r	--	--	--	--	--	--	--	--	--	U	--

Source: Modified from Garcia et al., 2017

[a] Values in parentheses represent ambiguous estimates; U = Undetected; -- = Not estimated.

Figure 9-1 presents the locations of hydraulic connections identified during the Pahute Mesa MWATs by Garcia et al. (2017). Drawdowns were detected at distances greater than 3 miles (4.8 km) from pumping wells and propagated across HSUs and major structures, suggesting that fracturing is pervasive within the Bench area, and individual faults do not have a significant influence on the flow field. However, the analysis of hydraulic conductivity data presented in Section 5.2.3 identified a correlation between proximity to faults at a distance of less than 1,000 ft and hydraulic conductivity. Also, a steepening of the hydraulic gradient is seen in the western part of the SCCC near the West Boxcar fault. In addition, the Purse fault appears to behave as a structural barrier to groundwater flow (Section 8.6.1).

9.5 Drawdown Uncertainty

Drawdowns were classified as detected, ambiguous, or absent based on the signal-to-noise ratio and other aspects (e.g., correlations) within the water-level data. The signal-to-noise ratio is defined as the ratio of maximum drawdown in a well during an aquifer test to the RMS error of the model fit. Drawdown detection becomes ambiguous when the signal-to-noise ratio is low, or where correlation exists between environmental fluctuations and pumping signals. Correlation between the pumping signal and environmental fluctuations becomes apparent where observed drawdown can be approximated by a linear trend during all or part of the period of analysis. Correlation typically is possible as hydraulic diffusivity decreases; distance between observation and pumping well increases; or recovery is truncated. Correlation is unlikely where sharply defined pumping signals exist, or significant recovery has been observed (Garcia et al., 2013). Drawdown was classified as detected where the signal-to-noise ratio was greater than 10; drawdown was above a detection threshold of 0.05 ft; and correlation with environmental water-level fluctuations was unlikely. Drawdown was classified as ambiguous when the signal-to-noise ratio ranged between 2 and 10 (Garcia et al., 2017).

The noise in the water-level data that cannot be captured by the water-level models can be interpreted as the drawdown uncertainty and is specific to each well. The ambiguous drawdowns have the greatest uncertainty, and the uncertainty in the drawdown is inversely proportional to the signal-to-noise ratio. The magnitude of drawdown observations can vary greatly due to the proximity of the observation well to the pumped well, pumping rate, and hydraulic properties of the aquifer. During model calibration, the observation weights must be adjusted with a scaling factor so that the

contribution to the overall objective function from each drawdown observation is approximately the same. The uncertainty in the drawdowns will be considered in the calculation of observation and weights, and will be inversely proportional to the square of the signal-to-noise ratio as:

$$\frac{1}{((Noise)^2 + ScaleFactor)} \qquad (9\text{-}1)$$

9.6 Summary

The primary objective of the drawdown data analysis was to identify stress response data from the MWATs for use in the Pahute Mesa CAU flow model. Well development and aquifer testing along with the water-level monitoring in observation wells provide data for a total of 16 MWATs. Hydraulic connections between more than 200 pumping-observation well pairs were estimated from the MWATs for use in CAU model calibration.

10.0 LATERAL BOUNDARY FLUXES

Determining the hydraulic boundaries of the area to be modeled is required to ensure that the area through which test-related radionuclides may migrate is captured in the numerical flow and transport model. Inflow and outflow, if any, across the hydraulic boundaries is important, as it will affect the flow paths through the hydraulic basin.

10.1 Objectives

The specific objective is to identify the boundaries of the PM-OV groundwater basin and the groundwater fluxes across those boundaries. This basin definition will be used to define the area for which a groundwater flow and transport model will be generated to simulate the potential migration of Pahute Mesa test-related contaminants.

10.2 Approach

USGS has completed a number of hydrologic studies in the PM-OV area and has documented an estimated extent of the PM-OV groundwater basin (Fenelon et al., 2016). This study combines knowledge of the surrounding groundwater basins, basin discharges, hydrostratigraphy, groundwater elevations, and chloride mass-balance analyses to define the PM-OV groundwater basin boundaries and associated boundary fluxes. The basin delineations developed were tested through the development of a single-layer, steady-state, groundwater flow model to match groundwater elevations, basin discharge volumes, and transmissivities.

10.3 Basin Delineation

The PM-OV groundwater basin is the area over which recharge occurs, moves downgradient, and discharges in Oasis Valley. An estimated 5,900 acre-ft/yr of groundwater discharges in Oasis Valley. Subsurface discharge from Oasis Valley to the Amargosa Desert through alluvium in southern Oasis Valley is estimated at about another 100 acre-ft/yr, and an additional estimated 300 acre-ft/yr of surface water in the Amargosa River flows southward out of Oasis Valley (Fenelon et al., 2016). The

PM-OV groundwater basin does not include the area into which subsurface flow moves into the Amargosa Desert or surface flow out of the Oasis Valley occurring via the Amargosa River. With the exception of the relatively small volume of outflow described above, the basin is modeled as a closed system defined by no-flow boundaries.

The basin boundaries were defined by iteratively working with regional water balances and groundwater modeling of the PM-OV basin (Fenelon et al., 2016). This process led to the development of eight potential basin boundaries that eventually were resolved to the single most likely. The most likely basin boundary is shown in Figure 10-1.

The basin flow modeling balanced recharge against the estimated basin discharge with the recharge being applied to the groundwater flow model using three different approaches: a modified Maxey-Eakin method (Maxey and Eakin, 1951; Avon and Durbin, 1994), the INFILv3 model (Hevesi, 2006), and the Basin Characterization Model (Heilweil and Brooks, 2011).

10.4 Boundary Uncertainty

A total of eight PM-OV basin boundaries were developed using the iterative method briefly described above. Figure 10-2 shows the various basin boundaries considered. Figure 10-2 shows that although the boundary definition along the southeast was consistent, there was significant variation in the placement to the north and northwest.

Each of the alternative basin boundary definitions was considered in turn. Water levels, basin water balances, hydrostratigraphy, chloride mass-balance analyses, and the results of numerical modeling eliminated all but the basin delineation presented in Figure 10-1.

10.5 Conclusion

The PM-OV groundwater basin has been delineated and will define the flow and transport model developed to estimate potential migration of Pahute Mesa test-related contaminants. With the exception of a relatively small amount of discharge out of the basin to the Amargosa Desert and Amargosa River, the boundaries of the basin are no-flow boundaries.

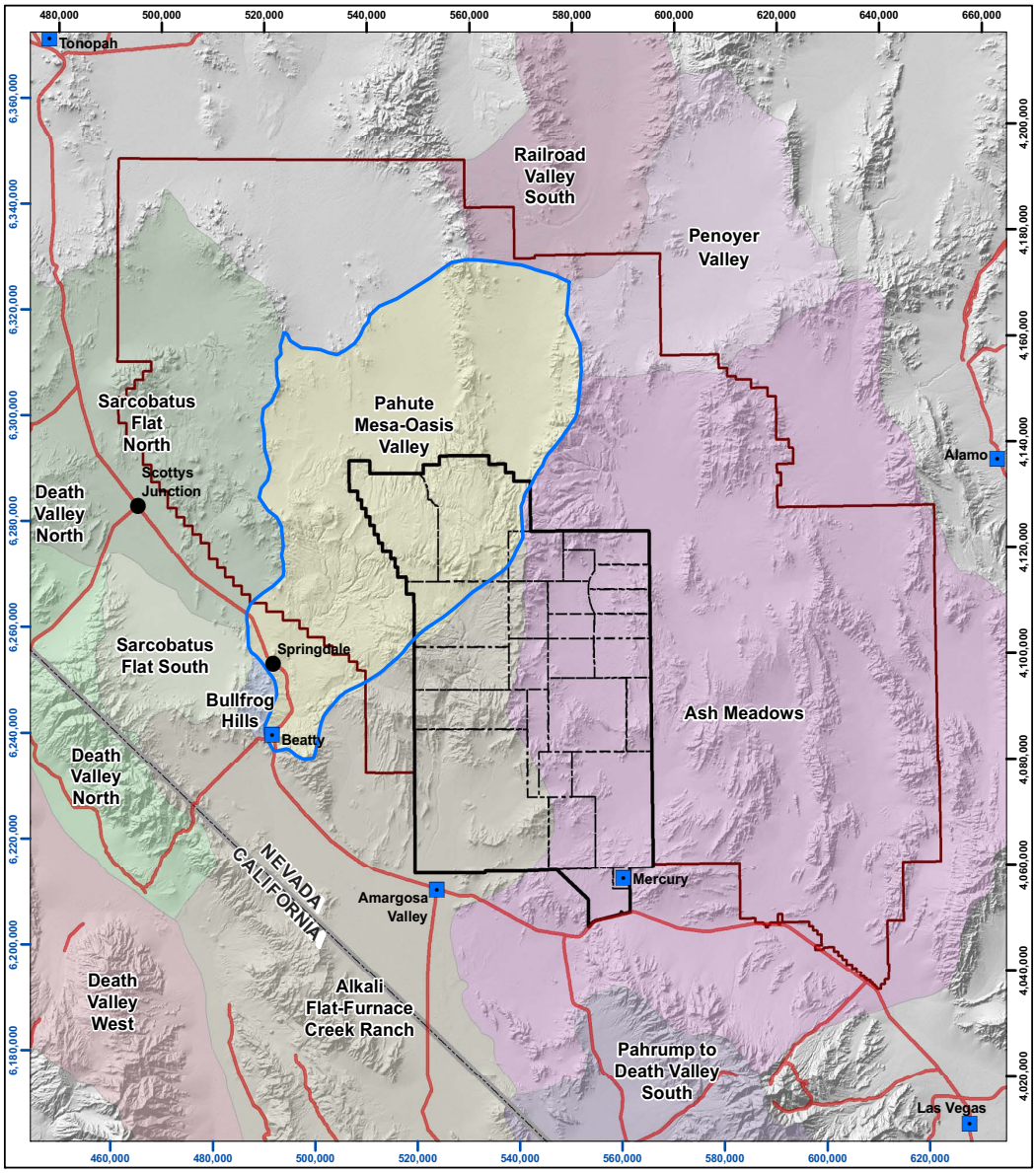

Figure 10-1
PM-OV Groundwater Basin and Surrounding Basins

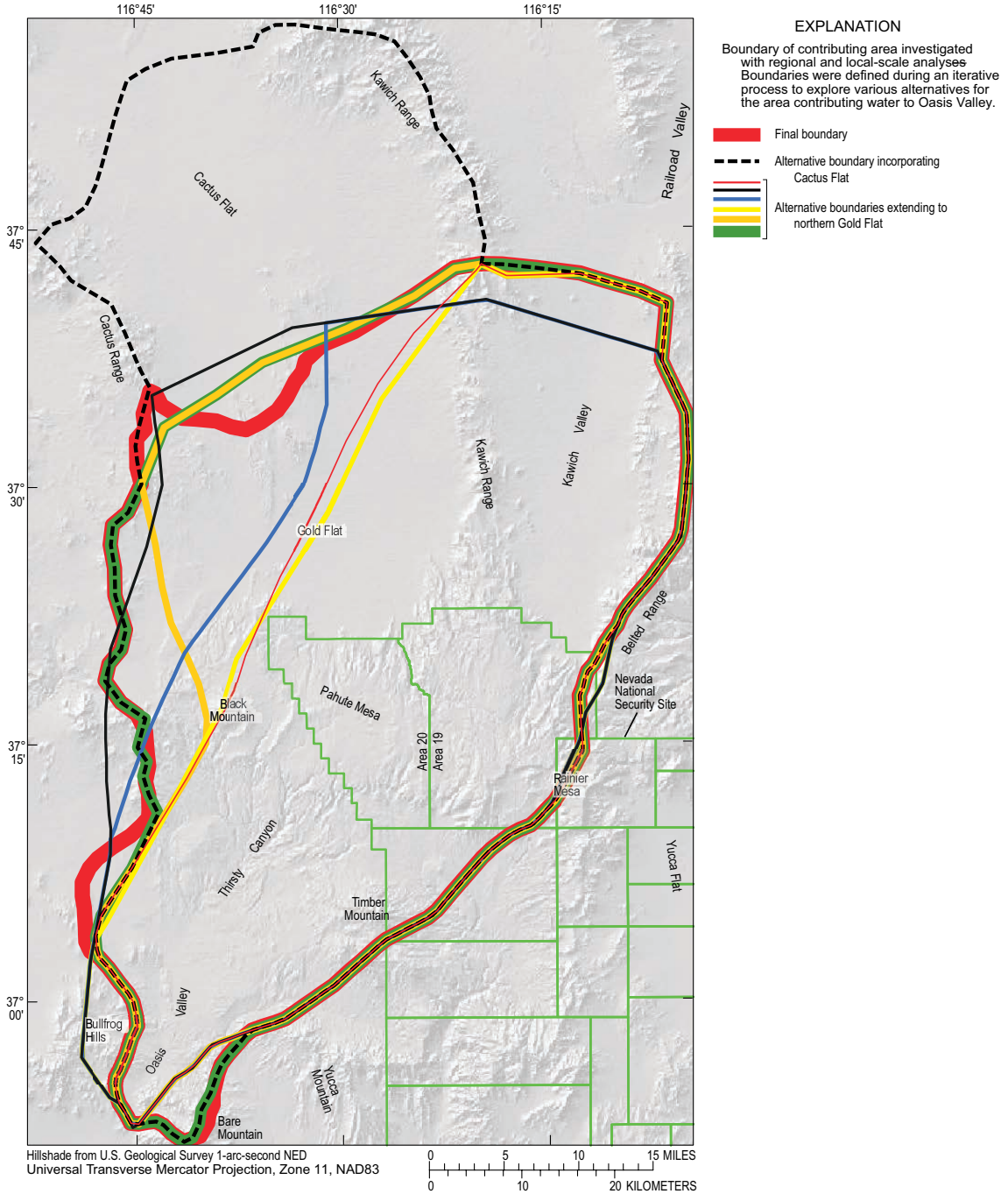

Figure 10-2
Boundaries Considered for the PM-OV Groundwater Basin
Source: Fenelon et al., 2016

To quote the conclusions drawn in Fenelon et al. (2016) regarding delineation of the PM-OV groundwater basin:

> *"The Pahute Mesa–Oasis Valley groundwater basin has been delineated consistently with regional and local constraints. The final Pahute Mesa–Oasis Valley groundwater basin is regionally consistent with adjacent bounding basins, because boundaries are perpendicular to water-level contours and recharge estimates balance measured groundwater discharge in the analyzed basins. Observed conditions in the final delineated Pahute Mesa–Oasis Valley groundwater basin were matched closely with a one-layer, groundwater-flow model to demonstrate local consistency. Simulated water levels, groundwater discharge, and transmissivities matched observed conditions within the measurement errors of each observation type."*

Also from Fenelon et al. (2016):

> *"Transport of radionuclides from Pahute Mesa can be assessed sufficiently within the final PM-OV groundwater basin because water passing through nuclear-test affected areas will discharge to Oasis Valley. The boundary is relatively certain because seven alternative boundaries were considered prior to determining the final Pahute Mesa–Oasis Valley groundwater basin. All 85 nuclear test locations were well within the 8 boundaries that were investigated."*

11.0 GROUNDWATER CHEMISTRY

Groundwater flow system evaluations consider groundwater chemistry data because they provide a means for determining the origin, pathway, and timescale of groundwater flow that is independent of estimates based on conventional hydraulic data. Groundwater chemistry and hydraulic data reflect distinct but complementary aspects of a groundwater flow system, and are therefore considered together to develop a consistent, comprehensive, and defensible flow system assessment. A geochemical evaluation of the PM-OV flow system is presented in the Phase I HDD (SNJV, 2004a), which describes groundwater chemistry data in the western portion of the NNSS, areas upgradient of the NNSS to the north, and downgradient areas as far south as the Amargosa Desert and as far southwest as Death Valley (Figure 11-1). Additional Phase I geochemical evaluations by Kwicklis et al. (2005) and Kwicklis (2009) were completed following publication of SNJV (2004a). Kwicklis et al. (2005) built on the previous evaluations using additional data and a different geochemical modeling approach. Kwicklis (2009) used carbon-14 (^{14}C) data to estimate groundwater ages.

A Phase II geochemistry evaluation for the PM-OV flow system was recently completed (Navarro, 2020). The Phase II evaluation focused on a smaller area within the PM-OV flow system where an additional 11 wells were drilled and additional groundwater sampling was performed in support of the NNSS Integrated Groundwater Sampling Plan (DOE/EMNV, 2019). The overall objective of the evaluation, as identified in the CAIP (NNSA/NFO, 2014), was to reduce uncertainty for the conceptual flow model used for transport modeling. To accomplish this objective, geochemical and isotopic parameters were examined to build an understanding of potential groundwater sources and flow paths within the vicinity of the Phase II focus area (Figure 11-2). Groundwater flow paths identified during Phase I were revised based on the new data. The usefulness of ^{14}C data for estimating travel times along the potential groundwater flow paths was also evaluated. Geochemical and isotopic data were also used to evaluate the revised groundwater flow system boundaries presented in Fenelon et al. (2016).

This section presents a summary of the Phase I (Section 11.1) and Phase II (Section 11.2) geochemical evaluations. Conclusions are presented in Section 11.3.

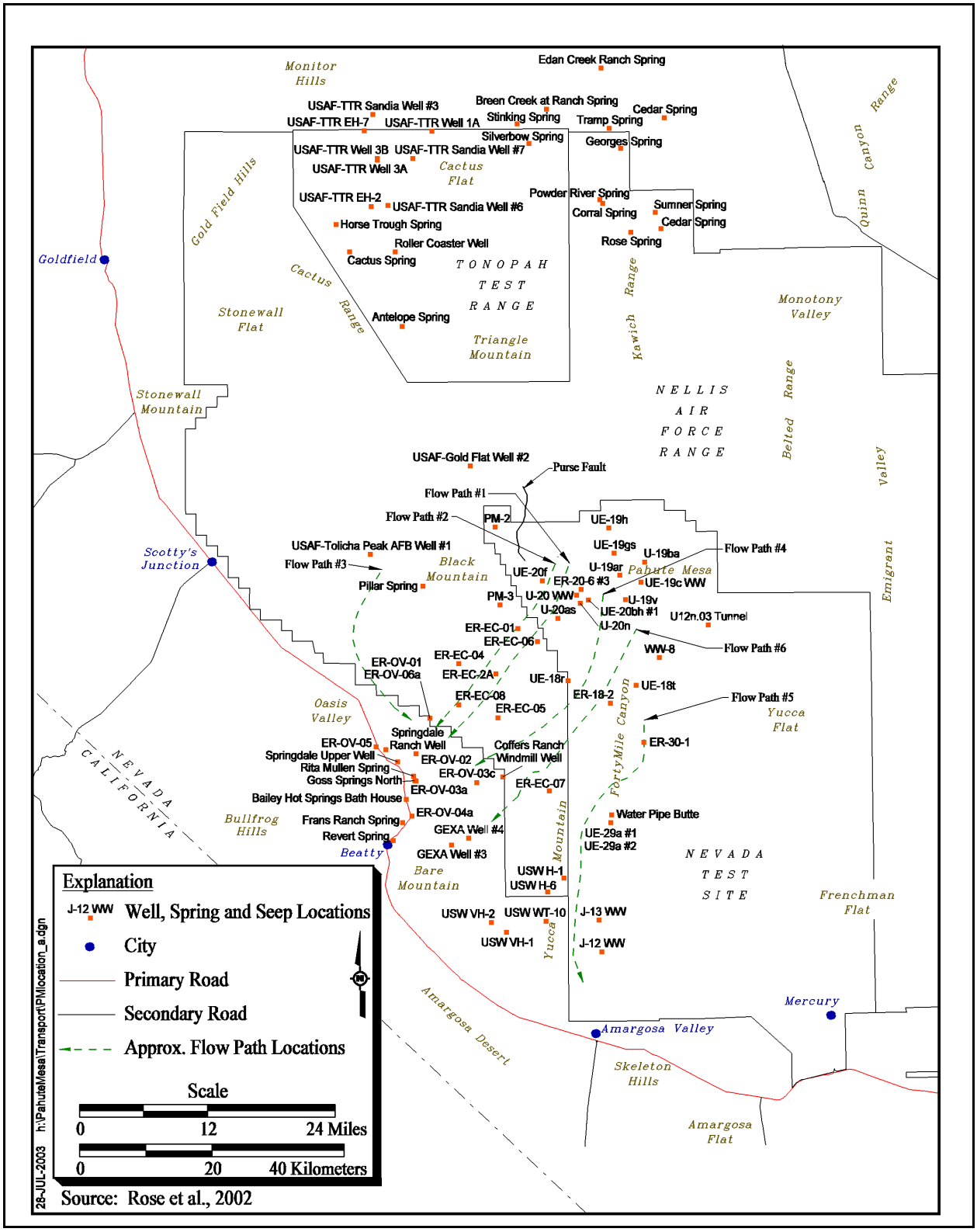

Figure 11-1
Locations Included in the Phase I PM-OV Geochemical Evaluation
Source: SNJV, 2004a

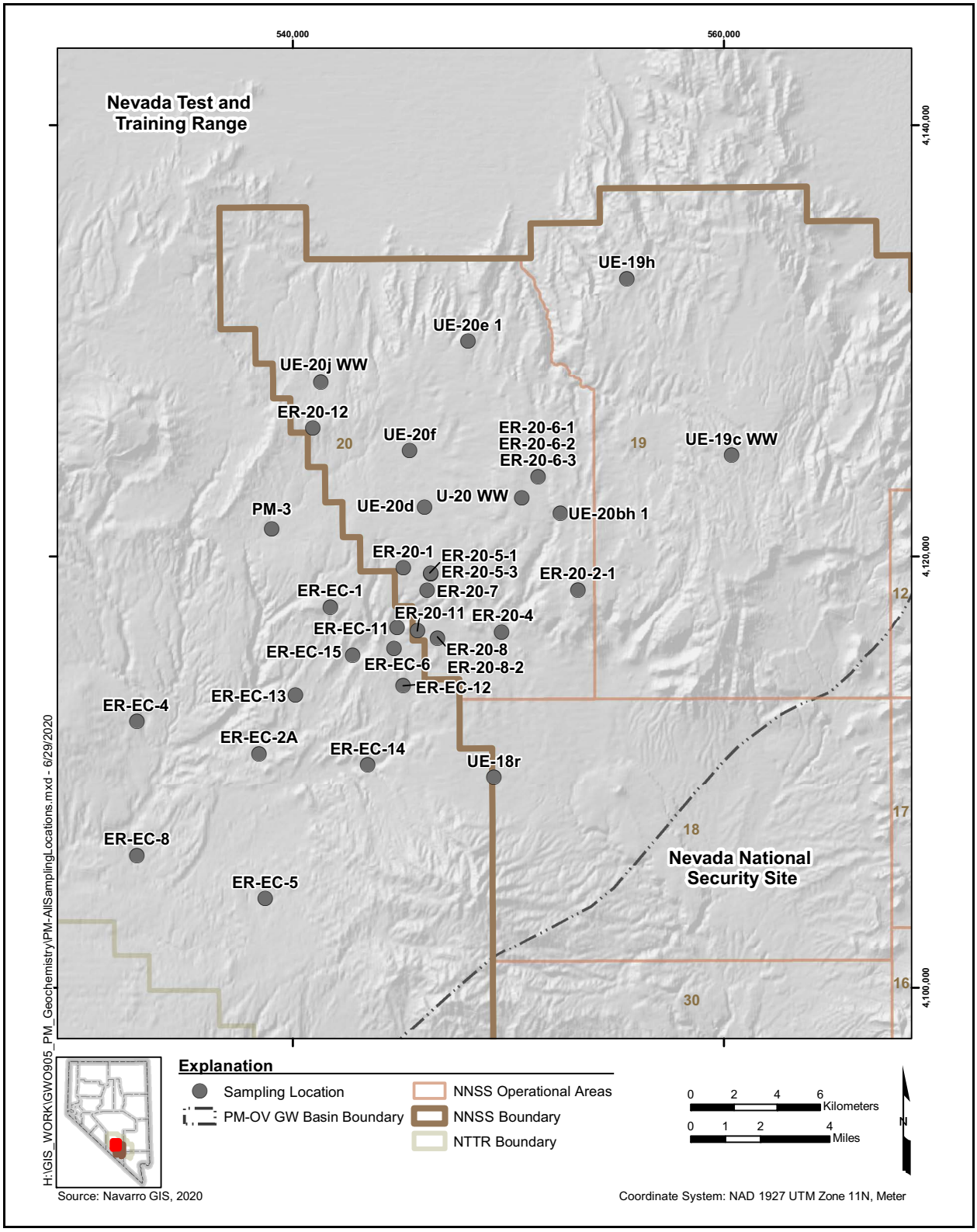

Figure 11-2
Locations Included in the Phase II PM-OV Geochemical Evaluation
Source: Navarro, 2020

11.1 Phase I Geochemical Evaluations

The Phase I dataset described in SNJV (2004a) consists of results for more than 1,800 sampling events conducted on 316 different well, spring, and seep locations (Figure 11-1). The dataset includes general chemical parameters, major ions, minor and trace elements, and stable and radioactive environmental isotopes. Representative data were selected based on data quality, distribution, and completeness of the necessary parameter suite. Variations in the water chemistry and isotopic composition were identified for the geographic subregions within the flow system (SNJV, 2004a).

SNJV (2004a) also summarized the geochemical investigation by Rose et al. (2006). Note that the work described in Rose et al. (2006) was completed and documented in a draft report in 2002, but the document was not finalized until 2006. Rose et al. (2006) expanded on an earlier investigation by Thomas et al. (2002) by including data from newly drilled UGTA wells on the NTTR (i.e., ER-EC wells). Both investigations used the NETPATH computer program (Plummer et al., 1994) for developing geochemical models to identify potential groundwater flow paths and mixing relations, and to evaluate groundwater travel times.

Additional Phase I geochemical evaluations by Kwicklis et al. (2005) and Kwicklis (2009) were completed following publication of SNJV (2004a). Kwicklis et al. (2005) built on the evaluations described in Thomas et al. (2002) and Rose et al. (2006) using additional data collected from the area south of Oasis Valley in the northwest Amargosa Desert, from Crater Flat, and from Yucca Mountain. Kwicklis et al. (2005) also applied a different code, PHREEQC (Parkhurst and Appelo, 1999), so that chemical and isotopic analytical uncertainty could be considered during model development. Inclusion of additional data south of the Pahute Mesa CAU flow model area enabled the fate of water leaving the PM-OV flow system to be better defined. Groundwater ^{14}C ages and travels times between wells were estimated by Kwicklis (2009) for the Pahute Mesa CAU flow model domain using the geochemical models previously developed for the PM-OV flow system.

11.1.1 Phase I Data Evaluation

Evaluation of the Phase I geochemical and isotopic dataset is summarized in this subsection. This evaluation focuses on geochemical investigations that took place after SNJV (2004a) and that were published by Kwicklis et al. (2005) and Kwicklis (2009). For more detailed information, the reader is

referred to the original reports (Thomas et al. [2002], Rose et al. [2006], Kwicklis et al. [2005], and Kwicklis [2009]). Sampling locations included in the Kwicklis et al. (2005) evaluation, categorized by the geographic area, are shown in Figure 11-3. Kwicklis et al. (2005) identified three distinct groundwater types in the PM-OV flow system based on conservative tracer (Cl, SO_4, δ^2H, and $\delta^{18}O$) data:

- Northernmost Thirsty Canyon area (e.g., ER-EC-1 and ER-EC-4) groundwater characterized by relatively light δ^2H compositions and high Cl concentrations.
- Pahute Mesa (e.g., U-20 WW and UE-19c WW) groundwater characterized by relatively light δ^2H compositions and relatively dilute Cl concentrations.
- Upper Fortymile Wash area (e.g., UE-29a#1 and UE-29a#2) groundwater characterized by dilute Cl and heavier δ^2H composition. Some groundwater (e.g., ER-18-2) has distinctly lighter δ^2H compositions, suggesting multiple sources of groundwater in this area.

The compositions of other groundwaters are generally intermediate between these end-members, indicating that they are a mixture of groundwater from these sources (Figure 11-4).

Figure 11-4 shows that Thirsty Canyon groundwaters lie along a trend defined by ER-EC-1 and ER-EC-4 and Pahute Mesa area wells. Downgradient of these Thirsty Canyon groundwaters, many Oasis Valley area groundwaters appear to lie along the same trend in Cl concentration but have a somewhat heavier δ^2H composition (Figure 11-4), suggesting that an isotopically heavier component has mixed with Thirsty Canyon groundwater in the Oasis Valley area. Potential sources of this isotopically heavier component include local recharge from surface runoff (represented by UE-29a#1 and UE-29a#2), groundwater from the northwest (represented by USAF Tolicha Peak Well #1 [Tolicha Peak Well] and ER-OV-05 wells), or from north of the NNSS (represented by Cedar Pass well).

The geographic distribution of Cl, SO_4, δ^2H, and $\delta^{18}O$ compositions in groundwater further illustrate the following trends (Figure 11-5).

- Relatively dilute groundwater from Pahute Mesa flows southwest toward Thirsty Canyon, where it mixes with more concentrated groundwater flowing from the north.
- Thirsty Canyon groundwater mixes with more dilute water to form Oasis Valley groundwater.

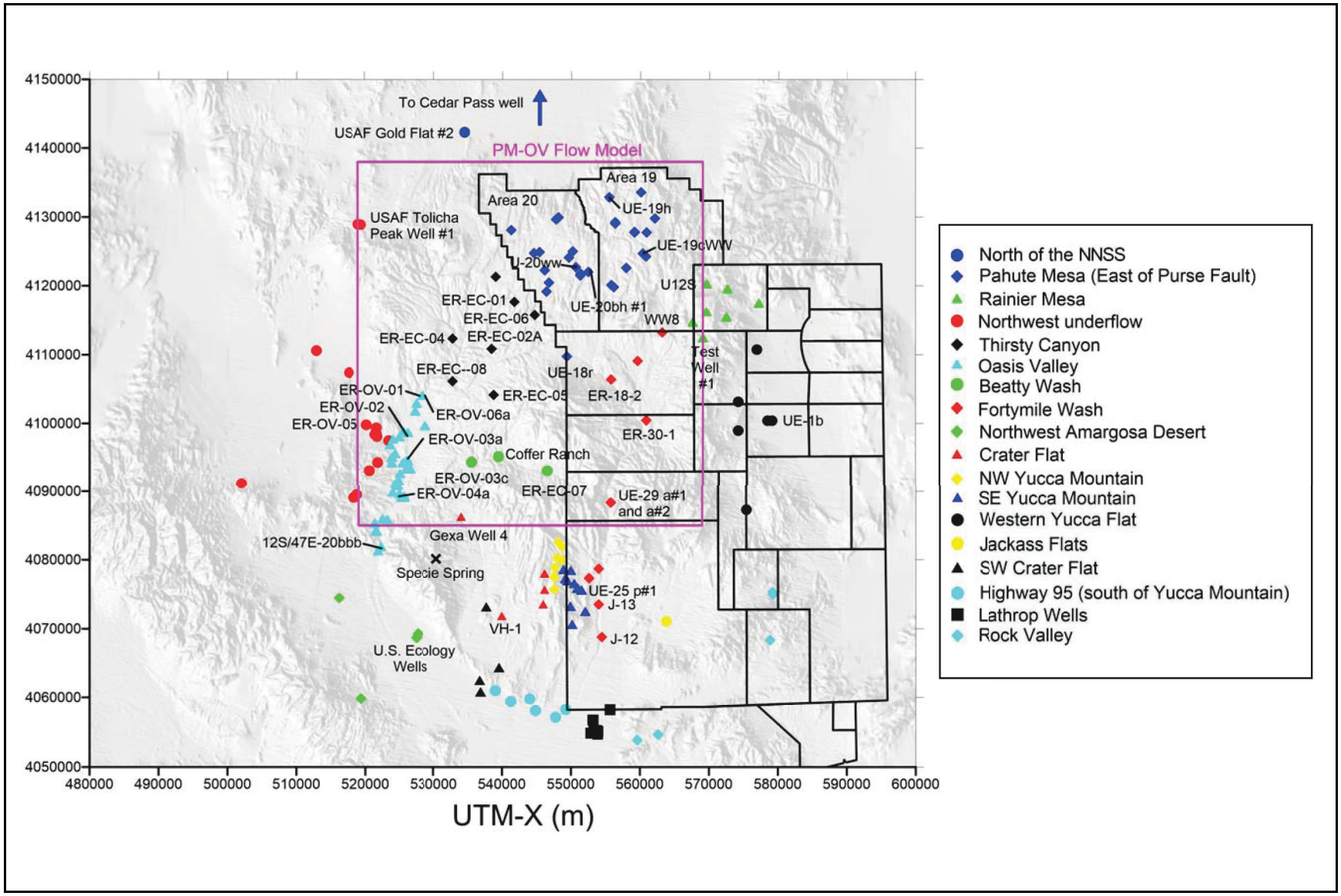

Figure 11-3
Key Wells Used for Phase I PM-OV Geochemistry Investigations
Source: Modified from Kwicklis et al., 2005

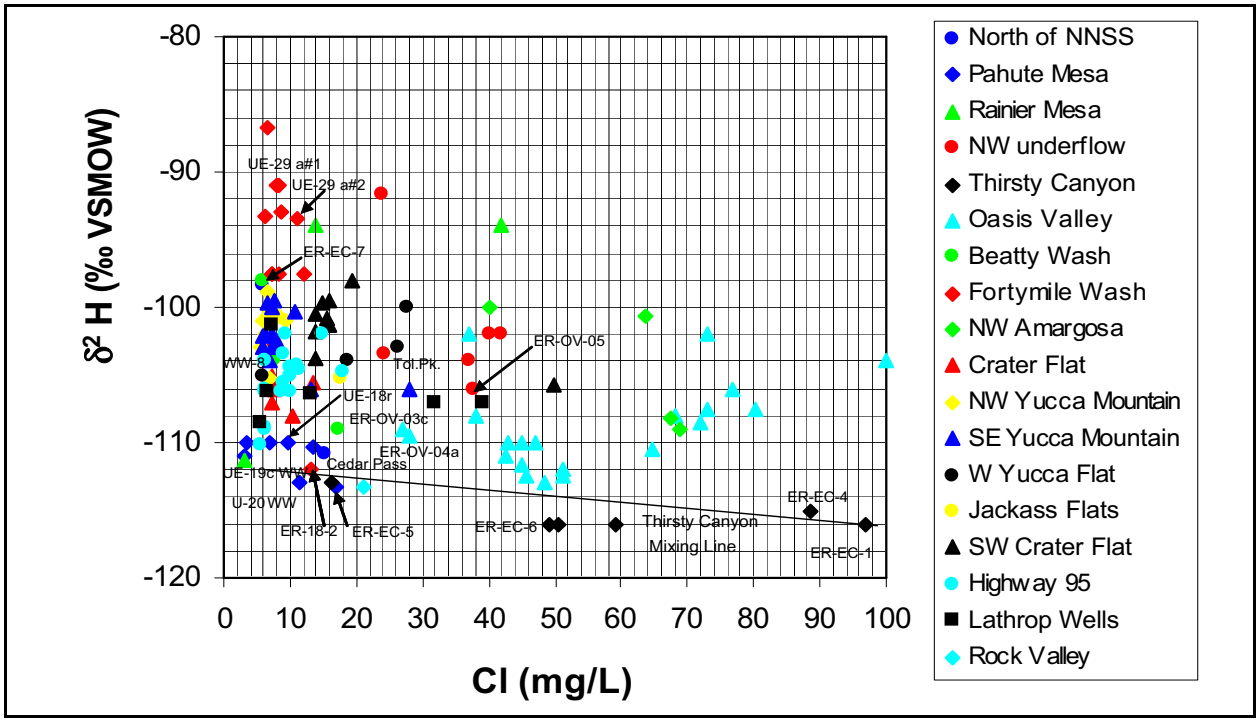

Figure 11-4
δ²H versus Cl for the Wells Included in the Phase I PM-OV Investigation
Source: Modified from Kwicklis et al., 2005

- Groundwater Cl and SO_4 concentrations are relatively constant southward from Pahute Mesa through Timber Mountain and into the Yucca Mountain area.

- Isotopically lighter groundwater from Pahute Mesa appears to flow around the western margin of the resurgent Timber Mountain dome toward Thirsty Canyon and Oasis Valley, with some groundwater possibly flowing through lower Beatty Wash into northwestern Crater Flat.

- Groundwater beneath Fortymile Wash, upper Beatty Wash, and Yucca Mountain is too isotopically heavy to include a large fraction of groundwater from Pahute Mesa.

- Groundwater from upper Beatty Wash likely flows southeast through northeast Yucca Mountain toward Fortymile Wash based on δ^2H and $\delta^{18}O$ compositions.

11.1.2 Phase I Flow Path Evaluation

Potential flow paths were identified based on the spatial trends identified using the conservative tracer data. Inverse water-rock reaction geochemical models were developed to determine potential proportions of groundwater from various upgradient wells that may be present in groundwater at a

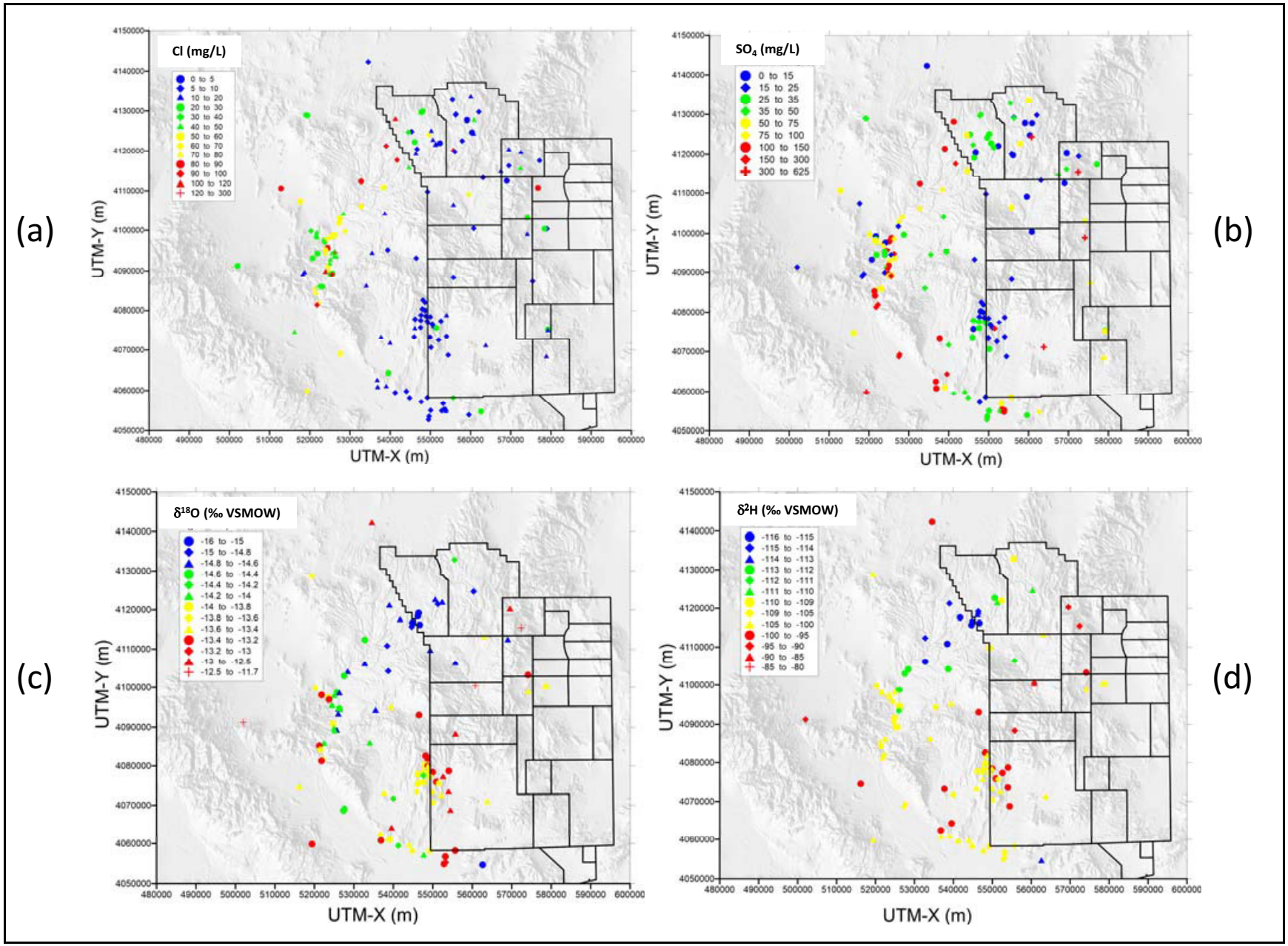

Figure 11-5
Spatial Trends within the PM-OV Flow System: (a) Cl, (b) SO_4, (c) $\delta^{18}O$, and (d) $\delta^{2}H$
Source: Kwicklis et al., 2005

downgradient well, and identify the nature and extent of water-rock interactions that may have affected the composition of the groundwater between the upgradient and downgradient wells. Water-rock interactions were estimated from the reactive species (pH, cations, silica, alkalinity and $\delta^{13}C$) once the effects of mixing were established. The reactive components considered by these models therefore potentially limit the number of possible mixing models estimated from non-reactive species to a smaller numbers of models for which plausible water-rock interaction models can also be found. Six flow paths were identified by Rose et al. (2006) and were further tested by Kwicklis et al. (2005) using conservative tracer and inverse water-rock reaction geochemical modeling techniques (Figure 11-6). These flow paths are summarized below:

- **Flow Path 1** represents groundwater flowing southwest from western Pahute Mesa through Thirsty Canyon to Oasis Valley. Oasis Valley groundwater is represented by ER-OV-3a in the geochemical models used to evaluate this flow path. Mixing of Pahute Mesa groundwater from UE-19h (14 to 65 percent) or U-20 WW (0 to 48 percent) with ER-EC-1 groundwater (29 to 47 percent) north of Thirsty Canyon was required to produce groundwater compositions consistent with ER-OV-03a. Local recharge from surface water runoff, represented by Well UE-29a#2, is a minor contributor (0 to 8 percent) to these models.

- **Flow Path 2** represents western Pahute Mesa groundwater flowing toward Oasis Valley and mixing with groundwater flowing from north of the NNSS. Oasis Valley groundwater was represented by ER-OV-01 in the geochemical models used to evaluate this flow path. Groundwater from ER-EC-6 was identified as the primary source (55 to 93 percent) of ER-OV-01 groundwater. Cedar Pass Well, representing groundwater from north of the NNSS (0 to 31 percent); USAF Tolicha Peak Well #1, representing potential groundwater flow from the northwest corner of the PM-OV flow domain (0 to 16 percent); local recharge represented by Well UE-29a#2 (0 to 6 percent); and Thirsty Canyon Well ER-EC-4 (0 to 20 percent) were identified as potential minor contributors. Geochemical models developed for ER-EC-6 identified ER-EC-1 and U-20 WW as roughly equal contributors, with a possible minor contribution of groundwater from the vicinity of UE-19h.

- **Flow Path 3** represents groundwater flowing from northwest Oasis Valley (represented by Well ER-OV-05) as a minor component in some downgradient Oasis Valley groundwaters. Two model categories were developed for this flow path. The first model category required groundwater from north of the NNSS (the Cedar Pass well) and a relatively large component of local recharge (represented by groundwater from UE-29a#2). The second model category required groundwater from the Tolicha Peak area, with a smaller amount of groundwater from Thirsty Canyon (ER-EC-4). Both model categories include a significant mixing fraction of ER-EC-4 groundwater.

- **Flow Path 4** represents groundwater from Pahute Mesa flowing southwest through Timber Mountain and lower Beatty Wash toward the Oasis Valley discharge area (represented by

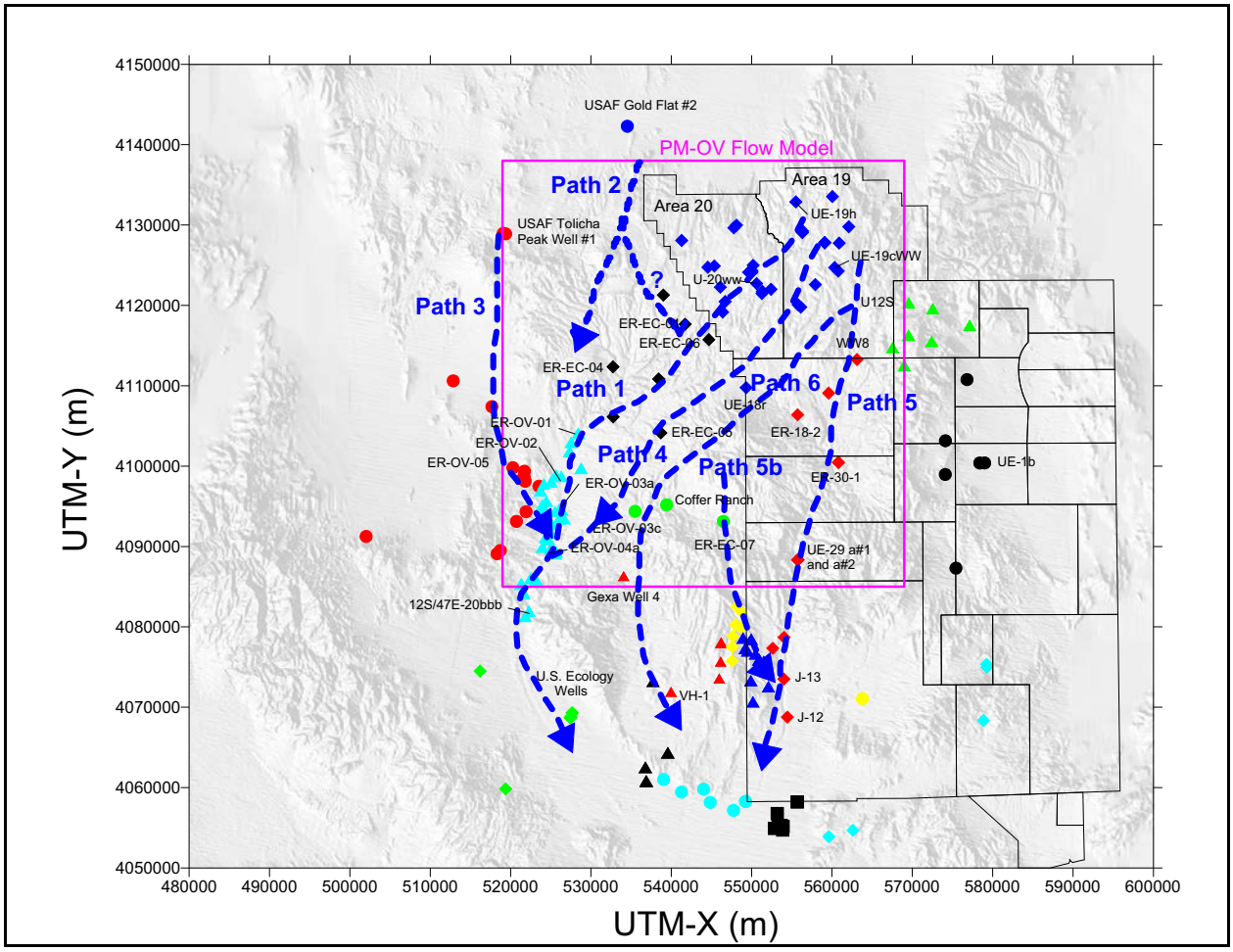

Figure 11-6
Phase I Groundwater Flow Paths
Source: Kwicklis et al., 2005

groundwater from ER-OV-04a). The model results suggest that most of the groundwater at ER-OV-04a originates from lower Beatty Wash near ER-OV-03c. The sources for groundwater at ER-OV-03c were subsequently investigated, and were observed to primarily be groundwater from ER-EC-5 and Timber Mountain recharge and surface runoff down Beatty Wash. Groundwater at ER-EC-5 was observed to be derived predominantly from UE-18r, with smaller amounts of groundwater from U-20 WW and ER-EC-1.

- **Flow Path 5** represents southward groundwater flow from Area 19 through Fortymile Canyon and along Fortymile Wash into western Jackass Flats. Western Jackass Flats groundwater is represented by J-12 WW and J-13 WW. Groundwater originates primarily from the vicinity of WW-8 (36 to 64 percent) and UE-29a#1 (22 to 60 percent), with a minor contribution from ER-18-2 (2 to 6 percent) and possibly from ER-30-1 (0 to 16 percent). This flow path is inconsistent with the Fenelon et al. (2016) flow-system boundaries and is revised in Section 11.2.4. An additional flow path, 5b, represents southeasterly groundwater flow from

upper Beatty Wash across northeast Yucca Mountain toward Fortymile Wash. Upper Beatty Wash groundwater was represented by ER-EC-7.

- **Flow Path 6** represents groundwater flow from the vicinity of Area 19 on Pahute Mesa beneath Timber Mountain and lower Beatty Wash and into northwest Crater Flat (represented by Well USW VH-1). Groundwater in lower Beatty Wash (represented by ER-OV-03c and Coffer Ranch Windmill Well), with at most a minor fraction contributed by groundwater in upper Beatty Wash (ER-EC-07), was identified as sources of USW VH-1 groundwater. Successful models required the $\delta^{13}C$ constraint be relaxed. ER-OV-03c was previously shown to primarily represent Pahute Mesa groundwater that moved through the vicinity of UE-18r in northern Timber Mountain. Coffer Ranch Windmill Well models indicated contribution from WW-8 (up to 84 percent) along with smaller amounts of groundwater from ER-18-2, UE-18r, and ER-EC-07. Alternatively, Coffer Ranch Windmill Well can result from Pahute Mesa groundwater mixing with groundwater flow down Beatty Wash or from Timber Mountain recharge depending on whether ER-EC-07 groundwater is interpreted to represent recharge at Timber Mountain in general, or groundwater that is characteristic of upper Beatty Wash.

11.1.3 Estimation of Groundwater ^{14}C Ages

Kwicklis (2009) calculated groundwater ^{14}C ages using chemical and $\delta^{13}C$-based methods to correct for the incorporation of "dead" carbon through calcite dissolution and isotopic exchange (Figure 11-7). Groundwater ages are variable along the flow paths and actually decrease near Oasis Valley. Similar variability was observed along Flow Path 5 in Fortymile Canyon, where groundwater appears to be dominated by local recharge. Groundwater in Fortymile Canyon is considerably younger than Pahute Mesa groundwater because high infiltration rates beneath the Fortymile Canyon/Wash area and shallow depths to groundwater (<30 m) enable net infiltration to reach the groundwater quickly (days to weeks) after run-off events. Elsewhere beneath Pahute Mesa, the significant depth to groundwater (>600 m) and relatively small net infiltration rates (5 to 10 mm/yr) result in long travel times through the unsaturated zone. Corrected ^{14}C ages of between ~11,000 and 18,000 years were reported for groundwater beneath Pahute Mesa in Areas 19 and 20, indicating a predominantly Pleistocene origin for the groundwater. Groundwater ^{14}C ages in Thirsty Canyon are also between about 12,000 and 18,000 years, although they do not vary along Flow Path 1 in a systematic manner (Figure 11-7).

Kwicklis (2009) concluded that reliable travel times cannot be estimated using ^{14}C groundwater data. Differences between ^{14}C activities along groundwater flow paths are generally too small relative to its

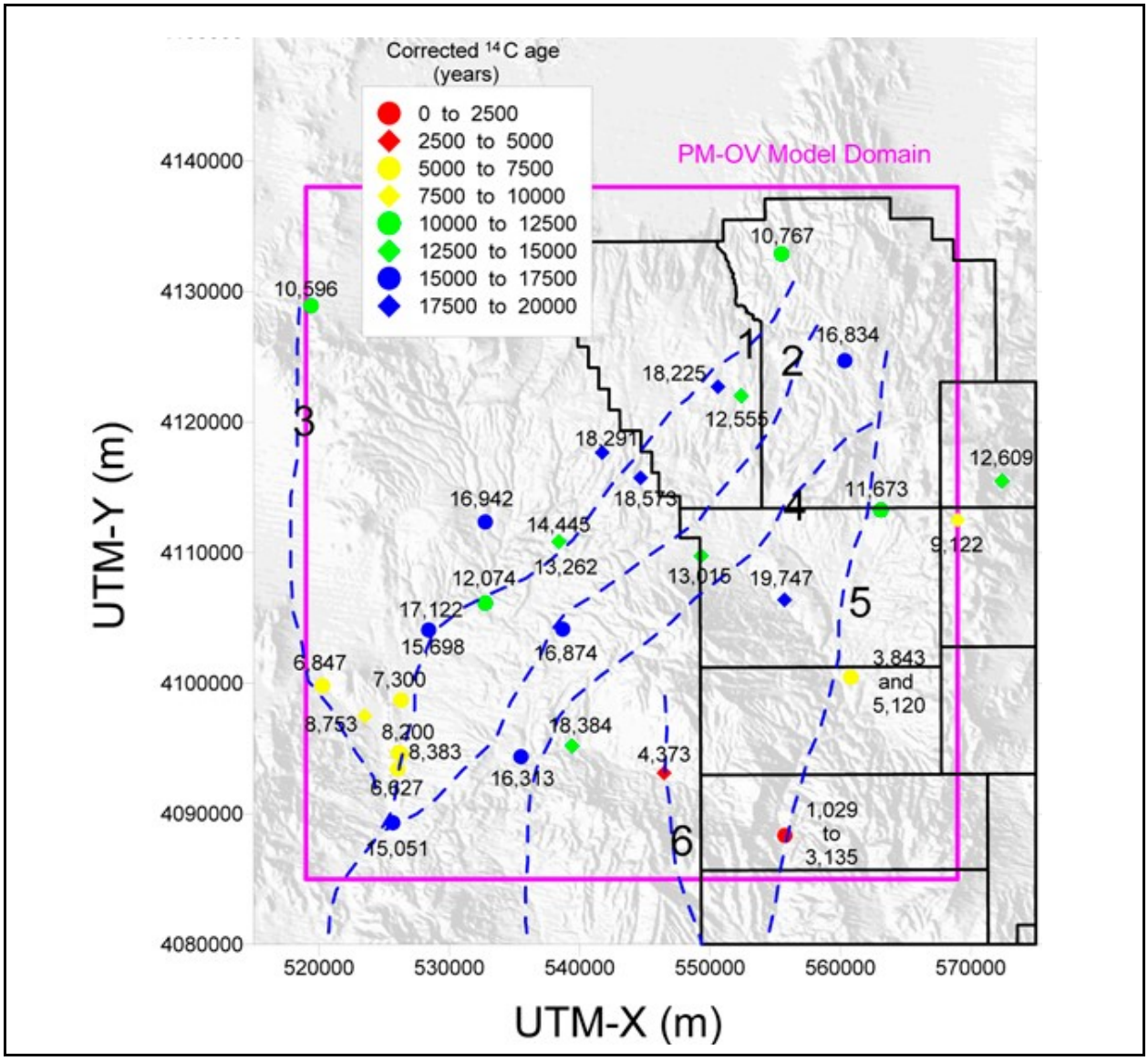

Figure 11-7
Groundwater ^{14}C Ages Superimposed on Flow Paths
Source: Kwicklis, 2009

5,730-year half life. Groundwater ages near Oasis Valley have been influenced by shallow groundwater interaction with soil gas that reset the groundwater ^{14}C ages and caused the shallow groundwater to appear artificially young, a conclusion also reached by White and Chuma (1987). The ^{14}C ages for the study area indicates that most groundwater is at least several thousand years old, and groundwater with ^{14}C ages <5,000 years occurs only in upper Beatty Wash and lower Fortymile Wash (Figure 11-7). Younger ages near Oasis Valley relative to upgradient areas are not indications of significant local recharge, but provide evidence of the interaction of shallow groundwater with soil

$^{14}CO_2$ near the discharge areas. Elsewhere, the absence of younger groundwater ages is suggestive of long unsaturated-zone residence times and/or low infiltration rates (Kwicklis, 2009).

11.2 Phase II Geochemical Evaluation

The Phase II geochemistry evaluation (Navarro, 2020) focused on new groundwater geochemical and isotopic data collected from wells drilled as part of the Phase II characterization effort in Area 20, the Bench area, and the northwest Timber Mountain moat area (Figure 11-2). The following subsections provide a summary of the geochemistry evaluation described in Navarro (2020). A description of the dataset is presented (Section 11.2.1) along with summaries of the conclusions of the data evaluation (Section 11.2.2); PHREEQC and NETPATH inverse water-rock geochemical reaction models (Section 11.2.3); PM-OV flow system boundaries (Section 11.2.5); and groundwater travel time estimates (Section 11.2.5). Refinements of the Phase I groundwater flow paths are also presented (Section 11.3).

11.2.1 Phase II Geochemistry Dataset

New data from the Phase II wells and other locations sampled in support of the NNSS Integrated Groundwater Sampling Plan (DOE/EMNV, 2019) were combined with previously reported data from the UGTA Groundwater Chemistry Database (Navarro, 2019b). A dataset was then developed to best represent the groundwater chemistry from each sampled completion interval for each well included in the investigation (Navarro, 2020). Samples from a total of 54 locations are included in the dataset; 37 are separate locations (Figure 11-2). Ten of these locations (ER-20-8, ER-20-12, ER-EC-2a, ER-EC-6, ER-EC-11, ER-EC-12, ER-EC-13, ER-EC-14, ER-EC-15, and PM-3) provide samples for multiple depth intervals. The parameter suites include the following (Navarro, 2020):

- Field parameters (temperature, pH, specific conductance, dissolved oxygen)
- Major ions (HCO_3, Cl, SO_4, F, Br, Na, K, Ca, and Mg)
- Environmental isotopes (δ^2H, $\delta^{18}O$, $\delta^{13}C$, ^{14}C, $\delta^{34}S$, $^{36}Cl/Cl$)
- Noble gases (He, Ne, Ar, Kr, Xe, and $^3He/^4He$)
- Radionuclides (^3H, ^{14}C, ^{36}Cl, ^{90}Sr, ^{99}Tc, ^{129}I, ^{137}Cs, $^{239/240}Pu$)

For most analytes, averages were calculated for each location and for each sample collection method (e.g., pumped samples collected from the wellhead, depth discrete bailed samples). Outliers were identified and removed from the calculated average. Charge balances (Hem, 1985) were calculated as

an indication of data quality. The most recent sample was selected for radionuclides. Averages for pumped wellhead samples were selected for the final dataset when available. A more detailed description of the dataset development is presented in Navarro (2020).

11.2.2 Phase II Data Evaluation

The dissolved constituents in groundwater provide a record of the minerals encountered as water moves through an aquifer; therefore, the major-ion characteristics of groundwater can provide insight on groundwater source areas and flow directions. A Piper diagram, illustrating the relative major-ion concentrations in groundwater samples, is presented in Figure 11-8. The Piper diagram presents relative concentrations in percent milliequivalents per liter (% meq/L), and is used to classify various groundwater chemistry types (or facies). Figure 11-8 shows that the groundwater is dominated by Na+K, which is characteristic of waters that have dissolved volcanic rhyolitic lava, ash-fall and ash-flow tuffs, and associated volcanic alluvium (Schoff and Moore, 1964; Thomas et al., 2002; Rose et al., 2006). Groundwater anions range from being dominated by HCO_3 to having relatively equal concentrations of all three anions (HCO_3/SO_4/Cl). The groundwater in the western portion of the study area has a distinct major-ion composition (Na-HCO_3/Cl/SO_4 type), which reflects higher relative concentrations of Cl and SO_4 (Figure 11-8). An evaluation of major-ion variability within each well sampling multiple depth intervals is presented in Navarro (2020). Although chemical variability exists across sampling depths in some wells, no consistent study-area-wide vertical trends are obvious through visual inspection of the major-ion data.

The concentrations of Cl and SO_4 in groundwater samples increase systematically from east to west within the Phase II study area (Figures 11-9 and 11-10). High SO_4 and Cl concentrations are observed in the northwestern/western portion (e.g., UE-20j WW, PM-3, ER-EC-1, and ER-20-12), and the most dilute concentrations of Cl and SO_4 are found in the eastern portion of the study area (e.g., UE-19c WW, ER-20-2-1, UE-20bh 1, and ER-20-4) consistent with that observed during the Phase I investigation (Figures 11-5, 11-9, and 11-10). Figure 11-11 shows a strong correlation ($R^2 = 0.93$) between SO_4 and Cl exists within the study area. This correlation indicates similar sources for the high-SO_4, high-Cl water. Navarro (2020) showed that the Cl and SO_4 concentration contours are oriented roughly perpendicular to hydraulic head contours, as would be expected for flow paths in an approximately isotropic medium (Figures 11-9 and 11-10). The potential flow paths represented by

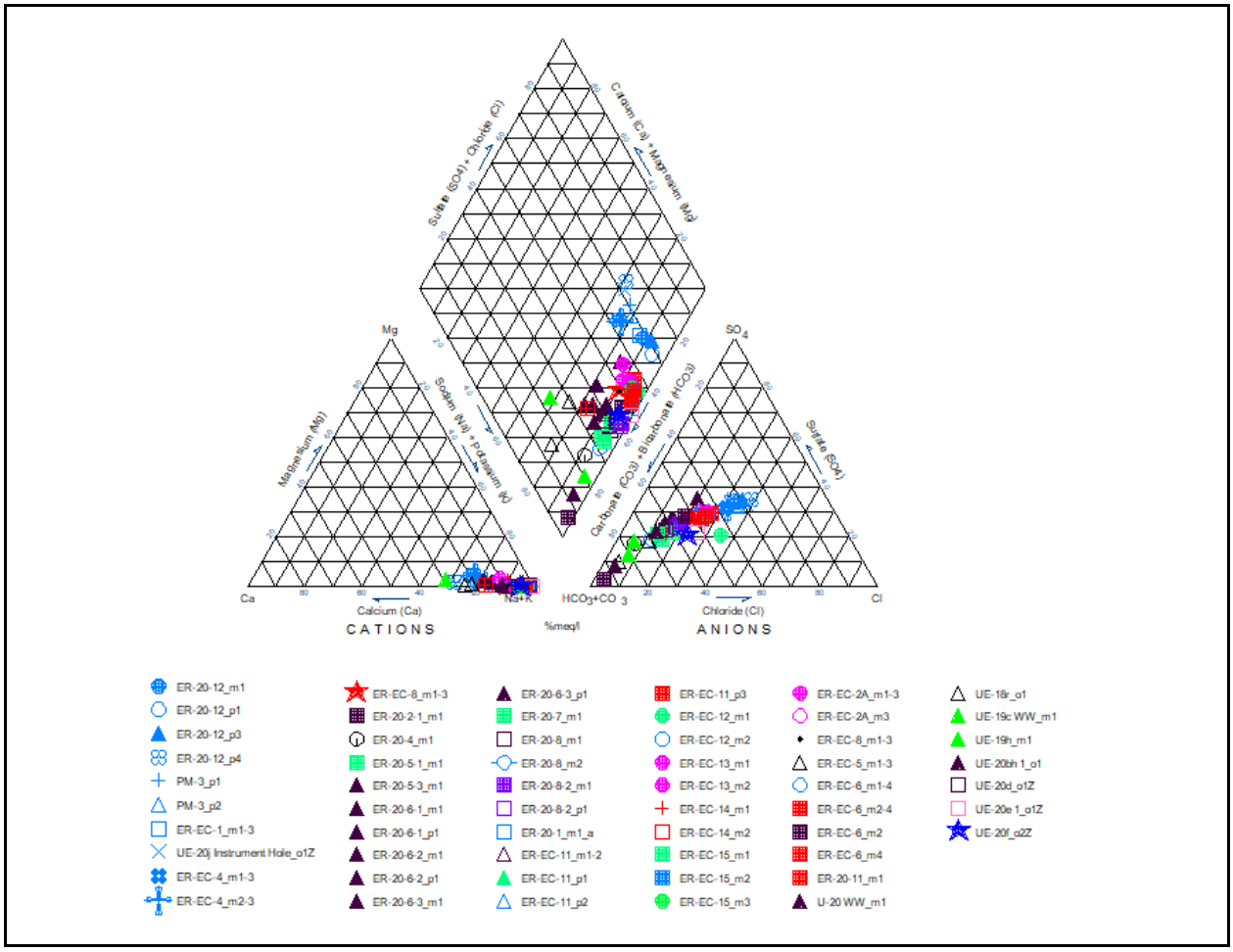

Figure 11-8
Piper Diagram

the Cl concentration contours converge from both the northwest and northeast in the hydraulic trough formed in western Area 20 by the Purse and West Purse faults on the west and the West Boxcar fault on the east, and then turn sharply west in the northwest TMCC (Figures 11-9 and 11-10). Navarro (2020) attributed the nonalignment of flow paths to head contours in the northwest part of the NNSS to sparsity of head data in this area and the assumed continuity in Cl concentrations across the Purse fault by the contouring software versus the assumed hydraulically discontinuous heads in this area represented using hand-drawn head contours (Blankennagel and Weir, 1973; Laczniack et al., 1996; Fenelon et al., 2016).

Groundwater samples from the study area contain very similar δ^2H and $\delta^{18}O$ values (Figure 11-12). The stable isotopic ratios of groundwater are originally derived from the stable isotopic ratios of

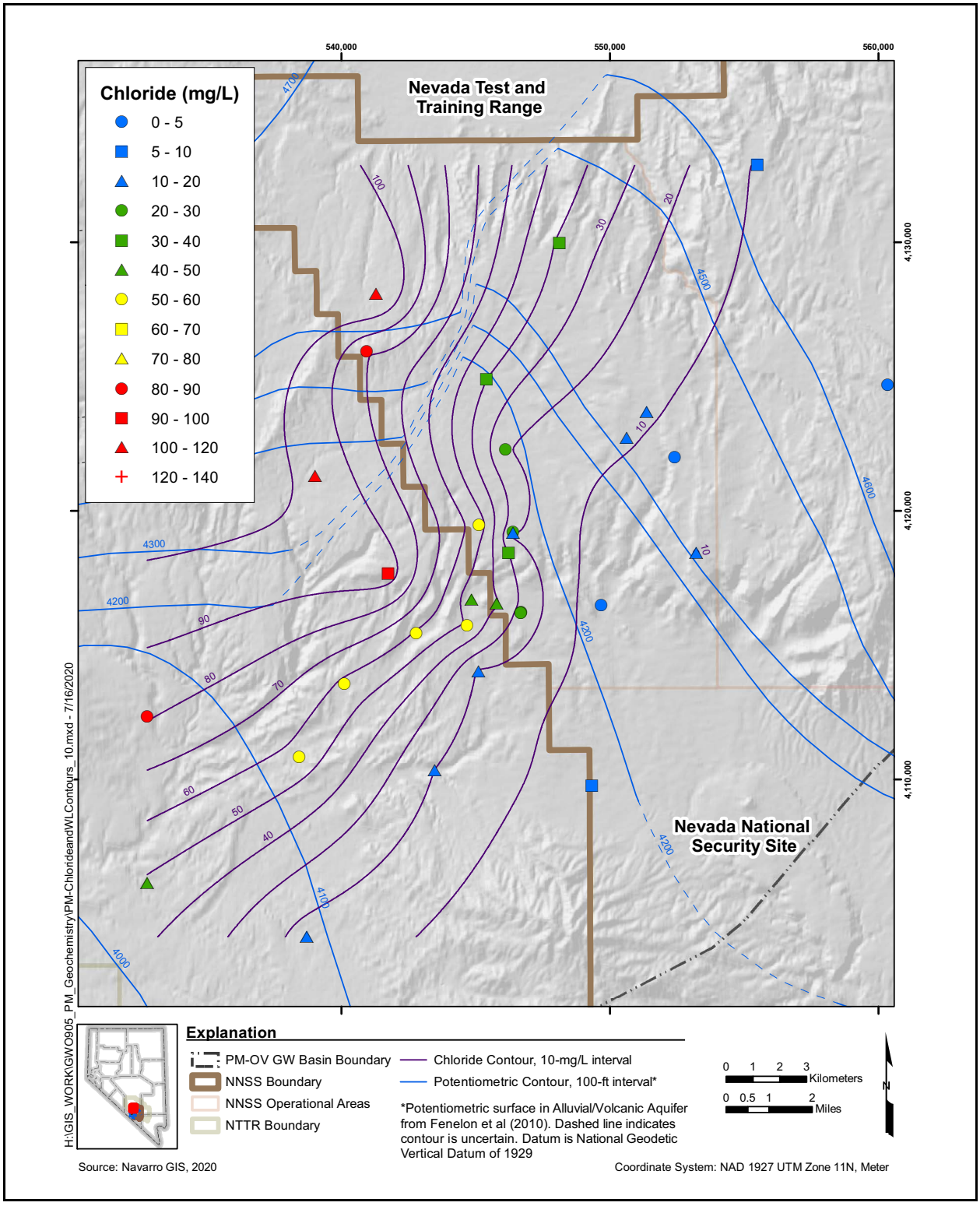

Figure 11-9
Chloride and Hydraulic-Head Contours

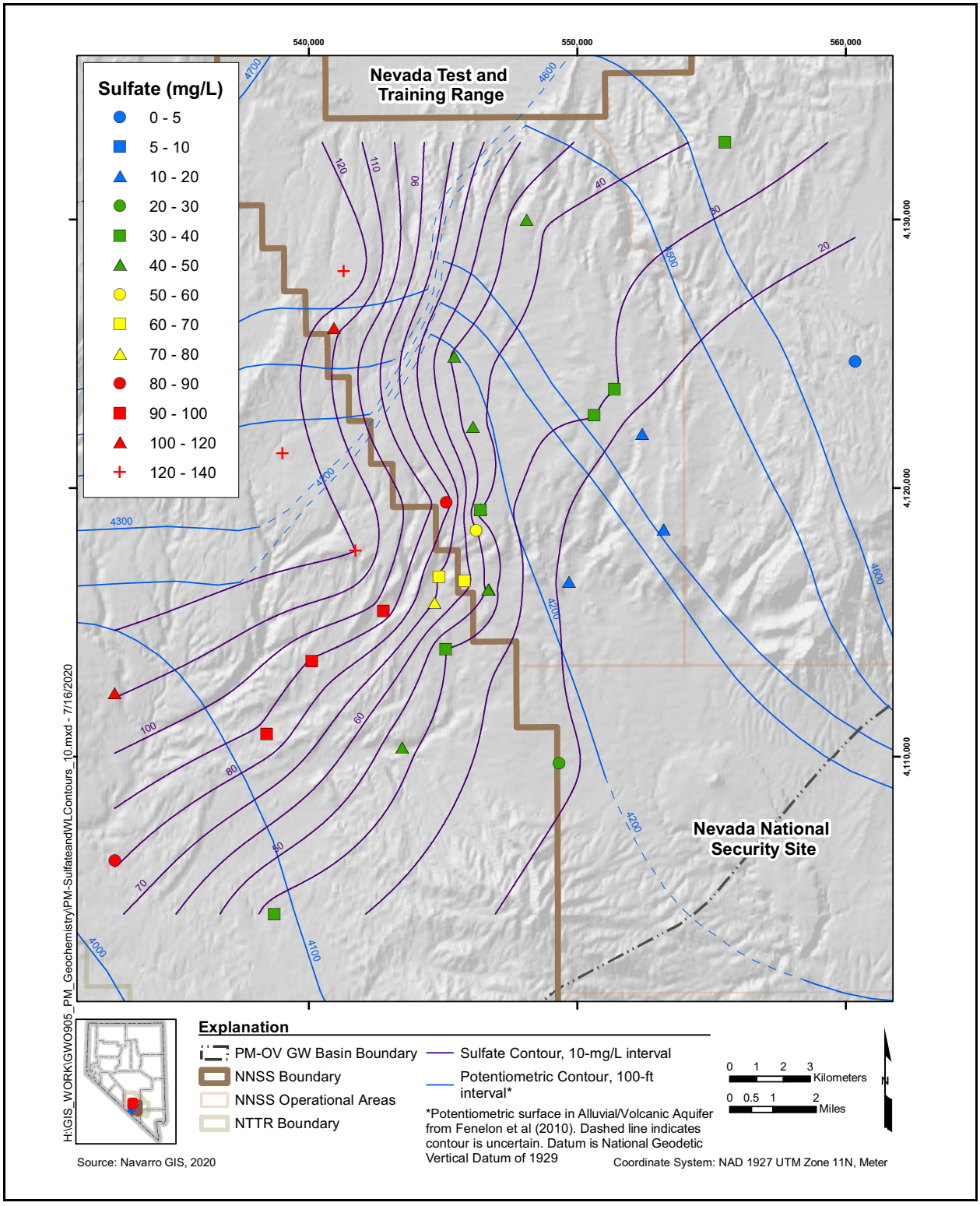

Figure 11-10
Sulfate and Hydraulic-Head Contours

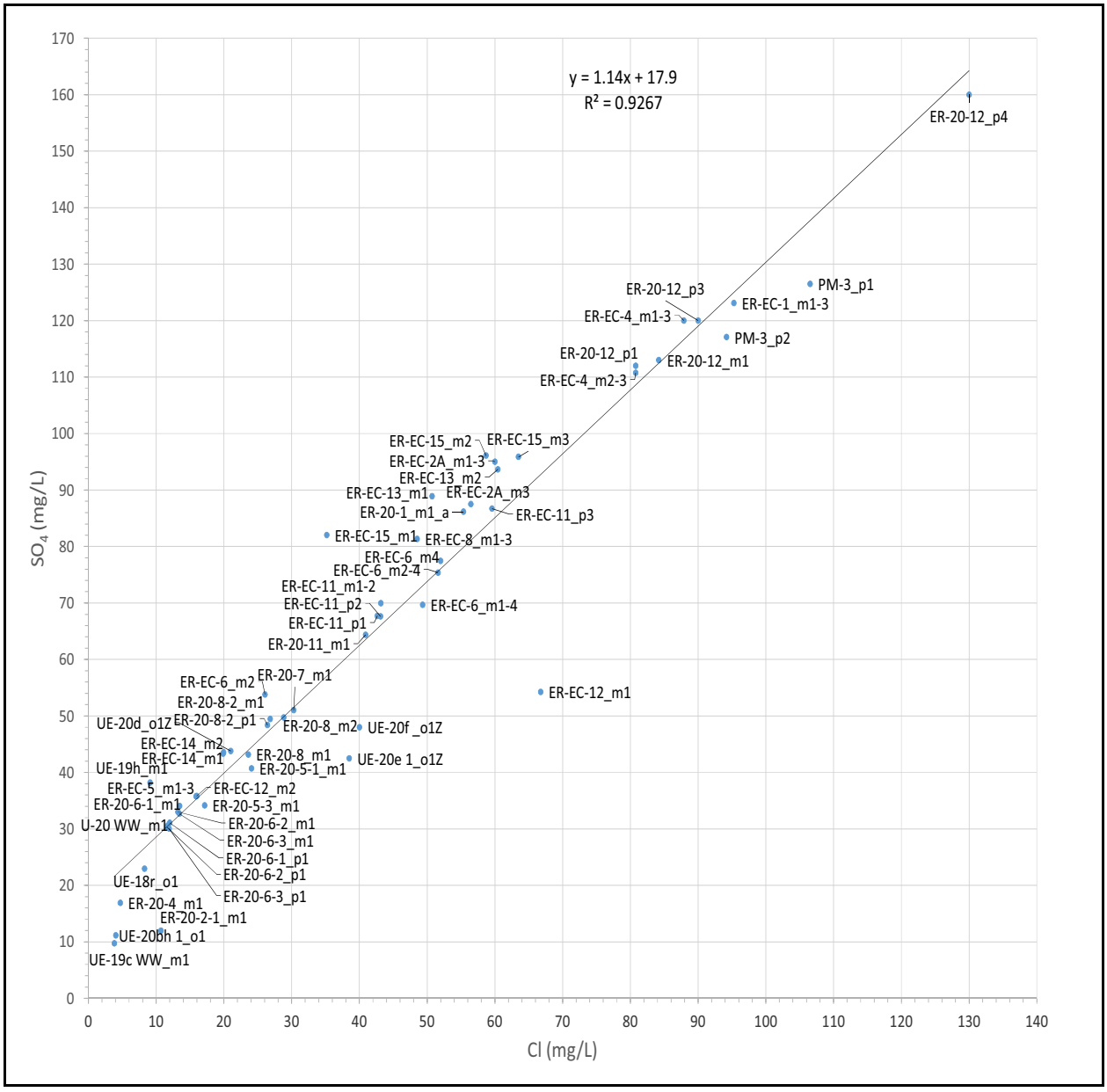

Figure 11-11
SO_4 versus Cl Concentrations with Regression Line

groundwater recharge. If sampled before they undergo significant post-discharge evaporation, perched springs in the recharge area often provide stable isotopic ratios that are representative of modern local groundwater recharge. No springs exist on Pahute Mesa; the closest springs considered representative of local recharge are found on Rainier Mesa. The isotopic ratios of groundwater from these springs along with samples from Rainier Mesa tunnels (U-12 tunnels) after the tunnels were plugged are shown in Figure 11-12. Figure 11-12 also presents the global meteoric water line

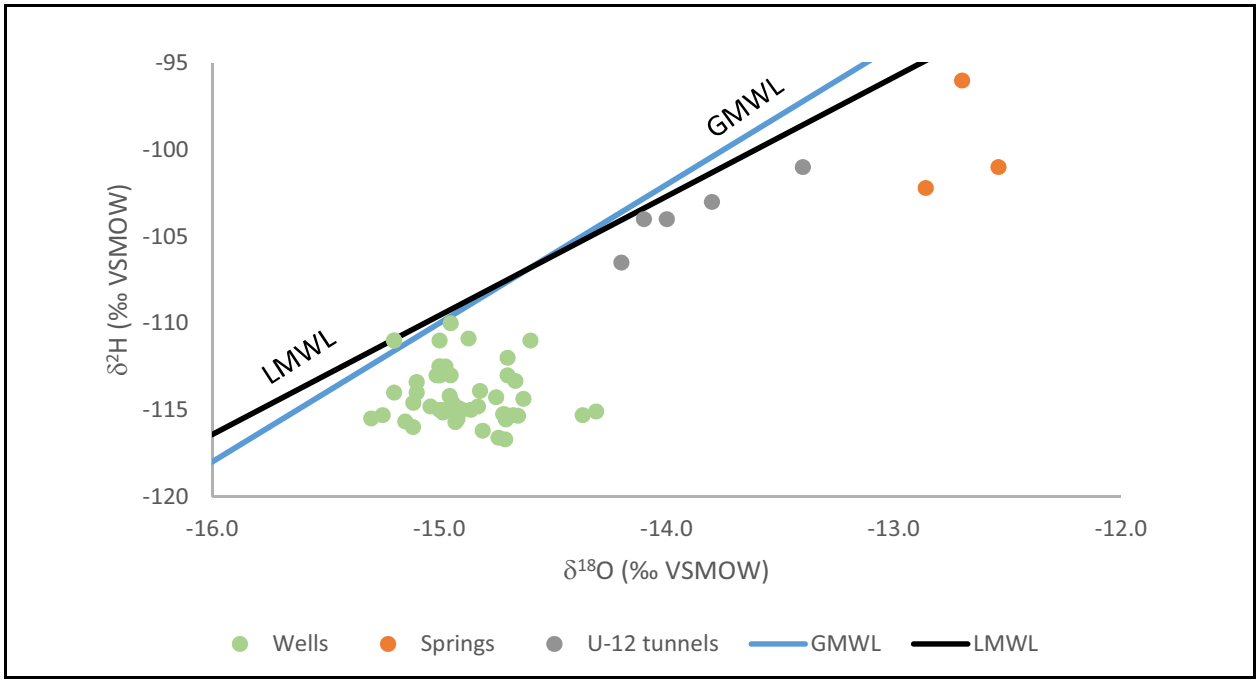

Figure 11-12
δ²H versus δ¹⁸O

(GMWL) (Craig, 1961) and local meteoric water line (LMWL) (Ingraham et al., 1991). As shown in Figure 11-12, Pahute Mesa area groundwater is isotopically distinct from modern local recharge. Groundwater δ^2H and $\delta^{18}O$ values are isotopically lighter than modern local recharge (represented by the spring and tunnel samples) and groundwater values offset to the right of the LMWL and GMWL (e.g., Claassen, 1985; White and Chuma, 1987). The current Pahute Mesa conceptual model of the groundwater system assumes that Pahute Mesa groundwater was recharged under different climatic conditions than those of today (Navarro, 2020), although minor contributions occur to this day.

Groundwater dissolved inorganic carbon (DIC) concentrations and $\delta^{13}C$ increase along the groundwater flow path from Pahute Mesa to Thirsty Canyon (Figure 11-13). Groundwater in western Pahute Mesa and Thirsty Canyon, in many cases, are isotopically heavier than expected for volcanic rock aquifers. This is attributed to interaction with secondary calcite fracture linings likely derived from Paleozoic carbonate rock present at the time of volcanism. The $\delta^{13}C$ and $\delta^{18}O$ signatures of the fracture lining calcite along with the high temperature of formation indicate that they were precipitated from groundwater equilibrated with Paleozoic carbonate rock under hydrothermal conditions following volcanic activity (Benedict et al., 2000; Thomas et al., 2002). The $\delta^{13}C$ of fracture lining calcite in Pahute Mesa (most values clustering between +1 and +4 ‰, Benedict et al.,

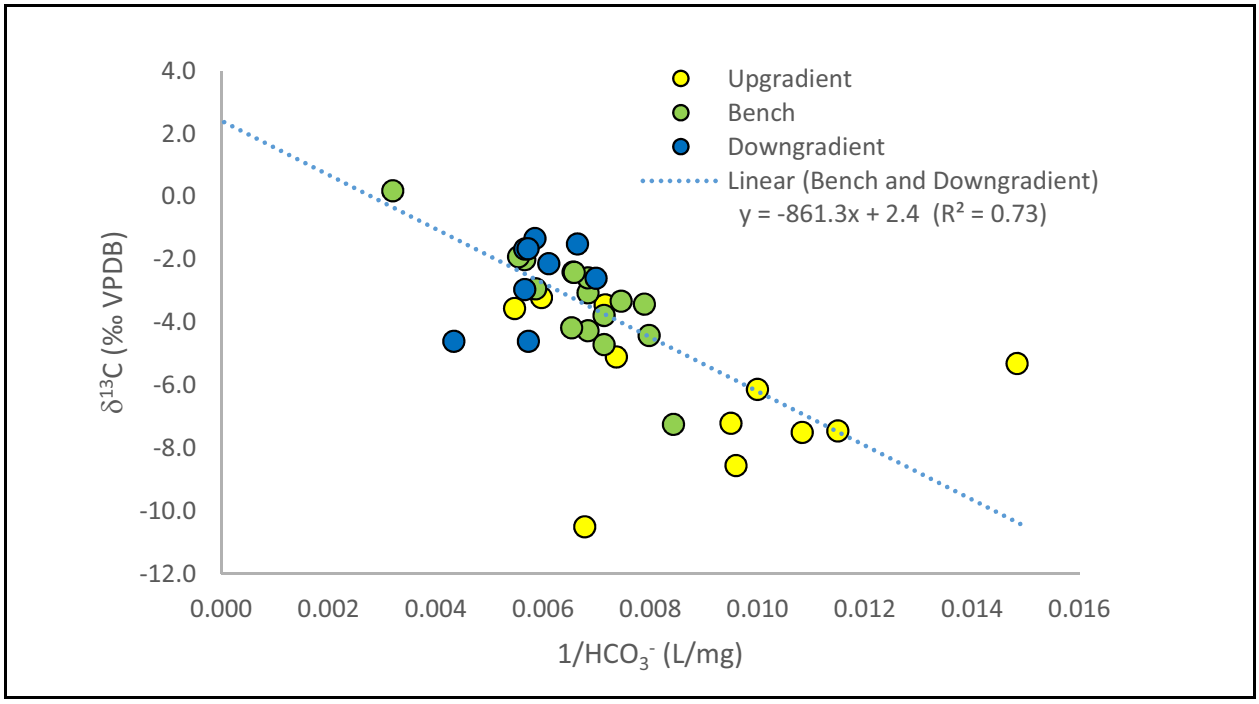

Figure 11-13
$\delta^{13}C$ versus $1/HCO_3^-$ for Pahute Mesa and Thirsty Canyon Groundwater

Note: HCO_3^- concentrations increase to the left. At infinite HCO_3^- concentrations, a trendline through the Bench and Downgradient well data intersects the Y-axis at 2.4 ‰, the average $\delta^{13}C$ value of the source carbonate rock for these wells.

2000; Thomas et al., 2002) are consistent with the $\delta^{13}C$ estimated for source carbonate rock (2.4 ‰) based on the trend of groundwater $\delta^{13}C$ versus $1/HCO_3^-$ for the study area groundwater (Figure 11-13). Substantial CO_2 input to groundwater from the mantle in the PM-OV groundwater basin is not supported by the low mantle CO_2 concentrations (less than 2 millimoles per liter [mmol/L]) calculated based on $^3He/^4He$ measurements (Navarro, 2020). Navarro (2020) also showed that there is no consistent pattern in groundwater $\delta^{13}C$ values with depth, HSU, or transmissivity of the sampled zone.

Upgradient of testing in Area 19 and eastern Area 20 and downgradient of the Bench area, DIC ^{14}C values are generally low (5.9 to 12.1 percent modern carbon [pmc]). In the Bench area, where known testing contamination is present, DIC ^{14}C values tend to be higher even in wells not thought to be impacted by testing (15.9 to 32.2 pmc, Figure 11-14). This variability of DIC ^{14}C across Pahute Mesa and Thirsty Canyon along with the known testing contamination are problematic for estimating groundwater velocities. Several wells in this dataset are known to be impacted by testing based on the presence of ^3H in the groundwater (ER-20-5-1, ER-20-5-3, ER-20-6-1, ER-20-6-2, ER-20-6-3,

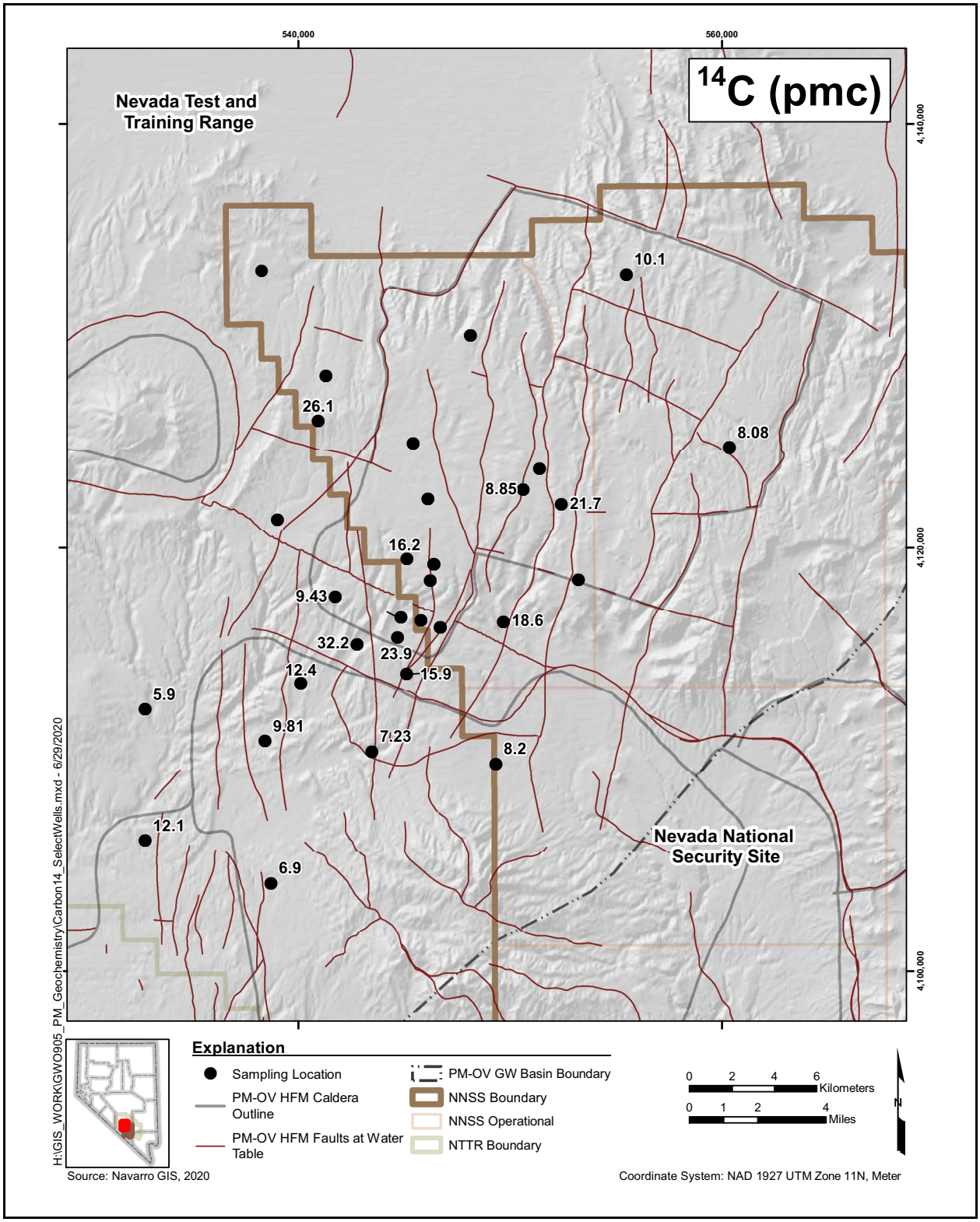

Figure 11-14
Spatial Distribution of Naturally Occurring (non-test-contaminated) DIC ^{14}C in the Vicinity of Pahute Mesa

ER-20-7, ER-20-8, ER-20-8-2, ER-20-11, ER-20-12, ER-EC-6, ER-EC-11, PM-3, and possibly UE-19h). The DIC ^{14}C values are likely to be elevated in these test-impacted groundwater. In addition, samples shown to have anomalously high ^{14}C values were identified (ER-EC-13_m1, ER-EC-14_m1, and ER-EC-15_m3), therefore warranting caution before using the data for water-rock reaction modeling to estimate groundwater ages.

Navarro (2020) also presented an evaluation of dissolved noble gas (He, Ne, Ar, Kr, and Xe) groundwater data. The elemental abundances of the heavier noble gases (Ne, Ar, Kr, Xe) are directly related to the temperature and altitude of the groundwater recharge location. Five possible recharge and re-equilibration scenarios to explain observed recharge temperatures were derived using noble gas recharge temperatures (NGRTs):

1. Groundwater recharge occurred under Pleistocene climate conditions with water-table temperatures at or below the present-day mean annual air temperature.
2. Groundwater recharge occurred locally under Holocene climatic and water-table conditions. As a result, NGRTs are close to the present-day water-table temperature.
3. Groundwater recharge occurs primarily under present-day climatic conditions.
4. Groundwater is focused over shallow geological barriers that cause re-equilibration of NGRTs at present-day water-table conditions (effectively resetting the noble gas thermometer). In this scenario, NGRTs upgradient of the flow barrier reflect recharge conditions, while NGRTs downgradient of the flow barrier reflect present-day water-table conditions.
5. Groundwater is a mixture of various recharge sources.

Table 11-1 presents NGRTs for sampling locations within the study area with available noble gas data. The associated recharge and re-equilibration scenarios are also presented (Table 11-1). NGRTs in groundwater beneath Pahute Mesa are consistently much cooler than present-day water-table temperatures and reflect recharge under Pleistocene climate conditions. Elevated noble gas temperatures in the Thirsty Canyon area (ER-EC wells) are probably the result of re-equilibration based also on their $\delta^{18}O$ signature similar to Pleistocene recharge (Navarro, 2020).

Navarro (2020) evaluated $^{36}Cl/Cl$ ratios and $\delta^{34}S$ data to determine the source of the high SO_4 and Cl in the northwestern/western part of the study area. Navarro (2020) interpreted the high SO_4 and Cl to originate from salts derived from the ocean and deposited with precipitation in the late Pleistocene.

Table 11-1
Noble Gas Recharge Temperatures and Interpretations

ISPID	NGRT (°C)	Interpretation
ER-EC-1_m1-3	20.3	Re-equilibration (Scenario 4) or mixed (Scenario 5)
ER-EC-2A_m3	31.3	Re-equilibration (Scenario 4)
ER-EC-4_m2-3	32.1	Re-equilibration (Scenario 4)
ER-EC-5_m1-3	30.7	Re-equilibration (Scenario 4)
ER-EC-6_m1-4	19.6	Re-equilibration (Scenario 4) or mixed (Scenario 5)
ER-EC-7_m1-2	21.7	Local recharge (Scenario 2)
ER-EC-8_m1-3	40.7	Re-equilibration (Scenario 4)
ER-EC-11_m1-2	22.0	Re-equilibration (Scenario 4) or mixed (Scenario 5)
ER-EC-12_m1	14.6	Local recharge (Scenario 2) or mixed (Scenario 5)
ER-EC-12_m2	21.4	Re-equilibration (Scenario 4)
ER-EC-13_m1	31.5	Re-equilibration (Scenario 4)
ER-EC-13_m2	27.3	Mixed (Scenario 5)
ER-EC-14_m1	33.8	Re-equilibration (Scenario 4)
ER-EC-14_m2	32.3	Re-equilibration (Scenario 4)
ER-EC-15_m1	15.4	Mixed (Scenario 5)
ER-EC-15_m2	13.9	Mixed (Scenario 5)
ER-EC-15_m3	26.0	Re-equilibration (Scenario 4) (geothermal) [a]
ER-20-5-3_m1	14.7	Mixed (Scenario 5)
ER-20-6-2_p1	12.6	Pleistocene recharge (Scenario 1)
ER-20-6-3_p1	12.1	Pleistocene recharge (Scenario 1)
UE-19c WW_m1	12.4	Pleistocene recharge (Scenario 1)
U-20 WW_m1	21.5	Re-equilibration (Scenario 4)

[a] Geothermal refers to samples with an unusually high measured temperature at the water table.

ISPID = Integrated Sampling Plan Identifier

It was first determined that the source could not have been the LCA or an ancient hydrothermal mineral source based on $^{36}Cl/Cl$ ratios. The source was further refined to be seawater-derived salts deposited within the past several million years based on $\delta^{34}S$ data (Clark and Fritz, 1997, Fig. 6-2) as described below.

The $^{36}Cl/Cl$ ratios observed in groundwater of the study area are relatively constant across a wide range of Cl concentrations and tend to be larger than the estimated present-day ratio in precipitation

(490×10^{-15}; Fabryka-Martin et al., 1993) (Figure 11-15). This relatively consistent pattern is not observed for groundwater of the LCA, where a decreasing trend in $^{36}Cl/Cl$ ratios with respect to 1/Cl (or increasing Cl concentrations) is interpreted to indicate groundwater dissolution of ^{36}Cl-free Cl in the carbonate rock matrix (Moran and Rose, 2003; Kwicklis and Farnham, 2014); any ^{36}Cl originally present in the carbonate rock would have decayed to near zero since deposition ~300 million years ago, given the half-life of ^{36}Cl of 301,000 years. Reconstruction of meteoric $^{36}Cl/Cl$ deposition near the NNSS based on packrat midden data indicates that $^{36}Cl/Cl$ ratios in precipitation was higher by a factor of as much as 2 compared to present day over the past 40,000 years (Figure 11-16; Plummer et al., 1997; Kwicklis and Farnham, 2014). Meteoric $^{36}Cl/Cl$ ratios have been near their present-day values for the past ~10,000 years, reaching a maximum of about twice their present-day values between 10,000 and 15,000 years ago, and between 40 and 60 percent greater than their present-day values between 15,000 and 20,000 years ago (Figure 11-16). Many of the measured groundwater $^{36}Cl/Cl$ ratios are larger than the estimated present-day ratio in precipitation (490×10^{-15}), consistent with an inferred Pleistocene origin for the groundwater. This is especially true for the more dilute samples (e.g., from UE-18r, ER-20-4, UE-20bh 1, and UE-19c WW), which have $^{36}Cl/Cl$ ratios comparable to those estimated for the period between 15,000 and 20,000 years ago. However, the highest Cl concentration samples (e.g., samples from ER-EC-4, ER-EC-8, ER-EC-1, and ER-EC-15) have $^{36}Cl/Cl$ ratios roughly comparable to the meteoric ratios shown in over the last 10,000 years. The $^{36}Cl/Cl$ ratios of the highest Cl groundwater indicate that either the dissolved Cl originated from salts deposited in the last 10,000 years, or that the dissolved salts initially had higher $^{36}Cl/Cl$ values but are old enough (perhaps hundreds of thousands of years) to have undergone some radioactive decay of ^{36}Cl.

Sulfur isotope ratios ($\delta^{34}S$) of groundwater SO_4 were measured on many samples in the study area (Figure 11-17). Although there have been many recent $\delta^{34}S$ measurements reported, the dataset is far from complete. No $\delta^{34}S$ data exist for ER-EC-5, UE-18r, UE-19c WW, UE-19h, U-20 WW, UE-20bh 1, and ER-20-6 (-1, -2, -3). The relationship between $\delta^{34}S$ and $1/SO_4$ indicates that there is a strong trend toward heavier $\delta^{34}S$ at higher SO_4 concentrations (lower $1/SO_4$ values) and that the mineral S-source has a $\delta^{34}S$ of about 20.4 ‰ (Figure 11-17). If Cl and SO_4 are derived from the same source (which their strong correlation with each other would suggest), modern seawater was identified as the only possible source of the heavy $\delta^{34}S$ in the high SO_4 groundwater (Navarro, 2020). Although termed "modern seawater," the $\delta^{34}S$ of seawater has been near 20 ‰ for the past several

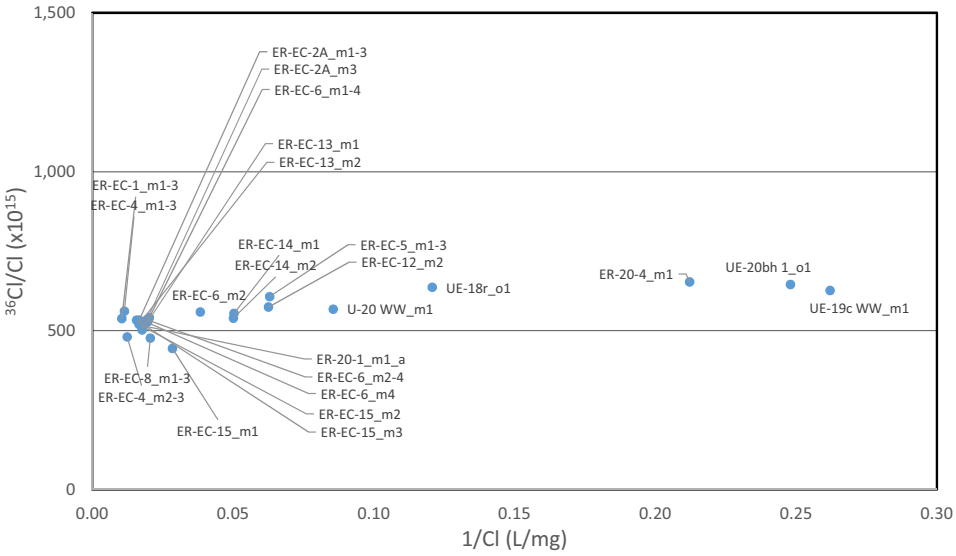

Figure 11-15
Plot of ^{36}Cl/Cl Ratios versus Inverse Cl Concentrations

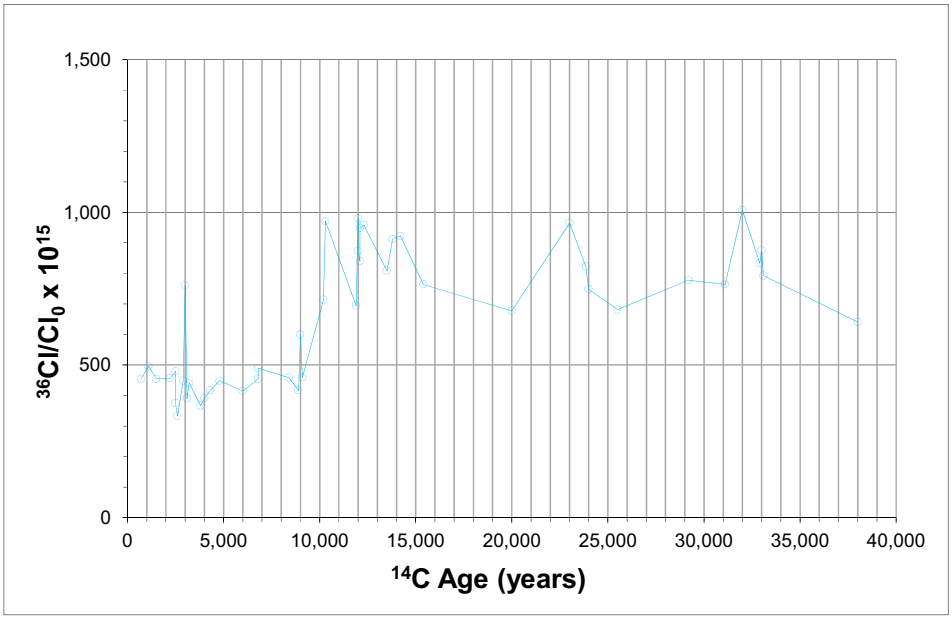

Figure 11-16
Reconstructed Record of Past Meteoric Deposition ^{36}Cl/Cl in the Vicinity of the NNSS
Source: Kwicklis and Farnham (2014), based on packrat midden from Plummer et al. (1997)

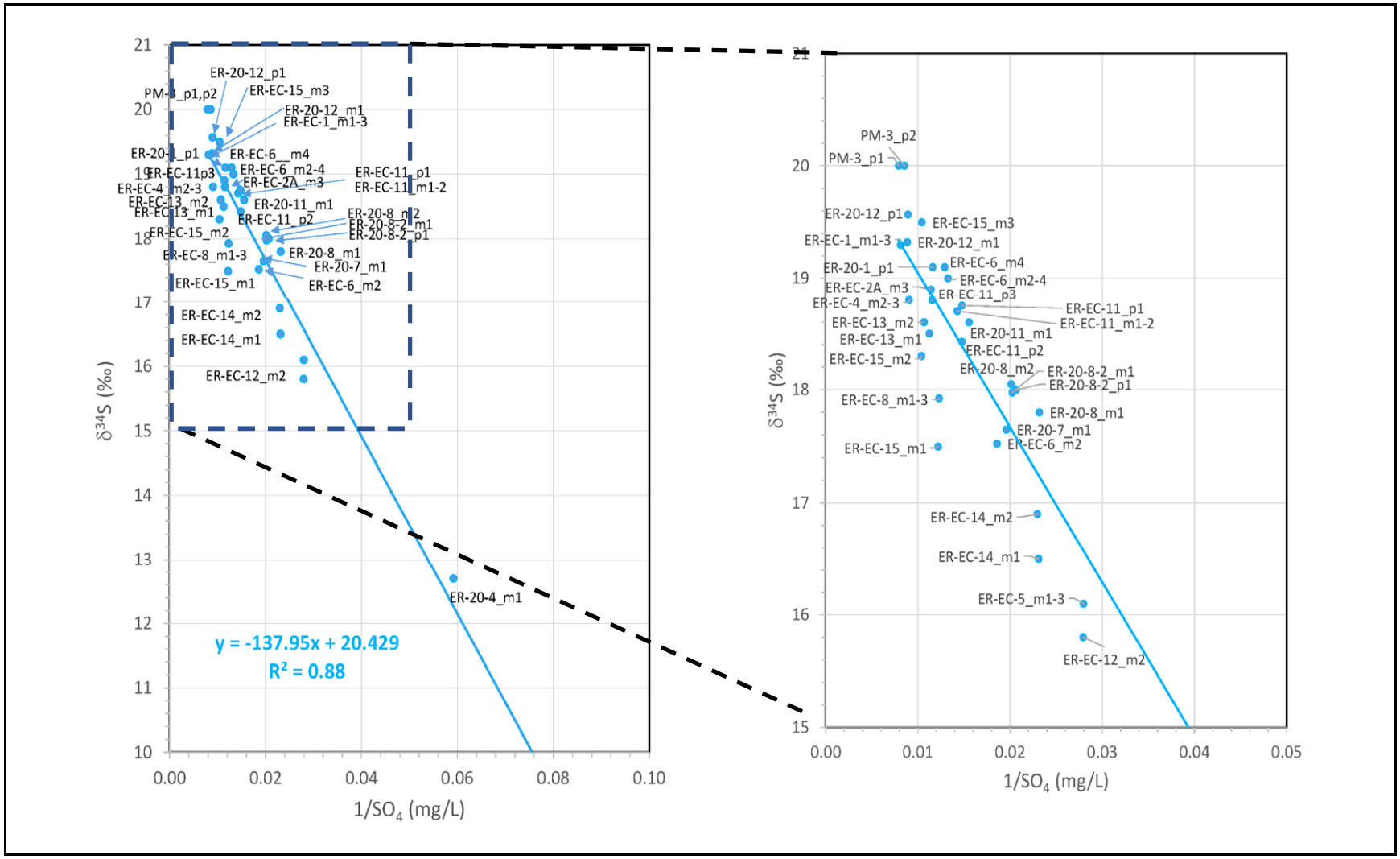

Figure 11-17
Scatterplot of $\delta^{34}S$ versus $1/SO_4$

Note: The y-intercept in the fitted regression line is 20.4 ‰. Because $1/SO_4 = 0$ at infinite SO_4 concentrations, or essentially a solid mineral, the regression line indicates the influence of a mineral S-source with a $\delta^{34}S$ of about 20.4 ‰.

million years, despite evidence for large variations in the $\delta^{34}S$ of seawater in the more distant past (Clark and Fritz, 1997, Figure 6-2).

One possible explanation that is consistent with all the geochemical and isotopic evidence is the periodic appearance and disappearance of playa lakes in Gold Flat north of Pahute Mesa during the late Pleisocene (Navarro, 2020). The occurrence of such lakes centered around the present-day Gold Flat playa dry lake is documented in Dickerson and Malczyk (2014) based on evidence for strand lines and wave-cut benches. Carbon-14 dates from tufa deposits associated with the lake range from 15,620 to 18,200 years, although the lake may have persisted much longer based on other regional evidence from lakes and wetlands. A similar lake existed in Kawich Valley to the east of the Kawich Range during the late Pleistocene. As the climate oscillated in the late Pleistocene between wetter and drier conditions, playa lakes may have intermittently dried out, leaving deposits of salts containing Cl and SO_4 that were originally derived from sea spray deposited by precipitation. Evaporation would be expected to concentrate ^{36}Cl and ^{35}Cl and ^{34}S and ^{32}S equally, leaving the $^{36}Cl/Cl$ and $\delta^{34}S$ ratios unchanged from the ratios in precipitation. The pore water largely evaporated as well during the dry periods, leaving little evidence of the highly fractionated water that formed on the playa as it dried out. During the next wet period, the salts deposited during the earlier dry period were flushed down to the groundwater by the next influx of water as the playa filled. This water would contain high salt concentrations of Cl and SO_4 but have very little evidence for the fractionation of $\delta^{18}O$ and $\delta^{2}H$, as would be expected if the high Cl and SO_4 concentrations were due to ET of pore water in the root zone. In other words, the surface water that deposited the salts and the water that flushed the salts to the groundwater were different waters that occurred at different periods in time. Little evidence of the water that produced the playa deposits exists because of its near-complete ET; evidence for the groundwater that flushed the salts to the water table is present in the groundwater system that can be observed west of the NNSS today.

Another scenario that also offers a plausible explanation of the high Cl and SO_4 concentrations and minimal evidence for evaporation in the $\delta^{18}O$ and $\delta^{2}H$ composition is that groundwater which recharged at higher elevations in the Kawich Range or other ranges upgradient from Gold Flat playa dissolved salts as it flowed toward Pahute Mesa beneath the present-day playa.

The more dilute SO_4 groundwater, presumably also derived from sea spray, has a much lower $\delta^{34}S$ (Figure 11-17). This dilute groundwater with lower $\delta^{34}S$ then moves west, where it encounters the more concentrated groundwater with $\delta^{34}S$ near 20 ‰. The mixed groundwater then has $\delta^{34}S$ values between 13 and 20 ‰, resulting in the trend observed in Figure 11-17. The large Cl and SO_4 gradient shown in Figures 11-9 and 11-10 represents the interface between two flow systems (Figure 11-18): dilute groundwater moving westward from the higher elevation recharge areas of eastern Pahute Mesa and Rainier Mesa; and the high-Cl, high-SO_4 groundwater moving south from playa lakes that formed in Gold Flat during the late Pleistocene. The two flow systems converge and to some degree mix in the southern part of Area 20 before moving southwestward around the northwest flank of Timber Mountain. The similarity in the ^{18}O and $\delta^{2}H$ of both the dilute and the more concentrated groundwater, along with their distinctly lighter character compared to modern-day recharge, confirms that both infiltrated under a cooler, pluvial climate.

11.2.3 Phase II Flow Path Evaluation

PHREEQC and NETPATH inverse water-rock geochemical reaction models were run to determine whether the flow paths inferred from Cl and SO_4 contours are feasible when other conservative and non-conservative species are considered. These models are used to identify the fractions of groundwaters from different upgradient areas, as represented by samples from particular wells, that could be present in groundwater at a downgradient well. A mass-balance calculation is performed for each chemical element or isotope, along with each element or isotope that is contained in a mineral phase that is listed as a potential chemical reactant.

Navarro (2020) investigated the 13 flow paths shown in Figure 11-19. The inverse models chosen involved potential mixing end-members that are permitted by the hydraulic gradients and involve upgradient wells lying near the Cl and SO_4 contours bracketing the downgradient well. The source of each sampled interval was investigated with multiple intervals were sampled (ER-EC-6, ER-EC-13, ER-EC-14, ER-EC-15, and ER-20-8).

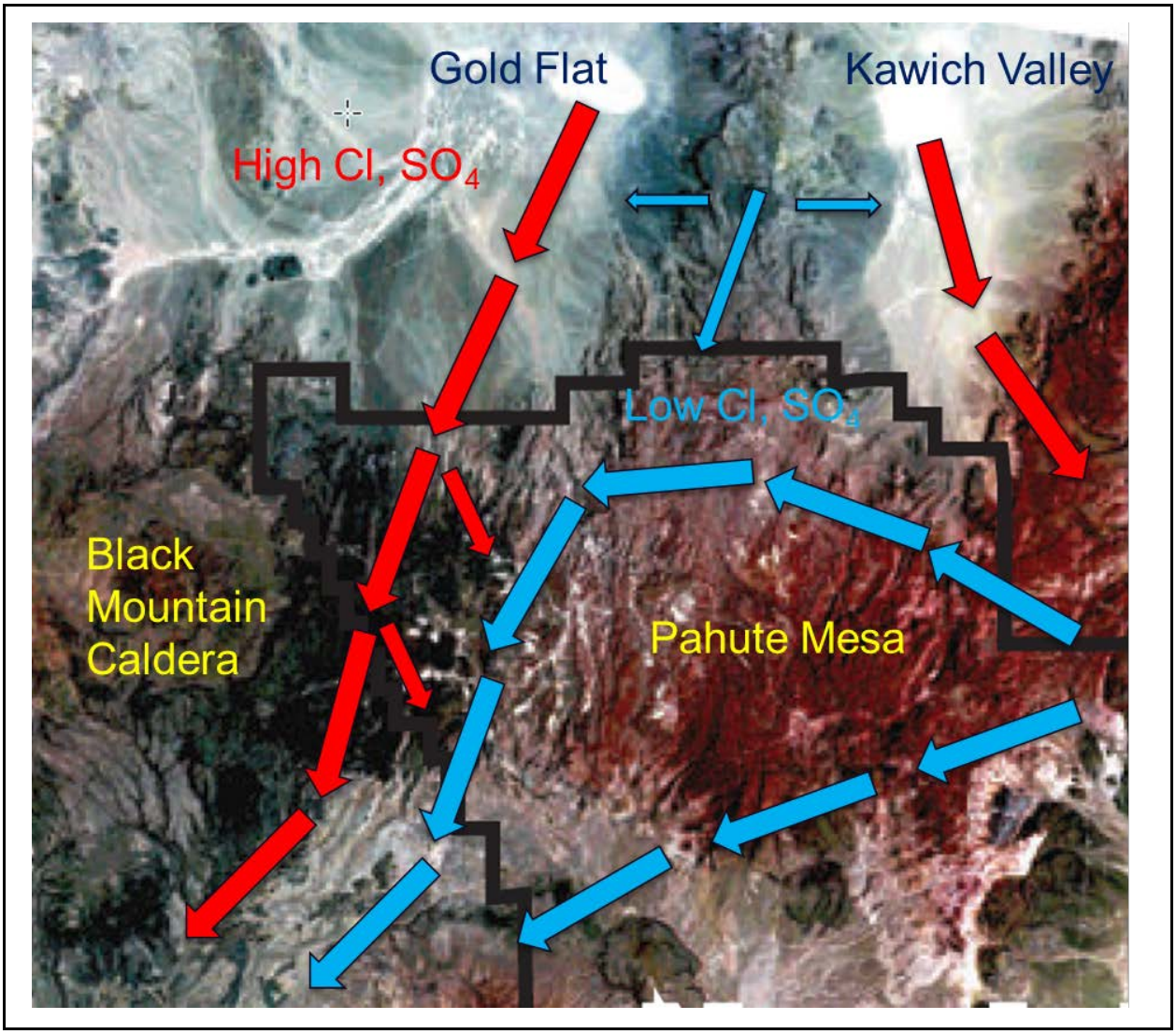

Figure 11-18
Conceptualization of the How the High and Low Concentration Groundwater from Gold Flat and Eastern Pahute Mesa Converge and Mix in Western Area 20 To Create the Large Gradients in Cl and SO_4 Shown in Figures 11-9 and 11-10

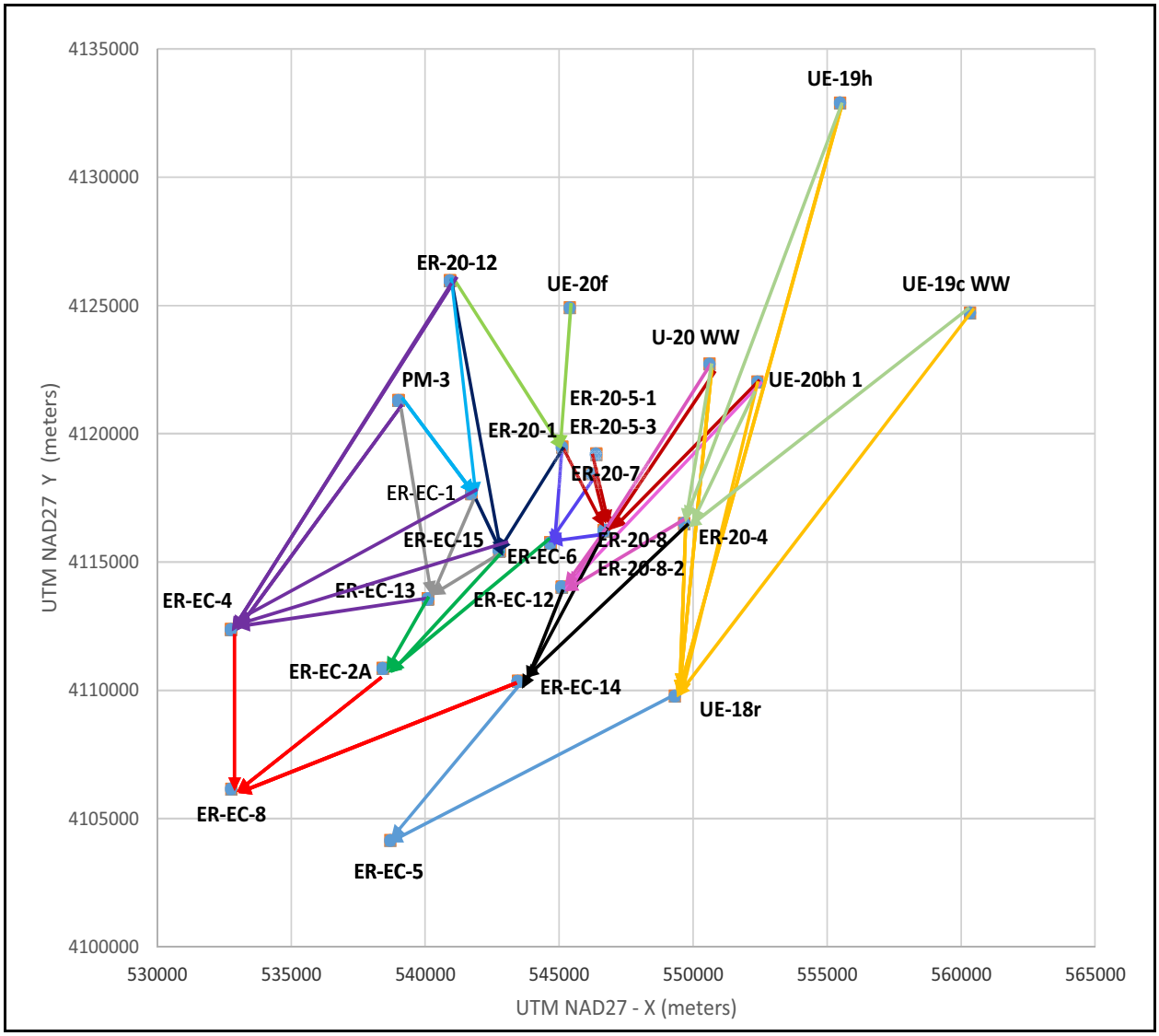

Figure 11-19
Inverse Mixing and Reaction Models Tested with PHREEQC and NETPATH

The PHREEQC and NETPATH results are combined for each flow path in Table 11-2. Multiple models involving different combinations of wells and water-rock geochemical reactions were identified that could explain the groundwater composition at each downgradient well, so the fractions of groundwater from different upgradient wells that contribute groundwater span a range of values. Distinct groundwaters can combine in different ways to explain the groundwater composition at the downgradient well. The inverse modeling results indicate the following:

- Most ER-EC-8 models identified ER-EC-2a as the primary groundwater source (70–80%), with the remaining component from ER-EC-14 (20–30%). Alternatively, models were

Table 11-2
Summary of PHREEQC and NETPATH Inverse Water-Rock Reaction Geochemical Models

Flow Path	Model [a]
1	ER-EC-8 = ER-EC-2A (0-79) + ER-EC-4 (0-47) + ER-EC-14 (21-60)
2	ER-EC-2A = ER-EC-6 (0-73) + ER-EC-13 (0-77) + ER-EC-15 (0-100)
3	ER-EC-4 = ER-EC-1 (0-57) + ER-EC-13 [b] (17-56) + ER-EC-15 (0) + ER-20-12 (4-71) + PM-3 [c] (0-51)
4	ER-EC-5 = ER-EC-14 (50-66) + UE-18r (34-50)
5	UE-18r = ER-20-4 (0-16) [d] + UE-19c WW (0-37) + UE-19h (7-54) + U-20 WW (22-54) + UE-20bh 1 (0-34)
6a	ER-EC-14_m1 = ER-EC-12 [e] (6-39) + ER-20-4 (4-50) + ER-20-8 [f] (42-73)
6b	ER-EC-14_m2 = ER-EC-12 [e] (0-28) + ER-20-4 (22-37) + ER-20-8 [f] (50-63)
7	ER-EC-12_m2 = ER-20-4 (0-35) + ER-20-8 [f] (26-68) + U-20 WW (0-73) + UE-20bh 1 (0-52)
8a	ER-20-8_m1 = ER-20-1 (6-27) + ER-20-5 [g] (37-94) + ER-20-7 (2-22) + U-20 WW (0-12) + UE-20bh 1 [d] (0-36)
8b	ER-20-8_m2 = ER-20-1 (0-43) + ER-20-5 [g] (3-77) + ER-20-7 (0-78) + U-20 WW (0-20) + UE-20bh 1 [d] (0-17)
8c	ER-20-8-2_m1 [h] = ER-20-1 (0-3) + ER-20-5 [g] (9-60) + ER-20-7 (21-73) + U-20 WW (0-24) + UE-20bh 1 [d] (0-18)
9	ER-20-1 = ER-20-12 (35-100) + UE-20f (0-65)
10	ER-EC-1 = ER-20-12 (17-100) + PM-3 [c] (0-83)
11a	ER-EC-13_m1 = ER-EC-1 (0) + ER-EC-15 [i] (78-100) + PM-3 [c] (0-22)
11b	ER-EC-13_m2 = ER-EC-1 (0-30) + ER-EC-15 [i] (26-96) + PM-3 [c] (0-35)
12a	ER-EC-15_m2 = ER-EC-1 (0-17) + ER-20-1 (65-92) + ER-20-12 (0-35)
12b	ER-EC-15_m3 = ER-EC-1 (0-20) + ER-20-1 (13-80) + ER-20-12 (0-87)
13a	ER-EC-6_m2 [j, k] = ER-20-1 (0-11) + ER-20-7 (0-48) + ER-20-8 [b] (52-100)
13b	ER-EC-6_m4 [j, k] = ER-20-1 (61-100) + ER-20-7 (0-7) + ER-20-8 [b] (0-39)
14	ER-20-4 = UE-19c WW (58-83) + UE-19h (4-17) + U-20 WW (0-8) + UE-20bh 1 (0-30) [l]

[a] Numbers in parenthesis indicate the percentages of groundwater in the upgradient well present at a specified interval in the downgradient well.
[b] The contributions from PM-3_p1 and PM-3_p 2 are summed.
[c] The contributions from ER-EC-13_m1 and ER-EC-13_m2 are summed
[d] Well was not included as a potential mixing end-member in the NETPATH model.
[e] The contributions from ER-EC-12_m1 and ER-EC-12_m2 are summed.
[f] The contributions from ER-20-8 and ER-20-8-2 are summed.
[g] The contributions from ER-20-5-1 and ER-20-5-3 are summed.
[h] PHREEQC results reported; model was not run using NETPATH.
[i] The contributions from ER-EC-15_m1, ER-EC-15_m2, and ER-EC-15_m3 are summed.
[j] No NETPATH models were identified likely because NETPATH doesn't allow for analytical uncertainty.
[k] ER-EC-06 (_m2 and _m4) models were also tested with PHREEQC (not NETPATH) using ER-20-5-1 and ER-20-5-3 instead of ER-20-8 and without S isotopes as a constraint. The contribution of ER-20-5-3 in these models is similar to ER-20-8 in the models reported here.
[l] Only NETPATH models were identified for ER-20-4; no PHREEQC models were found even after adding WW-8 and TW-1 as potential mixing components.

identified that required ER-EC-4 (40–47%) combined with ER-EC-14 (60%), or ER-EC-4 (5–20%) combined with ER-EC-2a (40%) and ER-EC-14 (40%). Groundwater from ER-EC-14_m1 and ER-EC-14_m2 substitute for each other in the models.

- Most ER-EC-2a models identified the deep zone of ER-EC-13 (ER-EC-13_m1), shallow zones of ER-EC-6 (ER-EC-6_m2-4 or ER-EC-6_m4), and shallow zones of ER-EC-15 (ER-EC-15_m2 or ER-EC-15_m3) as the groundwater source. Other models required

ER-EC-15_m2 (69–73%) with the remaining component (25–31%) primarily from ER-EC-6_m2-4. Substitution of ER_EC-13_m1 for ER-EC-15 in these models is not surprising considering that ER_EC-13_m1 can be derived solely from ER-EC-15 groundwaters (see below).

- ER-EC-4 groundwater may include groundwater that has flowed southwest from PM-3 and ER-EC-01. All PHREEQC models indicated the presence of ER-EC-13_m1 (40–60%) and either PM-3_p2 or ER-EC-1 (0 to 60%). NETPATH Models included PM-3_p1, ER-20-12_m1, ER-EC-1, and ER-EC-13. This is not surprising given the convergent nature of the hydraulic gradient in the vicinity of ER-EC-04 and the fact that groundwater at all of these wells is ultimately derived from the vicinity of ER-20-12.

- ER-EC-5 models indicate ER-EC-14 (50–65%) and UE-18r (35–50%) as the groundwater source. Groundwater from ER-EC-14_m1 and ER-EC-14_m2 substitute for each other in the models.

- UE-18r models identified UE-19h and U-20 WW as the groundwater source sometimes with contributions of either ER-20-4 or UE-20bh 1 groundwater, implying strong north–south groundwater flow. However, smaller amount of groundwater from UE-19c WW can also be present, implying some southwest flow.

- ER-20-1 groundwater is composed of ER-20-12 groundwater, along with groundwater from the northern part of the trough at UE-20f. ER-20-1 groundwater can be traced further downgradient to ER-EC-15 and the shallow interval of ER-EC-06 (ER-EC-06_m4), before moving southwest toward ER-EC-13, ER-EC-2A, and ER-EC-04. On the eastern side of the hydraulic trough, groundwater appears to flow more north–south between upgradient Wells UE-20bh 1, U-20 WW, and UE-19h; and downgradient Well UE-18r.

- ER-20-8 and ER-20-8-2 models indicate that ER-20-5 and ER-20-7 are the dominant groundwater contributors rather than wells east of the Boxcar fault such as U-20 WW and UE-20bh 1, although groundwater from these wells is also permissible in small amounts.

- ER-EC-12 (ER-EC-12_m2) models indicate that ER-20-8 is the dominant contributor which then combines with other groundwater from east of the Boxcar fault from ER-20-4, U-20 WW, or UE-20bh 1 before moving southwest toward ER-EC-14. At ER-EC-14, ER-EC-12_m2 mixes in small amounts with much larger percentages of groundwater from vicinity of ER-20-8 and ER-20-4.

- ER-EC-06, located in the center of the hydraulic trough, appears to received flow from multiple directions, with the groundwater in the lower zone (ER-EC-06_m2) being supplied primarily from the northeast in the vicinity of ER-20-8 or ER-20-7 and ER-20-5, and groundwater in the upper zone (ER-EC-06_m4) being supplied primarily by groundwater to the north in the vicinity of ER-20-1. Groundwater from ER-EC-06 shows up as a potential mixing component of groundwater at ER-EC-2A along with groundwater from ER-EC-13 and ER-EC-15.

From this analysis, the Cl and SO_4 contours shown in Figures 11-9 and 11-10 can be thought of as broadly reflecting flow paths that converge in the hydraulic trough formed in Area 20. However, the steep gradient in Cl and SO_4 that coincides with the trough arises through mixing of dilute groundwater moving west from eastern Pahute Mesa with more concentrated groundwater moving south from areas north of Pahute Mesa and, as such, the contour lines also represent variable amounts of these end-members in the mixture.

11.2.4 Phase II Evaluation of PM-OV Flow System Boundaries

As part of the Phase II evaluation, the PM-OV flow system boundaries presented in Fenelon et al. (2016) (Figures 2-1 and 11-20) were evaluated to determine whether they are consistent with hydrogeochemical data. Navarro (2020) presents an evaluation of the Timber Mountain segment (Figure 11-21) and of two segments, Railroad Valley and Cactus Flat, located in the northern portion (Figure 11-22) of the PM-OV groundwater basin of the no-flow boundary. The Timber Mountain segment of the boundary precludes the previously hypothesized groundwater flow path southward from testing areas along Fortymile Canyon into Fortymile Wash and Jackass Flat.

Navarro (2020) reported water chemical and isotopic data in general agreement with groundwater flow directions described in Fenelon et al. (2016). Higher concentrations of SO_4 and isotopically heavier $\delta^{13}C$ are observed on the western side of the Timber Mountain segment when compared to the eastern side of the no-flow model boundary (Figure 11-21). The lower SO_4 and lighter $\delta^{13}C$ on the east side of the Timber Mountain segment of the no-flow model boundary are consistent with stable isotopic data, indicating mixing of deep groundwater from the vicinity of Rainier Mesa with local recharge and with water-rock reactions involving calcite and gypsum as groundwater flows south–southwestward toward Jackass Flat. Water chemical and isotopic data indicate two distinct geochemical evolutionary flow paths along either side of the Timber Mountain no-flow model boundary. The existence of this no-flow boundary precludes previously hypothesized groundwater flow from eastern Pahute Mesa (Area 19) southward along Fortymile Canyon into Fortymile Wash and Jackass Flat. Kwicklis et al. (2005) and Rose et al. (2006) suggested a leaky boundary from Beatty Wash to Crater Flat in the southern portion of the Timber Mountain no-flow model boundary, which was based upon water-rock reaction models. However, for these models to work, the $\delta^{13}C$ constraint had to be removed, which makes the proposed leaky boundary in this area uncertain.

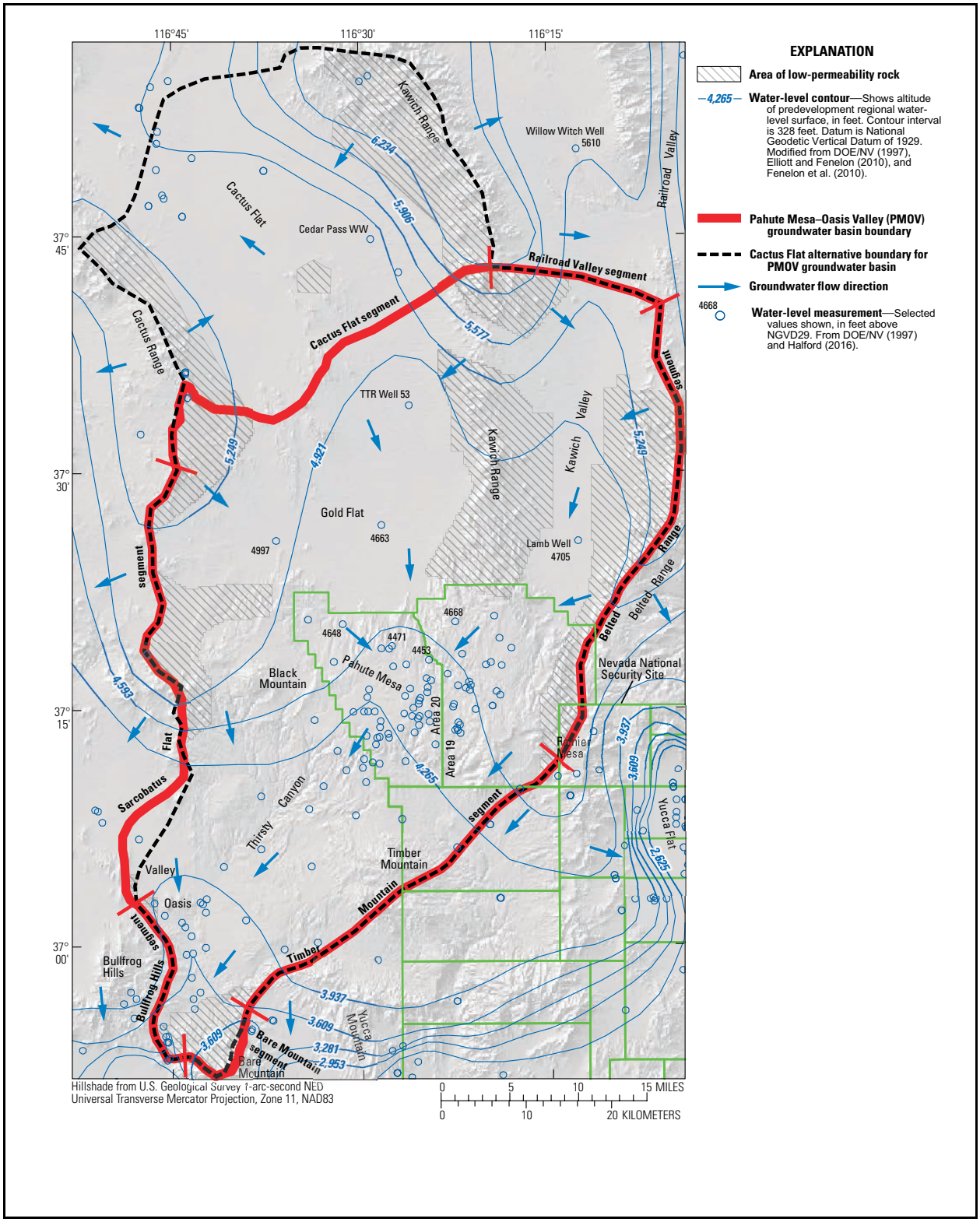

Figure 11-20
PM-OV Groundwater Basin
Source: Fenelon et al., 2016

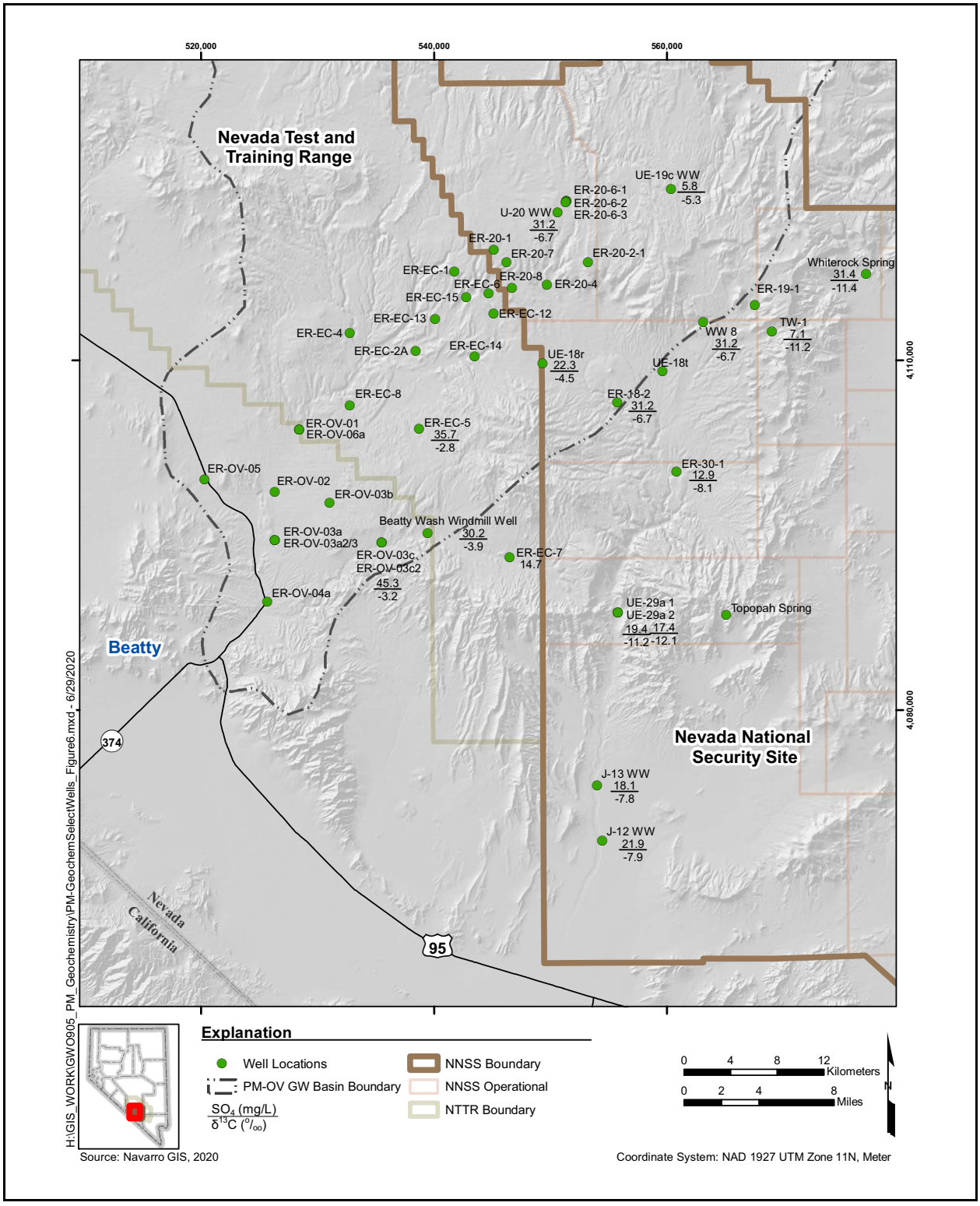

Figure 11-21
Spatial Distribution of $\delta^{13}C$ and SO_4 along Both Sides of the Timber Mountain Segment of the No-Flow Model Boundary

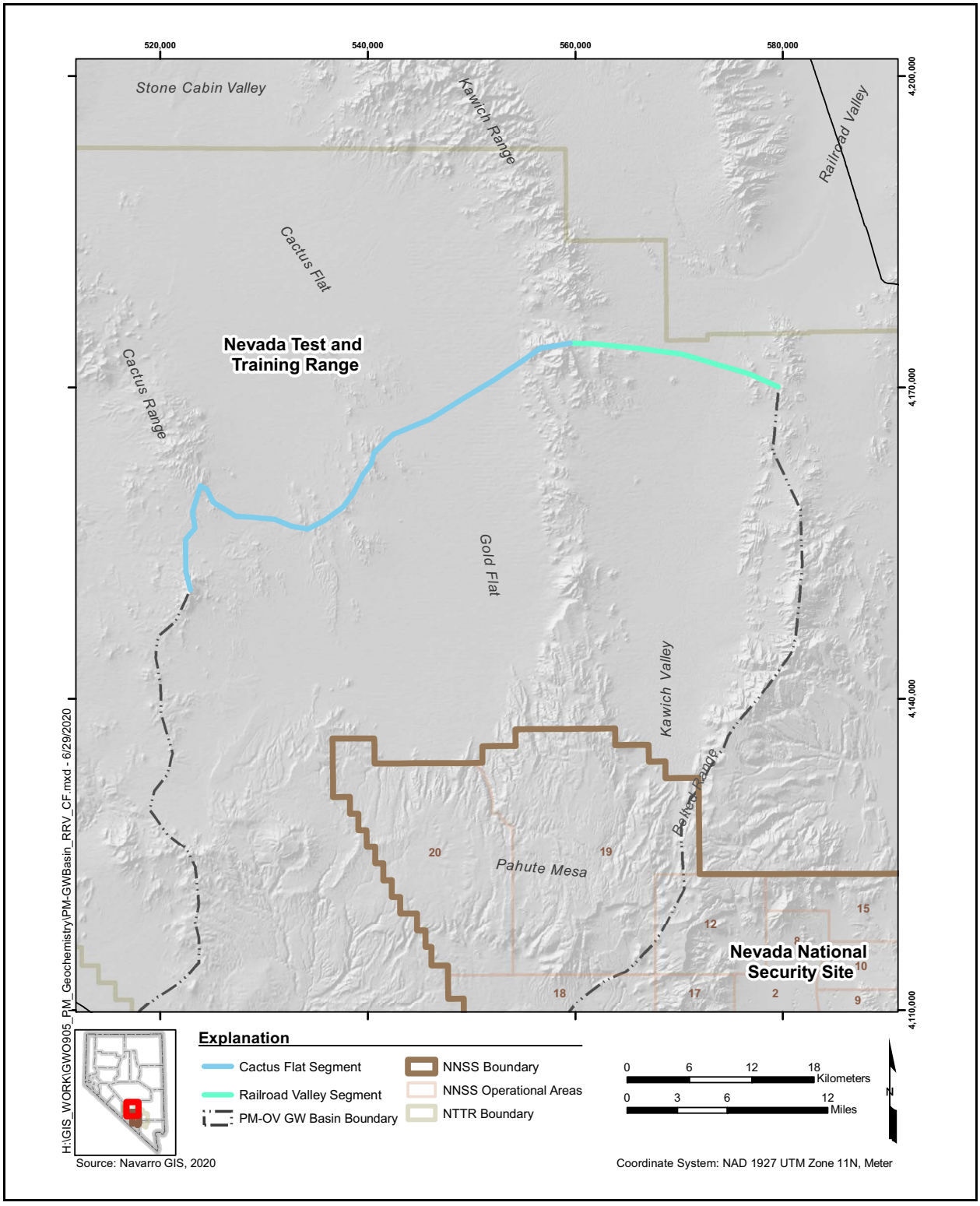

Figure 11-22
Railroad Valley and Cactus Flat Segments of the PM-OV Groundwater Basin
Source: Fenelon et al., 2016

Water chemical and isotopic data are in general agreement with the proposed northern no-flow boundaries for the PM-OV groundwater basin in Fenelon et al. (2016). Although the stable isotopes $\delta^{2}H$ and $\delta^{18}O$ indicate groundwater could flow southward across the Railroad Valley and Cactus Flat segments of the no-flow boundaries, Cl and SO_4 concentrations in Areas 19 and 20 of Pahute Mesa suggest that this is less likely. More complicated processes (i.e., groundwater flow, mixing of valley groundwater with local recharge, water-rock reactions, and other sources of Cl and SO_4 such as an older saline playa lake) are required to explain the concentrations of these major solutes in Pahute Mesa (Areas 19 and 20) groundwater. The observed changes in Cl and SO_4 concentrations across the proposed no-flow boundaries are not consistent with large amounts of groundwater flowing from the north into Pahute Mesa.

11.2.5 Groundwater Travel Times

Similar to the Phase I evaluation, the average (composite) groundwater travel time between the upgradient wells in the mixture and the downgradient well is estimated after taking into account the water-rock geochemical reactions that may have introduced ^{14}C-free carbon into the groundwater. In general, groundwater velocity estimates from ^{14}C could not be made in southern Area 20 and downgradient areas. In Area 20, groundwater ^{14}C often included contributions of test-derived ^{14}C, which biased the travel-time estimates between wells. Downgradient of the areas affected by test-derived ^{14}C, past studies (e.g., Kwicklis, 2009) have concluded that either the difference between ^{14}C activities was too small to allow a reliable estimate of travel times or, close to the discharge areas in Oasis Valley, the groundwater had interacted with ^{14}C in soil CO_2, which reset the groundwater ^{14}C ages and caused the shallow groundwater to appear artificially young. Estimated noble gas recharge temperatures and $^{3}He/^{4}He$ ratios presented in this study support the hypothesis that groundwater re-equilibrated with shallow soil gas in the Oasis Valley area.

11.3 Conclusions

Understanding of the groundwater flow system near Pahute Mesa at the NNSS was updated with new groundwater hydrochemical and isotopic data collected from wells drilled in Area 20, the Bench area, and the northwest Timber Mountain moat area as part of the Phase II characterization effort (Navarro, 2020). Groundwater flow paths defined by Cl and SO_4 contours indicate convergent flow into a hydraulic trough in southern Area 20 that is created by a combination of low- and

high-permeability faults. Steep gradients in Cl and SO_4 within this trough reflect the convergence of higher-concentration groundwater flowing south from Gold Flat into western Pahute Mesa, where it mixes with more dilute groundwater flowing west from high-elevation recharge areas in eastern Pahute Mesa and possibly the Belted Range. The groundwater from Gold Flat appears to have been recharged in the late Pleistocene, when the presently dry Gold Flat playa lake alternately dried out and deposited salts, and then re-dissolved these salts as the playa lake refilled in response to climate oscillations. High stand of the lake was about 30 ft above the present playa surface and occurred between 18 and 15 thousand years ago based on ^{14}C dating of submarine tufa deposits, roughly the ^{14}C age of the high-Cl and -SO_4 groundwater presently flowing south along the western boundary of the NNSS. The groundwater hypothesized to be recharged at Gold Flat playa in the late Pleistocene is characterized by $^{36}Cl/Cl$ ratios and $\delta^{34}S$ values that indicate the elevated Cl and SO_4 in the groundwater originated from salts derived from the ocean and deposited with precipitation in the late Pleistocene rather than from an ancient mineral source such as a hydrothermal deposit. The extremely light $\delta^{18}O$ and $\delta^{2}H$ of this groundwater relative to modern precipitation is also consistent with a late pluvial origin for the groundwater. The dilute groundwater flowing west from eastern Pahute Mesa is also late Pleistocene groundwater based on its ^{14}C age and its similarly light $\delta^{18}O$ and $\delta^{2}H$ relative to modern precipitation. The continued presence of late Pleistocene groundwater beneath Pahute Mesa, despite evidence for a dynamic saturated flow system from the rapid migration of test-generated ^{3}H, is attributed to long residence times of high-elevation infiltration in the thick (>600-m) unsaturated zone beneath Pahute Mesa. In the case of the more concentrated pluvial playa lake groundwater, its continued presence beneath western Pahute Mesa is attributed to the small volume of recharge north of Pahute Mesa that is presently available to displace the Pleistocene groundwater, and to the slow transport out of Gold Flat through high-porosity alluvium. The flow paths identified by the Cl and SO_4 contours and tested with geochemical mixing and reaction models such as PHREEQC and NETPATH can help site future downgradient monitoring wells by locating them along Cl and SO_4 contour lines having similar concentration as those observed in presently contaminated upgradient wells.

In general, groundwater velocity estimates from ^{14}C could not be made in southern Area 20 and downgradient areas. In Area 20, groundwater ^{14}C often included contributions of test-derived ^{14}C, which biased the travel-time estimates between wells. Downgradient of the areas affected by test-derived ^{14}C, past studies (e.g., Kwicklis, 2009) have concluded that either the difference between

^{14}C activities was too small to allow a reliable estimate of travel times or, close to the discharge areas in Oasis Valley, the groundwater had interacted with ^{14}C in soil CO_2, which reset the groundwater ^{14}C ages and caused the shallow groundwater to appear artificially young. Estimated noble gas recharge temperatures and $^{3}He/^{4}He$ ratios presented in this study support the hypothesis that groundwater re-equilibrated with shallow soil gas in the Oasis Valley area.

More regional groundwater geochemical and isotopic data were also examined to evaluate the boundaries of the PM-OV groundwater basin defined by USGS (Fenelon et al., 2016). In general, the groundwater geochemical and isotopic data support the interpretation from hydrologic and geologic data that groundwater from Pahute Mesa does not flow directly south from Pahute Mesa beneath Timber Mountain toward Yucca Mountain, but instead flows around the northwest margin of Timber Mountain toward Oasis Valley and lower Beatty Wash. Some unknown, but probably minor, fraction of this groundwater flows across lower Beatty Wash into northwest Crater Flat, but most flows toward Oasis Valley as interpreted by USGS from hydraulic head contours. Steep hydraulic gradients between Beatty Wash and areas to the south indicate that southerly flow beneath Timber Mountain is prevented by structural or stratigraphic features to the south of Timber Mountain rather than beneath Timber Mountain itself. Groundwater south of Timber Mountain in upper Beatty Wash and northwest Yucca Mountain has distinctly heavier $\delta^{18}O$ and $\delta^{2}H$ than Pahute Mesa groundwater, and was probably derived by local recharge on Timber Mountain itself.

Refinement to Phase I flow path interpretations resulted from new data from Phase II wells, new data for Phase I and other Pahute Mesa wells (including new $\delta^{34}S$ results), and revised delineation of PM-OV groundwater basin (Fenelon et al., 2016). The data collected as part of the Phase II geochemistry investigations were combined with data previously reported in Kwicklis et al. (2005) to produce the composite maps of groundwater Cl and $\delta^{2}H$ shown in Figure 11-23. A comparison between the original flow paths shown in Figure 11-6 with the revised flow paths shown in Figure 11-23 indicates several significant changes:

- The flow path from Gold Flat into western Pahute Mesa (Path 6) was added to explain the high Cl and SO_4 groundwater observed in western Pahute Mesa. Flow Path 5 marks the western limit of the unmixed dilute groundwater flowing west from eastern Pahute Mesa. Flow Path 5 trends north–south through southern Area 20 and the Bench, and then turns sharply west in the northwest TMCC. Between Flow Paths 5 and 6 is a mixing zone of intermediate concentration groundwater where these two groundwater systems come together

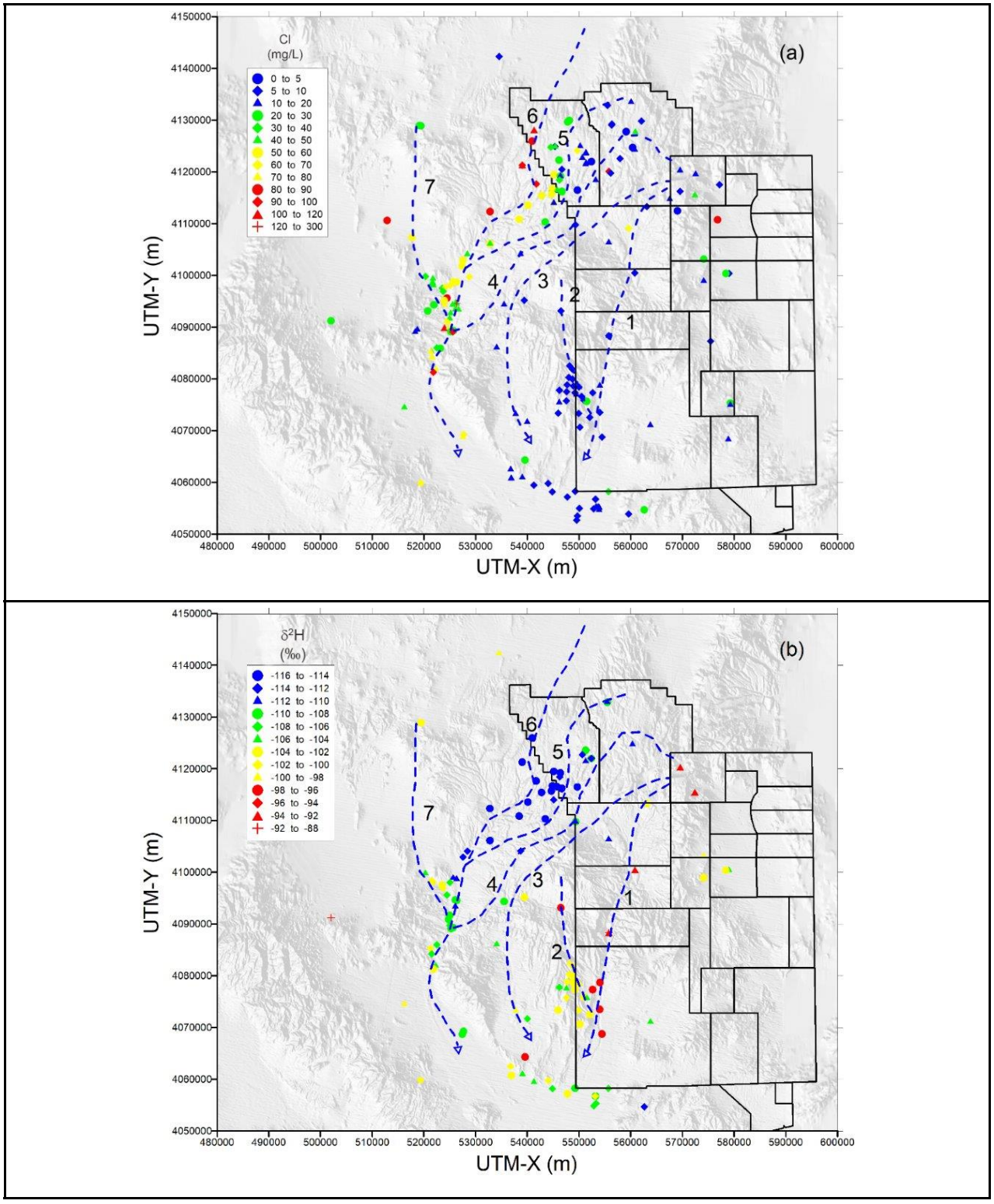

Figure 11-23
Revised Flow Paths Shown with (a) Cl and (b) δ^2H of Wells and Springs Included in the Phase I PM-OV Investigation

in a hydraulic trough in southern Area 20 of the NNSS before flowing through the Thirsty Canyon Area toward Oasis Valley.

- The flow path from Pahute Mesa along Fortymile Canyon into western Jackass Flat (Path 1) was refined to include only a Rainier Mesa source. Previously, this flow path had allowed for the possibility of groundwater flow along Fortymile Canyon from locations as far north as Well UE-19c in Area 19 of Pahute Mesa. This flow path was revised based on hydrologic and geochemical studies at Rainier Mesa (Fenelon et al., 2005; Hershey et al., 2008) which showed that lateral flow from perched systems at Rainier Mesa spread out radially from the high-elevation recharge areas, preventing groundwater from the Area 19 testing locations from flowing south through Fortymile Canyon. This flow path was also revised based on the PM-OV flow system boundary evaluation summarized in Section 11.2.4.

- Flow Path 4 allows for more eastward and even northern flow from the Rainier Mesa area in response to diverted infiltration spreading radially outward from Rainier Mesa, as depicted in Hershey et al. (2008) and DOE/EMNV (2018a). However, as presented in Kwicklis et al. (2005), groundwater along nearby Flow Path 3 continues across lower Beatty Wash into northwest Crater Flat and eventually is pushed by recharge on Bare Mountain southeastward across Crater Flat and through southern Yucca Mountain.

- Like Flow Path 3, Flow Paths 2 and 7 are essentially unchanged from the Kwicklis et al. (2005) study. Note that Flow Path 2 begins on Timber Mountain, indicating that this is the expected path that Timber Mountain recharge takes as it flows from the recharge area. This interpretation was based primarily on the similarity in $\delta^{18}O$ and $\delta^{2}H$ values of groundwater in upper Beatty Wash and northwest Yucca Mountain to modern recharge beneath Fortymile Canyon (though it is upgradient from Fortymile Canyon), and its dissimilar character to Pahute Mesa groundwater.

12.0 REFERENCES

Anderson, J.R., E.E. Hardy, J.T. Roach, and R.E. Witmer. 1976. *A Land Use and Land Cover Classification System for Use with Remote Sensor Data,* Professional Paper 964. Denver, CO: U.S. Geological Survey.

Andraski, B.J. 1997. "Soil-water Movement Under Natural-Site and Waste-Site Conditions—A Multiple-Year Field Study in the Mojave Desert, Nevada." In *Water Resources Research*, Vol. 33(8): pp. 1901–1916. Washington, DC: American Geophysical Union.

Avon, L., and T.J. Durbin. 1994. "Evaluation of the Maxey-Eakin Method for Estimating Recharge to Ground-Water Basins in Nevada." In *Journal of the American Water Resources Association*, Vol. 30(1): pp. 99–111.

BN, see Bechtel Nevada.

Bechtel Nevada. 2002. *Hydrostratigraphic Model and Alternatives for the Groundwater Flow and Contaminant Transport Model of Corrective Action Units 101 and 102: Central and Western Pahute Mesa, Nye County, Nevada,* DOE/NV/11718-646. Prepared for U.S. Department of Energy, National Nuclear Security Administration Nevada Operations Office. Las Vegas, NV.

Belcher, W.R., and D.S. Sweetkind eds. 2010. *Death Valley Regional Groundwater Flow System, Nevada and California—Hydrogeologic Framework and Transient Groundwater Flow Model,* Professional Paper 1711. Reston, VA: U.S. Geological Survey.

Benedict, F.C., Jr., T.P. Rose, and X. Zhou. 2000. *Mineralogical, Chemical, and Isotopic Characterization of Fracture-Coating Minerals in Borehole Samples from Western Pahute Mesa and Oasis Valley, Nevada*, UCRL-ID-152919. Livermore, CA: Lawrence Livermore National Laboratory.

Benjamin, J.R., and C.A. Cornell. 1970. *Probability, Statistics, and Decision for Civil Engineers*. New York, NY: McGraw-Hill Book Co.

Blakely, R.J., and D.A. Ponce. 2001. *Map Showing Depth to Pre-Cenozoic Basement in the Death Valley Ground-water Model Area, Nevada and California*. Miscellaneous Field Studies Map MF-2381-E. Scale 1:250,000. Denver, CO: U.S. Geological Survey.

Blankennagel, R.K. 1967. *Hydraulic Testing Techniques of Deep Drill Holes at Pahute Mesa, Nevada Test Site*, Open-File Report 67-18. Prepared in cooperation with the U.S. Atomic Energy Commission. Washington, DC: U.S. Geological Survey.

Blankennagel, R.K., and J.E. Weir, Jr. 1973. *Geohydrology of the Eastern Part of Pahute Mesa, Nevada Test Site, Nye County, Nevada*, Professional Paper 712-B. Denver, CO: U.S. Geological Survey.

Bowen, I.S. 1926. "The Ratio of Heat Losses by Conduction and by Evaporation from Any Water Surface." In *Physical Review*, Vol. 27: pp. 779–787. New York, NY: American Physical Society.

Bradbury, K.R., and M.A. Muldoon. 1990. "Hydraulic Conductivity Determinations in Unlithified Glacial and Fluvial Materials." In *Ground Water and Vadose Zone Monitoring,* ASTM STP 1053. pp. 138–151. D.M. Nielsen and A.I. Johnson eds. Philadelphia, PA: American Society for Testing and Materials.

Bredehoeft, J.D. 1967. "Response of Well-Aquifer Systems to Earth Tides." In *Journal of Geophysical Research*, Vol. 72(12): pp. 3,075–3,087.

Butler, J.J. Jr., and J.M. Healey. 1998. "Relationship Between Pumping-Test and Slug-Test Parameters: Scale Effect or Artifact?" In *Groundwater*, Vol. 36(2): pp. 305–313.

CFR, see *Code of Federal Regulations*.

Caine, J.S., J.P. Evans, and C.B. Forster. 1996. "Fault Zone Architecture and Permeability Structure." In *Geology*, Vol. 24(11): pp. 1025–1028.

Carle, S.F. 2016. *Spreadsheet for Estimation of Uncertainty of Potentiometric Head from Variation of Water Temperature and Gravity Within the Water Column of Pahute Mesa Boreholes,* LLNL-MI-693218. Livermore, CA: Lawrence Livermore National Laboratory.

Cas, R.A.F., and J.V. Wright. 1987. *Volcanic Successions: Modern and Ancient.* London, UK: Allen and Unwin.

Claassen, H.C. 1985. *Sources and Mechanisms of Recharge for Ground Water in the West-Central Amargosa Desert, Nevada—A Geochemical Interpretation*, Professional Paper 712-F. Alexandria, VA: U.S. Geological Survey.

Clark, I., and P. Fritz. 1997. *Environmental Isotopes in Hydrogeology*. Boca Raton, FL: CRC Press.

Code of Federal Regulations. 2019. Title 40 CFR, Part 141, "National Primary Drinking Water Regulations." Washington, DC: U.S. Government Printing Office.

Cooper, C.A., R.L. Hershey, J.M. Healey, and B.F. Lyles. 2013. *Estimation of Groundwater Recharge at Pahute Mesa Using the Chloride Mass-Balance Method*, DOE/NV/0000939-09; Publication No. 45251. Reno, NV: Desert Research Institute, Water Resources Center.

Craig, H. 1961. "Isotopic Variations in Meteoric Waters." In *Science*, Vol. 133(3465): pp. 1702–1703. Washington, DC: American Association for the Advancement of Science.

Cutillo, P.A., and J.D. Bredehoeft. 2011. "Estimating Aquifer Properties from the Water Level Response to Earth Tides." In *Ground Water*, Vol. 49(4): pp. 600–610.

Czarnecki, J.B. 1997. *Geohydrology and Evapotranspiration at Franklin Lake Playa, Inyo County, California, with a Section on Estimating Evapotranspiration using the Energy-Budget Eddy-correlation Technique by D.I. Stannard,* Water-Supply Paper 2377. Denver, CO: U.S. Geological Survey.

DOE, see U.S. Department of Energy.

DOE/EMNV, see U.S. Department of Energy Environmental Management Nevada Program.

DOE/NV, see U.S. Department of Energy, Nevada Operations Office.

Dynamic Graphics, see Dynamic Graphics, Inc.

Dagan, G. 1986. "Statistical Theory of Groundwater Flow and Transport: Pore to Laboratory, Laboratory to Formation, and Formation to Regional Scale." In *Water Resources Research*, Vol. 22(95): pp. 120S-135S.

Decision Engineering. 1996. *Crystal Ball Software*, Version 4.0 for Windows. Denver, CO.

DeMeo, G.A., R.J. Laczniak, and W.E. Nylund. 1999. "Estimating Evapotranspiration Rates in Death Valley, California." In *Proceedings of Conference on Status of Geologic Research and Mapping in Death Valley National Park, Las Vegas, Nevada*, April 9–11, Open-File Report 99-153, p. 68. Denver, CO: U.S. Geological Survey.

Dickerson, R., and N. Malczyk. 2014. "Quaternary Geologic Studies on Playas of the Nevada Test and Training Range in Support of the Nellis AFB Training Mission," pp.159–176. In *Geological Society of America Reviews in Engineering Geology Volume XXII.* R.S. Harmon, S.E. Baker, and E.V. McDonald eds. Boulder, CO.

Doherty, J. 2018. "Methodologies and Software for PEST-Based Model Predictive Uncertainty Analysis." Brisbane, Australia: Watermark Numerical Computing. Available at Iwww.pesthomepage.org\Downloads.php?file=pest_uncert.zip. As accessed on 2 January.

Dynamic Graphics, Inc. 2015. *EarthVision 9.1: Software for 3D Modeling & Visualization.* Alameda, CA.

Dynamic Graphics, Inc. 2019. *EarthVision 10: Software for 3D Modeling & Visualization*. Alameda, CA.

Ekren, E.B., R.E. Anderson, C.L. Rogers, and D.C. Noble. 1971. *Geology of Northern Nellis Air Force Base Bombing and Gunnery Range, Nye County, Nevada,* Professional Paper 651. Washington, DC: U.S. Geological Survey.

Elliott, P.E., and J.M. Fenelon. 2010. *Database of Groundwater Levels and Hydrograph Descriptions for the Nevada Test Site Area, Nye County, Nevada*, *1941–2010,* Data Series 533. Reston, VA: U.S. Geological Survey. (Version 9.0 released in February 2019).

Elliott, P.E., and M.T. Moreo. 2018. *Update to the Groundwater Withdrawals Database for the Death Valley Regional Groundwater Flow System, Nevada and California*, *1913–2010*. Reston, VA: U.S. Geological Survey.

FFACO, see *Federal Facility Agreement and Consent Order.*

Fabryka-Martin, J.T, S.J. Wightman, W.J. Murphy, M.P. Wickham, M.W. Caffee, G.J. Nimz, J.R. Southon, and P. Sharma. 1993. "Distribution of Chlorine-36 in the Unsaturated Zone at Yucca Mountain: An Indicator of Fast Transport Paths." In *Conference Proceeding, FOCUS '93: Site Characterization and Model Validation*, 26–29 September. Las Vegas, NV.

Federal Facility Agreement and Consent Order. 1996 (as amended March 2010). Agreed to by the State of Nevada; U.S. Department of Energy, Environmental Management; U.S. Department of Defense; and U.S. Department of Energy, Legacy Management. Appendix VI, which contains the Underground Test Area Strategy, was last modified June 2014, Revision No. 5.

Fenelon, J.M. 2005. *Analysis of Ground-Water Levels and Associated Trends in Yucca Flat, Nevada Test Site, Nye County, Nevada, 1951–2003*, Scientific Investigations Report 2005-5175. Carson City, NV: U.S. Geological Survey.

Fenelon, J.M. 2010. *Quality Assurance and Analysis of Water Levels in Wells on Pahute Mesa and Vicinity, Nevada Test Site, Nye County, Nevada.* Water-Resources Investigations Report 00-4014. Carson City, NV. U.S. Geological Survey.

Fenelon, J.M., Geological Survey. 2015a. Personal communication to P. Martian (Navarro) regarding steady-state water level data for the Pahute Mesa/Oasis Valley groundwater system, 10 August. Henderson, NV.

Fenelon, J.M., Geological Survey. 2015b. Personal communication to P. Martian (Navarro) regarding steady-state water level data for the Pahute Mesa/Oasis Valley groundwater system, 12 August. Henderson, NV.

Fenelon, J.M., Geological Survey. 2015c. Personal communication to P. Martian (Navarro) regarding steady-state water level data for the Pahute Mesa/Oasis Valley groundwater system, 14 August. Henderson, NV.

Fenelon, J.M., K.J. Halford, and M.T. Moreo. 2016. *Delineation of the Pahute Mesa–Oasis Valley Groundwater Basin, Nevada,* Scientific Investigations Report 2015–5175. Carson City, NV: U.S. Geological Survey.

Ferguson, J.F., A.H. Cogbill, and R.G. Warren. 1994. "A Geophysical-Geological Transect of the Silent Canyon Caldera Complex, Pahute Mesa, Nevada." In J*ournal of Geophysical Research: Solid Earth*, Vol. 99(B3): pp. 4323–4339.

Finnegan, D.L., S.M. Bowen, J.L. Thompson, C.M. Miller, P.L. Baca, L.F. Olivas, C.G. Geoffrion, D.K. Smith, W. Goishi, B.K. Esser, J.W. Meadows, N. Namboodiri, and J.F. Wild. 2016. *Nevada National Security Site Underground Radionuclide Inventory, 1951–1992: Accounting for Radionuclide Decay through September 30, 2012,* LA-UR-16-21749. Los Alamos, NM: Los Alamos National Laboratory.

Freeze, R.A., and J.A. Cherry. 1979. *Groundwater.* Englewood Cliffs, NJ: Prentice Hall.

Freeze, R.A., J. Massmann, L. Smith, T. Sperling, and B. James. 1990. "Hydrogeological Decision Analysis: I. A Framework." In *Groundwater*, Vol. 28(5): pp. 738–766. Columbus, OH: Groundwater Publishing Co.

Fridrich, C.J., S.A. Minor, J.L. Slate, and P.L. Ryder. 2007. *Geologic Map of Oasis Valley Spring-Discharge Area and Vicinity, Nye County, Nevada*, Scientific Investigations Map 2957, 25 p., scale 1:50,000. Denver, CO: U.S. Geological Survey.

Frus, R.J., and K.J. Halford. 2018. *Documentation of Single-Well Aquifer Tests and Integrated Borehole Analyses, Pahute Mesa and Vicinity, Nevada,* Scientific Investigations Report 2018-5096. Reston, VA: U.S. Geological Survey.

Garcia, C.A., K.J. Halford, and J.M. Fenelon. 2013. "Detecting Drawdowns Masked by Environmental Stresses with Water-Level Models." In *Groundwater,* Vol. 51(3): pp. 322–332.

Garcia, C.A., T.R. Jackson, K.J. Halford, D.S. Sweetkind, N.A. Damar, J.M. Fenelon, and S.R. Reiner. 2017. *Hydraulic Characterization of Volcanic Rocks in Pahute Mesa Using an Integrated Analysis of 16 Multiple-Well Aquifer Tests, Nevada National Security Site, 2009–14,* Scientific Investigations Report 2016-5151. Carson City, NV: U.S. Geological Survey.

Gay, L.W., and L.J. Fritschen. 1979. "An Energy Budget Analysis of Water Use by Saltcedar." In *Water Resources Research*, Vol. 15(6): pp. 1589–1592. Washington, DC: American Geophysical Union.

Grauch, V.J.S., D.A. Sawyer, C.J. Fridrich, and M.R. Hudson. 1999. *Geophysical Framework of the Southwestern Nevada Volcanic Field and Hydrogeologic Implications,* Professional Paper 1608. Denver, CO: U.S. Geological Survey.

Halford, K.J., U.S. Geological Survey. 2011. Memorandum to Bonnie Thompson, USGS/NNSA Program Manager, Henderson, Nevada, regarding an assessment of flow logs in piezometers for ER-20-8 #2 and ER-EC-11, Pahute Mesa, Nevada National Security Site, 9 March. Las Vegas, NV.

Halford, K.J. 2016. *Model Archive of Pahute-Mesa Oasis Valley Groundwater Flow Model*, U.S. Geological Survey Data Release. Carson City, NV.

Halford, K., C.A. Garcia, J. Fenelon, and B. Mirus. 2016. *Advanced Methods for Modeling Water-Levels and Estimating Drawdowns with SeriesSEE, an Excel Add-In,* Techniques and Methods Report 4-F4, Version 1.1. Reston, VA: U.S. Geological Survey.

Halford, K.J., and T.R. Jackson. 2020. *Groundwater Characterization and Effects of Pumping in the Death Valley Regional Groundwater Flow System, Nevada and California, with Special Reference to Devils Hole*, Professional Paper 1863. Reston, VA: U.S. Geological Survey.

Heilweil, V.M., and L.E. Brooks eds. 2011. *Conceptual Model of the Great Basin Carbonate and Alluvial Aquifer System*, Scientific Investigations Report 2010-5193. Salt Lake City, UT: U.S. Geological Survey.

Hem, J.D. 1985. *Study and Interpretation of the Chemical Characteristics of Natural Water*, Water-Supply Paper 2254, Third Edition, p. 118. Denver, CO: U.S. Geological Survey.

Hershey, R.L., J.B. Paces, M.J. Singleton, E.M. Kwicklis, D.L. Decker, W.M. Fryer, and S. Earman. 2008. *Geochemical and Isotopic Evaluation of Groundwater Movement in Corrective Action Unit 99: Rainier Mesa and Shoshone Mountain, Nevada Test Site*, DOE/NV/26383-10; Publication No. 45229. Las Vegas, NV: Desert Research Institute.

Hevesi, J.A. 2006. *Net Infiltration of the Death Valley Regional Ground-Water Flow System, Nevada and California*. As accessed at http://water.usgs.gov/GIS/metadata/usgswrd/XML /pp1711_rch_model1.xml. Reston, VA: U.S. Geological Survey.

Hevesi, J.A., A.L. Flint, and L.E. Flint. 2003. *Simulation of Net Infiltration and Potential Recharge Using a Distributed-Parameter Watershed Model of the Death Valley Region, Nevada and California.* Water-Resources Investigations Report 03-4090. Sacramento, CA: U.S. Geological Survey.

Hildenbrand, T.G., V.E. Langenheim, E.A. Mankinen, and E.H. McKee. 1999. *Inversion of Gravity Data To Define the Pre-Tertiary Surface and Regional Structures Possibly Influencing Ground-Water Flow in the Pahute Mesa-Oasis Valley Region, Nye County, Nevada,* Open-File Report 99-49. Menlo Park, CA: U.S. Geological Survey.

Houser, F.N., R.E. Davis, and W.L. Emerick. 1961. *Geologic Reconnaissance of Granite Intrusive Masses at Gold Meadows, Tem Piute, and Trappman's Camp, Lincoln and Nye Counties, Nevada, and Comparison with Climax Stock of the Nevada Test Site,* TEI-793; Open File Report 61-70. Washington, DC: U.S. Geological Survey.

IT, see IT Corporation.

Ingraham, N.L., B.F. Lyles, R.L. Jacobson, and J.W. Hess. 1991. "Stable Isotopic Study of Precipitation and Spring Discharge in Southern Nevada." In *Journal of Hydrology*, Vol. 125(3–4): pp. 243–258.

IT Corporation. 1996a. *Groundwater Recharge and Discharge Data Documentation Package (Underground Test Area Subproject Phase I Data Analysis Documentation, Volume III*). Prepared for the U.S. Department of Energy, Nevada Operations Office. Las Vegas, NV.

IT Corporation. 1996b. *Hydrologic Parameter Data Documentation Package (Underground Test Area Subproject Phase 1 Data Analysis Documentation, Volume IV).* Prepared for the U.S. Department of Energy, Nevada Operations Office. Las Vegas, NV.

IT Corporation. 1996c. *Potentiometric Data Documentation Package (Underground Test Area Subproject Phase 1 Data Analysis Documentation, Volume II).* Prepared for the U.S. Department of Energy, Nevada Operations Office. Las Vegas, NV.

IT Corporation. 1996d. *Regional Geologic Model Data Documentation Package (Underground Test Area Subproject Phase 1 Data Analysis Documentation, Volume I).* Prepared for the U.S. Department of Energy, Nevada Operations Office. Las Vegas, NV.

IT Corporation. 1998. *Report and Analysis of the BULLION Forced-Gradient Experiment,* Rev. 0, DOE/NV/13052-042; ITLV/13052-042; UC-700. Las Vegas, NV.

Jackson, T.R., and J.M. Fenelon. 2018. *Conceptual Framework and Trend Analysis of Water-Level Responses to Hydrologic Stresses, Pahute Mesa–Oasis Valley Groundwater Basin, Nevada, 1966–2016*, Scientific Investigation Report 2018-5064. Reston, VA: U.S. Geological Survey.

Jackson, T.R., and K.J. Halford. 2019. Written communication. Subject: *Groundwater Characterization and Effects of Pumping in the Death Valley Regional Groundwater Flow System, Nevada and California, with Special Reference to Devils Hole.* Reston, VA: U.S. Geological Survey.

Johnson, M.J. 1993. *Micrometeorological Measurements at Ash Meadows and Corn Creek Springs, Nye and Clark Counties, Nevada, 1986-87*, Open-File Report 92-650. Denver, CO: U.S. Geological Survey.

Kane, M.F., M.W. Webring, and B.K. Bhattacharyya. 1981. *A Preliminary Analysis of Gravity and Aeromagnetic Surveys of the Timber Mountain Area, Southern Nevada,* Open-File Report 81-189. Denver, CO: U.S. Geological Survey.

Kwicklis, E. 2009. "Appendix D: Evaluation of Groundwater Travel Times in the PM-OV Flow System from ^{14}C Data." In *Phase I Transport Model of Corrective Action Units 101 and 102: Central and Western Pahute Mesa, Nevada Test Site, Nye County, Nevada*, S-N/99205--111. Las Vegas, NV: Stoller-Navarro Joint Venture.

Kwicklis, E., and I. Farnham. 2014. "Testing the ^{14}C Ages and Conservative Behavior of Dissolved ^{14}C in a Carbonate Aquifer in Yucca Flat, Nevada (USA), Using ^{36}Cl from Groundwater and Packrat Middens." In *Hydrogeology Journal*, Vol. 22(6): pp. 1359–1381.

Kwicklis, E.M., T.P. Rose, and F.C. Benedict, Jr. 2005. *Evaluation of Groundwater Flow in the Pahute Mesa–Oasis Valley Flow System Using Groundwater Chemical and Isotopic Data*, LA-UR-05-4344. Los Alamos, NM: Los Alamos National Laboratory.

Laczniak, R.J., U.S. Geological Survey. 1996. Personal communication to O. Drici (IT Corporation) regarding groundwater discharge in Ash Meadows and Oasis Valley, 13 February. Las Vegas, NV.

Laczniak, R.J., J.C. Cole, D.A. Sawyer, and D.A. Trudeau. 1996. *Summary of Hydrogeologic Controls on Ground-Water Flow at the Nevada Test Site, Nye County, Nevada,* Water-Resources Investigations Report 96-4109. Carson City, NV: U.S. Geological Survey.

Laczniak, R.J., G.A. DeMeo, S.R. Reiner, J.L. Smith, and W.E. Nylund. 1999. *Estimates of Ground-Water Discharge as Determined from Measurements of Evapotranspiration, Ash Meadows Area, Nye County, Nevada,* Water-Resources Investigations Report 99-4079. Carson City, NV: U.S. Geological Survey.

Laczniak, R.J., J.L. Smith, P.E. Elliott, G.A. DeMeo, M.A. Chatigny, and G. Roemer. 2001. *GroundWater Discharge Determined from Estimates of Evapotranspiration, Death Valley Regional Flow System, Nevada and California*, Water-Resources Investigations Report 01-4195. Carson City, NV: U.S. Geological Survey.

Langevin, C.D., J.D. Hughes, E.R. Banta, R.G. Niswonger, S. Panday, and A.M. Provost. 2017. *Documentation for the MODFLOW 6 Groundwater Flow Model: U.S. Geological Survey Techniques and Methods, Book 6, Chapter A55*. Available at https://doi.org/10.3133/tm6A55.

Lee, C.H. 1912. *An Intensive Study of the Water Resources of a Part of Owens Valley, California,* Water-Supply Paper 294. Washington, DC: U.S. Geological Survey.

Lu, Z., E. Kwicklis, T. Miller, and M. Bourret. 2020. Written communication. Subject: *Development and Calibration of the Pahute Mesa Bench Area Groundwater Flow and Tritium Transport Model, Nevada National Security Site*. Los Alamos, NM: Los Alamos National Laboratory.

Maldonado, F. 1977. *Summary of the Geology and Physical Properties of the Climax Stock, Nevada Test Site*, Open-File Report-77-356. Denver, CO: U.S. Geological Survey.

Malmberg, G.T., and T.E Eakin. 1962. *Ground-Water Appraisal of Sarcobatus Flat and Oasis Valley, Nye and Esmeralda Counties, Nevada: Nevada Department of Conservation and Natural Resources,* Ground-Water Resources-Reconnaissance Series Report 10, p 39. Carson City, NV: U.S. Geological Survey.

Mankinen, E.A., T.G. Hildenbrand, G.L. Dixon, E.H. McKee, C.J. Fridrich, and R.J. Laczniak. 1999. *Gravity and Magnetic Study of the Pahute Mesa and Oasis Valley Region, Nye County, Nevada,* Open-File Report 99-303, Version 1.0. Reston, VA: U.S. Geological Survey.

Mankinen, E.A., T.G. Hildenbrand, C.J. Fridrich, E.H. McKee, and C.J. Schenkel. 2003. *Geophysical Setting of the Pahute Mesa-Oasis Valley Region, Southern Nevada*, Report 50. Reno, NV: Nevada Bureau of Mines and Geology.

Maxey, G.B., and T.E. Eakin. 1951. "Ground Water in Railroad, Hot Creek, Reveille, Kawich, and Penoyer Valleys, Nye, Lincoln, and White Pine Counties, Nevada." In *Contributions to the Hydrology of Eastern Nevada,* Water Resources Bulletin No. 12. pp. 127–171. Carson City, NV: State of Nevada, Office of the State Engineer/U.S. Geological Survey.

McKinley, P.W., M.P. Long, and L.V. Benson. 1991. *Chemical Analyses of Water From Selected Wells and Springs in the Yucca Mountain Area, Nevada and Southeastern California,* Open-File Report 90-355. Denver, CO: U.S. Geological Survey.

Middleton, R.S., E.M. Kwicklis, K.H. Birdsell, D.G. Levitt, and J. Hevesi. 2019. *Net Infiltration Models for the Pahute Mesa Area*, LA-UR-16-27513, Rev 1. Los Alamos, NM: Los Alamos National Laboratory.

Moran, J.E., and T.P. Rose. 2003. "A Chlorine-36 Study of Regional Groundwater Flow and Vertical Transport in Southern Nevada." In *Environmental Geology*, Vol. 43(5): 592–605.

Navarro GIS, see Navarro Geographic Information Systems.

N-I, see Navarro-Intera, LLC.

NNSA/NFO, see U.S. Department of Energy, National Nuclear Security Administration Nevada Field Office.

NSTec, see National Security Technologies, LLC.

National Security Technologies, LLC. 2014. Written communication. Subject: *Phase II Hydrostratigraphic Framework Model for Corrective Action Units 101 and 102 Central and Western Pahute Mesa, Nye County Nevada*. November. Las Vegas, NV.

Navarro. 2015. *Pahute Mesa Well Development and Testing Analyses for Wells ER-EC-14 and ER-EC-15, Nevada National Security Site, Nye County, Nevada*, N/2653--006. Las Vegas, NV.

Navarro. 2018. *Pahute Mesa Well Development and Testing Analyses for Wells ER-EC-12 and ER-EC-13, Nevada National Security Site, Nye County, Nevada*, Rev. 0, N/0002653--051. Las Vegas, NV.

Navarro. 2019a. Written communication. "PM_Extended_HFM_ovpmv28." UGTA Technical Data Repository Database Identification Number UGTA-4-2028, Las Vegas, NV.

Navarro. 2019b. Written communication. Subject: "UGTA Geochemistry Database," UGTA Technical Data Repository Database Identification Number UGTA-4-129. Las Vegas, NV.

Navarro. 2020. Written communication. Subject: *Phase II Geochemical and Isotopic Evaluation of Groundwater Flow in the Pahute Mesa–Oasis Valley Flow System, Nevada*. Las Vegas, NV

Navarro Geographic Information Systems. 2019–2020. ESRI ArcGIS Software.

Navarro-Intera, LLC. 2012. *Pahute Mesa Well Development and Testing Analyses for Wells ER-20-8 and ER-20-4, Nevada National Security Site, Nye County, Nevada,* Rev. 0, N-I/28091--061. Las Vegas, NV.

Navarro-Intera, LLC. 2013. *Phase I Flow and Transport Model Document for Corrective Action Unit 97: Yucca Flat/Climax Mine, Nevada National Security Site, Nye County, Nevada*, Rev. 1, N-I/ 28091--080. Las Vegas, NV.

Navarro-Intera, LLC. 2014. Written communication. Subject: *Pahute Mesa Well Development and Testing Analyses for Wells ER-EC-12 and ER-EC-13*, *Nevada National Security Site, Nye County, Nevada*. Las Vegas, NV.

Neuman, S.P. 1990. "Universal Scaling of Hydraulic Conductivities and Dispersivities in Geologic Media." In *Water Resources Research*, Vol. 26(8): pp. 1749–1758. Washington, DC: American Geophysical Union.

Nichols, W.D. 1993. "Estimating Discharge of Shallow Groundwater by Transpiration from Greasewood in the Northern Great Basin." In *Water Resources Research*, Vol. 29(8): pp. 2771–2778. Washington, DC: American Geophysical Union.

Nichols, W.D. 2001. *Regional Ground-Water Evapotranspiration and Ground-Water Budgets, Great Basin, Nevada*, Professional Paper 1628. Denver, CO: U.S. Geological Survey.

Nichols, W.D., R.J. Laczniak, G.A. DeMeo, and T.R. Rapp. 1997. *Estimated Ground-Water Discharge by Evapotranspiration, Ash Meadows Area, Nye County, Nevada*, *1994*, Water-Resources Investigations Report 97-4025. Denver, CO: U.S. Geological Survey.

Oberlander, P.L., D. McGraw, and C. E. Russell. 2007. *Hydraulic Conductivity With Depth for Underground Test Area (UGTA) Wells,* DOE/NV/26383-08; Publication No. 45228. Las Vegas, NV: Desert Research Institute, Water Resources Center.

Parkhurst, D.L., and C.A.J. Appelo. 1999. *User's Guide to PHREEQC (Version 2)–A Computer Program for Speciation, Batch-Reaction, One-Dimensional Transport, and Inverse Geochemical Calculations,* Water-Resources Investigations Report 99-4259. Denver, CO: U.S. Geological Survey.

Plummer, L.N., E.C. Prestemon, and D.L. Parkhurst. 1994. *An Interactive Code (NETPATH) for Modeling Net Geochemical Reactions Along a Flow Path*, Version 2.0, Water-Resources Investigations Report 94-4169. Denver, CO: U.S. Geological Survey.

Plummer, M.A., F.M. Phillips, J. Fabryka-Martin, H.J. Turin, P.E. Wigand, and P. Sharma. 1997. "Chlorine-36 in Fossil Rat Urine: An Archive of Cosmogenic Nuclide Deposition during the Past 40,000 Years." In *Science,* Vol. 277(5325): pp. 538–541.

Pottorff, E.J., S.J. Erikson, and M.E. Campana. 1987. *Hydrologic Utility of Borehole Temperatures in Areas 19 and 20, Pahute Mesa, Nevada Test Site*, Publication No. 45275. Las Vegas, NV: Desert Research Institute.

PRISM Climate Group. 2012. "PRISM Climate Data, 30-Year Normals, Norm81m dataset." Created July 2012: Accessed May 2014 at http://prism.oregonstate.edu. Corvallis, Oregon State University.

Prothro, L.B., and S.L. Drellack, Jr. 1997. *Nature and Extent of Lava-Flow Aquifers Beneath Pahute Mesa, Nevada Test Site,* DOE/NV-11718-156. Las Vegas, NV: Bechtel Nevada.

Prothro, L.B., S.L. Drellack, and J.M. Mercadante. 2009a. *A Hydrostratigraphic System for Modeling Groundwater Flow and Radionuclide Migration at the Corrective Action Unit Scale, Nevada Test Site and Surrounding Areas, Clark, Lincoln, and Nye Counties, Nevada*, DOE/NV/25946--630. Las Vegas, NV: National Security Technologies, LLC.

Prothro, L.B., S.L. Drellack, D.N. Haugstad, H.E. Huckins-Gang, and M.J. Townsend. 2009b. *Observations on Faults and Associated Permeability Structures in Hydrogeologic Units at the Nevada Test Site*, DOE/NV/25946--690. Las Vegas, NV: National Security Technologies, LLC.

RamaRao, B.S., A.M. Lavenue, G. de Marsily, and M.G. Marietta. 1995. "Pilot Point Methodology for Automated Calibration of an Ensemble of Conditionally Simulated Transmissivity Fields 1. Theory and Computational Experiments." In *Water Resources Research*, Vol. 31(3): pp. 475–493.

Rawling, G.C., L.B. Goodwin, and J.L. Wilson. 2001. "Internal Architecture, Permeability Structure, and Hydrologic Significance of Contrasting Fault-Zones Types." In *Geology,* Vol. 29(1): pp. 43–46.

Reeves, D.M., K.D. Smith, R. Parashar, C. Collins, and K.M. Heintz. 2017. *Investigating the Influence of Regional Stress on Fault and Fracture Permeability at Pahute Mesa, Nevada National Security Site*, DOE/NV/0000939-41; Publication No. 45275. Las Vegas, NV: Desert Research Institute.

Reiner, S.R. 2007. *Ground-Water Temperature Data, Nevada Test Site and Vicinity, Nye, Clark, and Lincoln Counties, Nevada, 2000–2006,* Data Series 269. Carson City, NV: U.S. Geological Survey.

Reiner, S.R., R.J. Laczniak, G.A. DeMeo, J. LaRue Smith, P.E. Elliott, W.E. Nylund, and C.J. Fridrich. 2002. *Ground-Water Discharge Determined from Measurements of Evapotranspiration, Other Available Hydrologic Components, and Shallow Water-Level Changes, Oasis Valley, Nye County, Nevada,* Water-Resources Investigations Report 01-4239. Carson City, NV: U.S. Geological Survey.

Robinson, T.W. 1958. *Phreatophytes*, Water-Supply Paper 1423. Washington DC: U.S. Geological Survey.

Rose, T.P., F.C. Benedict, J.M Thomas, W.S. Sicke, R.L. Hershey, J.B. Paces, I.M. Farnham, and Z.E. Peterman. 2002. *Geochemical Data Analysis and Interpretation of the Pahute Mesa - Oasis Valley Groundwater Flow System, Nye County, Nevada*. Lawrence Livermore National Laboratory report attached to a memorandum to files by W. Drici (Stoller-Navarro Joint Venture), 23 February 2004. Las Vegas, NV.

Rose, T.P., F.C. Benedict, Jr., J.M. Thomas, W.S. Sicke, R.L. Hershey, J.B. Paces, I.M. Farnham, and Z.E. Peterman. 2006. *Geochemical Data Analysis and Interpretation of the Pahute Mesa–Oasis Valley Groundwater Flow System, Nye County, Nevada, August 2002*, UCRL-TR-224559. Livermore, CA: Lawrence Livermore National Laboratory.

Rovey, C.W., II, and D.S. Cherkauer. 1995. "Scale Dependency of Hydraulic Conductivity Measurements." In *Ground Water*, Vol. 33(5): pp. 769–780.

Rush, F.E. 1970. *Regional Ground-Water Systems in the Nevada Test Site Area, Nye, Lincoln, and Clark Counties, Nevada,* Division of Water Resources, Reconnaissance Series, Report 54, p. 21. Carson City, NV: Nevada Department of Conservation and Natural Resources, Division of Hydrologic Sciences.

Russell, C.E., D. McGraw, and P.L. Oberlander, 2011. *Evaluation of Borehole Flow Logging for Underground Test Area Well ER-20-8#2,* DOE/NV/26383-LTR2011-01. Las Vegas, NV: Desert Research Institute, Water Resources Center.

SNJV, see Stoller-Navarro Joint Venture.

Sawyer, D.A., R.J. Fleck, M.A. Lanphere, R.G. Warren, D.E. Broxton, and M.R. Hudson. 1994. "Episodic Caldera Volcanism in the Miocene Southwestern Nevada Volcanic Field: Revised Stratigraphic Caldera Framework, $^{40}Ar/^{39}Ar$ Geochronology, and Implications for Magmatism and Extension." In *Geological Society of America Bulletin*, Vol. 106(10): pp. 1304–1318.

Schoff, S.L., and J.E. Moore. 1964. *Chemistry and Movement of Ground Water, Nevada Test Site*, Report TEI-838. Denver, CO: U.S. Geological Survey.

Slate, J.L., M.E. Berry, P.D. Rowley, C.J. Fridrich, K.S. Morgan, J.B. Workman, O.D. Young, G.L. Dixon, V.S. Williams, E.H. McKee, D.A. Ponce, T.G. Hildenbrand, W.C. Swadley, S.C. Lundstrom, E.B. Ekren, R.G. Warren, J.C. Cole, R.J. Fleck, M.A. Lanphere, D.A. Sawyer, S.A. Minor, D.J. Grunwald, R.J. Laczniak, C.M. Menges, J.C. Yount, and A.S. Jayko. 1999. *Part A. Digital Geologic Map of the Nevada Test Site and Vicinity, Nye, Lincoln, and Clark Counties, Nevada, and Inyo County, California, Revision 4*, Open-File Report 99-554-A, scale 1:120,000. Denver, CO: U.S. Geological Survey.

Snyder, R.P. 1977. *Geology of the Gold Meadows Stock, Nevada Test Site* (Areas 12-26), Open-File Report 474-179. Denver, CO: U.S. Geological Survey.

Stoller-Navarro Joint Venture. 2004a. *Hydrologic Data for the Groundwater Flow and Contaminant Transport Model of Corrective Action Units 101 and 102: Central and Western Pahute Mesa, Nye County, Nevada*, Rev. 0, S-N/99205--002, Shaw/13052-204. Las Vegas, NV.

Stoller-Navarro Joint Venture. 2004b. *Transferability of Data Related to the Underground Test Area Project, Nevada Test Site, Nye County, Nevada*, Rev. 0, S-N/99205--020. Las Vegas, NV

Stoller-Navarro Joint Venture. 2004c. *Unclassified Source Term and Radionuclide Data for the Groundwater Flow and Contaminant Transport Model of Corrective Action Units 101 and 102: Central and Western Pahute Mesa, Nye County, Nevada*, Rev. 0, S-N/99205--022. Las Vegas, NV.

Stoller-Navarro Joint Venture. 2006. *Groundwater Flow Model of Corrective Action Units 101 and 102: Central and Western Pahute Mesa, Nevada Test Site, Nye County, Nevada,* Rev. 0, S-N/99205--076. Las Vegas, NV.

Stoller-Navarro Joint Venture. 2007. *Addendum to the Groundwater Flow Model of Corrective Action Units 101 and 102: Central and Western Pahute Mesa, Nevada Test Site, Nye County, Nevada*, Rev. 0, S-N/99205--076-ADD. Las Vegas, NV.

Stoller-Navarro Joint Venture. 2009a. *Central and Western Pahute Mesa Phase II Hydrogeologic Investigation Wells Drilling and Completion Criteria,* Rev. 0, S-N/99205--120. Las Vegas, NV.

Stoller-Navarro Joint Venture. 2009b. *Phase I Transport Model of Corrective Action Units 101 and 102: Central and Western Pahute Mesa, Nevada Test Site, Nye County, Nevada*, Rev. 1, S-N/99205--111. Las Vegas, NV.

Sweetkind, D.S., and R.M. Drake, II. 2007. *Characteristics of Fault Zones in Volcanic Rocks near Yucca Flat, Nevada Test Site, Nevada*, Open-File Report 2007-1293. Reston, VA: U.S. Geological Survey.

Theis, C.V. 1935. "The Relation between the Lowering of the Piezometric Surface and the Rate and Duration of Discharge of a Well Using Groundwater Storage." In *Eos, Transactions American Geophysical Union,* Vol. 16(2): pp. 519–524.

Thomas, J.M., F.C. Benedict, Jr., T.P. Rose, R.L. Hershey, J.B. Paces, Z.E. Peterman, I.M. Farnham, K.H. Johannesson, A.K. Singh, K.J. Stetzenbach, G.B. Hudson, J.M. Kenneally, G.F. Eaton, and D.K. Smith. 2002. *Geochemical and Isotopic Interpretations of Groundwater Flow in the Oasis Valley Flow System, Southern Nevada*, DOE/NV/11508-56; Publication No. 45190. Las Vegas, NV: Desert Research Institute.

USGS, see U.S. Geological Survey.

USGS and DOE, see U.S Geological Survey and U.S. Department of Energy.

U.S. Department of Energy, Nevada Operations Office. 1997. *Regional Groundwater Flow and Tritium Transport Modeling and Risk Assessment of the Underground Test Area, Nevada Test Site, Nevada,* DOE/NV--477, UC-700. Las Vegas, NV.

U.S. Department of Energy, Nevada Operations Office. 1999. *Corrective Action Investigation Plan for Corrective Action Units 101 and 102, Central and Western Pahute Mesa, Nevada Test Site, Nevada,* Rev. 1, DOE/NV--516. Las Vegas, NV.

U.S. Department of Energy, National Nuclear Security Administration Nevada Field Office. 2014. *Record of Technical Change to Phase II Corrective Action Investigation Plan for Corrective Action Units 101 and 102: Central and Western Pahute Mesa, Nevada Test Site, Nye County, Nevada,* DOE/NV--1312-Rev. 2; Technical Change No. DOE/NV--1312-Rev. 2 ROTC 2, 25 November. Las Vegas, NV.

U.S. Department of Energy, National Nuclear Security Administration Nevada Field Office. 2015a. *Underground Test Area Activity Quality Assurance Plan, Nevada National Security Site, Nevada*, Rev. 2, DOE/NV--1450-REV.2. Las Vegas, NV.

U.S. Department of Energy, National Nuclear Security Administration Nevada Field Office. 2015b. *United States Nuclear Tests, July 1945 through September 1992,* DOE/NV-209, Rev. 16. Las Vegas, NV.

U.S. Department of Energy, National Nuclear Security Administration Nevada Field Office. 2016. *Completion Report for Well ER-20-12, Corrective Action Units 101 and 102: Central and Western Pahute Mesa*, DOE/NV--1549. Las Vegas, NV.

U.S. Department of Energy Environmental Management Nevada Program. 2018a. *Rainier Mesa/Shoshone Mountain Flow and Transport Model Report Nevada National Security Site, Nevada*, Rev. 1. DOE/NV-1588, Las Vegas, NV.

U.S. Department of Energy, Environmental Management Nevada Program. 2018b. *Record of Technical Change to Underground Test Area Activity Quality Assurance Plan, Nevada National Security Site, Nevada*, Rev. 2, DOE/NV--1450-REV.2; Technical Change No. DOE/NV--1450-REV.2-ROTC-1,5 February. Las Vegas, NV.

U.S. Department of Energy Environmental Management Nevada Program. 2019. *Record of Technical Change to Nevada National Security Site Integrated Groundwater Sampling Plan*, Rev. 1, DOE/NV--1525-REV. 1; ROTC No. DOE/NV--1525-REV.1-ROTC 1, 5 February. Las Vegas, NV.

U.S. Department of Energy, Environmental Management Nevada Program. 2020a. *Pahute Mesa-Oasis Valley Hydrostratigraphic Framework Model for Corrective Action Units 101 and 102: Central and Western Pahute Mesa, Nye County, Nevada*, Rev. 0, DOE/EMNV--0014. Las Vegas, NV.

U.S. Department of Energy Environmental Management Nevada Program. 2020b. *Update to the Phase II Corrective Action Investigation Plan for Corrective Action Units 101 and 102, Central and Western Pahute Mesa, Nevada National Security Site, Nye County, Nevada,* Rev. 1, DOE/EMNV--0018. Las Vegas, NV.

U.S. Geological Survey. 2008a. *Documentation of Computer Program INFIL3.0 – A Distributed-Parameter Watershed Model to Estimate Net Infiltration Below the Root Zone,* Scientific Investigations Report 2008-5006, 99 p. Reston, VA: U.S. Geological Survey.

U.S. Geological Survey. 2008b. *USGS Groundwater Software INFIL3.0 – A Grid-Based, Distributed-Parameter Watershed Model to Estimate Net Infiltration Below the Root Zone.* As accessed at https://water.usgs.gov/nrp/gwsoftware/Infil/Infil.html.

U.S. Geological Survey. 2015. National Water Information System (NWISWeb) http://waterdata.usgs.gov/nwis.

U.S. Geological Survey. 2019. "FloPy: Python Package for Creating, Running, and Post-Processing MODFLOW-Based Models." Accessed at http://https://www.usgs.gov/software/flopy-python-package-creating-running-and-post-processing-modflow-based-models on 8 August.

U.S. Geological Survey and U.S. Department of Energy. 2019. "USGS/U.S. Department of Energy Cooperative Studies in Nevada" web page. As accessed at http://nevada.usgs.gov/doe_nv on 24 July.

Watermark Computing, see Watermark Numerical Computing and Waterloo Hydrogeologic.

Walker, G.E. 1962. *Ground Water in the Climax Stock, Nevada Test Site, Nye County, Nevada*, USGS-TEI-813. Washington, DC: U.S. Geological Survey.

Walker, G.E., and T.E. Eakin. 1963. *Geology and Ground Water of Amargosa Desert, Nevada-California,* Ground-Water Resources - Reconnaissance Series Report 14. Denver, CO: Nevada Department of Conservation and Natural Resources and U.S. Geological Survey.

Warren, R.G., D.A. Sawyer, F.M. Byers, Jr., and G.L. Cole. 2000a. *A Petrographic/Geochemical Database and Stratigraphic and Structural Framework for the Southwestern Nevada Volcanic Field,* LA-UR-00-3791. Los Alamos, NM: Los Alamos National Laboratory.

Warren, R.G., G.L. Cole, and D. Walther. 2000b. *A Structural Block Model for the Three-Dimensional Geology of the Southwestern Nevada Volcanic Field*, LA-UR-00-5866. Los Alamos, NM: Los Alamos National Laboratory Report.

Watermark Numerical Computing and Waterloo Hydrogeologic. 2000. *Visual PEST User's Manual (Includes PEST2000 & WinPEST) - Graphical Model-Independent Parameter Estimation.* Ontario, Canada; and Tampa, FL.

Weeks, E.P., H.L. Weaver, G.S. Campbell, and B.D. Tanner. 1987. *Water Use by Saltcedar and by Replacement Vegetation in The Pecos River Flood Plain Between Acme and Artesia, New Mexico,* Professional Paper 491-G, p. 33. Denver, CO: U.S. Geological Survey.

White, W.N. 1932. *A Method of Estimating Ground-Water Supplies Based on Discharge by Plants and Evaporation from Soil,* Water-Supply Paper 659-A, p. 165. Denver, CO: U.S. Geological Survey.

White, A.F. 1979. *Geochemistry of Ground Water Associated with Tuffaceous Rocks, Oasis Valley, Nevada*, Professional Paper 712-E. Denver, CO: U.S. Geological Survey.

White, A.F., and N.J. Chuma. 1987. "Carbon and Isotopic Mass Balance Models of Oasis Valley-Fortymile Canyon Groundwater Basin, Southern Nevada." In *Water Resources Research*, Vol. 23(4): pp. 571–582. Washington, DC: American Geophysical Union.

Winograd, I.J., and W. Thordarson. 1975. *Hydrogeologic and Hydrochemical Framework, South-Central Great Basin, Nevada-California, with Special Reference to the Nevada Test Site,* Professional Paper 712-C. Washington, DC: U.S. Geological Survey.

Wurtz, J., and K. Day. 2018. Written communication. Subject: "Pahute Mesa Phase II HFM: Thirsty Canyon Lineament Alternative." Las Vegas, NV: Navarro Research and Engineering.

Young, A.A., and H.F. Blaney. 1942. *Use of Water by Native Vegetation,* Division of Water Resources Bulletin 50, 154 p. Sacramento, CA: California Department of Public Works.

Appendix A

Hydrostratigraphic Model Supporting Information

A.1.0 DESCRIPTION OF THE PM-OV MODEL LAYERS

Brief descriptions of the HSUs used to construct the PM-OV model are provided in Table A-1. They are listed in approximate order from surface to basement, although some are laterally rather than vertically contiguous, and not all units are present in all parts of the model area.

Table A-1
HSUs of the PM-OV HFM
(Page 1 of 14)

Model Layer Number	HSU (Symbol)	Dominant HGU(s) [a]	Stratigraphic Unit Map Symbols [b]	General Description
77	alluvial aquifer (AA) (this term is also used to designate an HGU)	AA	Qay, QTc, Qs, Qam, QTa, QTu, Qb, Tgy, Tgc, Tgm, Tgyx, Tt	Consists mainly of alluvium that fills extensional basins such as Gold Flat, Crater Flat, Kawich Valley, and Sarcobatus Flat. Also includes generally older Tertiary gravels, tuffaceous sediments, and nonwelded tuffs (where thin) that partially fill other basins such as Oasis Valley and the moat of the TMCC. In the eastern moat area of the TMCC, includes intercalated partially welded ash-flow tuff of the Thirsty Canyon Group.
76	younger volcanic composite unit (YVCM)	LFA, WTA, VTA	Typ	A minor unsaturated HSU that consists of Pliocene to late Miocene basaltic rocks at Thirsty Mountain and Buckboard Mesa.
75	Thirsty Canyon volcanic aquifer (TCVA)	WTA, LFA, lesser VTA	Ttg, Tth, Tts, Ttt, Ttp, Ttc	Consists mainly of welded ash-flow tuff and lava of the Thirsty Canyon Group. Unit is very thick within the Black Mountain caldera. Also is present east and south of the caldera, including the northwestern moat area of the TMCC and the northern portion of the Oasis Valley basin.
74	detached volcanics composite unit (DVCM)	WTA, LFA, TCU	Tf through Tq	Consists of a very complex distribution of lavas and tuffs that form a relatively thin, highly extended interval above the FC-BH detachment fault in the southwestern portion of the model area. Unit is locally hydrothermally altered.
73	detached volcanics aquifer (DVA)	WTA, LFA	Tgyx, Tf, Tma, Tmr	Consists of welded ash-flow tuff and lava assigned to the Ammonia Tanks Tuff and units of the Volcanics of Fortymile Canyon. Although (like the DVCM) the DVA also overlies the FC-BH detachment fault, it is considered a separate HSU because of the preponderance of WTAs and LFAs that compose the HSU and much smaller degree of hydrothermal alteration present.
72	Shoshone Mountain lava-flow aquifer (SMLFA)	LFA	Tfs	Rhyolitic lava and related dikes, plugs, tuff, and tuff breccias of the rhyolite of Shoshone Mountain. According to Slate et al. (1999): “Forms a volcanic dome straddling the southeastern topographic margin of the Rainier Mesa caldera.” A topographically prominent, but unsaturated HSU.
71	Fortymile Canyon composite unit (FCCM)	TCU	Tfu, Tfs, Tfd, Tfr, Tfb, Tfl, Tff	Consists mainly of zeolitic to quartzo-feldspathic nonwelded and bedded tuffs of the Volcanics of Fortymile Canyon that encapsulate intercalated rhyolite lava flows and welded tuffs which are assigned to different and separate HSUs. The FCCM is generally confined within the moat of the TMCC, where the unit forms a “depositional” ring around the Timber Mountain resurgent dome. Unit is thickest within the northwestern moat of the TMCC where measured thicknesses are 917 m (3,008 ft) at Well ER-EC-2a and greater than 500 m (1,640 ft) at Well ER-EC-13.

Table A-1
HSUs of the PM-OV HFM
(Page 2 of 14)

Model Layer Number	HSU (Symbol)	Dominant HGU(s) [a]	Stratigraphic Unit Map Symbols [b]	General Description
70	Fortymile Canyon upper mafic lava-flow aquifer (FCUMLFA)	LFA	Tfd, Tft, Tfb	Consists of as many as 12 individual flows of dense to scoriaceous trachybasalt, basaltic trachyandisite, and trachyandesite assigned to the lavas of Dome Mountain. Exposed extensively in the southeastern Timber Mountain moat (Tfd in Slate et al., 1999) where it forms a high volcanic edifice (i.e., Dome Mountain). Encountered in Well ER-30-1 (116.4–217.3-m [382–713-ft] depth interval). Saturated only in its northernmost extent in the eastern Timber Mountain moat. Modeled as a property model within the FCCM.
69	Fortymile Canyon upper lava-flow aquifer 1 (FCULFA1)	LFA, lesser VTA	Tfbw	Consists of a single buried, but shallow, rhyolitic lava flow of the rhyolite of Beatty Wash. Modeled as having limited extent beneath the northwestern Timber Mountain moat. Known only from a single occurrence in Well ER-EC-13 (6.1–147.8-m [20–485-ft] depth interval). Mostly unsaturated, but very basal portions maybe saturated in places. Modeled as a property model within the FCCM.
68	Fortymile Canyon upper lava-flow aquifer 2 (FCULFA2)	LFA	Tfbw	Consists of a single rhyolitic lava flow of the rhyolite of Beatty Wash exposed in the northwestern Timber Mountain moat. Also encountered in Well ER-EC-2a (0–227.4-m [0–746-ft] depth interval). Conceptualized and modeled as an isolated LFA, but could possibly correlate to, and connect with, FCULFA1. Mostly unsaturated, but basal portion is likely saturated in most places. Modeled as a property model within the FCCM.
67	Fortymile Canyon upper lava-flow aquifer 3 (FCULFA3)	LFA	Tfbw	Consists of a single buried rhyolitic lava flow of the rhyolite of Beatty Wash. Known only from a single occurrence in UE-18r (137.2–286.5-m [450–940-ft] depth interval). Conceptualized and modeled as an isolated LFA of limited extent beneath the northern Timber Mountain moat. Unsaturated. Modeled as a property model within the FCCM.
66	Fortymile Canyon upper lava-flow aquifer 4 (FCULFA4)	LFA, lesser TCU	Tfb	Consists of a buried sequence of rhyolitic lava-flow lithologies of the Beatty Wash Formation that likely represent 2 stacked individual flow units beneath the northwestern Timber Mountain moat. Known only from a single occurrence in Well ER-EC-13 (505.4–771.1-m [1,658–2,530-ft] depth interval). Conceptualized and modeled as having limited extent. Saturated. Modeled as a property model within the FCCM.
65	Fortymile Canyon upper lava-flow aquifer 5 (FCULFA5)	LFA	Tfbw	Consist of a single buried rhyolitic lava flow of the rhyolite of Beatty Wash occurring beneath the southwestern Timber Mountain moat. Known only from a single occurrence in the MYJO Coffer well (387.1–433.4-m [1,270–1,422-ft] depth interval). Conceptualized and modeled as an isolated LFA of limited extent. Saturated. Modeled as a property model within the FCCM.

Table A-1
HSUs of the PM-OV HFM
(Page 3 of 14)

Model Layer Number	HSU (Symbol)	Dominant HGU(s) [a]	Stratigraphic Unit Map Symbols [b]	General Description
64	Fortymile Canyon upper lava-flow aquifer 6 (FCULFA6)	LFA, lesser TCU	Tfb	Consists of a thick and extensive sequence of rhyolitic lava flows of the Beatty Wash Formation, and that outcrop along Beatty Wash in the southern Timber Mountain moat. Encountered in Well ER-EC-7 (12.5–422.5-m [41–1,386-ft] depth interval). Lower portions saturated. Modeled as a property model within the FCCM.
63	Fortymile Canyon upper lava-flow aquifer 7 (FCULFA7)	LFA, lesser TCU	Tf	Consists of a buried sequence of rhyolitic lava flows of the Volcanics of Fortymile Canyon, and that occur beneath the southern Timber Mountain moat. Known only from a single occurrence in the lower portion of Well ER-EC-7 (352.0–422.5-m [1,155–1,386-ft] depth interval). Conceptualized and modeled as an isolated LFA with limited extent. Modeled as a property model within the FCCM.
62	Fortymile Canyon welded-tuff aquifer 1 (FCWTA1)	WTA	Tfb	Consists of a buried interval welded ash-flow tuff of the Beatty Wash Formation that occurs in the northwestern portion of the Timber Mountain moat. Known only from a single occurrence in Well ER-EC-2a (830.9–867.5-m [2,726–2,846-ft] depth interval). Conceptualized and modeled as an isolated WTA of limited extent. Modeled as a property model within the FCCM.
61	Fortymile Canyon welded-tuff aquifer (FCWTA)	WTA, lesser VTA and TCU	Tfb	Consists mostly of partially to moderately welded ash-flow tuff that occurs in the lower portion of the Volcanics of Fortymile Canyon in the southwestern portion of the TMCC. Exposed along the west side of the Transvaal Hills where it is 30 to 60 m (100–200 ft) thick and consists of moderately welded tuff in upper part grading to nonwelded vitric tuff (i.e., VTA) at base (Lipman et al., 1966). West of the Transvaal Hills the unit is deeply buried and much thicker, and consists of at least 2 separate welded ash-flow tuff units with the upper unit described as moderately welded and the lower unit as partially welded. The buried portion is known only from a single occurrence in the MYJO Coffer well (529.4–776.3-m [1,737–2,547-ft] depth interval). Zeolitic or quartzo-feldspathic bedded tuff of unknown thickness likely occurs between the 2 buried ash-flow tuff intervals. Mostly saturated except for portions near surface exposures in the Transvaal Hills.

Table A-1
HSUs of the PM-OV HFM
(Page 4 of 14)

Model Layer Number	HSU (Symbol)	Dominant HGU(s) [a]	Stratigraphic Unit Map Symbols [b]	General Description
60	Fortymile Canyon lower lava-flow aquifer (FCLLFA)	LFA, lesser TCU	Tff	Consists of rhyolitic to trachytic lava flows that likely straddle the stratigraphic contact between the Fortymile Canyon and Timber Mountain Groups. The HSU includes two geographically separate occurrences. Between the Transvaal Hills and Timber Mountain the HSU correlates to the rhyodacite of Fleur-de-lis Ranch where it has a maximum exposed thickness of approximately 300 m (1,000 ft) along the west side of Timber Mountain (Slate et al., 1999). Farther west in Oasis Valley basin the lava flows correlate to the rhyodacite of Fleur-de-Lis Ranch and trachyte of East Cat Canyon. This buried occurrence is known only from a single occurrence in the MYJO Coffer well (776.3–855.0-m [2,547–2,805-ft] depth interval). Zeolitic or quartzo-feldspathic bedded tuff of unknown thickness likely occurs between these two units in Oasis Valley basin. Saturated within the Oasis Valley basin, but portions near surface exposures along the west side of Timber Mountain are unsaturated.
59	Fortymile Canyon lower mafic lava-flow aquifer (FCLMLFA)	LFA	Tfbb	Consists of basaltic lava that occurs at the base of the Volcanics of Fortymile Canyon in the eastern Timber Mountain moat. Modeled as having no surface exposure, but may correlate to exposures of older basalt mapped by Byers et al. (1966) in Fortymile Canyon. HSU penetrated in Well ER-30-1 from the depths 289.6–365.2 m (950–1,198 ft) where it directly overlies welded Ammonia Tanks Tuff. Saturated.
58	Ammonia Tanks mafic lava-flow aquifer (ATMLFA)	LFA	Tmay	Consists of trachytic lava flows exposed along the eastern flank of Timber Mountain, and modeled as extending into the subsurface of the southeastern Timber Mountain moat. Maximum exposed thickness is 150 m (490 ft) (Slate et al., 1999). Includes a small isolated rhyolite dome on the northern flank of Timber Mountain. Deeper portions are saturated.

Table A-1
HSUs of the PM-OV HFM
(Page 5 of 14)

Model Layer Number	HSU (Symbol)	Dominant HGU(s) [a]	Stratigraphic Unit Map Symbols [b]	General Description
57	Buttonhook Wash welded-tuff aquifer (BWWTA)	WTA	Tmaw	Consists of welded ash-flow tuff assigned to the tuff of Crooked Canyon and tuff of Buttonhook Wash. Exposed along the base of Timber Mountain (Tmb and Tmc in Byers et al., 1976). Unit is not exposed or encountered outside the margins of the TMCC. Interpreted to be in the subsurface of the southern and northwestern moat area (1,400.3–1,410.0 m [4,594–4,626-ft] depth in Well ER-EC-2a), and between Timber Mountain and the Transvaal Hills. A relatively thin subsurface occurrence is present in Well ER-EC-8 (439.5–448.7-m [1,442–1,472-ft] depth interval), and indicating that a portion of the unit flowed over or around the northern end of the Transvaal Hills. Unit is not present in MYJO Coffer #1, and thus its presence west of the Transvaal Hills is limited to the area around ER-EC-8. Consists of landslide breccia in Well ER-EC-5 (246.9–305.4-m [810–1,002-ft] depth) that is sourced from Timber Mountain during resurgent doming (DOE/NV, 2004), and thus may be a poor aquifer in this area. An isolated occurrence is also located in the northeastern Timber Mountain moat (262.7–328.0-m [862–1,076-ft] depth in Well ER-18-2). Becomes saturated at deeper levels away from exposures along Timber Mountain. Maximum exposed thickness is 250 m (820 ft) (Slate et al., 1999). Note: Surface exposures in model are mainly from Byers et al. (1976).
56	Buttonhook Wash confining unit (BWCU)	TCU	Tmaw	Zeolitic nonwelded tuff that occurs between the welded ash-flow tuffs of the Tuff of Buttonhook Wash and Ammonia Tanks Tuff. BWCU has a distribution similar to the BWWTA. Exposures of BWCU are probably present along the western base of Timber Mountain underlying BWWTA (e.g., Tmfu and Tmfl in Lipman et al. [1966]), but are not demarcated/mapped in the model. Maximum cumulative thickness of Tmfu and Tmfl in Lipman et al. (1966) is 83.8 m (275 ft).
55	Ammonia Tanks welded-tuff aquifer (ATWTA)	WTA	Tma	Welded ash-flow tuff assigned to the Ammonia Tanks Tuff. Very thick within the structural margins of the Ammonia Tanks caldera. Thinner, but still thick and extensive within the topographic low formed by the Rainier Mesa caldera. Exposed in the Transvaal Hills and on Timber Mountain. Includes nonwelded zones in the eastern portion of the Ammonia Tanks caldera (Tmb, Tmd, Tmf in Carr and Quinlivan [1966]). This heterogeneity is addressed with the inclusion of ATCCU as a property model within the ATWTA HSU. All units assigned as Tma in Slate et al. (1999) that occur within the margins of the TMCC represent ATWTA surface exposures (with the exception of those units at the base of Timber Mountain that may be assigned to BWWTA after Byers et al. [1976]).

Table A-1
HSUs of the PM-OV HFM
(Page 6 of 14)

Model Layer Number	HSU (Symbol)	Dominant HGU(s) [a]	Stratigraphic Unit Map Symbols [b]	General Description
54	Ammonia Tanks caldera confining unit (ATCCU)	TCU	Tma	Mostly nonwelded tuff exposed on the eastern portion of Timber Mountain (Tmb in Carr and Quinlivan [1966]). Expected to be altered where saturated. Modeled only in the subsurface beneath the northeastern and southeastern portions of the Ammonia Tanks caldera. This unit provides a conceptualization of the known heterogeneity in the upper and middle portions of the intra-caldera Ammonia Tanks Tuff in the eastern portion of the Ammonia Tanks caldera. It is addressed through the use of a property model within the ATWT HSU. Exposed along the eastern side of Timber Mountain where it is unsaturated and grouped within the ATWT aquifer due to the complex fault-controlled exposures on Timber Mountain. Grouped with Tma and Tml in Slate et al. (1999) and Byers et al. (1976), respectively. Present in UE-18r (897.6–1,027.2 m [2,945–3,370 ft]) as 129.5 m (425 ft) of potassic nonwelded tuff.
53	Timber Mountain upper welded-tuff aquifer (TMUWTA)	WTA, lesser LFA and TCU	Tmap	Unit consists predominately of extra-caldera welded ash-flow tuff of the mafic-poor member of the Ammonia Tanks Tuff. Known only from a single occurrence in Well ER-EC-4 where it is 265.8-m (872-ft) thick. The top of the unit at Well ER-EC-4 consists of 3.7 m (12 ft) of mafic lava (i.e., LFA) overlying 15.8 m (52 ft) of zeolitic to quartzo-feldspathic bedded and nonwelded tuff (i.e., TCU). The remaining 89% of the HSU consists of welded ash-flow tuff (i.e. WTA). The HSU is conceptualized as occurring within the northern portion of the Oasis Valley basin of Fridrich et al. (2007) south of the Black Mountain caldera, and between the Hogback fault on the west and the TMCC on the east. Although poorly constrained, this conceptualization is based on the thick extra-caldera occurrence in Well ER-EC-4, which suggests deposition within a structural basin. Mostly saturated except for westernmost portion.
52	Tannenbaum Hill lava-flow aquifer (THLFA)	LFA, minor VTA and TCU	Tmat	Composed entirely of rhyolitic lava of the rhyolite of Tannenbaum Hill. Main occurrence is on the Bench, and just outside the northwestern structural boundary of the TMCC. Mostly unsaturated, but very basal portions become saturated locally.
51	Tannenbaum Hill composite unit (THCM)	Mostly TCU, lesser WTA	Tmat	Zeolitic tuff and lesser welded ash-flow tuff of the rhyolite of Tannenbaum Hill that occurs stratigraphically below Tannenbaum Hill lava and above the rhyolite of Fluorspar Canyon. Distribution is similar to the THLFA. Lower portions to end to be saturated.

Table A-1
HSUs of the PM-OV HFM
(Page 7 of 14)

Model Layer Number	HSU (Symbol)	Dominant HGU(s) [a]	Stratigraphic Unit Map Symbols [b]	General Description
50	Tannenbaum Hill confining unit (THCU)	TCU	Tmat, Tmab, Tmrb	Nonwelded tuff and tuff breccia occurring between the Tannenbaum Hill lava and Rainier Mesa Tuff (1,184.5–1,367.0-m [3,886–4,485-ft] depth in well UE-18r). Also includes nonwelded, bedded tuffs assigned to the bedded Ammonia Tanks Tuff (Tmab) and bedded Rainier Mesa Tuff (Tmrb) of Ferguson et al. (1994). Nonwelded tuffs are assumed to be zeolitic because of the unit's deep intra-caldera location below the water table. It is also assumed that thin nonwelded and bedded tuffs are always present between the Ammonia Tanks and Rainier Mesa Tuffs within the TMCC as observed in numerous drills holes on Pahute Mesa. As a result, the unit is present in an intervening position everywhere the Ammonia Tanks Tuff overlies the Rainier Mesa Tuff within the TMCC. Thin unmapped exposures of THCU are assumed to be present in the Transvaal Hills. Mostly saturated, except for elevated occurrences such as Timber Mountain, Transvaal Hills, and portions of the Bench.
49	Timber Mountain welded-tuff aquifer (TMWTA)	WTA, minor VTA	Tmr, Tma	Consists mainly of welded ash-flow tuff of the Rainier Mesa Tuff where it occurs outside the Rainier Mesa caldera (i.e., extra-caldera). Includes minor amounts of unsaturated welded ash-flow tuff and vitric bedded tuff of the overlying Ammonia Tanks Tuff outside the limit of the TMUWTA (e.g., in eastern Pahute Mesa). Mostly unsaturated except for deeper portions in the extreme northwest portion of Pahute Mesa, southern portions of the Bench, and in the Oasis Valley basin between the western margins of the TMCC and the Hogback fault.
48	Timber Mountain lower vitric-tuff aquifer (TMLVTA)	VTA	Tmr, Tmrh, Tmrf, Tp	Consists mainly of vitric (i.e., unaltered) nonwelded and bedded tuffs of the lower portion of the Timber Mountain Group. These include the basal nonwelded portion of the Rainier Mesa Tuff, and nonwelded and bedded tuffs of the underlying tuff of Holmes Road and tuff of Fluorspar Canyon. Locally includes minor intervals of vitric lithologies at the top the underlying Paintbrush Group. Mostly unsaturated except for western portions on Pahute Mesa where the lower portion becomes saturated.

Table A-1
HSUs of the PM-OV HFM
(Page 8 of 14)

Model Layer Number	HSU (Symbol)	Dominant HGU(s) [a]	Stratigraphic Unit Map Symbols [b]	General Description
47	Rainier Mesa welded-tuff aquifer (RMWTA)	WTA	Tmr, Tmc	Thick and extensive intra-caldera welded ash-flow tuff assigned to the Rainier Mesa Tuff. Exposed only in the Transvaal Hills, where it also includes debris-flow breccia (Tmc in Slate et al. [1999]) for this study. Present everywhere within the structural margins of the Rainier Mesa caldera. Includes both the mafic-rich and mafic-poor members of Ferguson et al. (1994). Modeled thickness is approximately 1,200 m (4,000 ft). Fridrich et al. (2007) shows intra-caldera Rainier Mesa Tuff up to 2,500 m (8,000 ft) thick. Maximum exposed intra-caldera thickness is 500 m (1,640 ft) but base is not exposed (Slate et al., 1999). Mostly saturated, except for elevated occurrences such as Timber Mountain, Transvaal Hills, and portions of the Bench where the uppermost portions are unsaturated.
46	Fluorspar Canyon confining unit (FCCU)	TCU	Tmrf	Consists of zeolitic, nonwelded tuff of the rhyolite of Fluorspar Canyon. Locally, includes minor zeolitic lithologies (e.g., pumiceous lava) of the underlying top-most portion of the Paintbrush Group. HSU is confined to the Bench, where it has been structurally down-dropped below the water table, resulting in zeolitic alteration of the unit. On Pahute Mesa to the north, the rhyolite of Fluorspar Canyon is structurally higher, occurring mostly above the water table, and thus is vitric, and assigned to the TMLVTA. Mostly saturated except uppermost portions that are locally unsaturated.
45	Windy Wash aquifer (WWA)	LFA	Tmw	Minor unsaturated HSU consisting of the lava-flow lithofacies of the rhyolite of Windy Wash. Occurs locally along the western (down-thrown) side of the West Greeley fault in Area 20.
44	Paintbrush composite unit (PCM)	WTA, LFA, TCU	Tpc, Tp	Consists mostly of units of the Paintbrush Group that occur in the southern portion of the model area in the vicinity of the Claim Canyon caldera. Unit is dominated by thick, strongly welded Tiva Canyon Tuff within the Claim Canyon caldera. Outside the caldera this unit is more variable, consisting of welded and nonwelded tuff and rhyolitic lava assigned to various formations of the Paintbrush Group. Stratigraphically equivalent units of the Paintbrush Group that occur in the northern portion of the model area beneath Pahute Mesa have been grouped into seven separate HSUs.
43	Comb Peak aquifer (CPA)	LFA	Tpk	Consists of the LFA lithofacies of the rhyolite of Comb Peak at Pahute Mesa. HSU known from only 2 subsurface occurrences in Wells ER-EC-1 and ER-EC-15, where it is interpreted to consist of a single rhyolite lava flow. TCU-like lithofacies (e.g., zeolitic pumiceous lava) that occur at the top and base of the flow are grouped with the hydrostrigraphically adjacent FCCU and UPCU. Mostly saturated on the Bench. Unsaturated north of the Bench on Pahute Mesa.

Table A-1
HSUs of the PM-OV HFM
(Page 9 of 14)

Model Layer Number	HSU (Symbol)	Dominant HGU(s) [a]	Stratigraphic Unit Map Symbols [b]	General Description
42	Post-Benham Paintbrush confining unit (PBPCU)	TCU	Tp	Zeolitic nonwelded tuff, bedded tuff, and pumiceous lava that locally separates the BA from the CPA. Saturated on the Bench. Unsaturated north of the Bench on Pahute Mesa.
41	Benham aquifer (BA)	LFA	Tpb	Lava-flow lithofacies of the rhyolite of Benham. Occurs north of the TMCC and beneath the southwestern portion of Pahute Mesa.
40	upper Paintbrush confining unit (UPCU)	TCU	Tp	Zeolitic nonwelded tuff, bedded tuff, and pumiceous lava that separate the SPA and TCA from overlying aquifers (e.g., BA and CPA).
39	Scrugham Peak aquifer (SPA)	LFA	Tps	Consists of the LFA lithofacies of the rhyolite of Scrugham Peak. HSU is exposed along the south face of Pahute Mesa, and was encountered in Wells ER-20-8 and ER-20-8-2. Zeolitic pumiceous lava that occurs at the top and of the flow in these wells are group with the overlying UPCU.
38	Middle Paintbrush confining unit (MPCU)	TCU	Tp	Zeolitic nonwelded and bedded tuff that separate the TCA and the overlying SPA.
37	Tiva Canyon aquifer (TCA)	WTA	Tpc	The welded ash-flow lithofacies of the Pahute Mesa lobe of the Tiva Canyon Tuff beneath Pahute Mesa. Only saturated west of the Boxcar fault.
36	Paintbrush vitric-tuff aquifer (PVTA)	VTA	Pre-Tmr tuffs, Tp	Typically includes all vitric, nonwelded and bedded tuff units below the Rainier Mesa Tuff to the top of a Paintbrush lava (e.g., Tpb or Tpe) but may extend to base of Paintbrush Tuff in eastern Area 19 where Tpe or Tpr lavas are not present. May also include the vitric pumiceous top of the Tpe lava. Unit occurs in the northern portion of the model area beneath Pahute Mesa.
35	lower Paintbrush confining unit (LPCU)	TCU	Tpe, Tpd, Tpt	Consists of zeolitic bedded and nonwelded tuffs that occur stratigraphically between the Tiva Canyon Tuff and the welded Topopah Spring Tuff. This mainly includes the rhyolite of Delirium Canyon and the bedded and nonwelded Topopah Spring Tuff.
34	Paintbrush lava-flow aquifer (PLFA)	LFA	Tpd, Tpe, Tpr	Lava-flow lithofacies of the rhyolite of Delirium Canyon (Tpd), rhyolite of Echo Peak (Tpe), and rhyolite of Silent Canyon (Tpr). Also includes moderately to densely welded ash-flow tuff of Tpe. Unit occurs in the northern portion of the model area beneath Pahute Mesa.

Table A-1
HSUs of the PM-OV HFM
(Page 10 of 14)

Model Layer Number	HSU (Symbol)	Dominant HGU(s) [a]	Stratigraphic Unit Map Symbols [b]	General Description
33	Topopah Spring aquifer (TSA)	WTA	Tpt	The welded ash-flow lithofacies of the Topopah Spring Tuff in southern Area 20.
32	Yucca Mountain Crater Flat composite unit (YMCFCM)	LFA, WTA, TCU	Tc, Th	Includes all units of the Crater Flat Group and Calico Hills Formation that occur in the southern portion of the model area in the vicinity of Yucca Mountain. Stratigraphically equivalent units that occur in the northern portion of the model area beneath Pahute Mesa have been grouped into nine separate HSUs.
31	Calico Hills vitric-tuff aquifer (CHVTA)	VTA	Th (Tac)	Structurally high, vitric, nonwelded tuffs of the Calico Hills Formation. Present in the northern portion of the model area beneath the eastern portion of Area 19. May become partly zeolitic in the lower portions.
30	Calico Hills zeolitic composite unit (CHZCM)	TCU	Th	Formerly in the Phase I HFM, the CHZCM consisted of a complex distribution of rhyolite lava flows (i.e., LFAs) intercalated within thick and extensive mostly zeolitic and quartzo-feldspathic nonwelded and bedded tuffs (i.e., TCUs) of the Calico Hills Formation. In the Phase II model, the LFAs have been demarcated and modeled as separate property models within the CHZCM. Although the composite unit designation for the CHZCM is retained in the Phase II HFM, the unit is conceptualized in the Phase II HFM as consisting entirely of TCU. In addition, the Phase I CHCU HSU has been merged with the CHZCM in the Phase II HFM. The CHZCM is present in the northern portion of the model area beneath most of eastern and central Area 20, west of the West Greeley fault. The CHZCM is mostly saturated, particularly west of the Boxcar fault. East of the Boxcar fault, the upper portion of the HSU is above the water table.
29	Calico Hills lava-flow aquifer 1 (CHLFA1)	LFA	Th	The uppermost LFA property model within the CHZCM. Conceptualized as a single rhyolite lava flow of the Calico Hills Formation. Mainly occurs as a north–south-elongated flow between the West Greeley and Boxcar faults. Only the lower portion saturated west of the West Greeley fault.
28	Calico Hills lava-flow aquifer 2 (CHLFA2)	LFA, very minor TCU	Th	An LFA property model within the CHZCM. Although modeled as a single flow, very thin zeolitic bedded tuff observed within the CHLFA2 interval in U-20aj suggests that the property model may consist locally of 2 separate flows. Occurs in the northern portion of Pahute Mesa, mostly west of the West Greeley fault. Mostly unsaturated. Lower portion saturated in some places.

Table A-1
HSUs of the PM-OV HFM
(Page 11 of 14)

Model Layer Number	HSU (Symbol)	Dominant HGU(s) [a]	Stratigraphic Unit Map Symbols [b]	General Description
27	Calico Hills lava-flow aquifer 3 (CHLFA3)	LFA, minor TCU	Th	An LFA property model within the CHZCM. Although modeled as a single flow, the lithofacies distribution within drill holes penetrating the unit suggests that the property model may consist of more than one flow. Some of the lithofacies are described as zeolitic which likely imparts TCU-like properties to portions of the flow, although these TCU-like portions appear to thin and thus minor in occurrence. Similar in size and occurrence to CHLFA2. Fully saturated only west of the Boxcar fault. Lower portion saturated between the West Greeley and Boxcar faults. Mostly unsaturated east of the West Greeley fault.
26	Calico Hills lava-flow aquifer 4 (CHLFA4)	LFA	Th	An LFA property model within the CHZCM. Modeled as a single flow. Occurs as a north–south-elongated flow straddling the West Greeley fault. Mostly fully saturated west of the West Greeley fault. Portions become unsaturated east of the West Greeley fault.
25	Calico Hills lava-flow aquifer 5 (CHLFA5)	LFA	Th	The lowermost and most extensive LFA property model within the CHZCM. Modeled as a single flow. Occurs mainly west of the West Greeley fault. Saturated.
24	Inlet aquifer (IA)	LFA	Tci	Lava-flow lithofacies of the rhyolite of Inlet. Occurs as two thick isolated deposits beneath Pahute Mesa in the northern portion of the model area.
23	Crater Flat composite unit (CFCM)	Mostly LFA, intercalated with TCU	Tc, Tcpj, Tcps, Tcg	Includes welded tuff and lava flow lithofacies of the tuff of Jorum (Tcpj), the rhyolite of Sled (Tcps), and the andesite of Grimy Gulch (Tcg). Occurs in central Area 20 in the northern portion of the model area.
22	Crater Flat confining unit (CFCU)	TCU	Tc	Includes all zeolitic, nonwelded and bedded units below the Calico Hills Formation (Th) to the top of the Bullfrog Tuff (Tcb). Occurs mainly in Area 19 in the northern portion of the model area.
21	Kearsarge aquifer (KA)	LFA	Tcpk	Minor HSU that consists of the lava-flow lithofacies of rhyolite of Kearsarge. Unit is present as a small isolated occurrence in the northeastern portion of the model area.
20	Stockade Wash aquifer (SWA)	WTA	Tcbs	Consists of partially welded ash-flow tuff of the Stockade Wash lobe of the Bullfrog Tuff. Occurs along the eastern margin of the model area where it is extensively exposed. Mostly unsaturated.
19	Lower vitric-tuff aquifer 2 (LVTA2)	VTA	Tc	Two very small, unsaturated occurrences of vitric bedded tuff below the SWA in the extreme eastern portion of the model area.

Table A-1
HSUs of the PM-OV HFM
(Page 12 of 14)

Model Layer Number	HSU (Symbol)	Dominant HGU(s) [a]	Stratigraphic Unit Map Symbols [b]	General Description
18	Bullfrog confining unit (BFCU)	TCU	Tcb	Major confining unit in the northern portion of the model area. Unit consists of thick intra-caldera, zeolitic, mostly nonwelded tuff of the Bullfrog Formation.
17	Belted Range aquifer (BRA)	LFA and WTA, with lesser TCU	Tb, Tbg, Tbgs, Tbq	Consists of welded ash-flow tuff and lava of the Belted Range Group (Tb) above the Grouse Canyon Tuff (Tbg), but may also include the lava flow lithofacies of the comendite of Split Ridge (Tbgs) and the comendite of Quartet Dome (Tbq) where present. Occurs in the northern portion of the model area.
16	Pre-Belted Range composite unit (PBRCM)	TCU, WTA, LFA	Tr, Tn, Tq, Tu, To, Tk, Te	Laterally extensive and locally very thick HSU that includes all the volcanic rocks older than the Belted Range Group.
15	subcaldera volcanic confining unit (SCVCU)	TCU	Tm, Tp, Tc, and older, undifferentiated tuffs	A highly conjectural unit that is modeled as consisting of highly altered volcanic rocks that occur stratigraphically between the Rainier Mesa Tuff and basement rocks (ATICU and RMICU) within the deeper portions of the TMCC.
14	lower clastic confining unit - thrust plate (LCCU1)	CCU	Cc, Cz, Czw, Zs	Late Proterozoic to Early Cambrian siliciclastic rocks that occur within the hanging wall of the Belted Range thrust fault.
13	lower carbonate aquifer - thrust plate (LCA3)	CA	Dg through Cc	Cambrian through Devonian, mostly limestone and dolomite, rocks that occur in the hanging wall of the Belted Range thrust fault.
12	upper clastic confining unit (UCCU)	CCU	MDc, MDe	Late Devonian through Mississippian siliciclastic rocks. Present in the eastern third of the model area.
11	lower carbonate aquifer (LCA)	CA	Dg through Cc	Cambrian through Devonian mostly limestone and dolomite. Widespread throughout the model area.
10	lower clastic confining unit (LCCU)	CCU	Cc, Cz, Czw, Zs, Zj	Late Proterozoic through Early Cambrian siliciclastic rocks. Widespread throughout the model area.

Table A-1
HSUs of the PM-OV HFM
(Page 13 of 14)

Model Layer Number	HSU (Symbol)	Dominant HGU(s) [a]	Stratigraphic Unit Map Symbols [b]	General Description
9	Silent Canyon intrusive confining unit (SCICU)	IICU	Tc, Tb	Although modeled as single intrusive masses beneath the Silent Canyon and Redrock Valley calderas the actual nature of these units is unknown. They may consist exclusively of igneous intrusive rocks, or older volcanic and pre-Tertiary sedimentary rocks that are intruded to varying degrees by igneous rocks ranging in composition from granite to basalt.
8	Redrock Valley intrusive confining unit (RVICU)	IICU	Tori	
7	Mesozoic granite confining unit (MGCU)	GCU	Kg	Consists of granitic rocks that comprise the Gold Meadows stock along the northeastern margin of the model area.
6	Black Mountain intrusive confining unit (BMICU)	IICU	Not Defined	Although modeled as single intrusive masses beneath each of the Black Mountain, Ammonia Tanks, Rainier Mesa, and Claim Canyon calderas, and the Calico Hills area, the actual nature of these units is unknown. They may consist exclusively of igneous intrusive rocks, or older volcanic and pre-Tertiary sedimentary rocks that are intruded to varying degrees by igneous rocks ranging in composition from granite to basalt.
5	Calico Hills intrusive confining unit (CHICU)	IICU	Not Defined	
4	Claim Canyon intrusive confining unit (CCICU)	IICU	Not Defined	
3	Rainier Mesa intrusive confining unit (RMICU)	IICU	Not Defined	

Table A-1
HSUs of the PM-OV HFM
(Page 14 of 14)

Model Layer Number	HSU (Symbol)	Dominant HGU(s) [a]	Stratigraphic Unit Map Symbols [b]	General Description
2	Ammonia Tanks intrusive confining unit (ATICU)	IICU	Not Defined	Although modeled as single intrusive masses beneath each of the Black Mountain, Ammonia Tanks, Rainier Mesa, and Claim Canyon calderas, and the Calico Hills area, the actual nature of these units is unknown. They may consist exclusively of igneous intrusive rocks, or older volcanic and pre-Tertiary sedimentary rocks that are intruded to varying degrees by igneous rocks ranging in composition from granite to basalt.
1	Pahute Mesa Northern Extension intrusive confining unit (PMNICU)	IICU	Not Defined	Modeled as individual intrusive confining units for the Mount Helen Caldera and Cathedral Ridge Calderas

[a] See Table 2-2 for definitions of HGUs.
[b] See Tables 4-1 and 4-2 of the PM-OV HFM (DOE/EMNV, 2020) for definitions of stratigraphic unit map symbols.

A.2.0 REFERENCES

Byers, F.M., Jr., C.L. Rogers, W.J. Carr, and S.J. Luft. 1966. *Geologic Map of the Buckboard Mesa Quadrangle, Nye County, Nevada*, Map GQ-552, scale 1:24,000. Washington, DC: U.S. Geological Survey

Byers, F.M., Jr., W.J. Carr, R.L. Christiansen, P.W. Lipman, P.P. Orkild, and W.D. Quinlivan. 1976. *Geologic Map of the Timber Mountain Caldera Area, Nye County, Nevada,* Map, I-891, scale 1:48,000. Reston, VA: U.S. Geological Survey

Carr, W.J., and W.D. Quinlivan. 1966. *Geologic Map of the Timber Mountain Quadrangle, Nye County, Nevada*, Map GQ-503, scale 1:24,000. Washington, DC: U.S. Geological Survey.

DOE/EMNV, see U.S. Department of Energy Environmental Management Nevada Program.

Ferguson, J.F., A.H. Cogbill, and R.G. Warren. 1994. "A Geophysical-Geological Transect of the Silent Canyon Caldera Complex, Pahute Mesa, Nevada." In J*ournal of Geophysical Research: Solid Earth*, Vol. 99(B3): pp. 4323–4339.

Fridrich, C.J., S.A. Minor, J.L. Slate, and P.L. Ryder. 2007. *Geologic Map of Oasis Valley Spring-Discharge Area and Vicinity, Nye County, Nevada*, Scientific Investigations Map 2957, 25 p., scale 1:50,000. Denver, CO: U.S. Geological Survey.

Lipman, P. W., W. D. Quinlivan, W. J. Carr, and R. E. Anderson, 1966. *Geologic Map of the Thirsty Canyon SE Quadrangle, Nye County, Nevada*. U.S. Geological Survey Geologic Quadrangle Map GQ-489, scale, 1:24,000

Navarro. 2019. Written communication. Subject: "PM_Extended_HFM_ovpmv28." UGTA Technical Data Repository Database Identification Number UGTA-4-2028, Las Vegas, NV.

Slate, J.L., M.E. Berry, P.D. Rowley, C.J. Fridrich, K.S. Morgan, J.B. Workman, O.D. Young, G.L. Dixon, V.S. Williams, E.H. McKee, D.A. Ponce, T.G. Hildenbrand, W.C. Swadley, S.C. Lundstrom, E.B. Ekren, R.G. Warren, J.C. Cole, R.J. Fleck, M.A. Lanphere, D.A. Sawyer, S.A. Minor, D.J. Grunwald, R.J. Laczniak, C.M. Menges, J.C. Yount, and A.S. Jayko. 1999. *Part A. Digital Geologic Map of the Nevada Test Site and Vicinity, Nye, Lincoln, and Clark Counties, Nevada, and Inyo County, California, Revision 4*, Open-File Report 99-554-A, scale 1:120,000. Denver, CO: U.S. Geological Survey.

U.S. Department of Energy, National Nuclear Security Administration Nevada Site Office. 2004. *Completion Report for Well ER-EC-8*, DOE/NV/11718--435, UC-700. Prepared by Bechtel Nevada. Las Vegas, NV.

U.S. Department of Energy Environmental Management Nevada Program. 2020. *Pahute Mesa-Oasis Valley Hydrostratigraphic Framework Model for Corrective Action Units 101 and 102: Central and Western Pahute Mesa, Nye County, Nevada*, Rev. 0, DOE/EMNV--014; Las Vegas, NV.

Appendix B

Use of Non-Direct Data

B.1.0 INTRODUCTION

The UGTA Activity is modeling flow and transport in aquifers of the NNSS and surrounding areas that have been contaminated from underground testing of nuclear devices. Modeling is used as a method of forecasting how the hydrogeologic system, including the underground test cavities, will behave over time with the goal of assessing the migration of radionuclides away from these cavities. To this end, flow and transport models are being developed over a range of scales for the UGTA CAUs. For the Central and Western Pahute Mesa CAUs, the predominant hydrologic flow pathways from the test cavities are through locally hydrologically conductive Cenozoic volcanic rocks that were erupted and deposited during multiple eruptive cycles of the TMCC and SCCC (Christensen et al., 1977; Byers et al., 1976 and 1989; Broxton et al., 1989; Sawyer et al., 1994). Probability distributions for flow and transport parameters for these rocks are required input for the models.

A major effort of the UGTA Activity is to compile and assess the suitability of the existing data for these models. Modeling of the UGTA CAUs is not a common groundwater contaminant modeling problem. Most groundwater contamination problems consist of migration of contaminants from relatively well-characterized sources over short flow paths through shallow aquifers. There is often some information about contaminant distribution as a result of monitoring and site characterization. In contrast, the Pahute Mesa CAU model will require prediction of contaminant movement through deep aquifers in a large system (tens of kilometers on a side). Information about sources and radionuclide distribution in the aquifer is sparse. Test cavities on Pahute Mesa are as deep as 1,450 m, making extensive characterization of the source and contaminant migration difficult and expensive.

Using experience from other sites to reduce parameter uncertainty is an appropriate approach when developing models in a sparse data environment (Freeze et al., 1990). This approach incorporates flow and transport parameter data from investigations of similar environments when developing prior distributions for parameters to be used in modeling the study area. Utilization of such existing data can be both a cost-effective and necessary step to a modeling effort in a sparse data environment.

The UGTA QAP, Rev. 2 (NNSA/NSO, 2015) requires the justification of non-direct datasets and data sources used in support of UGTA models. All data used in the modeling will be reviewed in relation to the QAP requirements; however, the following general acceptance criteria were developed to guide use of the non-direct data most commonly used:

1. **UGTA data documents** present flow and transport model data, including data quality assessments, data analyses to derive expected values or probability distributions, and parameter uncertainty estimates. The documents are developed under the QAP requirements in place at the time of their preparation and were reviewed by the Preemptive Review (PER) Committees, DOE, and NDEP. The data in these documents are considered to be valid for use.

2. **Peer-reviewed literature,** including handbooks of physical or chemical constants, are considered acceptable and do not require additional source acceptance justification. These documents have received sufficient technical reviews.

3. **UGTA-sponsored technical reports** completed before the current QAP (NNSA/NSO, 2015) have adequately justified their data sources and datasets, and the technical reviews have been sufficient to justify the results and conclusions. The documents were generally reviewed by the PER Committees (or predecessor), DOE, and NDEP.

4. **Historical NNSS (or NTS) data** produced by LANL, LLNL, USGS, and contractors have applied sufficient QA and/or technical review to justify the use of the data. Data contained in the USGS Rock-Property Database (USGS, 2020; and previous versions) and the Database of NNSS Groundwater Levels and Hydrograph Descriptions (Elliott and Fenelon, 2010; and previous versions) have been formally accepted by UGTA.

5. **Other DOE programs** such as the Yucca Mountain Project, and the Low-Level Radioactive Waste Management programs in Areas 3 and 5 of the NNSS in Nevada and the Waste Isolation Project Plant (WIPP) in New Mexico were developed under QA programs equivalent to UGTA's and thereby satisfy current UGTA requirements.

6. **USGS data**, reports, and analyses are used in the development of UGTA documents. USGS is an UGTA Activity participant, and the information used was developed for the project. USGS works under a QA program that meets the UGTA Activity QAP requirements, and no further justification is necessary for use of this organization's information.

7. **Other federal or international entities—**such as the National Oceanic and Atmospheric Administration, International Atomic Energy Agency, and European Space Agency—have sufficient internal review and QA procedures, and no further justification is necessary.

8. **UGTA databases** developed and updated in compliance with QA procedures existing at the time of compilation are sufficient to justify the data, even if the data were originally generated from a non-UGTA entity, such as the weapons program and the Routine Radiological Environmental Monitoring Program.

9. **Non-direct data from other non-UGTA reports** that are cited to provide the overall scientific context for the UGTA generated work but are not used directly in the models do not require any further justification.

B.2.0 REFERENCES

Broxton, D.E., R.G. Warren, F.M. Byers, and R.B. Scott. 1989. "Chemical and Mineralogic Trends within the Timber Mountain–Oasis Valley Caldera Complex, Nevada: Evidence for Multiple Cycles of Chemical Evolution in a Long-Lived Silicic Magma System." In *Journal of Geophysical Research: Solid Earth*, Vol. 94(B5): pp. 5961–5985.

Byers, F.M., Jr., W.J. Carr, R.L. Christiansen, P.W. Lipman, P.P. Orkild, and W.D. Quinlivan. 1976. *Geologic Map of the Timber Mountain Caldera Area, Nye County, Nevada,* Map, I-891, scale 1:48,000. Reston, VA: U.S. Geological Survey

Byers, F.M., Jr., W.J. Carr, and P.P. Orkild. 1989. "Volcanic Centers of Southwestern Nevada: Evolution and Understanding, 1960–1988." In *Journal of Geophysical Research: Solid Earth,* Vol. 94(B5): pp. 5908–5924.

Christiansen, R.L., P.W. Lipman, W.J. Carr, F.M. Byers, Jr., P.P. Orkild, and K.A. Sargent. 1977. "Timber Mountain-Oasis Valley Caldera Complex of Southern Nevada." In *Geological Society of America Bulletin*, Vol. 88(7): pp. 943–959.

Elliott, P.E., and J.M. Fenelon. 2010. *Database of Groundwater Levels and Hydrograph Descriptions for the Nevada Test Site Area, Nye County, Nevada*, *1941–2010,* Data Series 533. Reston, VA: U.S. Geological Survey. (Version 9.0 released in February 2019).

Freeze, R.A., J. Massmann, L. Smith, T. Sperling, and B. James. 1990. "Hydrogeological Decision Analysis: 1. A Framework." In *Ground Water*, Vol. 28(5): 738–766.

NNSA/NFO, see U.S. Department of Energy, National Nuclear Security Administration Nevada Field Office.

Sawyer, D.A., R.J. Fleck, M.A. Lanphere, R.G. Warren, D.E. Broxton, and M.R. Hudson. 1994. "Episodic Caldera Volcanism in the Miocene Southwestern Nevada Volcanic Field: Revised Stratigraphic Caldera Framework, $^{40}Ar/^{39}Ar$ Geochronology, and Implications for Magmatism and Extension." In *Geological Society of America Bulletin*, Vol. 106(10): pp. 1304–1318.

USGS, see U.S. Geological Survey.

U.S. Department of Energy, National Nuclear Security Administration Nevada Field Office. 2015. *Underground Test Area Activity Quality Assurance Plan, Nevada National Security Site, Nevada*, Rev. 2, DOE/NV--1450-REV.2. Las Vegas, NV.

U.S. Geological Survey. 2020. "Mercury Core Library and Data Center, Rock-Property Database." As accessed at http://nevada.usgs.gov/mercury/ on 1 May. Mercury, NV.

Appendix C

Steady-State Hydraulic Head, Gradient, and Spring Data for Pahute Mesa

C.1.0 INTRODUCTION

This appendix contains summary information on the well construction, hydraulic heads, hydraulic gradients, and spring elevations. Section 8.0 describes the compilation and analysis of water-level data to derive hydraulic heads that are used to calibrate the Pahute Mesa Phase II flow model.

C.1.1 Hydraulic Head and Gradient Data Summary

General site information for wells, boreholes or completions located within the Phase II HFM is presented in Table C-1. For wells, boreholes, or completions, the general site information of interest includes location, land-surface elevation, EOI, and hydrostratigraphy. For springs, site information of interest includes location, land surface elevation and the HSUs to a depth of 100 m bgs. Site information for regional springs located within the Phase II HFM is presented in Table C-2. Table C-3 summarizes the steady-state hydraulic heads determined for each site in the Pahute Mesa Phase II HFM. Also included in this table is the number, minimum, maximum, and standard deviation of the measurements used to determine the steady-state values along with the uncertainties assigned to each steady-state head. Table C-4 contains the hydraulic gradient between well pairs for the wells aligned with the general direction of flow toward Oasis Valley. Well pairs were selected as the well pair with the minimum of distance between wells within 4 to 20 km of each other.

The distance between wells used to select well pairs was determined from the parametric uncertainty analysis presented in Section 8.5.3. All water-level data within various distances of each well were identified, and a plane was fit through the data using linear regression. Water-level uncertainty was introduced to the calculations using a Monte Carlo sampling approach. The easting, northing, and elevation represent the variables X, Y, and Z in the equation of a plane $ax+by+cz+d=0$. Setting the z variable to zero provides the equation for the line of strike at $z=0$ $ax+by+d=0$. The strike azimuth can be calculated from the arctan of the X-Y plane derivative as $arctan(x/y)$ or as $arctan(-b/a)$. The strike azimuth is the orientation of the horizontal line within a plane and is perpendicular to the dip azimuth, which is the direction of flow.

Table C-5 presents an example of the data and plane fit to water levels surrounding Well ER-18-2. Two wells are within 10 km of Well ER-18-2, providing three points for linear regression to a plane.

The resulting dip azimuth from this example is 207.537 degrees. To illustrate the effect of water-level uncertainty on the dip azimuth, in this example, the uncertainty is added to the Well UE-18t water level and subtracted the ER-30-1 water level, while keeping ER-18-2 water level the same; resulting in a dip azimuth of 207.538 degrees. The small difference between the dip azimuth calculation with and without uncertainty suggests that the water-level uncertainty has an insignificant effect on the direction of flow calculation at a scale of 10 km at this location. To reduce large number precision error in the linear regression calculation, the water-level coordinates can be translated without changing the direction of flow by subtracting the minimum of the easting, northing, and elevation from the water-level coordinates.

Table C-1
Site Information for Selected Wells and Boreholes Located in the Pahute Mesa Area and Vicinity
(Page 1 of 13)

Well Name	NWIS ID	ISPID	UTM Easting (m) [a]	UTM Northing (m) [b]	Land Surface Elevation (m amsl) [b]	Total Depth (m bgs) [c]	Effective Open Interval Top Elevation (m amsl) [d]	Effective Open Interval Bottom Elevation (m amsl) [e]	Primary HSU [f]	Secondary HSU [g]
Beatty Middle Well	365619116483901	None	516696.6	4087999.0	1,252.7	213.4	1,237.8 [h, i]	1,039.4 [h]	DVCM	None
Beatty Summit Well	365527116475301	None	517912.2	4086306.7	1,183.2	213.4	1,143.6 [h, i]	969.9 [h]	DVCM	None
Beatty Upper Indian Well	365709116481101	None	517510.1	4089325.6	1,292.4	211.2	1,238.4 [h, i]	1,081.1 [h]	DVCM	None
Beatty Wash Terrace Well	365640116431501	Beatty Wash Terrace Well_m1	524857.8	4088542.8	1,051.6	22.9	1,034.8	1,028.7	DVCM	None
Beatty Wash Windmill Well	370014116332501	229 S11 E48 01 1 Beatty Wash Windmill Well_s1	539402.8	4095210.4	1,338.1	146.3	1,235.4 [i]	1,191.8	RMWTA	None
Beatty Water Test Hole	365457116515801	None	521328.8	4085359.4	1,025.7	53.3	1,001.3 [h, i]	972.3 [h]	DVCM	AA
Beatty Well No.1	365524116444001	Beatty Wtr Swr-Well 1_m1	521378.4	4085328.7	1,025.7	61.0	996.7 [i]	964.7	DVCM	AA
Beatty Well No. 2	365409116452301	None	521578.9	4084312.3	1,005.8	59.4	999.7 [h, i]	946.4 [h]	DVCM	AA
Beatty Well No. 3	365420116453001	Beatty Wtr Swr-Well 3_m1	521653.5	4084158.4	1,002.8	91.4	981.5	911.4	DVCM	None
BGC-1 Well	365358116452001	Beatty GID BGC-1 Well_g	521778.9	4083542.5	996.7	22.9	991.8 [h, i]	973.8 [h]	DVCM	AA
BGC-2 Well	365355116451401	None	521927.6	4083450.4	994.0	22.9	990.6 [h, i]	971.1 [h]	DVCM	AA
BLM Springdale	370648116473001	BLM Spdale_m1	518460.2	4107292.5	1,229.9	0.0	1,201.2 [h, i]	1,194.2 [h]	TCVA	None
Boiling Pot Rd Well	365934116431601	None	524817.4	4093904.4	1,103.4	3.7	1,102.8 [h, i]	1,099.6 [h]	AA	None
CDH-61	365239116490701	None	516165.5	4081095.7	1,015.3	304.8	807.7 [h, i]	710.5 [h]	LCA3	None
Central Beatty Well	365431116452501	None	521652.5	4084559.0	1,005.8	8.2	1,001.9 [h, i]	997.6 [h]	AA	None
Crater Flat 1 (CF-1)	365520116370301	Crater Flat 1_m1	534267.4	4085956.4	1,198.1	487.7	1,010.1 [h, i]	710.5 [h]	PCM	AA
Crater Flat 1a (CF-1a)	365445116383901	Crater Flat 1a_m1	531648.6	4084929.3	1,243.9	213.4	1,202.7 [h, i]	1,030.5 [h]	DVCM	PCM
ER-12-1 (1641-1846 ft)	371106116110401	ER-12-1_m5	572411.5	4115492.8	1,773.1	1,093.6	1,272.9	1,210.4	UCCU	LCA3
ER-12-1 (1641-3414 ft)	371106116110407	ER-12-1_m1-5	572411.5	4115492.8	1,773.1	1,093.6	1,272.9	732.5	UCCU	LCA3/LCA
ER-12-1 (1883-1940 ft)	371106116110405	ER-12-1_m4	572411.5	4115492.8	1,773.1	1,093.6	1,199.1	1,181.7	UCCU	None
ER-12-1 (2449-2602 ft)	371106116110404	ER-12-1_m3	572411.5	4115492.8	1,773.1	1,093.6	1,026.6	980.0	UCCU	None
ER-12-1 (2958-3212 ft)	371106116110403	ER-12-1_m2	572411.5	4115492.8	1,773.1	1,093.6	871.5	794.0	UCCU	None
ER-12-1 (3309-3414 ft)	371106116110402	ER-12-1_m1	572411.5	4115492.8	1,773.1	1,093.6	764.5	732.5	UCCU	LCA
ER-12-1 (brhl)	371106116110406	ER-12-1_o1Z	572411.5	4115492.8	1,773.1	1,093.6	1,302.1 [i]	679.4	UCCU	LCA/LCA3
ER-12-3 main	371142116125102	ER-12-3_m1	569748.4	4116592.1	2,252.7	1,496.0	1,158.2	756.8	LCA3	None
ER-12-3 piezometer	371142116125101	ER-12-3_p1	569748.4	4116592.1	2,252.7	1,496.0	1,821.6	1,582.2	PBRCM	None
ER-12-4 main	371311116105902	ER-12-4_m1	572473.2	4119345.6	2,098.2	1,132.3	1,149.8	965.8	LCA3	None
ER-12-4 piezometer	371311116105901	ER-12-4_p1	572473.2	4119345.6	2,098.2	1,132.3	1,538.5	1,492.2	PBRCM	None
ER-18-2	370615116222401	ER-18-2_m1	555724.7	4106388.5	1,657.2	762.0	1,245.4	895.2	RMWTA	None
ER-19-1-1 (deep)	371043116142101	ER-19-1_m1	567541.5	4114743.5	1,871.4	1,095.8	893.0	786.3	LCCU1	None
ER-19-1-2 (middle)	371043116142102	ER-19-1_m2	567541.5	4114743.5	1,871.4	1,095.8	1,094.2	1,036.9	PBRCM	None

Table C-1
Site Information for Selected Wells and Boreholes Located in the Pahute Mesa Area and Vicinity
(Page 2 of 13)

Well Name	NWIS ID	ISPID	UTM Easting (m) [a]	UTM Northing (m) [b]	Land Surface Elevation (m amsl) [b]	Total Depth (m bgs) [c]	Effective Open Interval Top Elevation (m amsl) [d]	Effective Open Interval Bottom Elevation (m amsl) [e]	Primary HSU [f]	Secondary HSU [g]
ER-19-1-3 (shallow)	371043116142103	ER-19-1_m3	567541.5	4114743.5	1,871.4	1,095.8	1,474.9	1,438.0	PBRCM	None
ER-20-1	371321116292301	ER-20-1_p1	545113.2	4119467.9	1,883.9	629.4	1,277.7 [i]	1,254.5	TCA	None
ER-20-2-1	371246116240101	ER-20-2-1_p1	553210.7	4118447.2	2,043.7	769.3	1,348.1	1,275.6	CHZCM	None
ER-20-4 borehole	371143116262502	ER-20-4_m1	549676.1	4116492.4	1,748.4	1,066.5	1,283.8	681.9	CFCU	CHLFA1/CHLFA4
ER-20-4 deep	371143116262503	ER-20-4_p1	549676.1	4116492.4	1,748.4	1,066.5	1,012.3	818.7	CFCU	CHLFA4
ER-20-4 shallow	371143116262504	ER-20-4_p2	549676.1	4116492.4	1,748.4	1,066.5	1,284.7 [i]	1,036.4	CHLFA1	CHLFA4
ER-20-5-1 (3-in string)	371312116283801	ER-20-5-1_p1	546385.8	4119208.3	1,902.5	860.5	1,217.0	1,093.3	TSA	CHZCM
ER-20-5-3	371311116283801	ER-20-5-3_m1	546384.8	4119176.8	1,902.5	1,308.8	882.1	709.6	CHLFA5	None
ER-20-6-1 (3-in string)	371537116251501	ER-20-6-1_p1	551363.0	4123691.8	1,973.5	975.4	1,230.7	1,075.3	CHLFA3	None
ER-20-6-2 (3-in string)	371536116251601	ER-20-6-2_p1	551328.0	4123661.7	1,973.6	975.4	1,237.8	1,076.0	CHLFA3	None
ER-20-6-3 (3-in string)	371533116251801	ER-20-6-3_p1	551295.7	4123578.9	1,970.8	975.4	1,228.3	1,115.3	CHLFA3	None
ER-20-7	371247116284502	ER-20-7_m1	546218.3	4118429.8	1,892.5	894.9	1,193.9	997.5	TSA	CHZCM/LPCU
ER-20-7 (120-2208 ft)	371247116284501	ER-20-7_m2Z	546218.3	4118429.8	1,892.5	894.9	1,220.7	1,210.6	LPCU	None
ER-20-8 deep	371135116282602	ER-20-8_p1	546686.3	4116218.3	1,782.6	1,049.1	846.8	733.3	CHZCM	LPCU/TSA
ER-20-8 intermediate	371135116282603	ER-20-8_p2	546686.3	4116218.3	1,782.6	1,049.1	1,038.8	886.4	TCA	LPCU/MPCU
ER-20-8 main	371135116282601	ER-20-8_o1Z	546686.3	4116218.3	1,782.6	1,049.1	1,274.4 [i]	733.3	SPA	TCA/LPCU
ER-20-8 shallow	371135116282604	ER-20-8_p3	546686.3	4116218.3	1,782.6	1,049.1	1,146.0	1,127.2	SPA	None
ER-20-8-2	371135116282701	ER-20-8-2_m1	546672.8	4116211.4	1,782.7	712.6	1,270.5	1,069.9	SPA	UPCU/MPCU
ER-20-11	371146116290301	ER-20-11_m1	545778.7	4116550.4	1,778.2	915.6	997.3	862.6	BA	UPCU/FCCU
ER-20-12 (m1)	371652116321801	ER-20-12_m1	540925.1	4125952.8	1,907.6	1,384.8	714.0	522.9	PBRCM	None
ER-20-12 (p1)	371652116321802	ER-20-12_p1	540925.1	4125952.8	1,907.6	1,384.8	888.6	772.2	BRA	CHZCM
ER-20-12 (p2)	371652116321803	ER-20-12_p2	540925.1	4125952.8	1,907.6	1,384.8	977.0	945.3	CHZCM	None
ER-20-12 (p3)	371652116321804	ER-20-12_p3	540925.1	4125952.8	1,907.6	1,384.8	1,142.5	1,009.3	CHLFA5	CHZCM
ER-20-12 (p4)	371652116321805	ER-20-12_p4	540925.1	4125952.8	1,907.6	1,384.8	1,415.8	1,210.5	TMLVTA	TMWTA
ER-30-1-1 deep	370301116185801	ER-30-1_m1	560804.6	4100463.0	1,416.5	434.6	1,210.2	1,175.7	FCCM	None
ER-30-1-2 shallow	370301116185802	ER-30-1_m2	560804.6	4100463.0	1,416.5	434.6	1,237.5	1,225.1	FCCM	None
ER-EC-1	371223116314701	ER-EC-1_m1-3	541729.8	4117659.7	1,836.6	1,524.0	1,148.4	361.4	CHZCM	CFCM/LPCU
ER-EC-2A (1635-2236 ft)	370852116340502	ER-EC-2A_m3	538420.8	4110841.3	1,494.1	1,516.1	995.8	812.6	FCCM	None
ER-EC-2A (1635-4973 ft)	370852116340501	ER-EC-2A_m1-3	538420.8	4110841.3	1,494.1	1,516.1	995.8	-22.1	FCWTA1	FCCM/BWCU
ER-EC-4 (952-2295 ft)	370935116375302	ER-EC-4_m2-3	532759.4	4112356.0	1,450.7	1,062.8	1,160.6	751.2	TCVA	TMUWTA/FCCM
ER-EC-4 (952-3487 ft)	370935116375301	ER-EC-4_o1Z	532759.4	4112356.0	1,450.7	1,062.8	1,222.6 [i]	387.9	TMUWTA	TCVA/FCCM

Table C-1
Site Information for Selected Wells and Boreholes Located in the Pahute Mesa Area and Vicinity
(Page 3 of 13)

Well Name	NWIS ID	ISPID	UTM Easting (m) [a]	UTM Northing (m) [b]	Land Surface Elevation (m amsl) [b]	Total Depth (m bgs) [c]	Effective Open Interval Top Elevation (m amsl) [d]	Effective Open Interval Bottom Elevation (m amsl) [e]	Primary HSU [f]	Secondary HSU [g]
ER-EC-5	370504116335201	ER-EC-5_m1-3	538701.7	4104137.1	1,547.5	762.0	1,191.2	785.5	ATWTA	None
ER-EC-6 (1581-3820 ft)	371120116294802	ER-EC-6_m2-4	544673.4	4115728.8	1,708.2	1,524.0	1,218.7	543.9	BA	TSA/LPCU
ER-EC-6 (1581-5000 ft)	371120116294801	ER-EC-6_m1-4	544673.4	4115728.8	1,708.2	1,524.0	1,218.7	213.2	CFCM	BA/CHZCM
ER-EC-6 deep	371120116294803	ER-EC-6_m2_a1	544673.4	4115728.8	1,708.2	1,524.0	674.3	543.9	CHZCM	TSA
ER-EC-6 intermediate	371120116294804	ER-EC-6_m3_a2	544673.4	4115728.8	1,708.2	1,524.0	1,056.6	943.2	UPCU	TCA
ER-EC-6 shallow	371120116294805	ER-EC-6_m4_a3	544673.4	4115728.8	1,708.2	1,524.0	1,218.7	1,114.5	BA	FCCU
ER-EC-7	365910116284401	ER-EC-7_m1-2	546483.7	4093127.5	1,464.7	422.5	1,191.9	1,042.2	FCULFA7	FCULFA6/FCCM
ER-EC-8	370610116375301	ER-EC-8_m1-3	532763.8	4106141.8	1,320.9	609.6	1,128.2	711.3	FCCM	ATWTA/BWCU
ER-EC-11 deep	371151116294102	ER-EC-11_p1	544839.1	4116703.1	1,724.0	1,264.3	629.8	459.5	TSA	CHZCM
ER-EC-11 intermediate	371151116294103	ER-EC-11_p2	544839.1	4116703.1	1,724.0	1,264.3	749.9	692.3	TCA	None
ER-EC-11 main	371151116294101	ER-EC-11_m1-2	544839.1	4116703.1	1,724.0	1,264.3	779.2	459.5	TSA	TCA/LPCU
ER-EC-11 shallow	371151116294104	ER-EC-11_p3	544839.1	4116703.1	1,724.0	1,264.3	907.9	800.5	BA	FCCU
ER-EC-11 water table	371151116294105	ER-EC-11_p4	544839.1	4116703.1	1,724.0	1,264.3	1,273.8 [i]	1,249.5	TMWTA	None
ER-EC-12 deep	371024116293102	ER-EC-12_p1	545099.1	4114013.6	1,686.2	1,240.2	523.3	445.9	CFCU	CHZCM
ER-EC-12 intermediate	371024116293103	ER-EC-12_p2	545099.1	4114013.6	1,686.2	1,240.2	714.5	537.1	TSA	CHZCM
ER-EC-12 shallow	371024116293104	ER-EC-12_p3	545099.1	4114013.6	1,686.2	1,240.2	1,121.1	849.8	TCA	LPCU/TMWTA
ER-EC-13 deep	371010116325402	ER-EC-13_p1	540102.3	4113553.2	1,577.4	914.4	894.6	760.5	FCULFA4	None
ER-EC-13 intermediate	371010116325403	ER-EC-13_p2	540102.3	4113553.2	1,577.4	914.4	1,018.1	926.3	FCULFA4	None
ER-EC-13 shallow	371010116325404	ER-EC-13_p3	540102.3	4113553.2	1,577.4	914.4	1,268.4	1,111.0	FCCM	None
ER-EC-14 deep	370825116302402	ER-EC-14_p1	543466.5	4110337.9	1,580.7	724.8	1,004.9	855.8	RMWTA	None
ER-EC-14 main	370825116302401	ER-EC-14_m1-2	543466.5	4110337.9	1,580.7	724.8	1,185.9	855.8	RMWTA	None
ER-EC-14 shallow	370825116302403	ER-EC-14_p2	543466.5	4110337.9	1,580.7	724.8	1,185.9	1,061.3	RMWTA	None
ER-EC-15 deep	371110116310502	ER-EC-15_p1	542769.3	4115426.7	1,635.3	991.8	796.4	643.3	TSA	CHZCM/CFCU
ER-EC-15 intermediate	371110116310503	ER-EC-15_p2	542769.3	4115426.7	1,635.3	991.8	992.7	895.5	TCA	LPCU/UPCU
ER-EC-15 shallow	371110116310504	ER-EC-15_p3	542769.3	4115426.7	1,635.3	991.8	1,214.4	1,096.1	CPA	PBPCU
ER-OV-01	370504116404901	ER-OV-01_p1	528416.9	4104084.5	1,221.4	54.9	1,178.1	1,166.6	TCVA	None
ER-OV-02	370210116421501	ER-OV-02_p1	526310.3	4098715.9	1,182.7	61.0	1,133.9	1,121.8	FCCM	None
ER-OV-03a	365956116421601	ER-OV-03a_p1	526298.4	4094586.8	1,170.8	76.5	1,110.5	1,094.3	DVA	None
ER-OV-03a2	365956116421602	ER-OV-03a2/3_p1	526298.4	4094586.8	1,170.6	250.2	1,000.0	971.0	DVA	None
ER-OV-03a3	365956116421603	ER-OV-03a2/3_p2	526298.4	4094586.8	1,170.6	250.2	1,143.8	1,121.9	DVA	None
ER-OV-03b	370139116390501	ER-OV-03b_p1	531007.7	4097776.6	1,290.1	121.9	1,182.5	1,168.2	AA	None

Table C-1
Site Information for Selected Wells and Boreholes Located in the Pahute Mesa Area and Vicinity
(Page 4 of 13)

Well Name	NWIS ID	ISPID	UTM Easting (m) [a]	UTM Northing (m) [b]	Land Surface Elevation (m amsl) [b]	Total Depth (m bgs) [c]	Effective Open Interval Top Elevation (m amsl) [d]	Effective Open Interval Bottom Elevation (m amsl) [e]	Primary HSU [f]	Secondary HSU [g]
ER-OV-03c	365948116360401	ER-OV-03c_p1	535494.1	4094373.8	1,276.6	165.2	1,125.5	1,111.5	ATWTA	None
ER-OV-03c2	365948116360402	ER-OV-03c2_p1	535494.1	4094373.8	1,276.8	97.8	1,194.5	1,178.9	ATWTA	None
ER-OV-04a	365705116424201	ER-OV-04A_p1	525671.7	4089315.6	1,063.2	46.0	1,036.1	1,017.2	DVCM	None
ER-OV-05	370246116461901	ER-OV-05_p1	520279.7	4099808.7	1,199.3	61.0	1,157.8	1,138.3	AA	None
ER-OV-06a	370504116404902	ER-OV-06a_p1	528416.9	4104084.5	1,221.5	163.4	1,072.7	1,058.1	FCCM	None
ER-OV-06a2	370504116404903	ER-OV-06a2_p1	528416.9	4104084.5	1,221.3	21.6	1,207.9	1,201.5	TCVA	None
Gold Flat 1	372642116281301	None	546857.8	4144166.9	1,565.1	148.1	1,421.3 [h, i]	1,417.0 [h]	AA	None
Gold Flat 2	372543116363501	Gold Flat 2_m1Z	534530.4	4142288.5	1,594.1	115.8	1,523.1 [i]	1,505.7	TCVA	AA
Gold Flat 2a	372543116363502	Gold Flat 2_m1	534530.5	4142281.1	1,594.1	115.8	1,517.9	1,484.4	TCVA	BRA
Gold Flat 3	372543116363503	None	534530.5	4142262.0	1,594.1	125.0	1,522.8 [h, i]	1,469.1 [h]	TCVA	BRA
Hagestad1 (1600-1904 ft)	371131116125902	Hagestad 1 (1600-1904 ft)_m1	569542.3	4116259.7	2,281.5	591.6	1,793.8	1,701.2	PBRCM	None
Hagestad1 (1874-1904 ft)	371131116125901	Hagestad 1 (1874-1904 ft)_m2	569542.3	4116259.7	2,281.5	591.6	1,710.3	1,701.2	PBRCM	None
Hammel Mine Well	373228116472001	None	518650.4	4154718.7	1,688.6	37.5	1,652.3 [h, i]	1,651.1 [h]	PBRCM	None
Lamb Well	372438116123601	None	569898.2	4142355.8	1,635.3	213.4	1,434.1 [h, i]	1,421.9 [h]	AA	None
Lower Indian Springs Well	365642116474501	Lower Indian Springs Well_g	518179.5	4088587.5	1,228.3	0.0	1,228.3 [h, i]	1,227.3 [h]	Outside_HFM	Outside_HFM
Narrows South Well 1	365247116451801	None	521834.0	4081354.9	969.3	38.4	963.5 [h, i]	930.9 [h]	UCCU	None
Narrows South Well 2	365253116450801	None	522081.0	4081540.4	969.3	36.6	963.5 [h, i]	932.7 [h]	UCCU	None
NC-GWE-OV-01	370022116431501	None	524924.0	4095397.7	1,122.2	0.0	1,122.3 [h, i]	1,122.2 [h]	AA	None
NC-GWE-OV-02	365752116432301	None	524739.7	4090779.2	1,079.7	0.0	1,075.9 [h, i]	1,074.9 [h]	AA	DVCM
OVM ET Well	370039116432401	None	524613.8	4095906.7	1,124.9	4.0	1,124.1 [h, i]	1,120.9 [h]	AA	None
OVU-Dune Well	370301116421101	None	526404.2	4100287.8	1,183.5	5.2	1,181.4 [h, i]	1,178.4 [h]	AA	None
OVU-Lower ET Well	370242116422901	None	525961.4	4099700.9	1,176.8	3.4	1,175.3 [h, i]	1,173.4 [h]	AA	None
OVU-Middle ET Well	370249116424101	None	525664.3	4099915.7	1,175.3	3.4	1,174.4 [h, i]	1,171.9 [h]	AA	None
P Ranch Well	365802116432201	228 S11 E47 21ACC 1P Ranch Well_o1	524677.4	4091069.0	1,094.2	0.0	1,094.2 [h, i]	1,093.2 [h]	Outside_HFM	Outside_HFM
Perlite Canyon Ranch Well	365604116430901	None	525009.5	4087433.9	1,069.8	53.3	1,039.1 [h, i]	1,016.5 [h]	AA	None
Pioneer Road Seep Well	365929116434701	None	524051.6	4093748.1	1,112.5	2.2	1,112.2 [h, i]	1,110.3 [h]	AA	None
PM-1 (7543-7858 ft)	371649116242102	PM-1_o1	552668.1	4125925.2	1,998.8	2,395.1	-300.3	-396.3	BRA	None
PM-2	372042116340501	PM-2_m1-o7	538256.7	4133028.2	1,704.4	2,678.6	940.6	-974.2	PBRCM	None
PM-3 (1647 ft)	371421116333701	PM-3_o2Z	539011.8	4121281.4	1,774.8	920.2	1,331.7 [i]	1,272.8	UPCU	None
PM-3 (3019 ft)	371421116333702	PM-3_o1Z	539011.8	4121281.4	1,774.8	920.2	1,325.8	854.6	LPCU	UPCU/TCA
PM-3-1 (1919-2144 ft)	371421116333703	PM-3_p1	539011.8	4121281.4	1,774.8	920.2	1,204.2	1,106.7	TCA	LPCU/UPCU

Table C-1
Site Information for Selected Wells and Boreholes Located in the Pahute Mesa Area and Vicinity
(Page 5 of 13)

Well Name	NWIS ID	ISPID	UTM Easting (m) [a]	UTM Northing (m) [b]	Land Surface Elevation (m amsl) [b]	Total Depth (m bgs) [c]	Effective Open Interval Top Elevation (m amsl) [d]	Effective Open Interval Bottom Elevation (m amsl) [e]	Primary HSU [f]	Secondary HSU [g]
PM-3-2 (1442-1667 ft)	371421116333704	PM-3_p2	539011.8	4121281.4	1,774.8	920.2	1,325.8	1,260.6	UPCU	None
Springdale ET Deep Well	370113116434901	None	523993.1	4096952.6	1,132.1	2.8	1,132.3 [h, i]	1,129.3 [h]	AA	None
Springdale ET Shallow Well	370113116434902	None	523993.1	4096952.6	1,132.1	2.8	1,131.7 [h, i]	1,129.3 [h]	AA	None
Springdale Lower Well	370113116435301	None	523894.2	4096952.3	1,130.8	3.5	1,129.6 [h, i]	1,127.3 [h]	AA	None
Springdale Upper Well	370131116440801	Spdale Upper Well_m1	523522.0	4097506.0	1,150.6	0.0	1,143.3 i	1,122.9	AA	None
Springdale Windmill Well	370218116455201	None	521469.2	4098301.7	1,179.6	36.6	1,175.3 [h, i]	1,143.0 [h]	AA	DVCM
Tolicha Peak Well	371832116470101	None	519167.8	4128971.1	1,731.3	611.1	1,524.9 [h, i]	1,120.1 [h]	TMWTA	TMLVTA/TCVA
TTR Antelope Mine 1	373622116434601	TTR Antelope Mine 1_mine1	523896.0	4161883.0	1,935.5	0.0	0.0 [h]	1,928.7 [h]	PBRCM	None
TTR Antelope Mine 2	373622116434701	TTR Antelope Mine 2_mine1	523876.7	4161946.8	1,937.3	0.0	0.0 [h]	1,929.3 [h]	PBRCM	None
TTR Antelope Mine 3	373623116434701	TTR Antelope Mine 3_mine1	523866.9	4161956.9	1,939.1	0.0	0.0 [h]	1,929.0 [h]	PBRCM	None
TTR Sulfide Mine	373446116433301	TTR Sulfide Mine_mine1	524197.0	4158978.4	1,868.4	0.0	0.0 [h]	1,851.9 [h]	PBRCM	None
TTR Well 53	373420116260201	TTR Well 53_g	549982.0	4158293.7	1,583.4	243.7	1,442.0 [h, i]	1,339.7 [h]	AA	None
TW-1 (0-560 ft)	370929116132301	TW-1_o7Z	569000.3	4112499.1	1,876.3	1,282.0	1,751.1 [i]	1,705.6	PBRCM	None
TW-1 (0-1615 ft)	370929116132302	TW-1_o6Z	569000.3	4112499.1	1,876.3	1,282.0	1,749.6 [i]	1,384.0	PBRCM	None
TW-1 (0-3731 ft)	370929116132305	TW-1_o4Z	569000.3	4112499.1	1,876.3	1,282.0	1,451.7	739.1	PBRCM	LCA3
TW-1 (1615-1840 ft)	370929116132303	TW-1_o5Z	569000.3	4112499.1	1,876.3	1,282.0	1,384.0	1,315.5	PBRCM	None
TW-1 (1615-3300 ft)	370929116132307	TW-1_o3Z	569000.3	4112499.1	1,876.3	1,282.0	1,294.1	870.4	PBRCM	None
TW-1 (1615-4206 ft)	370929116132311	TW-1_m1	569000.3	4112499.1	1,876.3	1,282.0	1,294.1	594.3	PBRCM	LCA3
TW-1 (3700-3731 ft)	370929116132304	TW-1_o2Z	569000.3	4112499.1	1,876.3	1,282.0	748.5	739.1	LCA3	None
TW-1 (3700-4206 ft)	370929116132309	TW-1_o1Z	569000.3	4112499.1	1,876.3	1,282.0	748.5	594.3	LCA3	None
U-12e.03-1 (430 ft)	371122116122201	None	570468.7	4115979.9	2,299.7	679.4	1,879.7 [h, i]	1,620.3 [h]	PBRCM	None
U-12e.03-1 (682 ft)	371122116122202	None	570468.7	4115979.9	2,299.7	679.4	1,727.0 [h, i]	1,620.3 [h]	PBRCM	None
U-12e.03-1 (834 ft)	371122116122203	None	570468.7	4115979.9	2,299.7	679.4	1,658.1 [h, i]	1,620.3 [h]	PBRCM	None
U-12e.06-1R	371052116125201	U-12e.06-1 R/C-Ex._g	569742.7	4115040.6	2,308.3	969.3	1,414.9 [h, i]	1,339.0 [h]	PBRCM	None
U-12e.M1UG (1501 ft)	371106116123001	U-12e.M1 (UG Ex.)_g	570276.1	4115486.7	2,297.9	878.1	1,424.6 [h, i]	1,419.8 [h]	LCA3	None
U-12e.M1UG (19 ft)	371106116123002	None	570276.1	4115486.7	2,297.9	878.1	1,877.6 [h, i]	1,419.8 [h]	PBRCM	LCA3
U-12e.M1UG (631 ft)	371106116123003	None	570276.1	4115486.7	2,297.9	878.1	1,885.2 [h, i]	1,419.8 [h]	PBRCM	LCA3
U-12e.M1UG (777 ft)	371106116123004	None	570276.1	4115486.7	2,297.9	878.1	1,860.8 [h, i]	1,419.8 [h]	PBRCM	LCA3
U-12g.06PS1V	371028116123002	None	570275.6	4114312.5	2,324.4	449.3	1,875.7 [h, i]	1,875.1 [h]	PBRCM	None
U-12n Vent Hole 2	371213116130501	U-12n Vent Hole 2_o1	569390.2	4117536.8	2,241.5	381.6	1,868.4 i	1,859.9	PBRCM	None
U-12n.10 Vent Hole	371228116122001	U-12n.10 Vent Hole_o1	570500.6	4118007.6	2,218.9	378.0	1,858.4 [h, i]	1,841.0 [h]	PBRCM	None

Table C-1
Site Information for Selected Wells and Boreholes Located in the Pahute Mesa Area and Vicinity
(Page 6 of 13)

Well Name	NWIS ID	ISPID	UTM Easting (m) [a]	UTM Northing (m) [b]	Land Surface Elevation (m amsl) [b]	Total Depth (m bgs) [c]	Effective Open Interval Top Elevation (m amsl) [d]	Effective Open Interval Bottom Elevation (m amsl) [e]	Primary HSU [f]	Secondary HSU [g]
U-12q	371153116134601	None	568379.0	4116931.2	2,259.6	653.5	1,706.9 [h, i]	1,606.1 [h]	PBRCM	None
U-12s (1480 ft)	371342116125102	U-12s_o1	569567.1	4120287.2	2,070.9	486.5	1,786.7 [i]	1,619.8	MGCU	None
U-12s (1596 ft)	371342116125101	U-12s_o2Z	569567.1	4120287.2	2,070.9	486.5	1,776.4 [i]	1,584.4	MGCU	None
U-19ab	371512116193101	None	559842.3	4122993.3	2,111.8	685.8	1,495.0 [h, i]	1,426.0 [h]	BFCU	CFCU
U-19ab 2	371513116193001	None	559863.9	4123006.0	2,112.2	731.5	1,498.1 [h, i]	1,380.7 [h]	BFCU	CFCU
U-19ac	371653116181901	None	561575.0	4126107.6	2,145.2	701.0	1,446.0 [h, i]	1,444.2 [h]	KA	None
U-19adPS1A	371613116211701	U-19ad PS 1A_m1	557215.8	4124859.1	2,028.7	795.2	1,295.1	1,233.5	CHVTA	None
U-19ae	371410116221301	None	555867.2	4121059.2	2,064.9	832.1	1,369.8 [h, i]	1,232.8 [h]	CHZCM	None
U-19af	371423116220401	None	556079.0	4121450.4	2,045.2	670.6	1,375.6 [h, i]	1,374.6 [h]	CHZCM	None
U-19ai	371929116185501	None	560675.0	4130919.1	2,055.0	632.5	1,428.9 [h, i]	1,422.5 [h]	BFCU	None
U-19aj	371812116193201	None	559768.3	4128539.0	2,100.3	670.6	1,432.6 [h, i]	1,429.8 [h]	BFCU	None
U-19aq	371341116222901	None	555471.6	4120144.1	2,072.2	662.9	1,428.9 [h, i]	1,409.2 [h]	PLFA	CHZCM
U-19ar	371643116212001	None	557127.2	4125777.8	2,044.2	670.6	1,399.3 [h, i]	1,373.7 [h]	PLFA	None
U-19aS (2813 ft)	371630116221202	None	555856.7	4125370.8	2,060.7	1,092.4	1,392.6 [h, i]	968.3 [h]	CFCU	BFCU/CHVTA
U-19au	371509116223601	None	555278.5	4122855.6	1,991.6	670.6	1,358.5 [h, i]	1,321.0 [h]	CHVTA	None
U-19au1	371509116223602	None	555285.5	4122848.9	1,990.9	660.5	1,357.9 [h, i]	1,330.4 [h]	CHVTA	None
U-19ax	371750116182401	None	561462.4	4127859.1	2,129.2	670.6	1,467.9 [h, i]	1,458.6 [h]	BFCU	None
U-19ay	371632116211301	None	557311.4	4125422.5	2,045.8	657.1	1,396.9 [h, i]	1,388.7 [h]	PLFA	None
U-19az	371339116221601	U-19az_o1	555779.1	4120082.3	2,058.3	649.2	1,424.6 [h, i]	1,409.0 [h]	PLFA	None
U-19ba	371746116184601	None	560899.2	4127735.7	2,144.9	664.5	1,488.6 [h, i]	1,480.5 [h]	KA	BFCU
U-19ba1	371746116184701	U-19ba 1_o1Z	560892.5	4127744.0	2,145.1	713.2	1,430.7 [h, i]	1,429.7 [h]	BFCU	None
U-19ba2	371745116184701	None	560883.1	4127723.3	2,145.6	713.2	1,432.3 [h, i]	1,431.3 [h]	BFCU	None
U-19ba3	371746116184702	None	560882.8	4127757.5	2,145.1	713.2	1,441.1 [h, i]	1,431.9 [h]	BFCU	None
U-19bg	371621116213501	None	556762.5	4125085.0	2,039.5	657.5	1,395.7 [h, i]	1,382.1 [h]	PLFA	CHVTA
U-19bg1	371620116213501	None	556762.3	4125074.2	2,040.3	685.8	1,394.5 [h, i]	1,354.5 [h]	CHVTA	PLFA
U-19bh	371349116222001	U-19bh_o1	555683.6	4120389.2	2,062.9	654.7	1,427.4 [i]	1,408.1	PLFA	None
U-19bj	371736116184701	U-19bj_o1	560900.3	4127416.1	2,144.1	656.2	1,492.9 [i]	1,487.9	KA	None
U-19bk	371714116230301	U-19bk_o1	554585.7	4126723.0	2,033.0	670.0	1,428.3 [i]	1,363.0	CHVTA	None
U-19c (2656 ft)	371554116185303	None	560769.4	4124276.4	2,143.5	968.3	1,430.1 [h, i]	1,175.1 [h]	BRA	CFCU
U-19d2	372054116191901	U-19d 2_g	560056.4	4133534.8	2,091.1	2,343.6	1,427.7 [h, i]	-252.5 [h]	BRA	PBRCM
U-19d2 (675-4633 ft)	372054116191902	None	560056.4	4133534.8	2,091.1	2,343.6	1,427.1 [i]	679.0	BRA	None

Table C-1
Site Information for Selected Wells and Boreholes Located in the Pahute Mesa Area and Vicinity
(Page 7 of 13)

Well Name	NWIS ID	ISPID	UTM Easting (m) [a]	UTM Northing (m) [b]	Land Surface Elevation (m amsl) [b]	Total Depth (m bgs) [c]	Effective Open Interval Top Elevation (m amsl) [d]	Effective Open Interval Bottom Elevation (m amsl) [e]	Primary HSU [f]	Secondary HSU [g]
U-19d2 (2362-2560 ft)	372054116191915	None	560056.4	4133534.8	2,091.1	2,343.6	1,371.2	1,310.8	BRA	None
U-19d2 (2500-2698 ft)	372054116191914	None	560056.4	4133534.8	2,091.1	2,343.6	1,329.1	1,268.8	BRA	None
U-19d2 (2884-3082 ft)	372054116191912	None	560056.4	4133534.8	2,091.1	2,343.6	1,212.1	1,151.7	BRA	None
U-19d2 (3088-3286 ft)	372054116191911	None	560056.4	4133534.8	2,091.1	2,343.6	1,149.9	1,089.5	BRA	None
U-19d2 (3285-3483 ft)	372054116191910	None	560056.4	4133534.8	2,091.1	2,343.6	1,089.8	1,029.5	BRA	None
U-19d2 (3844-4042 ft)	372054116191907	None	560056.4	4133534.8	2,091.1	2,343.6	919.5	859.1	BRA	None
U-19d2 (4123-4321 ft)	372054116191905	None	560056.4	4133534.8	2,091.1	2,343.6	834.4	774.1	BRA	None
U-19e (5050 ft)	371748116195901	U-19e_o1Z	559100.8	4127774.9	2,108.9	1,539.2	1,430.4 [h, i]	569.7 [h]	BRA	BFCU
U-19g (3079-3197 ft)	371836116215104	None	556340.5	4129244.1	2,052.4	1,003.4	1,114.0	1,078.0	BRA	None
U-19g (3132-3250 ft)	371836116215103	None	556340.5	4129244.1	2,052.4	1,003.4	1,097.8	1,061.8	BRA	None
U-19g (liner)	371836116215101	U-19g_m1Z	556340.5	4129244.1	2,052.4	1,003.4	1,424.0 [h, i]	1,049.0 [h]	BFCU	BRA/CFCU
U-19x	371401116220601	None	556020.5	4120757.9	2,066.8	679.7	1,392.0 [h, i]	1,387.1 [h]	PLFA	None
U-20WW (2528 ft)	371505116254502	U-20 WW_o1Z	550614.2	4122711.6	1,971.3	996.1	1,351.5 [i]	1,200.8	CHZCM	CHLFA1
U-20WW (cased)	371505116254501	U-20 WW_m1	550614.2	4122711.6	1,971.3	996.1	1,279.1	975.2	CHLFA4	CHZCM
U-20a (2177 ft)	371434116255101	None	550480.6	4121740.0	1,987.2	774.2	1,328.6 [h, i]	1,213.0 [h]	CHLFA4	CHLFA1
U-20a 2 WW	371434116251601	U-20a 2 WW_o1Z	551333.3	4121743.1	1,972.5	1,371.6	1,343.3 [h, i]	600.9 [h]	CHLFA4	CHLFA1
U-20a 2 WW (860-2404 ft)	371434116251614	None	551333.3	4121743.1	1,972.5	1,371.6	1,342.6 [i]	1,239.8	CHLFA1	CHLFA4
U-20a 2 WW (2404-2608 ft)	371434116251613	None	551333.3	4121743.1	1,972.5	1,371.6	1,239.8	1,177.6	CHLFA4	None
U-20a 2 WW (2492-2682 ft)	371434116251612	None	551333.3	4121743.1	1,972.5	1,371.6	1,213.0	1,155.1	CHLFA4	None
U-20a 2WW (2895-3085 ft)	371434116251610	None	551333.3	4121743.1	1,972.5	1,371.6	1,090.1	1,032.2	CHLFA4	None
U-20a 2 WW (3090-3280 ft)	371434116251609	None	551333.3	4121743.1	1,972.5	1,371.6	1,030.7	972.8	CHLFA4	None
U-20a 2 WW (3460-3650 ft)	371434116251607	None	551333.3	4121743.1	1,972.5	1,371.6	917.9	860.0	CHLFA4	None
U-20a 2 WW (3648-3838 ft)	371434116251606	None	551333.3	4121743.1	1,972.5	1,371.6	860.6	802.7	CHLFA4	None
U-20a 2 WW (3848-4038 ft)	371434116251605	None	551333.3	4121743.1	1,972.5	1,371.6	799.7	741.8	CHLFA4	None
U-20a 2 WW (4048-4238 ft)	371434116251604	None	551333.3	4121743.1	1,972.5	1,371.6	738.7	680.8	CHLFA4	None
U-20a 2 WW (4355-4500 ft)	371434116251602	None	551333.3	4121743.1	1,972.5	1,371.6	645.1	600.9	CHLFA4	None
U-20aa	371822116281701	None	546837.5	4128745.2	1,931.4	1,294.5	1,361.5 [h, i]	636.9 [h]	CHLFA3	CFCM/CHLFA5
U-20ad	371723116271901	None	548286.4	4126944.4	1,940.5	716.3	1,360.3 [h, i]	1,224.2 [h]	CHZCM	CHLFA2
U-20ae	371523116283900	None	546343.2	4123232.1	1,886.3	716.3	1,280.2 [h, i]	1,170.1 [h]	UPCU	None
U-20ag	371328116274601	None	547672.1	4119690.0	1,900.1	670.6	1,285.6 [h, i]	1,229.6 [h]	BA	None
U-20ah	371521116252001	None	551224.8	4123206.5	1,964.5	701.0	1,354.2 [h, i]	1,263.5 [h]	CHLFA1	None

Table C-1
Site Information for Selected Wells and Boreholes Located in the Pahute Mesa Area and Vicinity
(Page 8 of 13)

Well Name	NWIS ID	ISPID	UTM Easting (m) [a]	UTM Northing (m) [b]	Land Surface Elevation (m amsl) [b]	Total Depth (m bgs) [c]	Effective Open Interval Top Elevation (m amsl) [d]	Effective Open Interval Bottom Elevation (m amsl) [e]	Primary HSU [f]	Secondary HSU [g]
U-20ai	371551116262501	U-20ai_o1Z	549637.4	4124115.3	1,982.2	656.5	1,356.4 [h, i]	1,325.6 [h]	CHLFA3	None
U-20aj	371802116273601	None	547855.4	4128162.0	1,933.9	566.0	1,369.5 [h, i]	1,367.9 [h]	CHLFA2	None
U-20ak	371452116292101	None	545315.4	4122286.9	1,900.5	640.1	1,278.3 [h, i]	1,260.4 [h]	BA	None
U-20al	371612116295101	U-20aL_o1Z	544545.9	4124748.1	1,866.5	609.6	1,302.7 [h, i]	1,256.9 [h]	UPCU	None
U-20am	371604116243801	None	552255.9	4124536.1	2,009.6	670.6	1,356.7 [h, i]	1,339.1 [h]	CHLFA4	None
U-20an	371750116262701	None	549804.3	4127791.8	1,969.5	617.5	1,363.1 [h, i]	1,352.0 [h]	CHLFA3	None
U-20ao	371416116282201	U-20ao_o1Z	546767.7	4121179.9	1,913.8	655.3	1,317.7 [h, i]	1,258.5 [h]	BA	None
U-20ap	371547116244201	None	552166.8	4124002.5	2,018.1	655.3	1,366.4 [h, i]	1,362.8 [h]	CHZCM	None
U-20aq	371553116300401	None	544396.2	4124138.0	1,876.0	579.1	1,302.1 [h, i]	1,296.9 [h]	UPCU	None
U-20ar1	371852116281701	None	546841.1	4129690.7	1,926.1	696.5	1,364.6 [h, i]	1,229.7 [h]	CHLFA2	CHZCM/TMLVTA
U-20as	371313116274201	U-20as_g	547764.6	4119233.6	1,898.0	640.1	1,284.4 [h, i]	1,257.9 [h]	UPCU	None
U-20at1	371452116303301	None	543540.1	4122270.4	1,902.2	669.6	1,284.4 [h, i]	1,232.5 [h]	LPCU	TCA
U-20av	371359116252301	None	551172.7	4120677.7	1,970.1	640.1	1,337.5 [h, i]	1,330.1 [h]	LPCU	None
U-20aw	371658116244401	None	552097.9	4126211.3	2,007.1	640.1	1,371.3 [h, i]	1,367.0 [h]	CHZCM	None
U-20ax	371350116264701	None	549116.8	4120396.4	1,992.2	670.6	1,329.8 [h, i]	1,321.6 [h]	CHLFA1	None
U-20ay	371536116262801	None	549562.4	4123673.3	1,987.4	640.1	1,360.9 [h, i]	1,347.4 [h]	CHLFA3	None
U-20az	371352116243401	None	552392.3	4120468.5	2,003.4	685.8	1,345.1 [h, i]	1,317.6 [h]	CHZCM	None
U-20bb (1900 ft)	371452116293901	None	544857.9	4122285.3	1,897.8	676.7	1,367.6 [h, i]	1,221.1 [h]	PBPCU	UPCU/BA
U-20bb (2220 ft)	371452116293902	None	544857.9	4122285.3	1,897.8	676.7	1,284.1 [h, i]	1,221.1 [h]	PBPCU	UPCU/BA
U-20bb1	371452116293903	None	544858.2	4122265.3	1,897.7	714.8	1,279.6 [h, i]	1,182.9 [h]	UPCU	BA/PBPCU
U-20bc	371547116292601	None	545158.2	4123977.8	1,873.4	609.6	1,303.0 [h, i]	1,263.8 [h]	UPCU	None
U-20bd (2100 ft)	371542116251201	None	551420.2	4123847.5	1,976.7	689.2	1,417.0 [h, i]	1,287.5 [h]	UPCU	CHZCM/LPCU
U-20bd (2261 ft)	371542116251203	None	551420.2	4123847.5	1,976.7	689.2	1,355.4 [h, i]	1,287.5 [h]	CHZCM	LPCU/UPCU
U-20bd 1	371542116251301	None	551402.8	4123864.9	1,976.8	732.1	1,355.4 [h, i]	1,244.7 [h]	CHZCM	LPCU/CHLFA3
U-20bd 2	371542116251202	None	551437.6	4123857.4	1,977.2	746.8	1,356.1 [h, i]	1,230.5 [h]	CHZCM	CHLFA3/LPCU
U-20be	371332116254101	None	550733.4	4119853.1	1,978.6	676.7	1,303.6 [h, i]	1,302.0 [h]	CHZCM	None
U-20bf	371444116263001	None	549522.6	4122042.5	1,988.0	685.8	1,339.0 [h, i]	1,302.2 [h]	CHLFA1	None
U-20bg	371414116242901	U-20bg_o1	552511.8	4121139.2	2,001.7	670.6	1,350.3 [i]	1,331.1	CHZCM	None
U-20c (12-4800 ft)	371353116282507	None	546698.7	4120477.8	1,914.4	1,463.0	1,275.3 [h, i]	451.4 [h]	CHZCM	CHZCM/CHLFA5
U-20e	371851116273801	U-20e_o1Z	547789.3	4129655.0	1,925.1	1,174.4	1,360.3 [h, i]	750.7 [h]	CHLFA3	CHLFA5/CHLFA2
U-20f	371617116291801	U-20f_o1Z	545355.2	4124900.3	1,864.4	1,280.8	1,276.2 [h, i]	583.6 [h]	CHLFA5	UPCU/CHZCM

Table C-1
Site Information for Selected Wells and Boreholes Located in the Pahute Mesa Area and Vicinity
(Page 9 of 13)

Well Name	NWIS ID	ISPID	UTM Easting (m) [a]	UTM Northing (m) [b]	Land Surface Elevation (m amsl) [b]	Total Depth (m bgs) [c]	Effective Open Interval Top Elevation (m amsl) [d]	Effective Open Interval Bottom Elevation (m amsl) [e]	Primary HSU [f]	Secondary HSU [g]
U-20i	371744116272101	None	548243.0	4127580.9	1,941.6	1,434.1	1,361.2 [h, i]	507.6 [h]	CFCM	CHLFA3/CHLFA5
U-20i (4397-4545 ft)	371744116272105	None	548243.0	4127580.9	1,941.6	1,434.1	601.4	556.3	CFCM	None
U-20i (4520-4668 ft)	371744116272104	None	548243.0	4127580.9	1,941.6	1,434.1	563.9	518.8	CFCM	None
U-20m (3710-3920 ft)	371802116320304	None	541289.7	4128104.3	1,799.2	1,264.0	668.4	604.4	PBRCM	None
U-20n	371434116251301	None	551424.4	4121743.0	1,974.1	1,301.2	1,352.7 [h, i]	672.9 [h]	CHLFA4	CHZCM
U-20n PS1DD-H (4309 ft)	371433116251301	U-20n PS 1D_o3Z	551149.9	4121479.1	1,971.5	1,377.7	690.7	658.1	CHLFA4	None
U-20y (1925 ft)	371315116282702	None	546651.3	4119291.1	1,907.0	793.1	1,340.8 [h, i]	1,114.0 [h]	TSA	LPCU/TCA
U-20y (2602 ft)	371315116282701	None	546651.3	4119291.1	1,907.0	793.1	1,277.1 [h, i]	1,114.0 [h]	TSA	LPCU
UE-12n 15A	371226116125201	None	569703.1	4117954.5	2,246.1	589.5	1,840.7 [h, i]	1,656.6 [h]	PBRCM	MGCU
UE-12t6 (1378 ft)	371332116112801	UE-12t-6_o2Z	571753.7	4119988.8	2,105.3	445.3	1,841.0 [i]	1,685.4	PBRCM	None
UE-12t6 (1461 ft)	371332116112802	UE-12t-6_o1	571753.7	4119988.8	2,105.3	445.3	1,853.2 [i]	1,659.9	PBRCM	None
UE-12t7	371307116103801	None	572584.2	4120449.5	2,121.7	515.7	1,865.7 [h, i]	1,606.0 [h]	PBRCM	None
UE-17c	370616116090801	None	575340.0	4106606.2	1,473.6	178.6	1,317.7 [h, i]	1,295.0 [h]	AA	UCCU
UE-18r	370806116264001	UE-18r_o1	549321.8	4109762.2	1,688.0	1,525.2	1,191.5	162.8	ATWTA	ATCCU/THCU
UE-18r (1648-1848 ft)	370806116264019	UE-18r_o18Z	549321.8	4109762.2	1,688.0	1,525.2	1,185.7	1,124.8	ATWTA	None
UE-18r (1859-2059 ft)	370806116264017	UE-18r_o16Z	549321.8	4109762.2	1,688.0	1,525.2	1,121.4	1,060.5	ATWTA	None
UE-18r (2000-2200 ft)	370806116264016	UE-18r_o15Z	549321.8	4109762.2	1,688.0	1,525.2	1,078.4	1,017.5	ATWTA	None
UE-18r (2193-2393 ft)	370806116264015	UE-18r_o14Z	549321.8	4109762.2	1,688.0	1,525.2	1,019.6	958.7	ATWTA	None
UE-18r (2408-2608 ft)	370806116264014	UE-18r_o13Z	549321.8	4109762.2	1,688.0	1,525.2	954.1	893.1	ATWTA	None
UE-18r (2616-2816 ft)	370806116264013	UE-18r_o12Z	549321.8	4109762.2	1,688.0	1,525.2	890.7	829.7	ATWTA	None
UE-18r (2796-2996 ft)	370806116264012	UE-18r_o11Z	549321.8	4109762.2	1,688.0	1,525.2	835.8	774.9	ATWTA	ATCCU
UE-18r (3002-3202 ft)	370806116264011	UE-18r_o10Z	549321.8	4109762.2	1,688.0	1,525.2	773.0	712.1	ATCCU	None
UE-18r (3442-3642 ft)	370806116264009	UE-18r_o8Z	549321.8	4109762.2	1,688.0	1,525.2	638.9	578.0	THLFA	ATCCU
UE-18r (3849-4049 ft)	370806116264007	UE-18r_o6Z	549321.8	4109762.2	1,688.0	1,525.2	514.9	453.9	THCU	THLFA
UE-18r (4051-4251 ft)	370806116264006	UE-18r_o5Z	549321.8	4109762.2	1,688.0	1,525.2	453.3	392.3	THCU	None
UE-18t	370741116194501	UE-18t_o1	559591.4	4109095.1	1,585.3	792.5	1,306.7 [i]	792.8	RMWTA	ATWTA/THCU
UE-19b 1 (2190-2374 ft)	371852116175708	None	562090.7	4129796.6	2,073.2	1,371.6	1,405.7	1,349.7	BRA	None
UE-19b 1 (2361-2559 ft)	371852116175707	None	562090.7	4129796.6	2,073.2	1,371.6	1,353.6	1,293.3	BRA	None
UE-19b 1 (2556-2754 ft)	371852116175706	None	562090.7	4129796.6	2,073.2	1,371.6	1,294.2	1,233.8	BRA	None
UE-19b 1 (2754-2952 ft)	371852116175705	None	562090.7	4129796.6	2,073.2	1,371.6	1,233.8	1,173.5	BRA	None
UE-19b 1 (3758-3956 ft)	371852116175702	None	562090.7	4129796.6	2,073.2	1,371.6	927.8	867.5	BRA	None

Table C-1
Site Information for Selected Wells and Boreholes Located in the Pahute Mesa Area and Vicinity
(Page 10 of 13)

Well Name	NWIS ID	ISPID	UTM Easting (m) [a]	UTM Northing (m) [b]	Land Surface Elevation (m amsl) [b]	Total Depth (m bgs) [c]	Effective Open Interval Top Elevation (m amsl) [d]	Effective Open Interval Bottom Elevation (m amsl) [e]	Primary HSU [f]	Secondary HSU [g]
UE-19b 1 WW	371852116175701	UE-19b 1_o1Z	562090.7	4129796.6	2,073.2	1,371.6	1,428.0 [h, i]	701.6 [h]	BRA	None
UE-19c (2421-4520 ft)	371608116191001	UE-19c WW_o1-8Z	560338.8	4124701.6	2,143.7	2,587.4	1,405.8	766.0	BRA	None
UE-19c (2884-3082 ft)	371608116191009	UE-19c WW_o7Z	560338.8	4124701.6	2,143.7	2,587.4	1,264.6	1,204.3	BRA	None
UE-19c (3078-3284 ft)	371608116191008	UE-19c WW_o6Z	560338.8	4124701.6	2,143.7	2,587.4	1,205.5	1,142.7	BRA	None
UE-19c WW	371608116191002	UE-19c WW_m1	560338.8	4124701.6	2,143.7	2,587.4	1,405.8	-443.8	BRA	PBRCM
UE-19e WW	371750116195901	UE-19e/Inst._o1Z	559100.4	4127835.9	2,108.8	1,830.3	1,432.9 [h, i]	278.5 [h]	BFCU	None
UE-19fS (2565-4779 ft)	371329116220302	None	556107.6	4119780.7	2,052.9	2,118.4	1,271.1	596.2	BRA	BFCU
UE-19fS (2750-2908 ft)	371329116220314	None	556107.6	4119780.7	2,052.9	2,118.4	1,214.7	1,166.5	IA	CFCU/CHZCM
UE-19fS (2908-3066 ft)	371329116220313	None	556107.6	4119780.7	2,052.9	2,118.4	1,166.5	1,118.4	IA	None
UE-19fS (3060-3218 ft)	371329116220312	None	556107.6	4119780.7	2,052.9	2,118.4	1,120.2	1,072.0	IA	None
UE-19fS (3520-3678 ft)	371329116220309	None	556107.6	4119780.7	2,052.9	2,118.4	980.0	931.8	IA	None
UE-19fS (3680-3838 ft)	371329116220308	None	556107.6	4119780.7	2,052.9	2,118.4	931.2	883.1	IA	None
UE-19fS (4298-4456 ft)	371329116220304	None	556107.6	4119780.7	2,052.9	2,118.4	742.9	694.7	IA	None
UE-19fS (4464-4779 ft)	371329116220303	None	556107.6	4119780.7	2,052.9	2,118.4	692.3	596.2	CFCU	IA
UE-19gS (2650-4508 ft)	371830116215300	UE-19gs_m2Z	556306.1	4129056.8	2,048.0	2,286.0	1,240.3	674.0	CFCU	BFCU
UE-19gS (2650-7500 ft)	371830116215303	None	556306.1	4129056.8	2,048.0	2,286.0	1,240.3	-238.0	BRA	BFCU
UE-19gS (2802-2970 ft)	371830116215305	None	556306.1	4129056.8	2,048.0	2,286.0	1,194.0	1,142.8	BRA	PBRCM/BFCU
UE-19gS (6920-7118 ft)	371830116215322	None	556306.1	4129056.8	2,048.0	2,286.0	-61.2	-121.5	BRA	None
UE-19h (2321-2396 ft)	372034116222512	UE-19h_o8Z	555488.5	4132881.6	2,066.6	1,129.3	1,359.1	1,336.3	BRA	None
UE-19h (2321-3705 ft)	372034116222501	UE-19h_o1-8Z	555488.5	4132881.6	2,066.6	1,129.3	1,359.1	937.3	BRA	None
UE-19h (2408-2604 ft)	372034116222511	UE-19h_o7Z	555488.5	4132881.6	2,066.6	1,129.3	1,332.6	1,272.9	BRA	None
UE-19h (2566-2762 ft)	372034116222510	UE-19h_o6Z	555488.5	4132881.6	2,066.6	1,129.3	1,284.5	1,224.7	BRA	None
UE-19h (2765-2961 ft)	372034116222509	UE-19h_o5Z	555488.5	4132881.6	2,066.6	1,129.3	1,223.8	1,161.0	BRA	None
UE-19h (2833-3029 ft)	372034116222508	UE-19h_o4Z	555488.5	4132881.6	2,066.6	1,129.3	1,203.1	1,143.3	BRA	None
UE-19h (3030-3226 ft)	372034116222507	UE-19h_o3Z	555488.5	4132881.6	2,066.6	1,129.3	1,143.0	1,083.3	BRA	None
UE-19h (3220-3416 ft)	372034116222506	UE-19h_o2Z	555488.5	4132881.6	2,066.6	1,129.3	1,085.1	1,025.4	BRA	None
UE-19h (3420-3705 ft)	372034116222505	UE-19h_o1Z	555488.5	4132881.6	2,066.6	1,129.3	1,024.2	937.3	BRA	None
UE-19h (recompleted)	372034116222504	UE-19h_m1	555488.5	4132881.6	2,066.6	1,129.3	1,423.1 [i]	1,369.5	BRA	None
UE-19i (2910-3068 ft)	371459116204810	None	557922.3	4122592.1	2,084.5	2,438.4	1,197.5	1,149.4	BFCU	None
UE-19i (3222-3380 ft)	371459116204808	None	557922.3	4122592.1	2,084.5	2,438.4	1,102.4	1,054.3	BFCU	None
UE-19i (3298-3456 ft)	371459116204807	None	557922.3	4122592.1	2,084.5	2,438.4	1,079.3	1,031.1	BFCU	None

Table C-1
Site Information for Selected Wells and Boreholes Located in the Pahute Mesa Area and Vicinity
(Page 11 of 13)

Well Name	NWIS ID	ISPID	UTM Easting (m) [a]	UTM Northing (m) [b]	Land Surface Elevation (m amsl) [b]	Total Depth (m bgs) [c]	Effective Open Interval Top Elevation (m amsl) [d]	Effective Open Interval Bottom Elevation (m amsl) [e]	Primary HSU [f]	Secondary HSU [g]
UE-19i (3460-3618 ft)	371459116204806	None	557922.3	4122592.1	2,084.5	2,438.4	1,029.9	981.7	BFCU	None
UE-19i (4100-4258 ft)	371459116204802	None	557922.3	4122592.1	2,084.5	2,438.4	834.8	786.7	BFCU	None
UE-19z (2225 ft)	371758116193602	None	559665.0	4128109.0	2,099.4	853.4	1,458.8 [h, i]	1,245.9 [h]	BFCU	None
UE-19z (2800 ft)	371758116193601	None	559665.0	4128109.0	2,099.4	853.4	1,429.5 [h, i]	1,245.9 [h]	BFCU	None
UE-20ab	371623116243701	None	552284.4	4125130.2	2,005.8	777.2	1,357.9 [h, i]	1,228.5 [h]	CHLFA3	CHLFA4
UE-20av	371401116252001	None	551258.9	4120728.1	1,968.5	796.7	1,319.8 [h, i]	1,171.7 [h]	CHLFA4	LPCU/CHZCM
UE-20bh 1	371442116243301	UE-20bh 1_o1	552402.2	4122007.3	2,022.8	856.5	1,349.0 [i]	1,166.3	CHLFA5	CHZCM
UE-20c (3210 ft)	371352116281801	None	546865.6	4120450.4	1,915.1	1,630.1	1,266.7 [h, i]	285.0 [h]	CHZCM	CHZCM/CHLFA5
UE-20d	371452116284901	UE-20d_o1Z	546102.8	4122275.1	1,905.9	1,369.2	1,273.8 [h, i]	536.8 [h]	CHZCM	CHLFA5/UPCU
UE-20d (2578-2776 ft)	371452116284908	None	546102.8	4122275.1	1,905.9	1,369.2	1,120.1	1,059.8	TCA	LPCU
UE-20d (3074-3272 ft)	371452116284907	None	546102.8	4122275.1	1,905.9	1,369.2	969.0	908.6	TSA	CHZCM
UE-20e 1 (1500-2766 ft)	371901116272510	None	548110.3	4129980.8	1,919.4	1,949.2	1,360.9 [i]	1,076.3	CHLFA3	CHZCM/CHLFA2
UE-20e 1 (1500-3600 ft)	371901116272502	None	548110.3	4129980.8	1,919.4	1,949.2	1,362.8 [i]	822.1	CHLFA3	CHLFA5/CHZCM
UE-20e 1 (1500-6395 ft)	371901116272501	UE-20e 1_o1Z	548110.3	4129980.8	1,919.4	1,949.2	1,365.5 [i]	-29.8	CHLFA3	BRA/CFCM
UE-20e 1 (2774-2972 ft)	371901116272509	None	548110.3	4129980.8	1,919.4	1,949.2	1,073.8	1,013.5	CHLFA3	None
UE-20e 1 (3480-3678 ft)	371901116272507	None	548110.3	4129980.8	1,919.4	1,949.2	858.7	798.3	CHLFA5	None
UE-20e 1 (4020-4218 ft)	371901116272506	None	548110.3	4129980.8	1,919.4	1,949.2	694.1	633.7	CHZCM	CFCM
UE-20e 1 (4540-6395 ft)	371901116272503	None	548110.3	4129980.8	1,919.4	1,949.2	535.6	-29.8	BRA	CFCM
UE-20f (4350-4543 ft)	371617116291703	None	545400.8	4124900.3	1,864.2	4,171.5	538.4	479.5	IA	None
UE-20f (4456-13686 ft)	371617116291701	UE-20f_o1Z	545400.8	4124900.3	1,864.2	4,171.5	506.1	-2,307.2	PBRCM	BFCU/BRA
UE-20f (4568-4766 ft)	371617116291725	None	545400.8	4124900.3	1,864.2	4,171.5	471.9	411.6	IA	None
UE-20f (5051-5249 ft)	371617116291724	None	545400.8	4124900.3	1,864.2	4,171.5	324.7	264.4	IA	None
UE-20h (2575-2743 ft)	371618116260215	None	550196.6	4124975.0	1,998.5	2,196.7	1,213.6	1,162.4	CHLFA4	None
UE-20h (2741-2909 ft)	371618116260214	None	550196.6	4124975.0	1,998.5	2,196.7	1,163.0	1,111.8	CHLFA4	None
UE-20h (2900-3068 ft)	371618116260213	None	550196.6	4124975.0	1,998.5	2,196.7	1,114.5	1,063.3	CHLFA4	None
UE-20h (3042-3210 ft)	371618116260212	None	550196.6	4124975.0	1,998.5	2,196.7	1,071.3	1,020.0	CHLFA4	CHZCM
UE-20h (3350-3518 ft)	371618116260211	None	550196.6	4124975.0	1,998.5	2,196.7	977.4	926.2	CHZCM	None
UE-20h (3522-7207 ft)	371618116260203	None	550196.6	4124975.0	1,998.5	2,196.7	924.9	-198.2	BFCU	CHZCM/CFCU
UE-20h (3705-3873 ft)	371618116260209	None	550196.6	4124975.0	1,998.5	2,196.7	869.2	818.0	CHZCM	None
UE-20h (3892-4060 ft)	371618116260208	None	550196.6	4124975.0	1,998.5	2,196.7	812.2	761.0	CHZCM	None
UE-20h (4070-4238 ft)	371618116260207	None	550196.6	4124975.0	1,998.5	2,196.7	757.9	706.7	CHZCM	None

Table C-1
Site Information for Selected Wells and Boreholes Located in the Pahute Mesa Area and Vicinity
(Page 12 of 13)

Well Name	NWIS ID	ISPID	UTM Easting (m) [a]	UTM Northing (m) [b]	Land Surface Elevation (m amsl) [b]	Total Depth (m bgs) [c]	Effective Open Interval Top Elevation (m amsl) [d]	Effective Open Interval Bottom Elevation (m amsl) [e]	Primary HSU [f]	Secondary HSU [g]
UE-20h (4500-4676 ft)	371618116260205	None	550196.6	4124975.0	1,998.5	2,196.7	626.9	573.2	CHZCM	None
UE-20h WW	371618116260201	UE-20h Emplacement Hole_o1Z	550196.6	4124975.0	1,998.5	2,196.7	1,356.4 [h, i]	-198.2 [h]	CHZCM	BFCU/CHLFA4
UE-20j (1858-2056 ft)	371801116320313	None	541284.9	4128082.4	1,799.2	1,734.3	1,232.9	1,172.5	BRA	BFCU
UE-20j (2051-2249 ft)	371801116320312	None	541284.9	4128082.4	1,799.2	1,734.3	1,174.0	1,113.7	BRA	None
UE-20j (2253-2461 ft)	371801116320311	None	541284.9	4128082.4	1,799.2	1,734.3	1,112.5	1,049.1	PBRCM	BRA
UE-20j (2670-2868 ft)	371801116320309	None	541284.9	4128082.4	1,799.2	1,734.3	985.4	925.0	PBRCM	None
UE-20j (2957-3155 ft)	371801116320308	None	541284.9	4128082.4	1,799.2	1,734.3	897.9	837.5	PBRCM	None
UE-20j (3147-3345 ft)	371801116320307	None	541284.9	4128082.4	1,799.2	1,734.3	840.0	779.6	PBRCM	None
UE-20j (3359-3557 ft)	371801116320306	None	541284.9	4128082.4	1,799.2	1,734.3	775.4	715.0	PBRCM	None
UE-20j (3487-3685 ft)	371801116320305	None	541284.9	4128082.4	1,799.2	1,734.3	736.3	676.0	PBRCM	None
UE-20j (3634-3832 ft)	371801116320304	None	541284.9	4128082.4	1,799.2	1,734.3	691.5	631.2	PBRCM	None
UE-20j WW	371801116320301	UE-20j Instrument Hole_o1Z	541284.9	4128082.4	1,799.2	1,734.3	1,411.8 [h, i]	64.9 [h]	PBRCM	BRA
UE-20n 1 (2834 ft)	371425116251902	UE-20n 1_o2	551273.3	4121483.8	1,969.2	1,005.8	1,261.2	1,108.5	CHLFA4	None
UE-20p ST-2	372024116312003	None	542331.5	4132503.3	1,692.5	1,524.0	1,422.8 [h, i]	168.5 [h]	PBRCM	TMWTA/BRA
UE-25 WT 6	365340116264601	UE-25 WT 6_p1	549361.5	4083092.1	1,314.7	383.1	946.5	931.6	YMCFCM	None
UE-25 WT 16	365239116253401	UE-25 WT 16_p1	551157.1	4081222.4	1,210.5	521.2	700.2	689.3	YMCFCM	None
UE-25 WT 18	365207116264201	None	549472.5	4080225.1	1,336.3	622.7	730.6 [h, i]	713.6 [h]	YMCFCM	None
UE-29a 1 HTH	365629116222601	UE-29a 1_o1	555758.1	4088341.3	1,214.4	65.5	1,188.7 [i]	1,148.9	PCM	YMCFCM
UE-29a 2 HTH	365629116222602	UE-29a 2_p1	555749.4	4088345.9	1,214.5	421.5	1,127.6	793.0	YMCFCM	None
USAF TTR Cedar Pass R-1 WW	374241116264601	None	548821.3	4173733.2	1,736.1	236.2	1,608.1 [h, i]	1,499.9 [h]	AA	None
USWG-1	365200116272901	None	548298.6	4080017.8	1,325.9	1,828.8	754.1 [h, i]	-502.9 [h]	YMCFCM	PBRCM
USWG-2	365322116273501	USW G-2_m1	548138.6	4082553.9	1,553.7	1,830.6	1,019.9 [i]	761.8	YMCFCM	None
USW UZ-N91	365624116222901	UE-29 UZN 91_m1	555687.2	4088202.5	1,203.8	28.7	1,176.6	1,175.1	PCM	None
USW WT-24	365301116271301	None	548690.9	4081897.6	1,493.6	863.8	840.3 [h, i]	629.8 [h]	YMCFCM	None
Ute Springs Drainage Well	365713116425301	None	525399.0	4089561.3	1,063.8	3.3	1,062.8 [h, i]	1,060.5 [h]	AA	None
WW-8 (1770-2031 ft)	370956116172102	WW-8_o7Z	563113.0	4113274.6	1,735.7	1,673.4	1,409.4 [i]	1,370.6	BRA	None
WW-8 (2031-2053 ft)	370956116172105	WW-8_o5Z	563113.0	4113274.6	1,735.7	1,673.4	1,116.7	1,110.0	PBRCM	None
WW-8 (2031-5490 ft)	370956116172133	WW-8_m1	563113.0	4113274.6	1,735.7	1,673.4	1,116.7	62.4	PBRCM	LCCU1
WW-8 (2053-2249 ft)	370956116172104	WW-8_o4Z	563113.0	4113274.6	1,735.7	1,673.4	1,110.0	1,050.2	PBRCM	None
WW-8 (30-1198 ft)	370956116172103	WW-8_o6Z	563113.0	4113274.6	1,735.7	1,673.4	1,196.2	1,116.7	BRA	PBRCM
WW-8 (30-2031 ft)	370956116172101	WW-8_m26	563113.0	4113274.6	1,735.7	1,673.4	1,410.3 [i]	1,116.7	BRA	PBRCM

Table C-1
Site Information for Selected Wells and Boreholes Located in the Pahute Mesa Area and Vicinity
(Page 13 of 13)

Well Name	NWIS ID	ISPID	UTM Easting (m) [a]	UTM Northing (m) [b]	Land Surface Elevation (m amsl) [b]	Total Depth (m bgs) [c]	Effective Open Interval Top Elevation (m amsl) [d]	Effective Open Interval Bottom Elevation (m amsl) [e]	Primary HSU [f]	Secondary HSU [g]
WW-8 (3333-3429 ft)	370956116172106	WW-8_o3Z	563113.0	4113274.6	1,735.7	1,673.4	719.8	690.6	PBRCM	None
WW-8 (3428-3524 ft)	370956116172107	WW-8_o2Z	563113.0	4113274.6	1,735.7	1,673.4	690.9	661.6	PBRCM	None

[a] UTM Zone 11, NAD 1927 in meters.
[b] Land-surface elevation in meters above mean sea level; source is Fenelon (2015).
[c] Total drilled depth in meters below ground surface; source is the UGTA Borehole Index Database (Navarro, 2019).
[d] Effective open interval top elevation in meters above mean sea level; calculated as land-surface elevation minus depth to top of EOI.
[e] Effective open interval bottom in meters above mean sea level; calculated as land-surface elevation minus depth to bottom of EOI.
[f] Primary HSU is defined as the thickest HSU within well screen.
[g] Secondary HSU is defined as the second-thickest HSU within the well screen.
[h] Well is an open borehole or the well screen interval is unknown, and the well is assumed to have an open borehole.
[i] Water table occurs the top of the open interval, and the depth to water defines the top of the EOI.

amsl = Above mean sea level
NAD = North American Datum
UTM = Universal Transverse Mercator

Table C-2
Site Information for Selected Springs Located in the Pahute Mesa Area and Vicinity
(Page 1 of 3)

Spring Name	UTM Easting (m) [a]	UTM Northing (m) [a]	Land Surface Elevation (m amsl) [b]	Land Surface Accuracy (m) [b]	HSU at Land Surface	HSU at Land Surface Thickness (m)	Other HSUs within 100 m of Land Surface
Beatty_Springs	523017.8	4086384.0	1,023.5	6.1	AA	100.0	None
Burrell_Hot_Spring	524963.0	4090290.0	1,080.2	6.1	AA	6.1	DVCM
Colson_Pond	527348.7	4103023.0	1,211.6	6.1	AA	4.3	TCVA/FCCM
Crystal_Springs1	521467.9	4092988.0	1,209.1	6.1	AA	28.3	DVCM
Crystal_Springs2	521978.3	4093217.5	1,189.0	6.1	AA	76.8	DVCM
Goss_Springs1	525448.6	4094296.8	1,121.7	6.1	DVA	100.0	None
Goss_Springs2	526061.8	4094123.8	1,161.9	6.1	DVA	100.0	None
Goss_Springs3	526239.7	4093964.0	1,157.6	6.1	DVA	100.0	None
Goss_Springs4	525213.8	4094516.5	1,120.4	6.1	DVA	100.0	None
Goss_Springs5	525407.2	4094285.0	1,120.4	6.1	DVA	100.0	None
Goss_Springs6	525276.3	4094412.0	1,121.1	6.1	DVA	100.0	None
Goss_Springs_north1	526087.0	4094638.3	1,170.7	6.1	DVA	100.0	None
Goss_Springs_north2	526155.3	4094613.0	1,169.8	6.1	DVA	100.0	None
Hot_Springs1	524871.0	4091777.0	1,095.8	6.1	DVCM	100.0	None
Hot_Springs2	524818.4	4091827.0	1,094.2	6.1	DVCM	100.0	None
Hot_Springs3	524796.9	4091880.5	1,094.8	6.1	DVCM	100.0	None
Hot_Springs4	524793.8	4092087.3	1,094.5	6.1	AA	6.1	DVCM
Hot_Springs5	524905.3	4091745.5	1,095.8	6.1	DVCM	100.0	None
Hot_Springs6	524983.0	4091639.0	1,094.2	6.1	AA	2.5	DVCM
Hot_Springs7	524805.5	4091853.8	1,094.2	6.1	DVCM	100.0	None
Long_Spring_NE_area	524984.0	4097835.5	1,150.9	6.1	DVA	100.0	None
Lower_Indian_Springs1	518303.5	4088623.0	1,237.5	6.1	AA	10.0	DVCM
Lower_Indian_Springs2	518183.5	4088554.5	1,227.4	6.1	AA	8.4	DVCM
Middle_Indian_Spring	517830.1	4089114.8	1,270.1	6.1	AA	1.4	DVCM
NE_unnamed_spring1	525816.6	4098790.0	1,170.4	6.1	AA	6.2	DVA

Table C-2
Site Information for Selected Springs Located in the Pahute Mesa Area and Vicinity
(Page 2 of 3)

Spring Name	UTM Easting (m) [a]	UTM Northing (m) [a]	Land Surface Elevation (m amsl) [b]	Land Surface Accuracy (m) [b]	HSU at Land Surface	HSU at Land Surface Thickness (m)	Other HSUs within 100 m of Land Surface
NE_unnamed_spring2	525907.2	4098491.5	1,169.8	6.1	AA	24.2	DVA
NE_unnamed_spring3	525511.4	4099477.0	1,169.8	6.1	AA	23.0	DVA
NE_unnamed_spring4	525730.7	4098967.0	1,169.8	6.1	AA	3.2	DVA
NE_unnamed_spring5	525667.6	4098872.3	1,168.9	6.1	AA	0.4	DVA
NE_unnamed_spring6	525792.8	4099357.5	1,173.5	6.1	AA	13.9	DVA
NE_unnamed_spring7	525567.8	4099378.0	1,169.8	6.1	AA	14.0	DVA
NE_unnamed_spring8	525831.1	4099022.3	1,172.0	6.1	AA	5.4	DVA
NE_unnamed_spring9	525701.7	4099607.0	1,173.5	6.1	AA	33.3	DVA
NE_unnamed_spring10	525677.2	4099285.0	1,172.3	6.1	AA	6.8	DVA
northern_Ute_Springs1	524693.8	4091137.0	1,093.9	6.1	AA	5.1	DVCM
northern_Ute_Springs2	524683.0	4091104.0	1,094.2	6.1	AA	3.2	DVCM
northern_Ute_Springs3	524830.0	4091095.0	1,083.6	6.1	AA	12.3	DVCM
northern_Ute_Springs4	524618.2	4090806.5	1,086.0	6.1	AA	3.0	DVCM
nr_Torrance_Spring	524377.3	4095278.8	1,122.6	6.1	AA	66.9	DVCM
NW_unnamed_spring1	523498.3	4097309.5	1,140.6	6.1	AA	89.0	DVCM
NW_unnamed_spring2	523865.5	4097042.0	1,133.3	6.1	AA	73.4	DVCM
NW_unnamed_spring3	523725.8	4096884.8	1,133.6	6.1	AA	75.2	DVCM
NW_unnamed_spring_nr_Springdale1	522500.4	4097850.5	1,157.9	6.1	AA	69.5	DVCM
NW_unnamed_spring_nr_Springdale2	521896.4	4098249.5	1,172.9	6.1	AA	41.3	DVCM
NW_unnamed_spring_nr_Springdale3	521831.5	4098080.5	1,171.3	6.1	AA	35.9	DVCM
Oleo_Rd_N_of_Goss_Springs	525941.4	4095322.3	1,170.1	6.1	DVA	100.0	None
Revert_Springs1	522827.0	4085634.8	1,030.8	6.1	AA	37.8	DVCM
Revert_Springs2	522822.9	4085589.0	1,032.4	6.1	AA	26.2	DVCM
Revert_Springs3	522817.5	4085554.3	1,033.9	6.1	AA	14.9	DVCM
seep_nr_Crystal_Springs1	521613.2	4093484.0	1,198.2	6.1	AA	73.4	DVCM

Table C-2
Site Information for Selected Springs Located in the Pahute Mesa Area and Vicinity
(Page 3 of 3)

Spring Name	UTM Easting (m) [a]	UTM Northing (m) [a]	Land Surface Elevation (m amsl) [b]	Land Surface Accuracy (m) [b]	HSU at Land Surface	HSU at Land Surface Thickness (m)	Other HSUs within 100 m of Land Surface
seep_nr_Crystal_Springs2	522011.4	4093397.5	1,186.9	6.1	AA	100.0	None
seep_S._of_Goss_Springs1	525370.5	4093587.5	1,114.0	6.1	AA	48.8	DVCM
seep_S._of_Goss_Springs2	525385.5	4093655.8	1,118.6	6.1	AA	55.6	DVCM
seep_W._of_Goss_Springs	524015.4	4093754.3	1,114.0	6.1	AA	66.5	DVCM
seep_W_of_Beatty_Spring1	522235.2	4086269.8	1,024.7	6.1	AA	52.9	DVCM
seep_W_of_Beatty_Spring2	522286.6	4086271.3	1,023.5	6.1	AA	52.7	DVCM
south_of_Ute_Springs1	525093.5	4088996.8	1,061.3	6.1	AA	3.1	DVCM
south_of_Ute_Springs2	524249.7	4088281.5	1,058.9	6.1	AA	16.4	DVCM
south_of_Ute_Springs3	525104.4	4089020.0	1,060.7	6.1	AA	3.3	DVCM
south_of_Ute_Springs4	525080.7	4088973.0	1,062.2	6.1	AA	3.4	DVCM
Specie_Spring	530399.2	4080151.5	1,341.1	6.1	DVCM	100.0	None
spring_N_of_Beatty_Spring	523363.8	4086649.5	1,025.0	6.1	AA	42.3	DVCM
Torrance_Spring	524499.8	4095480.3	1,121.1	6.1	AA	69.2	DVCM
unnamed_Bullfrog_Hills_spring	516294.3	4087011.5	1,283.2	6.1	AA	2.3	DVCM
unnamed_spring_nr_Narrows	522286.5	4082046.5	972.3	6.1	AA	1.6	UCCU
unnamed_spring_S_of_Beatty	521926.4	4083013.5	988.5	6.1	DVCM	62.7	UCCU
Upper_Indian_Spring	517440.2	4089309.0	1,289.3	6.1	AA	4.1	DVCM
Ute_Springs1	524910.2	4089881.5	1,072.9	6.1	AA	0.9	DVCM
Ute_Springs2	525105.9	4089860.0	1,074.1	6.1	AA	7.5	DVCM
Ute_Springs3	524986.3	4089892.0	1,072.3	6.1	AA	2.4	DVCM
Ute_Springs4	525019.2	4090082.3	1,075.6	6.1	AA	6.1	DVCM

[a] UTM Zone 11, NAD 1927 in meters; source is Fenelon (2015).
[b] Land-surface elevation in meters above mean sea level; source is Fenelon (2015).

Table C-3
Summary of Hydraulic Heads at Sites within Pahute Mesa Area and Vicinity
(Page 1 of 17)

Well Reporting Name	Average Steady-State Hydraulic Head (m amsl) [a]	Count	Minimum Hydraulic Head (m amsl)	Maximum Hydraulic Head (m amsl)	Standard Deviation (m)	Land Surface Accuracy (m) [a]	Water-Level Measurement Accuracy (m) [a]	Water-Level Variability Accuracy (m)	Temperature Uncertainty (m)	Total Hydraulic Head Uncertainty (m) [b]
Beatty Middle Well	1,237.8	1	1,237.8	1,237.8	0.00	6.10	1.52	2.00 [c]	0.30 [d]	6.61
Beatty Summit Well	1,143.6	1	1,143.6	1,143.6	0.00	6.10	1.52	2.00 [c]	0.26 [d]	6.60
Beatty Upper Indian Well	1,238.4	1	1,238.4	1,238.4	0.00	6.10	1.52	2.00 [c]	0.24 [d]	6.60
Beatty Wash Terrace Well	1,045.5	100	1,045.0	1,046.4	0.35	6.10	0.30	1.39 [e]	0.04 [d]	6.28
Beatty Wash Windmill Well	1,235.4	3	1,235.2	1,235.2	0.02	3.05	0.30	2.00 [c]	0.07 [d]	3.66
Beatty Water Test Hole	1,001.3	1	1,001.3	1,001.3	0.00	6.10	1.52	2.00 [c]	0.04 [d]	6.60
Beatty Well No.1	996.7	1	996.7	996.7	0.00	6.10	1.52	2.00 [c]	0.05 [d]	6.60
Beatty Well No. 2	999.7	1	999.7	999.7	0.00	6.10	1.52	2.00 [c]	0.08 [d]	6.60
Beatty Well No. 3	997.9	1	997.9	997.9	0.00	6.10	1.52	2.00 [c]	0.15 [d]	6.60
BGC-1 Well	991.8	1	991.8	991.8	0.00	6.10	0.30	2.00 [c]	0.03 [d]	6.43
BGC-2 Well	990.6	13	990.1	990.9	0.29	6.10	0.30	2.00 [c]	0.03 [d]	6.43
BLM Springdale	1,201.2	63	1,201.3	1,201.4	0.02	3.05	0.30	0.09 [e]	0.01 [d]	3.07
Boiling Pot Rd Well	1,102.8	42	1,102.4	1,103.3	0.28	6.10	0.30	2.00 [c]	0.00 [d]	6.43
CDH-61	807.7	1	807.6	807.6	0.00	6.10	1.52	2.00 [c]	0.15 [d]	6.60
Central Beatty Well	1,001.9	15	1,001.3	1,002.6	0.43	6.10	0.30	1.27 [e]	0.01 [d]	6.25
Crater Flat 1 (CF-1)	1,010.1	15	1,010.0	1,010.1	0.04	0.30	0.30	2.00 [c]	0.45 [d]	2.10
Crater Flat 1a (CF-1a)	1,202.7 [f]	1	1,202.7	1,202.7	0.00	0.30	1.52	2.00 [c]	0.26 [d]	2.55
ER-12-1 (1641-1846 ft)	1,308.5	81	1,302.9	1,310.4	1.55	0.30	0.30	7.45 [e]	0.20 [d]	7.63
ER-12-1 (1641-3414 ft)	1,302.7	2	1,301.8	1,303.4	1.08	0.30	1.52	2.00 [c]	0.90 [d]	2.90
ER-12-1 (1883-1940 ft)	1,321.9	1	1,322.0	1,322.0	0.00	0.30	30.48	2.00 [c]	0.39 [d]	30.55
ER-12-1 (2449-2602 ft)	1,335.9	1	1,336.0	1,336.0	0.00	0.30	30.48	2.00 [c]	1.00 [d]	30.56
ER-12-1 (2958-3212 ft)	926.0	1	926.0	926.0	0.00	0.30	30.48	2.00 [c]	0.28 [d]	30.55
ER-12-1 (3309-3414 ft)	931.2	1	931.2	931.2	0.00	0.30	30.48	2.00 [c]	0.55 [d]	30.55

Table C-3
Summary of Hydraulic Heads at Sites within Pahute Mesa Area and Vicinity
(Page 2 of 17)

Well Reporting Name	Average Steady-State Hydraulic Head (m amsl) [a]	Count	Minimum Hydraulic Head (m amsl)	Maximum Hydraulic Head (m amsl)	Standard Deviation (m)	Land Surface Accuracy (m) [a]	Water-Level Measurement Accuracy (m) [a]	Water-Level Variability Accuracy (m)	Temperature Uncertainty (m)	Total Hydraulic Head Uncertainty (m) [b]
ER-12-1 (brhl)	1,302.1	4	1,301.8	1,302.8	0.38	0.30	1.52	2.00 [c]	0.93 [d]	2.73
ER-12-3 main	1,305.2	47	1,303.1	1,305.8	0.70	0.30	0.30	2.00 [c]	1.04 [d]	2.40
ER-12-3 piezometer	1,873.6	34	1,873.3	1,873.7	0.12	0.30	0.30	2.00 [c]	0.52 [d]	2.12
ER-12-4 main	1,316.4	32	1,315.5	1,316.9	0.38	0.30	0.30	2.00 [c]	0.78 [d]	2.23
ER-12-4 piezometer	1,809.9	1	1,809.9	1,809.9	0.00	0.30	0.30	2.00 [c]	0.88 [d]	2.23
ER-18-2	1,288.1	53	1,287.9	1,288.4	0.16	0.30	0.30	0.52 [e]	0.65 [d]	0.96
ER-19-1-1 (deep)	1,330.1	32	1,329.4	1,331.8	0.62	0.30	0.30	2.35 [e]	1.47 [d]	2.88
ER-19-1-2 (middle)	1,522.2	37	1,521.5	1,523.2	0.56	0.30	0.30	1.68 [e]	1.37 [d]	2.28
ER-19-1-3 (shallow)	1,565.1	65	1,564.2	1,565.6	0.40	0.30	0.30	1.35 [e]	0.33 [d]	1.51
ER-20-1	1,277.7	78	1,277.6	1,278.1	0.10	0.30	0.30	0.53 [e]	0.03 [d]	0.70
ER-20-2-1	1,350.9	22	1,350.7	1,350.9	0.08	3.05	0.30	2.00 [c]	0.05 [g]	3.66
ER-20-4 borehole	1,284.7	5	1,284.2	1,285.1	0.32	0.30	1.52	2.00 [c]	0.91 [d]	2.71
ER-20-4 deep	1,284.7	21	1,284.6	1,284.8	0.08	0.30	0.30	2.00 [c]	1.11 [d]	2.33
ER-20-4 shallow	1,284.7	6	1,284.7	1,284.8	0.05	0.30	0.30	2.00 [c]	0.37 [d]	2.08
ER-20-5-1 (3-in string)	1,276.5	1	1,276.4	1,276.4	0.00	0.30	1.52	2.00 [c]	0.04 [g]	2.53
ER-20-5-3	1,277.1	4	1,277.0	1,277.3	0.10	0.30	0.30	2.00 [c]	1.44 [d]	2.51
ER-20-6-1 (3-in string)	1,357.0	92	1,356.5	1,357.2	0.18	0.30	0.30	0.78 [e]	0.61 [d]	1.10
ER-20-6-2 (3-in string)	1,356.7	57	1,356.5	1,357.1	0.16	0.30	0.30	0.63 [e]	0.60 [d]	0.99
ER-20-6-3 (3-in string)	1,356.7	51	1,356.3	1,357.0	0.15	0.30	0.30	0.64 [e]	0.55 [d]	0.97
ER-20-7	1,275.9	7	1,275.8	1,276.1	0.10	0.30	0.30	2.00 [c]	0.54 [d]	2.12
ER-20-7 (120-2208 ft)	1,276.8	1	1,276.8	1,276.8	0.00	0.30	1.52	2.00 [c]	0.18 [d]	2.54
ER-20-8 deep	1,274.7	7	1,274.4	1,274.6	0.07	0.30	0.30	2.00 [c]	1.45 [d]	2.51
ER-20-8 intermediate	1,274.7	18	1,274.6	1,274.8	0.05	0.30	0.30	2.00 [c]	0.94 [d]	2.26

Table C-3
Summary of Hydraulic Heads at Sites within Pahute Mesa Area and Vicinity
(Page 3 of 17)

Well Reporting Name	Average Steady-State Hydraulic Head (m amsl) [a]	Count	Minimum Hydraulic Head (m amsl)	Maximum Hydraulic Head (m amsl)	Standard Deviation (m)	Land Surface Accuracy (m) [a]	Water-Level Measurement Accuracy (m) [a]	Water-Level Variability Accuracy (m)	Temperature Uncertainty (m)	Total Hydraulic Head Uncertainty (m) [b]
ER-20-8 main	1,274.4	1	1,274.5	1,274.5	0.00	0.30	0.30	2.00 [c]	0.81 [d]	2.20
ER-20-8 shallow	1,274.4	9	1,274.3	1,274.5	0.08	0.30	0.30	2.00 [c]	0.41 [d]	2.09
ER-20-8-2	1,274.4	22	1,274.3	1,274.6	0.05	0.30	0.30	2.00 [c]	0.31 [d]	2.07
ER-20-11	1,273.8	7	1,273.5	1,273.8	0.08	0.30	0.30	2.00 [c]	1.03 [d]	2.30
ER-20-12 (m1)	1,344.5	1	1,344.5	1,344.5	0.00	0.30	0.30	2.00 [c]	2.18 [d]	2.99
ER-20-12 (p1)	1,341.4	1	1,341.4	1,341.4	0.00	0.30	0.30	2.00 [c]	1.53 [d]	2.56
ER-20-12 (p2)	1,336.5	1	1,336.5	1,336.5	0.00	0.30	0.30	2.00 [c]	1.13 [d]	2.34
ER-20-12 (p3)	1,336.5	1	1,336.5	1,336.5	0.00	0.30	0.30	2.00 [c]	0.78 [d]	2.19
ER-20-12 (p4)	1,415.8	1	1,415.8	1,415.8	0.00	0.30	0.30	2.00 [c]	0.31 [d]	2.07
ER-30-1-1 deep	1,279.2	2	1,279.3	1,279.4	0.05	0.30	0.30	2.00 [c]	0.26 [d]	2.07
ER-30-1-2 shallow	1,279.2	1	1,279.3	1,279.3	0.00	0.30	0.30	2.00 [c]	0.14 [d]	2.05
ER-EC-1	1,271.0	42	1,270.9	1,271.2	0.06	0.30	0.30	0.26 [e]	1.55 [d]	1.64
ER-EC-2A (1635-2236 ft)	1,264.0	39	1,264.1	1,264.3	0.05	0.30	0.30	2.00 [c]	1.08 [d]	2.32
ER-EC-2A (1635-4973 ft)	1,266.1	3	1,266.1	1,266.3	0.10	0.30	0.30	2.00 [c]	2.34 [d]	3.11
ER-EC-4 (952-2295 ft)	1,222.6	54	1,222.4	1,222.6	0.06	0.30	0.30	0.25 [e]	0.80 [d]	0.95
ER-EC-4 (952-3487 ft)	1,222.6	11	1,222.4	1,222.5	0.02	0.30	0.30	2.00 [c]	1.25 [d]	2.40
ER-EC-5	1,237.8	62	1,237.5	1,238.0	0.15	0.30	0.30	0.52 [e]	0.75 [d]	1.03
ER-EC-6 (1581-3820 ft)	1,273.8	39	1,273.6	1,273.8	0.05	0.30	0.30	2.00 [c]	1.18 [d]	2.37
ER-EC-6 (1581-5000 ft)	1,273.8	13	1,273.6	1,273.7	0.05	0.30	0.30	2.00 [c]	1.67 [d]	2.64
ER-EC-6 deep	1,273.5	4	1,273.5	1,273.5	0.03	0.30	0.30	2.00 [c]	1.99 [d]	2.86
ER-EC-6 intermediate	1,273.8	4	1,273.6	1,273.7	0.04	0.30	0.30	2.00 [c]	0.82 [d]	2.21
ER-EC-6 shallow	1,273.8	4	1,273.8	1,273.8	0.03	0.30	0.30	2.00 [c]	0.32 [d]	2.08
ER-EC-7	1,237.2	63	1,236.7	1,237.4	0.19	0.30	0.30	0.64 [e]	0.36 [d]	0.88

Table C-3
Summary of Hydraulic Heads at Sites within Pahute Mesa Area and Vicinity
(Page 4 of 17)

Well Reporting Name	Average Steady-State Hydraulic Head (m amsl) [a]	Count	Minimum Hydraulic Head (m amsl)	Maximum Hydraulic Head (m amsl)	Standard Deviation (m)	Land Surface Accuracy (m) [a]	Water-Level Measurement Accuracy (m) [a]	Water-Level Variability Accuracy (m)	Temperature Uncertainty (m)	Total Hydraulic Head Uncertainty (m) [b]
ER-EC-8	1,222.6	50	1,222.4	1,222.7	0.07	0.30	0.30	0.32 [e]	0.91 [d]	1.07
ER-EC-11 deep	1,274.1	6	1,273.8	1,274.1	0.12	0.30	0.30	2.00 [c]	2.19 [d]	3.00
ER-EC-11 intermediate	1,273.8	23	1,273.7	1,274.6	0.19	0.30	0.30	2.00 [c]	1.66 [d]	2.64
ER-EC-11 main	1,274.1	2	1,274.1	1,274.2	0.06	0.30	0.30	2.00 [c]	1.96 [d]	2.84
ER-EC-11 shallow	1,273.8	9	1,273.7	1,274.1	0.17	0.30	0.30	2.00 [c]	1.26 [d]	2.41
ER-EC-11 water table	1,273.8	1	1,273.8	1,273.8	0.00	0.30	0.30	2.00 [c]	0.04 [d]	2.05
ER-EC-12 deep	1,272.2	1	1,272.1	1,272.1	0.00	0.30	0.30	2.00 [c]	2.36 [d]	3.13
ER-EC-12 intermediate	1,271.6	1	1,271.7	1,271.7	0.00	0.30	0.30	2.00 [c]	1.94 [d]	2.82
ER-EC-12 shallow	1,271.0	17	1,270.9	1,271.2	0.07	0.30	0.30	2.00 [c]	0.86 [d]	2.22
ER-EC-13 deep	1,269.5	2	1,269.4	1,269.4	0.04	0.30	0.30	2.00 [c]	1.33 [d]	2.44
ER-EC-13 intermediate	1,269.5	13	1,269.3	1,269.4	0.03	0.30	0.30	2.00 [c]	0.89 [d]	2.24
ER-EC-13 shallow	1,269.5	1	1,269.3	1,269.3	0.00	0.30	0.30	2.00 [c]	0.24 [d]	2.06
ER-EC-14 deep	1,268.9	3	1,268.8	1,268.9	0.06	0.30	0.30	2.00 [c]	1.02 [d]	2.29
ER-EC-14 main	1,268.9	2	1,268.9	1,268.9	0.02	0.30	0.30	2.00 [c]	0.74 [d]	2.18
ER-EC-14 shallow	1,268.9	8	1,268.8	1,268.9	0.06	0.30	0.30	2.00 [c]	0.44 [d]	2.10
ER-EC-15 deep	1,273.5	2	1,273.4	1,273.5	0.00	0.30	0.30	2.00 [c]	1.66 [d]	2.64
ER-EC-15 intermediate	1,272.8	2	1,272.9	1,272.9	0.01	0.30	0.30	2.00 [c]	0.99 [d]	2.28
ER-EC-15 shallow	1,272.2	12	1,272.1	1,272.4	0.10	0.30	0.30	2.00 [c]	0.35 [d]	2.08
ER-OV-01	1,215.8	74	1,215.8	1,216.1	0.06	0.30	0.30	0.22 [e]	0.13 [d]	0.52
ER-OV-02	1,174.1	74	1,173.9	1,174.2	0.07	0.30	0.30	0.32 [e]	0.14 [d]	0.57
ER-OV-03a	1,153.1	73	1,152.0	1,153.6	0.43	0.30	0.30	1.60 [e]	0.15 [d]	1.72
ER-OV-03a2	1,122.0	69	1,121.7	1,122.1	0.09	0.30	0.30	0.39 [e]	0.41 [d]	0.73
ER-OV-03a3	1,152.8	72	1,151.9	1,153.5	0.43	0.30	0.30	1.62 [e]	0.06 [d]	1.74

Table C-3
Summary of Hydraulic Heads at Sites within Pahute Mesa Area and Vicinity
(Page 5 of 17)

Well Reporting Name	Average Steady-State Hydraulic Head (m amsl) [a]	Count	Minimum Hydraulic Head (m amsl)	Maximum Hydraulic Head (m amsl)	Standard Deviation (m)	Land Surface Accuracy (m) [a]	Water-Level Measurement Accuracy (m) [a]	Water-Level Variability Accuracy (m)	Temperature Uncertainty (m)	Total Hydraulic Head Uncertainty (m) [b]
ER-OV-03b	1,184.5	69	1,184.4	1,184.9	0.08	0.30	0.30	0.47 [e]	0.03 [d]	0.66
ER-OV-03c	1,211.3	74	1,211.3	1,211.5	0.04	0.30	0.30	0.24 [e]	0.28 [d]	0.58
ER-OV-03c2	1,211.3	79	1,211.3	1,211.5	0.04	0.30	0.30	0.22 [e]	0.07 [d]	0.51
ER-OV-04a	1,055.8	73	1,055.7	1,056.2	0.13	0.30	0.30	0.47 [e]	0.09 [d]	0.67
ER-OV-05	1,189.6	72	1,189.5	1,189.6	0.03	0.30	0.30	0.15 [e]	0.12 [d]	0.49
ER-OV-06a	1,216.8	85	1,216.8	1,217.1	0.06	0.30	0.30	0.28 [e]	0.45 [d]	0.70
ER-OV-06a2	1,215.8	67	1,215.6	1,215.8	0.04	0.30	0.30	0.16 [e]	0.03 [d]	0.48
Gold Flat 1	1,421.3	1	1,421.2	1,421.2	0.00	1.52	1.52	2.00 [c]	0.01 [d]	2.94
Gold Flat 2	1,523.1	11	1,522.5	1,523.3	0.21	1.52	0.30	0.82 [e]	0.03 [d]	1.77
Gold Flat 2a	1,523.4	1	1,523.4	1,523.4	0.00	1.52	0.30	2.00 [c]	0.07 [d]	2.54
Gold Flat 3	1,522.8	2	1,522.9	1,522.9	0.04	3.05	0.30	2.00 [c]	0.08 [d]	3.66
Hagestad1 (1600-1904 ft)	1,842.5	22	1,841.4	1,843.8	0.67	0.30	0.30	2.00 [c]	0.29 [d]	2.18
Hagestad1 (1874-1904 ft)	1,804.1	1	1,804.1	1,804.1	0.00	0.30	0.30	2.00 [c]	0.30 [d]	2.07
Hammel Mine Well	1,652.3 [f]	32	1,652.3	1,652.5	0.05	0.76	0.30	0.22 [e]	0.00 [d]	0.86
Lamb Well	1,434.1	1	1,434.1	1,434.1	0.00	3.05	1.52	2.00 [c]	0.02 [d]	3.95
Lower Indian Springs Well	1,228.3	8	1,228.2	1,228.3	0.03	6.10	0.30	2.00 [c]	0.00 [d]	6.43
Narrows South Well 1	963.5	2	963.2	963.9	0.52	6.10	0.30	0.73 [e]	0.05 [d]	6.17
Narrows South Well 2	963.5	53	963.3	964.5	0.25	6.10	0.30	1.21 [e]	0.05 [d]	6.23
NC-GWE-OV-01	1,122.3	1	1,122.2	1,122.2	0.00	0.76	1.52	2.00 [c]	0.00 [d]	2.63
NC-GWE-OV-02	1,075.9	1	1,076.0	1,076.0	0.00	0.76	1.52	2.00 [c]	0.00 [d]	2.63
OVM ET Well	1,124.1	46	1,123.6	1,124.9	0.37	0.30	0.30	2.00 [c]	0.00 [d]	2.08
OVU-Dune Well	1,181.4	37	1,181.3	1,181.7	0.12	3.05	0.30	2.00 [c]	0.00 [d]	3.66
OVU-Lower ET Well	1,175.3	31	1,175.0	1,176.0	0.31	3.05	0.30	2.00 [c]	0.00 [d]	3.68

Table C-3
Summary of Hydraulic Heads at Sites within Pahute Mesa Area and Vicinity
(Page 6 of 17)

Well Reporting Name	Average Steady-State Hydraulic Head (m amsl) [a]	Count	Minimum Hydraulic Head (m amsl)	Maximum Hydraulic Head (m amsl)	Standard Deviation (m)	Land Surface Accuracy (m) [a]	Water-Level Measurement Accuracy (m) [a]	Water-Level Variability Accuracy (m)	Temperature Uncertainty (m)	Total Hydraulic Head Uncertainty (m) [b]
OVU-Middle ET Well	1,174.4	26	1,173.9	1,175.0	0.36	3.05	0.30	2.00 [c]	0.00 [d]	3.68
P Ranch Well	1,094.2	1	1,094.2	1,094.2	0.00	6.10	0.30	2.00 [c]	0.00 [d]	6.43
Perlite Canyon Ranch Well	1,039.1	1	1,039.1	1,039.1	0.00	6.10	0.30	2.00 [c]	0.03 [d]	6.43
Pioneer Road Seep Well	1,112.2	43	1,111.7	1,112.6	0.25	6.10	0.30	2.00 [c]	0.00 [d]	6.43
PM-1 (7543-7858 ft)	1,359.4	63	1,358.4	1,360.5	0.50	0.30	0.30	2.13 [e]	7.59 [g]	7.91
PM-2	1,442.6	29	1,442.5	1,442.6	0.03	0.30	0.30	2.00 [c]	4.38 [d]	4.84
PM-3 (1647 ft)	1,331.7	1	1,331.6	1,331.6	0.00	0.30	1.52	2.00 [c]	0.03 [g]	2.53
PM-3 (3019 ft)	1,330.5	20	1,329.6	1,331.0	0.41	0.30	0.30	2.00 [c]	0.15 [g]	2.10
PM-3-1 (1919-2144 ft)	1,330.5	78	1,329.7	1,330.9	0.27	0.30	0.30	1.22 [e]	0.04 [g]	1.33
PM-3-2 (1442-1667 ft)	1,331.4	136	1,330.4	1,331.5	0.22	0.30	0.30	1.09 [e]	0.01 [g]	1.20
Springdale ET Deep Well	1,132.3	60	1,131.9	1,132.8	0.28	0.30	0.30	2.00 [c]	0.00 [d]	2.07
Springdale ET Shallow Well	1,131.7	57	1,131.2	1,132.2	0.36	0.30	0.30	2.00 [c]	0.00 [d]	2.08
Springdale Lower Well	1,129.6	58	1,128.3	1,130.8	0.81	3.05	0.30	2.00 [c]	0.00 [d]	3.75
Springdale Upper Well	1,143.3	113	1,143.1	1,143.6	0.10	3.05	0.30	0.47 [e]	0.03 [d]	3.11
Springdale Windmill Well	1,175.3	44	1,175.1	1,175.4	0.09	3.05	0.30	2.00 [c]	0.05 [d]	3.66
Tolicha Peak Well	1,524.9	1	1,524.9	1,524.9	0.00	3.05	1.52	2.00 [c]	0.61 [d]	4.00
TTR Antelope Mine 1	1,929.7	50	1,928.5	1,932.1	0.77	6.10	0.30	3.62 [e]	2.90 [d]	7.71
TTR Antelope Mine 2	1,930.3 [f]	49	1,928.9	1,933.3	0.89	6.10	0.30	4.38 [e]	2.90 [d]	8.11
TTR Antelope Mine 3	1,930.0	50	1,928.3	1,933.0	0.93	6.10	0.30	4.74 [e]	2.90 [d]	8.31
TTR Sulfide Mine	1,852.9 [f]	49	1,851.1	1,854.5	0.86	3.05	0.30	3.41 [e]	2.78 [d]	5.43
TTR Well 53	1,442.0	1	1,442.0	1,442.0	0.00	1.52	1.52	2.00 [c]	0.15 [d]	2.94
TW-1 (0-560 ft)	1,751.1 [f]	1	1,751.2	1,751.2	0.00	0.30	1.52	2.00 [c]	0.07 [d]	2.54
TW-1 (0-1615 ft)	1,749.6	2	1,749.6	1,749.7	0.04	0.30	1.52	2.00 [c]	0.55 [d]	2.59

Table C-3
Summary of Hydraulic Heads at Sites within Pahute Mesa Area and Vicinity
(Page 7 of 17)

Well Reporting Name	Average Steady-State Hydraulic Head (m amsl) [a]	Count	Minimum Hydraulic Head (m amsl)	Maximum Hydraulic Head (m amsl)	Standard Deviation (m)	Land Surface Accuracy (m) [a]	Water-Level Measurement Accuracy (m) [a]	Water-Level Variability Accuracy (m)	Temperature Uncertainty (m)	Total Hydraulic Head Uncertainty (m) [b]
TW-1 (0-3731 ft)	1,563.3	3	1,563.3	1,563.7	0.17	0.30	0.30	2.00 [c]	1.40 [d]	2.49
TW-1 (1615-1840 ft)	1,564.2	2	1,564.2	1,564.4	0.11	0.30	0.30	2.00 [c]	0.64 [d]	2.15
TW-1 (1615-3300 ft)	1,437.1	8	1,437.0	1,437.7	0.23	0.30	0.30	2.00 [c]	1.06 [d]	2.32
TW-1 (1615-4206 ft)	1,430.4	88	1,428.9	1,431.3	0.58	0.30	0.30	2.36 [e]	1.46 [d]	2.87
TW-1 (3700-3731 ft)	1,271.6	1	1,271.6	1,271.6	0.00	0.30	1.52	2.00 [c]	1.58 [d]	2.99
TW-1 (3700-4206 ft)	1,277.4	5	1,277.2	1,277.3	0.06	0.30	0.30	2.00 [c]	1.82 [d]	2.74
U-12e.03-1 (430 ft)	1,879.7	1	1,879.8	1,879.8	0.00	3.05	1.52	2.00 [c]	0.39 [d]	3.97
U-12e.03-1 (682 ft)	1,727.0	1	1,727.0	1,727.0	0.00	3.05	1.52	2.00 [c]	0.16 [d]	3.96
U-12e.03-1 (834 ft)	1,658.1	1	1,658.1	1,658.1	0.00	3.05	1.52	2.00 [c]	0.06 [d]	3.95
U-12e.06-1R	1,414.9	1	1,658.1	1,658.1	0.00	0.30	0.30	2.00 [c]	0.11 [d]	2.05
U-12e.M1UG (1501 ft)	1,424.6	1	1,424.7	1,424.7	0.00	3.05	0.30	2.00 [c]	0.01 [d]	3.66
U-12e.M1UG (19 ft)	1,877.6	1	1,877.5	1,877.5	0.00	3.05	0.30	2.00 [c]	0.69 [d]	3.73
U-12e.M1UG (631 ft)	1,885.2	1	1,885.3	1,885.3	0.00	3.05	1.52	2.00 [c]	0.70 [d]	4.02
U-12e.M1UG (777 ft)	1,860.8	1	1,860.9	1,860.9	0.00	3.05	0.30	2.00 [c]	0.66 [d]	3.72
U-12g.06PS1V	1,875.7	1	1,875.7	1,875.7	0.00	0.30	1.52	2.00 [c]	0.00 [d]	2.53
U-12n Vent Hole 2	1,868.4	1	1,868.4	1,868.4	0.00	0.30	4.57	2.00 [c]	0.01 [d]	5.00
U-12n.10 Vent Hole	1,858.4	1	1,858.4	1,858.4	0.00	0.30	4.57	2.00 [c]	0.03 [d]	5.00
U-12q	1,706.9	2	1,706.9	1,706.9	0.00	3.05	0.30	2.00 [c]	0.15 [d]	3.67
U-12s (1480 ft)	1,786.7	225	1,783.1	1,797.0	4.34	0.30	0.30	13.85 [e]	0.25 [d]	14.52
U-12s (1596 ft)	1,776.4	1	1,776.4	1,776.4	0.00	0.30	1.52	2.00 [c]	0.29 [d]	2.55
U-19ab	1,495.0 [f]	3	1,494.9	1,495.5	0.30	0.30	1.52	2.00 [c]	0.10 [d]	2.55
U-19ab 2	1,498.1 [f]	1	1,498.0	1,498.0	0.00	0.30	0.30	2.00 [c]	0.18 [d]	2.06
U-19ac	1,446.0	1	1,446.0	1,446.0	0.00	0.30	1.52	2.00 [c]	0.00 [d]	2.53

Table C-3
Summary of Hydraulic Heads at Sites within Pahute Mesa Area and Vicinity
(Page 8 of 17)

Well Reporting Name	Average Steady-State Hydraulic Head (m amsl) [a]	Count	Minimum Hydraulic Head (m amsl)	Maximum Hydraulic Head (m amsl)	Standard Deviation (m)	Land Surface Accuracy (m) [a]	Water-Level Measurement Accuracy (m) [a]	Water-Level Variability Accuracy (m)	Temperature Uncertainty (m)	Total Hydraulic Head Uncertainty (m) [b]
U-19adPS1A	1,393.2	1	1,393.1	1,393.1	0.00	0.30	1.52	2.00 [c]	0.39 [d]	2.56
U-19ae	1,369.8 [f]	2	1,369.3	1,369.9	0.43	0.30	1.52	2.00 [c]	0.21 [d]	2.58
U-19af	1,375.6 [f]	1	1,375.6	1,375.6	0.00	1.52	1.52	2.00 [c]	0.00 [d]	2.94
U-19ai	1,428.9	10	1,428.3	1,429.8	0.46	0.30	1.52	2.00 [c]	0.01 [d]	2.58
U-19aj	1,432.6 [f]	1	1,432.5	1,432.5	0.00	0.30	1.52	2.00 [c]	0.00 [d]	2.53
U-19aq	1,428.9 [f]	4	1,428.4	1,429.4	0.38	0.30	1.52	2.00 [c]	0.03 [d]	2.56
U-19ar	1,399.3	2	1,399.3	1,399.6	0.22	0.30	1.52	2.00 [c]	0.04 [d]	2.54
U-19aS (2813 ft)	1,392.6	3	1,392.6	1,392.6	0.00	0.30	0.30	2.00 [c]	0.44 [g]	2.10
U-19au	1,358.5	8	1,358.3	1,358.6	0.12	0.30	0.30	2.00 [c]	0.06 [d]	2.05
U-19au1	1,357.9	2	1,358.0	1,358.0	0.00	0.30	0.30	2.00 [c]	0.04 [d]	2.05
U-19ax	1,467.9	1	1,467.9	1,467.9	0.00	0.30	0.30	2.00 [c]	0.01 [d]	2.05
U-19ay	1,396.9	3	1,396.9	1,397.0	0.05	0.30	0.30	2.00 [c]	0.01 [d]	2.05
U-19az	1,424.6 [f]	16	1,424.4	1,424.6	0.08	0.30	0.30	2.00 [c]	0.02 [d]	2.05
U-19ba	1,488.6 [f]	10	1,488.7	1,488.9	0.05	0.30	0.30	2.00 [c]	0.01 [d]	2.05
U-19ba1	1,430.7	1	1,430.7	1,430.7	0.00	0.30	0.30	2.00 [c]	0.00 [d]	2.05
U-19ba2	1,432.3	1	1,432.3	1,432.3	0.00	0.30	0.30	2.00 [c]	0.00 [d]	2.05
U-19ba3	1,441.1	1	1,441.1	1,441.1	0.00	0.30	0.30	2.00 [c]	0.01 [d]	2.05
U-19bg	1,395.7	1	1,395.7	1,395.7	0.00	0.30	0.30	2.00 [c]	0.02 [d]	2.05
U-19bg1	1,394.5	6	1,394.3	1,394.7	0.15	0.30	0.30	2.00 [c]	0.06 [d]	2.06
U-19bh	1,427.4 [f]	57	1,424.8	1,429.2	1.14	0.30	0.30	4.37 [e]	0.03 [d]	4.54
U-19bj	1,492.9 [f]	1	1,492.8	1,492.8	0.00	0.30	0.30	2.00 [c]	0.01 [d]	2.05
U-19bk	1,428.3 [f]	86	1,427.7	1,428.4	0.18	0.30	0.30	0.74 [e]	0.04 [g]	0.89
U-19c (2656 ft)	1,430.1	1	1,430.2	1,430.2	0.00	0.30	1.52	2.00 [c]	0.38 [d]	2.56

Table C-3
Summary of Hydraulic Heads at Sites within Pahute Mesa Area and Vicinity
(Page 9 of 17)

Well Reporting Name	Average Steady-State Hydraulic Head (m amsl) [a]	Count	Minimum Hydraulic Head (m amsl)	Maximum Hydraulic Head (m amsl)	Standard Deviation (m)	Land Surface Accuracy (m) [a]	Water-Level Measurement Accuracy (m) [a]	Water-Level Variability Accuracy (m)	Temperature Uncertainty (m)	Total Hydraulic Head Uncertainty (m) [b]
U-19d2	1,427.7	1	1,427.6	1,427.6	0.00	0.30	0.30	2.00 [c]	2.52 [d]	3.25
U-19d2 (675-4633 ft)	1,427.1	2	1,427.1	1,427.1	0.00	0.30	4.57	2.00 [c]	1.12 [d]	5.12
U-19d2 (2362-2560 ft)	1,433.8 [f]	2	1,428.7	1,433.8	3.60	0.30	4.57	2.00 [c]	0.28 [d]	6.17
U-19d2 (2500-2698 ft)	1,427.4	3	1,427.5	1,427.5	0.00	0.30	4.57	2.00 [c]	0.39 [d]	5.02
U-19d2 (2884-3082 ft)	1,427.7	6	1,427.5	1,427.6	0.05	0.30	4.57	2.00 [c]	0.74 [d]	5.05
U-19d2 (3088-3286 ft)	1,427.7	1	1,427.7	1,427.7	0.00	0.30	4.57	2.00 [c]	0.92 [d]	5.08
U-19d2 (3285-3483 ft)	1,427.4	5	1,427.3	1,427.3	0.00	0.30	4.57	2.00 [c]	1.10 [d]	5.12
U-19d2 (3844-4042 ft)	1,427.4	1	1,427.3	1,427.3	0.00	0.30	4.57	2.00 [c]	1.61 [d]	5.25
U-19d2 (4123-4321 ft)	1,428.3	1	1,428.4	1,428.4	0.00	0.30	4.57	2.00 [c]	1.87 [d]	5.34
U-19e (5050 ft)	1,430.4	5	1,428.6	1,432.3	1.29	0.30	1.52	2.00 [c]	0.12 [g]	2.85
U-19g (3079-3197 ft)	1,424.3	1	1,424.2	1,424.2	0.00	0.30	0.30	2.00 [c]	0.63 [g]	2.14
U-19g (3132-3250 ft)	1,426.5	1	1,426.6	1,426.6	0.00	0.30	0.30	2.00 [c]	0.67 [g]	2.16
U-19g (liner)	1,424.0	4	1,423.3	1,424.8	0.88	0.30	1.52	2.00 [c]	0.38 [g]	2.71
U-19x	1,392.0 [f]	1	1,392.0	1,392.0	0.00	0.30	1.52	2.00 [c]	0.01 [d]	2.53
U-20WW (2528 ft)	1,351.5	2	1,351.4	1,351.4	0.00	0.30	1.52	2.00 [c]	0.11 [g]	2.54
U-20WW (cased)	1,351.5	4	1,351.1	1,351.7	0.26	0.30	0.30	2.00 [c]	0.32 [g]	2.09
U-20a (2177 ft)	1,328.6	1	1,328.7	1,328.7	0.00	0.30	0.30	2.00 [c]	0.17 [d]	2.06
U-20a 2 WW	1,343.3	11	1,342.7	1,345.3	0.71	0.30	0.30	2.53 [e]	1.11 [d]	2.89
U-20a 2 WW (860-2404 ft)	1,342.6	3	1,342.6	1,342.6	0.00	0.30	0.30	2.00 [c]	0.15 [d]	2.06
U-20a 2 WW (2404-2608 ft)	1,342.3	10	1,342.3	1,342.5	0.06	0.30	0.30	2.00 [c]	0.40 [d]	2.09
U-20a 2 WW (2492-2682 ft)	1,342.3	5	1,342.0	1,342.8	0.44	0.30	0.30	2.00 [c]	0.47 [d]	2.15
U-20a 2WW (2895-3085 ft)	1,342.3	2	1,342.2	1,342.2	0.00	0.30	0.30	2.00 [c]	0.84 [d]	2.22
U-20a 2 WW (3090-3280 ft)	1,342.3	4	1,342.4	1,342.4	0.00	0.30	0.30	2.00 [c]	1.02 [d]	2.29

Table C-3
Summary of Hydraulic Heads at Sites within Pahute Mesa Area and Vicinity
(Page 10 of 17)

Well Reporting Name	Average Steady-State Hydraulic Head (m amsl) [a]	Count	Minimum Hydraulic Head (m amsl)	Maximum Hydraulic Head (m amsl)	Standard Deviation (m)	Land Surface Accuracy (m) [a]	Water-Level Measurement Accuracy (m) [a]	Water-Level Variability Accuracy (m)	Temperature Uncertainty (m)	Total Hydraulic Head Uncertainty (m) [b]
U-20a 2 WW (3460-3650 ft)	1,350.6	1	1,350.5	1,350.5	0.00	0.30	0.30	2.00 [c]	1.38 [d]	2.47
U-20a 2 WW (3648-3838 ft)	1,349.3	12	1,349.3	1,349.4	0.04	0.30	0.30	2.00 [c]	1.55 [d]	2.57
U-20a 2 WW (3848-4038 ft)	1,348.7	1	1,348.6	1,348.6	0.00	0.30	0.30	2.00 [c]	1.73 [d]	2.68
U-20a 2 WW (4048-4238 ft)	1,346.6	2	1,346.5	1,346.5	0.00	0.30	0.30	2.00 [c]	1.91 [d]	2.80
U-20a 2 WW (4355-4500 ft)	1,352.1	2	1,352.2	1,352.2	0.00	0.30	0.30	2.00 [c]	2.19 [d]	3.00
U-20aa	1,361.5	1	1,361.6	1,361.6	0.00	0.30	1.52	2.00 [c]	0.25 [g]	2.55
U-20ad	1,360.3	1	1,360.2	1,360.2	0.00	0.30	1.52	2.00 [c]	0.12 [g]	2.54
U-20ae	1,280.2 [f]	1	1,280.1	1,280.1	0.00	0.30	1.52	2.00 [c]	0.17 [d]	2.54
U-20ag	1,285.6	4	1,285.3	1,285.6	0.15	0.30	1.52	2.00 [c]	0.08 [d]	2.54
U-20ah	1,354.2	12	1,352.5	1,355.8	1.02	0.30	1.52	2.00 [c]	0.14 [d]	2.74
U-20ai	1,356.4	8	1,355.2	1,357.0	0.55	0.30	0.30	2.00 [c]	0.05 [d]	2.12
U-20aj	1,369.5	1	1,369.5	1,369.5	0.00	0.30	1.52	2.00 [c]	0.00 [d]	2.53
U-20ak	1,278.3	8	1,277.8	1,279.3	0.52	0.30	0.30	2.00 [c]	0.03 [d]	2.12
U-20al	1,302.7 [f]	1	1,302.7	1,302.7	0.00	0.30	1.52	2.00 [c]	0.07 [d]	2.54
U-20am	1,356.7	1	1,356.8	1,356.8	0.00	0.30	1.52	2.00 [c]	0.03 [d]	2.53
U-20an	1,363.1	12	1,362.3	1,363.9	0.41	0.30	0.30	2.00 [c]	0.02 [d]	2.09
U-20ao	1,317.7 [f]	14	1,316.7	1,319.5	0.79	0.30	0.30	2.00 [c]	0.09 [d]	2.20
U-20ap	1,366.4 [f]	2	1,366.4	1,366.4	0.04	0.30	0.30	2.00 [c]	0.01 [d]	2.05
U-20aq	1,302.1 [f]	10	1,301.5	1,302.7	0.43	0.30	0.30	2.00 [c]	0.01 [d]	2.09
U-20ar1	1,364.6	10	1,363.6	1,365.9	0.66	0.30	0.30	2.00 [c]	0.20 [d]	2.16
U-20as	1,284.4	5	1,284.4	1,284.7	0.12	0.30	0.30	2.00 [c]	0.04 [d]	2.05
U-20at1	1,284.4	4	1,284.0	1,284.6	0.29	0.30	1.52	2.00 [c]	0.08 [d]	2.55
U-20av	1,337.5 [f]	1	1,337.5	1,337.5	0.00	0.30	0.30	2.00 [c]	0.01 [d]	2.05

Table C-3
Summary of Hydraulic Heads at Sites within Pahute Mesa Area and Vicinity
(Page 11 of 17)

Well Reporting Name	Average Steady-State Hydraulic Head (m amsl) [a]	Count	Minimum Hydraulic Head (m amsl)	Maximum Hydraulic Head (m amsl)	Standard Deviation (m)	Land Surface Accuracy (m) [a]	Water-Level Measurement Accuracy (m) [a]	Water-Level Variability Accuracy (m)	Temperature Uncertainty (m)	Total Hydraulic Head Uncertainty (m) [b]
U-20aw	1,371.3 [f]	10	1,371.3	1,371.6	0.10	0.30	0.30	2.00 [c]	0.01 [d]	2.05
U-20ax	1,329.8 [f]	37	1,329.5	1,330.4	0.24	0.30	0.30	2.00 [c]	0.01 [d]	2.06
U-20ay	1,360.9 [f]	9	1,360.9	1,361.1	0.06	0.30	0.30	2.00 [c]	0.02 [d]	2.05
U-20az	1,345.1	1	1,345.1	1,345.1	0.00	0.30	0.30	2.00 [c]	0.04 [d]	2.05
U-20bb (1900 ft)	1,367.6 [f]	1	1,367.7	1,367.7	0.00	0.30	0.30	2.00 [c]	0.22 [d]	2.06
U-20bb (2220 ft)	1,284.1	1	1,284.0	1,284.0	0.00	0.30	0.30	2.00 [c]	0.09 [d]	2.05
U-20bb1	1,279.6	17	1,279.4	1,279.9	0.16	0.30	0.30	2.00 [c]	0.14 [d]	2.06
U-20bc	1,303.0 [f]	23	1,302.9	1,303.4	0.13	0.30	0.30	2.00 [c]	0.06 [d]	2.06
U-20bd (2100 ft)	1,417.0 [f]	1	1,417.0	1,417.0	0.00	0.30	0.30	2.00 [c]	0.19 [d]	2.06
U-20bd (2261 ft)	1,355.4	7	1,355.4	1,355.6	0.05	0.30	0.30	2.00 [c]	0.10 [d]	2.05
U-20bd 1	1,355.4	6	1,355.3	1,355.9	0.20	0.30	0.30	2.00 [c]	0.17 [d]	2.07
U-20bd 2	1,356.1	2	1,356.0	1,356.2	0.17	0.30	0.30	2.00 [c]	0.19 [d]	2.07
U-20be	1,303.6	5	1,303.5	1,303.7	0.07	0.30	0.30	2.00 [c]	0.00 [d]	2.05
U-20bf	1,339.0 [f]	1	1,338.9	1,338.9	0.00	0.30	0.30	2.00 [c]	0.06 [d]	2.05
U-20bg	1,350.3	88	1,350.1	1,350.3	0.05	0.30	0.30	0.24 [e]	0.03 [d]	0.51
U-20c (12-4800 ft)	1,275.3	1	1,275.3	1,275.3	0.00	0.30	1.52	2.00 [c]	0.41 [g]	2.57
U-20e	1,360.3	1	1,360.3	1,360.3	0.00	0.30	1.52	2.00 [c]	0.70 [g]	2.63
U-20f	1,276.2	1	1,276.1	1,276.1	0.00	0.30	1.52	2.00 [c]	1.04 [d]	2.74
U-20i	1,361.2	1	1,361.3	1,361.3	0.00	0.30	1.52	2.00 [c]	1.28 [d]	2.84
U-20i (4397-4545 ft)	1,362.2	6	1,362.2	1,362.3	0.04	0.30	1.52	2.00 [c]	2.35 [d]	3.46
U-20i (4520-4668 ft)	1,361.8	2	1,362.0	1,362.0	0.00	0.30	1.52	2.00 [c]	2.46 [d]	3.53
U-20m (3710-3920 ft)	1,414.3	1	1,414.3	1,414.3	0.00	0.30	1.52	2.00 [c]	0.36 [g]	2.56
U-20n	1,352.7	3	1,352.3	1,353.5	0.63	0.30	1.52	2.00 [c]	0.02 [g]	2.61

Table C-3
Summary of Hydraulic Heads at Sites within Pahute Mesa Area and Vicinity
(Page 12 of 17)

Well Reporting Name	Average Steady-State Hydraulic Head (m amsl) [a]	Count	Minimum Hydraulic Head (m amsl)	Maximum Hydraulic Head (m amsl)	Standard Deviation (m)	Land Surface Accuracy (m) [a]	Water-Level Measurement Accuracy (m) [a]	Water-Level Variability Accuracy (m)	Temperature Uncertainty (m)	Total Hydraulic Head Uncertainty (m) [b]
U-20n PS1DD-H (4309 ft)	1,349.0	3	1,348.8	1,349.4	0.30	0.30	1.52	2.00 [c]	2.02 [d]	3.25
U-20y (1925 ft)	1,340.8 [f]	1	1,340.7	1,340.7	0.00	0.30	1.52	2.00 [c]	0.34 [d]	2.56
U-20y (2602 ft)	1,277.1	8	1,276.4	1,277.9	0.47	0.30	1.52	2.00 [c]	0.13 [g]	2.58
UE-12n 15A	1,840.7	4	1,840.4	1,841.3	0.39	0.30	0.30	2.00 [c]	0.28 [d]	2.11
UE-12t6 (1378 ft)	1,841.0	1	1,840.9	1,840.9	0.00	0.30	0.30	2.00 [c]	0.23 [d]	2.06
UE-12t6 (1461 ft)	1,853.2	51	1,847.1	1,858.9	3.75	0.30	0.30	11.76 [e]	0.29 [d]	12.36
UE-12t7	1,865.7	1	1,865.6	1,865.6	0.00	0.30	0.30	2.00 [c]	0.39 [d]	2.09
UE-17c	1,317.7	1	1,317.7	1,317.7	0.00	0.30	0.30	2.00 [c]	0.03 [d]	2.05
UE-18r	1,272.2	67	1,269.8	1,272.6	0.53	0.30	0.30	2.88 [e]	1.79 [d]	3.46
UE-18r (1648-1848 ft)	1,269.8	4	1,269.6	1,269.7	0.04	0.30	1.52	2.00 [c]	0.34 [d]	2.56
UE-18r (1859-2059 ft)	1,269.8	2	1,269.9	1,269.9	0.00	0.30	1.52	2.00 [c]	0.54 [d]	2.59
UE-18r (2000-2200 ft)	1,269.8	4	1,269.8	1,269.8	0.03	0.30	1.52	2.00 [c]	0.67 [d]	2.62
UE-18r (2193-2393 ft)	1,269.8	7	1,269.9	1,269.9	0.02	0.30	1.52	2.00 [c]	0.84 [d]	2.67
UE-18r (2408-2608 ft)	1,270.1	1	1,270.1	1,270.1	0.00	0.30	1.52	2.00 [c]	1.04 [d]	2.74
UE-18r (2616-2816 ft)	1,269.8	10	1,269.6	1,269.9	0.10	0.30	1.52	2.00 [c]	1.23 [d]	2.82
UE-18r (2796-2996 ft)	1,269.8	1	1,269.7	1,269.7	0.00	0.30	1.52	2.00 [c]	1.39 [d]	2.89
UE-18r (3002-3202 ft)	1,269.8	1	1,269.8	1,269.8	0.00	0.30	1.52	2.00 [c]	1.58 [d]	2.99
UE-18r (3442-3642 ft)	1,269.8	8	1,269.6	1,269.7	0.04	0.30	1.52	2.00 [c]	1.98 [d]	3.22
UE-18r (3849-4049 ft)	1,269.8	1	1,269.7	1,269.7	0.00	0.30	1.52	2.00 [c]	2.36 [d]	3.46
UE-18r (4051-4251 ft)	1,269.8	2	1,269.5	1,269.8	0.17	0.30	1.52	2.00 [c]	2.54 [d]	3.59
UE-18t	1,306.7	79	1,305.9	1,307.1	0.31	0.30	0.30	1.18 [e]	0.77 [d]	1.51
UE-19b 1 (2190-2374 ft)	1,425.5	4	1,425.5	1,425.6	0.02	0.30	4.57	2.00 [c]	0.12 [g]	5.00
UE-19b 1 (2361-2559 ft)	1,425.5	3	1,425.4	1,425.4	0.00	0.30	4.57	2.00 [c]	0.27 [g]	5.01

Table C-3
Summary of Hydraulic Heads at Sites within Pahute Mesa Area and Vicinity
(Page 13 of 17)

Well Reporting Name	Average Steady-State Hydraulic Head (m amsl) [a]	Count	Minimum Hydraulic Head (m amsl)	Maximum Hydraulic Head (m amsl)	Standard Deviation (m)	Land Surface Accuracy (m) [a]	Water-Level Measurement Accuracy (m) [a]	Water-Level Variability Accuracy (m)	Temperature Uncertainty (m)	Total Hydraulic Head Uncertainty (m) [b]
UE-19b 1 (2556-2754 ft)	1,425.5	6	1,425.5	1,425.5	0.02	0.30	4.57	2.00 [c]	0.46 [g]	5.02
UE-19b 1 (2754-2952 ft)	1,428.0	1	1,428.0	1,428.0	0.00	0.30	4.57	2.00 [c]	0.64 [g]	5.04
UE-19b 1 (3758-3956 ft)	1,427.1	1	1,427.2	1,427.2	0.00	0.30	4.57	2.00 [c]	1.80 [g]	5.31
UE-19b 1 WW	1,428.0	2	1,427.9	1,428.0	0.04	0.30	0.30	2.00 [c]	1.14 [g]	2.35
UE-19c (2421-4520 ft)	1,428.0	6	1,428.0	1,428.4	0.21	0.30	0.30	2.00 [c]	0.00 [g]	2.06
UE-19c (2884-3082 ft)	1,428.0	6	1,427.9	1,428.0	0.01	0.30	0.30	2.00 [c]	0.03 [g]	2.05
UE-19c (3078-3284 ft)	1,428.0	3	1,428.1	1,428.1	0.02	0.30	0.30	2.00 [c]	0.02 [g]	2.05
UE-19c WW	1,430.7	64	1,430.5	1,431.4	0.12	0.30	0.30	0.89 [e]	3.42 [g]	3.56
UE-19e WW	1,432.9	3	1,432.7	1,433.0	0.19	0.30	0.30	2.00 [c]	1.73 [d]	2.69
UE-19fS (2565-4779 ft)	1,350.3	5	1,350.2	1,350.4	0.06	0.30	0.30	2.00 [c]	1.25 [d]	2.40
UE-19fS (2750-2908 ft)	1,351.5	3	1,351.3	1,351.4	0.04	0.30	0.30	2.00 [c]	0.48 [d]	2.11
UE-19fS (2908-3066 ft)	1,351.2	2	1,351.1	1,351.1	0.00	0.30	0.30	2.00 [c]	0.63 [d]	2.14
UE-19fS (3060-3218 ft)	1,351.5	2	1,351.6	1,351.6	0.02	0.30	0.30	2.00 [c]	0.77 [d]	2.19
UE-19fS (3520-3678 ft)	1,350.9	2	1,350.7	1,350.8	0.02	0.30	0.30	2.00 [c]	1.18 [d]	2.37
UE-19fS (3680-3838 ft)	1,351.2	3	1,351.1	1,351.1	0.02	0.30	0.30	2.00 [c]	1.33 [d]	2.44
UE-19fS (4298-4456 ft)	1,349.7	3	1,349.5	1,349.6	0.02	0.30	0.30	2.00 [c]	1.89 [d]	2.79
UE-19fS (4464-4779 ft)	1,349.0	3	1,349.1	1,349.1	0.00	0.30	0.30	2.00 [c]	2.11 [d]	2.94
UE-19gS (2650-4508 ft)	1,425.5	5	1,425.4	1,425.6	0.12	0.30	0.30	2.00 [c]	1.41 [d]	2.49
UE-19gS (2650-7500 ft)	1,424.9	1	1,424.9	1,424.9	0.00	0.30	0.30	2.00 [c]	2.77 [d]	3.45
UE-19gS (2802-2970 ft)	1,425.2	3	1,425.4	1,425.4	0.00	0.30	0.30	2.00 [c]	0.77 [d]	2.19
UE-19gS (6920-7118 ft)	1,424.6	1	1,424.5	1,424.5	0.00	0.30	0.30	2.00 [c]	4.55 [d]	4.99
UE-19h (2321-2396 ft)	1,423.7	5	1,423.8	1,423.8	0.00	0.30	0.30	2.00 [c]	0.23 [d]	2.06
UE-19h (2321-3705 ft)	1,422.8	3	1,422.9	1,423.0	0.05	0.30	0.30	2.00 [c]	0.82 [d]	2.21

Table C-3
Summary of Hydraulic Heads at Sites within Pahute Mesa Area and Vicinity
(Page 14 of 17)

Well Reporting Name	Average Steady-State Hydraulic Head (m amsl) [a]	Count	Minimum Hydraulic Head (m amsl)	Maximum Hydraulic Head (m amsl)	Standard Deviation (m)	Land Surface Accuracy (m) [a]	Water-Level Measurement Accuracy (m) [a]	Water-Level Variability Accuracy (m)	Temperature Uncertainty (m)	Total Hydraulic Head Uncertainty (m) [b]
UE-19h (2408-2604 ft)	1,422.8	1	1,422.9	1,422.9	0.00	0.30	0.30	2.00 [c]	0.36 [d]	2.08
UE-19h (2566-2762 ft)	1,423.4	1	1,423.3	1,423.3	0.00	0.30	0.30	2.00 [c]	0.51 [d]	2.11
UE-19h (2765-2961 ft)	1,422.8	3	1,422.8	1,422.8	0.00	0.30	0.30	2.00 [c]	0.69 [d]	2.16
UE-19h (2833-3029 ft)	1,422.8	5	1,422.7	1,422.8	0.03	0.30	0.30	2.00 [c]	0.75 [d]	2.18
UE-19h (3030-3226 ft)	1,422.8	7	1,423.0	1,423.0	0.00	0.30	4.57	2.00 [c]	0.93 [d]	5.09
UE-19h (3220-3416 ft)	1,423.1	6	1,423.1	1,423.1	0.02	0.30	0.30	2.00 [c]	1.10 [d]	2.33
UE-19h (3420-3705 ft)	1,423.1	8	1,423.0	1,423.0	0.00	0.30	0.30	2.00 [c]	1.33 [d]	2.44
UE-19h (recompleted)	1,423.1	83	1,423.0	1,423.3	0.06	0.30	0.30	0.36 [e]	0.05 [g]	0.58
UE-19i (2910-3068 ft)	1,406.7 [f]	1	1,406.6	1,406.6	0.00	0.30	0.30	2.00 [c]	0.06 [g]	2.05
UE-19i (3222-3380 ft)	1,409.1 [f]	1	1,409.2	1,409.2	0.00	0.30	0.30	2.00 [c]	0.11 [g]	2.05
UE-19i (3298-3456 ft)	1,398.4 [f]	1	1,398.6	1,398.6	0.00	0.30	0.30	2.00 [c]	0.21 [g]	2.06
UE-19i (3460-3618 ft)	1,398.7	1	1,398.9	1,398.9	0.00	0.30	0.30	2.00 [c]	0.40 [g]	2.09
UE-19i (4100-4258 ft)	1,408.8	1	1,408.9	1,408.9	0.00	0.30	0.30	2.00 [c]	1.24 [g]	2.40
UE-19z (2225 ft)	1,458.8 [f]	1	1,458.7	1,458.7	0.00	0.30	1.52	2.00 [c]	0.32 [d]	2.55
UE-19z (2800 ft)	1,429.5	6	1,429.1	1,429.7	0.26	0.30	1.52	2.00 [c]	0.28 [d]	2.56
UE-20ab	1,357.9	1	1,357.8	1,357.8	0.00	0.30	1.52	2.00 [c]	0.19 [d]	2.54
UE-20av	1,319.8	1	1,319.7	1,319.7	0.00	0.30	0.30	2.00 [c]	0.22 [d]	2.06
UE-20bh 1	1,349.0	1	1,349.1	1,349.1	0.00	0.30	0.30	2.00 [c]	0.01 [g]	2.05
UE-20c (3210 ft)	1,266.7	1	1,266.9	1,266.9	0.00	0.30	0.30	2.00 [c]	1.47 [d]	2.52
UE-20d	1,273.8	20	1,273.4	1,274.4	0.18	0.30	0.30	2.00 [c]	1.11 [d]	2.34
UE-20d (2578-2776 ft)	1,272.5	4	1,272.4	1,272.4	0.00	0.30	1.52	2.00 [c]	0.05 [g]	2.53
UE-20d (3074-3272 ft)	1,275.9	1	1,275.9	1,275.9	0.00	0.30	1.52	2.00 [c]	0.04 [g]	2.53
UE-20e 1 (1500-2766 ft)	1,360.9	5	1,361.0	1,361.0	0.03	0.30	1.52	2.00 [c]	0.43 [d]	2.57

Table C-3
Summary of Hydraulic Heads at Sites within Pahute Mesa Area and Vicinity
(Page 15 of 17)

Well Reporting Name	Average Steady-State Hydraulic Head (m amsl) [a]	Count	Minimum Hydraulic Head (m amsl)	Maximum Hydraulic Head (m amsl)	Standard Deviation (m)	Land Surface Accuracy (m) [a]	Water-Level Measurement Accuracy (m) [a]	Water-Level Variability Accuracy (m)	Temperature Uncertainty (m)	Total Hydraulic Head Uncertainty (m) [b]
UE-20e 1 (1500-3600 ft)	1,362.8	1	1,362.8	1,362.8	0.00	0.30	1.52	2.00 [c]	0.81 [d]	2.66
UE-20e 1 (1500-6395 ft)	1,365.5	1	1,365.5	1,365.5	0.00	0.30	0.30	2.00 [c]	1.96 [g]	2.84
UE-20e 1 (2774-2972 ft)	1,361.8	1	1,362.0	1,362.0	0.00	0.30	1.52	2.00 [c]	0.95 [d]	2.71
UE-20e 1 (3480-3678 ft)	1,360.0	2	1,360.0	1,360.0	0.00	0.30	1.52	2.00 [c]	1.40 [g]	2.90
UE-20e 1 (4020-4218 ft)	1,361.8	1	1,362.0	1,362.0	0.00	0.30	1.52	2.00 [c]	1.98 [g]	3.22
UE-20e 1 (4540-6395 ft)	1,364.0	6	1,363.9	1,363.9	0.03	0.30	1.52	2.00 [c]	3.63 [g]	4.43
UE-20f (4350-4543 ft)	1,298.1	1	1,298.1	1,298.1	0.00	0.30	1.52	2.00 [c]	1.00 [g]	2.72
UE-20f (4456-13686 ft)	1,322.8	3	1,321.7	1,324.1	1.22	0.30	0.30	2.00 [c]	17.93 [g]	18.09
UE-20f (4568-4766 ft)	1,298.8	1	1,298.7	1,298.7	0.00	0.30	1.52	2.00 [c]	0.82 [g]	2.66
UE-20f (5051-5249 ft)	1,298.1	1	1,298.2	1,298.2	0.00	0.30	1.52	2.00 [c]	0.65 [g]	2.62
UE-20h (2575-2743 ft)	1,354.8	1	1,355.0	1,355.0	0.00	0.30	4.57	2.00 [c]	0.50 [d]	5.02
UE-20h (2741-2909 ft)	1,353.6	1	1,353.7	1,353.7	0.00	0.30	4.57	2.00 [c]	0.65 [d]	5.04
UE-20h (2900-3068 ft)	1,353.6	1	1,353.5	1,353.5	0.00	0.30	4.57	2.00 [c]	0.79 [d]	5.06
UE-20h (3042-3210 ft)	1,353.9	2	1,353.9	1,354.0	0.04	0.30	4.57	2.00 [c]	0.92 [d]	5.08
UE-20h (3350-3518 ft)	1,355.4	1	1,355.3	1,355.3	0.00	0.30	4.57	2.00 [c]	1.21 [d]	5.14
UE-20h (3522-7207 ft)	1,355.1	7	1,355.2	1,355.3	0.06	0.30	4.57	2.00 [c]	2.98 [d]	5.82
UE-20h (3705-3873 ft)	1,355.1	1	1,355.0	1,355.0	0.00	0.30	4.57	2.00 [c]	1.53 [d]	5.23
UE-20h (3892-4060 ft)	1,354.5	16	1,353.6	1,355.0	0.59	0.30	4.57	2.00 [c]	1.70 [d]	5.31
UE-20h (4070-4238 ft)	1,353.3	2	1,353.3	1,353.3	0.00	0.30	4.57	2.00 [c]	1.86 [d]	5.33
UE-20h (4500-4676 ft)	1,355.4	1	1,355.3	1,355.3	0.00	0.30	4.57	2.00 [c]	2.27 [d]	5.49
UE-20h WW	1,356.4	2	1,356.0	1,357.0	0.69	0.30	0.30	2.00 [c]	2.33 [d]	3.18
UE-20j (1858-2056 ft)	1,421.9	1	1,422.0	1,422.0	0.00	0.30	0.30	2.00 [c]	0.16 [g]	2.06
UE-20j (2051-2249 ft)	1,421.3	1	1,421.3	1,421.3	0.00	0.30	0.30	2.00 [c]	0.16 [g]	2.06

Table C-3
Summary of Hydraulic Heads at Sites within Pahute Mesa Area and Vicinity
(Page 16 of 17)

Well Reporting Name	Average Steady-State Hydraulic Head (m amsl) [a]	Count	Minimum Hydraulic Head (m amsl)	Maximum Hydraulic Head (m amsl)	Standard Deviation (m)	Land Surface Accuracy (m) [a]	Water-Level Measurement Accuracy (m) [a]	Water-Level Variability Accuracy (m)	Temperature Uncertainty (m)	Total Hydraulic Head Uncertainty (m) [b]
UE-20j (2253-2461 ft)	1,420.7	1	1,420.8	1,420.8	0.00	0.30	0.30	2.00 [c]	0.15 [g]	2.06
UE-20j (2670-2868 ft)	1,417.0	1	1,417.1	1,417.1	0.00	0.30	0.30	2.00 [c]	0.10 [g]	2.05
UE-20j (2957-3155 ft)	1,414.3	4	1,414.3	1,414.4	0.03	0.30	0.30	2.00 [c]	0.04 [g]	2.05
UE-20j (3147-3345 ft)	1,414.3	3	1,414.1	1,414.2	0.05	0.30	0.30	2.00 [c]	0.02 [g]	2.05
UE-20j (3359-3557 ft)	1,414.0	1	1,413.8	1,413.8	0.00	0.30	0.30	2.00 [c]	0.09 [g]	2.05
UE-20j (3487-3685 ft)	1,413.4	2	1,413.5	1,413.5	0.02	0.30	0.30	2.00 [c]	0.14 [g]	2.06
UE-20j (3634-3832 ft)	1,413.4	2	1,413.4	1,413.4	0.02	0.30	0.30	2.00 [c]	0.17 [g]	2.06
UE-20j WW	1,411.8	4	1,411.8	1,412.1	0.12	0.30	0.30	2.00 [c]	2.02 [d]	2.88
UE-20n 1 (2834 ft)	1,349.7	1	1,349.7	1,349.7	0.00	0.30	0.30	2.00 [c]	0.49 [d]	2.11
UE-20p ST-2	1,422.8	1	1,422.9	1,422.9	0.00	0.30	1.52	2.00 [c]	1.88 [d]	3.16
UE-25 WT 6	1,035.1	51	1,034.8	1,035.3	0.10	0.30	0.30	0.56 [e]	0.29 [d]	0.78
UE-25 WT 16	738.2	172	737.6	741.2	0.56	0.30	0.30	3.59 [e]	0.13 [d]	3.66
UE-25 WT 18	730.6	38	730.5	730.9	0.10	0.30	0.30	2.00 [c]	0.03 [d]	2.05
UE-29a 1 HTH	1,188.7	277	1,187.0	1,193.4	1.44	0.30	0.30	6.43 [e]	0.06 [d]	6.60
UE-29a 2 HTH	1,186.6	296	1,185.4	1,190.4	1.08	0.30	0.30	5.07 [e]	0.68 [d]	5.25
USAF TTR Cedar Pass R-1 WW	1,608.1	1	1,608.1	1,608.1	0.00	1.52	1.52	2.00 [c]	0.16 [d]	2.94
USWG-1	754.1	1	754.2	754.2	0.00	0.30	1.52	2.00 [c]	1.89 [d]	3.16
USWG-2	1,019.9	59	1,019.3	1,020.9	0.31	0.30	0.30	1.56 [e]	0.39 [d]	1.70
USW UZ-N91	1,187.2	297	1,186.2	1,191.9	1.11	0.30	0.30	5.75 [e]	0.03 [d]	5.87
USW WT-24	840.3	36	839.7	840.9	0.31	0.30	0.30	2.00 [c]	0.32 [d]	2.10
Ute Springs Drainage Well	1,062.8	43	1,062.0	1,063.8	0.63	6.10	0.30	2.00 [c]	0.00 [d]	6.46
WW-8 (1770-2031 ft)	1,409.4	2	1,409.4	1,409.6	0.13	0.30	4.57	2.00 [c]	0.06 [d]	5.00
WW-8 (2031-2053 ft)	1,410.3	3	1,410.3	1,410.3	0.02	0.30	4.57	2.00 [c]	0.89 [d]	5.08

Table C-3
Summary of Hydraulic Heads at Sites within Pahute Mesa Area and Vicinity
(Page 17 of 17)

Well Reporting Name	Average Steady-State Hydraulic Head (m amsl) [a]	Count	Minimum Hydraulic Head (m amsl)	Maximum Hydraulic Head (m amsl)	Standard Deviation (m)	Land Surface Accuracy (m) [a]	Water-Level Measurement Accuracy (m) [a]	Water-Level Variability Accuracy (m)	Temperature Uncertainty (m)	Total Hydraulic Head Uncertainty (m) [b]
WW-8 (2031-5490 ft)	1,409.4	1	1,409.4	1,409.4	0.00	0.30	0.30	2.00 [c]	2.46 [d]	3.20
WW-8 (2053-2249 ft)	1,409.7	4	1,409.8	1,409.9	0.03	0.30	4.57	2.00 [c]	0.99 [d]	5.10
WW-8 (30-1198 ft)	1,409.7	3	1,409.7	1,409.7	0.00	0.30	4.57	2.00 [c]	0.76 [d]	5.06
WW-8 (30-2031 ft)	1,410.3	2	1,410.2	1,410.3	0.06	0.30	0.30	2.00 [c]	0.44 [d]	2.10
WW-8 (3333-3429 ft)	1,407.9	3	1,407.8	1,407.9	0.05	0.30	4.57	2.00 [c]	2.11 [d]	5.43
WW-8 (3428-3524 ft)	1,407.6	3	1,407.3	1,407.9	0.28	0.30	4.57	2.00 [c]	2.19 [d]	5.47

[a] Source: Fenelon, 2015
[b] Total uncertainty includes 0.5 ft of borehole deviation uncertainty.
[c] 2-m estimated water-level uncertainty because less than 10 years of monitoring data are available.
[d] No temperature profile data are available and temperature uncertainty is estimated as 0.3% of water column height m/m.
[e] Water-level variability is observed range in hydrograph.
[f] Water level is anomalously elevated.
[g] Water level is anomalously depressed.

Table C-4
Hydraulic Gradient between Well Pairs
(Page 1 of 4)

Upgradient Well	Primary Open Interval HSU	Downgradient Well	Primary Open Interval HSU	Gradient (m/m)	Distance between Wells (m)	Gradient Classification [a]
Beatty Wash Terrace Well	DVCM	Beatty Well No.1	DVCM	0.0103	4,737	Medium
Beatty Wash Windmill Well	RMWTA	Crater Flat 1 (CF-1)	PCM	0.0213	10,583	High
Crater Flat 1 (CF-1)	PCM	Narrows South Well 2	UCCU	0.0036	12,962	Low
Crater Flat 1a (CF-1a)	DVCM	Narrows South Well 2	UCCU	0.0236	10,150	High
ER-18-2	RMWTA	ER-EC-7	FCULFA7	0.0031	16,163	Low
ER-19-1-2 (middle)	PBRCM	UE-18t	RMWTA	0.0221	9,753	High
ER-20-1	TCA	ER-EC-15 shallow	CPA	0.0012	4,672	Low
ER-20-2-1	CHZCM	ER-20-4 deep	CFCU	0.0164	4,039	High
ER-20-4 deep	CFCU	ER-EC-12 shallow	TCA	0.0026	5,205	Low
ER-20-5-1 (3-in string)	TSA	ER-EC-15 shallow	CPA	0.0008	5,233	Low
ER-20-5-3	CHLFA5	ER-EC-15 shallow	CPA	0.0009	5,209	Low
ER-20-6-1 (3-in string)	CHLFA3	U-20ag	BA	0.0131	5,444	Medium
ER-20-6-2 (3-in string)	CHLFA3	U-20ag	BA	0.0132	5,398	Medium
ER-20-6-3 (3-in string)	CHLFA3	U-20ag	BA	0.0134	5,315	Medium
ER-20-7	TSA	ER-EC-15 shallow	CPA	0.0008	4,573	Low
ER-20-8 shallow	SPA	ER-EC-14 deep	RMWTA	0.0008	6,704	Low
ER-20-8-2	SPA	ER-EC-14 deep	RMWTA	0.0008	6,692	Low
ER-20-11	BA	ER-EC-13 deep	FCULFA4	0.0007	6,419	Low
ER-20-12 (p4)	TMLVTA	PM-3-1 (1919-2144 ft)	TCA	0.0169	5,048	High
ER-30-1-1 deep	FCCM	UE-29a2 HTH	YMCFCM	0.0071	13,129	Medium
ER-EC-1	CHZCM	ER-EC-13 deep	FCULFA4	0.0003	4,417	Low
ER-EC-2A (1635-2236 ft)	FCCM	ER-EC-8	FCCM	0.0056	7,354	Medium
ER-EC-4 (952-2295 ft)	TCVA	ER-OV-06a	FCCM	0.0006	9,342	Low
ER-EC-5	ATWTA	ER-OV-03b	AA	0.0053	9,983	Medium
ER-EC-6 (1581-3820 ft)	BA	ER-EC-13 deep	FCULFA4	0.0008	5,062	Low
ER-EC-7	FCULFA7	Crater Flat 1 (CF-1)	PCM	0.0160	14,166	High
ER-EC-8	FCCM	ER-OV-06a	FCCM	0.0012	4,809	Low
ER-EC-11 intermediate	TCA	ER-EC-13 deep	FCULFA4	0.0008	5,689	Low
ER-EC-12 shallow	TCA	ER-EC-14 deep	RMWTA	0.0005	4,022	Low
ER-EC-13 deep	FCULFA4	ER-EC-8	FCCM	0.0045	10,430	Low
ER-EC-14 deep	RMWTA	ER-EC-5	ATWTA	0.0040	7,820	Low
ER-EC-15 shallow	CPA	ER-EC-2A (1635-2236 ft)	FCCM	0.0013	6,319	Low

Table C-4
Hydraulic Gradient between Well Pairs
(Page 2 of 4)

Upgradient Well	Primary Open Interval HSU	Downgradient Well	Primary Open Interval HSU	Gradient (m/m)	Distance between Wells (m)	Gradient Classification [a]
ER-OV-02	FCCM	Pioneer Road Seep Well	AA	0.0113	5,457	Medium
ER-OV-03b	AA	NC-GWE-OV-01	AA	0.0095	6,532	Medium
ER-OV-03c	ATWTA	Crater Flat 1a (CF-1a)	DVCM	0.0008	10,198	Low
ER-OV-04a	DVCM	Beatty Well No.1	DVCM	0.0101	5,859	Medium
ER-OV-06a	FCCM	OVU-Dune Well	AA	0.0082	4,297	Medium
Hagestad1 (1600-1904 ft)	PBRCM	UE-18t	RMWTA	0.0437	12,262	High
Lamb Well	AA	U-19d2	BRA	0.0005	13,216	Low
NC-GWE-OV-02	AA	Beatty Well No.1	DVCM	0.0124	6,404	Medium
OVU-Dune Well	AA	Springdale Upper Well	AA	0.0095	4,006	Medium
OVU-Lower Well	AA	OVM ET Well	AA	0.0127	4,026	Medium
P Ranch Well	Outside_HFM	Beatty Water Test Hole	DVCM	0.0140	6,619	Medium
Perlite Canyon Ranch Well	AA	Beatty Well No.1	DVCM	0.0101	4,197	Medium
PM-1 (7543-7858 ft)	BRA	U-20a (2177 ft)	CHLFA4	0.0065	4,723	Medium
PM-3-1 (1919-2144 ft)	TCA	ER-EC-4 (952-2295 ft)	TCVA	0.0099	10,898	Medium
U-12s (1480 ft)	MGCU	ER-19-1-2 (middle)	PBRCM	0.0448	5,902	High
U-19ac	KA	UE-19i (3460-3618 ft)	BFCU	0.0093	5,069	Medium
U-19ai	BFCU	UE-19gS (2650-7500 ft)	BRA	0.0008	4,749	Low
U-19aj	BFCU	U-19bg1	CHVTA	0.0083	4,587	Medium
U-19ar	PLFA	U-20bd2	CHZCM	0.0072	6,005	Medium
U-19aS (2813 ft)	CFCU	U-20bd2	CHZCM	0.0078	4,671	Medium
U-19au	CHVTA	UE-20n1 (2834 ft)	CHLFA4	0.0021	4,234	Low
U-19au1	CHVTA	UE-20n1 (2834 ft)	CHLFA4	0.0019	4,238	Low
U-19ay	PLFA	UE-20bh1	CHLFA5	0.0080	5,981	Medium
U-19bg1	CHVTA	UE-20bh1	CHLFA5	0.0085	5,331	Medium
U-19d2	BRA	UE-19gS (2650-7500 ft)	BRA	0.0005	5,841	Low
U-19e (5050 ft)	BRA	U-19aS (2813 ft)	CFCU	0.0094	4,038	Medium
U-20WW (cased)	CHLFA4	U-20ag	BA	0.0156	4,217	High
U-20a (2177 ft)	CHLFA4	U-20y (2602 ft)	TSA	0.0113	4,545	Medium
U-20a2WW (4355-4500 ft)	CHLFA4	U-20ag	BA	0.0158	4,197	High
U-20aa	CHLFA3	UE-20f (4456-13686 ft)	PBRCM	0.0094	4,105	Medium
U-20ad	CHZCM	U-20bc	UPCU	0.0133	4,312	Medium
U-20ag	BA	ER-EC-11 intermediate	TCA	0.0029	4,117	Low

Table C-4
Hydraulic Gradient between Well Pairs
(Page 3 of 4)

Upgradient Well	Primary Open Interval HSU	Downgradient Well	Primary Open Interval HSU	Gradient (m/m)	Distance between Wells (m)	Gradient Classification [a]
U-20ah	CHLFA1	U-20ag	BA	0.0137	4,999	Medium
U-20ai	CHLFA3	U-20c (12-4800 ft)	CHZCM	0.0173	4,676	High
U-20ak	BA	ER-EC-1	CHZCM	0.0012	5,854	Low
U-20am	CHLFA4	UE-20d	CHZCM	0.0126	6,555	Medium
U-20an	CHLFA3	UE-20f (4456-13686 ft)	PBRCM	0.0077	5,268	Medium
U-20ar1	CHLFA2	U-20aq	UPCU	0.0103	6,067	Medium
U-20as	UPCU	ER-EC-6 (1581-3820 ft)	BA	0.0023	4,673	Low
U-20at1	LPCU	ER-EC-1	CHZCM	0.0027	4,953	Low
U-20az	CHZCM	ER-20-4 deep	CFCU	0.0125	4,815	Medium
U-20bb1	UPCU	ER-EC-1	CHZCM	0.0015	5,568	Low
U-20bd (2261 ft)	CHZCM	U-20ag	BA	0.0125	5,597	Medium
U-20bd1	CHZCM	U-20ag	BA	0.0125	5,599	Medium
U-20bd2	CHZCM	U-20ag	BA	0.0126	5,616	Medium
U-20be	CHZCM	ER-20-8 shallow	SPA	0.0054	5,440	Medium
U-20bf	CHLFA1	ER-20-5-1 (3-in string)	TSA	0.0148	4,228	Medium
U-20bg	CHZCM	U-20as	UPCU	0.0129	5,115	Medium
U-20c (12-4800 ft)	CHZCM	ER-EC-11 intermediate	TCA	0.0004	4,208	Low
U-20i	CFCM	U-20bc	UPCU	0.0123	4,743	Medium
U-20n	CHLFA4	U-20ag	BA	0.0157	4,277	High
U-20y (2602 ft)	TSA	ER-EC-6 (1581-3820 ft)	BA	0.0008	4,074	Low
UE-18r	ATWTA	ER-EC-5	ATWTA	0.0029	12,018	Low
UE-18t	RMWTA	ER-18-2	RMWTA	0.0039	4,720	Low
UE-19cWW	BRA	U-19au1	CHVTA	0.0135	5,382	Medium
UE-19eWW	BFCU	U-19aS (2813 ft)	CFCU	0.0099	4,074	Medium
UE-19fS (2750-2908 ft)	IA	ER-20-4 deep	CFCU	0.0092	7,223	Medium
UE-19gS (2650-7500 ft)	BRA	PM-1 (7543-7858 ft)	BRA	0.0136	4,800	Medium
UE-19h (recompleted)	BRA	PM-1 (7543-7858 ft)	BRA	0.0085	7,506	Medium
UE-19i (3460-3618 ft)	BFCU	U-20az	CHZCM	0.0090	5,924	Medium
UE-19z (2800 ft)	BFCU	U-19bg1	CHVTA	0.0083	4,199	Medium
UE-20ab	CHLFA3	U-20bf	CHLFA1	0.0046	4,142	Low
UE-20av	CHLFA4	ER-20-4 deep	CFCU	0.0078	4,522	Medium
UE-20bh1	CHLFA5	U-20ag	BA	0.0120	5,267	Medium

Table C-4
Hydraulic Gradient between Well Pairs
(Page 4 of 4)

Upgradient Well	Primary Open Interval HSU	Downgradient Well	Primary Open Interval HSU	Gradient (m/m)	Distance between Wells (m)	Gradient Classification [a]
UE-20d	CHZCM	ER-EC-1	CHZCM	0.0004	6,358	Low
UE-20e1 (1500-6395 ft)	CHLFA3	UE-20f (4456-13686 ft)	PBRCM	0.0074	5,758	Medium
UE-20hWW	CHZCM	UE-20d	CHZCM	0.0168	4,904	High
UE-20jWW	PBRCM	PM-3-1 (1919-2144 ft)	TCA	0.0113	7,171	Medium
UE-20n1(2834 ft)	CHLFA4	U-20ag	BA	0.0159	4,023	High
Ute Springs Drainage Well	AA	Beatty Well No.1	DVCM	0.0113	5,838	Medium

[a] Low gradient is less than 0.005; medium gradient is 0.005 to 0.015; and high gradient is greater than 0.015.

Table C-5
Example Calculation of the Direction of Flow

Well	ER-30-1-1	ER-18-2	UE-18t	Minimum Value
Easting (m)	560804.6	555724.7	559591.4	555724.7
Northing (m)	4100463.0	4106388.5	4109095.1	4100463.0
Water-Level Uncertainty (m)	2.1	1.0	1.5	--
Water Elevation (m)	1,279.2	1,288.1	1,306.7	1,279.2
Water Elevation with Uncertainty (m)	1,277.1	1,288.1	1,308.2	1,277.1
Distance from ER-30-1-1 (m)	0.0	7,804.9	8,716.9	--
Coordinates with minimum value subtracted for fitting to a plane in translated coordinates				
Easting (m)	5079.9	0.0	3866.7	--
Northing (m)	0.0	5925.5	8632.1	--
Water Elevation (m)	0.0	8.9	27.5	--
Water Elevation with Uncertainty (m)	0.0	11.0	31.1	--
Plane Equation Coefficients	**Without Uncertainty**	**With Uncertainty**		
a	-22791591.7	-22780267.2	--	--
b	-43710507.5	-43692219.9	--	--
c	30055736.3	30045068.6	--	--
d	-437509232.2	-453787213.0	--	--
Dip Azimuth (degrees)	207.538	207.537	--	--

-- = Not applicable

C.2.0 REFERENCES

Fenelon, J.M., U.S. Geological Survey. 2015. Personal communication to P. Martian (Navarro) regarding steady-state water level data for the Pahute Mesa/Oasis Valley groundwater system, 10 August. Henderson, NV.

Navarro. 2019. Written communication. Subject: "UGTA Borehole Index Database," UGTA Technical Data Repository Database Identification Number UGTA-4-127. Las Vegas, NV.

Appendix D

Nevada Division of Environmental Protection Comments

(5 Pages)

NEVADA ENVIRONMENTAL MANAGEMENT OPERATIONS ACTIVITY
DOCUMENT REVIEW SHEET

1. Document Title/Number: Hydrologic Data for the Groundwater Flow and Contaminant Transport Model of Corrective Action Units 101 and 102: Central and Western Pahute Mesa, Nye County, Nevada, Revision 0, September 2020				2. Document Date: Draft - September 2020
3. Revision Number: Rev. 0				4. Originator/Organization: Navarro
5. Responsible EM Nevada Program Activity Lead: John Myers				6. Date Comments Due: 11/12/2020
7. Review Criteria:				
8. Reviewer/Organization Phone No.: Christine Anders, NDEP				9. Reviewer's Signature:
10. Comment Number/Location		11. Type[a]	12. Comment	13. Comment Response
1.	General Comment		As aquifer tests use pumping to obtain the data presented in the document, please replace the term "pump test data" and "pumping tests" (terms used inconsistently in the Report) with "pump-scale aquifer tests" and "slug-scale aquifer tests" where appropriate throughout the document. These terms are used in other reports to indicate the scale of measure.	Changed as suggested.
2.	Page 3-2, Section 3.1, First Partial Paragraph, First Partial Sentence		Please change "SWDA" to "SDWA".	Changed to SDWA.
3.	Page 3-10, Section 3.6.5, Third Paragraph, Fourth Sentence		Will the adjustments within discrete HSU and fault zones be heterogeneous or homogeneous? Please clarify in the text	Text was clarified to state the following: "Initial model calibrations will assume HSU and fault zones are homogeneous. Heterogeneity will be added to the HSU and fault zones as needed to calibrate the model."
4.	Page 3-11, Section 3 .6.5, First Partial Paragraph, First Partial Sentence		Is the recharge distribution a calibration variable? Please clarify in the text.	Text was clarified to state the following: "Initially, the model will be calibrated to data by adjusting the conductivities and storativities using a fixed recharge distribution obtained from the cited literature. If this calibration is found to be unsatisfactory, the recharge distribution may then be treated as a calibration variable to obtain a better match to the observed data."
5.	Page 4-7, Section 4.2.2, First Full Bullet, first Sentence.		" ... if sufficient data are present in the original study ... " Please provide a reference for the original study in the text.	The section cited lays out the general transfer methodology. As such, it does not refer to any specific or referenceable data. If data transfer is used for a specific data type presented elsewhere in the document, specific references are provided. A parenthetical was added to the revised bullet (see comment #6) informing the reader that data references will be located within specific data discussions, as appropriate.
6.	Page 4-7, Section 4.2.2, First Full Bullet, Second Sentence		Why is the incorporation and transfer of data from other areas into the existing dataset needed if sufficient data is present in the original study. Please explain in the text.	Text clarified to read: "Finally, if sufficient data for the purpose of statistical comparison are present in the original study area, a comparison can be made of the datasets (data references are located within the specific data discussions, as appropriate). If it can be shown that the two datasets have comparable distributions, data from the original study can be augmented with those from other areas. While this approach is unlikely to substantially alter measures of central tendency, adding additional comparable data may provide increased confidence in the estimation of the range of uncertainty in the data."

[a]Comment Types: M = Mandatory, S = Suggested.
Return Document Review Sheets to Environmental Management Nevada Program Operations Activity, Attn: QAC, M/S NSF 505

NEVADA ENVIRONMENTAL MANAGEMENT OPERATIONS ACTIVITY
DOCUMENT REVIEW SHEET

1. Document Title/Number: Hydrologic Data for the Groundwater Flow and Contaminant Transport Model of Corrective Action Units 101 and 102: Central and Western Pahute Mesa, Nye County, Nevada, Revision 0, September 2020				2. Document Date: Draft - September 2020
3. Revision Number: Rev. 0				4. Originator/Organization: Navarro
5. Responsible EM Nevada Program Activity Lead: John Myers				6. Date Comments Due: 11/12/2020
7. Review Criteria:				
8. Reviewer/Organization Phone No.: Christine Anders, NDEP				9. Reviewer's Signature:
10. Comment Number/Location		11. Type[a]	12. Comment	13. Comment Response
7.	Page 5-5, Section 5.2.2.1, Fourth Bullet, Fifth Sentence:.		Please provide a reference for determining the hydraulic conductivity from flow logging data in the text.	The reference to Oberlander et al. (2007) was added as follows: "Where flow logging data are available, the logging under stressed conditions is also used to determine the hydraulic conductivity within individual HSUs (Oberlander et al., 2007)."
8.	Page 5-21, Section 5.2.2.5, Second Full Paragraph, Seventh Sentence:		Please include a reference for the maximum unclassified yield for the HANDLEY, BOXCAR and MUENSTER detonations in the text.	Reference was added (NNSA/NFO, 2015b).
9.	Page 5-27, Section 5.2.2.6, Figure 5-10		Please add to figure title "for pump-scale aquifer test data."	Figure title was changed to "Hydraulic Conductivity from Pump-Scale Aquifer Tests versus Distance to Faults."
10	Page 5-29, Section 5.3, Second Paragraph, Fifth Sentence		Please explain in the text why values used for porosity were taken from the Phase I Flow and Transport Model document for CAU 97: Yucca Flat/Climax Mine.	Changed the text as follows: "The values used for porosity were taken from the YF/CM Phase I flow and transport model document (N-I, 2013). Although this report was prepared for YF/CM, the estimates for the volcanics given in the report are not exclusive to YF/CM; they are based on sitewide data. In addition, the report provides estimates of porosity for the LCA that are not available at this time from Pahute Mesa data. These parameter values are listed in Table 5-11."
11	Page 7-27, Section 7.6.2, Figure 7-4:		Please make the blue and orange labels below the bars larger to aid the reader.	Changed as suggested.

[a]Comment Types: M = Mandatory, S = Suggested.
Return Document Review Sheets to Environmental Management Nevada Program Operations Activity, Attn: QAC, M/S NSF 505

NEVADA ENVIRONMENTAL MANAGEMENT OPERATIONS ACTIVITY
DOCUMENT REVIEW SHEET

1. Document Title/Number: Hydrologic Data for the Groundwater Flow and Contaminant Transport Model of Corrective Action Units 101 and 102: Central and Western Pahute Mesa, Nye County, Nevada, Revision 0, September 2020				2. Document Date: Draft - September 2020
3. Revision Number: Rev. 0				4. Originator/Organization: Navarro
5. Responsible EM Nevada Program Activity Lead: John Myers				6. Date Comments Due: 11/12/2020
7. Review Criteria:				
8. Reviewer/Organization Phone No.: Christine Anders, NDEP				9. Reviewer's Signature:
10. Comment Number/Location		11. Type[a]	12. Comment	13. Comment Response
12	Page 8-12, Section 8.5.3, Second Full Paragraph, Third Sentence		Please provide the method used to reduce uncertainty in gradient and gradient direction based on the regression for all the wells. Also, provide the reference for the report where this method has been validated because Appendix C, titled Steady-State Hydraulic Head, Gradient, and Spring Data for Pahute Mesa, does not contain any information concerning the method. Please clarify in text.	Replaced the first two paragraphs of Section 8.5.3 with the following: "Uncertainty in water levels imparts uncertainty in the water-level gradients and the inferred direction of water flow. If the magnitude of water-level uncertainty is large compared to the water-level difference between wells, the direction of flow cannot be reliably ascertained. Because the water-level difference between wells generally increases with distance between wells, the relative uncertainty in the estimates of flow direction is expected to decrease with increasing well spacing. For example, the distance between Wells ER-20-11 and ER-EC-15 is approximately 3 km, and the steady-state water-level difference between these wells is approximately 2 m, which is approximately the same as the water-level uncertainty at these wells. In contrast, the distance between Wells ER-20-11 and ER-EC-8 is approximately 17 km, and the steady-state water-level difference between these wells is approximately 50 m, suggesting the flow direction and gradient can be more reliably estimated at a scale of 17 km compared to 3 km. The relationship between distance and flow direction uncertainty was investigated by calculating the horizontal gradient direction over various length scales (2, 5, and 10 km) from the water-level data that Fenelon (2015a) used to construct the potentiometric surface map of Pahute Mesa. For wells with multiple completions, preference was given to heads from wells open to transmissive intervals; or wells with long open intervals, heads with low uncertainty, and heads consistent with surrounding wells (Fenelon 2015a). All water-level data within various distances of each well were identified, and a plane was fit through the data using linear regression. The azimuth and the dip of the resulting plane were used to approximate the flow direction and gradient. Uncertainty in the gradient calculations was introduced by sampling 1,000 realizations assuming the total water-level uncertainty is a uniform random variable with the distribution bounds of -1/2 the total water-level uncertainty to +1/2 the total uncertainty. Each realization results in a unique flow direction and gradient estimate. The 2.5 percentile and 97.5 percentile values of the calculated gradient and dip azimuth capture the 95th percentile interval and are used to estimate the uncertainty range of the horizontal gradient.

[a]Comment Types: M = Mandatory, S = Suggested.
Return Document Review Sheets to Environmental Management Nevada Program Operations Activity, Attn: QAC, M/S NSF 505

NEVADA ENVIRONMENTAL MANAGEMENT OPERATIONS ACTIVITY
DOCUMENT REVIEW SHEET

1. Document Title/Number: Hydrologic Data for the Groundwater Flow and Contaminant Transport Model of Corrective Action Units 101 and 102: Central and Western Pahute Mesa, Nye County, Nevada, Revision 0, September 2020				2. Document Date: Draft - September 2020
3. Revision Number: Rev. 0				4. Originator/Organization: Navarro
5. Responsible EM Nevada Program Activity Lead: John Myers				6. Date Comments Due: 11/12/2020
7. Review Criteria:				
8. Reviewer/Organization Phone No.: Christine Anders, NDEP				9. Reviewer's Signature:
10. Comment Number/Location		11. Type[a]	12. Comment	13. Comment Response
				The uncertainty discussed here is the parametric uncertainty in the gradient direction resulting from uncertainty in the water-level data assuming the potentiometric surface is a plane at the scale of the calculation. This is not a complete assessment of flow direction uncertainty and should not be interpreted as such. This approach does not address conceptual uncertainties such as those arising due to recharge variability or the amount of available data in various regions of Pahute Mesa. These sources of uncertainty can be addressed during the flow model development and calibration using alternate calibrated models, sensitivity studies, or NSMC analysis (Doherty et al., 2010)."
13	Page 8-13, Section 8.5.3, Figure 8-4, 10-km Length Scale		The black (97.5%) arrow directions are not clear in this figure: a. Are they lost below the red (2.5%) arrows or are they in the same direction as the red (2.5%)? b. Please explain in the text why the variation is changing between the different scale lengths.	When both arrows are not apparent, that is due to overlapping direction. a. Yes; when the 2.5% and 97.5% arrows are essentially the same, the red arrow plots on top of and obscures the black arrow. A note has been added to the figure. b. Section 8.5.3, first paragraph text clarified, and example added; see response to Comment 12. Figure 8-4 caption modified as follows "**Pahute Mesa Gradient Direction Uncertainty at Specific Wells Estimated Using Neighboring Wells within 2, 5, and 10 km** Note: Locations with a single red arrow have nearly identical 2.5 and 97.5 percentile gradient directions."
14	Page 8-15, Section 8.6.1, Figure 8-5		In this figure there are no wells plotted in the far northwest corner of Pahute Mesa, whereas in Figures 8-6 and 8-7 (pages 8-16 and 8-17 respectively), there are wells plotted in this area. Please explain this inconsistency in the text.	Section 8.6.1, Paragraph 4, added the following explanation: "Fewer gradient locations are illustrated in Figure 8-5 compared to Figures 8-6 and 8-7 because at some locations, there are no wells within 2 km of one another."
15	Page 9-4, Section 9.4, Figure 9-2		The horizontal scale needs to include the appropriate dates that are presented on Figure 6 from Garcia et al., 2017. Please add the dates to the figure.	Figure was revised as requested.
16	Figures 8-6 and 8-7 (pages 8-16 and 8-17)		Wells are plotted in the far northwest corner of Pahute Mesa but on Figure 8-5 (page 8-15), wells are not plotted in this location. Please explain the inconsistency in the text.	Section 8.6.1, Paragraph 4, added the following explanation: "Fewer gradient locations are illustrated in Figure 8-5 compared to Figures 8-6 and 8-7 because at some locations, there are no wells within 2 km of one another."

[a]Comment Types: M = Mandatory, S = Suggested.
Return Document Review Sheets to Environmental Management Nevada Program Operations Activity, Attn: QAC, M/S NSF 505

NEVADA ENVIRONMENTAL MANAGEMENT OPERATIONS ACTIVITY
DOCUMENT REVIEW SHEET

1. Document Title/Number: Hydrologic Data for the Groundwater Flow and Contaminant Transport Model of Corrective Action Units 101 and 102: Central and Western Pahute Mesa, Nye County, Nevada, Revision 0, September 2020				2. Document Date: Draft - September 2020
3. Revision Number: Rev. 0				4. Originator/Organization: Navarro
5. Responsible EM Nevada Program Activity Lead: John Myers				6. Date Comments Due: 11/12/2020
7. Review Criteria:				
8. Reviewer/Organization Phone No.: Christine Anders, NDEP				9. Reviewer's Signature:
10. Comment Number/Location		11. Type[a]	12. Comment	13. Comment Response
17	Figures 8-6 and 8-7 (pages 8-16 and 8-17) And Table C-4		Are the head gradient locations associated with specific well locations? In the figures, the colored circles indicate magnitudes of hydraulic gradient but circles are normally used to indicate well locations. Having an explanation in the text in regard to head gradients in relationship to well locations will be helpful. Table C-4 gradients are given between well pairs. So that is another reason to clarify the figures	Section 8.6.1, Paragraph 4, added the following explanation: "that are located at the well location used to calculate the gradient." Section 8.5.3, Paragraph 2, added the following explanation: "The uncertainty analysis described here was used to select appropriate distances between the well pairs used in the model calibration. Hydraulic head gradients between various well pairs are reported in Table C-4." Section 8.6.1, Paragraph 4, after the first sentence, added the following explanation: "At each well location, the mean value for the appropriate scale was used from the uncertainty realizations described above." Replaced the title of Figure 8-4 with "Pahute Mesa Gradient Direction Uncertainty at Specific Wells Estimated Using Neighboring Wells within 2, 5, and 10 km."
18	Appendix C, page C-39 of HDD-NDEP-changebars.pdf attached to the recent modified Document Review Sheet, Table C-5:		For clarity, please remove the green x's around each entry on Table C-5, if these are not automatically removed when accept track changes is applied.	These will be removed by the final edit.
19	Table C-5		Please add units for the distance from ER-30-1-1	Units of (m) added in Table C-5.
Below are changes identified during the Navarro editorial process				
	Figures 5-8a, 5-8b, and 5-8c		Figure captions do not accurately represent the contents.	Titles of these figures changed to: "Hydraulic Conductivity versus Depth for Dominant HGUs within Each Well."

[a]Comment Types: M = Mandatory, S = Suggested.
Return Document Review Sheets to Environmental Management Nevada Program Operations Activity, Attn: QAC, M/S NSF 505

Plate 1

Correlation of Stratigraphic and Hydrostratigraphic Units of the Pahute Mesa-Oasis Valley Hydrostratigraphic Framework Model

Plate 1
Correlation of Stratigraphic and Hydrostratigraphic Units of the Pahute Mesa-Oasis Valley Hydrostratigraphic Framework Model

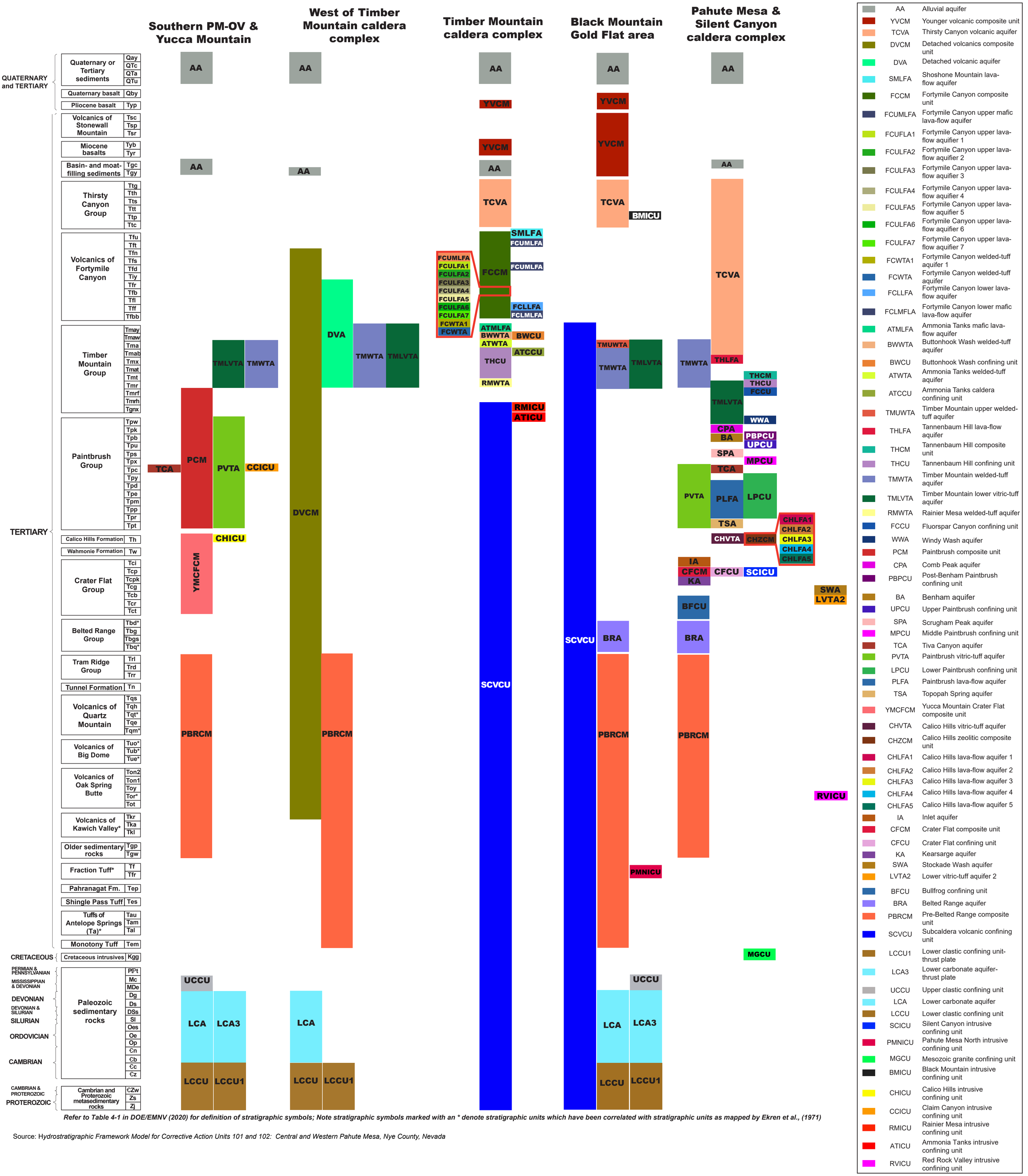

AA	Alluvial aquifer
YVCM	Younger volcanic composite unit
TCVA	Thirsty Canyon volcanic aquifer
DVCM	Detached volcanics composite unit
DVA	Detached volcanic aquifer
SMLFA	Shoshone Mountain lava-flow aquifer
FCCM	Fortymile Canyon composite unit
FCUMLFA	Fortymile Canyon upper mafic lava-flow aquifer
FCUFLA1	Fortymile Canyon upper lava-flow aquifer 1
FCULFA2	Fortymile Canyon upper lava-flow aquifer 2
FCULFA3	Fortymile Canyon upper lava-flow aquifer 3
FCULFA4	Fortymile Canyon upper lava-flow aquifer 4
FCULFA5	Fortymile Canyon upper lava-flow aquifer 5
FCULFA6	Fortymile Canyon upper lava-flow aquifer 6
FCULFA7	Fortymile Canyon upper lava-flow aquifer 7
FCWTA1	Fortymile Canyon welded-tuff aquifer 1
FCWTA	Fortymile Canyon welded-tuff aquifer
FCLLFA	Fortymile Canyon lower lava-flow aquifer
FCLMFLA	Fortymile Canyon lower mafic lava-flow aquifer
ATMLFA	Ammonia Tanks mafic lava-flow aquifer
BWWTA	Buttonhook Wash welded-tuff aquifer
BWCU	Buttonhook Wash confining unit
ATWTA	Ammonia Tanks welded-tuff aquifer
ATCCU	Ammonia Tanks caldera confining unit
TMUWTA	Timber Mountain upper welded-tuff aquifer
THLFA	Tannenbaum Hill lava-flow aquifer
THCM	Tannenbaum Hill composite unit
THCU	Tannenbaum Hill confining unit
TMWTA	Timber Mountain welded-tuff aquifer
TMLVTA	Timber Mountain lower vitric-tuff aquifer
RMWTA	Rainier Mesa welded-tuff aquifer
FCCU	Fluorspar Canyon confining unit
WWA	Windy Wash aquifer
PCM	Paintbrush composite unit
CPA	Comb Peak aquifer
PBPCU	Post-Benham Paintbrush confining unit
BA	Benham aquifer
UPCU	Upper Paintbrush confining unit
SPA	Scrugham Peak aquifer
MPCU	Middle Paintbrush confining unit
TCA	Tiva Canyon aquifer
PVTA	Paintbrush vitric-tuff aquifer
LPCU	Lower Paintbrush confining unit
PLFA	Paintbrush lava-flow aquifer
TSA	Topopah Spring aquifer
YMCFCM	Yucca Mountain Crater Flat composite unit
CHVTA	Calico Hills vitric-tuff aquifer
CHZCM	Calico Hills zeolitic composite unit
CHLFA1	Calico Hills lava-flow aquifer 1
CHLFA2	Calico Hills lava-flow aquifer 2
CHLFA3	Calico Hills lava-flow aquifer 3
CHLFA4	Calico Hills lava-flow aquifer 4
CHLFA5	Calico Hills lava-flow aquifer 5
IA	Inlet aquifer
CFCM	Crater Flat composite unit
CFCU	Crater Flat confining unit
KA	Kearsarge aquifer
SWA	Stockade Wash aquifer
LVTA2	Lower vitric-tuff aquifer 2
BFCU	Bullfrog confining unit
BRA	Belted Range aquifer
PBRCM	Pre-Belted Range composite unit
SCVCU	Subcaldera volcanic confining unit
LCCU1	Lower clastic confining unit-thrust plate
LCA3	Lower carbonate aquifer-thrust plate
UCCU	Upper clastic confining unit
LCA	Lower carbonate aquifer
LCCU	Lower clastic confining unit
SCICU	Silent Canyon intrusive confining unit
PMNICU	Pahute Mesa North intrusive confining unit
MGCU	Mesozoic granite confining unit
BMICU	Black Mountain intrusive confining unit
CHICU	Calico Hills intrusive confining unit
CCICU	Claim Canyon intrusive confining unit
RMICU	Rainier Mesa intrusive confining unit
ATICU	Ammonia Tanks intrusive confining unit
RVICU	Red Rock Valley intrusive confining unit

*Refer to Table 4-1 in DOE/EMNV (2020) for definition of stratigraphic symbols; Note stratigraphic symbols marked with an * denote stratigraphic units which have been correlated with stratigraphic units as mapped by Ekren et al., (1971)*

Source: H*ydrostratigraphic Framework Model for Corrective Action Units 101 and 102: Central and Western Pahute Mesa, Nye County, Nevada*

DISTRIBUTION

	Copies
W.R. Wilborn Environmental Management Nevada Program 100 N. City Parkway, Suite 1750 Las Vegas, NV 89106	1 electronic media
John Myers Environmental Management Nevada Program 100 N. City Parkway, Suite 1750 Las Vegas, NV 89106	1 electronic media
Chris Andres State of Nevada Nevada Division of Environmental Protection 375 E. Warm Springs Road, Suite 200 Las Vegas, NV 89119	1 electronic media
Michelle Bourret Los Alamos National Laboratory Bikini Atoll Road, SM-30, MS T003 Los Alamos, NM 87545	1 electronic media
Ed Kwicklis Los Alamos National Laboratory Bikini Atoll Road, SM-30, MS T003, EES-16 Los Alamos, NM 87545	1 electronic media
Andrew Tompson Lawrence Livermore National Laboratory 7000 East Avenue, L-103 Livermore, CA 94550-9909	1 electronic media
Mavrik Zavarin Lawrence Livermore National Laboratory 7000 East Avenue, L-103 Livermore, CA 94550-9909	1 electronic media
Jeff V. Sanders U.S. Geological Survey 160 N. Stephanie Street Henderson, NV 89074	1 electronic media

	Copies
Tracie Jackson U.S. Geological Survey 160 N. Stephanie Street Henderson, NV 89074	1 electronic media
Ken Ortego Mission Support and Test Services, LLC P.O. Box 98521, M/S NLV 082 Las Vegas, NV 89193-8521	1 electronic media
Chuck E. Russell Desert Research Institute 755 E. Flamingo Las Vegas, NV 89119	1 electronic media
Karl Pohlmann Desert Research Institute 755 E. Flamingo Las Vegas, NV 89119	1 electronic media
Mark Hausner Desert Research Institute 2215 Raggio Parkway Reno, NV 89512	1 electronic media
Ken Rehfeldt Navarro 100 N. City Parkway, Suite 1750 Las Vegas, NV 89106	1 electronic media
Sharad Kelkar Navarro 100 N. City Parkway, Suite 1750 Las Vegas, NV 89106	1 electronic media
Irene Farnham Navarro 100 N. City Parkway, Suite 1750 Las Vegas, NV 89106	1 electronic media

	Copies
Brian Haight Navarro 100 N. City Parkway, Suite 1750 Las Vegas, NV 89106	1 electronic media
John Londergan Navarro 100 N. City Parkway, Suite 1750 Las Vegas, NV 89106	1 electronic media
Jeff Wurtz Navarro 100 N. City Parkway, Suite 1750 Las Vegas, NV 89106	1 electronic media
Environmental Management Records Environmental Management Nevada Program 100 N. City Parkway, Suite 1750 Las Vegas, NV 89106	1 electronic media
Navarro Central Files 100 N. City Parkway, Suite 1750 Las Vegas, NV 89106	1 electronic media